The Dissertation Committee for Daniel Joseph Lang Miller Certifies that this is the approved version of the following dissertation:

Assessment of Fouling in Native and Surface-Modified Water Purification Membranes

Committee:

Benny D. Freeman, Supervisor

Donald R. Paul, Co-Supervisor

Christopher W. Bielawski

Christopher J. Ellison

Andrew D. Ellington

Assessment of Fouling in Native and Surface-Modified Water Purification Membranes

by

Daniel Joseph Lang Miller, B.S.Ch.E.

Dissertation

Presented to the Faculty of the Graduate School of

The University of Texas at Austin

in Partial Fulfillment

of the Requirements

for the Degree of

Doctor of Philosophy

The University of Texas at Austin

May 2013

Dedication

To my family

Acknowledgements

I am deeply indebted to a number of individuals for their support during my studies. My advisors, Drs. Benny Freeman and Don Paul, have enabled my work, provided technical advice, and lent their encouragement on a daily basis. Their extraordinary generosity has allowed me to carry out experiments without restriction, pursue courses of study that interest me, and attend conferences worldwide. Their advice has contributed immeasurably to my work ethic, my writing and speaking skills, and my personal and professional development. For these things, I am extremely grateful.

A few individuals have made particularly significant contributions to my work. First, Sirirat "Peach" Kasemset has been an indispensible laboratory partner. She is easily the most careful, thorough, and rigorous experimentalist I have ever met. Yet, she is a constant source of optimism, light-heartedness, and good will for me and everyone else in the laboratory. It has been inspirational to work alongside of her and her ebullient daily attitude will be missed. Second, Dr. Dan Dreyer and his advisor, Dr. Chris Bielawski, enabled the work on polydopamine structural characterization. Dan's comprehensive knowledge of spectroscopic techniques, outstanding writing, and thorough experimental approach have given me the opportunity to expand my doctoral work into fields that would have otherwise been impossible to explore. Without them, that work would not have even approached the outcome that it ultimately reached. Third, Dr. Hans Vrouwenvelder at WETSUS in Leeuwarden, the Netherlands, helped to spearhead the biofouling studies. He is a wealth of membrane fouling knowledge and was exceptionally generous in facilitating my studies overseas. Finally, Dr. Bryan McCloskey served as my mentor when I was beginning in the lab. His patience,

thoughtfulness, and inspiring ideas were invaluable to me as I was beginning my journey. Bryan was responsible, along with Dr. Ho Bum Park, for initiating the investigation of polydopamine-modified membranes, and without them, this project may have never happened.

Thanks are also in order for many of my colleagues who have also become some of my closest personal friends. Dr. Tom Murphy, Grant Offord, and Kevin Tung all began their graduate school journeys with me in the laboratories of Drs. Paul and Freeman, and they have remained fixtures throughout my studies here. Dr. Adam Stephens has been a colleague, a comrade, and a never-ending wellspring of humor. David Sanders has been a lunch companion, traveling companion, and sports-watching companion. I've had the pleasure of climbing mountains with Zach Smith, driving the Amalfi Coast with Dr. Geoff Geise, and spinning around dance floors with Katrina Czenkush. Other present and past lab mates, including Dr. Norman Horn, Dr. Brandon Rowe, Dr. Hua "Richard" Li, Dr. Claudio Ribeiro, Dr. Kristofer Gleason, Dr. Victor Kusuma, Dr. Hao Ju, Dr. Alyson Sagle, Dr. Liz Van Wagner, Dr. Wei Xie, Hee Jeung Oh, and Joe Cook have helped shape my graduate school experience.

A few individuals outside the lab should also be recognized. Dr. Julie Baker, my junior year high school chemistry teacher, was a Ph.D. chemical engineer herself and encouraged me to pursue this field of study. Sherry Reynolds and her indefatigable husband, Kevin, have shown me exceptional generosity of time and talent and have provided me with countless hours of instruction, challenge, and fulfillment. Kate Williams has been the bedrock of encouragement and support in my personal life throughout graduate school. Finally, and perhaps most importantly, I extend my most heartfelt appreciation to my parents, who spurred my interest in science at an early age and have undyingly supported me since.

Assessment of Fouling in Native and Surface-Modified Water Purification Membranes

Daniel Joseph Lang Miller, Ph.D.

The University of Texas at Austin, 2013

Co-Supervisors: Benny D. Freeman and Donald R. Paul

Fouling is a major obstacle to the implementation of membranes in water purification applications. Hydrophilization of the membrane surface tends to mitigate fouling because hydrophobic interactions between foulants and the membrane are reduced. Polydopamine was deposited onto membranes to render their surfaces hydrophilic. The chemical structure of polydopamine, which was previously ambiguous, was investigated by many spectroscopic techniques. While previously thought to consist of covalently-linked monomers, polydopamine was found to be an aggregate of partly-oxidized dopamine units linked by strong, non-covalent secondary interactions. Polydopamine was also used as a platform for the molecular conjugation of other anti-fouling materials, such as poly(ethylene glycol), to the membrane surface.

Membrane fouling was assessed by constant permeate flux crossflow filtration with an oil/water emulsion feed. The threshold flux—the flux at which the rate of fouling significantly increases—was determined by a well-established flux stepping technique. Membrane resistance evolution during fouling was compared for constant flux and constant transmembrane pressure operation using unmodified membranes. Below the threshold flux (slow fouling), good agreement in resistance evolution was found between the two operational modes; above the threshold flux, significant deviation was observed.

The effect of polydopamine and polydopamine-*g*-poly(ethylene glycol) surface modifications was studied under constant flux crossflow fouling conditions. The surface modifications were found to increase the membrane resistance, resulting in higher transmembrane pressures in the modified membranes than in the unmodified membranes at fluxes below the threshold flux. Modified membranes were also compared to unmodified membranes with the same pure water permeance (same initial resistance). In this case, the modified membranes had lower transmembrane pressures during fouling than the unmodified membranes, suggesting that a preferred method of membrane surface modification is to begin with a membrane of higher permeance than required, and then surface-modify it to achieve the desired permeance.

The efficacy of polydopamine and polydopamine-*g*-poly(ethylene glycol) surface modifications in reducing biofouling was also evaluated. Modified membranes showed reduced protein and bacterial adhesion in short-term tests, which are commonly used to assess biofouling propensity. However, long-term operation under hydrodynamic conditions mimicking those of an industrial module showed no benefit of the hydrophilic coatings in limiting biofouling.

Table of Contents

List of Tables

List of Figures

Chapter 1: Introduction

1.1 Goals of the Dissertation

Fouling is a significant challenge facing the use of polymeric membranes in water purification applications [1–3]. Many porous membranes are made of hydrophobic polymers through a phase inversion process [3], so hydrophobic solutes in the feed water, such as emulsified oils, readily accumulate on the membrane surface or within its porous structure through strong hydrophobic interactions [4]. Such fouling typically decreases membrane productivity, requiring increased energy expenditure or cleaning frequency [5]. Surface modification is a common approach to attempt to mitigate membrane fouling [6]. Surface modifications frequently aim to make the membrane surface more hydrophilic [7]. Hydrophilic surfaces are hypothesized to attract a strongly-bound layer of water molecules, which may act as a buffer to the adhesion of hydrophobic foulants [8]. Historically, hydrophilic surface modifications may take the form of thin, highly-permeable dense films, such as crosslinked poly(ethylene glycol) (PEG)-based coatings [1,2,5,9], or grafted molecules, such as PEG brushes [10–12]. While the application of such modifications are often effective in improving membrane hydrophilicity, they also typically reduce the membrane permeance, as the coating or grafted material contributes to the overall mass transfer resistance of the membrane [5,9,12–15]. Additionally, many methods require specific chemistries or exotic preparation, such as plasma treatment, to achieve grafting to the polymer backbone [16,17].

Polydopamine (PD) deposition has recently been used to hydrophilize a variety of materials [18]. PD may be deposited under mild conditions from buffered, aqueous dopamine solution and forms a robust, thin layer on nearly any surface in contact with the solution [18,19]. Due to the non-specific nature of its deposition, PD offers the ability to surface-modify a variety of different membranes or membrane modules. PD can also act

as a surface primer, facilitating the grafting of other molecules, such as poly(ethylene glycol) monoamine (PEG-NH_2), to a PD modified surface [18,20]. Many types of membranes, including microfiltration (MF), ultrafiltration (UF), nanofiltration (NF), and reverse osmosis (RO), have shown improved resistance to fouling by emulsified oil after modification with PD or PD-*g*-PEG [21,22].

This dissertation describes a fundamental investigation of fouling and fouling alleviation in porous, polymeric membranes used for water filtration. The goals were to:

(1) Characterize the chemical structure of polydopamine, which was heretofore ambiguous

(2) Compare membrane fouling under constant transmembrane pressure and constant flux conditions

(3) Evaluate the efficacy of polydopamine-based surface modifications in mitigating membrane fouling by model oil emulsions, produced water from hydraulic fracturing, and biofoulants

1.2 INTRODUCTION TO THE DISSERTATION

An overview of world water shortages, porous membranes, and membrane fouling is given in Chapter 2. Methods of membrane formation and surface modification strategies are covered. A special emphasis is given to emulsified oil foulants, which are employed widely in these studies. Hydraulic fracturing operations, which are increasingly utilizing mobile membrane skids to purify large volumes of oily wastewater for reuse, are briefly described. The chapter concludes with a discussion of membrane transport during fouling, including the recently developed concepts of critical and threshold fluxes.

1.2.1 Polydopamine as an Agent for Surface Modification

Polydopamine has drawn interest recently as a universal surface modification agent for use in a broad range of biotechnology [23–25], electrochemistry [26,27], nanotechnology [28,29], and membrane [21,22,30] applications, as described in Chapter 3. As elegantly demonstrated by Messersmith and co-workers, various substrates, including metals, metal oxides, ceramics, synthetic polymers, and a wide range of other hydrophilic and hydrophobic materials, may be coated with polydopamine *via* treatment of a surface with a tris(hydroxymethyl)aminomethane hydrochloride (TRIS HCl) buffered dopamine solution [18,19]. The polydopamine coatings obtained from this methodology are typically thin (tens of nm), highly robust and have shown utility as a platform for the conjugation of synthetic polymers [19,30] or biomolecules [20,31], and for electroless metallization [18]. Unlike other techniques, such as layer-by-layer assembly, monolayer self-assembly, and Langmuir-Blodgett deposition, surfaces modification with polydopamine requires only a single step [19].

Despite its remarkable properties and ease of preparation, the molecular structure of polydopamine has yet to be unambiguously determined, making further optimization difficult. In their report on surface modification by dip-coating substrates in dopamine solutions, Messersmith and co-workers suggested a structure (I) wherein oxidized and cyclized dopamine monomers were covalently joined *via* aryl-aryl linkages (Figure 1.1) [18]; similar covalent models (II/III) have been proposed by others [32–34]. Such structures are not without precedent as similar bonding schemes had been postulated for eumelanins (a class of pigments biosynthesized in melanocytes [35]) derived from various catecholamine monomers [36–39]. Chapter 3 surveys the investigation of natural and synthetic melanins since their discovery in the nineteenth century. Early spectroscopic studies were confounded by the fact that they focused on natural

eumelanins, which were often contaminated with proteinaceous materials and other organic impurities [40]. To simplify such experiments, synthetic eumelanins have been employed *in lieu* of natural samples. HPLC and UV-vis absorption studies of purified tyrosine proposed that cyclization of the catecholamine to the indoline-like cyclodopa was followed by further oxidation to dopachrome, and ultimately covalent coupling to form oligomeric eumelanins (Figure 1.2), although the precise mechanistic details of the associated processes were not disclosed [41]. Due to the poor solubility of eumelanins, early reports concluded that the presence of these oligomers indicated that the eumelanin product contained mixtures of covalent polymers and non-covalent aggregates [42]. Such a mixed structural model has been supported more recently through DFT calculations, X-ray analyses, and mass spectroscopy studies, which have suggested that covalently-bound oligomers (such as IV) stack through π-π and other non-covalent interactions to form larger supramolecular complexes, rather than traditional, covalently-coupled polymers [35,43].

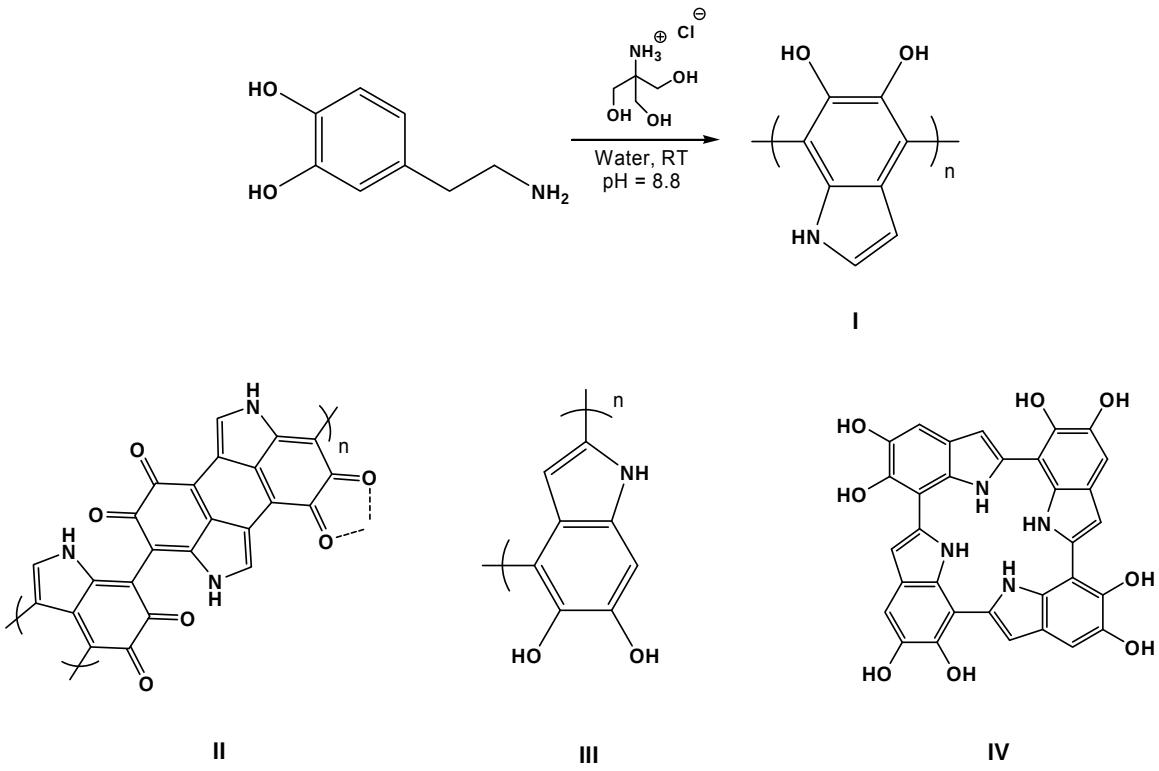

Figure 1.1. (Top) Synthesis and structure of polydopamine as proposed by Messersmith and others [18–20,31,32], and (bottom) other proposed structures of polydopamine [35,44–47].

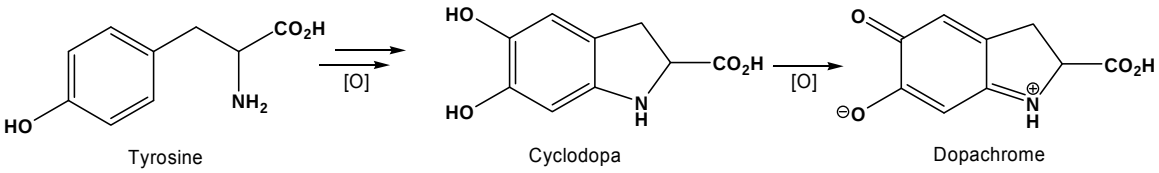

Figure 1.2. Proposed mechanism for the oxidative cyclization of tyrosine.

In contrast to the models described above, scrutiny of the literature reveals that dopamine may polymerize in a manner similar to that of hydroquinone (*p*-benzenediol) and catechol (*o*-benzenediol) [39,48–51]. In addition to the structural parallels between benzenediols and catecholamines, such as an aryl core and *ortho*- or *para*-substituted diol

functionality (*meta*-substituted benzenediols and catecholamines are unreactive under aqueous, alkaline conditions), monomers in both systems can undergo autoxidation. For example, hydroquinone and catechol polymerize under conditions similar to those for the formation of polydopamine and other synthetic eumelanins (alkaline, aqueous media under an aerobic atmosphere) to afford insoluble, polymeric products [48]. Reaction of the two aforementioned diols proceeds *via* autoxidation, forming *p*-benzoquinone and *o*-benzoquinone, respectively [51–53]. After formation, discrete carbonyl-containing species react with residual diols *via* charge-transfer, hydrogen bonding, and π-stacking interactions, resulting in 1:1 complexes commonly referred to as quinhydrones (see Figure 1.3) [48,54,55]. The bimolecular quinhydrone complexes are known to further react with one another *via* identical non-covalent processes, resulting in oligomeric or polymeric aggregates, though some disagreement exists regarding their structures [56,57]. While a non-covalent model of quinhydrones is the most widely adopted, covalent bonding with aryl linkages in the backbone formed *via* ionic and radical processes has also been suggested [56,57].

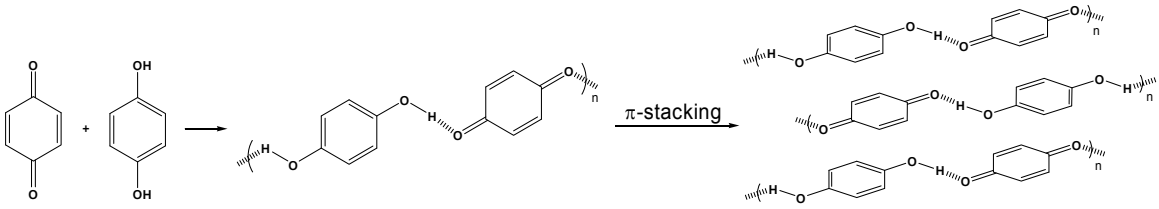

Figure 1.3. Formation of quinhydrones through 1:1 complexation of benzoquinones and diols, and subsequent π-stacking leads to multi-dimensional polymeric materials [48].

Sharing many of the complexities of quinhydrones, a significant amount of effort has been invested in identifying the structure of polydopamine. However, no definitive model exists. Thus, in an effort to provide direction for further optimization of polydopamine for use in surface modifications, a comprehensive study of the polymer's

structure and bonding was undertaken and is described in Chapter 5. Based on a wide range of spectroscopic evidence, a structural model for synthetic polydopamine wherein the monomers are linked primarily through non-covalent interactions is proposed. Also, because polydopamine is comprised of reactants that are similar to the catecholamine precursors of natural eumelanins, it is further proposed that polydopamine may serve as a model for broadly understanding structure and bonding patterns of synthetic and naturally-occurring eumelanins [58].

1.2.2 Membrane Fouling

Membrane fouling behavior is commonly characterized in crossflow experiments, where a feed solution passes tangentially along the membrane surface and permeate flow through the membrane is perpendicular to the feed flow [3]. Crossflow filtration may be performed in one of two operational modes: constant transmembrane pressure (TMP) or constant permeate flux. In a constant TMP experiment, the transmembrane pressure is fixed, often by applying a steady feed pressure and leaving the permeate open to the atmosphere. As the membrane fouls, membrane mass transfer resistance increases, and permeate flux decreases. This flux decrease, the metric by which fouling is measured, causes changes in the hydrodynamic environment and the concentration of solutes at the membrane surface [59,60]. Such variable conditions can complicate comparisons of different membranes or the modeling of fouling phenomena [60]. The convective flow of solutes toward the membrane surface can be better controlled by imposing a constant permeate flux and monitoring the transmembrane pressure change required to maintain a steady permeation rate [59,61]. Constant flux experiments, therefore, eliminate the variable hydrodynamics inherent to constant TMP experiments [60]. Despite this advantage of constant flux studies, they are less commonly reported in the literature than constant TMP experiments, likely due to the added complexity and more challenging

operation of laboratory constant flux crossflow systems relative to their constant TMP counterparts. Critically, however, most industrial water purification processes using microfiltration and ultrafiltration membranes are operated at constant flux [62,63], as are many biochemical processes [59], so laboratory evaluation of membrane fouling under constant flux conditions could be helpful to further understand fouling under conditions closer to those used in industry.

Constant flux crossflow systems are also useful in critical and threshold flux determination. Many definitions of critical flux can be found in the literature [59,61,64–70], but it is often considered the maximum permeate flux at which negligible fouling accumulates on the membrane; these definitions are expounded upon in Chapter 2. A number of critical and threshold flux determination methods are described in the literature [64], but the most common are flux stepping procedures where the transmembrane pressure is monitored over constant flux intervals [66]. The flux is increased from one interval to the next, and the critical or threshold flux is typically determined graphically using the resultant TMP data [65,66]. A constant flux crossflow apparatus, therefore, facilitates straightforward determination of the membrane critical and threshold fluxes.

Chapter 4 describes, in detail, the design and operation of a laboratory-scale crossflow system for evaluation of constant permeate flux membrane fouling behavior. In studies utilizing simpler system designs based on those found in the current literature, the permeate flow rate stability was poor. To combat this issue, a feedback control scheme was implemented to ensure that the permeate flux was rigorously maintained at a constant rate. Automatic control of the permeate rate also facilitates critical and threshold flux determination by simply raising the flux setpoint at desired intervals, allowing for rapid critical flux screening. This instrument was found suitable for studies

on microfiltration (MF) or ultrafiltration (UF) membranes with a variety of foulants. Validation of system operation, including comparison to another constant flux fouling study, is presented in Chapter 6.

Although both constant TMP and, to a lesser degree, constant flux fouling studies have been reported, there are few direct comparisons of membrane fouling under both operational modes. In their work describing the critical flux concept, Field *et al*. provided qualitative observations of constant TMP and constant flux measurements [59]. They observed that the total mass transfer resistance of the membrane and foulant was generally low for constant flux experiments and high for constant TMP experiments, presumably due to the rapid fouling at the beginning of constant TMP experiments. Marshall, Munro, and Trägårdh developed a crossflow system capable of operating in constant flux or constant TMP modes [71]. They filtered skimmed milk with both ultrafiltration and microfiltration membranes. Although their study focused mainly on a comparison of ultrafiltration and microfiltration fouling, they also identified experimental conditions where ultrafiltration membrane resistances developed similarly in constant flux and constant TMP fouling studies. Decloux *et al.* considered the operation of ultrafiltration and microfiltration membranes under both control modes, finding the constant flux operation resulted in less severe fouling than constant TMP operation, resulting in a reduced frequency of cleaning [72]. A few publications, including two very recent reports [73,74], have focused on methods for predicting the fouling propensity of certain solutions and have, to this end, evaluated fouling under both constant flux and constant TMP operation. Kanani and Ghosh developed a model to predict permeate flux decline in constant TMP operation by assuming that the flux decline is comprised of many sequential constant flux steps [75]. Model parameters were obtained from constant flux experiments, which offer an unchanging hydrodynamic environment at the

membrane surface, facilitating the capture of data related to concentration polarization and fouling phenomena. Further investigation of fouling phenomena at constant flux and constant TMP is, however, warranted. As noted by Sioutopoulos and Karabelas, "uncertainty exists as to whether the more common constant-pressure UF and RO laboratory tests provide fouling resistances representative of conditions prevailing in the constant flux mode of commercial plant operation" [74].

Chapter 7 compares constant flux and constant TMP fouling of unmodified ultrafiltration membranes being used to filter an emulsified oil solution. The resistance to permeation, which increases due to foulant accumulation on the membrane [71], is calculated as a function of the permeate volume processed per unit membrane area. Experiments were performed such that the initial flux in a constant TMP test was equal to the flux imposed in the corresponding constant flux test (and, consequently, the initial TMP in the constant flux experiment was equal to the TMP imposed in the constant TMP experiment). Agreement between the experimental protocols was good at low fluxes but not at high fluxes. The threshold flux, as recently defined by Field and Pearce [76], was found to separate the flux regime of good agreement from that of poor agreement. The weak form of the critical flux was also observed.

Following this fundamental study of fouling on unmodified membranes, attention turned to the evaluation of polydopamine-based surface modifications for fouling mitigation. Like most open literature studies reporting the fouling performance of surface-modified membranes, studies on PD and PD-*g*-PEG modified membranes have focused on constant transmembrane pressure experiments, where the transmembrane pressure (TMP) is fixed, and fouling is evaluated by monitoring permeate flux decline over time [21,22]. This technique is widely used in laboratory fouling studies [9,13,21]. However, many industrial membrane-based water purification systems operate at

constant permeate flux to ensure a steady rate of product water production [62,72]. In this operational mode, the permeate flux is fixed, and the TMP is increased over time, as the membrane fouls, to maintain the desired permeate flux [61]. Aside from the similarity with industrial practice, constant flux operation has several other benefits. As permeate flux declines in a constant TMP experiment, the rate of permeate flow through the membrane pores also decreases. Therefore, the rate at which foulants are brought to the membrane surface by permeate convection varies continuously during the experiment as the membrane fouls. Therefore, the observed fouling behavior is not only the result of interaction between foulants and the membrane surface (important when evaluating the effect of fouling-resistant surface modifications), but it is also a result of the changing hydrodynamic environment and solute concentration near the membrane [59,60]. This variability complicates comparison of membranes (such as modified membranes against their unmodified counterparts) and modeling of fouling phenomena [60]. An additional benefit of constant flux experiments is that the critical and threshold fluxes of a membrane may be determined by slowly increasing the flux through a series of constant flux steps [61]. The threshold flux contributes valuable information to the determination of sustainable fluxes for industrial operation [76]. However, very few reports describing the influence of surface modification of membranes on their on fouling resistance at constant flux operation are available [14].

Chapter 8 describes constant flux fouling studies on PD and PD-*g*-PEG modified polysulfone UF membranes. Fouling was compared among modified and unmodified membranes at six different fluxes. The threshold flux for each membrane was evaluated by three different parameters obtained from flux stepping experiments and analyzed in the context of constant flux fouling experiments. Additionally, due to the decrease in intrinsic membrane permeance caused by the application of the PD and PD-*g*-PEG

coatings, modified membranes were compared to another polysulfone UF membrane with a smaller pore size, and this membrane had comparable pure water permeance to that of the modified membranes.

In an effort to extend laboratory tests of polydopamine-coated membranes to an industrial scenario with a complex, highly fouling feed water, a field study involving purification of flowback water from hydraulic fracturing operations was performed. This pilot study is discussed in Chapter 9. The non-specific deposition of polydopamine permits modification of membrane modules *in situ*, depositing PD on the membrane surface, feed spacers, and all wetted parts [77]. Ultrafiltration and reverse osmosis membrane modules were modified with polydopamine; ultrafiltration modules were further modified by grafting PEG to the polydopamine coating. Previous work has demonstrated improved UF fouling resistance when PEG was grafted to the PD coating [21]; in the case of RO, the grafted PEG layer contributed significantly increased mass transfer resistance [30], so the RO modules were coated only with PD in this study. Modules were used to purify saline hydraulic fracturing flowback water from wells in the Barnett shale play in north Texas. The UF modules were used primarily to remove residual suspended solids and organics (especially emulsified oils) from the pretreated raw feed, and the RO modules were used mainly to desalinate the UF permeate. The fouling behavior of PD (and PD-*g*-PEG) modified UF and RO modules was compared to that of unmodified modules.

In addition to emulsified oil fouling, biofouling represents a major limitation in the use of membranes for water purification. Biofouling occurs when the growth of microorganisms, typically as a biofilm, becomes substantial enough to increase feed channel pressure drop, to reduce permeate flux, and to compromise rejection properties of a membrane installation [78]. Cells and organic macromolecules are so ubiquitous in

industrial water streams that surfaces in contact with water are covered with a conditioning film within seconds; biofilm development quickly follows as cells adhere easily to the conditioning film [79]. Biofilm growth provides a number of advantages to its constituent organisms over growth in the planktonic state, including enhanced nutrient access, improved antimicrobial resistance, and synergistic associations with nearby cells [80]. Biofilms are notoriously difficult to prevent or to eliminate. Employment of anti-biofouling strategies, such as antimicrobial compounds or turbulent hydrodynamic conditions, tends to select for organisms resistant to that particular countermeasure, resulting in the development of very robust biofilms. Chlorination has been successfully used to control microbial growth [81], but chlorine's deleterious effects on some membranes (most notably thin film composite polyamide-based reverse osmosis membranes) [82] forces costly de-chlorination before membrane treatment and re-chlorination before end use.

The use of biocides and cleaning protocols for biofouling control may be reduced by membranes resistant to biofouling. Hydrophilic, smooth surfaces have historically shown resistance to protein and bacterial adhesion [83]. Because of their successes in reducing fouling when applied to membranes in previous studies, polydopamine and polydopamine-*g*-PEG membrane coatings are of interest as potential anti-biofouling surface modifications.

The biofouling susceptibility of membranes modified with polydopamine and with polydopamine-*g*-poly(ethylene glycol) was assessed at WETSUS in Leeuwarden, the Netherlands. This study is described in Chapter 10. Coated membranes were challenged with short-term batch adhesion of proteins and bacteria and with continuous biofilm growth experiments in a membrane fouling simulator. The results were used to assess the effectiveness of membrane modification for biofouling control and to evaluate

the appropriateness of short-term adhesion tests in determining the biofouling potential of the modified membranes and spacers.

1.3 REFERENCES

[1] H. Ju, B.D. McCloskey, A.C. Sagle, V.A. Kusuma, B.D. Freeman, Preparation and characterization of crosslinked poly(ethylene glycol) diacrylate hydrogels as fouling-resistant membrane coating materials, Journal of Membrane Science 330 (1-2) (2009) 180–188.

[2] A.C. Sagle, H. Ju, B.D. Freeman, M.M. Sharma, PEG-Based Hydrogel Membrane Coatings, Polymer 50 (3) (2009) 756–766.

[3] R.W. Baker, Membrane Technology and Applications, 2nd ed., John Wiley & Sons, West Sussex, England, 2004.

[4] J. Mueller, Y. Cen, R.H. Davis, Crossflow Microfiltration of Oily Water, Journal of Membrane Science 129 (2) (1997) 221–235.

[5] H. Ju, B.D. McCloskey, A.C. Sagle, Y.-H. Wu, V.A. Kusuma, B.D. Freeman, Crosslinked Poly(ethylene oxide) Fouling Resistant Coating Materials for Oil/Water Separation, Journal of Membrane Science 307 (2) (2008) 260–267.

[6] G.M. Geise, H.-S. Lee, D.J. Miller, B.D. Freeman, J.E. McGrath, D.R. Paul, Water Purification by Membranes: The Role of Polymer Science, Journal of Polymer Science Part B: Polymer Physics 48 (15) (2010) 1685–1718.

[7] D. Rana, T. Matsuura, Surface modifications for antifouling membranes, Chemical Reviews 110 (4) (2010) 2448–71.

[8] M. Elimelech, W.A. Phillip, The Future of Seawater Desalination: Energy, Technology, and the Environment, Science 333 (6043) (2011) 712–7.

[9] A.C. Sagle, E.M. Van Wagner, H. Ju, B.D. McCloskey, B.D. Freeman, M.M. Sharma, PEG-Coated Reverse Osmosis Membranes: Desalination Properties and Fouling Resistance, Journal of Membrane Science 340 (1-2) (2009) 92–108.

[10] A. Roosjen, H.J. Kaper, H.C. van der Mei, W. Norde, H.J. Busscher, Inhibition of adhesion of yeasts and bacteria by poly(ethylene oxide)-brushes on glass in a parallel plate flow chamber, Microbiology 149 (11) (2003) 3239–3246.

[11] A. Roosjen, H.C. van der Mei, H.J. Busscher, W. Norde, Microbial Adhesion to Poly(ethylene oxide) Brushes: Influence of Polymer Chain Length and Temperature, Langmuir 20 (25) (2004) 10949–55.

[12] M. Ulbricht, H. Matuschewski, A. Oechel, H.-G. Hicke, Photo-induced graft polymerization surface modifications for the preparation of hydrophilic and low-proten-adsorbing ultrafiltration membranes, Journal of Membrane Science 115 (1) (1996) 31–47.

[13] E.M. Van Wagner, A.C. Sagle, M.M. Sharma, Y.-H. La, B.D. Freeman, Surface Modification of Commercial Polyamide Desalination Membranes using Poly(ethylene glycol) Diglycidyl Ether to Enhance Membrane Fouling Resistance, Journal of Membrane Science 367 (1-2) (2011) 273–287.

[14] J. Meier-Haack, S. Derenko, J. Seng, Fouling Reduction by Graft-Modification with Hydrophilic Polymers, Separation Science and Technology 42 (13) (2007) 2881–2889.

[15] J. Louie, I. Pinnau, I. Ciobanu, K. Ishida, A. Ng, M. Reinhard, Effects of Polyether–Polyamide Block Copolymer Coating on Performance and Fouling of Reverse Osmosis Membranes, Journal of Membrane Science 280 (1-2) (2006) 762–770.

[16] M. Ulbricht, G. Belfort, Surface modification of ultrafiltration membranes by low temperature plasma. I. Treatment of polyacrylonitrile, Journal of Applied Polymer Science 56 (3) (1995) 325–343.

[17] M. Ulbricht, G. Belfort, Surface modification of ultrafiltration membranes by low temperature plasma II. Graft polymerization onto polyacrylonitrile and polysulfone, Journal of Membrane Science 111 (2) (1996) 193–215.

[18] H. Lee, S.M. Dellatore, W.M. Miller, P.B. Messersmith, Mussel-Inspired Surface Chemistry for Multifunctional Coatings, Science 318 (5849) (2007) 426–430.

[19] H. Lee, Y. Lee, A.R. Statz, J. Rho, T.G. Park, P.B. Messersmith, Substrate-Independent Layer-by-Layer Assembly by Using Mussel-Adhesive-Inspired Polymers, Advanced Materials 20 (9) (2008) 1619–1623.

[20] H. Lee, J. Rho, P.B. Messersmith, Facile Conjugation of Biomolecules onto Surfaces via Mussel Adhesive Protein Inspired Coatings, Advanced Materials 21 (4) (2009) 431–434.

[21] B.D. McCloskey, H.B. Park, H. Ju, B.W. Rowe, D.J. Miller, B.D. Freeman, A Bioinspired Fouling-Resistant Surface Modification for Water Purification Membranes, Journal of Membrane Science 413-414 (2012) 82–90.

[22] S. Kasemset, A. Lee, D.J. Miller, B.D. Freeman, M.M. Sharma, Effect of polydopamine deposition conditions on fouling resistance, physical properties, and permeation properties of reverse osmosis membranes in oil/water separation, Journal of Membrane Science 425-426 (2013) 208–216.

[23] S.H. Ku, J.S. Lee, C.B. Park, Spatial Control of Cell Adhesion and Patterning through Mussel-Inspired Surface Modification by Polydopamine, Langmuir 26 (6) (2010) 15104–15108.

[24] S.H. Ku, J. Ryu, S.K. Hong, H. Lee, C.B. Park, General functionalization route for cell adhesion on non-wetting surfaces, Biomaterials 31 (9) (2010) 2535–41.

[25] J. Ryu, S.H. Ku, H. Lee, C.B. Park, Mussel-Inspired Polydopamine Coating as a Universal Route to Hydroxyapatite Crystallization, Advanced Functional Materials 20 (13) (2010) 2132–2139.

[26] T. Luczak, Preparation and characterization of the dopamine film electrochemically deposited on a gold template and its applications for dopamine sensing in aqueous solution, Electrochimica Acta 53 (19) (2008) 5725–5731.

[27] Y. Zhang, H. Wang, J. Nie, H. Zhou, G. Shen, R. Yu, Mussel-inspired fabrication of encoded polymer films for electrochemical identification, Electrochemistry Communications 11 (10) (2009) 1936–1939.

[28] B. Fei, B. Qian, Z. Yang, R. Wang, W. Liu, C. Mak, et al., Coating carbon nanotubes by spontaneous oxidative polymerization of dopamine, Carbon 46 (13) (2008) 1795–1797.

[29] H. Hu, B. Yu, Q. Ye, Y. Gu, F. Zhou, Modification of carbon nanotubes with a nanothin polydopamine layer and polydimethylamino-ethyl methacrylate brushes, Carbon 48 (8) (2010) 2347–2353.

[30] B.D. McCloskey, H.B. Park, H. Ju, B.W. Rowe, D.J. Miller, B.J. Chun, et al., Influence of Polydopamine Deposition Conditions on Pure Water Flux and Foulant Adhesion Resistance of Reverse Osmosis, Ultrafiltration, and Microfiltration Membranes, Polymer 51 (15) (2010) 3472–3485.

[31] T. a Morris, A.W. Peterson, M.J. Tarlov, Selective binding of RNase B glycoforms by polydopamine-immobilized concanavalin A, Analytical Chemistry 81 (13) (2009) 5413–20.

[32] F. Yu, S. Chen, Y. Chen, H. Li, L. Yang, Y. Chen, et al., Experimental and theoretical analysis of polymerization reaction process on the polydopamine membranes and its corrosion protection properties for 304 Stainless Steel, Journal of Molecular Structure 982 (1-3) (2010) 152–161.

[33] X.-B. Yin, D.-Y. Liu, Polydopamine-based permanent coating capillary electrochromatography for auxin determination, Journal of Chromatography A 1212 (1-2) (2008) 130–136.

[34] L. Zhang, J. Shi, Z. Jiang, Y. Jiang, S. Qiao, J. Li, et al., Bioinspired preparation of polydopamine microcapsule for multienzyme system construction, Green Chemistry 13 (2) (2011) 300.

[35] E. Kaxiras, A. Tsolakidis, G. Zonios, S. Meng, Structural Model of Eumelanin, Physical Review Letters 97 (21) (2006) 218102/1–218102/4.

[36] M.D. Hawley, S. V Tatawawadi, S. Piekarski, R.N. Adams, Electrochemical studies of the oxidation pathways of catecholamines, Journal of the American Chemical Society 89 (2) (1967) 447–50.

[37] M.D. Hawley, S. V. Tatawawadi, S. Piekarski, R.N. Adams, Additions and Corrections - Electrochemical Studies of the Oxidation Pathways of

Catecholamines, Journal of the American Chemical Society 90 (4) (1968) 1093–1093.

[38] M.M. Jastrzebska, K. Stepień, J. Wilczok, M. Porebska-Budny, T. Wilczok, Semiconductor properties of melanins prepared from catecholamines, General Physiology and Biophysics 9 (4) (1990) 373–83.

[39] D.C.S. Tse, R.L. McCreery, R.N. Adams, Potential oxidative pathways of brain catecholamines, Journal of Medicinal Chemistry 19 (1) (1976) 37–40.

[40] M.B. Clark, J.A. Gardella, T.M. Schultz, D.G. Patil, L. Salvati, Solid-state analysis of eumelanin biopolymers by electron spectroscopy for chemical analysis, Analytical Chemistry 62 (9) (1990) 949–956.

[41] S. Ito, A chemist's view of melanogenesis, Pigment Cell Research 16 (3) (2003) 230–6.

[42] M. d'Ischia, A. Napolitano, A. Pezzella, P. Meredith, T. Sarna, Chemical and structural diversity in eumelanins: unexplored bio-optoelectronic materials, Angewandte Chemie International Edition 48 (22) (2009) 3914–21.

[43] J.A. Swift, Speculations on the molecular structure of eumelanin, International Journal of Cosmetic Science 31 (2) (2009) 143–50.

[44] A. Postma, Y. Yan, Y. Wang, A.N. Zelikin, E. Tjipto, F. Caruso, Self-Polymerization of Dopamine as a Versatile and Robust Technique to Prepare Polymer Capsules, Chemistry of Materials 21 (14) (2009) 3042–3044.

[45] B. Yu, D.A. Wang, Q. Ye, F. Zhou, W. Liu, Robust polydopamine nano/microcapsules and their loading and release behavior, Chemical Communications (44) (2009) 6789–91.

[46] J. Ryu, S.H. Ku, M. Lee, C.B. Park, Bone-like peptide/hydroxyapatite nanocomposites assembled with multi-level hierarchical structures, Soft Matter 7 (16) (2011) 7201.

[47] S. Kang, M. Elimelech, Bioinspired single bacterial cell force spectroscopy, Langmuir 25 (17) (2009) 9656–9.

[48] A.O. Patil, W.T. Pennington, G.R. Desiraju, D.Y. Curtin, I.C. Paul, Recent Studies on the Formation and Properties of Quinhydrone Complexes, Molecular Crystals and Liquid Crystals 134 (1) (1986) 279–304.

[49] W.H. Harrison, W.W. Whisler, B.J. Hill, Catecholamine oxidation and ionization properties indicated from the H+ release, tritium exchange, and spectral changes which occur during ferricyanide oxidation, Biochemistry 7 (9) (1968) 3089–94.

[50] S. Senoh, C.R. Creveling, S. Udenfriend, B. Witkop, Chemical, Enzymatic and Metabolic Studies on the Mechanism of Oxidation of Dopamine, Journal of the American Chemical Society 81 (23) (1959) 6236–6240.

[51] F. Cataldo, On the Structure of Macromolecules Obtained by Oxidative Polymerization of Polyhydroxyphenols and Quinones, Polymer International 46 (4) (1998) 263–268.

[52] A. V Ragimov, I.I. Ragimov, B.A. Mamedov, S.A. Guseinov, B.I. Liogon'kii, On features of the oligomerization of hydroquinone under auto-oxidation, Polymer Science USSR 24 (10) (1982) 2434–2440.

[53] M.T.I.W. Schüsler-Van Hees, G.M.J. Beijersbergen Van Henegouwen, P. Stoutenberg, Autoxidation of catechol(amine)s, Pharmaceutisch Weekblad Scientific Edition 7 (6) (1985) 245–251.

[54] D. Bijl, H. Kainer, A.C. Rose-Innes, Stabilization of Free Radicals by Adsoption: Detection by Paramagnetic Resonance, Nature 174 (4435) (1954) 830–831.

[55] H.R. Devlin, I.J. Harris, Mechanism of the oxidation of aqueous phenol with dissolved oxygen, Industrial & Engineering Chemistry Fundamentals 23 (4) (1984) 387–392.

[56] A. Furlani, M. V Russo, F. Cataldo, Oxidative polymerization of p-benzoquinone and hydroquinone. Conductivity of doped and undoped polymerization products, Synthetic Metals 29 (1) (1989) 507–510.

[57] A. V Ragimov, B.A. Mamedov, B.I. Liogon'kii, The alkali initiated polymerization of p-benzoquinone, Polymer Science USSR 19 (11) (1977) 2922–2928.

[58] F. Bernsmann, A. Ponche, C. Ringwald, J. Hemmerlé, J. Raya, B. Bechinger, et al., Characterization of Dopamine−Melanin Growth on Silicon Oxide, Journal of Physical Chemistry C 113 (19) (2009) 8234–8242.

[59] R.W. Field, D. Wu, J.A. Howell, B.B. Gupta, Critical flux concept for microfiltration fouling, Journal of Membrane Science 100 (3) (1995) 259–272.

[60] P. Aimar, J.A. Howell, M. Turner, Effects of concentration boundary layer development on the flux limitations in ultrafiltration, Chemical Engineering Research and Design 67 (3) (1989) 255–261.

[61] R. Chan, V. Chen, The effects of electrolyte concentration and pH on protein aggregation and deposition: critical flux and constant flux membrane filtration, Journal of Membrane Science 185 (2) (2001) 177–192.

[62] B. Alspach, S. Adham, T. Cooke, P. Delphos, J. Garcia-Aleman, J. Jacangelo, et al., Microfiltration and ultrafiltration membranes for drinking water, Journal of the American Water Works Association 100 (12) (2008) 84–97.

[63] R. Field, Fundamentals of Fouling, in: K.-V. Pinemann, S.P. Nunes (Eds.), Membrane Technology: Membranes for Water Treatment, Volume 4, Wiley-VCH, Weinheim, Germany, 2010: pp. 1–24.

[64] P. Bacchin, P. Aimar, R.W. Field, Critical and sustainable fluxes: Theory, experiments and applications, Journal of Membrane Science 281 (1-2) (2006) 42–69.

[65] P.S. Beier, G. Jonsson, Critical Flux Determination by Flux-Stepping, AIChE Journal 56 (7) (2010) 1739–1747.

[66] K.Y.-J. Choi, B.A. Dempsey, Bench-scale evaluation of critical flux and TMP in low-pressure membrane filtration, Journal of the American Water Works Association 97 (7) (2005) 134–143.

[67] J.A. Howell, Sub-critical flux operation of microfiltration, Journal of Membrane Science 107 (1-2) (1995) 165–171.

[68] D.. Kwon, S. Vigneswaran, A.. Fane, R.B. Aim, Experimental determination of critical flux in cross-flow microfiltration, Separation and Purification Technology 19 (3) (2000) 169–181.

[69] P. Le Clech, B. Jefferson, I.S. Chang, S.J. Judd, Critical flux determination by the flux-step method in a submerged membrane bioreactor, Journal of Membrane Science 227 (1-2) (2003) 81–93.

[70] S. Metsämuuronen, J. Howell, M. Nyström, Critical flux in ultrafiltration of myoglobin and baker's yeast, Journal of Membrane Science 196 (1) (2002) 13–25.

[71] A.D. Marshall, P.A. Munro, G. Trägårdh, The effect of protein fouling in microfiltration and ultrafiltration on permeate flux, protein retention and selectivity: A literature review, Desalination 91 (1) (1993) 65–108.

[72] M. Decloux, L. Tatoud, Importance of the control mode in ultrafiltration: case of raw cane sugar remelt, Journal of Food Engineering 44 (2) (2000) 119–126.

[73] L.-N. Sim, Y. Ye, V. Chen, A.G. Fane, Comparison of MFI-UF constant pressure, MFI-UF constant flux and Crossflow Sampler – Modified Fouling Index Ultrafiltration (CFS-MFIUF), Water Research 45 (4) (2010) 1639–1650.

[74] D.C. Sioutopoulos, A.J. Karabelas, Correlation of organic fouling resistances in RO and UF membrane filtration under constant flux and constant pressure, Journal of Membrane Science 407-408 (2012) 34–46.

[75] D.M. Kanani, R. Ghosh, A constant flux based mathematical model for predicting permeate flux decline in constant pressure protein ultrafiltration, Journal of Membrane Science 290 (1-2) (2007) 207–215.

[76] R.W. Field, G.K. Pearce, Critical, sustainable and threshold fluxes for membrane filtration with water industry applications, Advances in Colloid and Interface Science 164 (1-2) (2011) 38–44.

[77] B.D. McCloskey, Novel Surface Modifications and Materials for Fouling Resistant Water Purification Membranes, The University of Texas at Austin, 2009.

[78] J.S. Vrouwenvelder, S.A. Manolarakis, J.P. van der Hoek, J.A.M. van Paassen, W.G.J. van der Meer, J.M.C. van Agtmaal, et al., Quantitative biofouling diagnosis in full scale nanofiltration and reverse osmosis installations, Water Research 42 (19) (2008) 4856–68.

[79] H.-C. Flemming, Biofouling in water systems--cases, causes and countermeasures, Applied Microbiology and Biotechnology 59 (6) (2002) 629–40.

[80] S.L. Percival, J.T. Walker, P.R. Hunter, Microbiological Aspects of Biofilms and Drinking Water, CRC Press, Boca Raton, FL, 2000.

[81] H.F. Ridgway, C.A. Justice, C. Whittaker, D.G. Argo, B.H. Olson, Biofilm fouling of RO membranes - its nature and effect on treatment of water for reuse, Journal of the American Water Works Association 76 (6) (1984) 94–102.

[82] T. Knoell, Chlorine's Impact on the Performance and Properties of Polyamide Membranes, Ultrapure Water UP230324 (2006) 24–30.

[83] M. Pasmore, P. Todd, S. Smith, D. Baker, J. Silverstein, D. Coons, et al., Effects of ultrafiltration membrane surface properties on Pseudomonas aeruginosa biofilm initiation for the purpose of reducing biofouling, Journal of Membrane Science 194 (1) (2001) 15–32.

Chapter 2: Membrane Background, Fouling, and Transport

2.1 World Water Resources

Less than one percent of all freshwater on earth is usable by humans. Most freshwater is inaccessibly locked into polar icecaps or permanent mountain snow cover. Freshwater as a whole only constitutes 2.5% of Earth's water—the vast majority is saltwater (97%) in the ocean, and the small remainder is brackish water (0.5%) found in surface estuaries and salty underground aquifers [1]. Of the freshwater that humans consume, 70% is used for irrigation, 20% is allocated for industry, and only 10% finds domestic use [2]. Clearly, the latter figure is not enough since 1.2 billion people worldwide are without safe drinking water and 2.6 billion lack adequate sanitation [3]. Diarrheal diseases alone result in 1.8 million deaths each year, 88% of which are attributable to unsafe drinking water and inadequate sanitation [4]. The World Health Organization publishes comprehensive reports on acceptable levels of microorganisms, chemicals, and other impurities found in drinking water [5].

With water use growing twice as rapidly as population over the last century [6], an improvement in these circumstances is unlikely. The lack of safe water resources has impacts beyond human health, however. By the year 2050, the world's population is expected to increase by 3 billion people and roughly 2.7 billion of these people will be in developing countries where the economic impact of poor water and sanitation availability

---

This chapter adapted from:

G. M. Geise, H.-S. Lee, D. J. Miller, B. D. Freeman, J. E. McGrath, D. R. Paul. Water Purification by Membranes: The Role of Polymer Science, Journal of Polymer Science Part B: Polymer Physics, 48 (15) (2010) 1685-1718. © 2010 Wiley Periodicals, Inc.

D. J. Miller, X. Huang, H. Li, S. Kasemset, A. Lee, D. Agnihotri, T. Hayes, D. R. Paul, B. D. Freeman, Fouling-Resistant Membranes for the Treatment of Flowback Water from Hydraulic Shale Fracturing: a Pilot Study, Journal of Membrane Science, 437 (2013) 265-275. © 2013 Elsevier Ltd.

is devastating [6]. The overall annual loss in Africa due to a lack of clean water and basic sanitation is estimated at $28 billion (5% of GDP) [6]. In the southeastern Asia countries of Indonesia, Cambodia, the Philippines, and Vietnam, $9 billion (2% of GDP) is lost each year [6]. Because there is such a significant negative economic impact of substandard water access and sanitation there are tremendous benefits from appropriate investments. The World Health Organization estimates a return of $3 - $34 for every $1 invested in safe drinking water and sanitation depending upon the nation and region [7]. Clearly, such efforts should be at the forefront of agendas in developing nations during the 21st century.

Freshwater availability is also inextricably linked to energy production. Webber recently described the vicious cycle linking water purification and energy production [7]. Delivery of one million gallons of clean water from a lake or river requires 1.4 megawatt-hours of energy; desalination raises that figure to 9.8 – 16.5 megawatt-hours for the same amount of clean water derived from seawater. One megawatt-hour of electricity produced using coal or oil, however, requires 21,000 – 50,000 gallons of water; nuclear plants require 25,000 – 60,000 gallons of water to make the same amount of electricity. Gasoline vehicles consume 7 – 14 gallons of water for every 100 miles they travel; more "environmentally-friendly" vehicle technologies consume even more water: 24 gallons per 100 miles for plug-in hybrids, 42 gallons per 100 miles for hydrogen-fuel cell vehicles, and up to 6,200 gallons per 100 miles for vehicles running on ethanol [7]. Development of energetically efficient methods of water purification will be key to finding solutions within this cycle.

Agriculture consumes 70% of all human freshwater withdrawals. Water shortages, therefore, will limit food production and place pressure on food imports. The growing population, as noted above, will also drive up the demand for food. Increased

energy costs contribute to elevated fertilizer costs which, in turn, raise food prices [4]. The link between water and food supplies can be illustrated by examining how much water is consumed during the production of various food products. A single hamburger, for example, requires 635 gallons of water. A glass of milk requires 53 gallons, a single egg requires nearly 36 gallons, and a slice of bread requires 10.5 gallons [8]. Safe freshwater availability, therefore, remains important not only for human consumption but also to maintain a sufficient food supply.

With the current and future pressures on water supply, low-cost, high-efficiency means of water purification from a variety of sources will be of utmost importance. Many of the most arid and water-stressed regions of the world lie near water sources that have not been traditionally accessed to provide large volumes of clean water. The world's oceans could easily satisfy human water needs with appropriate purification and desalination. The high osmotic pressure of seawater makes desalination an energy-intensive process with current technology. Brackish water does not require as much desalination and may represent a more energetically favorable source. Many other non-traditional sources require different types of separation. Singapore is breaking new ground in reclaiming public wastewater and purifying it for human re-consumption with its NEWater program [9]. Petroleum refining produces large volumes of wastewater that contains residual oil and refining byproducts. Each barrel of refined oil generates 7-10 barrels of wastewater [10]. Each of these sources may become important contributors to water for human consumption, but each has unique separation requirements. Membranes represent an energetically efficient solution for carrying out many of these separations.

2.2 Filtration (Porous) Membranes and Processes

Molecules pass through RO membranes primarily by a solution-diffusion mechanism as discussed in a later section. Microfiltration (MF) and ultrafiltration (UF)

membranes operate exclusively by pore-flow, while NF membranes show a combination of solution-diffusion and pore-flow character. This section will discuss MF, UF, and NF membranes. The four major types of polymer membranes and conventional filtration (CF) materials effectively remove particles of sizes that are shown in Figure 2.1.

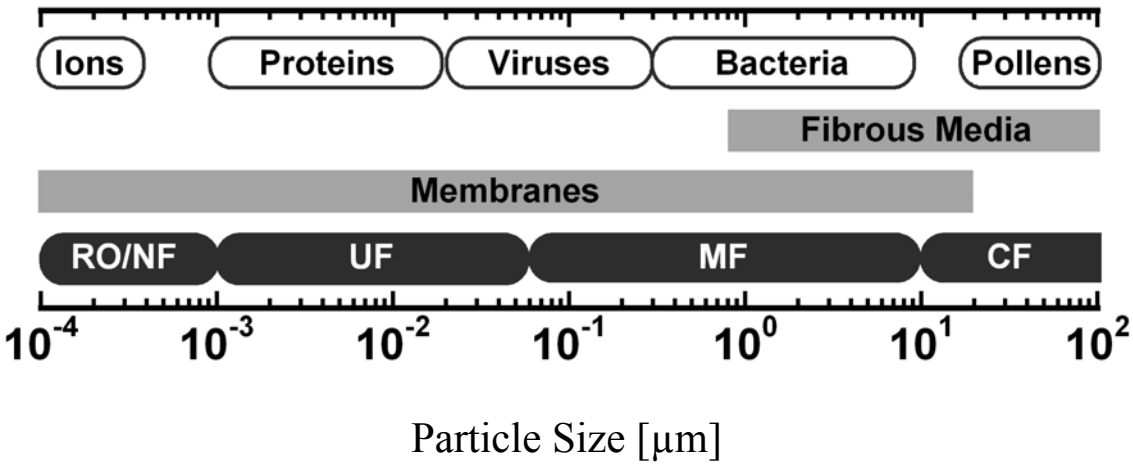

Figure 2.1. Size of particles removed by RO, NF, UF, and MF membranes along with conventional filtration

Filtration membranes may have a relatively uniform pore structure throughout the thickness; such symmetrical structures act as depth filters. Alternatively, the membrane may consist of a thin layer with fine pores (active layer or 'skin') overlaying a thicker layer with larger pores to provide mechanical support but little resistance to water flow; such asymmetric membranes are sometimes called screen filters because the separation of particulates occurs at the surface of the membrane in a very thin, selective layer. Unlike screen filters, where rejection of large solutes takes place on the membrane surface, depth filters capture solute particles within the membrane. Depth filters may capture particles by several mechanisms, including simple size sieving, adsorption, Brownian diffusion,

and electrostatic adsorption. Sieving typically accounts for only a small fraction of the membrane's rejection [11].

2.2.1 Formation of a Pore-Flow Membrane

The oldest and most common technique for forming porous polymeric membranes consists of forming a concentrated solution of the polymer in a solvent with subsequent immersion into a liquid bath, typically water or a mixture with the solvent, in which the solvent is miscible but the polymer is not. Water vapor adsorption from a humid atmosphere, solvent evaporation, or some combination of techniques may be used in place of immersion in the liquid bath [12]. Methods were summarized by Pinnau and Koros [13]. Under proper conditions a film is formed comprised of a continuous phase of solid polymer and an interconnecting phase of voids, chambers, or pores through which liquids can flow. The distribution of phases during solvent exchange dictates the physical structure of the solid membrane [14]. Anisotropic membranes are created by contacting the top surface of the cast film with the non-solvent first, creating a finely porous selective skin layer. The precipitated skin layer slows the penetration of non-solvent into the film, causing polymer below the skin layer to precipitate more slowly. As a result, the substructure is more porous than the skin layer. In the membrane literature this process has been called "phase inversion" [15]; structures of this type were being studied more than a century ago. An analogous procedure is used to make fibers by wet spinning [16–18] where the solidification step is called "coagulation." The pore structure, *i.e.*, pore size, shape and volume, is affected by many factors. There is a sizable body of literature devoted to analysis of the phase inversion or coagulation process [19–26]; however, the practice is still largely an empirical art.

Early membranes made in this way consisted of a similar pore structure through the entire membrane, and because of their thickness such membranes had low fluxes.

Loeb and Sourirajan [27] introduced a solvent evaporation step prior to precipitating the polymer; the polymer concentration gradient in the nascent film leads to a gradation of pore size upon phase inversion. This effectively gives a "thin skin" with very fine pores, *i.e.* the separating layer, overlaying a substrate consisting of much larger pores that provide mechanical support but relatively little resistance to water flow. With a wet annealing step, Loeb and Sourirajan were able to make the first practical reverse osmosis membrane.

The polymer solution can be cast in batch mode to make laboratory membranes or in a continuous fashion and used to form commercial membranes. The solution can be cast on a fabric or other porous substrate for additional support. An analogous process with an evaporation step, known as dry-jet wet spinning, is used to make hollow fiber membranes [28].

The most important membrane preparation process is the Loeb-Sourirajan process described in 1963 [27]. The Loeb-Sourirajan process utilizes water as the phase inversion non-solvent and was originally used to produce cellulose acetate reverse osmosis membranes. Today, reverse osmosis and nanofiltration membranes are usually of the polyamide thin-film composite type which will be discussed later. The Loeb-Sourirajan process is, however, still the predominant method of making ultrafiltration and microfiltration membranes. Common ultrafiltration membrane materials include cellulose acetate [29], polyacrylonitrile, poly(ether imides) [30], aromatic polyamides, polysulfone, poly(ether sulfone) [30], poly(vinylidene fluoride), and poly(vinyl pyrrolidone) [31]. Early microfiltration membranes were nitrocellulose and cellulose acetate [12]; materials used more recently are poly(vinylidene fluoride), polysulfone, polyamide, poly(tetrafluoroethylene) [12,30], and polyethylene [30].

Several other methods of producing pore-flow membranes have been reported. Thermally-induced phase separation (TIPS) bears some similarity to the phase inversion process but utilizes a temperature decrease rather than a non-solvent to coagulate the polymer. A polymer solution is spread on a support and one face of the film is cooled, initiating phase separation. The rest of the film is gradually cooled and phase inversion gradually propagates to form an isotropic or anisotropic porous membrane [32]. To create the selective surface layer in the case of anisotropic membranes, solvent evaporation at the selective surface is sometimes used to enhance the phase inversion process rather than only a simple thermal gradient in the solvent. TIPS also makes a number of polymers accessible for membrane formation that cannot be used in the traditional phase inversion technique [33]. TIPS has been carried out on a number of different polymers including homopolymers such as polypropylene and diphenyl ether [34] and copolymers such as poly(ethylene-co-acrylic acid) [33]. Connected pore structures form at low polymer concentrations; as polymer concentration and cooling rate increased, pore size is found to decrease [20]. When evaporation is used to create anisotropic membranes, the polymer molecular weight does not significantly affect the cell size of the selective layer and therefore does not greatly influence the membrane performance [35].

Pore flow membranes have also been created without solvent by stretching melt-cast polymer films. This process was developed extensively by Celanese to produce the product Celgard® based on polypropylene and is described in several patents [36,37]. These patents are directed at medical dressings and battery separators and cover a wide range of polymers. W.L. Gore also applied the stretching technique to production of porous fabrics made of polytetrafluoroethylene [38]. The process begins with a precursor film which shows row-nucleated lamellar morphology. The precursor film is typically

annealed to eliminate any inconsistencies in the crystal structure. Stretching is then carried out at low temperature to introduce voids and subsequently at high temperature to enlarge those voids [39]. The morphology of the precursor film is of utmost importance for the success of the stretching technique. The crystals form as a result of stress and elongation induced during the extrusion process and their formation is a strong function of processing conditions and, most importantly, polymer molecular weight [40]. A critical molecular weight for crystal formation is known to exist which is dependent on shear rate and temperature up to a particular shear rate after which it is independent of process conditions [41]. High molecular weights were found to increase pore size and pore uniformity, leading to high water vapor transmission in polypropylene membranes [39]. In the case of poly(vinylidene fluoride) membranes, the necessary crystalline structure in the precursor film was found to form most readily when a blend of low- and high-molecular weight polymer was used [42].

Another type of solvent-less membrane formation is track etching. By this technique, a polymer film is bombarded with α-particles to create "tracks" through the film. The film is then immersed in a chemical etchant to create straight-through circular pores. Polycarbonate membranes have been formed by this technique. Unlike membranes prepared by the other methods described here, track-etch membranes are typically of a very uniform thickness and have precisely-defined pore diameters. As a result of the unity tortuosity and the uniform thickness (which allows the membrane to be exceedingly thin everywhere), the porosity of a track-etch membrane may be significantly lower than that of a solvent-cast membrane but both membranes may show similar permeability [43].

Semi-porous nanofiltration membranes bear a strong compositional similarity to reverse osmosis membranes. Both reverse osmosis and nanofiltration membranes,

though formerly produced by the Loeb-Sourirajan process from cellulose acetate, are today thin-film composite membranes. Soon after Loeb and Sourirajan published their phase inversion method, Francis [44] developed composite membranes. Petersen provided an extensive review of composite reverse osmosis and nanofiltration membranes [45]. Composite membranes consist of an ultra-thin selective layer atop a porous support backing. These two components are almost always of differing chemical compositions (unlike Loeb-Sourirajan integrally-skinned membranes) and may therefore be optimized for their particular roles. Cellulose acetate was initially used as the support material; polysulfone and polyethersulfone (PES) are the backings of choice now. The composite structure may be formed in a number of ways, including laminating together separately-formed backing and selective layers, but the vast majority of nanofiltration membranes are produced by interfacial polymerization of a set of monomers on the support surface. Linear aromatic polyamides are one of the few polymers with the necessary solute rejection and flux characteristics for the selective layer [45].

2.2.2 Applications of Pore-Flow Membranes

Membranes are used for sterilization in a variety of applications. Microfiltration membranes are often assembled into disposable cartridges which are typically used for short periods of time before being replaced. The pharmaceutical and microelectronics industries have been extensive users of microfilters over the past several decades. Microfiltration cartridges are typically used to sterilize injectable drug solutions because 200 nm microfilters are able to remove virtually all bacteria. Filters are sterilized by autoclaving or other means after manufacture and immediately before use. In the electronics industry, microfilters are used to polish ultrapure water before use. Filters with 100 nm pores are used to remove any contamination from piping between the water treatment facility and end-use point [12].

The food and beverage industry extensively employs MF and UF membranes. In wine and beer purification applications, microfilters remove yeast and bacterial cells to clarify the final product [46,47]. Because of the low cost of wine and beer relative to products such as pharmaceuticals, pre-filters are often used to extend the lives of the MF membranes [12]. Drinking water treatment is an ever-growing application for microfilters. MF/UF plants have been in use for approximately two decades in bringing surface water into compliance with USA EPA drinking water guidelines [12,48]. Similar guidelines exist in Europe. Hollow fiber membrane modules which are backflushed frequently are typically found in these applications [12].

Cheese production is another well-known application of membranes. Instead of traditional coagulation processes, which results in significant difficult-to-dispose whey production, MF or UF is used to concentrate proteins in milk for the direct production of yogurt and soft cheeses or for further processing in the production of hard cheeses [49,50]. When traditional coagulation is used, UF membranes are used to concentrate whey proteins and remove lactose concentrate and salts. The whey proteins are valuable and can be reused where they used to be discharged prior to ultrafiltration development [12]. Fruit juices, including apple, pear, orange, and grape, are all clarified using ultrafiltration. Crude filtration is performed immediately after crushing the fruit; ultrafiltration produces a perfectly clear, nearly-sterile product [12,51].

The first industrial UF application was the recovery of electrocoat automotive paint. Automotive paint is an emulsion of charged paint particles. Metal parts are coated by applying a charge opposite that of the paint particles. After electrocoating, the pieces are rinsed to remove excess paint. The rinse water becomes contaminated with otherwise reusable paint particles. Additionally, the quality of the paint emulsion is degraded by ionic species which migrate from the metal cleaning process prior to painting. The

electrostatic nature and high solids content of the paint emulsions make for difficult filtration as significant fouling layers readily develop on the membrane, resulting in low fluxes. Unlike MF, UF tends to be expensive, but the high value of the paint makes the ultrafiltration process worthwhile [12].

Industrial UF systems are used to separate oil/water emulsions and to recover process water. Machining operations often use oil/water emulsions for lubrication and cooling. Ultrafiltration is used to separate water from the oil for safe disposal after use. Cleaning process water in-house and recycling it leads to reduced municipal water costs. Ultrafiltration has the added benefit of effectively operating at elevated temperatures. Since many industrial process streams are hot, ultrafiltration provides a means of cleaning streams without the energetic expense of cooling and re-heating [12].

NF membranes have been developed to fill market niches between RO and UF membranes. The polymeric matrix of NF membranes is more open than that of their RO counterparts, affording them some degree of porous flow while maintaining some salt selectivity. Reverse osmosis membranes provide very high salt rejections but low fluxes; nanofiltration membranes do not reject as much salt but do provide much higher fluxes. NF membranes typically reject of 20-80% of sodium chloride present, but reject much more of the large divalent salt ions. Molecular weight cutoffs for organic solutes are 200-1000 Da. The looser structure of the NF membranes allows them to operate at trans-membrane pressures that are much lower than those of RO systems. Most applications of NF membranes are in final polishing of already clean water. Low levels of contaminants may be readily removed from drinking water as a final step at a water treatment plant or at the end-use facility. Municipal water may be softened by removal of multivalent cations such as sulfate [12].

2.2.3 Fouling in Pore-Flow Membranes

A significant hurdle to the widespread implementation of membranes for liquid purification is fouling. Fouling is the deposition of colloidal or particulate matter in a membrane's pores or on its surface that leads to changes in membrane transport characteristics (Figure 2.2a) [52]. As water containing particulates, colloids, macromolecules, or microbes is filtered through a membrane, the foreign material deposits inside the porous structure and onto the surface of the membrane, creating a cake layer which drastically reduces water flux and affects overall membrane rejection performance (Figure 2.2b). Because of fouling, the flux declines, which results in significant increases in the cost of membrane operation due to required membrane cleaning, periodic membrane replacement, and increased energy input to achieve high flux.

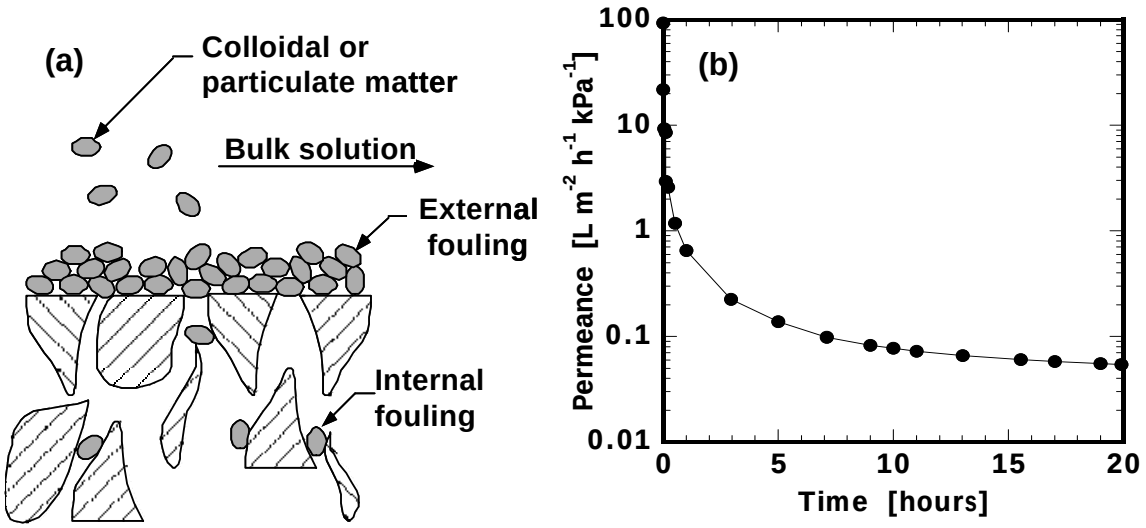

Figure 2.2. (a) Schematic of particulate fouling in porous water purification membranes [53] (b) Conventional MF membrane in crossflow protein filtration with 1 g/L Bovine Serum Albumin (BSA) in pH 7.4, phosphate-buffered solution, 25 cm/s crossflow, transmembrane pressure = 1,000 kPa (145 psi), 0. 2 μm nominal pore size poly(vinylidene fluoride) (PVDF) membrane

Pore-flow membranes may experience two kinds of fouling: surface and internal [53], as shown in Figure 2.2a. Surface fouling is caused by particulate adsorption to the membrane surface while internal fouling is the result of foulant entrainment in the membrane pores. Non-porous reverse osmosis membranes, in contrast, undergo surface fouling only. Internal fouling is sometimes called irreversible fouling because the particles entrained in the membrane cannot be removed, even with harsh chemical or mechanical cleaning. Surface fouling may be either reversible or irreversible. Reversible surface fouling consists of foulants that may be removed by cleaning. Some particulates, especially after extended exposure to the membrane surface, are so strongly adsorbed to the membrane surface that they cannot be removed, constituting irreversible surface fouling.

Surface modification has developed as a popular means of reducing the fouling propensity of many types of membranes [54]. Surface modification aims to change the

surface properties of the membrane while maintaining its selective structure [55]. By reducing fouling, flux is maintained at a high level. Resistance to fouling also lessens the need to clean the membranes. Cleaning can be accomplished in many ways, such as through backpulsing, gas sparging, increasing shear at the membrane surface, or UV radiation. Chemical agents such as ozone, acids, bases, or chlorine may be employed, but these compounds may pose deleterious environmental consequences or even degrade the membrane structure, such as in the case of chlorine compounds and polyamide membranes. To maximize output and minimize the need for membrane cleaning, membrane modifications aim to alter the surface properties of membranes to make fouling less likely.

Surface properties such as surface hydrophilicity, charge, roughness are known to affect membrane fouling [56–59]. Hydrophilic and smooth surfaces typically show the best resistance to fouling. Negatively charged membrane surfaces may reduce some forms of fouling by electro-statically repelling negatively charged foulants [60]. However, negatively charged membrane surfaces may attract positively charged foulants; thus, un-charged membranes may exhibit a reduced tendency toward fouling. In measuring and quantifying surface properties, it is important to consider the effect of feed composition on surface properties as these properties are often measured under ideal and low TDS conditions [60,61].

In water treatment, hydrophilic membranes show reduced fouling because of their affinity for water. Water is strongly bound to a highly hydrophilic membrane surface [62]; foulants interact only with this water layer and not with the membrane surface. If the membrane surface is hydrophobic, water near the membrane can be easily displaced by foulants and hydrophobic-hydrophobic interactions bind the foulant to the membrane surface. To increase the surface hydrophilicity of a membrane, two types of surface

modifications have appeared in the literature. Hydrophilic moieties may be coated or grafted to the membrane surface as shown in Figure 2.3.

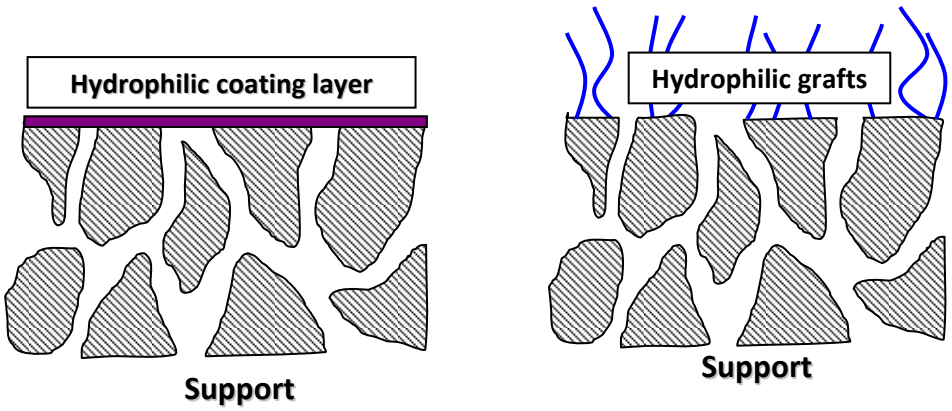

Figure 2.3. Membrane surface modification by hydrophilic coating (left) or grafting (right).

In either case, additional mass transfer resistance is introduced to the membrane surface, so highly hydrophilic polymers (to permit high water uptake into the surface layer) are typically used. The hydrophilic coating layer is nonporous and therefore must be very thin to avoid introducing catastrophic mass transfer limitations. Dense coatings, however, eliminate entrainment of foulants inside the membrane. Grafting of hydrophilic chains may be used as an alternative to the dense coating layer. The mass transfer limitations imposed by grafting modification are typically less than in the case of the coating layer, but foulants may still be able to find their way inside the membrane structure.

Hydrophilic polymers can be grafted directly to membranes surfaces by a variety of methods. Chemical grafting to the surface provide a more stable structure than simple adsorption of hydrophilic polymers to the membrane, which has shown some prevention of protein fouling in microfiltration and ultrafiltration [63,64]. Grafting can be achieved

by inducing polymerization from the membrane surface or by tethering polymer chains to the surface. Plasma-induced polymerization techniques have been used to graft polyamides or poly(acrylic acid) to porous membrane surfaces [65]. This technique has also been reported on polyethylene surfaces [66], polycarbonate [67] and poly(vinylidene fluoride) [65] microfilters, and poly(vinyl chloride) [68], poly(acrylonitrile), and polysulfone ultrafilters [55]. Photo-initiated graft polymerization has been used to attach a variety of monomers to poly(ether sulfone) membranes by inducing radical formation in the PES backbone [69,70]. Photo-induced graft polymerization and subsequent crosslinking has been utilized to attach epoxy diacrylates to ultrafilters [71]. Photo-grafting acrylic acid, 2-hydroxyethyl methacrylate, and poly(ethylene glycol) methacrylate derivatives have also seen use in photo-induced polymerization onto poly(acrylonitrile) flat-sheet membranes [72,73]. Grafting by photo-polymerization has been carried out on membrane architectures other than flat sheets such as microporous hollow fibers [74,75]. Polymer chains may also be tethered to the surface to form a graft structure. Dextran derivatives were grafted to ultrafiltration membranes to reduce protein fouling [64]. Poly(ethylene glycol) (PEG) has proven to be extremely popular for use with this technique. Photo-induced grafting requires surface [76–78] or PEG functionalization [78–80] to achieve a covalent link between the surface and the polymer chain.

Dense hydrophilic coating layers have also been used to induce fouling resistance. Due to their notorious propensity for fouling, ultrafiltration membranes have been a popular substrate for such coating layers [81]. Composite ultrafiltration membranes have been formed by crosslinking thin layers of poly(vinyl alcohol) on the membrane surfaces [82,83]. Poly(ethylene glycol) has also been used in the same manner [84]. Crosslink

density in the coating layer may be manipulated by varying the polymer/solvent ratio in the thin-film casting solution [85,86].

Membrane surface modifications explored to date, however, are not without limitations. Many modification techniques are membrane-specific. For example, photo-grafting induces radical formation on the backbone of PES [69,70] to which hydrophilic moieties may be grafted, as noted previously. Unfortunately, photo-grafting is not effective on other common membrane materials such as poly(vinylidene fluoride) (PVDF), poly(tetrafluoroethylene) (PTFE) and polyamides since, unlike PES, these polymers do not readily form surface radicals under UV irradiation. Other modification strategies such as plasma treatment [55,87–89] and multi-step organic reactions [90] may be difficult or expensive to apply in a manufacturing environment.

Measurement of the zeta potential is becoming a popular means of characterizing the surface of modified membranes. The zeta potential describes the potential induced between the membrane surface and the shear plane of fluid moving past the surface. As noted previously, uncharged surfaces typically show good fouling resistance. The zeta potential, therefore, can be used to predict the fouling resistance of a membrane. Surfaces become charged by ionization of chemical functionalities on the surface or by adsorption of charged particles. The pK, isoelectric point, and charge density all affect the zeta potential of a surface. The zeta potential has also been found, however, to depend on membrane pore diameter and surface roughness. Interaction of membrane surface with foulants, therefore, can only be compared among well-defined membranes [91].

2.3 HYDRAULIC FRACTURING: A TARGET INDUSTRY FOR MEMBRANE-BASED WASTEWATER REUSE

Most of the fouling studies described herein were conducted with oily water emulsions, a simple, model feed that is commonly used as a laboratory analogue for the complex, highly-fouling mixtures that are found in many industry effluents [92–98]. Hydraulic fracturing of oil and natural gas wells is responsible for the production of vast quantities of oily wastewater. Hydraulic fracturing has been used to enhance the productivity of oil and gas wells since its introduction by Standard Oil in 1949 [99]. Its application, especially in the recovery of natural gas from shale fields in North America, has grown intensely over the past decade [100]. A map of major gas shale basins in the United States is shown in Figure 2.4. Once a wellbore is created in a rock bed containing petroleum or gas reservoirs, fluid is pumped into the well at a pressure sufficient to fracture the rock, permitting extraction of the petroleum or gas. Hydraulic fracturing has dramatically increased in popularity over the last decade with some reports suggesting that 60% of all wells drilled today undergo fracking [99]. The substantial reduction in the price of natural gas, relative to oil, during the past few years has been attributed in large measure to the use of hydraulic fracturing, which has greatly increased the estimated supply of accessible natural gas in the U.S. [101].

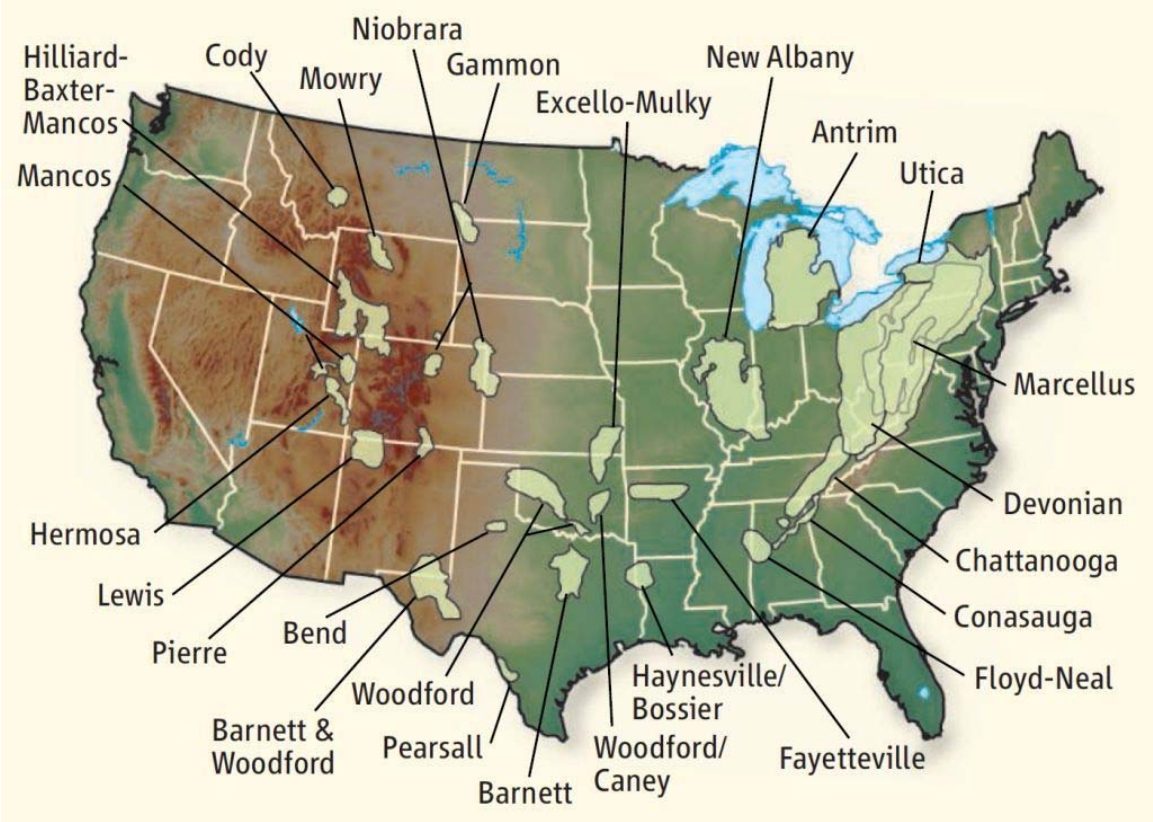

Figure 2.4. Map of shale gas basins in the United States [102].

Hydraulic fracturing is often utilized in conjunction with another enabling technology, horizontal drilling. Horizontal drilling extends wells considerable distances into portions of a reservoir that would otherwise be inaccessible with only a vertical well. The first horizontal wells were drilled in the 1930s, but the technical complexity, risk, and cost of horizontal drilling were not outweighed by the relatively modest gains in well productivity. Hydraulic fracturing was used to save many horizontal wells facing abandonment [103]. As recent developments have improved horizontal drilling techniques, these two technologies have synergistically promoted the development of one another. Very large, highly productive shale gas reservoirs may now be conveniently accessed through a single well bore [104].

Water is, by far, the most common fracturing fluid—96% of all fractured wells employ an aqueous fluid. "Frac jobs" for shale gas production in the Marcellus basin, for example, require about 1 million gallons of water for vertical wells and 3-6 million gallons for horizontal wells [105]. The tremendous water requirement of hydraulic fracturing creates two problems: fresh water demand is high and used water disposal is expensive [100]. The location of wells in remote areas often means that water must be trucked to the sites. Transportation costs to wells in arid regions, such as North Dakota, Texas, and Colorado, are high enough that on-site water treatment is already being used [106]. About 10-30% of the fracking water returns to the surface as "flowback" water with the released oil or gas [106]. Disposal of used fracking water in an injection well costs $1.50 - $2.00/bbl, and the cost of transportation to the disposal site may add up to $4.00/bbl [106] to this expense. The substantial demand for fresh water to fracture wells and high disposal costs may both be addressed by reuse of flowback water. While no standards exist for fracturing water quality, flowback water is typically not suitable for direct reuse due to high salt content. Barium, iron, strontium, and sulfates contribute to scaling that may obstruct fractures, reducing well productivity. Additionally, certain injection water additives are not compatible with high salinity or other impurities commonly found in flowback water [106,107]. Fracturing water must be able to carry particulate fracturing proppants (such as sand) into the shale fissures; therefore, gelling agents are often added to increase viscosity [108]. Frictional forces between the fluid and the fissure walls increase due to this increase in viscosity, so friction-reducing components are added to fracking water. Desalination to remove the salts that interfere with these additives, therefore, is critical if flowback water is to be reused in more fracturing [109]. Enabling the use of saline water for fracturing would reduce the expenses associated with flowback water reuse, but currently only a limited number of

such gelling and friction reduction additives are available [110]. Typical composition ranges of flowback water from the Barnett (Texas) and Marcellus (Appalachian) shale plays are shown in Table 2.1.

Parameter	Barnett (5 locations)		Marcellus (19 locations)	
	Range	Median	Range	Median
pH	6.6 - 8.0	7.1	5.8 – 7.2	6.6
Total Dissolved Solids (mg/L)	23,600 – 98,900	36,100	38,500 – 238,000	67,300
Alkalinity (mg/L $CaCO_3$)	238 – 1,630	610	48.8 - 327	138
Total Suspended Solids (mg/L)	36.8 - 253	133	10.8 – 3,220	99
Total Organic Carbon (mg/L)	9.5 – 99.1	18.1	3.7 - 323	62.8
Biochemical Oxygen Demand (mg/L)	92.6 – 1,480	319	6.2 – 1,950	138
Chloride (mg/L)	16,500 – 72,400	22,200	26,400 – 148,000	41,850
Bicarbonate (mg/L $CaCO_3$)	145 – 994	372	29.8 - 162	74
Sulfate (mg/L)	145 – 1,300	1080	< 0.031 - 106	25.9
Calcium (mg/L)	454 – 6,680	1,020	1,440 – 23,500	4,950
Barium (mg/L)	1.5 – 16.8	2.11	21.4 – 13,900	686
Iron (mg/L)	11.8 – 76.7	17.8	10.8 - 180	39
Sodium (mg/L)	7,420 – 25,300	15,500	10,700 – 65,100	18,000
Magnesium (mg/L)	75.3 - 757	156	135 – 1,550	559

Table 2.1. Composition ranges of Barnett and Marcellus flowback waters [111].

The small footprint of membrane units makes them attractive for on-site flowback water purification systems. For example, many flowback water treatment scenarios

require relatively short term (*e.g.*, several weeks [112]) access to water purification due to the transitory nature of flowback water. Having small footprint water purification systems, which allows them to be mobile, could be advantageous since the water purification system could be moved from site to site as new wells are completed. [105] Reverse osmosis (RO), nanofiltration (NF), ultrafiltration (UF), and microfiltration (MF) are all increasingly being used to treat oily produced water [57,92,95]. MF and UF membranes are typically used to remove oils and other organics while NF and RO membranes are suited to removal of dissolved solids such as salts. For desalination, membrane systems are typically more energy-efficient than traditional thermal technologies and produce permeate of consistent quality regardless of influent stream composition [95]. Membranes may be used in combination, such as MF/UF pretreatment followed by RO desalination, or together with other technologies, such as gravity separation or flocculation systems [95]. With mixtures as complex as hydraulic fracturing flowback water, membrane fouling becomes a significant hurdle to implementation of membrane-based purification systems. Mixtures of salt, oils, particulates, and other contaminants often cause significant and irreversible deterioration of permeate flux, requiring aggressive chemical cleaning that shortens membrane lifetime. Water purification membranes are typically made of hydrophobic polymers and, as a result, oil and grease tend to be highly fouling due to hydrophobic-hydrophobic interactions between the membrane surface and the foulant.

2.4 MEMBRANE TRANSPORT DURING FOULING

The permeate flux through a porous membrane is often described as the applied transmembrane pressure driving force (TMP) divided by the resistance to mass transfer, R [113]:

$$J = \frac{\text{TMP}}{R} \qquad [2.1]$$

For pure water filtration, R represents the resistance to mass transfer associated with the clean membrane. During fouling, the resistance to permeation increases due to various mechanisms, such as pore plugging, cake layer formation, concentration polarization, osmotic pressure, etc. [114]. The resistance can be calculated by a resistance-in-series model. In this way, the total resistance may be described by individual resistances, including the resistance of the membrane itself, the resistance due to adsorption fouling, and the resistances due to reversible and irreversible fouling. For clarity, "adsorption fouling" refers to the spontaneous adsorption of foulant to the membrane surface that occurs *even under zero flux conditions*. "Reversible fouling" and "irreversible fouling" refer to the accumulation of foulant that is brought to the membrane *during operation; that is, when the permeate flux is greater than zero.* In the cases of reversible and irreversible fouling, as defined here, foulant is therefore brought to the membrane by convection due to the permeate flux through the pores [113,115,116]. In constant TMP operation, the increase in mass transfer resistance causes the flux to decline; in constant flux operation, TMP increases as R increases. Therefore, the change in resistance during fouling provides a simple macroscopic variable for comparing constant flux and constant TMP experimental results.

If the flux is sufficiently low, mechanisms such as Brownian diffusion, shear-induced diffusion, axial transport along the surface, and inertial lift can act to remove foulant particles as they reach the membrane surface due to permeate convection through the pores [52,115]. Under these conditions, the total resistance remains constant, and the permeate flux scales linearly with TMP. At relatively high fluxes, the aforementioned foulant removal mechanisms cannot overcome the inexorable flow of foulant towards the membrane surface, so foulant accumulates on, and perhaps in, the membrane during

filtration, and the resistance increases with time. The flux no longer scales linearly with TMP and, eventually, a limiting flux is reached where further increases in TMP do not produce increases in flux [12].

Field *et al.* introduced the concept of critical flux—the maximum flux that can be achieved with slight or negligible fouling—to distinguish the regime of invariant resistance from that where resistance changes with flux [117]. The exact value of the critical flux depends upon foulant properties (*e.g.*, concentration and particle size), membrane properties (*e.g.*, pore size and material), and crossflow velocity [118]. Two forms of the critical flux are further defined: the strong form and the weak form [118]. At fluxes below the strong form of the critical flux, the only contribution to R is that of the clean, unfouled membrane itself; *i.e.*, fouling does not contribute to the resistance to permeation:

$$J = \frac{\mathrm{TMP}}{R_m} \qquad \text{for } J < J_{cs} \qquad [2.2]$$

where J is the flux, TMP is the transmembrane pressure, R_m is the membrane resistance, and J_{cs} is the strong form of the critical flux. For the weak form of the critical flux, the resistance to permeation is given by the sum of the membrane resistance and resistance from adsorption of foulant to the membrane surface:

$$J = \frac{\mathrm{TMP}}{R_m + R_{ads}} \qquad \text{for } J < J_{cw} \qquad [2.3]$$

where R_{ads} is the resistance due to adsorption, and J_{cw} is the weak form of the critical flux. The resistance due to adsorption reflects foulant whose adsorption to the membrane occurs spontaneously and independently of flux [119]. Therefore, whether a particular membrane/foulant system exhibits the strong form of the critical flux or the weak form of the critical flux is dictated by whether foulant adsorption to the membrane is a significant

contributor to resistance. Because such adsorption occurs spontaneously and independently of flux (and even in the absence of flux) [119], a membrane/foulant system will show either the strong form or the weak form of the critical flux, but not both.

At fluxes above the two forms of the critical flux, the resistance to permeation is increased due to reversible and irreversible fouling:

$$J = \frac{\text{TMP}}{R_m + R_{rev} + R_{irrev}} \qquad \text{for } J > J_{cs} \qquad [2.4]$$

$$J = \frac{\text{TMP}}{R_m + R_{ads} + R_{rev} + R_{irrev}} \qquad \text{for } J > J_{cw} \qquad [2.5]$$

where R_{rev} is the resistance due to reversible fouling and R_{irrev} is the resistance due to irreversible fouling. As noted previously, R_{rev} and R_{irrev} refer to resistances due to permeate-driven fouling of the membrane.

A third form of the critical flux, the critical flux for irreversibility, has also been described. It refers to the flux at which the feed fluid irreversibly transforms from a dispersed phase to aggregates on the membrane surface, triggered by flux-induced concentration enhancement [118]. Once such aggregation occurs, the original membrane properties may only be recovered by cleaning or other protocols [118]. This phenomenon is examined in more detail in the Appendix.

The definitions of the weak and strong forms of the critical flux require that the total resistance not vary with time at fluxes below the critical flux. However, it is possible that an invariant resistance during filtration may never be achieved, even at extremely low fluxes. LeClech *et al.* reported a scenario in which a zero rate of TMP increase with time was never observed during constant flux microfiltration of sewage, so a critical flux could not be identified. They did observe, however, a regime of linearity in the TMP/flux relationship at low fluxes, and deviation from linearity at high fluxes. In

the regime of linearity, the (non-zero) rate of fouling was constant at several low fluxes. In the regime of non-linearity, the rate of fouling increased with increasing flux. The threshold flux has recently been defined as the flux at which the rate of fouling significantly increases [119]. The threshold flux and the critical flux are, therefore, conceptually similar, since below either of them, the TMP scales linearly with flux, and above either of them, the rate of fouling increases appreciably. Experimentally, flux stepping protocols, which will be described later, can be used to identify the threshold or critical flux. However, a threshold flux can be distinguished from a critical flux by observing the rate of fouling below the flux in question. If the TMP does not increase with time, the identified flux is a critical flux; if the transmembrane pressure slowly rises at the same rate at several low fluxes, the flux is a threshold flux [119].

2.5 REFERENCES

[1] Vital Water Graphics: An Overview of the State of the World's Fresh and Marine Waters, United Nations Environment Programme, Nairobi, Kenya, 2008.

[2] The United Nations World Water Development Report 3: Facts and Figures, The United Nations Educational, Scientific, and Cultural Organization (2009).

[3] M. a Shannon, P.W. Bohn, M. Elimelech, J.G. Georgiadis, B.J. Mariñas, A.M. Mayes, Science and technology for water purification in the coming decades, Nature 452 (7185) (2008) 301–10.

[4] Water, Sanitation, and Hygiene Links to Health: Facts and Figures, World Health Organization (2004).

[5] Guidelines for Drinking-water Quality, 4th ed., World Health Organization, Geneva, Switzerland, 2011.

[6] The United Nations World Water Development Report 3, The United Nations Educational, Scientific, and Cultural Organization, Paris, France, 2009.

[7] M.E. Webber, Catch-22: Water vs. Energy, Scientific American 18 (4) (2008) 34–41.

[8] Producing Food, Food and Agricultrure Organization of the United Nations (2009).

[9] H. Seah, T.P. Tan, M.L. Chong, J. Leong, NEWater—multi safety barrier approach for indirect potable use, Water Science & Technology: Water Supply 8 (5) (2008) 573.

[10] J.A. Veil, M.G. Puder, D. Elcock, R.J. Redweik, A White Paper Describing Produced Water from Production of Crude Oil, Natural Gas, and Coal Bed Methane, 2004.

[11] T.H. Meltzer, Filtration in the Pharmaceutical Industry, Marcel Dekker, New York, 1987.

[12] R.W. Baker, Membrane Technology and Applications, 2nd ed., John Wiley & Sons, West Sussex, England, 2004.

[13] I. Pinnau, W.J. Koros, Structures and gas separation properties of asymmetric polysulfone membranes made by dry, wet, and dry/wet phase inversion, Journal of Applied Polymer Science 43 (8) (1991) 1491–1502.

[14] I. Pinnau, Recent advances in the formation of ultrathin polymeric membranes for gas separations, Polymers for Advanced Technologies 5 (11) (1994) 733–744.

[15] R.E. Kesting, Synthetic Polymeric Membranes, McGraw-Hill, New York, 1971.

[16] J.P. Craig, J.P. Knudsen, V.F. Holland, Characterization of Acrylic Fiber Structure, Textile Research Journal 32 (6) (1962) 435–448.

[17] J.P. Knudsen, The Influence of Coagulation Variables on the Structure and Physical Properties of an Acrylic Fiber, Textile Research Journal 33 (1) (1963) 13–20.

[18] D.R. Paul, Diffusion during the coagulation step of wet-spinning, Journal of Applied Polymer Science 12 (3) (1968) 383–402.

[19] L. Broens, D.M. Koenhen, C.A. Smolders, On the mechanism of formation of asymmetric ultra- and hyper-filtration membranes, Desalination 22 (1-3) (1977) 205–219.

[20] D.M. Koenhen, M.H. V. Mulder, C. A. Smolders, Phase separation phenomena during the formation of asymmetric membranes, Journal of Applied Polymer Science 21 (1) (1977) 199–215.

[21] W.R. Burghardt, L. Yilmaz, A.J. McHugh, Glass transition, crystallization and thermoreversible gelation in ternary PPO solutions; relationship to asymmetric membrane formation, Polymer 28 (12) (1987) 2085–2092.

[22] C. Cohen, G.B. Tanny, S. Prager, Diffusion-controlled formation of porous structures in ternary polymer systems, Journal of Polymer Science: Polymer Physics Edition 17 (3) (1979) 477–489.

[23] H. Bokhorst, F.W. Altena, C.A. Smolders, Formation of asymmetric cellulose acetate membranes, Desalination 38 (1981) 349–360.

[24] M. H. V. Mulder, J.O. Hendrikman, J.G. Wijmans, C. A. Smolders, A rationale for the preparation of asymmetric pervaporation membranes, Journal of Applied Polymer Science 30 (7) (1985) 2805–2820.

[25] J.. Wijmans, J. Kant, M.H.. Mulder, C. A. Smolders, Phase separation phenomena in solutions of polysulfone in mixtures of a solvent and a nonsolvent: relationship with membrane formation, Polymer 26 (10) (1985) 1539–1545.

[26] G.E. Gaides, A.J. McHugh, Gelation in an amorphous polymer: a discussion of its relation to membrane formation, Polymer 30 (11) (1989) 2118–2123.

[27] S. Loeb, S. Sourirajan, Sea Water Demineralization by Means of an Osmotic Membrane, Advances in Chemistry Series 38 (1963) 117–132.

[28] W.S. Ho, K.K. Sirkar, Membrane Handbook, Van Nostrand Reinhold, New York, 1992.

[29] C. Combe, E. Molis, P. Lucas, R. Riley, M.. Clark, The effect of CA membrane properties on adsorptive fouling by humic acid, Journal of Membrane Science 154 (1) (1999) 73–87.

[30] M. Ulbricht, Advanced functional polymer membranes, Polymer 47 (7) (2006) 2217–2262.

[31] I.M. Wienk, R.M. Boom, M. a. M. Beerlage, a. M.W. Bulte, C. a. Smolders, H. Strathmann, Recent advances in the formation of phase inversion membranes made from amorphous or semi-crystalline polymers, Journal of Membrane Science 113 (2) (1996) 361–371.

[32] G.T. Caneba, D.S. Soong, Polymer membrane formation through the thermal-inversion process. 1. Experimental study of membrane structure formation, Macromolecules 18 (12) (1985) 2538–2545.

[33] H. Matsuyama, S. Berghmans, D.R. Lloyd, Formation of hydrophilic microporous membranes via thermally induced phase separation, Journal of Membrane Science 142 (2) (1998) 213–224.

[34] H. Matsuyama, S. Berghmans, D.R. Lloyd, Formation of anisotropic membranes via thermally induced phase separation, Polymer 40 (9) (1999) 2289–2301.

[35] P.M. Atkinson, D.R. Lloyd, Anisotropic flat sheet membrane formation via TIPS: atmospheric convection and polymer molecular weight effects, Journal of Membrane Science 175 (2) (2000) 225–238.

[36] H.S. Bierenbaum, R.B. Plainfield, R. Isaacson, P.R. Lantos, Breathable Medical Dressing, U.S. Patent 3426754, 1969.

[37] H.T. Taskier, Hydrophilic Microporous Film, U.S. Patent 3853601, 1974.

[38] R.W. Gore, Process for Producing Porous Products, U.S. Patent 3953566, 1976.

[39] S. Tabatabaei, P. Carreau, A. Ajji, Microporous membranes obtained from polypropylene blend films by stretching, Journal of Membrane Science 325 (2) (2008) 772–782.

[40] F. Sadeghi, A. Ajji, P.J. Carreau, Analysis of row nucleated lamellar morphology of polypropylene obtained from the cast film process: Effect of melt rheology and process conditions, Polymer Engineering & Science 47 (7) (2007) 1170–1178.

[41] A. Nogales, B.S. Hsiao, R.H. Somani, S. Srinivas, A.H. Tsou, F.J. Balta-Calleja, et al., Shear-induced crystallization of isotactic polypropylene with different molecular weight distributions: in situ small- and wide-angle X-ray scattering studies, Polymer 42 (12) (2001) 5247–5256.

[42] F. Sadeghi, S.H. Tabatabaei, A. Ajji, P.J. Carreau, Effect of PVDF characteristics on extruded film morphology and porous membranes feasibility by stretching, Journal of Polymer Science Part B: Polymer Physics 47 (12) (2009) 1219–1229.

[43] H.K. Lonsdale, The Growth of Membrane Technology, Journal of Membrane Science 10 (2-3) (1982) 81–181.

[44] P.S. Francis, NTIS Report Number PB-177083, United States Department of Commerce (1966).

[45] R.J. Petersen, Composite reverse osmosis and nanofiltration membranes, Journal of Membrane Science 83 (1) (1993) 81–150.

[46] Q. Gan, R.W. Field, M.R. Bird, R. England, J.A. Howell, M.T. McKechnie, et al., Beer Clarification by Cross-Flow Microfiltration: Fouling Mechanisms and Flux Enhancement, Chemical Engineering Research and Design 75 (1) (1997) 3–8.

[47] P. Czekaj, F. López, C. Güell, Membrane fouling during microfiltration of fermented beverages, Journal of Membrane Science 166 (2) (2000) 199–212.

[48] K.J. Howe, M.M. Clark, Fouling of microfiltration and ultrafiltration membranes by natural waters, Environmental Science & Technology 36 (16) (2002) 3571–3576.

[49] E. Beuvier, K. Berthaud, S. Cegarra, A. Dasen, S. Pochet, S. Buchin, et al., Ripening and quality of Swiss-type cheese made from raw, pasteurized or microfiltered milk, International Dairy Journal 7 (5) (1997) 311–323.

[50] A.L. Zydney, Protein Separations Using Membrane Filtration: New Opportunities for Whey Fractionation, International Dairy Journal 8 (3) (1998) 243–250.

[51] C. Güell, R.H. Davis, Membrane fouling during microfiltration of protein mixtures, Journal of Membrane Science 119 (2) (1996) 269–284.

[52] G. Belfort, R.H. Davis, A.L. Zydney, The behavior of suspensions and macromolecular solutions in crossflow microfiltration, Journal of Membrane Science 96 (1-2) (1994) 1–58.

[53] B.D. Freeman, I. Pinnau, Gas and Liquid Separations Using Membranes: An Overview, in: I. Pinnau, B.D. Freeman (Eds.), Advanced Materials for Membrane Separations, 2004: pp. 1–23.

[54] K.B. Hvid, P.S. Nielsen, F.F. Stengaard, Preparation and characterization of a new ultrafiltration membrane, Journal of Membrane Science 53 (3) (1990) 189–202.

[55] M. Ulbricht, G. Belfort, Surface modification of ultrafiltration membranes by low temperature plasma II. Graft polymerization onto polyacrylonitrile and polysulfone, Journal of Membrane Science 111 (2) (1996) 193–215.

[56] J. Louie, I. Pinnau, I. Ciobanu, K. Ishida, A. Ng, M. Reinhard, Effects of Polyether–Polyamide Block Copolymer Coating on Performance and Fouling of Reverse Osmosis Membranes, Journal of Membrane Science 280 (1-2) (2006) 762–770.

[57] S. Mondal, S. Wickramasinghe, Produced Water Treatment by Nanofiltration and Reverse Osmosis Membranes, Journal of Membrane Science 322 (1) (2008) 162–170.

[58] E.M. Vrijenhoek, S. Hong, M. Elimelech, Influence of membrane surface properties on initial rate of colloidal fouling of reverse osmosis and nanofiltration membranes, Journal of Membrane Science 188 (1) (2001) 115–128.

[59] A.E. Chddress, S.S. Deshmukh, Effect ofhumic substances and anionic surfactants on the surface charge and performance of reverse osmosis membranes, Desalination 118 (1-3) (1998) 167–174.

[60] J. Yang, S. Lee, E. Lee, J. Lee, S. Hong, Effect of solution chemistry on the surface property of reverse osmosis membranes under seawater conditions, Desalination 247 (1-3) (2009) 148–161.

[61] Y. Shim, H.-J. Lee, S. Lee, S.-H. Moon, J. Cho, Effects of natural organic matter and ionic species on membrane surface charge, Environmental Science & Technology 36 (17) (2002) 3864–71.

[62] M. Elimelech, W.A. Phillip, The Future of Seawater Desalination: Energy, Technology, and the Environment, Science 333 (6043) (2011) 712–7.

[63] J.H. Hanemaaijer, T. Robbertsen, T. van den Boomgaard, J.W. Gunnink, Fouling of ultrafiltration membranes. The role of protein adsorption and salt precipitation, Journal of Membrane Science 40 (2) (1989) 199–217.

[64] B. Sivik, M. Wahlgren, Y. Miezis, A rheological screening method for membrane modifying polymers, Desalination 77 (1990) 181–193.

[65] H. Iwata, T. Matsuda, Preparation and properties of novel environment-sensitive membranes prepared by graft polymerization onto a porous membrane, Journal of Membrane Science 38 (2) (1988) 185–199.

[66] M. Suzuki, a. Kishida, H. Iwata, Y. Ikada, Graft copolymerization of acrylamide onto a polyethylene surface pretreated with glow discharge, Macromolecules 19 (7) (1986) 1804–1808.

[67] Y. Ito, S. Kotera, M. Inaba, K. Kono, Y. Imanishi, Control of pore size of polycarbonate membrane with straight pores by poly(acrylic acid) grafts, Polymer 31 (11) (1990) 2157–2161.

[68] F. Vigo, C. Uliana, M. Traverso, Poly(vinyl chloride) ultrafiltration membranes modified by glow discharge grafting of poly(acrylic acid), European Polymer Journal 27 (8) (1991) 779–783.

[69] M. Taniguchi, G. Belfort, Low protein fouling synthetic membranes by UV-assisted surface grafting modification: varying monomer type, Journal of Membrane Science 231 (1-2) (2004) 147–157.

[70] M. Taniguchi, J.E. Kilduff, G. Belfort, Low fouling synthetic membranes by UV-assisted graft polymerization: monomer selection to mitigate fouling by natural organic matter, Journal of Membrane Science 222 (1-2) (2003) 59–70.

[71] M. Zeni, I.R. Bellobono, F. Muffato, A. Polissi, E. Selli, E. Rastelli, Photosynthetic membranes. VI. Characterization of ultrafiltration membranes prepared by photografting zeolite-epoxy-diacrylate resin composites onto cellulose, Journal of Membrane Science 36 (1988) 277–295.

[72] M. Ulbricht, H. Matuschewski, A. Oechel, H.-G. Hicke, Photo-induced Graft Polymerization Surface Modifications for the Preparation of Hydrophilic and Low-proten-adsorbing Ultrafiltration Membranes, Journal of Membrane Science 115 (1) (1996) 31–47.

[73] M. Ulbricht, A. Oechel, C. Lehmann, G. Tomaschewski, H.-G. Hicke, Gas-phase photoinduced graft polymerization of acrylic acid onto polyacrylonitrile ultrafiltration membranes, Journal of Applied Polymer Science 55 (13) (1995) 1707–1723.

[74] C. Liu, C.R. Martin, Composite membranes from photochemical synthesis of ultrathin polymer films, Nature 352 (6330) (1991) 50–52.

[75] A. Parthasarathy, C.J. Brumlik, C.R. Martin, G.E. Collins, Interfacial polymerization of thin polymer films onto the surface of a microporous hollow-fiber membrane, Journal of Membrane Science 94 (1) (1994) 249–254.

[76] B. Wesslén, M. Kober, C. Freij-Larsson, a Ljungh, M. Paulsson, Protein adsorption of poly(ether urethane) surfaces modified by amphiphilic and hydrophilic polymers, Biomaterials 15 (4) (1994) 278–84.

[77] W.R. Gombotz, W. Guanghui, a. S. Hoffman, Immobilization of poly(ethylene oxide) on poly(ethylene terephthalate) using a plasma polymerization process, Journal of Applied Polymer Science 37 (1) (1989) 91–107.

[78] Y.C. Tseng, K. Park, Synthesis of photoreactive poly(ethylene glycol) and its application to the prevention of surface-induced platelet activation, Journal of Biomedical Materials Research 26 (3) (1992) 373–91.

[79] E. Uchida, Y. Uyama, Y. Ikada, Grafting of Water-Soluble Chains onto a Polymer Surface, Langmuir 10 (2) (1994) 481–485.

[80] H. Iwata, M.I. Ivanchenko, Y. Miyaki, Preparation of anti-oil stained membrane by grafting polyethylene glycol macromer onto polysulfone membrane, Journal of Applied Polymer Science 54 (1) (1994) 125–128.

[81] S.P. Nunes, M.L. Sforça, K.-V. Peinemann, Dense hydrophilic composite membranes for ultrafiltration, Journal of Membrane Science 106 (1-2) (1995) 49–56.

[82] R.H. Li, T.A. Barbari, Performance of poly(vinyl alcohol) thin-gel composite ultrafiltration membranes, Journal of Membrane Science 105 (1-2) (1995) 71–78.

[83] W.. Dai, T.. Barbari, Hydrogel membranes with mesh size asymmetry based on the gradient crosslinking of poly(vinyl alcohol), Journal of Membrane Science 156 (1) (1999) 67–79.

[84] H. Ju, B.D. McCloskey, A.C. Sagle, Y.-H. Wu, V.A. Kusuma, B.D. Freeman, Crosslinked Poly(ethylene oxide) Fouling Resistant Coating Materials for Oil/Water Separation, Journal of Membrane Science 307 (2) (2008) 260–267.

[85] H. Lin, T. Kai, B.D. Freeman, S. Kalakkunnath, D.S. Kalika, The Effect of Cross-Linking on Gas Permeability in Cross-Linked Poly(Ethylene Glycol Diacrylate), Macromolecules 38 (20) (2005) 8381–8393.

[86] H. Lin, E. Van Wagner, J.S. Swinnea, B.D. Freeman, S.J. Pas, A.J. Hill, et al., Transport and structural characteristics of crosslinked poly(ethylene oxide) rubbers, Journal of Membrane Science 276 (1-2) (2006) 145–161.

[87] P. Wang, K.L. Tan, E.T. Kang, K.G. Neoh, Plasma-induced immobilization of poly(ethylene glycol) onto poly(vinylidene fluoride) microporous membrane, Journal of Membrane Science 195 (1) (2002) 103–114.

[88] H. Yu, Y. Xie, M. Hu, J. Wang, S. Wang, Z. Xu, Surface modification of polypropylene microporous membrane to improve its antifouling property in MBR: CO plasma treatment, Journal of Membrane Science 254 (1-2) (2005) 219–227.

[89] H. Yu, M. Hu, Z. Xu, J. Wang, S. Wang, Surface modification of polypropylene microporous membranes to improve their antifouling property in MBR: NH plasma treatment, Separation and Purification Technology 45 (1) (2005) 8–15.

[90] A. Bhattacharya, B.N. Misra, Grafting: a versatile means to modify polymersTechniques, factors and applications, Progress in Polymer Science 29 (8) (2004) 767–814.

[91] T. Jimbo, M. Higa, N. Minoura, A. Tanioka, Surface Characterization of Poly(acrylonitrile) Membranes Graft-Polymerized with Ionic Monomers As Revealed by ζ Potential Measurement, Macromolecules 31 (4) (1998) 1277–1284.

[92] J. Mueller, Y. Cen, R.H. Davis, Crossflow Microfiltration of Oily Water, Journal of Membrane Science 129 (2) (1997) 221–235.

[93] A.B. Koltuniewicz, R.W. Field, T.C. Arnot, Cross-flow and dead-end microfiltration of oily-water emulsion. Part I: Experimental study and analysis of flux decline, Journal of Membrane Science 102 (1-3) (1995) 193–207.

[94] T.C. Arnot, R.W. Field, A.B. Koltuniewicz, Cross-flow and dead-end microfiltration of oily-water emulsions Part II. Mechanisms and modelling of flux decline, Journal of Membrane Science 169 (1) (2000) 1–15.

[95] M. Cheryan, N. Rajagopalan, Membrane Processing of Oily Streams. Wastewater Treatment and Waste Reduction, Journal of Membrane Science 151 (1) (1998) 13–28.

[96] A. Asatekin, A.M. Mayes, Oil industry wastewater treatment with fouling resistant membranes containing amphiphilic comb copolymers, Environmental Science & Technology 43 (12) (2009) 4487–92.

[97] W. Chen, Y. Su, J. Peng, X. Zhao, Z. Jiang, Y. Dong, et al., Efficient wastewater treatment by membranes through constructing tunable antifouling membrane surfaces, Environmental Science & Technology 45 (15) (2011) 6545–52.

[98] T. Mohammadi, M. Kazemimoghadam, M. Saadabadi, Modeling of membrane fouling and flux decline in reverse osmosis during separation of oil in water emulsions, Desalination 157 (1-3) (2003) 369–375.

[99] C.T. Montgomery, M.B. Smith, Hydraulic Fracturing: History of an Enduring Technology, Journal of Petroleum Technology 62 (12) (2010) 26–32.

[100] R. Beckwith, Hydraulic Fracturing: the Fuss, the facts, the Future, Journal of Petroleum Technology 62 (12) (2010) 34–41.

[101] C. Raasch, Falling Natural Gas Prices Hit States' Pocketbooks, USA Today (2012) 3B.

[102] R.A. Kerr, Not Under My Backyard, Thank You, Science 328 (5986) (2010) 1625.

[103] J. Surjaatmadja, B. McDaniel, L. Case, L. East, J. Pyecroft, Consideration for Future Stimulation Options Is Vital in Deciding Horizontal Well Drilling and Completion Schemes for Production Optimization, SPE Production & Operations 23 (2) (2008) 27–31.

[104] M.J. Economides, M. Nikolaou, Technologies for Oil and Gas Production: Present and Future, AIChE Journal 57 (8) (2011) 1974–1982.

[105] A.W. Gaudlip, L.O. Paugh, T.D. Hayes, Marcellus Shale Water Management Challenges in Pennsylvania, in: Proceedings of SPE Shale Gas Production Conference, Society of Petroleum Engineers, 2008.

[106] S. Rassenfoss, From Flowback to Fracturing: Water Recycling Grows in the Marcellus Shale, Journal of Petroleum Technology 63 (7) (2011) 48–51.

[107] J.-P. Nicot, B.R. Scanlon, Water Use for Shale-Gas Production in Texas, U.S., Environmental Science & Technology 46 (6) (2012) 3580–6.

[108] D. Gupta, B. Hlidek, Frac-Fluid Recycling and Water Conservation: A Case History, SPE Production & Operations 25 (1) (2010) 65–69.

[109] J. Bonapace, M. Giglio, J. Moggia, M. Krenz, Water Conservation: Reducing Freshwater Consumption by Using Produced Water for Base Fluid in Hydraulic Fracturing-Case Histories in Argentina, in: Proceedings of SPE Latin America and Caribbean Petroleum Engineering Conference, Society of Petroleum Engineers, 2012.

[110] M. Blauch, R. Myers, T. Moore, B. Lipinski, N. Houston, Marcellus Shale Post-Frac Flowback Waters - Where is All the Salt Coming from and What are the Implications?, in: Proceedings of SPE Eastern Regional Meeting, Society of Petroleum Engineers, 2009: pp. 1–20.

[111] T.D. Hayes, B.F. Severin, Characterization of Flowback Waters from the Marcellus and the Barnett Shale Regions. RPSEA Report 08122-05.09, 2012.

[112] G.E. King, Hydraulic Fracturing 101: What Every Representative, Environmentalist, Regulator, Reporter, Investor, University Researcher, Neighbor and Engineer Should Know About Estimating Frac Risk and Improving Frac Performance in Unconventional Gas and Oil Wells, in: Proceedings of SPE Hydraulic Fracturing Technology Conference, Society of Petroleum Engineers, 2012: pp. 1–80.

[113] P. Aimar, J.A. Howell, M. Turner, Effects of Concentration Boundary Layer Development on the Flux Limitations in Ultrafiltration, Chemical Engineering Research and Design 67 (3) (1989) 255–261.

[114] M. Taniguchi, J.E. Kilduff, G. Belfort, Modes of Natural Organic Matter Fouling during Ultrafiltration, Environmental Science & Technology 37 (8) (2003) 1676–1683.

[115] V. Chen, A.G. Fane, S. Madaeni, I.G. Wenten, Particle deposition during membrane filtration of colloids: transition between concentration polarization and cake formation, Journal of Membrane Science 125 (1) (1997) 109–122.

[116] D.. Kwon, S. Vigneswaran, A.. Fane, R.B. Aim, Experimental determination of critical flux in cross-flow microfiltration, Separation and Purification Technology 19 (3) (2000) 169–181.

[117] R.W. Field, D. Wu, J.A. Howell, B.B. Gupta, Critical Flux Concept for Microfiltration Fouling, Journal of Membrane Science 100 (3) (1995) 259–272.

[118] P. Bacchin, P. Aimar, R.W. Field, Critical and sustainable fluxes: Theory, experiments and applications, Journal of Membrane Science 281 (1-2) (2006) 42–69.

[119] R.W. Field, G.K. Pearce, Critical, Sustainable and Threshold Fluxes for Membrane Filtration with Water Industry Applications, Advances in Colloid and Interface Science 164 (1-2) (2011) 38–44.

Chapter 3: Polydopamine: Review of Chemistry and Applications

3.1 Polydopamine: a Novel, Bio-Inspired Surface Modification Agent

Recently, there has been significant interest in materials inspired by the adhesive secretions of mussels and other sessile marine organisms [1–4]. Able to anchor themselves firmly to nearly any underwater surface, these species have become the subject of interest for chemists, biochemists, and engineers who seek to understand the source of this remarkable aqueous adhesive behavior and port it to synthetic systems [5]. The chemistry behind these systems is complex, however, and there are many outstanding challenges which prevent the realization of synthetic systems that show the same adhesive properties as those produced by Nature. Here, the history and development of polydopamine and related compounds is reviewed, and some perspectives on the utility of these materials for various applications are offered.

Mussel adhesive secretions are largely comprised of proteins which typically contain a high proportion of lysine and L-3,4-dihydroxyphenylalanine (L-DOPA), compounds that feature free amino and catechol functional groups, respectively. These moieties are believed to be responsible for the protein's solidification and the ensuing adhesion of the mussel to a surface [1]. In organisms, these catecholamine precursors are enzymatically polymerized to afford highly robust, polymeric melanin products.[6–8] Synthetic melanins have been prepared using a variety of commercially available catechols and catecholamines as analogues of the biological systems, the most common being dopamine (1) and 3,4-dihydroxyphenylalanine (DOPA) (2), shown in Figure 3.1. Dopamine is a small molecule containing amino and catechol functionalities and has been advanced as a commercially viable analogue of the aforementioned naturally occurring melanins. Upon polymerization in alkaline buffer, dopamine is capable of strong

This chapter adapted from a manuscript co-written with D. R. Dreyer, for future publication.

adhesion to a variety of surfaces [1]. Many of the key features (*e.g.*, strong adhesion, intense pigmentation, light absorption, good electrical conductivity, etc.) observed in the biologically derived melanins are typically preserved in the synthetic melanins [9].

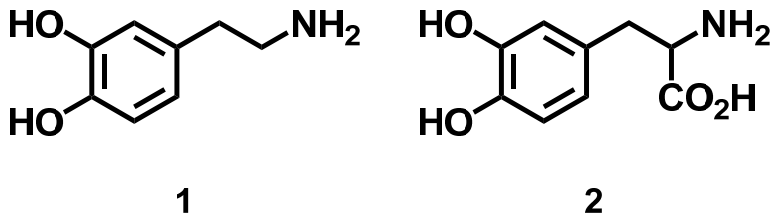

Figure 3.1. Small-molecule catecholamines used to prepare synthetic melanins. (1) dopamine and (2) DOPA.

Melanins have a long, storied, and controversial history in chemistry and biochemistry. Catecholamines and their polymer derivatives are ubiquitous in fields as diverse as nutrition science (*e.g.*, the browning of fruits and vegetables) [10], neuroscience (*e.g.*, the proposed link between catecholamine oxidation and neurodegenerative disease) [11], and botany (*e.g.*, the formation of melanin as a metabolite of catecholamines which can influence stress response and growth) [12]. Thus, the vast array of research into melanins provides fertile ground from which to draw insight into the chemistry of related synthetic materials, such as polydopamine. Indeed, no discussion of polydopamine would be complete without addressing the chemistry of melanins.

3.2 History and Background of Natural and Synthetic Melanins

3.2.1 Terminology

The terminology surrounding the melanins and derivatives thereof can be complex since much of the vernacular stems from antiquated origins. The term

"melanin" can be traced back to at least the 19th century in primarily an anthropological context (*e.g.*, human skin pigmentation) [13]. Since that time, and as the field of melanin chemistry has become more molecular in nature, the use of the term has broadened to the extent that it is not necessarily obvious whether or not a molecule or macromolecule may appropriately be considered a "melanin."

As of this writing, the IUPAC has yet to precisely define any of the terms below in their Compendium of Chemical Terminology (with the exception of "quinhydrone," as noted). Thus, the following terms are offered to improve the clarity of the accompanying discussions.

- Melanin: a general term used to describe dark pigments in biological systems that are commonly derived from the oxidation of tyrosine [14], although the molecules themselves can be prepared either naturally or synthetically [15,16]; it has been previously suggested (1953) that melanins share common chemical traits, including "resistance to solvents, bleaching when subjected to the action of oxidants, and the capacity to reduce ammoniacal solutions of silver nitrate" [17]
- Eumelanin: a black-brown subclass of melanins found in skin, hair, fur, and feathers; pheomelanins, in contrast, contain sulfur (from cysteine residues) and are typically yellow or red in color [14,16,18,19]
- Quinhydrone: "[from the IUPAC Compendium] molecular complexes of one equivalent amount of a quinone with one equivalent amount of the corresponding hydroquinone" [20]
- Polydopamine: a synthetic melanin prepared by the oxidative (typically aerobic) polymerization of dopamine (3-hydroxytyramine)

3.2.2 Discovery

Biological pigments have been of interest for many years, but the chemistry underlying these pigments was not the subject of direct investigation until the 19th century. Mammalian pigments were observed by Purkyně in the *substantia nigra* as early as 1838 [21] and by Simon in pig embryos in 1841 [22,23]. The isolation of these pigments was reported by Berzelius (1840) [24], who is often credited with first application of the term "melanin"[14], Mörner (1887) [25], and Landholt (1899) [23,26]. In 1895, Bourquelot and Bertrand recognized that blackening in various fungi was due to enzymatic action on tyrosine [27–29]. A variety of other plants and animals were found to possess similarly active enzymes, including cephalopods, insects, and amphibians [13]. In the early 20th century, Bloch showed that crude samples of human skin could catalyze the formation of melanin granules upon immersion in a solution of DOPA [30].

Beginning in 1928, Raper reported studies of the precise enzymatic processes responsible for this behavior [31], and in 1948 Mason refined these mechanisms [32]. The so-called Raper-Mason mechanism, which has since been widely adopted in understanding the polymerization behavior of catecholamines, will be discussed in greater detail below, but historically this work proved to be seminal in the development of a more molecular understanding of complex pigments and melanic polymers. The understanding of the chemistry and biochemistry displayed by melanin and eumelanin progressed after this time and has branched into several fields of chemistry [19,33], biology [34,35], and medicine [15,36]. Despite this broad importance, surprisingly little is known about melanins, primarily as a result of the difficulties associated with their isolation and characterization. In the sections that follow, a summary of some of the key findings will be presented, with a particular emphasis on those aspects that pertain to polydopamine as a specific and timely example.

3.3 Structure and Bonding in Polydopamine and Related Synthetic Melanins

3.3.1 Methods of Preparation

The synthetic approaches applied to melanin formation may be divided into two categories: enzymatic and non-enzymatic. Most of the ongoing development of polydopamine chemistry does not utilize the enzymatic approach, however. Catecholamines of many varieties are known to undergo oxidative polymerization under aerobic conditions [37,38]. As would be expected, therefore, the polymerization of dopamine can be suppressed under inert atmospheres [39]. Polymerization is readily initiated when dopamine is treated with a base under aerobic conditions. Similar behavior is seen when catechol (*o*-benzenediol) or hydroquinone (*p*-benzenediol) are exposed to alkaline, aerobic media [40–42], suggesting the polymerization behavior stems from reaction of the diol moiety (pK_a of catechol = 9.25 [43]; observed pK_a of dopamine = 8.89 [44]) with the base, rather than the free pendant amine (pK_a of benzeneethaneamine= 10.42 [45]).

Aside from molecular oxygen, various solution-based chemical oxidants such as ammonium persulfate ($(NH_4)_2S_2O_8$), sodium periodate ($NaIO_4$), and potassium chlorate ($KClO_3$) can polymerize dopamine as well [46]. These reactions have been shown to exhibit dependence on pH, similar to the aerobic oxidation. At pH < 7.0, dopamine exhibits minimal reactivity with all of the aforementioned chemical oxidants except ammonium persulfate; at pH > 8.5, however, all of the noted oxidants were able to initiate polymerization [46].

Mechanistically, there are multiple ways of understanding how the oxidative polymerization(s) may proceed, but each of the mechanisms results in products with significantly different structures. As has been the case for melanins over the years, the unique structure of polydopamine remains the subject of much debate. The proposed

structures of polydopamine may be divided into two broad categories: those that incorporate covalent linkages between the monomers and those that incorporate non-covalent linkages.

3.3.2 Structure and Bonding: Covalent Model

The initial steps of the tyrosinase-catalyzed oxidative polymerization of dopamine and other similar catecholamines are well known and generally accepted to proceed *via* the so-called Raper-Mason mechanism; the key transformations are shown in Figure 3.2 using tyrosine as a model compound. Notably, however, the final steps of the process (*i.e.*, the formation and structure of melanochrome and the final melanin product) were not well understood at the time this mechanism was proposed (1928, 1948). Unfortunately, these steps are essential for understanding the structure of the final product, and lie at the heart of the present literature debate on the subject.

With respect to the polymerization of dopamine *via* this mechanism [47,48], it is worth noting that dopamine lacks the carboxylic moiety present in tyrosine. The resulting inability to decarboxylate dopamine during its polymerization could lead to formation of the saturated indoline derivative, rather than unsaturated indole. Autoxidation of the indoline is possible, but would be anticipated to be slow, given the high stability of indolines to oxidative conditions [49]. The conversion of indolines to indoles typically requires strong oxidants (*e.g.*, hypochlorite and dimethyl sulfide [50]), or the use of metal catalysts (*e.g.*, cobalt [51], manganese [52], or gold compounds [53]).

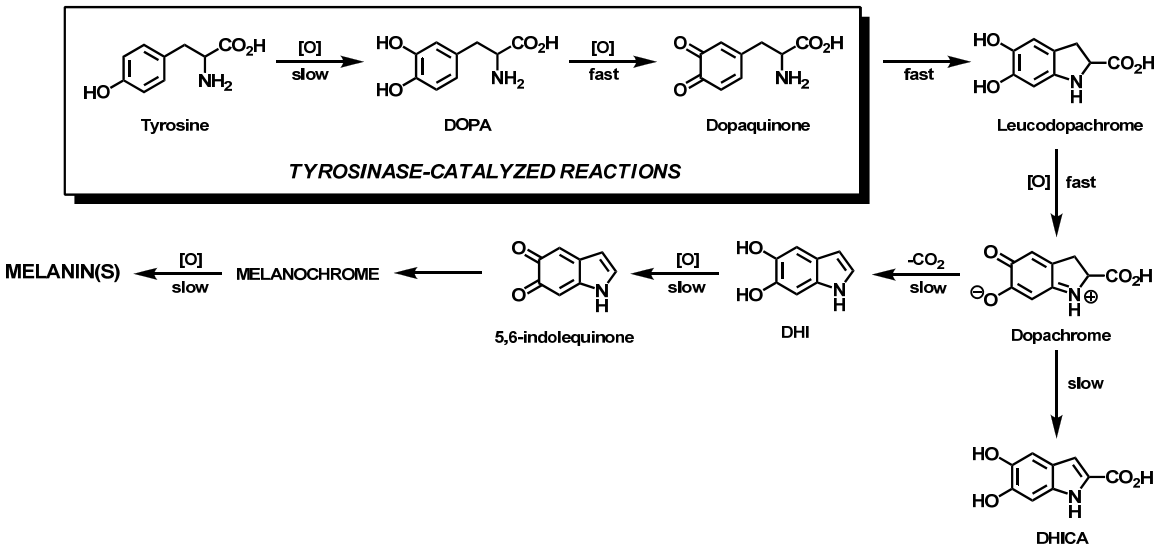

Figure 3.2. Tyrosinase-catalyzed oxidation and polymerization of tyrosine according to the Raper-Mason mechanism. DHI = 5,6-dihydroxyindole; DHICA = 5,6-dihydroxyindole-2-carboxylic acid.

According to the Raper-Mason mechanism, the key precursor of melanin is 5,6-dihydroxyindole (DHI), and much of the research in the field of DHI chemistry has been described by a team of researchers at the University of Naples. Through meticulous work spanning several decades, the Naples team has used many techniques (*e.g.*, chromatography, mass spectroscopy, and UV-vis spectroscopy) [54] to understand the reaction intermediates, the melanin polymers themselves, and the degradation products produced by reaction of melanin with various chemical agents.

The majority of the structural models of melanin proposed by the Naples team can be understood in terms of the reactivity of DHI with its oxidized form (5,6-indolequinone). In particular, it has been proposed that DHI can act as a nucleophile and the quinone can act as an electrophile (Figure 3.3) [13,55,56], affording new covalent linkages upon combination and leading to a variety of structures, including the 2,4', 4,4', 4,7', and 7,7' arrangements. Radical mechanisms have also been suggested as potential

sources of these covalent linkages, particularly for the formation of symmetrical species (*e.g.*, the 2,2' dimer) [13].

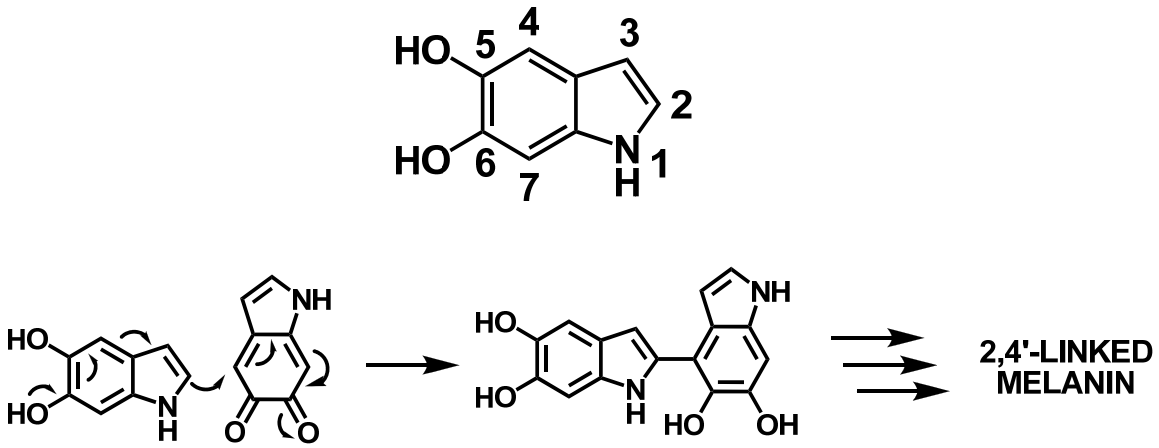

Figure 3.3. Numbering in DHI (top), and the proposed electron pushing schemes for the conversion of DHI and 5,6-indolequinone to the corresponding 2,4'-linked melanin polymer product (bottom).

The formation of the intermediates along these pathways has also been studied extensively by the Naples group [33]. One key approach employed toward this end has been protection of the catechol functionality *via* acetylation of the melanochrome intermediate(s) (Figure 3.4) [57–63], typically achieved using acetic anhydride and a base (*e.g.*, pyridine). Protection of the catechol moiety in this fashion allowed for isolation and characterization of the intermediate(s), as well as postulation about the subsequent reaction pathways leading to the final melanins. Subsequent hydrolysis of the acetylated derivatives under anaerobic conditions resulted in the reformation of the catechols (identified by UV-vis spectroscopy), and further exposure to an oxidizing atmosphere led to polymerization to the corresponding melanin. In sum, covalent linkages in polydopamine are believed to arise as a result of nucleophilic-electrophilic interactions between heterocycles of varying oxidation state, or from radical species generated *in situ*.

It has been further proposed that these small bound species undergo further bonding, analogous to a step-growth polymerization, or aggregation to form the final insoluble polymer product (see further discussion below of aggregation phenomena).

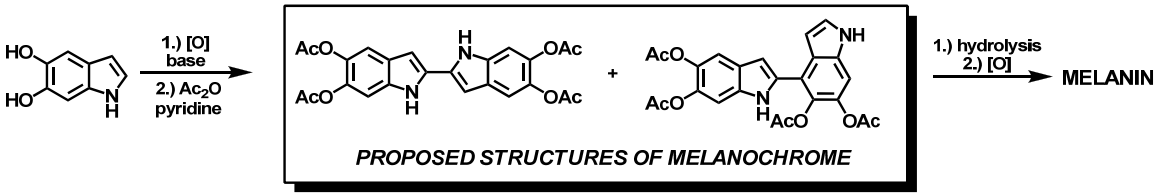

Figure 3.4. Proposed structures of melanochrome determined *via* isolation and characterization of the acetylated intermediates formed during oxidative polymerization of DHI.

3.3.3 Structure and Bonding: Non-Covalent Model

A comprehensive study that investigated the structure of powdered polydopamine samples has recently been reported [64]. Solid state ^{15}N NMR spectroscopy indicated the formation of a cyclized species (*e.g.*, indoline or indole), rather than the free amine, in contrast with some previously proposed models of polydopamine, which suggested to us that the majority of the monomer units remained uncyclized in the polymer product [13,65]. Further analysis of the polymer by ^{13}C NMR spectroscopy revealed several important features, including partial saturation of the bicyclic ring system (indicating the presence of an indoline-type structure rather than an indole) and oxidation (or partial oxidation) of the diol to a dione. The key question of whether or not covalent bonds existed (principally proposed to occur through the benzene moieties, as noted above) was addressed with the use of dopamine isotopically labeled with ^{13}C (99 atom%) only on the arene ring. A standard 1D cross-polarized (CP) spectrum of the sample revealed the presence of protons bound to the benzene core of the molecule. Crucially, this result

appeared to be inconsistent with the predominately covalent models that have been alternatively proposed.

Lacking spectroscopic evidence for the presence of aryl-aryl linkages in the as-prepared polydopamine powder, efforts turned toward investigating the nature of the bonding interaction between the monomers. Powder X-ray diffraction (PXRD) indicated the presence of ordered stacking (d-spacing = 3.8 Å) consistent with a variety of π-stacked structures [66,67]. Furthermore, analysis of the powder by electron paramagnetic resonance (EPR) spectroscopy showed the presence of stable free radicals present at low concentration in the polymer sample (less than 1 spin per 25 repeat units), consistent with a variety of other melanins (see discussion of radical character below) [68]. Collectively, these results suggested to us that the repeating units in polydopamine were held together *via* non-covalent bonds rather than covalent carbon-carbon bonds, as many of the previous models have proposed (Figure 3.5). The data indicate that these occur through a mixture of hydrogen bonding interactions (similar to the strong non-covalent interactions believed to be present in quinhydrones [69,70]), π-stacking, and charge transfer processes. As indicated by polydopamine's near complete insolubility and the exceptional stability of its coated forms, these non-covalent interactions are very strong (both between the monomer units and the underlying substrate, if present), as has been demonstrated for a variety of natural and synthetic polymer materials [71–77].

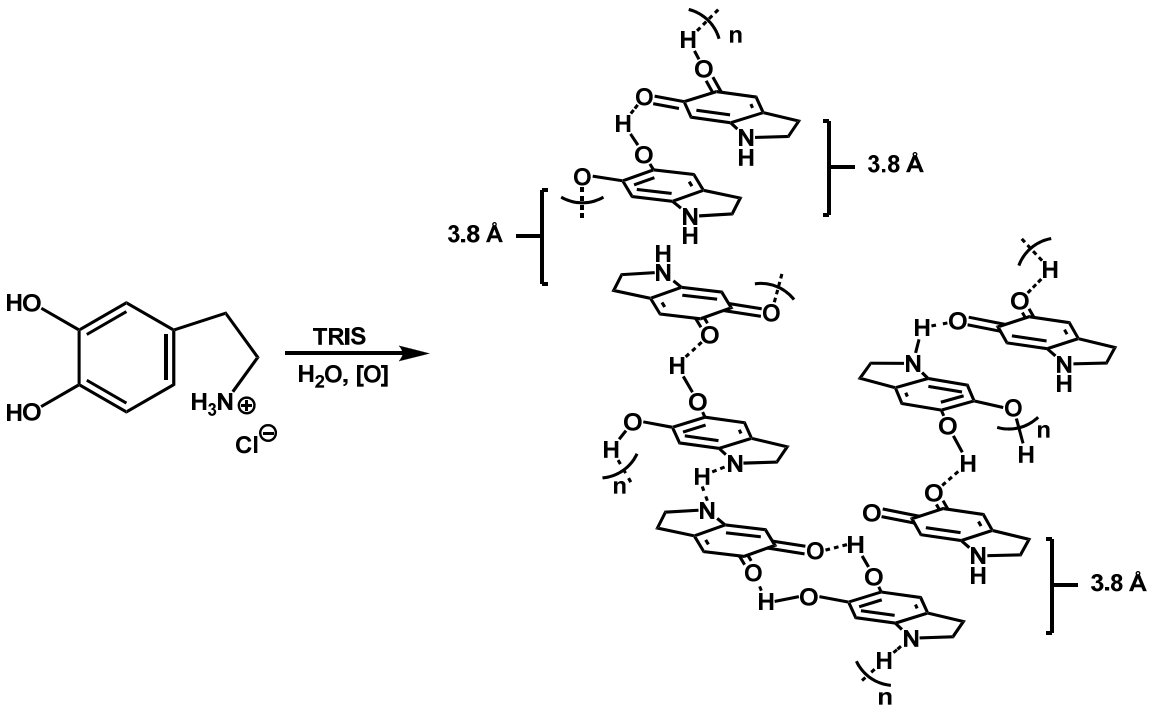

Figure 3.5. Proposed supramolecular structure of polydopamine, incorporating a combination of non-covalent hydrogen bonding, charge transfer and π-stacking interactions. Adapted from [64].

It has previously been shown that melanins may be degraded by exposure to hydrogen peroxide, molecular oxygen, peracetic acid (CH_3CO_3H), or alkaline potassium permanganate ($KMnO_4$) through an oxidative bleaching process [13,78–80]. As described above, these degradation products have been a crucial source of information on the structure of the parent polymers. Nicolaus and coworkers have suggested that the primary compound formed by treating sepiomelanin with the aforementioned oxidants is pyrrole-2,3,5-tricarboxylic acid (PTCA, 3) (Figure 3.6), identified *via* paper chromatography, in addition to trace amounts of the other di-, tri-, and tetracarboxylic acid derivatives of pyrrole [80]. Similarly, polydopamine was found to degrade by either aqueous sodium hypochlorite (NaOCl) or potassium meta-periodate (KIO_4) at room temperature over periods of several hours. The insoluble, darkly colored powder became

fully soluble, clear, and nearly colorless as reaction with either of these oxidants proceeded. In accordance with the non-covalent model of polydopamine and supported with FT-IR spectroscopy, this solubilization was proposed to have occurred *via* oxidation of the catechol functional groups, leading to the formation of 2,3-dihydro-indolo-5,6-quinone.

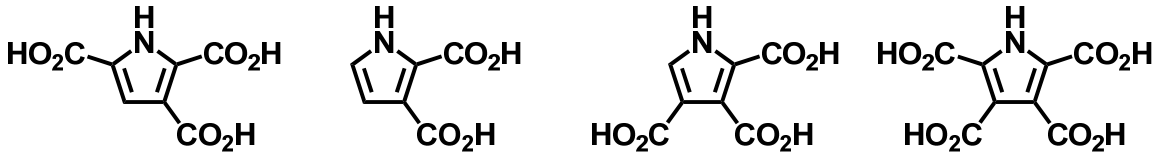

Figure 3.6. Product mixture obtained by treating sepiomelanin with either peracetic acid or alkaline potassium permanganate. The primary product was found to be pyrrole-2,3,5-tricarboxylic acid (PTCA, 3), with trace amounts of the other acids (4–6). Adapted from [80].

The proposed structural model of polydopamine differs significantly from the majority of models that have been previously suggested, though other studies have shown that non-covalent, supramolecular interactions are key components of polydopamine's structure [16,18]. Higher order secondary and tertiary interactions are known to be present in various melanins (similar to protein folding interactions), resulting in complex nanoaggregates and filaments (see Figure 3.7) [81,82]. The importance of secondary interactions in melanins formation is supported by the work of Tsolakidis and coworkers, who used density functional theory to describe a melanin model in which tetrameric or pentameric protomolecules stacked into supramolecular assemblies [83].

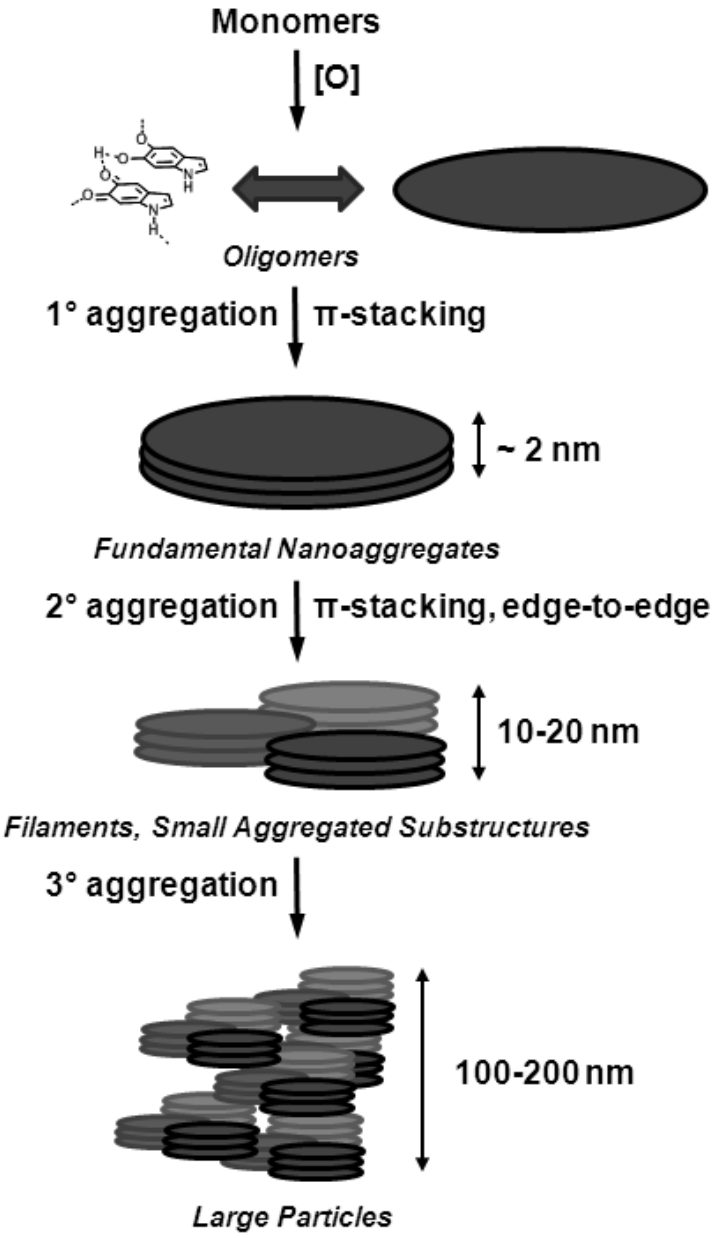

Figure 3.7. Schematic of primary, secondary, and tertiary ordering in melanins such as polydopamine. Adapted from [84,85].

While the debate surrounding this fundamental question of the material's structure and bonding is likely to continue, the non-covalent model presents a structure that is most consistent with the chemistry seen in other similar molecular architectures (*e.g.*,

quinhydrones, supramolecular polymers, proteins, etc.). A proper understanding of the polymer's structure is not merely an academic question: the ability to install orthogonal functionalities (*e.g.*, fluorophores, solubilizing polymers, etc.) into the monomer, while preserving its ability to undergo oxidative polymerization and adhesion, will depend on how the repeat units are linked in the polymer. While the models that rely on covalent coupling between the monomers suggest that substitution of the monomer at any position, particularly the aryl core, will impede its subsequent polymerization, the non-covalent model suggests that the catechol functionality is the crucial moiety. The non-covalent model also predicts that para substitution of the diol functionality (as in hydroquinone) will afford analogous products; ortho substitution of the diol may not be strictly required for the reaction to proceed. Though the para substituted diol derivative of dopamine is known (*i.e.*, 2,5-dihydroxyphenylethylamine), it has not been applied to polymerizations of the type described herein.

3.4 Physicochemical Properties of Polydopamine

3.4.1 Physical Properties

The unique structural properties of polydopamine and related melanins, described in the previous sections, endow these materials with a number of distinctive and useful physical properties. In addition to those previously discussed (*e.g.*, strong adhesion to a broand range of surfaces), electronic conductivity and broadband absorption of light are of particular interest and importance. Melanins as a broad class of molecules have long been known to exhibit semiconductive properties [86–90], even in the absence of chemical dopants. Arising from the material's unique structure and bonding, polydopamine exhibits conductivity properties that depend on a variety of factors, including temperature, hydration state, and exposure to light [89,91–93]. The key

semiconductor properties of polydopamine and other melanins are summarized in Table 3.1.

	Conductivity (T = 293K) σ_{293} (Ω^{-1} cm^{-1})	Thermal Activation Energy ΔEA (eV)	Preexponential Factor σ_o (Ω^{-1} cm^{-1})	Photocurrent Intensity ΔI_{ph} (A)
Polydopamine	$(5.1 \pm 0.1) \times 10^{-12}$	0.71 ± 0.01	8.0	*
Poly(adrenaline)	$(1.3 \pm 0.1) \times 10^{-12}$	0.68 ± 0.01	0.6	*
Poly(adrenochrome)	$(5.2 \pm 0.1) \times 10^{-12}$	0.73 ± 0.01	18.6	*
Poly(adrenolutin)	$(1.5 \pm 0.1) \times 10^{-10}$	0.62 ± 0.01	7.0	8.0×10^{-9}

* no photocurrent observed

Table 3.1: Summary of the electronic properties of polydopamine and related melanins prepared from catechol amines. Adapted from [92].

In addition to semiconductivity, polydopamine is known to strongly absorb light over a broad range of wavelengths [18,84]. Indeed, it is precisely this trait of melanins that makes them excellent photoprotectants. In addition to the absorption of light, it has also been proposed that the particulate nature of melanins leads to a combination of Rayleigh and Mie scattering, particularly at wavelengths below 300 nm [94]. Contributions of this scattering effect to the total optical attenuation range from < 6% between 210 and 325 nm (no scattering was observed at longer wavelengths in this study [95]) to 12–13.5% in the visible range [96]. Due to the broadband, monotonic nature of polydopamine's absorption profile, the determination of the electronic and molecular structure *via* optical spectroscopy has proved challenging. Likewise, efforts to measure the materials' band gap in amorphous samples have led to widely varying values, ranging from 1.3 eV to as much as 3.4 eV [89,93]. As with the semiconductor properties of the

materials, however, the measured band gaps show a dependence on preparation method, hydration state and temperature.

While polydopamine has strong absorption properties, as much as 99.9% of the absorbed energy is dissipated non-radiatively, primarily as phonons [18]. As such, synthetic melanin exhibits minimal fluorescence or phosphorescence, displaying quantum yields below 7×10^{-4} [97]. In the many reported studies of melanins' photophysical properties, it is apparent that polymers of this type do not possess a single, well-defined chromophore, but a mixture of light absorbing/emitting species [18]. As noted by Meredith and co-workers, the line shapes in the absorption and emission spectra of melanins do not mirror one another, in violation of the so-called "mirror-image rule" of well-defined organic chromophores [18]. While the absorption profiles for most melanins are broad and monotonic (see Figure 3.8), as previously described, the emission profiles are typically Gaussian.

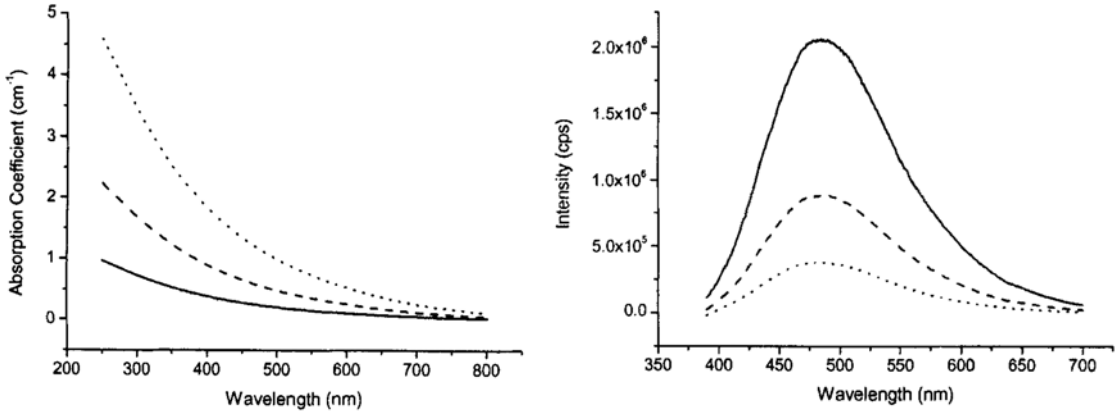

Figure 3.8. UV-vis absorption profiles (left) and photoluminescence emission profiles (right) for synthetic melanin prepared from tyrosine at three different concentrations: 0.005% (dotted line), 0.0025% (dashed line) and 0.001% (solid line) by weight concentration. Adapted from [97].

3.4.2 Chemical Properties

In addition to these desirable physical properties, polydopamine has certain chemical properties that are also remarkable. The most significant of these relate to the polymer's redox properties, which are relevant even in biological systems where eumelanins act as oxygen scavengers [98]. Paradoxically, polydopamine and other melanins can act both as reductants and as oxidants [15]. This divergent behavior is believed to stem from the fact that polydopamine possesses both oxidizing quinones and reducing catechols, both of which may participate in electron transfer reactions. For example, polydopamine rapidly oxidizes thiols (and amines to a lesser extent), converting the quinoidal moieties in the polymer to the corresponding catechols.[99,100] In contrast, polydopamine can electrolessly metallize Ag(0) [101], Au(0) [102], or other metals onto various surfaces by reduction of the corresponding metal salts from aqueous solutions. The reduction of the carbon-based material, graphene oxide, to graphene by the oxidative polymerization of dopamine has also been demonstrated [103–105].

Beyond the redox chemistry and its propensity to bind water [106] as well as various metal ions [5,107], polydopamine is resistant to most other chemical agents, giving rise to the previously described stability of deposited films. Polydopamine coatings may be modified through the attachment of polymers, but these reactions typically occur to relatively minimal extents and often require the presence of orthogonal functional groups. For example, it has been shown that amine-terminated poly(ethylene glycol) (PEG) may be conjugated to polydopamine coatings *via* condensation of the terminal amine and the carbonyls present in the quinones in polydopamine [108,109]. Similarly, PEG chains have been conjugated to polydopamine *via* attachment to the N–H position of the acyclic monomers [110]. In these and other strategies that have been

employed, however, the polydopamine coatings themselves remain largely intact, preventing disruption of the desirable adhesion.

The chemical inertness of polydopamine is also manifested by the presence of stable radical species, present both during and after the polymerization reaction [64]. Comprehensive EPR studies performed on poly(DOPA) have suggested the presence of more than one type of radical (*e.g.*, a semiquinone-type species and a species associated with defects in the polymer) [84,111]. The steady-state concentrations of radicals in these materials is proposed to be very low; on the order of 10^{17}–10^{18} g^{-1} [15].

3.4.3 Bulk Properties and Processing

Though polydopamine and other synthetic melanins can be isolated as a bulk powder [64], this form of the material is intractable and has no known uses other than for fundamental study. This powder is, however, considered representative of the coating material deposited on substrates in contact with alkaline dopamine solution and often used for characterization purposes [9]. Derivatives of polydopamine, such as those with polymers attached to them [112,113], can be prepared, and some of these have excellent solubility properties. However, such conjugates still readily deposit, and typically irreversibly, onto myriad surfaces. Polymerization initiators may also be anchored to polydopamine-coated surfaces for the preparation of surface-attached polymer brushes [39,114], representing an alternative to pre- and post-coating conjugation techniques described above.

In view of polydopamine's minimal to non-existent bulk processability, the majority of polydopamine applications (discussed in greater detail in section 3.5) focus on coatings [15,115]. Upon immersion of either hydrophilic or hydrophobic materials of a variety of shapes into alkaline solutions of dopamine, thin coatings are deposited and later characterized [1,4,116–119]. In general, the thickness of polydopamine films has

been found to increase with deposition time and temperature [120]. The observed water contact angles of coated substrates have been measured to be nearly uniform (θ = 50–60°), regardless of the underlying material (Figure 3.9), suggesting that the polydopamine top coat dominated the composite materials' surface properties.[46] Significant conversions of surface hydrophilicity have been reported using polydopamine on hydrophobic surfaces that include poly(vinylidene fluoride), poly(tetrafluoroethylene) (PTFE), poly(ethylene terephthalate) (PET), and poly(imide) [120]. Dopamine solution concentration and deposition time have also shown little effect on the surface hydrophilicity after modification [120]. When silica was used as a substrate, the film growth rate was found to be approximately 3.6 nm h^{-1} (see Figure 3.10), though decreasing the immersion time from 15 min to 5 min was found to increase the deposition rate to as much as 7 nm h^{-1} [9]. The resulting coatings were highly robust and were resistant to mechanical [121–125], chemical [1], and electrochemical degradation [122,124]. To remove these coatings, strongly alkaline or oxidizing solutions were typically required. Polydopamine coatings have shown good corrosion resistance when applied to stainless steel [118,126], copper [116], and silicon [122,124] substrates.

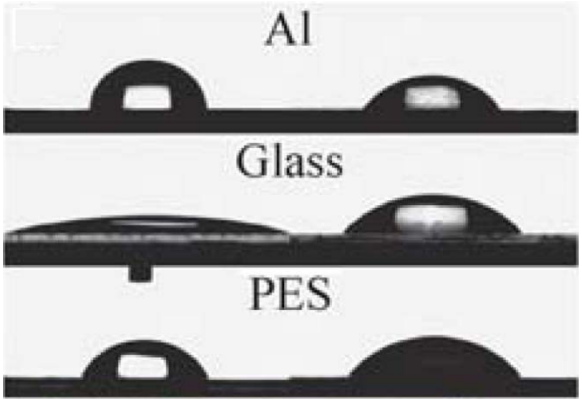

Figure 3.9. Water contact angles of polydopamine-free aluminum, glass, and poly(ether sulfone) (PES) (left), and the polydopamine-coated substrates (right). Adapted from [46].

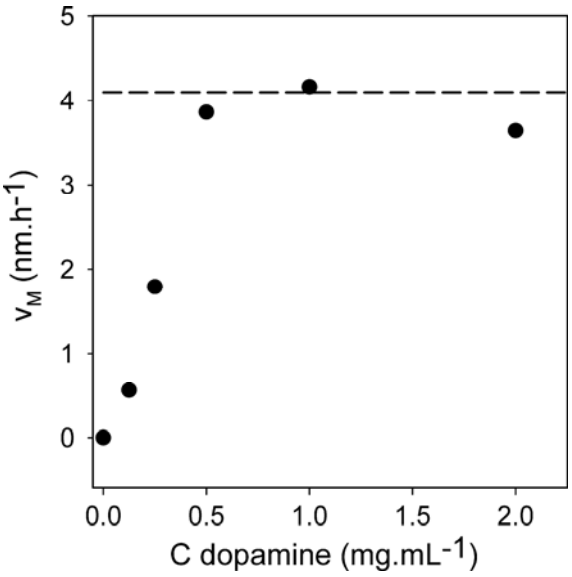

Figure 3.10. Polydopamine deposition rate (v_M) as a function of the initial buffered aqueous dopamine solution. Performed on silica substrates under normal atmosphere at pH 8.5 and 25°C for immersion times of 15 min. The horizontal line represents an observed plateauing of the deposition rate at higher concentrations. Adapted from [9].

The surface adhesion of polydopamine is believed to arise through non-covalent interactions (*e.g.*, hydrogen bonding, metal chelation, etc.) between the polymer and the surface onto which it is deposited, similar to other melanins. Using mica or titanium dioxide as a common substrate, it has been shown that the adhesion strength of melanin coatings varies with the number of hydrogen bonding partners. For example, films with a high DOPA content (a derivative of dopamine that contains an additional pendant carboxylic acid moiety; see 2) exhibited increased adhesion work (measured in mJ m^{-2}), as determined by various force measurement apparatus [127]. It is believed that in more

complex polymers, such as poly(DOPA), polydentate hydrogen bonding is enabled, allowing for even stronger adhesive properties. Films of this type are susceptible to attack by strong oxidants, however, presumably occurring through oxidative degradation of the repeat units, as well as the bonds that adhere the polymer to the surface.

3.5 APPLICATIONS OF POLYDOPAMINE

In the short time since Messersmith and coworkers' seminal report in 2007 describing coatings formed on substrates immersed in buffered, alkaline dopamine solution [1], polydopamine has found use in a variety of applications. Polydopamine coatings are typically tens of nanometers in thickness [120,128], meaning that substrates may be functionalized with very little change in their geometry. Most of these applications take advantage of polydopamine's ability to non-aggressively "prime" a surface, permitting further molecular conjugation, attachment of particles, or layer assembly. For example, Messersmith, described layer-by-layer assembly on PTFE, poly(ethylene) (PE), poly(carbonate) (PC), PET, poly(methyl methacrylate) (PMMA), silica, and gold surfaces using catechol-functionalized cationic and anionic polymers following polydopamine deposition [129]. By selective deposition into a particular pattern, polydopamine may also be used to spatially organize polymers, metals, small molecules, cells, and proteins on nearly any substrate [119,130]. The generation of materials with a broad array of functions has lent polydopamine to diverse applications, some of which will be described in the sections that follow.

3.5.1 Nanotechnology

Because of the non-specific nature of its deposition and that the thin coatings that can be readily prepared, preventing significant perturbation of the underlying nanostructure, polydopamine has been used to surface-modify a variety of nanomaterials.

Numerous reports of polydopamine-coated nanoparticles,[131–136] nanotubes [102,137–141], nanowires [142–144], nanoclays [145], and powders [125] of various compositions are found throughout the literature. These materials are typically surface-modified with polydopamine made simply by dispersing the nanomaterial substrates in a buffered dopamine solution. Polydopamine may also be used to attach nanomaterials to surfaces. Nanoparticles of silver [146–149], gold [147,150,151], and multimetallic [152] compositions may be formed on a polydopamine-coated surface through contact with an appropriate metallic solution. Kim and coworkers coated poly(dimethyl siloxane) (PDMS) with polydopamine and were subsequently able to anchor nanowires to the surface by spray-deposition, creating stretchable, optically-transparent, conductive films [153].

Microcapsule fabrication is found in a number of reports and involves the coating of a hard or soft microsphere with polydopamine and subsequent removal of the core, leaving a hollow polydopamine shell, as shown in Figure 3.11. The technique has been implemented on template cores made of poly(styrene) (PS) [154,155], silica [156], calcium carbonate [157], and emulsion droplets [158,159]. In the case of emulsion templates, the polydopamine shell thickness could be tuned by varying the emulsion concentration and by repeating the dopamine polymerization process [154]. The uptake and release behavior of such capsules using charged dyes has also been assessed and found to be pH-dependent [154] and, in the case of some cargo molecules, unidirectional [155].

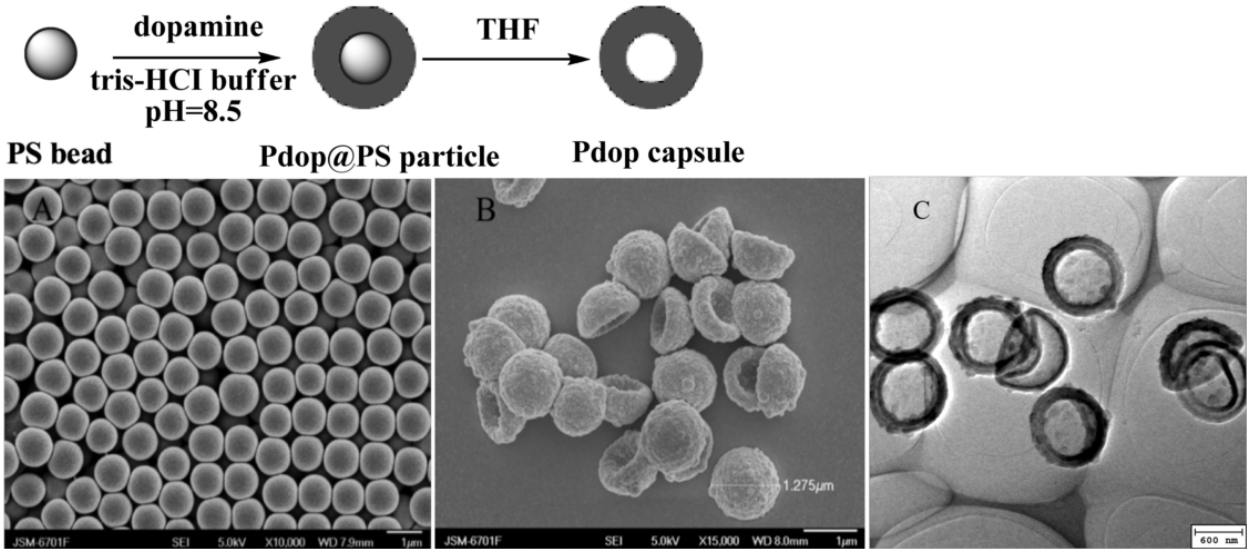

Figure 3.11. Polydopamine microcapsule formation. PS beads are coated with polydopamine by immersion in a buffered, alkaline dopamine solution (A). After formation of the polydopamine@PS particles, the PS is removed, leaving a hollow polydopamine capsule (SEM image, B and TEM image, C). Adapted from [154].

3.5.2 Biotechnology

Polydopamine has also found utility in many biotechnology related applications. Biomolecules (especially enzymes and other proteins) may be conjugated to nearly any polydopamine-treated surface. Direct entrapment of enzymes in polydopamine coatings has been reported by Jiang and coworkers [160]. Biomolecules may often be covalently conjugated to polydopamine coated surfaces through amine or imidazole moieties, which have been shown to react with polydopamine [4]. Indeed, polydopamine has enabled the conjugation of trypsin (a serine protease) to metals and polymers [4], proteins and antibodies to manganese carbonate microspheres [161], lipase to magnetic iron oxide nanoparticles [162], α-amylase to magnetic-chitin microparticles [163], bovine serum albumin to diamond-like carbon films [164], fibronectin to electrospun poly(ε-caprolactone) (PCL) [165], and bovine serum albumin to porous PE [166].

Biomolecule conjugation has been shown to improve substrate biocompatibility and can be used to enhance cellular adhesion, providing a route to construction of tissue scaffolds and improved biointegration of implants. Tissue scaffolds are often highly porous and the deposition of polydopamine from aqueous solutions provides a facile route to faciltiate biocompatibilization [167] of the entire surface area. For example, as noted above, the grafting of fibronectin to polydopamine-coated PCL improved cellular attachment to the modified PCL fibers [165]. Tethering vascular endothelial growth factor (VEGF) to polydopamine-coated titanium substrates resulted in increased attachment, viability, and proliferation of endothelial cells relative to an unmodified substrate [168,169]. Several studies, however, have noted that the polydopamine coating alone promotes cellular attachment to many substrates, even at short coating times [170]. Lee, Park, and co-workers found that mouse osteoblast [171] and human endothelial cell [172] adhesion and viability was improved on several non-wetting substrates such as PTFE, silicone rubber, PDMS, PE, and glass after coating with polydopamine. Polydopamine treatments have also enhanced the adhesion and proliferation of human mesenchymal stem cells on electrospun PMMA [173], rabbit chondrocytes on biodegradable polymers such as PCL, poly(L-lactide), poly(lactic-*co*-glycolic acid), and poly(urethane) [174], as well as bone marrow stromal cells on mesoporous silica scaffolds [175]. High surface area nanostructures, such as carbon nanotubes, have been coated with polydopamine to improve cellular compatibility for tissue scaffold applications [139,140,176]. Bone scaffolds and materials for ocular implants have been fabricated by hydroxyapatite crystallization on polydopamine-modified metals,[139] polymers,[107] and nanowires [177]. Cell adhesive peptides [178] and hydroxyapatite [179] have also been grafted to polydopamine-coated PMMA for improved biointegration of implants.

Polydopamine-promoted cell adhesion has been proposed for other applications. Shi and coworkers developed a simple gold/polypyrrole actuator coated with polydopamine to collect cells from aqueous media [180]. Preferential adhesion of cells to polydopamine over other substrates allows for cell patterning. Instead of complex protocols that require the use of adhesive proteins, patterned polydopamine may be deposited through lithographic [130,181] or microfluidic [182] techniques, resulting in spatial organization of adherent cells and proteins. Polydopamine may also be used to tether individual cells to surfaces. Choi and co-workers formed a polydopamine coating on individual yeast cells, allowing facile conjugation of avidin to the cell surface. The cells were then immobilized on a biotin-functionalized poly(ethylene glycol methacrylate) substrate [183]. Polydopamine modification of an AFM tip was shown to provide a straightforward means of studying single cell adhesion [184]. Even neuron interfaces have been functionalized with polydopamine [185].

While many investigators have been using polydopamine for molecular conjugation and cellular proliferation, others are using it as an intermediate to create surfaces resistant to protein and cell adhesion. PEG, in particular, has a long history of use in antifouling applications due to its strong affinity for water which effectively creates a steric barrier to foulant interaction with a surface [186]. Protein adhesion-resistant surfaces were fabricated by grafting PEG to polydopamine-coated PET, poly(L-lactide), and PS [187]. Electroless metallization of polydopamine-coated surfaces permitted the deposition of silver nanoparticles, which display antimicrobial properties [188,189]. Messersmith and coworkers were able to extend this methodology to a multilayered structure, where PC was coated with polydopamine and silver nanoparticles, then re-coated with polydopamine to which a thiol-terminated PEG was grafted. Release of silver from the coating was observed over seven days. The antimicrobial effect of the

silver and the steric hindrance to cell attachment provided by the PEG brushes reduced attachment and proliferation of both gram-positive and gram-negative bacteria [190]. Other antimicrobial compounds immobilized on a polydopamine layer include quaternary ammonium salts and ultrashort antimicrobial lipopeptides on glass slides [191], zwitterionic brushes on PTFE, PC, and PE [192], and carboxymethyl chitosan on medical silicone [193]. Ferreira and co-workers were able to attach silica nanoparticles functionalized with Amphotericin B, a powerful antifungal compound, to glass surfaces using polydopamine [194].

Bioseparations is another biotechnology area in which polydopamine has been successfully used. Molecular imprinting has attracted interest as a rapid, inexpensive means of producing materials capable of recognizing particular biomolecules. Ouyang and co-workers developed a method of producing molecularly imprinted polydopamine nanowires. Various template proteins were attached to the inside of pores in an alumina nanomold *via* epoxide functionality. The molds were then filled with a solution of dopamine and ammonium persulfate, forming solid polydopamine nanowires with imprints of the target molecule. Polydopamine nanowires capable of recognizing five different proteins were fabricated [195]. Other polydopamine-based molecularly imprinted architectures include nanoparticles [196,197] and monolithic columns for chromatography [198]. Electrochromographic columns have also been modified with polydopamine [199]; biological stationary phases, including lipids, cell membranes, and mitochondria, have subsequently been immobilized in polydopamine-coated columns [200]. Electroless metallization [201] and PEG grafting [109] approaches have been used to coat PDMS electrophoretic channels with polydopamine to create biofouling-resistant surfaces. Finally, Zhou and coworkers found that polydopamine films exhibited pH-tunable selectivity for permeation of charged molecules. At high pH, the films were

negatively charged and excluded anions; at low pH, the films were positively charged and excluded cations [202].

A variety of biosensors constructed with polydopamine have been reported. Simple devices in which an electrode was coated with polydopamine and a sensory moiety subsequently grafted to the polydopamine have been reported for the detection of nicotine [203], hydrogen peroxide [204], sulfate-reducing bacteria [205], and glucose [206]. Glucose receptors for medical or biofuel cell applications have also been developed by directly entrapping glucose oxidase in a polydopamine film cast on a gold electrode [207]. Composite sensors have been constructed by grafting glucose oxidase to polydopamine-coated carbon nanotubes which were then cast atop an electrode [208,209]. Polydopamine has also been used to prepare non-enzyme based glucose sensors by facilitating electroless metallization of a gold/Prussian blue nanocomposite with gold nanoparticles, to which a boronic acid-diol glucose binder was grafted [210]. Similar architectures, where polydopamine enables construction of a nanocomposite material on an electrode, have been reported for detection of ascorbic acid [147], hydrogen peroxide [211,212], and antigens (Figure 3.12) [213–216].

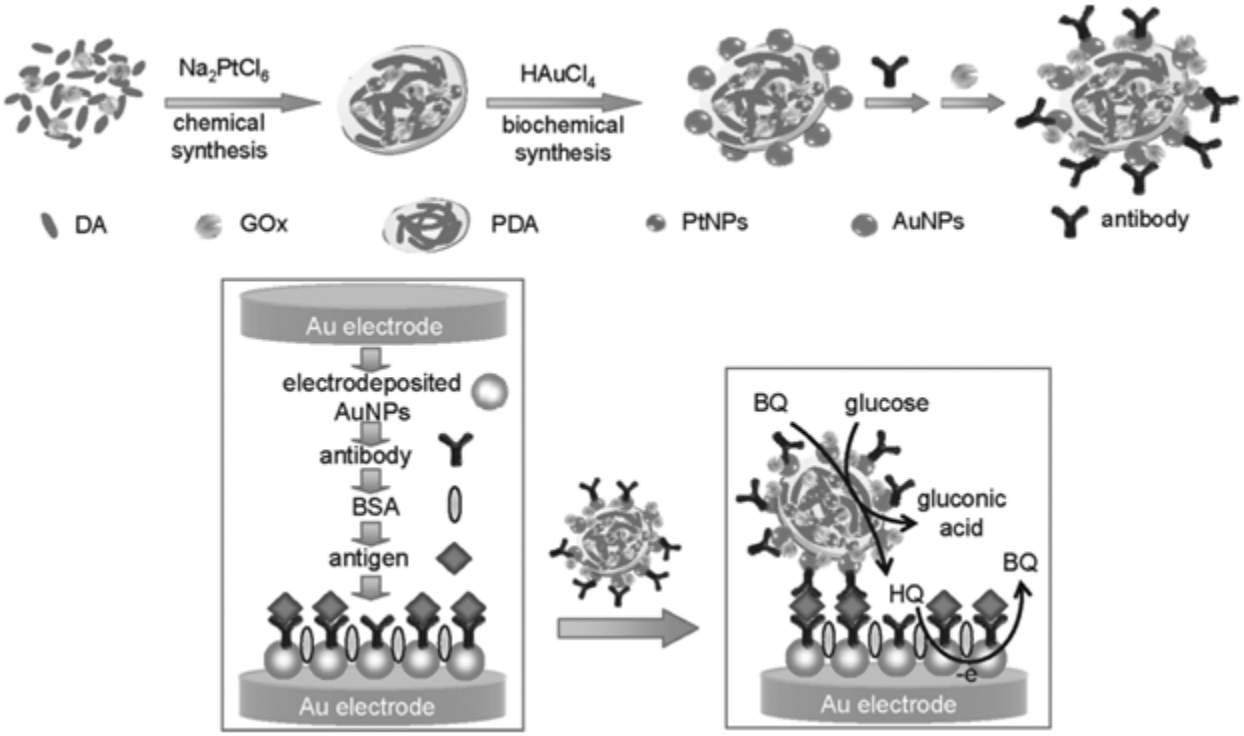

Figure 3.12. Polydopamine enables the fabrication of immunosensors. Polymeric bionanocomposites are constructed by mixing dopamine (DA), glucose oxidase (GOx), and Na_2PtCl_6; the platinum salt is reduced to yield platinum nanoparticles (PtNPs) and polydopamine-entrapped GOx. Gold nanoparticles (AuNPs) are then anchored to the polydopamine and used to attach antibodies, capable of interaction with the target antigen. Adapted from [213].

3.5.3 Membrane Separations

A final area of polydopamine application is membrane separations. Fouling represents a major obstacle in membrane-based water purification. The thin, hydrophilic nature of polydopamine coatings provides a means of imparting anti-fouling characteristics on a membrane while not imposing a significant mass transfer resistance that causes flux deterioration [128]. Many membrane surface modifications reported in the literature are challenging to implement industrially due to their complexity or specificity; polydopamine may prove to be a universal, aqueous-based solution [117].

Commercial membranes, including microfiltration, ultrafiltration, nanofiltration, and reverse osmosis membranes, have been modified with polydopamine, leading to improved fouling resistance when challenged with oil/water emulsions [217] and protein solutions [218]. Many membranes may be further modified by grafting PEG to a polydopamine coating, leading to further improvements in fouling resistance (Figure 3.13) [217]. Polydopamine and polydopamine-*g*-PEG modified membranes showed resistance to static protein [218] and bacteria [219] adhesion, but longer-term biofouling testing under flow conditions revealed no improvement over unmodified membranes [219,220].

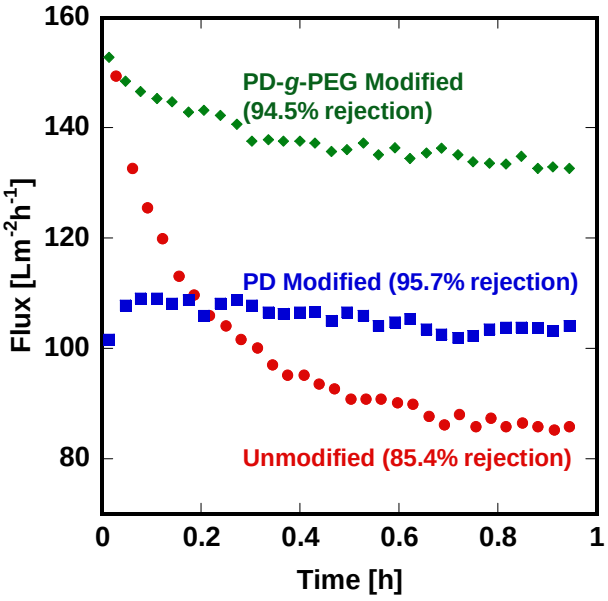

Figure 3.13. Oil-in-water emulsion fouling of unmodified, polydopamine modified (PD), and polydopamine-*g*-PEG modified (PD-*g*-PEG) PTFE microfiltration membranes (nominal pore size = 0.22 μm). Modified membranes show higher and more stable flux than the unmodified membrane. Modified membranes also show higher organic rejection due to pore constriction due to the polydopamine application. Adapted from [217].

Polydopamine has also been used in membrane fabrication. Composite membranes have been constructed with thin, defect-free skin layers of polydopamine atop a porous, hollow-fiber polysulfone support [221,222]. pH-responsive membranes were developed by grafting poly(acrylic acid) to a porous nylon support [114]. In addition to the use of polydopamine to form a selective layer, it has been used to facilitate the attachment of chitosan to poly(ether sulfone) ultrafiltration supports to form composite pervaporation membranes [223]. Improved pervaporation performance was also realized by coating PDMS membranes with polydopamine followed by electroless metallization to form silver/titanium dioxide microspheres [224]. Finally, Arena and coworkers was able to utilize commercial composite reverse osmosis membranes in a forward osmosis application by coating the underlying polysulfone ultrafiltration support membrane with polydopamine, achieving greatly increased water flux due to the hydrophilic surface modification [225].

3.6 OUTLOOK

Polydopamine has emerged in the last decade as a readily accessible synthetic melanin with structural, physical, and chemical properties shared by other melanins. Melanins as a whole have been subjects of study for well over a century and, as exemplified by the recent surge of interest in polydopamine, continue to exhibit surprising characteristics that have useful applications. Much of the contemporary interest stems from the polymer's ability to form highly robust coatings on diverse surfaces. The ensuing coatings are highly biocompatible, allowing polydopamine to serve as a general purpose surface modification agent for use in a range of biotechnological and nanotechnological applications.

Despite the practical significance of the polymer, the fundamental characterization of polydopamine remains challenging due to the limited scope of

characterization techniques available for its study, as well as its complex structure. Many of the structural models of polydopamine have proposed that the monomers are linked by covalent linkages, but new evidence indicates that non-covalent, supramolecular interactions may be dominant. Regardless of its structure, polydopamine exhibits a number of distinct physicochemical properties, including insolubility and broad chemical inertness (with the exception of strong oxidants or bases), semiconductive properties, strong light absorption, the ability to function both as a reductant and as an oxidant, and the presence of stable and persistent free radicals.

Contemporary interest in polydopamine has focused primarily on only a few of these features (*e.g.*, strong adhesion, resistance to fouling and corrosion, and conjugation of other molecules), leading to immediate applications in nanotechnology, biotechnology, and membrane science, but as the field continues to develop a broader array of utilities will likely emerge. Exploration of these new applications will require the intersection of diverse fields. For example, since the electronic and optoelectronic properties of polydopamine and other melanins were first discovered, it has been proposed that the materials may find utility in sensors, photovoltaics, energy storage devices, or photoprotective materials [84]. Few of these proposed applications have yet to be realized, however, and may depend on the development of derivatized forms of the dopamine monomer and/or polymer.

Both for reasons of fundamental curiosity and practical significance, polydopamine is likely to remain a subject of great interest in many research circles. Significant and essential questions remain, however, and the community is encouraged to pursue these questions (despite the difficulties associated with the material) in parallel with the ongoing development of the polymer's applications. Given the ubiquity of this

class of polymers in both natural and synthetic systems, the implications of advances in this field have a significance that few other broad classes of polymers can claim.

3.7 REFERENCES

[1] H. Lee, S.M. Dellatore, W.M. Miller, P.B. Messersmith, Mussel-Inspired Surface Chemistry for Multifunctional Coatings, Science 318 (5849) (2007) 426–430.

[2] L.M. McDowell, L.A. Burzio, J.H. Waite, J. Schaefer, Rotational Echo Double Resonance Detection of Cross-links Formed in Mussel Byssus under High-Flow Stress, Journal of Biological Chemistry 274 (29) (1999) 20293–20295.

[3] J.L. Dalsin, B.-H. Hu, B.P. Lee, P.B. Messersmith, Mussel adhesive protein mimetic polymers for the preparation of nonfouling surfaces, Journal of the American Chemical Society 125 (14) (2003) 4253–8.

[4] H. Lee, J. Rho, P.B. Messersmith, Facile Conjugation of Biomolecules onto Surfaces via Mussel Adhesive Protein Inspired Coatings, Advanced Materials 21 (4) (2009) 431–434.

[5] B.P. Lee, P.B. Messersmith, J.N. Israelachvili, J.H. Waite, Mussel-Inspired Adhesives and Coatings, Annual Review of Materials Research 41 (2011) 99–132.

[6] L.L. Iversen, The Catecholamines, Nature 214 (5083) (1967) 8–14.

[7] D.C.S. Tse, R.L. McCreery, R.N. Adams, Potential oxidative pathways of brain catecholamines, Journal of Medicinal Chemistry 19 (1) (1976) 37–40.

[8] M.D. Hawley, S. V Tatawawadi, S. Piekarski, R.N. Adams, Electrochemical studies of the oxidation pathways of catecholamines, Journal of the American Chemical Society 89 (2) (1967) 447–50.

[9] F. Bernsmann, A. Ponche, C. Ringwald, J. Hemmerlé, J. Raya, B. Bechinger, et al., Characterization of Dopamine−Melanin Growth on Silicon Oxide, Journal of Physical Chemistry C 113 (19) (2009) 8234–8242.

[10] R.F. Hurrell, P.-A. Finot, Nutritional consequences of the reactions between proteins and oxidized polyphenolic acids, Advances in Experimental Medicine and Biology 177 (1984) 423–435.

[11] L. Liu, K. Wakamatsu, S. Ito, P.R. Williamson, Catecholamine Oxidative Products, but Not Melanin, Are Produced by Cryptococcus neoformans during Neuropathogenesis in Mice, Infection and Immunity 67 (1) (1999) 108–112.

[12] A. Kulma, J. Szopa, Catecholamines are active compounds in plants, Plant Science 172 (3) (2007) 433–440.

[13] G. Prota, Melanins and Melanogenesis, Academic Press, Inc., San Diego, 1992.

[14] P.A. Riley, Melanin, International Journal of Biochemistry and Cell Biology 29 (11) (1997) 1235–1239.

[15] M.E. Lynge, R. van der Westen, A. Postma, B. Städler, Polydopamine--a nature-inspired polymer coating for biomedical science, Nanoscale 3 (12) (2011) 4916–28.

[16] A.A.R. Watt, J.P. Bothma, P. Meredith, The supramolecular structure of melanin, Soft Matter 5 (19) (2009) 3754.

[17] F.W. Jacobson, N. Millott, Phenolases and Melanogenesis in the Coelomic Fluid of the Echinoid Diadema antillarum Phillippi, Proceedings of the Royal Society of London B 141 (903) (1953) 231–47.

[18] P. Meredith, T. Sarna, The physical and chemical properties of eumelanin, Pigment Cell Research 19 (6) (2006) 572–94.

[19] J.A. Swift, Speculations on the molecular structure of eumelanin, International Journal of Cosmetic Science 31 (2) (2009) 143–50.

[20] IUPAC, Compendium of Chemical Terminology, 2nd ed., Blackwell Scientific Publications, Oxford, 1997.

[21] J.E. Purkyně, Bericht u̇ber die Versammlung deutscher Naturforscher und Aerzte in Prag im September 1837, Druck von G. Haase Sȯhne, Prague, 1838.

[22] G. Simon, Zür Entwickelungsgeschichte der Haare, Joh. Müllers Archiv Für Anatomie (1841) 367.

[23] J. Borovanský, History of Melanosome Research, in: P.A. Riley, J. Borovanský (Eds.), Melanins and Melanosomes: Biosynthesis, Biogenesis, Physiological, and Pathological Functions, Wiley-Blackwell, Weinheim, Germany, 2011: pp. 1–19.

[24] J.J. Berzelius, Lehrbuch der Chemie, Lehrbuch Der Chemie 9 (1840) 22–24.

[25] K.A.H. Mörner, Zur Kenntnis von der Farbstoffen der melanotischen Geschwülste, Zeitschrift Für Physiologische Chemie 11 (1887) 66–141.

[26] Landholt, Ueber das Melanin der Augenhäute, Hoppe-Seyler's Zeitschrift Für Physiologische Chemie 28 (1899) 192–211.

[27] E.E. Bourquelot, G. Bertrand, Sur la coloration des tissus et du suc de certains champignons au contact de l'air, Journal De Pharmacie Et De Chimie 3 (6) (1896) 177–182.

[28] E.E. Bourquelot, A. Bertrand, Le bleuissement et le noircissement des champignons, Comptes Rendus De l'Académie Des Sciences 2 (1895) 582–584.

[29] G. Bertrand, Sur une nouvelle oxydase, ou ferment solubleoxydant, d'origine vegetale, Comptes Rendus De l'Académie Des Sciences 122 (1896) 1215–1217.

[30] B. Bloch, Chemische Untersuchungen über das spezifische pigmentbildende Ferment der Haut, die Dopaoxydase, Zeitschrift Für Physiologische Chemie 98 (n.d.) 226–254.

[31] H.S. Raper, The Aerobic Oxidases, Physiological Reviews 8 (2) (1928) 245–282.

[32] H.S. Mason, The Chemistry of Melanin. III. Mechanism of Oxidation of 3,4-Dihydroxyphenylalanine by Tyrosinase, Journal of Biological Chemistry 172 (1948) 83–99.

[33] M. d'Ischia, A. Napolitano, A. Pezzella, 5,6-Dihydroxyindole Chemistry: Unexplored Opportunities Beyond Eumelanin, European Journal of Organic Chemistry 2011 (28) (2011) 5501–5516.

[34] S.S. Sulaimon, B.E. Kitchell, The biology of melanocytes, Veterinary Dermatology 14 (2) (2003) 57–65.

[35] K. Jimbow, W.C. Quevedo Jr., T.B. Fitzpatrick, G. Szabo, Some Aspects of Melanin Biology: 1950-1975, Journal of Investigative Dermatology 67 (1) (1976) 72–89.

[36] A.J. Miller, M.C. Mihm, Mechanisms of Disease: Melanoma, The New England Journal of Medicine 355 (1) (2006) 51–65.

[37] D.G. Graham, Oxidative Pathways for Catecholamines in the Genesis of Neuromelanin and Cytotoxic Quinones, Molecular Pharmacology 14 (4) (1978) 633–643.

[38] W.H. Harrison, W.W. Whisler, B.J. Hill, Catecholamine oxidation and ionization properties indicated from the H+ release, tritium exchange, and spectral changes which occur during ferricyanide oxidation, Biochemistry 7 (9) (1968) 3089–94.

[39] B. Zhu, S. Edmondson, Polydopamine-Melanin Initiators for Surface-Initiated ATRP, Polymer 52 (10) (2011) 2141–2149.

[40] S. Sánchez-Cortés, O. Francioso, J.. García-Ramos, C. Ciavatta, C. Gessa, Catechol polymerization in the presence of silver surface, Colloids and Surfaces A 176 (2-3) (2001) 177–184.

[41] A. Zhang, J. He, Y. Guan, Z. Li, Y. Zhang, J.X. Zhu, Oxidative polymerization of hydroquinone using deoxycholic acid supramolecular template, Science China Chemistry 55 (5) (2012) 830–835.

[42] A. Furlani, M. V Russo, F. Cataldo, Oxidative polymerization of p-benzoquinone and hydroquinone. Conductivity of doped and undoped polymerization products, Synthetic Metals 29 (1) (1989) 507–510.

[43] M.J. Sever, J.J. Wilker, Absorption spectroscopy and binding constants for first-row transition metal complexes of a DOPA-containing peptide, Dalton Transactions (6) (2006) 813–22.

[44] A. Bagheri Gh, Thermodynamic studies on complexation of dopamine with gadolinium(III) in water–ethanol system, Journal of Molecular Liquids 156 (2-3) (2010) 141–145.

[45] R.F. Jameson, G. Hunter, T. Kiss, A 1H nuclear magnetic resonance study of the deprotonation of L-dopa and adrenaline, Journal of the Chemical Society, Perkin Transactions 2 (7) (1980) 1105.

[46] Q. Wei, F. Zhang, J. Li, B. Li, C. Zhao, Oxidant-induced dopamine polymerization for multifunctional coatings, Polymer Chemistry 1 (9) (2010) 1430.

[47] S. Senoh, C.R. Creveling, S. Udenfriend, B. Witkop, Chemical, Enzymatic and Metabolic Studies on the Mechanism of Oxidation of Dopamine, Journal of the American Chemical Society 81 (23) (1959) 6236–6240.

[48] S. Senoh, B. Witkop, Formation and Rearrangements of Aminochromes from a New Metabolite of Dopamine and Some of its Derivatives, Journal of the American Chemical Society 81 (23) (1959) 6231–6235.

[49] J.A. Joule, K. Mills, Heterocyclic Chemistry, Wiley, Chichester, U.K., 2010.

[50] M. Kawase, Y. Miyake, Y. Kikugawa, Dehydrogenation of indolines to indoles via azasulphonium salts or N-chloramines, Journal of the Chemical Society, Perkin Transactions 1 (1984) 1401.

[51] A. Inada, Y. Nakamura, Y. Morita, An effective dehydrogenation of indolines to indoles with cobalt(II) Schiff's base complexes, Chemistry Letters 9 (10) (1980) 1287–1290.

[52] D.M. Ketcha, The manganese(III) acetate oxidation of N-protected indolines, Tetrahedron Letters 29 (18) (1988) 2151–2154.

[53] M.E. Kuehne, T.C. Hall, Oxidation of primary amines and indoline with palladium dichloride and gold trichloride, Journal of Organic Chemistry 41 (16) (1976) 2742–2746.

[54] A. Napolitano, A. Pezzella, G. Prota, R. Seraglia, P. Traldi, Structural Analysis of Synthetic Melanins from 5,6-Dihydroxyindole by Matrix-assisted Laser Desorption/Ionization Mass Spectrometry, Rapid Communications in Mass Spectrometry 10 (4) (1996) 468–472.

[55] M. d'Ischia, A. Napolitano, G. Prota, Oxidative Polymerization of 5,6-Dihydroxyindoles. Tracking the Biosynthetic Pathway to Melanin Pigments, Gazzetta Chimica Italiana 126 (12) (1996) 783–789.

[56] H. Okuda, K. Wakamatsu, S. Ito, T. Sota, Possible oxidative polymerization mechanism of 5,6-dihydroxyindole from ab initio calculations, Journal of Physical Chemistry A 112 (44) (2008) 11213–22.

[57] P. Palumbo, M. d'Ischia, G. Prota, Tyrosinase-promoted oxidation of 5, 6-dihydroxyindole-2-carboxylic acid to melanin. Isolation and characterization of oligomer intermediates, Tetrahedron 43 (18) (1987) 4203–4206.

[58] M.G. Corradoini, A. Napolitano, G. Prota, A biosynthetic approach to the structure of eumelanins. The isolation of oligomers from 5,6-dihydroxy-1-methylindole, Tetrahedron 42 (7) (1986) 2083–2088.

[59] M. d'Ischia, A. Napolitano, K. Tsiakas, G. Prota, New intermediates in the oxidative polymerisation of 5,6-dihydroxyindole to melanin promoted by the peroxidase/H_2O_2 system, Tetrahedron 46 (16) (1990) 5789–5796.

[60] P. Manini, M. D'Ischia, M. Milosa, G. Prota, Acid-Promoted Competing Pathways in the Oxidative Polymerization of 5,6-Dihydroxyindoles and Related Compounds: Straightforward Cyclotrimerization Routes to Diindolocarbazole Derivatives, Journal of Organic Chemistry 63 (20) (1998) 7002–7008.

[61] A. Pezzella, A. Napolitano, M. D'Ischia, G. Prota, Oxidative Polymerisation of 5,6-Dihydroxyindole-2-carboxylic Acid to Melanin: A New Insight, Tetrahedron 52 (23) (1996) 7913–7920.

[62] A. Pezzella, D. Vogna, G. Prota, Atropoisomeric melanin intermediates by oxidation of the melanogenic precursor 5,6-dihydroxyindole-2-carboxylic acid under biomimetic conditions, Tetrahedron 58 (19) (2002) 3681–3687.

[63] L. Panzella, A. Pezzella, A. Napolitano, M. D'Ischia, The first 5,6-dihydroxyindole tetramer by oxidation of 5,5',6,6'-tetrahydroxy- 2,4'-biindolyl and an unexpected issue of positional reactivity en route to eumelanin-related polymers, Organic Letters 9 (7) (2007) 1411–4.

[64] D.R. Dreyer, D.J. Miller, B.D. Freeman, D.R. Paul, C.W. Bielawski, Elucidating the Structure of Polydopamine, Langmuir 28 (15) (2012) 6428–6435.

[65] G.A. Swan, Structure, chemistry, and biosynthesis of the melanins, Progress in the Chemistry of Organic Natural Products 31 (1974) 521–582.

[66] T.F. Headen, C.A. Howard, N.T. Skipper, M.A. Wilkinson, D.T. Bowron, A.K. Soper, Structure of π-π Interactions in Aaromatic Liquids, Journal of the American Chemical Society 132 (16) (2010) 5735–42.

[67] M.O. Sinnokrot, C.D. Sherrill, High-accuracy quantum mechanical studies of pi-pi interactions in benzene dimers, The Journal of Physical Chemistry A 110 (37) (2006) 10656–68.

[68] B.-L.L. Seagle, K.A. Rezai, E.M. Gasyna, Y. Kobori, K.A. Rezaei, J.R. Norris, Time-resolved detection of melanin free radicals quenching reactive oxygen species, Journal of the American Chemical Society 127 (32) (2005) 11220–1.

[69] A.O. Patil, W.T. Pennington, G.R. Desiraju, D.Y. Curtin, I.C. Paul, Recent Studies on the Formation and Properties of Quinhydrone Complexes, Molecular Crystals and Liquid Crystals 134 (1) (1986) 279–304.

[70] J. Scheffer, Y.F. Wong, A.O. Patil, D.Y. Curtin, I.C. Paul, CPMAS (cross-polarization magic angle spinning) carbon-13 NMR spectra of quinones, hydroquinones, and their complexes. Use of CMR to follow a reaction in the solid state, Journal of the American Chemical Society 107 (17) (1985) 4898–4904.

[71] R.P. Sijbesma, F.H. Beijer, L. Brunsveld, B.J.B. Folmer, J.H.K.K. Hirschberg, R.F.M. Lange, et al., Reversible Polymers Formed from Self-Complementary Monomers Using Quadruple Hydrogen Bonding, Science 278 (5343) (1997) 1601–1604.

[72] H. Kautz, D.J.M. van Beek, R.P. Sijbesma, E.W. Meijer, Cooperative End-to-End and Lateral Hydrogen-Bonding Motifs in Supramolecular Thermoplastic Elastomers, Macromolecules 39 (13) (2006) 4265–4267.

[73] S. Yagai, T. Iwashima, T. Karatsu, A. Kitamura, Synthesis and noncovalent polymerization of self-complementary hydrogen-bonding supramolecular synthons: N,N'-disubstituted 4,6-diamino-pyrimidin-2(1H)-ones, Chemical Communications (9) (2004) 1114–1115.

[74] J. von Byern, I. Grunwald, Biological Adhesive Systems: From Nature to Technical and Medical Application, Springer, Vienna, 2010.

[75] A.R. Hirst, B. Escuder, J.F. Miravet, D.K. Smith, High-tech Applications of Self-Assembling Supramolecular Nanostructured Gel-Phase Materials: From Regenerative Medicine to Electronic Devices, Angewandte Chemie International Edition 47 (42) (2008) 8002–18.

[76] D.A. Uhlenheuer, K. Petkau, L. Brunsveld, Combining supramolecular chemistry with biology, Chemical Society Reviews 39 (8) (2010) 2817–2826.

[77] H. Cui, M.J. Webber, S.I. Stupp, Self-assembly of peptide amphiphiles: from molecules to nanostructures to biomaterials, Biopolymers 94 (1) (2010) 1–18.

[78] G.E. Orchard, E. Calonje, The Effect of Melanin Bleaching on Immunohistochemical Staining in Heavily Pigmented Melanocytic Neoplasms, The American Journal of Dermatopathology 20 (4) (1998) 357–361.

[79] W. Korytowski, T. Sarna, Bleaching of Melanin Pigments, The Journal of Biological Chemistry 265 (21) (1990) 12410–12416.

[80] M. Piattelli, E. Fattorusso, S. Magno, R.A. Nicolaus, The Structure of Melanins and Melanogenesis—III, Tetrahedron 19 (12) (1963) 2061–2072.

[81] G.W. Zajac, J.M. Gallas, J. Cheng, M. Eisner, S.C. Moss, A.E. Alvarado-Swaisgood, The fundamental unit of synthetic melanin: a verification by tunneling microscopy of X-ray scattering results, Biochimica Et Biophysica Acta 1199 (3) (1994) 271–278.

[82] K.B. Stark, J.M. Gallas, G.W. Zajac, J.T. Golab, S. Gidanian, T. McIntire, et al., Effect of stacking and redox state on optical absorption spectra of melanins --

comparison of theoretical and experimental results, Journal of Physical Chemistry B 109 (5) (2005) 1970–7.

[83] E. Kaxiras, A. Tsolakidis, G. Zonios, S. Meng, Structural Model of Eumelanin, Physical Review Letters 97 (21) (2006) 218102/1–218102/4.

[84] M. d'Ischia, A. Napolitano, A. Pezzella, P. Meredith, T. Sarna, Chemical and structural diversity in eumelanins: unexplored bio-optoelectronic materials, Angewandte Chemie International Edition 48 (22) (2009) 3914–21.

[85] C.M.R. Clancy, J.D. Simon, Ultrastructural Organization of Eumelanin from Sepia officinalis Measured by Atomic Force Microscopy, Biochemistry 40 (44) (2001) 13353–13360.

[86] H.C. Longuet-Higgins, On the origin of the free radical property of melanins, Archives of Biochemistry and Biophysics 86 (2) (1960) 231–232.

[87] J. McGinness, P. Corry, P. Proctor, Amorphous Semiconductor Switching in Melanins, Science 183 (4127) (1974) 853–855.

[88] J. Filatovs, J. McGinness, P. Corry, Thermal and electronic contributions to switching in melanins, Biopolymers 15 (11) (1976) 2309–12.

[89] P.R. Crippa, V. Cristofoletti, N. Romeo, A band model for melanin deduced from optical absorption and photoconductivity experiments, Biochimica Et Biophysica Acta - General Subjects 538 (1) (1978) 164–170.

[90] A. Pullman, B. Pullman, The band structure of melanins, Biochimica Et Biophysica Acta 54 (2) (1961) 384–385.

[91] M.M. Jastrzebska, H. Isotalo, J. Paloheimo, H. Stubb, Electrical conductivity of synthetic DOPA-melanin polymer for different hydration states and temperatures, Journal of Biomaterials Science, Polymer Edition 7 (7) (1996) 577–586.

[92] M.M. Jastrzebska, K. Stepień, J. Wilczok, M. Porebska-Budny, T. Wilczok, Semiconductor properties of melanins prepared from catecholamines, General Physiology and Biophysics 9 (4) (1990) 373–83.

[93] L. Morresi, M. Ficcadenti, N. Pinto, R. Murri, M. Cuccioloni, M. Angeletti, et al., Optical and electrical behavior of synthetic melanin thin films spray-coated, Energy Procedia 2 (1) (2010) 177–182.

[94] M.L. Wolbarsht, A.W. Walsh, G. George, Melanin, a unique biological absorber, Applied Optics 20 (13) (1981) 2184.

[95] J. Riesz, J. Gilmore, P. Meredith, Quantitative Scattering of Melanin Solutions, Biophysical Journal 90 (11) (2006) 4137–44.

[96] I.A. Vitkin, J. Woolsey, B.C. Wilson, R.R. Anderson, Optical and Thermal Characterization of Natural (Sepia officinalis) Melanin, Photochemistry and Photobiology 59 (4) (1994) 455–462.

[97] P. Meredith, J. Riesz, Radiative Relaxation Quantum Yields for Synthetic Eumelanin, Photochemistry and Photobiology 79 (2) (2004) 211.

[98] V. Horak, J.R. Gillette, A Study of the Oxidation-Reduction State of Synthetic 3,4-Dihydroxy-DL-phenylalanine Melanin, Molecular Pharmacology 7 (4) (1971) 429–33.

[99] M.J. LaVoie, B.L. Ostaszewski, A. Weihofen, M.G. Schlossmacher, D.J. Selkoe, Dopamine covalently modifies and functionally inactivates parkin, Nature Medicine 11 (11) (2005) 1214–21.

[100] C.J. Cooksey, E.J. Land, F.A.P. Rushton, C.A. Ramsden, P.A. Riley, Tyrosinase-Mediated Cytotoxicity of 4-Substituted Phenols: Use of QSAR to Forecast Reactivities of Thiols towards the Derived ortho -Quinones, Quantitative Structure-Activity Relationships 15 (6) (1996) 498–503.

[101] W. Wang, Y. Jiang, Y. Liao, M. Tian, H. Zou, L. Zhang, Fabrication of silver-coated silica microspheres through mussel-inspired surface functionalization, Journal of Colloid and Interface Science 358 (2) (2011) 567–574.

[102] B. Fei, B. Qian, Z. Yang, R. Wang, W. Liu, C. Mak, et al., Coating carbon nanotubes by spontaneous oxidative polymerization of dopamine, Carbon 46 (13) (2008) 1795–1797.

[103] Y. Mi, Z. Wang, X. Liu, S. Yang, H. Wang, J. Ou, et al., A simple and feasible in-situ reduction route for preparation of graphene lubricant films applied to a variety of substrates, Journal of Materials Chemistry 22 (16) (2012) 8036–8042.

[104] L.Q. Xu, W.J. Yang, K.-G. Neoh, E.-T. Kang, G.D. Fu, Dopamine-Induced Reduction and Functionalization of Graphene Oxide Nanosheets, Macromolecules 43 (20) (2010) 8336–8339.

[105] H. Liu, P. Xi, G. Xie, Y. Shi, F. Hou, L. Huang, et al., Simultaneous Reduction and Surface Functionalization of Graphene Oxide for Hydroxyapatite Mineralization, The Journal of Physical Chemistry C 116 (5) (2012) 3334–3341.

[106] M.G. Bridelli, P.R. Crippa, Infrared and water sorption studies of the hydration structure and mechanism in natural and synthetic melanin, The Journal of Physical Chemistry B 114 (29) (2010) 9381–90.

[107] J. Ryu, S.H. Ku, H. Lee, C.B. Park, Mussel-Inspired Polydopamine Coating as a Universal Route to Hydroxyapatite Crystallization, Advanced Functional Materials 20 (13) (2010) 2132–2139.

[108] L.A. Burzio, J.H. Waite, Cross-Linking in Adhesive Quinoproteins: Studies with Model Decapeptides, Biochemistry 39 (36) (2000) 11147–11153.

[109] R. Zeng, Z. Luo, D. Zhou, F. Cao, Y. Wang, A novel PEG coating immobilized onto capillary through polydopamine coating for separation of proteins in CE, Electrophoresis 31 (19) (2010) 3334–41.

[110] J.L. Dalsin, P.B. Messersmith, Bioinspired antifouling polymers, Materials Today 8 (9) (2005) 38–46.

[111] M. Pasenkiewicz-Gierula, R.C. Sealy, Analysis of the ESR spectrum of synthetic dopa melanin, Biochimica Et Biophysica Acta - General Subjects 884 (3) (1986) 510–516.

[112] L.Q. Xu, H. Jiang, K.-G. Neoh, E.-T. Kang, G.D. Fu, Poly(dopamine acrylamide)-co-poly(propargyl acrylamide)-modified titanium surfaces for "click" functionalization, Polymer Chemistry 3 (4) (2012) 920.

[113] M.D. Rubianes, M.C. Strumia, Polyethylenimine Functionalized with Dopamine: Characterization and Electrocatalytic Properties, Electroanalysis 22 (11) (2010) 1200–1206.

[114] C.Y. Li, W.C. Wang, F.J. Xu, L.Q. Zhang, W.T. Yang, Preparation of pH-sensitive membranes via dopamine-initiated atom transfer radical polymerization, Journal of Membrane Science 367 (1-2) (2011) 7–13.

[115] F. Bernsmann, V. Ball, F. Addiego, A. Ponche, M. Michel, J.J. de A. Gracio, et al., Dopamine-Melanin Film Deposition Depends on the Used Oxidant and Buffer Solution, Langmuir 27 (6) (2011) 2819–2825.

[116] S. Chen, Y. Chen, Y. Lei, Y. Yin, Novel strategy in enhancing stability and corrosion resistance for hydrophobic functional films on copper surfaces, Electrochemistry Communications 11 (8) (2009) 1675–1679.

[117] Z.-Y. Xi, Y.-Y. Xu, L.-P. Zhu, Y. Wang, B.-K. Zhu, A facile method of surface modification for hydrophobic polymer membranes based on the adhesive behavior of poly(DOPA) and polydopamine, Journal of Membrane Science 327 (1-2) (2009) 244–253.

[118] F. Yu, S. Chen, Y. Chen, H. Li, L. Yang, Y. Chen, et al., Experimental and theoretical analysis of polymerization reaction process on the polydopamine membranes and its corrosion protection properties for 304 Stainless Steel, Journal of Molecular Structure 982 (1-3) (2010) 152–161.

[119] B.H. Kim, D.H. Lee, J.Y. Kim, D.O. Shin, H.Y. Jeong, S. Hong, et al., Mussel-inspired block copolymer lithography for low surface energy materials of teflon, graphene, and gold, Advanced Materials 23 (47) (2011) 5618–22.

[120] J. Jiang, L. Zhu, L. Zhu, B. Zhu, Y. Xu, Surface characteristics of a self-polymerized dopamine coating deposited on hydrophobic polymer films, Langmuir 27 (23) (2011) 14180–7.

[121] H. Lee, N.F. Scherer, P.B. Messersmith, Single-molecule mechanics of mussel adhesion, Proceedings of the National Academy of Sciences of the United States of America 103 (35) (2006) 12999–3003.

[122] J. Ou, J. Wang, S. Liu, J. Zhou, S. Ren, S. Yang, Microtribological and electrochemical corrosion behaviors of polydopamine coating on APTS-SAM modified Si substrate, Applied Surface Science 256 (3) (2009) 894–899.

[123] J. Ou, J. Wang, S. Liu, J. Zhou, S. Yang, Self-Assembly and Tribological Property of a Novel 3-Layer Organic Film on Silicon Wafer with Polydopamine Coating as the Interlayer, Journal of Physical Chemistry C 113 (47) (2009) 20429–20434.

[124] J. Ou, J. Wang, Y. Qiu, L. Liu, S. Yang, Mechanical property and corrosion resistance of zirconia/polydopamine nanocomposite multilayer films fabricated via a novel non-electrostatic layer-by-layer assembly technique, Surface and Interface Analysis 43 (4) (2011) 803–808.

[125] H. Zhang, H. Hu, W. Ye, F. Zhou, Conferring polytetrafluoroethylene micropowders with hydrophilicity using dopamine chemistry and the application as water-based lubricant additive, Journal of Applied Polymer Science 122 (5) (2011) 3145–3151.

[126] F. Yu, S. Chen, H. Li, L. Yang, Y. Yin, Application of Self Assembled 6-aminohexanol layers for corrosion protection of 304 stainless steel surface, Thin Solid Films 520 (15) (2012) 4990–4995.

[127] T.H. Anderson, J. Yu, A. Estrada, M.U. Hammer, J.H. Waite, J.N. Israelachvili, The Contribution of DOPA to Substrate-Peptide Adhesion and Internal Cohesion of Mussel-Inspired Synthetic Peptide Films, Advanced Functional Materials 20 (23) (2010) 4196–4205.

[128] B.D. McCloskey, H.B. Park, H. Ju, B.W. Rowe, D.J. Miller, B.J. Chun, et al., Influence of Polydopamine Deposition Conditions on Pure Water Flux and Foulant Adhesion Resistance of Reverse Osmosis, Ultrafiltration, and Microfiltration Membranes, Polymer 51 (15) (2010) 3472–3485.

[129] H. Lee, Y. Lee, A.R. Statz, J. Rho, T.G. Park, P.B. Messersmith, Substrate-Independent Layer-by-Layer Assembly by Using Mussel-Adhesive-Inspired Polymers, Advanced Materials 20 (9) (2008) 1619–1623.

[130] H.-W. Chien, W.-H. Kuo, M.-J. Wang, S.-W. Tsai, W.-B. Tsai, Tunable Micropatterned Substrates Based on Polydopamine Deposition via Microcontact Printing, Langmuir 28 (13) (2012) 5775–82.

[131] J.-J. Feng, P.-P. Zhang, A.-J. Wang, Q.-C. Liao, J.-L. Xi, J.-R. Chen, One-step synthesis of monodisperse polydopamine-coated silver core–shell nanostructures for enhanced photocatalysis, New Journal of Chemistry 36 (1) (2012) 148.

[132] Z. Gao, N.I. Walton, A. Malugin, H. Ghandehari, I. Zharov, Preparation of dopamine-modified boron nanoparticles, Journal of Materials Chemistry 22 (3) (2012) 877–882.

[133] Z. Iqbal, S. Alsudir, M. Miah, E.P.C. Lai, Rapid CE-UV binding tests of environmentally hazardous compounds with polymer-modified magnetic nanoparticles, Electrophoresis (2011) 2181–2187.

[134] J. Si, H. Yang, Preparation and characterization of bio-compatible Fe3O4@Polydopamine spheres with core/shell nanostructure, Materials Chemistry and Physics 128 (3) (2011) 519–524.

[135] W. Wang, A. Zhang, L. Liu, M. Tian, L. Zhang, Dopamine-Induced Surface Functionalization for the Preparation of Al–Ag Bimetallic Microspheres, Journal of The Electrochemical Society 158 (4) (2011) D228.

[136] W. Wang, Y. Jiang, S. Wen, L. Liu, L. Zhang, Preparation and characterization of polystyrene/Ag core-shell microspheres--a bio-inspired polydopamine approach, Journal of Colloid and Interface Science 368 (1) (2012) 241–9.

[137] B. Çelen, D. Ekiz, E. Pişkin, G. Demirel, Green catalysts based on bio-inspired polymer coatings and electroless plating of silver nanoparticles, Journal of Molecular Catalysis A: Chemical 350 (1-2) (2011) 97–102.

[138] H. Hu, B. Yu, Q. Ye, Y. Gu, F. Zhou, Modification of carbon nanotubes with a nanothin polydopamine layer and polydimethylamino-ethyl methacrylate brushes, Carbon 48 (8) (2010) 2347–2353.

[139] M. Lai, K. Cai, L. Zhao, X. Chen, Y. Hou, Z. Yang, Surface functionalization of TiO2 nanotubes with bone morphogenetic protein 2 and its synergistic effect on the differentiation of mesenchymal stem cells, Biomacromolecules 12 (4) (2011) 1097–105.

[140] M. Lee, S.H. Ku, J. Ryu, C.B. Park, Mussel-inspired functionalization of carbon nanotubes for hydroxyapatite mineralization, Journal of Materials Chemistry 20 (40) (2010) 8848.

[141] W. Ye, H. Hu, H. Zhang, F. Zhou, W. Liu, Multi-walled carbon nanotube supported Pd and Pt nanoparticles with high solution affinity for effective electrocatalysis, Applied Surface Science 256 (22) (2010) 6723–6728.

[142] J. Feng, M. Sun, J. Li, L. Xu, X. Liu, S. Jiang, Polydopamine supported preparation method for solid-phase microextraction coatings on stainless steel wire, Journal of Chromatography A 1218 (23) (2011) 3601–7.

[143] J. Feng, M. Sun, L. Xu, J. Li, X. Liu, S. Jiang, Preparation of metal wire supported solid-phase microextraction fiber coated with multi-walled carbon nanotubes, Journal of Separation Science 34 (18) (2011) 2482–8.

[144] H. Jiang, L. Yang, C. Li, C. Yan, P.S. Lee, J. Ma, High–rate electrochemical capacitors from highly graphitic carbon–tipped manganese oxide/mesoporous carbon/manganese oxide hybrid nanowires, Energy & Environmental Science 4 (5) (2011) 1813.

[145] L. Yang, S.L. Phua, J.K.H. Teo, C.L. Toh, S.K. Lau, J. Ma, et al., A biomimetic approach to enhancing interfacial interactions: polydopamine-coated clay as reinforcement for epoxy resin, ACS Applied Materials & Interfaces 3 (8) (2011) 3026–32.

[146] S. Hong, J.S. Lee, J. Ryu, S.H. Lee, D.Y. Lee, D.-P. Kim, et al., Bio-inspired strategy for on-surface synthesis of silver nanoparticles for metal/organic hybrid nanomaterials and LDI-MS substrates, Nanotechnology 22 (49) (2011) 494020.

[147] F. Li, L. Yang, C. Zhao, Z. Du, Electroactive gold nanoparticles/polyaniline/polydopamine hybrid composite in neutral solution as high-performance sensing platform, Analytical Methods 3 (7) (2011) 1601.

[148] Y. Liao, B. Cao, W.-C. Wang, L. Zhang, D. Wu, R. Jin, A facile method for preparing highly conductive and reflective surface-silvered polyimide films, Applied Surface Science 255 (19) (2009) 8207–8212.

[149] Y. Long, J. Wu, H. Wang, X. Zhang, N. Zhao, J. Xu, Rapid sintering of silver nanoparticles in an electrolyte solution at room temperature and its application to fabricate conductive silver films using polydopamine as adhesive layers, Journal of Materials Chemistry 21 (13) (2011) 4875–4881.

[150] M. Zhang, X. He, L. Chen, Y. Zhang, Preparation of IDA-Cu functionalized core–satellite Fe3O4/polydopamine/Au magnetic nanocomposites and their application for depletion of abundant protein in bovine blood, Journal of Materials Chemistry 20 (47) (2010) 10696.

[151] W. Ye, D. Wang, H. Zhang, F. Zhou, W. Liu, Electrochemical growth of flowerlike gold nanoparticles on polydopamine modified ITO glass for SERS application, Electrochimica Acta 55 (6) (2010) 2004–2009.

[152] M. Sureshkumar, P.-N. Lee, C.-K. Lee, Stepwise assembly of multimetallic nanoparticles via self-polymerized polydopamine, Journal of Materials Chemistry 21 (33) (2011) 12316.

[153] T. Akter, W.S. Kim, Reversibly stretchable transparent conductive coatings of spray-deposited silver nanowires, ACS Applied Materials & Interfaces 4 (4) (2012) 1855–9.

[154] Q. Liu, B. Yu, W. Ye, F. Zhou, Highly selective uptake and release of charged molecules by pH-responsive polydopamine microcapsules, Macromolecular Bioscience 11 (9) (2011) 1227–34.

[155] B. Yu, D.A. Wang, Q. Ye, F. Zhou, W. Liu, Robust polydopamine nano/microcapsules and their loading and release behavior, Chemical Communications (44) (2009) 6789–91.

[156] A. Postma, Y. Yan, Y. Wang, A.N. Zelikin, E. Tjipto, F. Caruso, Self-Polymerization of Dopamine as a Versatile and Robust Technique to Prepare Polymer Capsules, Chemistry of Materials 21 (14) (2009) 3042–3044.

[157] L. Zhang, J. Shi, Z. Jiang, Y. Jiang, R. Meng, Y. Zhu, et al., Facile preparation of robust microcapsules by manipulating metal-coordination interaction between biomineral layer and bioadhesive layer, ACS Applied Materials & Interfaces 3 (2) (2011) 597–605.

[158] J. Cui, Y. Wang, A. Postma, J. Hao, L. Hosta-Rigau, F. Caruso, Monodisperse Polymer Capsules: Tailoring Size, Shell Thickness, and Hydrophobic Cargo Loading via Emulsion Templating, Advanced Functional Materials 20 (10) (2010) 1625–1631.

[159] H. Xu, X. Liu, D. Wang, Interfacial Basicity-Guided Formation of Polydopamine Hollow Capsules in Pristine O/W Emulsions – Toward Understanding of Emulsion Template Roles, Chemistry of Materials 23 (23) (2011) 5105–5110.

[160] Y. Zheng, L. Zhang, J. Shi, Y. Liang, X. Wang, Z. Jiang, Mussel-inspired surface capping and pore filling to confer mesoporous silica with high loading and enhanced stability of enzyme, Microporous and Mesoporous Materials 152 (2012) 122–127.

[161] J. Peng, L.-N. Feng, K. Zhang, J.-J. Li, L.-P. Jiang, J.-J. Zhu, Multifunctional manganese carbonate microspheres with superparamagnetic and fluorescent properties: synthesis and biological application, Chemistry 17 (39) (2011) 10916–23.

[162] Y. Ren, J.G. Rivera, L. He, H. Kulkarni, D.-K. Lee, P.B. Messersmith, Facile, high efficiency immobilization of lipase enzyme on magnetic iron oxide nanoparticles via a biomimetic coating, BMC Biotechnology 11 (2011) 63.

[163] M. Sureshkumar, C.-K. Lee, Polydopamine coated magnetic-chitin (MCT) particles as a new matrix for enzyme immobilization, Carbohydrate Polymers 84 (2) (2011) 775–780.

[164] C. Tao, S. Yang, J. Zhang, J. Wang, Surface modification of diamond-like carbon films with protein via polydopamine inspired coatings, Applied Surface Science 256 (1) (2009) 294–297.

[165] J. Xie, P.L. Michael, S. Zhong, B. Ma, M.R. MacEwan, C.T. Lim, Mussel inspired protein-mediated surface modification to electrospun fibers and their potential biomedical applications, Journal of Biomedical Materials Research A 100 (4) (2012) 929–38.

[166] L.-P. Zhu, J.-H. Jiang, B.-K. Zhu, Y.-Y. Xu, Immobilization of bovine serum albumin onto porous polyethylene membranes using strongly attached polydopamine as a spacer, Colloids and Surfaces B: Biointerfaces 86 (1) (2011) 111–8.

[167] J. Ou, J. Wang, D. Zhang, P. Zhang, S. Liu, P. Yan, et al., Fabrication and biocompatibility investigation of TiO(2) films on the polymer substrates obtained via a novel and versatile route, Colloids and Surfaces B: Biointerfaces 76 (1) (2010) 123–7.

[168] C.K. Poh, Z. Shi, T.Y. Lim, K.G. Neoh, W. Wang, The effect of VEGF functionalization of titanium on endothelial cells in vitro, Biomaterials 31 (7) (2010) 1578–85.

[169] W. Shen, K. Cai, Z. Yang, Y. Yan, W. Yang, P. Liu, Improved endothelialization of NiTi alloy by VEGF functionalized nanocoating, Colloids and Surfaces B: Biointerfaces 94 (2012) 347–53.

[170] Y.M. Shin, Y. Bin Lee, H. Shin, Time-dependent mussel-inspired functionalization of poly(L-lactide-co-ε-caprolactone) substrates for tunable cell behaviors, Colloids and Surfaces B: Biointerfaces 87 (1) (2011) 79–87.

[171] S.H. Ku, J. Ryu, S.K. Hong, H. Lee, C.B. Park, General functionalization route for cell adhesion on non-wetting surfaces, Biomaterials 31 (9) (2010) 2535–41.

[172] S.H. Ku, C.B. Park, Human endothelial cell growth on mussel-inspired nanofiber scaffold for vascular tissue engineering, Biomaterials 31 (36) (2010) 9431–7.

[173] N.G. Rim, S.J. Kim, Y.M. Shin, I. Jun, D.W. Lim, J.H. Park, et al., Mussel-inspired surface modification of poly(L-lactide) electrospun fibers for modulation of osteogenic differentiation of human mesenchymal stem cells, Colloids and Surfaces B: Biointerfaces 91 (2012) 189–97.

[174] W.-B. Tsai, W.-T. Chen, H.-W. Chien, W.-H. Kuo, M.-J. Wang, Polydopamine coating of scaffolds for articular cartilage tissue engineering, Acta Biomaterialia 7 (12) (2011) 4187–94.

[175] C. Wu, W. Fan, J. Chang, Y. Xiao, Mussel-inspired porous SiO_2 scaffolds with improved mineralization and cytocompatibility for drug delivery and bone tissue engineering, Journal of Materials Chemistry 21 (45) (2011) 18300.

[176] P. Yan, J. Wang, L. Wang, B. Liu, Z. Lei, S. Yang, The in vitro biomineralization and cytocompatibility of polydopamine coated carbon nanotubes, Applied Surface Science 257 (11) (2011) 4849–4855.

[177] J. Ryu, S.H. Ku, M. Lee, C.B. Park, Bone-like peptide/hydroxyapatite nanocomposites assembled with multi-level hierarchical structures, Soft Matter 7 (16) (2011) 7201.

[178] K.J. Jeong, L. Wang, C.F. Stefanescu, M.W. Lawlor, J. Polat, C.H. Dohlman, et al., Polydopamine coatings enhance biointegration of a model polymeric implant, Soft Matter 7 (18) (2011) 8305.

[179] L. Wang, K.J. Jeong, H.H. Chiang, D. Zurakowski, I. Behlau, J. Chodosh, et al., Hydroxyapatite for keratoprosthesis biointegration, Investigative Ophthalmology & Visual Science 52 (10) (2011) 7392–9.

[180] A. Liu, L. Zhao, H. Bai, H. Zhao, X. Xing, G. Shi, Polypyrrole actuator with a bioadhesive surface for accumulating bacteria from physiological media, ACS Applied Materials & Interfaces 1 (4) (2009) 951–5.

[181] K. Sun, Y. Xie, D. Ye, Y. Zhao, Y. Cui, F. Long, et al., Mussel-inspired anchoring for patterning cells using polydopamine, Langmuir 28 (4) (2012) 2131–6.

[182] S.H. Ku, J.S. Lee, C.B. Park, Spatial Control of Cell Adhesion and Patterning through Mussel-Inspired Surface Modification by Polydopamine, Langmuir 26 (6) (2010) 15104–15108.

[183] S.H. Yang, S.M. Kang, K.-B. Lee, T.D. Chung, H. Lee, I.S. Choi, Mussel-inspired encapsulation and functionalization of individual yeast cells, Journal of the American Chemical Society 133 (9) (2011) 2795–7.

[184] S. Kang, M. Elimelech, Bioinspired single bacterial cell force spectroscopy, Langmuir 25 (17) (2009) 9656–9.

[185] K. Kang, I.S. Choi, Y. Nam, A biofunctionalization scheme for neural interfaces using polydopamine polymer, Biomaterials 32 (27) (2011) 6374–80.

[186] E.M. Van Wagner, A.C. Sagle, M.M. Sharma, Y.-H. La, B.D. Freeman, Surface Modification of Commercial Polyamide Desalination Membranes using Poly(ethylene glycol) Diglycidyl Ether to Enhance Membrane Fouling Resistance, Journal of Membrane Science 367 (1-2) (2011) 273–287.

[187] O. Pop-Georgievski, Š. Popelka, M. Houska, D. Chvostová, V. Proks, F. Rypáček, Poly(ethylene oxide) layers grafted to dopamine-melanin anchoring layer: stability and resistance to protein adsorption, Biomacromolecules 12 (9) (2011) 3232–42.

[188] M. Sureshkumar, D.Y. Siswanto, C.-K. Lee, Magnetic antimicrobial nanocomposite based on bacterial cellulose and silver nanoparticles, Journal of Materials Chemistry 20 (33) (2010) 6948.

[189] H. Xu, X. Shi, H. Ma, Y. Lv, L. Zhang, Z. Mao, The preparation and antibacterial effects of dopa-cotton/AgNPs, Applied Surface Science 257 (15) (2011) 6799–6803.

[190] T.S. Sileika, H.-D. Kim, P. Maniak, P.B. Messersmith, Antibacterial performance of polydopamine-modified polymer surfaces containing passive and active components, ACS Applied Materials & Interfaces 3 (12) (2011) 4602–10.

[191] T. Shalev, A. Gopin, M. Bauer, R.W. Stark, S. Rahimipour, Non-leaching antimicrobial surfaces through polydopamine bio-inspired coating of quaternary ammonium salts or an ultrashort antimicrobial lipopeptide, Journal of Materials Chemistry 22 (5) (2012) 2026.

[192] J. Kuang, P.B. Messersmith, Universal surface-initiated polymerization of antifouling zwitterionic brushes using a mussel-mimetic Peptide initiator, Langmuir 28 (18) (2012) 7258–66.

[193] R. Wang, K.G. Neoh, Z. Shi, E.-T. Kang, P.A. Tambyah, E. Chiong, Inhibition of Escherichia coli and Proteus mirabilis adhesion and biofilm formation on medical grade silicone surface, Biotechnology and Bioengineering 109 (2) (2012) 336–45.

[194] C.S.O. Paulo, M. Vidal, L.S. Ferreira, Antifungal nanoparticles and surfaces, Biomacromolecules 11 (10) (2010) 2810–7.

[195] R. Ouyang, J. Lei, H. Ju, Surface molecularly imprinted nanowire for protein specific recognition, Chemical Communications (44) (2008) 5761–3.

[196] W.-H. Zhou, C.-H. Lu, X.-C. Guo, F.-R. Chen, H.-H. Yang, X.-R. Wang, Mussel-inspired molecularly imprinted polymer coating superparamagnetic nanoparticles for protein recognition, Journal of Materials Chemistry 20 (5) (2010) 880.

[197] R. Ouyang, J. Lei, H. Ju, Artificial receptor-functionalized nanoshell: facile preparation, fast separation and specific protein recognition, Nanotechnology 21 (18) (2010) 185502.

[198] M. Jia, L. Qin, X.-W. He, W.-Y. Li, Preparation and application of lysozyme imprinted monolithic column with dopamine as the functional monomer, Journal of Materials Chemistry 22 (2) (2012) 707.

[199] X.-B. Yin, D.-Y. Liu, Polydopamine-based permanent coating capillary electrochromatography for auxin determination, Journal of Chromatography A 1212 (1-2) (2008) 130–136.

[200] K. Martma, K.-L. Habicht, X.M. Ramirez, K. Tepp, T. Käämbre, O. Volobujeva, et al., Polydopamine as an adhesive coating for open tubular capillary electrochromatography, Electrophoresis 32 (9) (2011) 1054–60.

[201] R.-P. Liang, X.-Y. Meng, C.-M. Liu, J.-D. Qiu, PDMS microchip coated with polydopamine/gold nanoparticles hybrid for efficient electrophoresis separation of amino acids, Electrophoresis 32 (23) (2011) 3331–40.

[202] B. Yu, J. Liu, S. Liu, F. Zhou, Pdop layer exhibiting zwitterionicity: a simple electrochemical interface for governing ion permeability, Chemical Communications 46 (32) (2010) 5900–2.

[203] K. Liu, W.-Z. Wei, J.-X. Zeng, X.-Y. Liu, Y.-P. Gao, Application of a novel electrosynthesized polydopamine-imprinted film to the capacitive sensing of nicotine, Analytical and Bioanalytical Chemistry 385 (4) (2006) 724–9.

[204] L. Zheng, L. Xiong, D. Zheng, Y. Li, Q. Liu, K. Han, et al., Bilayer lipid membrane biosensor with enhanced stability for amperometric determination of hydrogen peroxide, Talanta 85 (1) (2011) 43–8.

[205] Y. Wan, D. Zhang, Y. Wang, P. Qi, B. Hou, Direct immobilisation of antibodies on a bioinspired architecture as a sensing platform, Biosensors & Bioelectronics 26 (5) (2011) 2595–600.

[206] F. Li, Y. Feng, L. Yang, L. Li, C. Tang, B. Tang, A selective novel non-enzyme glucose amperometric biosensor based on lectin-sugar binding on thionine modified electrode, Biosensors & Bioelectronics 26 (5) (2011) 2489–94.

[207] C. Chen, L. Wang, Y. Tan, C. Qin, F. Xie, Y. Fu, et al., High-performance amperometric biosensors and biofuel cell based on chitosan-strengthened cast thin films of chemically synthesized catecholamine polymers with glucose oxidase effectively entrapped, Biosensors & Bioelectronics 26 (5) (2011) 2311–6.

[208] Y. Tan, W. Deng, Y. Li, Z. Huang, Y. Meng, Q. Xie, et al., Polymeric bionanocomposite cast thin films with in situ laccase-catalyzed polymerization of dopamine for biosensing and biofuel cell applications, The Journal of Physical Chemistry B 114 (15) (2010) 5016–24.

[209] Y. Wang, L. Liu, M. Li, S. Xu, F. Gao, Multifunctional carbon nanotubes for direct electrochemistry of glucose oxidase and glucose bioassay, Biosensors & Bioelectronics 30 (1) (2011) 107–11.

[210] J. Li, Z. Wang, P. Li, N. Zong, F. Li, A sensitive non-enzyme sensing platform for glucose based on boronic acid–diol binding, Sensors and Actuators B: Chemical 161 (1) (2012) 832–837.

[211] C.-C. Lu, M. Zhang, A.-J. Li, X.-W. He, X.-B. Yin, 3,4-Dihydroxy-L-phenylalanine for Preparation of Gold Nanoparticles and as Electron Transfer Promoter in H2O2 Biosensor, Electroanalysis 23 (10) (2011) 2421–2428.

[212] A.-J. Wang, Q.-C. Liao, J.-J. Feng, Z.-Z. Yan, J.-R. Chen, In situ synthesis of polydopamine–Ag hollow microspheres for hydrogen peroxide sensing, Electrochimica Acta 61 (2012) 31–35.

[213] Y. Fu, P. Li, L. Bu, T. Wang, Q. Xie, X. Xu, et al., Chemical/Biochemical Preparation of New Polymeric Bionanocomposites with Enzyme Labels Immobilized at High Load and Activity for High-Performance Electrochemical Immunoassay, The Journal of Physical Chemistry C 114 (3) (2010) 1472–1480.

[214] Y. Fu, P. Li, T. Wang, L. Bu, Q. Xie, X. Xu, et al., Novel polymeric bionanocomposites with catalytic Pt nanoparticles label immobilized for high performance amperometric immunoassay, Biosensors & Bioelectronics 25 (7) (2010) 1699–704.

[215] G. Wang, H. Huang, G. Zhang, X. Zhang, B. Fang, L. Wang, Dual amplification strategy for the fabrication of highly sensitive interleukin-6 amperometric immunosensor based on poly-dopamine, Langmuir 27 (3) (2011) 1224–31.

[216] G. Wang, H. Huang, G. Zhang, X. Zhang, L. Wang, Dual functional electrochemical sensor based on Au–polydopamine–Fe3O4 nanocomposites, Analytical Methods 3 (11) (2011) 2475.

[217] B.D. McCloskey, H.B. Park, H. Ju, B.W. Rowe, D.J. Miller, B.D. Freeman, A Bioinspired Fouling-Resistant Surface Modification for Water Purification Membranes, Journal of Membrane Science 413-414 (2012) 82–90.

[218] S. Azari, L. Zou, Using zwitterionic amino acid l-DOPA to modify the surface of thin film composite polyamide reverse osmosis membranes to increase their fouling resistance, Journal of Membrane Science 401-402 (2012) 68–75.

[219] D.J. Miller, P.A. Araújo, P. Correia, M.M. Ramsey, J.C. Kruithof, M.C.M. van Loosdrecht, et al., Short-term adhesion and long-term biofouling testing of polydopamine and poly(ethylene glycol) surface modifications of membranes and feed spacers for biofouling control, Water Research 46 (12) (2012) 3737–3753.

[220] P.A. Araújo, D.J. Miller, P.B. Correia, M.C.M. van Loosdrecht, J.C. Kruithof, B.D. Freeman, et al., Impact of feed spacer and membrane modification by hydrophilic, bactericidal and biocidal coating on biofouling control, Desalination 295 (2012) 1–10.

[221] F. Pan, H. Jia, S. Qiao, Z. Jiang, J. Wang, B. Wang, et al., Bioinspired fabrication of high performance composite membranes with ultrathin defect-free skin layer, Journal of Membrane Science 341 (1-2) (2009) 279–285.

[222] B. Li, W. Liu, Z. Jiang, X. Dong, B. Wang, Y. Zhong, Ultrathin and Stable Active Layer of Dense Composite Membrane Enabled by Polydopamine, Langmuir 25 (13) (2009) 7368–74.

[223] J. Chen, X. Chen, X. Yin, J. Ma, Z. Jiang, Bioinspired fabrication of composite pervaporation membranes with high permeation flux and structural stability, Journal of Membrane Science 344 (1-2) (2009) 136–143.

[224] W. Liu, B. Li, R. Cao, Z. Jiang, S. Yu, G. Liu, et al., Enhanced pervaporation performance of poly (dimethyl siloxane) membrane by incorporating titania microspheres with high silver ion loading, Journal of Membrane Science 378 (1-2) (2011) 382–392.

[225] J.T. Arena, B. McCloskey, B.D. Freeman, J.R. McCutcheon, Surface modification of thin film composite membrane support layers with polydopamine: Enabling use of reverse osmosis membranes in pressure retarded osmosis, Journal of Membrane Science 375 (1-2) (2011) 55–62.

Chapter 4: Materials and Methods

4.1 POLYDOPAMINE CHARACTERIZATION

Unless otherwise noted, all reactions were performed under ambient conditions. All reagents were purchased from Acros Organics, TCI America, Sigma Aldrich, Alfa Aesar, or C/D/N Isotopes and were used without further purification. Solution state ^{1}H, ^{13}C and ^{15}N NMR spectra were collected on a Varian INOVA 500 MHz spectrometer. Chemical shifts (δ) are referenced downfield from CH_3NO_2 or $(CH_3)_4Si$ using the residual solvent peak as an internal standard (D_2O, 4.67 ppm for ^{1}H NMR). Solid state NMR (ssNMR) experiments were performed on a Bruker Avance-400 spectrometer equipped with standard 7-mm or 4-mm MAS probe heads at a spinning rate of 6 kHz. The ^{15}N, ^{13}C, and ^{1}H chemical shifts were referenced externally to CH_3NO_2 or TMS. The ^{15}N $\{^{1}H\}$ CP MAS NMR spectrum was recorded with a contact time of 1500 μs. The CP ^{13}C $\{^{1}H\}$ (cross-polarization from ^{1}H to ^{13}C) MAS NMR spectrum was recorded with a contact time of 1500 μs, a ^{1}H 90°-pulse of 4.5 μs, and a relaxation delay of 5 s over 700 consecutive scans. An additional evolution time (40 μs) was added to decrease the intensity of resonances associated with carbons bound to protons.

This chapter adapted from:

D.R. Dreyer, D.J. Miller, B.D. Freeman, D.R. Paul, C.W. Bielawski, Elucidating the Structure of Poly(dopamine), Langmuir 28 (15) (2012) 6428–6435.

D.J. Miller, D.R. Paul, B.D. Freeman., A crossflow filtration system for constant permeate flux membrane fouling characterization, Review of Scientific Instruments 84 (3) (2013) 035003.

D. J. Miller, X. Huang, H. Li, S. Kasemset, A. Lee, D. Agnihotri, T. Hayes, D. R. Paul, B. D. Freeman, Fouling-Resistant Membranes for the Treatment of Flowback Water from Hydraulic Shale Fracturing: a Pilot Study, Journal of Membrane Science, 437 (2013) 265-275.

D. J. Miller, P. A. Araújo, P.Correia, M. M. Ramsey, J. C. Kruithof, M. C. M. van Loosdrecht, B. D. Freeman, D. R. Paul, M. Whiteley, J. S. Vrouwenvelder, Short-term adhesion and long-term biofouling testing of polydopamine and poly(ethylene glycol) surface modifications of membranes and feed spacers for biofouling control, Water Research 46 (12) (2012) 3737-3753.

Deconvolution of the ^{13}C NMR spectrum was performed using PeakFit version 4.12 (Systat Software, Inc.). FT-IR analysis was performed using a Perkin Elmer BX spectrometer (KBr). Electron paramagnetic resonance (EPR) spectra were recorded in the solid state on a Bruker EMX+ CWEPR spectrometer. UV-vis spectra were recorded on a Perkin Elmer Lambda 35 spectrometer.

4.1.1 Preparation of polydopamine for Chemical Structure Characterization

A 500 mL Erlenmeyer flask was charged with 3-hydroxytyramine hydrochloride (dopamine HCl) (1.0 g, 5.3 mmol) and water (500 mL). To this solution was added tris(hydroxymethyl)aminomethane (TRIS) (0.3 g, 2.5 mmol). The reaction was magnetically stirred under ambient atmosphere, during which time the clear solution became brown. After 24 hours, the volume of the resultant suspension was reduced to 100 mL under vacuum, and the concentrated suspension was loaded into dialysis tubing (molecular weight cutoff: 6–8 kDa) and dialyzed against denionized water (500 mL) for 7 days. The water was changed at least twice every 24 hours. After dialysis, the solvent was removed under vacuum and the product was dried, affording the material as a dark brown, hygroscopic powder (0.0873 g, 11% yield).

4.1.2 Preparation of 95/5 (w/w) unlabeled-to-^{13}C labeled polydopamine.

A 500 mL Erlenmeyer flask was charged with 3-hydroxytyramine hydrochloride (dopamine HCl) (0.95 g, 5.3 mmol), 2-(3,4-dihydroxyphenyl-$^{13}C_6$)ethylamine HCl (99 atom%) (0.05 g, 0.3 mmol) and water (500 mL). To this solution was added tris(hydroxymethyl)aminomethane (TRIS) (0.3 g, 2.5 mmol). The reaction was magnetically stirred under an open atmosphere, during which time the clear solution became brown. After 24 hours of stirring, the volume of the resultant suspension was reduced to 100 mL under vacuum, and the concentrated suspension was loaded into

dialysis tubing (molecular weight cutoff: 6–8 kDa) and dialyzed against denionized water (500 mL) for 7 days The water was changed at least twice every 24 hours. After dialysis, the solvent was removed under vacuum and the product was dried, affording the material as a dark brown, hygroscopic powder (0.0952 g, 12% yield).

4.1.3 Solution State ^{13}C NMR of Dopamine HCl

^{13}C spectra of dopamine HCl were collected in a saturated solution (D_2O) for comparison to the solid state spectra of polydopamine.

4.1.4 Solid State ^{13}C NMR Spin-Lattice Relaxation

^{13}C spectra were collected on an unlabeled polydopamine sample at three different spin-lattice relaxation times (t_1 = 5, 15, and 20 s).

4.1.5 Solid State ^{13}C NMR with Internal Standard

Solid state ^{13}C NMR spectroscopy was performed on an unlabeled sample of polydopamine mixed with tetrabromomethane (CBr_4) in a 1.25 : 1 ratio (w/w). The spectrum was recorded with relaxation delay of 40 s at a pulse angle of 90° and integration over the range spanning 0–200 ppm (corresponding to the polydopamine).

4.1.6 Powder-X-ray Diffraction

Powder X-ray diffraction (PXRD) was performed in the solid state on an as-prepared polydopamine sample.

4.1.7 UV-Vis spectroscopy

Quartz microscope slides were obtained from Ted Pella and used as received. Before coating with polydopamine, a blank slide was scanned at wavelengths from 200–800 nm as a background. A solution of dopamine·HCl (2 mg/mL) and TRIS (0.6 mg/mL) was prepared as described above, and the quartz slide was immersed in the solution for 4

h to coat with polydopamine. After coating, the slide was rinsed gently with deionized water and air dried, and the as-prepared coated slide was measured in transmission mode.

4.1.8 FT-IR Spectroscopy

FT-IR spectroscopy was performed on the product recovered after reacting as-prepared polydopamine with aqueous NaOCl (5–6%), followed by removal of the solvent under vacuum, trituration in tetrahydrofuran (THF), and removal of the solvent. The freshly prepared resulting white solid was fabricated into a KBr pellet and analyzed in transmission mode.

4.1.9 Solid state EPR spectroscopy.

Solid state electron paramagnetic resonance (EPR) spectroscopy was used to determine the presence of free radicals in the polydopamine structure. In addition to characterizing the EPR-active, as-prepared polydopamine, polydopamine was analyzed in the presence of diphenylpicrylhydrazyl (DPPH) (sealed in a glass capillary packed into the polydopamine sample) to quantify the spin concentration.

4.2 LABORATORY FOULING STUDIES

4.2.1 Reagents

Dopamine HCl, Trizma HCl, ethanol, and isopropanol were obtained from Sigma Aldrich (St. Louis, MO). Sodium hydroxide, potassium chloride, and hydrochloric acid were purchased from Fisher Scientific (Pittsburgh, PA). Poly(ethylene glycol) monoamine (PEG-NH_2) was purchased from JenKem Technology (Allen, TX). Soybean oil (Wesson) was purchased from a local supermarket. Xiameter OFX-0193 non-ionic, silicone-based surfactant was obtained from Dow Corning (Midland, MI). This surfactant is identical to the DC193 surfactant employed in previous studies [1–3]. Polystyrene latex beads (3.0 μm diameter) were obtained from Sigma Aldrich (St. Louis,

MO).All chemicals were used as received. Ultrapure water was produced by a Millipore Milli-Q Advantage A10 water purification system (18.2 MΩ-cm at 25^{o}C, 1.2 ppb TOC) (Billerica, MA). TRIS buffer (15 mM) was prepared by combining Trizma HCl (2.634g) with ultrapure water (1 L) and adjusting the pH to 8.8 with sodium hydroxide.

4.2.2 Membranes

Polysulfone ultrafiltration (UF) membranes were used for most crossflow fouling studies. Rolls of PS-10 and PS-20 polysulfone UF membrane were purchased from Sepro Membranes, Inc. (Oceanside, CA). The rolls were stored in a cardboard tube. PS-10 and PS-20 membranes were similar except that PS-10 had a nominal molecular weight cutoff of 10 kDa, and PS-20 had a nominal molecular weight cutoff of 20 kDa. Membrane sheets approximately 20 cm x 28 cm were cut from the roll. Pretreatment to wet the porous structure was accomplished by immersing the membranes in ethanol overnight. The membrane sheets were carefully placed, selective side down, into a dish of ethanol so that they floated atop the ethanol, which wicked into the pores, allowing air to escape through the nonwoven backing. As the porous structure filled with ethanol, the membrane sheets sank to the bottom of the dish. After soaking in ethanol overnight, the membranes were transferred to a container of ultrapure water and soaked again overnight, changing the water at least once to promote exchange of ethanol for water in the pores.

Poly(vinylidene fluoride) (PVDF) microfiltration (MF) membranes (GVWP14250) from Millipore (Billerica, MA) were also used to validate the operation of the constant flux crossflow system. This hydrophilized membrane had a nominal pore size of 0.22 μm. PVDF membranes were pretreated by soaking in isopropanol overnight.

4.2.3 Membrane Modification

Acrylic plastic plates (20 cm x 28 cm x 0.6 cm) were obtained from Interstate Plastics (Austin, TX). Frames were fabricated from these plates by cutting out a 15 cm x 23 cm rectangle from the center of some of the plates. Rubber gaskets with the same dimensions as the plastic frames were purchased from Advanced Gasket & Supply (Ft. Worth, TX).

Pretreated PS-20 membrane sheets were modified at ambient conditions with polydopamine (PD). Some PS-20 sheets were reserved for use as unmodified, control membranes. No PS-10 UF membranes or PVDF MF membranes were modified. The polydopamine deposition procedure used to modify PS-20 membranes was similar to one previously reported [2,4]. Each membrane sheet to be modified with polydopamine was placed atop a plastic plate with its selective side facing up. A rubber gasket and matching plastic frame were placed on the membrane sample, and the stack was clamped together with large binder clips. A similar setup had previously been used to synthesize interfacial composite membranes [5]. Dopamine hydrochloride (200 mg) was dissolved in TRIS buffer (100 mL) and poured onto the membrane surface inside the gasket/frame. Typically, the membrane was placed on a rocking platform shaker (VWR International, Radnor, PA) for 60 minutes. (A few membranes, which will be discussed exclusively in Chapter 8, were modified with polydopamine for 75 minutes and will be referred to as "PD75 modified." Membranes referred to as "PD modified" were modified for 60 minutes.) As dopamine deposited on the membrane to form polydopamine, the membrane surface became brown. After the desired deposition time, the membrane sheet was removed from the plate/gasket/frame assembly and soaked in ethanol overnight to remove any weakly bound polydopamine from the membrane surface. Then, the

membrane sheet was soaked in ultrapure water overnight, changing the water at least once, to exchange the ethanol for water.

Poly(ethylene glycol) (PEG) was grafted to the surface of some of the polydopamine-modified PS-20 membrane sheets. Only PS-20 membrane sheets modified with polydopamine for 60 minutes were used for PEG grafting; sheets modified with polydopamine for 75 minutes were not used for PEG grafting. The PD modified membrane sheet was reassembled with the plate/gasket/frame, carefully aligning the edges of the PD modified portion of the membrane with the inner edges of the rubber gasket. TRIS buffer (100 mL) was warmed to 60°C before use. PEG-NH_2 (100 mg) was dissolved in the warm TRIS buffer and poured onto the membrane surface. The assembly was placed in an oven at 60°C for 60 minutes. After 60 minutes, the membrane sheet was removed from the plate/gasket/frame assembly and soaked in ultrapure water overnight to remove any weakly bound PEG-NH_2.

4.2.4 Pure Water Permeance

Pure water flux measurements were made in dead end filtration cells from Advantec MFS (Dublin, CA). Circular membrane samples (4.3 cm diameter) from pretreated membrane sheets (as described in section 4.2.2) were cut using a steel punch and rinsed in ultrapure water before measurement. Samples were clamped atop a porous plastic backing to provide mechanical support. The cell was filled with ultrapure water and pressurized to 2.1 barg (30 psig) with compressed air. Permeate exited at atmospheric pressure through a tube at the bottom of the cell into a beaker sitting on an electronic balance (Mettler Toledo, Columbus, OH). The balance was connected to a PC running LabVIEW, which automatically recorded the mass as a function of time; these data were used to calculate pure water permeance. Measurements were made on a

minimum of 25 samples cut from across the width (*i.e.*, transverse direction) of the membrane roll.

4.2.5 Foulant

A soybean oil emulsion was used as the foulant in most crossflow filtration experiments, following earlier studies [1–3,6]. The emulsion was prepared by combining oil and surfactant in a 9:1 ratio with enough ultrapure water to produce an overall emulsion concentration of 1500 ppm (1350 ppm soybean oil, 150 ppm surfactant). Emulsification was performed in a Waring laboratory blender (Torrington, CT) operated at 20,000 rpm for 180 seconds. Fresh emulsion was prepared immediately prior to each fouling experiment. The average oil droplet diameter was about 1.5 μm, with nearly all droplets in the range of 0.8 to 3.0 μm [7].

A polystyrene latex bead suspension was also used in conjunction with the PVDF MF membranes to validate the operation of the constant flux crossflow system. The latex suspension was prepared using 3.0 μm polystyrene beads. The concentration of beads was set to 200 mg/L to match conditions reported in an earlier study [8]. The polystyrene beads were first suspended in ~40 mL ultrapure water and sonicated for several hours to deagglomerate any particles which might have been agglomerated in the concentrated suspension supplied by the manufacturer. Afterwards, this solution was diluted with ultrapure water to the final concentration (200 mg/L). KCl was added to achieve an ionic concentration of 10^{-5} M and the pH was adjusted, if necessary, to 6.0 ± 0.5 using HCl or NaOH to inhibit agglomeration of the polystyrene particles during the fouling experiment.

4.2.6 Constant Flux Crossflow Fouling

4.2.6.1 Principle of Operation

Water permeation through a porous membrane is a pressure-driven process. The membrane mass transfer resistance (R) describes the relationship between the membrane flux (J) and the applied transmembrane pressure difference (TMP) [9]:

$$R = \frac{\text{TMP}}{J} \qquad [4.1]$$

When the membrane resistance increases, as when a membrane fouls during a constant flux experiment, the transmembrane pressure must increase to maintain constant flux. During a fouling experiment, where the membrane resistance may be continuously changing, this TMP increase can be achieved in two ways: (1) fix the permeate pressure and increase the feed pressure as required, or (2) fix the feed pressure and allow the permeate pressure to decrease. In method (1), the flux is indirectly controlled by manipulating the feed pressure. In a system such as the one described here, equipped with three sample cells for replicate testing, method (1) requires three independent feed lines, pumps, flow meters, and pressure regulators. Method (2), in contrast, is easily accomplished by directly regulating the permeate flow with a peristaltic pump on each permeate line. When the membrane mass transfer resistance is low, the permeate pump prevents unrestricted flow, and the permeate pressure is, consequently, very close to the feed pressure. As the membrane fouls and the mass transfer resistance increases, the permeate pressure decreases while the pump maintains the desired permeate flow rate, and the TMP rises.

To achieve rigorously constant flux, the permeate flow rate must be tracked continuously, often accomplished by measuring the permeate mass with an electronic balance [10–20]. However, to accurately calculate the flux, a number of mass readings

must be taken over a sufficient time interval, meaning that there is always some lag in the flux measurement. Additionally, if the permeate is collected on a balance, it cannot be continuously recycled to the feed tank, and the feed concentration will, therefore, vary as the experiment progresses, since one typically recirculates feed past one or more membrane cells from a finite volume of feed solution. If the permeate cannot be recycled to the feed tank of the system, then the system cannot easily be operated in continuous, steady operation because the feed concentration of the foulant will rise during the experiment. With a peristaltic pump regulating the permeate flow rate, as in method (2) above, a flow meter may be used to precisely measure the permeate flow rate, and this measured flow rate may be used to control the permeate pump speed. This flow meter is installed on the downstream side of the peristaltic permeate pump, where its pressure drop is inconsequential to the transmembrane pressure measured on the upstream side of the pump.

4.2.6.2 System Overview

A system diagram is shown in Figure 4.1. The system is designed to operate in total recycle mode (*i.e.*, the permeate and retentate streams are recycled to the feed tank) to ensure that the concentration of the fouling solution remains unchanged throughout an experiment. Pure water and the desired foulant solution are stored in feed tanks and pumped into the membrane test cells. Three cells are used to test sample replicates. Permeate flow rates are very small compared to the feed flow rate, so the feed concentration is virtually identical for all three cells. Single-ended pressure transducers were used to monitor the pressure on both the feed and reject sides of the membrane cell train. Differential pressure transducers monitored the transmembrane pressure of each sample cell. The high-pressure ports of the differential pressure transducers were connected to the feed line at the inlet to each cell and the low-pressure ports were

connected to the permeate line from each cell. The feed pressure was controlled with a backpressure regulator attached to the reject of the third cell. The pressure drop down the length of the membrane cell train was less than 0.07 bar (1 psi) at the flow rates used here. Valves were installed on each end of the train to prevent water from flowing into the cells while they were open for sample loading. The reject line was recycled to the feed tanks *via* a manifold. Permeate flow rates were regulated with a pump and flow meter on each of the three permeate lines. Permeate lines were also connected to the manifold for total recycle. The manifold permitted recycling to the pure water tank, recycling to the feed tank, or draining to a waste basin. A cartridge filter was installed on the recycle loop to remove residual foulant during system cleaning cycles and to maintain foulant-free feed water during pure water tests. A bypass was used to route fouling fluid around the filter during fouling experiments.

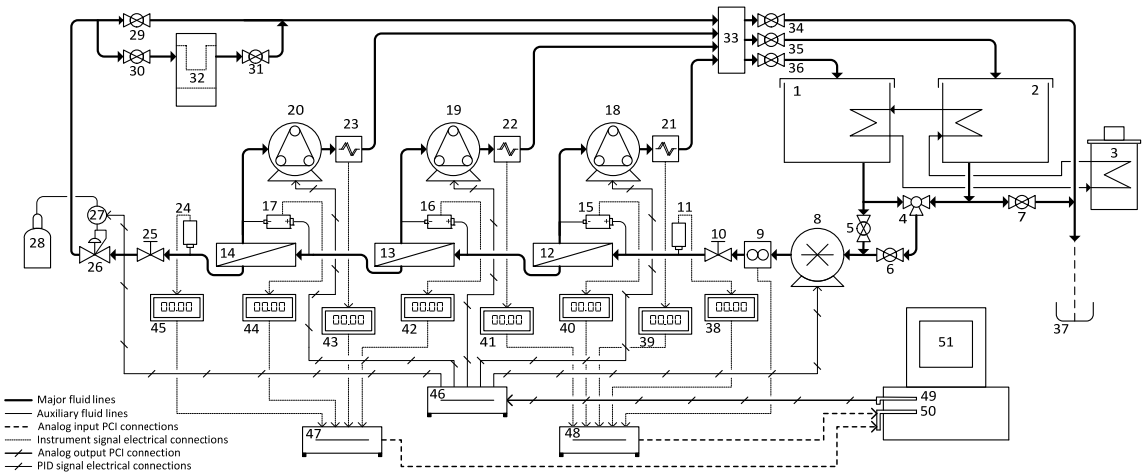

Figure 4.1. Constant flux crossflow fouling system schematic. Components identified by numerical labels are listed in Table 4.1.

No.	Description	Supplier	Cat. No.
1 – 2	Covered Feed Tank	U.S. Plastic Corp. (Lima, OH)	14200-0002
3	Heated Water Bath	Thermo Scientific (Tewksbury, MA)	NESLAB RTE 7
4	3-Way Valve	Cole-Parmer (Vernon Hills, IL)	01377-74
5 – 7	Ball Valve	Cole-Parmer	01377-03
8	Feed Pump	Cole-Parmer	Drive: 75211-30 Head: 07003-04
9	Feed Flow Meter	Brooks Instrument (Hatfield, PA)	BM02BSSPA2BVA
10	Screw-down Needle Valve	Swagelok (Solon, OH)	SS-1KS8
11	Feed Pressure Transducer	Omega Engineering (Stamford, CT)	PX209-060G5V
12 – 14	Membrane Sample Cell	Separations Systems Tech. (San Diego, CA)	--
15 – 17	Differential Pressure Transducer	Omega Engineering	PX409-030DWU5V
18 – 20	Permeate Pump	Cole-Parmer	Drive: 7523-80 Head: 7519-20 Cartridge: 7519-75
21 - 23	Permeate Flow Meter	Bronkhorst (Bethlehem, PA)	M13-ABD-11-0-S
24	Reject Pressure Transducer	Omega Engineering	PX209-060G5V
25	Screw-down Needle Valve	Swagelok	SS-1KS8

26	Back Pressure Regulator	Equilibar (Fletcher, NC)	EB1HF1
27	Air Regulator	Proportion Air (McCordsville, IN)	QPV1TFEE050AXL
28	Air Supply Cylinder	Airgas (Radnor, PA)	AI B300
29 - 31	Ball Valve	Cole-Parmer	01377-03
32	Cartridge Filter	Cole-Parmer	Housing: 29820-11 Filter: 01508-93
33	Manifold	Cole-Parmer	31522-51
34 - 36	Ball Valve	Cole-Parmer	01377-90
37	Drain	--	--
38 – 45	Process Meter	Omega Engineering	DP25B-E
46 – 48	Connector Block	National Instruments (Austin, TX)	SCB-68
49	Analog Output PCI Device	National Instruments	PCI-6713
50	Analog Input PCI Device	National Instruments	PCI-6224
51	Computer	Dell (Round Rock, TX)	Optiplex 360

Table 4.1. Constant flux crossflow fouling system components. Identification numbers correspond to those shown in Figure 4.1.

Figure 4.2. Photograph of the constant flux crossflow fouling system.

4.2.6.3 Construction Details

Major components, including their suppliers and catalog numbers, are listed in Table 4.1. Numerical identifiers in the following text correspond to those shown in Table 4.1 and Figure 4.1. Figure 4.2 is a photograph showing an overview of the system. The two covered feed tanks (1, 2) were used to hold pure water and foulant feed solution. Bulkhead fittings were installed near the bottom and top of each tank to allow feed flow and recycle. Each tank was equipped with a heating coil made of ¼" stainless steel tubing through which water flowed from an adjacent temperature controlled water bath (3). A three-way valve (4) was used to select the desired feed tank. Feed flowed directly into the feed pump (8), which was used to control the feed flow rate. A gear pump was chosen due to its ability to maintain smooth, non-pulsatile flow in the desired feed pressure range. A variety of pump heads suitable for a wide range of flowrates are available; the pump head chosen was capable of producing a flow range of 58.5 - 5850 mL/min. Gears may be made of either poly(*p*-phenylene sulfide) (PPS) or polyether ether ketone (PEEK). The less expensive PPS gears deteriorated in early trials and left

small, black particulates in the feed tanks. PEEK gears, though more expensive, have proven more reliable. The flow rate was monitored by an oval gear flowmeter (9), which is tolerant of pressures up to 10.3 barg (150 psig). Fiber-reinforced flexible tubing, capable of withstanding high fluid pressures, was used to connect the feed pump to the feed flow meter.

The three membrane sample cells (12 – 14) were machined at The University of Texas at Austin based on cells previously obtained from Separation Systems Technology (San Diego, CA). A detailed diagram of the top and bottom halves of the membrane test cell is shown in Figure 4.3. The feed flows into an inlet port, through a 90° bend, across the membrane surface in a rectangular flow path, through another 90° bend, and out an exit port. The flow path is 1.250" wide x 3.250" long x 0.101" deep (31.75 mm x 82.55 mm long x 2.565 mm). The membrane sits above the flow path, with its active side facing down, and it is sealed with a rectangular rubber O-ring, making 1" x 3" (25 mm x 78 mm, 1940 mm^2) of membrane surface area available for filtration. A piece of highly porous polypropylene (average pore size: 125 – 175 μm) obtained from Interstate Specialty Products (Sutton, MA) provided mechanical reinforcement for the membrane and has a negligible resistance to permeate flow. The permeate fluid passed through a port on the top of the cell.

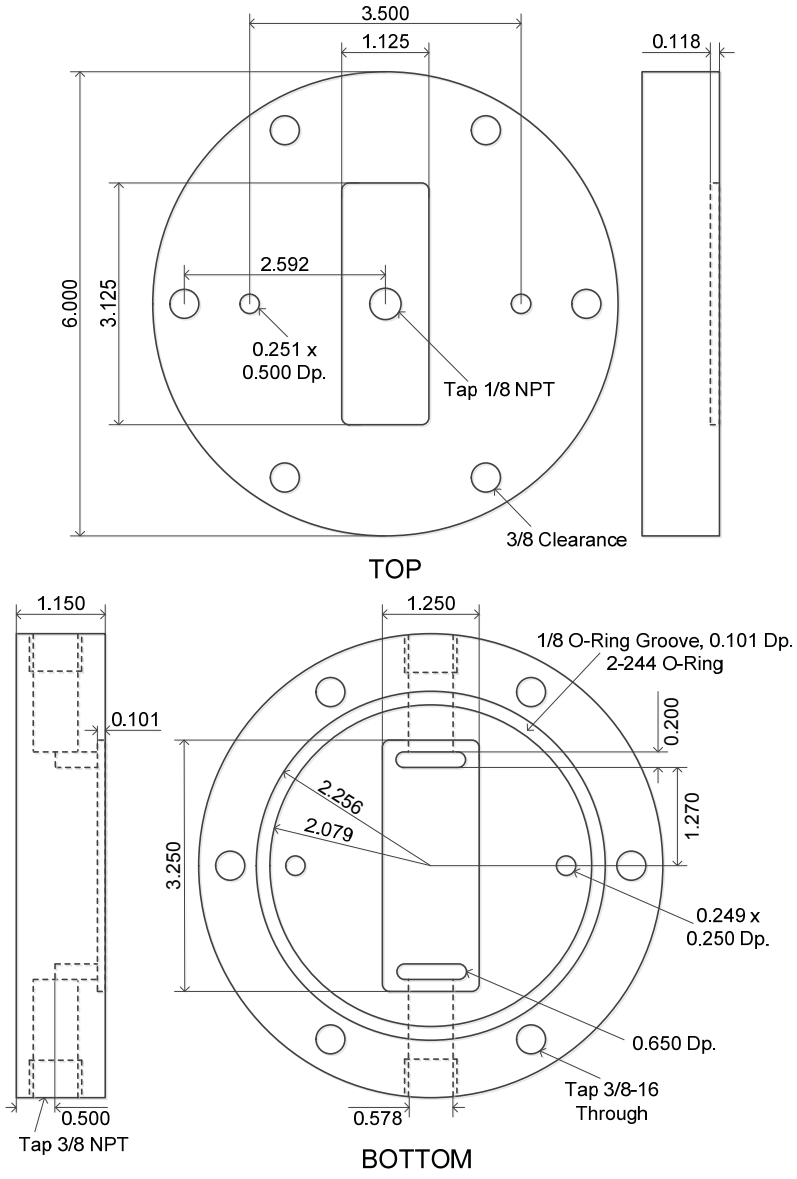

Figure 4.3. Diagram of top and bottom of membrane test cell; each half is viewed from the inside of the cell and from the side. The porous polypropylene reinforcement is inserted into the rectangular recess in the top half. The membrane is placed face down atop the rectangular flow channel on the bottom half, which also contains a rectangular rubber O-ring. All dimensions are shown in inches.

Feed (11) and reject (24) pressure transducers were 60 psig full scale (4.14 barg) single-ended models. Differential pressure transducers (15 – 17) were used to measure the transmembrane pressures. Fouling experiments were typically run until the transmembrane pressure difference was equal to the gauge feed pressure. UF and MF membranes were frequently run with feed pressures of 2.1 barg (30 psig), so 30 psi differential pressure transducers were selected. Other differential transducers were substituted if the feed pressure was changed. Accuracy of the PX409 series transducers is ±0.8% of full scale, so the use of transducers with the smallest usable full scale will give the most accurate results at low TMP values. All transducers had a 0 – 5 Vdc output which scaled linearly with their pressure range. Process meters were used to convert the signal voltage to a pressure reading and to provide a 24 Vdc excitation voltage. Snubbers were used on each pressure connection of both single-ended and differential pressure transducers to reduce damage to the transducers in the event of water hammer.

A backpressure regulator (BPR) (26) was installed downstream of the membrane cells. This BPR is used to adjust the feed pressure without significantly impacting the feed flow rate. The BPR contains a diaphragm that separates the water stream from a reference gas (air was used in this case). The pressure of the reference gas is controlled by an electronic regulator (27) mounted at the BPR reference inlet. The BPR diaphragm position changes according to the pressure of the reference gas (28), which consequently adjusts the feed pressure. The electronic gas regulator required 24 Vdc power and is controlled with a 0 – 10 Vdc analog input voltage.

The components of the membrane sample cell train were assembled, beginning with the feed needle valve (10) and working towards the reject backpressure regulator (26). Figure 4.4 shows, in detail, the fittings connected to one of the membrane sample cells. Stainless steel ½" tubing and compression fittings were used to connect the

components in the cell train. Single-ended pressure transducers (11, 24) were mounted vertically on the branch of a ½" tee. Differential pressure transducers (15 – 17) were mounted horizontally such that both ports were at the same level as the membrane samples inside the cells. High-pressure ports of the differential pressure transducers were connected to a ½" tee *via* a 90° elbow. A 90° elbow and compression-fit hose barb were attached to the low-pressure ports of the differential pressure transducers. Another compression-fit hose barb was attached to the branch of a ¼" stainless steel tee mounted on the permeate outlet of each sample cell. A short length of ⅛" polypropylene tubing was used to connect the low-pressure port of each differential pressure transducer with the sample cell permeate outlet; this line will later be referred to as the "permeate pressure transfer line." Aluminum hose collars were used to eliminate pressure leaks at the hose barbs. The permeate flow passed vertically into the permeate line attached to the ¼" tee with a hose barb.

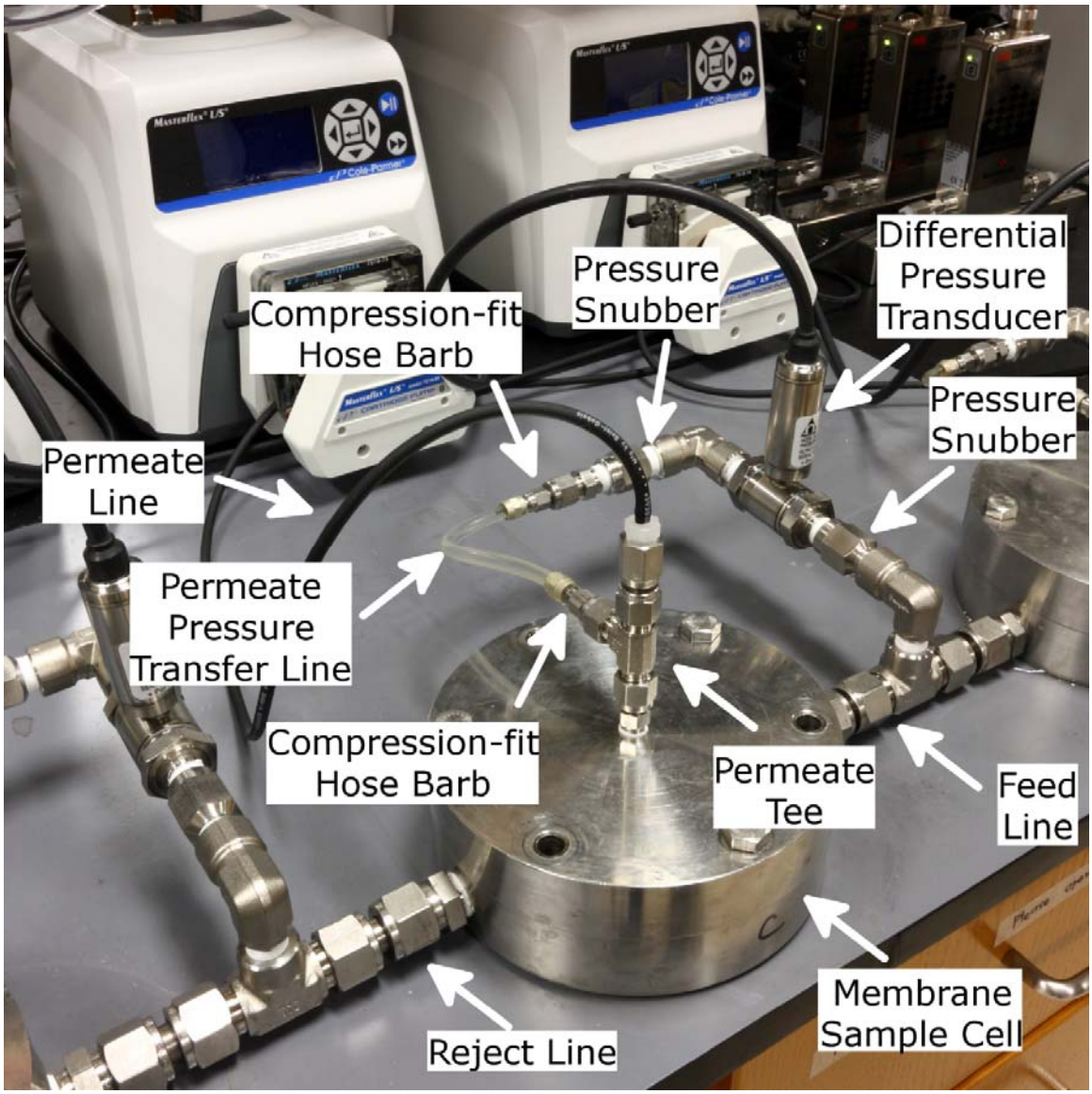

Figure 4.4. Detail of connections made to a membrane sample cell.

After passing through the BPR, the reject was near atmospheric pressure, so steel or fiber-reinforced tubing was not necessary. The reject line was flexible, clear ⅜" plastic tubing and was used to return reject fluid from the membrane train to the feed tanks. A manifold (33) was used to recombine the three permeate flows with the reject and recycle the fluid to the appropriate feed tank. Hose barbs of the appropriate sizes

were used to attach the reject and permeate lines to the manifold. Three valves (34 – 36) were also installed on the manifold to permit recycle to the pure water tank (1), recycle to the foulant tank (2), or drainage to a waste basin (37).

Three permeate pumps (18 – 20) were of the peristaltic type. Many different heads are available for Cole Parmer drives, including the common Easy-Load® styles, which were tested extensively. However, the three or four rollers of these heads cause significant pulsation when operated at speeds low enough to produce the desired permeate flow rates. Instead, cartridge-style heads were chosen because they are available with eight rollers to minimize pulsations at slow pump speeds. The cartridges have an occlusion adjustment knob which controls the volume of fluid pushed through the tubing with each roller pass. Loosening this adjustment increases fluid passage and the observed TMP; tightening it decreases fluid passage and the observed TMP. It is critical that the permeate pump effectively isolates the permeate side of the membrane from the atmospheric pressure of the permeate recycle to the feed tank and tightening the occlusion helps in this regard. However, a very tight occlusion causes premature tubing wear and, in some cases, can cause the tubing to become dislodged from the cartridge by the action of the rollers; greasing the rollers with a small amount of lubricant can help prevent these effects. In the adjustable range of 1 (tight) to 5 (loose), a setting of 2 was found to give the best, most repeatable performance. Permeate line tubing was size 14 peristaltic pump tubing. Smaller tubing sizes (*e.g.*, size 13) caused an appreciable pressure drop in the permeate line which affected the observed TMP. Larger tubing sizes (*e.g.*, size 16) required that the pump run very slowly, resulting in highly pulsatile permeate flow. Tubing was replaced frequently to promote efficient pump operation and prevent the deterioration of the tubing. Pump speeds were controlled with 0 – 10 Vdc input analog voltages.

Cavitation is sometimes a concern with peristaltic pumps. The required net positive suction head ($NPSH_R$) describes the frictional losses that result in a decrease in fluid pressure at the pump entrance. For small pumps such as those employed in the present apparatus, the required net positive suction head is typically 0.14-0.28 bar [21]. The available net positive suction head ($NPSH_A$) is the difference between the pump inlet pressure (P_{inlet}) and the fluid vapor pressure (P^*):

$$NPSH_A = P_{inlet} - P^* \quad [4.2]$$

As described in the proceeding sections, the permeate line pressure decreased during membrane fouling and experiments were typically stopped if the transmembrane pressure equaled the feed pressure, meaning that the minimum permeate pressure was atmospheric pressure (1.00 bar). The vapor pressure of water at 25°C is 0.03 bar [22], so the minimum $NPSH_A$ was 0.97 bar. To avoid cavitation, the available net positive suction head should remain greater than the required net positive suction head:

$$NPSH_A > NPSH_R \quad [4.3]$$

In this case, the minimum NPSHA (0.97 bar) was greater than NPSHR (0.14-0.28 bar), so cavitation was not a problem for these permeate peristaltic pumps.

Flow rates on the permeate lines were monitored by three Coriolis-style flow meters (21 – 23). Coriolis meters have high accuracy (even at very low flow rates), rapid response time, and they are not sensitive to the fluid being measured. Several other flow meter types were tested and found to be unsatisfactory. Variable area flow meters, though inexpensive, do not provide electronic reading of the flow rate. Differential pressure models, where the fluid is forced into laminar flow between thin metal plates over which the pressure drop is detected, provide electronic flow rate readings. However, they are most suitable for use with ultrapure water, as impurities (such as the soybean oil used in these studies) can foul the plates in the laminar flow element, causing inaccurate

and irregular readings. Thermal flow meters are not sensitive to the fluid and will not foul, but they generally have slow response times, making them unsuitable for feedback control of a pump as in this apparatus. The permeate tubing was attached directly to the inlet of the flow meters using an appropriate hose barb. Another hose barb was fitted to the flow meter outlet and size 16 clear Tygon tubing was used to carry permeate to the manifold (33) for recombination with the reject. Each flow meter was wired to a process meter (38 – 45) which provided 24 Vdc power and scaled the 0 – 10 Vdc analog output voltage from the flow meter to a flow rate.

4.2.6.4 System Control

National Instruments (NI) data acquisition hardware and LabVIEW software were used to collect and record data and to control instruments. Two NI PCI data acquisition devices (49, 50) were installed in a desktop computer (51) running Windows XP. One of the PCI devices was capable of outputting 0 – 10 Vdc analog voltage signals (49); the other device was capable of reading 0 – 10 Vdc analog voltage inputs and counting voltage pulse inputs (50). The PCI devices were connected to three terminal blocks (46 – 48) using cables provided by NI. The five pressure transducers and three permeate flow meters were connected to process meters (38 – 45) which scaled their voltage signals to pressure readings or flow rates according to their calibration certificates provided by the manufacturer. Each of the transducers and flow meters requires a 24 Vdc power supply, which was also provided by the process meters. These process meters were wired to the NI terminal blocks to pass the voltage signals to LabVIEW. Analog inputs were wired as differential inputs with the common wire referenced to ground for signal stability and consistency across all instruments. The Hall Effect sensor of the feed flow meter (9) was powered with a 5 Vdc voltage available on the NI terminal blocks. The flow meter produced 5 Vdc voltage pulses as its gears turned; the feed flow was, therefore, measured

by counting the frequency of voltage pulses. The feed flow meter was wired to a counter input on an NI terminal block (48) using a 1 kΩ pull-up resistor between the 5 Vdc supply and the counter input. The three permeate pumps, feed pump, and BPR were controlled with 0 – 10 Vdc analog voltage signals from one of the NI PCI devices (46). Output voltages were all referenced to ground for signal stability.

A program was written in LabVIEW 2010 with three primary functions: convert input signals to physical values, control instruments with a feedback control algorithm, and write data to an Excel spreadsheet. Pressure transducer and permeate flow meter voltages scaled linearly with their measurements, so multiplicative factors were used to calculate the feed pressure, reject pressure, transmembrane pressures, and permeate flow rates. Because the pressure drop down the three membrane cell train was low (<0.055 bar), the feed pressure for all three cells was taken as the average of the pressures measured by the feed (11) and reject (24) transducers. The permeate flow rates were converted to fluxes by dividing the flow rate by the membrane surface area available for permeation (19.4 cm^2). The feed flow rate was calculated by multiplying the frequency of voltage pulses from the oval gear flow meter by a scaling factor.

Proportional-Integral-Derivative (PID) control was facilitated by installation of the LabVIEW PID and Fuzzy Logic Toolkit. This toolkit includes built-in controllers that may be used to output voltage signals to instruments wired to NI data acquisition devices. Each controlled instrument could be toggled between manual control and automatic control. When in manual control mode, the output voltage to the instrument was specified by the user. In automatic control, the PID controller compared a process variable to a setpoint, and then calculated a voltage output based on proportional, integral, and derivative gains. Process disturbances could, therefore, be easily corrected; the importance of such control will be illustrated later. The feed pump, each of the three

permeate pumps, and the BPR were independently controlled using the feed flow rate, permeate flux, and average feed pressure measurements, respectively. Stable operation was achieved by careful selection of the gains. The derivative gain was usually set to zero, meaning that the system operated in proportional-integral feedback control only. Typical gain values, which were empirically found to produce stable system operation, are shown in Table 4.2, below.

Gain	Feed Pump	Permeate Pumps	BPR
Proportional (K_c)	0.050	0.010	0.010
Integral (T_i)	10.000	10.000	10.000
Derivative (T_o)	0.000	0.000	0.000

Table 4.2. PID control gains.

4.2.6.5 System Operation

One feed tank (1) was filled with ultrapure water while the other (2) was filled with the desired foulant solution. No stirring device was employed in the foulant feed tank, but the hold-up time (*i.e.*, the volume of fluid in the feed divided by the feed flow rate) was less than 10 minutes at the feed flow rates used in this study.

Membranes were cut into 4.0 cm x 9.0 cm (1.6 in x 3.5 in) coupons and loaded, selective side down, in the three sample cells (12 – 14). The three bolts used to secure the top of the sample cell were first finger-tightened only. Then, the feed (10) and reject (25) needle valves were opened and the permeate pressure transfer lines were disconnected at the compression fittings closest to each differential pressure transducer. The three bolts on each cell were then tightened with a crescent wrench. Without the relief afforded by opening the feed and reject valves and the permeate pressure transfer

lines to the atmosphere, pressure capable of deforming the membrane samples can develop in the cells while tightening the bolts. After all bolts were fully tightened, the permeate pressure transfer lines were re-connected. After loading membranes, the temperature control bath was turned on and adjusted to the desired temperature set point (typically 25°C). The fluid returning to the feed tank was within 1°C of the feed tank temperature.

The system was started by operating all instruments manually. Pure water was selected as the feed by opening valve 5, closing valve 6, and positioning valve 4 such that foulant from tank 2 was directed towards valve 6. Valve 36 was opened, and valves 34 and 35 were closed so that the water would be recycled to the water feed tank (1). Valves 30 and 31 were opened and valve 29 was closed, directing the reject through the activated carbon cartridge filter (32) so that the recirculating water was continuously filtered. The feed pump (8) was started at a voltage low enough to produce a flow rate below the desired feed flow. The setpoint was matched to the actual feed flow rate, and the system was switched to automatic control. Once stable operation was achieved under automatic control, the setpoint was increased to the desired feed flow and the PID controller automatically changed the pump voltage to match the feed flow setpoint. By starting each instrument in this fashion, the likelihood of unstable operation is minimized. Once the desired feed flow rate was achieved, the feed pressure setpoint was matched to the pressure produced by the feed pump. The BPR (26) was then switched to automatic control, and the feed pressure setpoint was adjusted to the desired feed pressure. The three permeate pumps (18 – 20) were started in a manner similar to the feed pump. First, a low voltage was manually applied to generate a permeate flux lower than that desired during the experiment. The setpoint was matched to the resultant flow rate, automatic control was switched on, and the setpoint was then adjusted to produce the desired flux.

By this point, all instruments were operating under automatic control with a pure water feed that matched the desired experimental feed flow, feed pressure, and permeate flux conditions. By this time, the temperature control bath (and pure water and foulant solution contained in their respective tanks) was at its target value. If the membrane samples were operating within 10% of the pure water permeance measured *via* dead end filtration (section 4.2.4), the experiment was continued. If the membranes were operating outside this range, the system was stopped, new membranes loaded, and the system re-started.

A fouling experiment was started by bypassing the cartridge filter, so that the foulant solution was not run through the filter, because this would alter the concentration of the foulant solution. The cartridge filter was bypassed by first opening the cartridge filter bypass valve (29) and then closing valves 30 and 31. The foulant solution was then introduced to the feed flow loop by first opening valve 6 and then closing valve 5 (in that order to avoid running the feed pump dry). The oil emulsion or latex suspension is visible as a moving front in the clear tubing; valve 35 was opened and valve 36 was closed so that the fouling solution was recycled to the foulant tank (2) immediately before this front reached the manifold (33) to avoid diluting the foulant in the tank. Fouling experiments could be run as an ordinary constant flux experiment, where the flux was maintained at the same rate for the entire experimental duration, or as a flux stepping experiment, where the flux was periodically increased. Flux stepping experiments, which are commonly used in the literature to determine a membrane's critical/threshold flux under a particular set of fouling conditions, were easily performed by increasing the permeate flux setpoints at desired time intervals.

System cleaning was initiated by closing recycle valves 35 and 36 and opening drain valves 7 and 34. The oil emulsions were only used for one experiment, so they

were always drained from the system at the end of the experiment. Latex bead emulsions could be reused. Valve 5 was closed and valve 4 was adjusted so that water from the pure water tank (1) was directed toward valve 6 to remove residual foulant in the tubing near the tanks. The system was flushed with water from the water feed tank (1) using the feed pump (8); this water was drained through the manifold (33). After flushing and draining the system, valves 10 and 25 were closed, the membrane cells opened, the samples removed, the cells closed again, and valves 10 and 25 again opened. Valve 5 was opened and valve 6 was closed. The pure water tank (1) was refilled with ultrapure water, valve 29 was closed, valves 30 and 31 were opened to direct recirculating water into the activated carbon filter, valve 36 was opened to recycle to the water tank (1), and valve 34 was closed. The feed pump (8) was used to recirculate pure water through the system; the three permeate pumps (18 – 20) were also turned on to flush the permeate lines. The system was cleaned in this manner, with the cartridge filter removing any residual foulant, for at least 30 minutes. The importance of rigorously cleaning the system after each experiment cannot be overstated; without such cleaning, residual foulant may accumulate in the system and cause membrane fouling during the startup of the next experiment, leading to artificially high TMP values.

Generally, constant flux fouling experiments with UF membranes (both PS-10 and PS-20) were carried out at a feed rate of 0.8 L/min, corresponding to a crossflow velocity of 0.18 m/s and a Reynolds number of approximately 1000 inside the flow channel of each test cell (Reynolds number was calculated by assuming that the flow channel consists of two parallel plates with large aspect ratios) [24]. The feed pressure was 2.1 bar (30 psig) and the feed was 1500 ppm soybean oil emulsion. A flux stepping experiment was also carried out with PVDF MF MF memrbanes and a styrene latex bead suspnsion. In this experiment, the feed pressure was 0.20 barg (2.9 psig), the crossflow

velocity was 0.2 m/s during fouling, and 0.5 m/s during five minute cleaning stages between fouling steps.

4.2.7 Constant Transmembrane Pressure Crossflow Fouling

Constant TMP fouling experiments were performed in a manner similar to those reported previously [1–3,23–25]. Constant TMP fouling experiments were performed only on unmodified PS-20 UF membranes for comparison to constant flux experiments (Chapter 7). The crossflow system employed was based on one purchased from Separations Systems Technologies (San Diego, CA). A 30 L feed tank was equipped with a heating coil connected to a water bath used to maintain a feed temperature of 25°C. A diaphragm pump from Texas Pump and Equipment (Wichita Falls, TX) was used to pump the feed solution into three stainless steel membrane sample cells in series. The feed flow rate was monitored using an oval gear flow meter from Brooks Instrument (Hatfield, PA). Single-ended pressure transducers from Omega Engineering (Stamford, CT) were used to monitor the feed and reject pressures. A backpressure regulator (BPR) from Equilibar (Fletcher, NC) was installed downstream of the three membrane sample cells. An electronic air regulator from Proportion Air, Inc. (McCordsville, IN) was mounted to the BPR and adjusted the BPR pressure based on readings from the feed pressure transducer by a LabVIEW program incorporating proportional/integral feedback control. Reject was continuously recycled to the feed tank.

Permeate from each sample cell was collected in a large beaker on an electronic mass balance. The change in mass was recorded as a function of time, and the permeate flux was calculated as follows:

$$J = \frac{\Delta M}{\rho_w A \Delta t} \qquad [4.4]$$

where J is the flux, ΔM is the mass of permeate collected in time Δt, ρ_w is the density of water, and A is the filtration area (19.4 cm^2). A differential pressure transducer (Omega Engineering) measured the difference between the feed and permeate pressures of each sample cell. A backpressure regulator (Equilibar) and electronic air regulator (Proportion Air, Inc.) was installed on each permeate line. In a scheme similar to that employed to control feed pressure, each permeate line BPR was operated in feedback control using the TMP reading from its respective differential pressure transducer. In this way, the TMP applied over each membrane was carefully and independently controlled. The TMP feedback control and all data collection, including mass of the permeate, the three transmembrane pressures, the feed pressure, and the feed flow rate, was recorded as a function of time by the same LabVIEW program mentioned above.

To begin a constant TMP fouling experiment, membrane sample coupons were loaded in the test cells and the feed tank was filled with 27 L of ultrapure water. The feed pump began circulation of the water at 0.8 L/min, corresponding to a crossflow velocity of 0.18 m/s and a Reynolds number of approximately 1000 inside the flow channel of each test cell (Reynolds number was calculated by assuming that the flow channel consists of two parallel plates with large aspect ratios) [24]. The feed pressure was 2.1 barg (30 psig) in all experiments, and the TMP across each sample cell was adjusted to produce a desired pure water flux. During startup with pure water operation, the recycled reject water was filtered using a Matrikx CTO Plus® activated carbon cartridge filter from KX Technologies (West Haven, CT) to remove any contaminants that might foul the membrane. The importance of continuous feed filtration during pure water permeation has been discussed elsewhere [24]. The membranes were operated with ultrapure water for a few minutes to ensure that all air was purged from the permeate lines. The manufacturer specifies a water permeance of 900 LMH/bar; dead end filtration tests

(section 4.2.4) have revealed a permeance range of approximately 600 – 1300 LMH/bar for small samples cut from the membrane roll. Typically, if the membranes were operating with ultrapure water near the middle of this range, *e.g.*, 800 – 1000 LMH/bar, the experiments were continued. If not, then the membranes were replaced, and the experiment was re-started.

Membrane fouling was initiated by adding 3 L of concentrated soybean oil emulsion to the 27 L of ultrapure water already in the feed tank sufficient to produce a 1500 ppm overall concentration, as described in section 3.1. The activated carbon cartridge filter was bypassed just before adding the foulant solution. As the membranes fouled, their flux decreases were tracked by the electronic balances.

4.2.8 Organic Rejection

Permeate and feed samples were taken during all crossflow fouling experiments. The total organic carbon (TOC) content of permeate and feed samples was measured by a Total Organic Carbon Analyzer from Shimadzu Scientific (Japan) to determine membrane rejection. The rejection was calculated as follows:

$$\Re = (1 - \frac{C_p}{C_f}) \times 100\% \qquad [4.5]$$

where $\Re$ is the rejection, C_p is the organic carbon concentration in the permeate, and C_f is the organic carbon concentration in the feed. The TOC instrument was calibrated using 10 ppm, 100 ppm, and 1000 ppm organic carbon standard solutions (Shimadzu). Calibration curves were constructed from measurements on the standard solutions and used to by the instrument software to determine TOC concentrations in the experimental samples.

4.3 PILOT STUDY

4.3.1 Membrane modules

Two UF modules were obtained from Mann+Hummel Ultra-Flo Pte, Ltd. (Portage, MI) and contained hydrophilized polyacrylonitrile hollow fibers. Six reverse osmosis (RO) modules were obtained from Hydranautics (Oceanside, CA). These RO modules consisted of spiral-wound, flat sheet membranes based on interfacial composite polyamides. Manufacturer specifications for both module types are recorded in Table 4.3.

Specification	Ultrafiltration	Reverse Osmosis
Manufacturer	Mann+Hummel	Hydranautics
Model Number	Ultra-Flo U630C	SWC3+
Material	hydrophilized polyacrylonitrile	composite polyamide
Architecture	hollow fiber (1.0 mm OD, 0.5 mm ID)	spiral-wound
Pore Size (μm)	0.1 - 0.01	N/A
Flow Direction	outside - in	N/A
Surface Area (m^2)	30	37
Pure Water Permeance (LMH/bar)	13 - 20	0.54
Product Quality	≤ 0.1 NTU	≤ 0.3% salt passage
Recovery	100% (dead end filtration)	10%
Maximum Feed Turbidity (NTU)	5	1
Feed pH Range	2 - 12	3 - 10
Maximum Feed Pressure (bar g)	3.5	83
Typical Feed Pressure (bar g)	2.5	55
Maximum Operating Temperature (°C)	50	45

Table 4.3. Specifications for UF and RO modules employed in the pilot study.

4.3.2 Module Modification

Dopamine HCl and Trizma HCl were purchased from Sigma Aldrich (St. Louis, MO). Sodium hydroxide was obtained from Fisher Scientific (Pittsburgh, PA), and

poly(ethylene glycol) monoamine (5000 Da) (PEG-NH_2) was purchased from JenKem Technology (Allen, TX). All chemicals were used as received.

One UF module and three RO modules were surface-modified with polydopamine using the following procedure. A module was flushed with ultrapure water overnight to fully wet the surfaces to be modified. TRIS buffer (15 mM) was prepared first by dissolving Trizma HCl (5.875g) in ultrapure water (2.5 L) and adjusting the pH of the resultant solution to 8.8 using sodium hydroxide pellets. Dopamine HCl (5 g) was dissolved in the TRIS buffer (2.5 L), and the resultant 2 g/L solution was poured into the feed side of a module. The modules were gently rolled back and forth for 60 minutes to ensure that the dopamine solution contacted all wetted surfaces on the membrane feed side. Every ten minutes, the feed inlet was opened to introduce fresh oxygen, as dopamine polymerization requires the presence of dissolved oxygen [26]. Residual dopamine was flushed from the module with ultrapure water.

The UF module was further modified by grafting PEG to the polydopamine coating. TRIS buffer (2.5 L, prepared as described above) was heated to 52°C. PEG-NH_2 (1.25 g) was dissolved in the TRIS buffer and this solution was poured into the feed end of the UF module. The module was gently rolled back and forth for 45 minutes to ensure that the PEG-NH_2 solution contacted all of the polydopamine-modified surfaces. After PEG grafting, the UF module was flushed with ultrapure water to remove residual PEG-NH_2 solution. PEG was not grafted to the polydopamine-treated RO modules because, as noted previously, grafted PEG creates a substantial mass transfer resistance on the surface of RO membranes, resulting in a flux loss that more than offsets any fouling-reducing benefit of the coating. After modification, the modules were filled with deionized water for storage until use.

4.3.3 Pilot System

The site of the pilot study was the Maggie Spain Water Reclamation Facility operated with the support of Devon Energy in the Barnett Shale region near Fort Worth, TX. Flowback water from hydraulically fractured natural gas wells in the Barnett Shale play was brought to the treatment facility by truck and stored in a lined pond before processing. Raw water was subjected to coagulation and sedimentation before treatment by the membrane systems. The feed water was pH-adjusted to a typical value of 5. Modified UF and RO modules were operated in parallel with unmodified, control modules. The RO reject was stored in a tank for off-site disposal. The RO permeate was collected in a finished water storage tank before being trucked back to the field for use in fracturing. A flowsheet of the pilot system is shown in Figure 4.5.

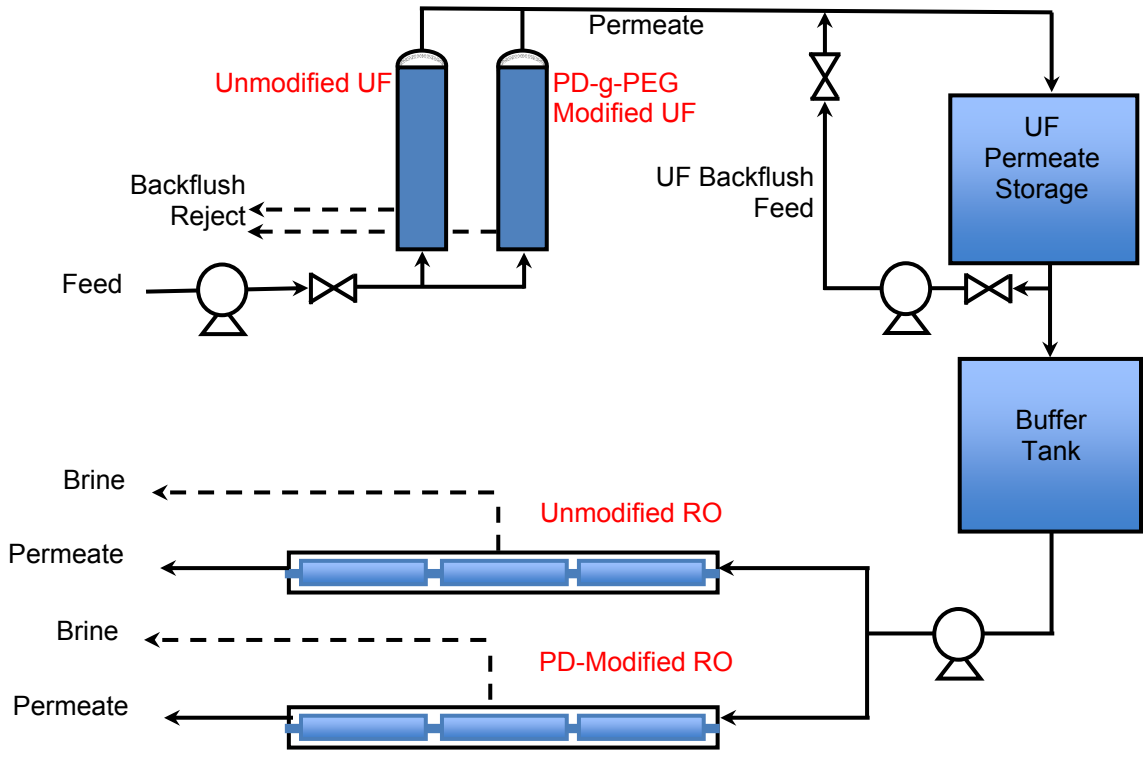

Figure 4.5. Pilot system process flow diagram.

Two UF modules were operated concurrently in parallel—one was surface modified as described above, and the second was an unmodified control. The UF units were operated continuously for a total of approximately 60 hours. The UF permeate was mixed, collected in a buffer tank, and used to feed the RO modules. The six RO membranes were divided into two trains consisting of three modules each—one train of PD-modified modules and one train of unmodified modules. Within each train, the three RO modules were connected through permeate core tubes in series, with concentrate from the first module feeding the second module, etc. The two RO trains were operated alternately for about 12 hours each during a total RO operation time of 100 hours. Therefore, each train operated four times. The unmodified train was operated for the first 12-hour block, followed by the modified train for the second 12-hour block, then the unmodified train for the third 12-hour block, the modified train in the fourth 12-hour block, and so on until the total 100-hour RO operating time had elapsed.

The UF modules were operated in dead-end mode with an initial feed flow of 21.9 L/min. The feed pump for the UF modules was run at a constant speed throughout the test; permeate flux and transmembrane pressure were allowed to vary as the membranes fouled. Permeate backwashing was performed for 30 seconds every 15 minutes due to the highly fouling nature of the UF feed. Two intensive cleaning procedures — chemically-enhanced hot water cleaning (HWC), performed daily, and traditional clean-in-place (CIP), preformed as needed, were used to recover UF flux. All cleaning solutions were prepared using RO permeate as solvent. The chemically-enhanced HWC step was a short version of the CIP procedure conducted to boost membrane performance. During the chemically-enhanced HWC cleaning procedure, heated caustic and then acid solutions were introduced from the feed side of the membrane fibers and circulated for a short period of time. Specifically, heated (52°C) caustic cleaning solution, prepared by

adjusting the pH of RO permeate water to 11.0 with sodium hydroxide, was first circulated through the UF modules for 15 minutes. Then, the cleaning solution pH was changed to 2.0 with citric acid and circulated for 15 more minutes. Finally, the modules were flushed with fresh RO permeate to remove the chemicals and dislodged foulants. During the traditional CIP process, a 1 wt% sodium hydroxide solution was circulated throughout the modules at 52°C for two hours. The modules were then flushed with RO permeate. Next, a 2 wt% citric acid solution (also heated to 52°C) was circulated through the modules for two hours. Finally, the modules were flushed with fresh RO permeate. During UF cleaning, feed flow to the RO train was maintained using water stored in the buffer tank (see Figure 4.5).

The RO modules were operated in crossflow with a feed flow of 56.7 L/min. The RO feed pump was operated at constant speed, which resulted in some variation in permeate flux and transmembrane pressure. Because the permeate flux was not held constant, recovery varied throughout the pilot study. Recovery was initially set at 50%, but during periods of high feed TDS concentrations, recovery decreased to as low as 10%. No chemical cleaning was performed on the RO modules.

Feed water turbidity, temperature, and RO feed and permeate conductivities were measured at 20-minute intervals. Turbidity was measured with an on-site nephelometer. Alkalinity, hardness, calcium concentration, and chloride concentration of the UF feed, UF permeate, RO feed, and RO permeate were measured frequently on-site using a drop-count titration test kit from Hach Company (Loveland, CO). RO membrane rejection is typically evaluated by measuring feed and permeate stream conductivity with in-line conductivity meters [27]. Conductivity meters, which had a maximum reading of 20,000 μS/cm, were calibrated using an 18,000 μS/cm (10,264 mg/L) NaCl standard solution

from Hach Company. Membrane rejection values were subsequently calculated from conductivity readings of feed and permeate streams.

4.4 BIOFOULING

4.4.1 Materials

Flat sheet PS-20 polysulfone UF membrane was purchased from Sepro Membranes, Inc (Oceanside, CA). Polypropylene feed spacer from a spiral wound TS80 nanofiltration membrane element was obtained from Trisep Corp. (Goleta, CA). Membrane samples were wetted with isopropanol for 10 minutes and soaked in deionized water for at least 30 minutes immediately before use. Dopamine HCl, Trizma HCl, isopropanol, ethanol, dimethyl sulfoxide, glycine buffer, bovine serum albumin, sodium acetate, sodium dihydrogen phosphate, and sodium nitrate were obtained from Sigma-Aldrich (St. Louis, Mo.). Sodium hydroxide and LB agar (Miller formulation) were purchased from Fisher Scientific (Pittsburgh, PA) and poly(ethylene glycol) monoamine (5000 Da.) from JenKem Technology (Allen, TX). Carbenicillin was obtained from Mediatech, Inc. (Manassas, VA) and NHS-rhodamine from Thermo Scientific (Rockford, IL). All chemicals were used as received. TRIS buffer (15mM), used throughout the membrane modifications, was prepared by dissolving Trizma HCl (2.634g/L) in deionized water and adjusting the pH of the resultant solution to 8.8 using sodium hydroxide (Fisher Scientific, Pittsburgh, PA).

4.4.2 Membrane modification

4.4.2.1 Membrane modification for short-term batch adhesion tests

PS-20 polysulfone UF membranes were modified with polydopamine and PEG for static protein and bacteria adhesion experiments. The membrane was placed, selective side up, on a clean glass plate. A thin coating of vacuum grease was applied to

the edge of a glass casting ring (~5" diameter) and the casting ring was pressed firmly onto the selective side of the membrane to anchor it in place. Dopamine (2 mg/mL) was dissolved in TRIS buffer (50 mL) and the solution was poured into the casting ring. The membrane was gently rocked, open to the atmosphere, for one hour to aerate the solution and to move it over the membrane surface. The membranes were immersed in ethanol for 10 minutes to remove any weakly-bound polydopamine and rinsed in deionized water for at least 30 minutes. If desired, PEG was grafted to the polydopamine-modified surface to create polydopamine-*g*-PEG-modified membranes. PEG-NH_2 (1 mg/mL) was dissolved in TRIS buffer (50 mL) heated to 60°C. This solution was poured into a 150 mm-diameter petri plate and the PD-modified membrane was floated, PD-modified side down, on the PEG-NH_2 solution for one hour in an oven at 60°C. After one hour, the membranes were rinsed with deionized water to remove unreacted PEG-NH_2. Membranes were stored in deionized water until use.

4.4.2.2 Membrane modification for continuous biofouling tests

PS-20 polysulfone UF membranes and polypropylene feed spacers were coated with polydopamine both *ex situ* prior to membrane fouling simulator assembly and *in situ* after membrane fouling simulator assembly. To coat membranes prior to assembly, membranes were floated, selective side down, atop dopamine solution (2 g/L, in TRIS buffer solution) for one hour with gentle rocking to agitate and aerate the solution during coating. Feed spacers were immersed in dopamine solution (2 g/L, in TRIS buffer solution) for one hour with gentle stirring. After one hour of contact with the dopamine solution, membranes and feed spacers were immersed in ethanol for 10 minutes to remove weakly-bound polydopamine and then rinsed with deionized water immediately prior to use. To coat membranes *in situ*, two membrane coupons were placed in the membrane fouling simulator channel sandwiching the feed spacer. The selective side of

the membrane coupons faced the spacer. A peristaltic pump (Masterflex, Cole Parmer, Vernon Hills, IL) was used to pump dopamine solution (2 g/L, in TRIS buffer solution) through the membrane fouling simulator for one hour at 5 L/min. The dopamine solution was recycled. After coating, ethanol was pumped through the membrane fouling simulator for 10 minutes to remove weakly-bound polydopamine. Finally, deionized water was pumped through the membrane fouling simulator for 30 minutes to remove the ethanol. Polydopamine coating was verified visually for membranes and feed spacers modified both *in situ* and *ex situ* by the characteristic browning of coated surfaces.

Poly(ethylene glycol) was also grafted to some of the polydopamine-coated membranes. PEG-NH_2 (1 g/L) was dissolved in TRIS buffer heated in an oven to 60°C. For those membranes modified *ex situ*, the membranes were floated, polydopamine-modified side down, atop the PEG-NH_2 solution with gentle rocking for one hour in an oven at 60°C. Feed spacers were immersed in PEG-NH_2 solution for one hour in an oven at 60°C. After PEG grafting, membranes and feed spacers were rinsed with deionized water immediately before use. For *in situ* PEG grafting, a membrane fouling simulator containing polydopamine-modified membranes and feed spacers was placed in an oven at 60°C and the PEG-NH_2 solution (1 g/L, in TRIS buffer solution) was pumped through the MFS for one hour at 5 L/min. The PEG-NH_2 solution was recycled. Deionized water was pumped through the membrane fouling simulator for 30 minutes immediately prior to use to remove any unreacted PEG-NH_2.

A schematic depiction of the membrane and feed spacer modification procedures is shown below in Figure 4.6.

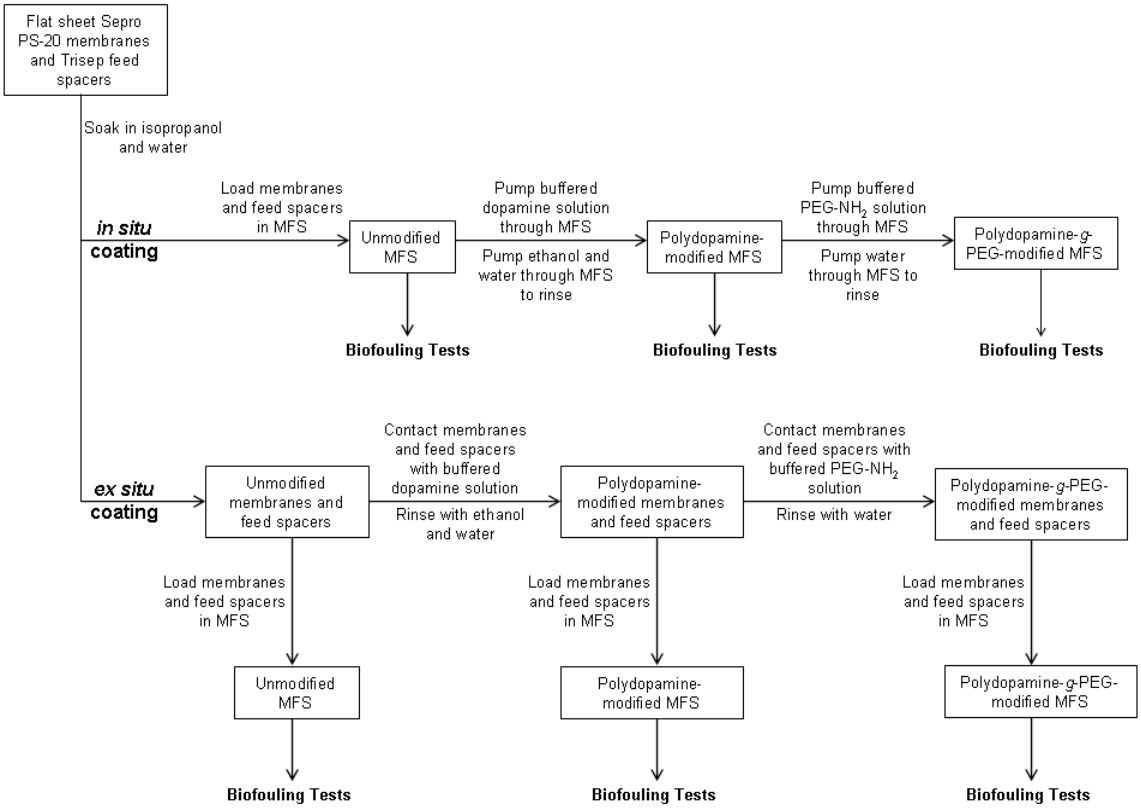

Figure 4.6. Schematic of *in situ* and *ex situ* membrane/feed spacer modification procedures.

4.4.3 Short-term batch adhesion tests

4.4.3.1 Protein adhesion test

Fluorescence measurement of surfaces exposed to fluorophore-tagged protein is an established means of comparing surface susceptibility to protein adhesion [28]. Bovine serum albumin (BSA), a common laboratory model globular protein, was tagged with NHS-rhodamine. BSA (40 mg) was dissolved in ultrapure water (5 mL) and NHS-rhodamine (8 mg) was dissolved in dimethyl sulfoxide (175 μL). An aliquot of the NHS-rhodamine solution (150 μL) was added to the BSA solution and was allowed to react for one hour; glycine buffer (50 μL) was then added to quench the reaction. The reaction

mixture was purified by elution through Sephadex columns (Thermo Scientific, Rockford, IL) followed by dialysis for 24 hours against ultrapure water in Slide-A-Lyzer dialysis cassettes (Thermo Scientific, Rockford, IL). The final BSA concentration was evaluated using UV spectrophotometry; the BSA suspension was diluted to 0.1 mg/mL. Unmodified, polydopamine-modified, and polydopamine-*g*-PEG-modified membranes were cut into 1"-diameter discs and loaded into dead-end cells (UHP 25, Advantec MFS, Dublin, CA) as shown in Figure 4.7. The BSA solution (2 mL) was dispensed into the dead-end cells. No pressure was applied to the solution and there was consequently no permeation through the membranes. The cells were covered for one hour at room temperature, after which time the BSA suspension was removed. The membranes were gently rinsed with deionized water (~10 mL) and air dried overnight. The fluorescence intensity of the samples was quantified with a fluorescent plate reader (Tecan Sapphire II, Mannedorf, Switzerland). Fluorescence of membrane samples with no protein exposure was measured and this background was subtracted from the sample fluorescence readings. High fluorescence indicates high protein adhesion.

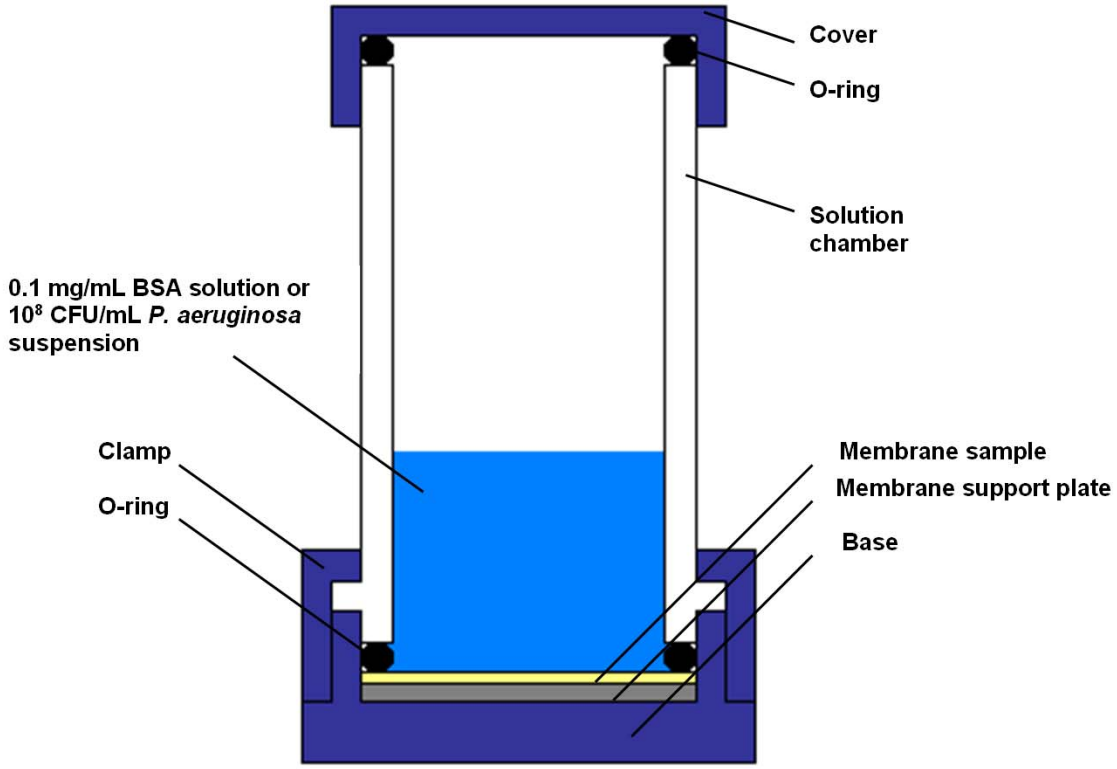

Figure 4.7. Dead-end cell used for protein and bacteria static adhesion experiments.

4.4.3.2 Bacteria adhesion test

P. aeruginosa, a Gram-negative, rod-shaped organism found in nearly all natural waters (Ramsey and Whiteley, 2004), was used to evaluate short-term bacteria adhesion to unmodified, polydopamine-modified, and polydopamine-*g*-PEG-modified membranes. A freezer stock of *lux*-producing *P. aeruginosa* strain PA14 was stored at -80°C.

Culture plates were prepared. LB agar (Miller formulation) was dissolved in deionized water according to manufacturer instruction, carbenicillin antibiotic (100 μg/mL) was added, and the mixture was autoclaved. (The *lux* plasmid employed provides resistance to the carbenicillin; inclusion of carbenicllin in the growth media ensures *lux* retention.) This mixture was poured into sterile petri plates and cooled. The

plates were stored at 4°C. Liquid LB media was prepared according to manufacturer instruction, carbenicillin was added (100 μg/mL), and the media was autoclaved.

Cells were grown by streaking a bit of the freezer stock on a culture plate and incubating overnight at 37°C. A single colony was picked from the plate and grown in liquid media (containing 100 μg/mL carbenicillin) overnight at 37°C with shaking. A 0.5 mL aliquot of the liquid culture was diluted with 4.5 mL fresh LB media without antibiotic and grown for about two hours at 37°C with shaking, until the optical density at 600 nm was in the range of 0.3 – 0.5. This dilution/growth procedure ensures that the bacteria are in log-phase growth during the experiment for maximum attachment and luminescence. The liquid culture was diluted with more fresh media to an optical density at 600 nm of 0.1 (approximately 10^8 CFU/mL).

Unmodified, polydopamine modified, and polydopamine-*g*-PEG modified membranes were cut into 1"-diameter discs and loaded into dead-end cells (UHP 25, Advantec MFS, Dublin, CA) as in the protein adhesion study (Figure 4.7). The bacteria suspension was dispensed into the dead-end cells (2 mL) and incubated at 37°C for one hour. No pressure was applied to the solution and there was consequently no permeation through the membranes. After one hour, the bacteria suspension was removed and the membranes were gently rinsed with ~10 mL deionized water. Four ¼"-diameter samples were cut out of each membrane and loaded into an opaque white 96-well plate. 100 μL fresh LB broth (no antibiotic) was dispensed into each cell to ensure that the bacteria would luminesce during the assay. Luminescence was measured in a Biotek Synergy HT plate reader running KC4 software. Luminescence of membrane samples with no bacteria exposure was measured and this background was subtracted from the sample luminescence readings. High luminescence indicates high bacterial adhesion.

4.4.4 Long-term continuous biofouling tests

4.4.4.1 The Membrane Fouling Simulator for biofouling tests

The membrane fouling simulator has been developed to simulate biofouling in spiral-wound modules [29]. Feed water flows into one end of the membrane fouling simulator, passes through a channel containing a feed spacer sandwiched between two membrane samples, and exits at the opposite end. The channel dimensions are 0.077 cm x 4.00 cm x 20.0 cm. With membranes and spacer in place, the hydrodynamics are similar to those found in spiral-wound modules [30]. In these experiments, no water permeated through the membranes; previous studies have shown that the presence or absence of permeate production has no effect on the measured feed channel pressure drop during biofouling experiments [31].

4.4.4.2 Biodegradable organic substrates for biofouling tests

Biodegradable organic compounds are requisite for biofilm growth and their presence in membrane filtration operations exacerbates biofouling [32]. The heterotrophic organisms comprising most biofilms [33] can metabolize many dissolved organics including anti-foulants such as anti-scaling compounds [34]. To simulate these dissolved organics and to promote biofilm growth within a reasonable laboratory experimental duration, substrate was dosed to the membrane fouling simulator feeds from a solution of acetate, dihydrogen phosphate, and nitrate to achieve a C:N:P ratio of 100:20:10. The typical C:N:P ratio in biomass is ~100:20:4.3; an excess of phosphorous was dosed to ensure that phosphate limitation, which has recently received interest as a biofouling control strategy [35], did not restrict biofouling in the membrane fouling simulators. Sodium acetate (4.608 g), sodium dihydrogen phosphate (0.518 g), and sodium nitrate (1.623 g) were dissolved into deionized water (5 L); sodium hydroxide was used to adjust the dosing solution to pH = 12. Substrate was dosed to each

membrane fouling simulator at 30 mL/hr using a calibrated peristaltic pump (Masterflex, Cole Parmer, Vernon Hills, IL), providing 0.500 mg/L C, 0.100 mg/L N, and 0.050 mg/L P in the membrane fouling simulator feeds. Substrate dosing levels were maintained throughout all three experiments. A negative control membrane fouling simulator was operated using unmodified membranes and spacer without substrate dosage.

4.4.5 Biofouling tests

Drinking water prepared from anaerobic groundwater (subsequently treated by aeration, rapid sand filtration, deacidification, softening and rapid sand filtration at treatment plant Spannenburg in the Netherlands) was used as membrane fouling simulator feed. The drinking water contained no residual disinfectant.

Three membrane fouling simulator experiments were carried out with polysulfone UF membranes and polypropylene feed spacers. In all three experiments, one membrane fouling simulator was operated with unmodified membranes and feed spacer without any substrate dosing as a negative control; another monitor was operated with unmodified membranes and feed spacer with substrate dosing as a positive control. A third monitor was operated with polydopamine modified membranes and feed spacers. The fourth monitor was operated with polydopamine-*g*-PEG modified membranes and feed spacers. In Experiments 1 and 2, membranes and feed spacers were modified *in situ*. Membrane and feed spacer samples were first loaded into two membrane fouling simulators and modified with polydopamine. One of these polydopamine-modified membrane fouling simulators was subsequently modified by PEG grafting. In Experiment 3, membrane and feed spacer modification was carried out prior to membrane fouling simulator assembly. Two sets of membrane and feed spacer samples were modified with polydopamine; PEG was subsequently grafted to one set of membrane and feed spacer samples. These

polydopamine modified and polydopamine-*g*-PEG modified membranes and feed spacers were then assembled into two membrane fouling simulators.

Fouling evolution was monitored *via* the feed channel pressure drop increase over the length of the monitor [36]. A differential pressure transducer (Deltabar S PMD70, Endress+Hauser, Reinach, Switzerland) measured the feed channel pressure drop by comparing the pressure at ports at the membrane fouling simulator inlet and outlet. Figure 4.8 shows a simplified schematic diagram of the experimental apparatus (a) and a photo of the setup at WETSUS in Leeuwarden, the Netherlands (b). Multiple membrane fouling simulators were used in parallel to compare unmodified and modified membranes and feed spacers with a negative control. Drinking water feed to each monitor was controlled at 16 L/hr with an adjustable valve and substrate dosing was checked gravimetrically at least once daily. Without temperature control, as in Experiment 1, the feed water was approximately 12°C. To warm the feed water in Experiments 2 and 3, accelerating microbial growth, feed water was passed through a coil immersed in a water tank heated with an electric heater. Heated feed water was approximately 20°C. At a temperature of 12°C biofilm was permitted to grow in the membrane fouling simulators for 250 hours or until the feed channel pressure drop reached at least 500 mbar. At a water temperature of 20°C, biofilm growth sufficient to produce a feed channel pressure drop of 500 mbar required about 100 hours.

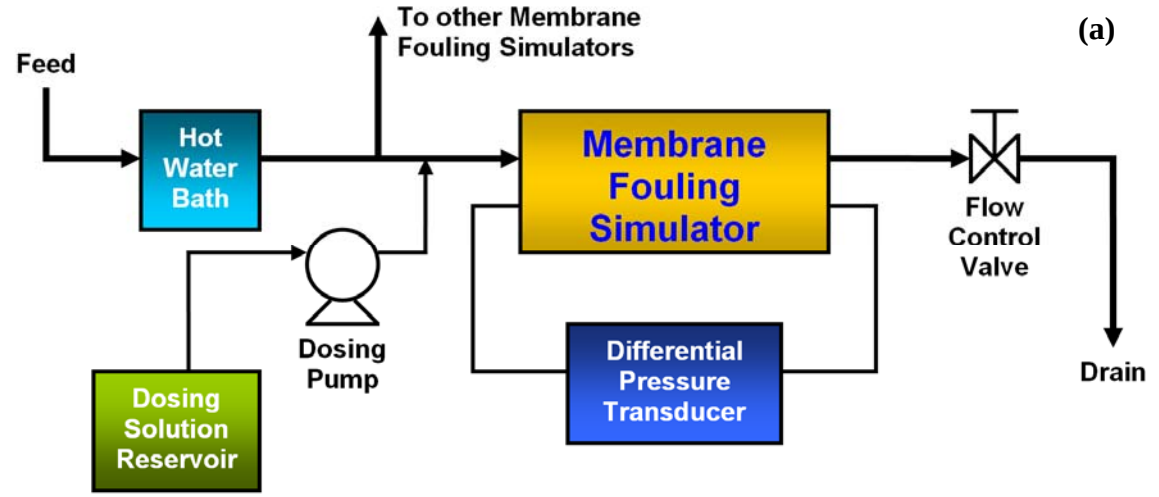

Figure 4.8. (a) Membrane fouling simulator experimental schematic. Eleven membrane fouling simulators were operated in parallel. In Experiment 1, the hot water bath was bypassed; in Experiments 2 and 3, where the feed water was heated to 20°C, the feed line was passed through a hot water bath. (b) Photo of the setup at WETSUS in Leeuwarden, the Netherlands.

After fouling, each membrane fouling simulator was disassembled to examine the accumulated biomass. From each membrane fouling simulator two samples (30 cm^2) of the membranes and feed spacers were cut out and placed in a centrifuge tube containing 30 ml sterile tap water for adenosine triphosphate (ATP) analysis and ultrapure water (mL) for total organic carbon (TOC) analysis. The centrifuge tubes were alternately sonicated using an ultrasonic cleaning bath (5510E-DTH, Bransonic, Danbury, CT) and agitated using a vortex mixer three times to dislodge the biomass from the membranes and feed spacers. Biomass suspensions were packed on ice and sent to Vitens (Leeuwarden, NL) for measurement of ATP and TOC concentrations. ATP concentration is a well-known metric of biomass growth as ATP is produced by all living cells and ATP is not associated with nonliving material [37]. TOC measures total organic carbon contained within the biofilm cells as well as from the extracellular polymeric substances [38,39], the sticky matrix of biopolymers that surrounds the cells [40].

4.4.6 Summary

A summary of the tests is shown in Table 4.4, below.

Study	Duration (h)	Temp. (°C)	Foulant	Evaluation Metric	Modified Material
Protein Adhesion	1	20	bovine serum albumin	fluorescence	membrane
Bacteria Adhesion	1	37	P. aeruginosa	luminescence	membrane
Biofouling (in situ coating)	250	12	autochthonous water population	pressure drop and biomass accumulation	membrane and spacer
Biofouling (in situ coating)	100	20	autochthonous water population	pressure drop and biomass accumulation	membrane and spacer
Biofouling (ex situ coating)	140	20	autochthonous water population	pressure drop and biomass accumulation	membrane and spacer

Table 4.4. Summary of experimental conditions in the biofouling studies.

4.5 REFERENCES

[1] S. Kasemset, A. Lee, D.J. Miller, B.D. Freeman, M.M. Sharma, Effect of Polydopamine Deposition Conditions on Fouling Resistance, Physical Properties, and Permeation Properties of Reverse Osmosis Membranes in Oil/Water Separation, Journal of Membrane Science 425-426 (2013) 208–216.

[2] B.D. McCloskey, H.B. Park, H. Ju, B.W. Rowe, D.J. Miller, B.D. Freeman, A Bioinspired Fouling-Resistant Surface Modification for Water Purification Membranes, Journal of Membrane Science 413-414 (2012) 82–90.

[3] H. Ju, B.D. McCloskey, A.C. Sagle, Y.-H. Wu, V.A. Kusuma, B.D. Freeman, Crosslinked Poly(ethylene oxide) Fouling Resistant Coating Materials for Oil/Water Separation, Journal of Membrane Science 307 (2) (2008) 260–267.

[4] B.D. McCloskey, H.B. Park, H. Ju, B.W. Rowe, D.J. Miller, B.J. Chun, et al., Influence of Polydopamine Deposition Conditions on Pure Water Flux and Foulant Adhesion Resistance of Reverse Osmosis, Ultrafiltration, and Microfiltration Membranes, Polymer 51 (15) (2010) 3472–3485.

[5] W. Xie, G.M. Geise, B.D. Freeman, H.-S. Lee, G. Byun, J.E. McGrath, Polyamide Interfacial Composite Membranes Prepared from m-Phenylene Diamine, Trimesoyl Chloride and a New Disulfonated Diamine, Journal of Membrane Science 403-404 (2012) 31–33.

[6] E.M. Van Wagner, A.C. Sagle, M.M. Sharma, Y.-H. La, B.D. Freeman, Surface Modification of Commercial Polyamide Desalination Membranes using Poly(ethylene glycol) Diglycidyl Ether to Enhance Membrane Fouling Resistance, Journal of Membrane Science 367 (1-2) (2011) 273–287.

[7] H. Ju, Water Transport Study in Crosslinked Poly (ethylene oxide) Hydrogels as Fouling-Resistant Membrane Coating Materials, The University of Texas at Austin, 2010.

[8] D.. Kwon, S. Vigneswaran, A.. Fane, R.B. Aim, Experimental determination of critical flux in cross-flow microfiltration, Separation and Purification Technology 19 (3) (2000) 169–181.

[9] P. Aimar, J.A. Howell, M. Turner, Effects of Concentration Boundary Layer Development on the Flux Limitations in Ultrafiltration, Chemical Engineering Research and Design 67 (3) (1989) 255–261.

[10] R.W. Field, D. Wu, J.A. Howell, B.B. Gupta, Critical Flux Concept for Microfiltration Fouling, Journal of Membrane Science 100 (3) (1995) 259–272.

[11] D. Wu, J.A. Howell, R.W. Field, Critical Flux Measurement for Model Colloids, Journal of Membrane Science 152 (1) (1999) 89–98.

[12] J.A. Howell, D. Wu, R.W. Field, Transmission of bovine albumin under controlled flux ultrafiltration, Journal of Membrane Science 152 (1) (1999) 117–127.

[13] P.S. Beier, G. Jonsson, Critical Flux Determination by Flux-Stepping, AIChE Journal 56 (7) (2010) 1739–1747.

[14] R. Chan, V. Chen, The Effects of Electrolyte Concentration and pH on Protein Aggregation and Deposition: Critical Flux and Constant Flux Membrane Filtration, Journal of Membrane Science 185 (2) (2001) 177–192.

[15] V. Chen, Performance of partially permeable microfiltration membranes under low fouling conditions, Journal of Membrane Science 147 (2) (1998) 265–278.

[16] K.Y.-J. Choi, B.A. Dempsey, Bench-scale Evaluation of Critical Flux and TMP in Low-pressure Membrane Filtration, Journal of the American Water Works Association 97 (7) (2005) 134–143.

[17] D. Hughes, R.W. Field, Crossflow filtration of washed and unwashed yeast suspensions at constant shear under nominally sub-critical conditions, Journal of Membrane Science 280 (1-2) (2006) 89–98.

[18] S. Metsämuuronen, M. Nyström, Critical flux in cross-flow ultrafiltration of protein solutions, Desalination 175 (1) (2005) 37–47.

[19] H.K. Vyas, R.J. Bennett, A.D. Marshall, Performance of crossflow microfiltration during constant transmembrane pressure and constant flux operations, International Dairy Journal 12 (5) (2002) 473–479.

[20] W. Youravong, M.J. Lewis, A.S. Grandison, Critical Flux in Ultrafiltration of Skimmed Milk, Food and Bioproducts Processing 81 (4) (2003) 303–308.

[21] R. Turton, R.C. Bailie, W.B. Whiting, J.A. Shaeiwitz, Analysis, Synthesis, and Design of Chemical Processes, 2nd ed., Prentice Hall PTR, Upper Saddle River, NJ, 2003.

[22] J.R. Elliot, C.T. Lira, Introductory Chemical Engineering Thermodynamics, Prentice Hall PTR, Upper Saddle River, NJ, 1999.

[23] A.C. Sagle, E.M. Van Wagner, H. Ju, B.D. McCloskey, B.D. Freeman, M.M. Sharma, PEG-Coated Reverse Osmosis Membranes: Desalination Properties and Fouling Resistance, Journal of Membrane Science 340 (1-2) (2009) 92–108.

[24] E.M. Van Wagner, A.C. Sagle, M.M. Sharma, B.D. Freeman, Effect of Crossflow Testing Conditions, including Feed pH and Continuous Feed Filtration, on Commercial Reverse Osmosis Membrane Performance, Journal of Membrane Science 345 (1-2) (2009) 97–109.

[25] B.D. McCloskey, H. Ju, B.D. Freeman, Composite Membranes Based on a Selective Chitosan−Poly(ethylene glycol) Hybrid Layer: Synthesis, Characterization, and Performance in Oil−Water Purification, Industrial & Engineering Chemistry Research 49 (1) (2010) 366–373.

[26] B. Zhu, S. Edmondson, Polydopamine-Melanin Initiators for Surface-Initiated ATRP, Polymer 52 (10) (2011) 2141–2149.

[27] Standard Test Methods for Operating Characteristics of Reverse Osmosis and Nanofiltration Devices, ASTM Standard D4194-03 (2008).

[28] M. Taylor, A.J. Urquhart, D.G. Anderson, P.M. Williams, R. Langer, M.R. Alexander, et al., A Methodology for Investigating Protein Adhesion and Adsorption to Microarrayed Combinatorial Polymers, Macromolecular Rapid Communications 29 (15) (2008) 1298–1302.

[29] J.S. Vrouwenvelder, S.M. Bakker, L.P. Wessels, J.A.M. van Paassen, The Membrane Fouling Simulator as a New Tool for Biofouling Control of Spiral-wound Membranes, Desalination 204 (1-3) (2007) 170–174.

[30] J.S. Vrouwenvelder, J.A.M. van Paassen, L.P. Wessels, A.F. van Dam, S.M. Bakker, The Membrane Fouling Simulator: A practical tool for fouling prediction and control, Journal of Membrane Science 281 (1-2) (2006) 316–324.

[31] J.S. Vrouwenvelder, D.A. Graf von der Schulenburg, J.C. Kruithof, M.L. Johns, M.C.M. van Loosdrecht, Biofouling of spiral-wound nanofiltration and reverse osmosis membranes: A feed spacer problem, Water Research 43 (3) (2009) 583–94.

[32] T. Griebe, H.-C. Flemming, Biocide-free antifouling strategy to protect RO membranes from biofouling, Desalination 118 (1-3) (1998) 153–156.

[33] H.-C. Flemming, Biofouling in Water Systems--Cases, Causes and Countermeasures, Applied Microbiology and Biotechnology 59 (6) (2002) 629–40.

[34] J.S. Vrouwenvelder, J.C. Kruithof, M.C.M. Van Loosdrecht, Integrated Approach for Biofouling Control, Water Science & Technology 62 (11) (2010) 2477–90.

[35] J.S. Vrouwenvelder, F. Beyer, K. Dahmani, N. Hasan, G. Galjaard, J.C. Kruithof, et al., Phosphate Limitation to Control Biofouling, Water Research 44 (11) (2010) 3454–66.

[36] J.S. Vrouwenvelder, J.A.M. van Paassen, J.C. Kruithof, M.C.M. van Loosdrecht, Sensitive pressure drop measurements of individual lead membrane elements for accurate early biofouling detection, Journal of Membrane Science 338 (1-2) (2009) 92–99.

[37] O. Holm-Hansen, C.R. Booth, The Measurement of Adenosine Triphosphate in the Ocean and its Ecological Significance, Limnology and Oceanography 11 (4) (1966) 510–519.

[38] S. Kim, S. Lee, S. Hong, Y. Oh, M. Seoul, J. Kweon, et al., Biofouling of reverse osmosis membranes: Microbial quorum sensing and fouling propensity, Desalination 247 (1-3) (2009) 303–315.

[39] C. Coufort, N. Derlon, J. Ochoa-Chaves, A. Liné, E. Paul, Cohesion and detachment in biofilm systems for different electron acceptor and donors, Water Science & Technology 55 (8-9) (2007) 421–428.

[40] H.-C. Flemming, T.R. Neu, D.J. Wozniak, The EPS Matrix: The “House of Biofilm Cells”, Journal of Bacteriology 189 (22) (2007) 7945–7.

Chapter 5: Elucidating the Structure of Polydopamine

5.1 Summary

Herein a new structure for polydopamine, a synthetic eumelanin that has found broad utility as an anti-fouling agent, is proposed. Commercially available 3-hydroxytyramine hydrochloride (dopamine HCl) was polymerized under aerobic, aqueous conditions using tris(hydroxymethyl)aminomethane (TRIS) as the base, affording a darkly colored powder product upon isolation. Solid state ^{13}C and ^{15}N NMR spectroscopy indicated that protons were bound to the aryl core of the polymer, in contrast to previously proposed models that incorporate aryl-aryl linkages between repeat units, suggesting that the bonds formed between monomers are non-covalent. The nature of these supramolecular bonds, as well as the resulting structure of the polymer, was probed by FT-IR and electron paramagnetic resonance (EPR) spectroscopies as well as powder X-ray diffraction (PXRD), which collectively indicated that the linkages between monomeric units in polydopamine consist primarily of strong hydrogen bonding, charge transfer, and π-stacking interactions.

5.2 Results and Discussion

Polydopamine was prepared in one step from commercially available 3-hydroxytyramine hydrochloride (dopamine HCl) by basifying the salt with tris(hydroxymethyl)aminomethane (TRIS) (Chapter 4) [1]. The as-prepared polydopamine powder was insoluble in water (both acidic and alkaline) and all common organic solvents. Therefore, solid state techniques were required to characterize the

---

This chapter adapted from: D.R. Dreyer, D.J. Miller, B.D. Freeman, D.R. Paul, C.W. Bielawski, Elucidating the Structure of Poly(dopamine), Langmuir 28 (15) (2012) 6428–6435.

structure of the material obtained. Efforts began with solid state nuclear magnetic resonance (ssNMR) spectroscopy. The solid state ^{15}N NMR spectrum of the as-prepared polydopamine showed a resonance at a chemical shift (δ) of -260 ppm (relative to CH_3NO_2) (Figure 5.1), consistent with the presence of cyclized, nitrogenous species such as the indole- or indoline-type structures [2] widely proposed in many eumelanins [3,4]. For comparison, the primary, uncyclized amines of dopamine HCl and TRIS exhibited ^{15}N NMR resonances at -349 ppm and -351 ppm, respectively, in solution (D_2O, relative to CH_3NO_2). The downfield shift of the ^{15}N resonance in polydopamine, as well as the absence of signals observed in the region that could be attributed to a primary amine, suggest that the dopamine underwent cyclization during the polymerization reaction and that the TRIS reagent was not incorporated into the polydopamine product to a significant extent.

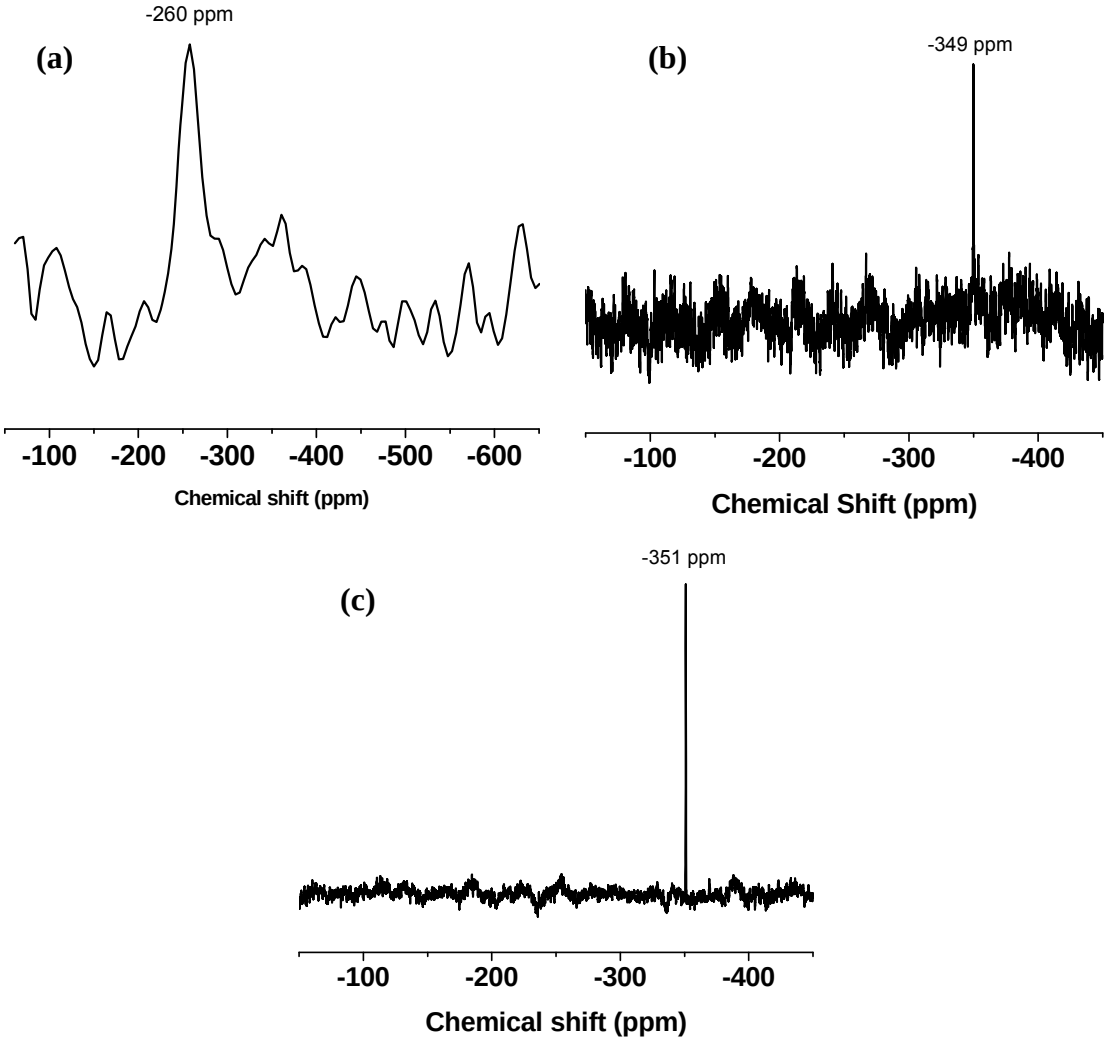

Figure 5.1. (a) solid state ^{15}N NMR spectra of polydopamine (400 MHz, spinning rate: 6 kHz), (b) solution state ^{15}N NMR of dopamine HCl (D_2O, 400 MHz), and (c) solution state ^{15}N NMR of TRIS (D_2O, 400 MHz). Chemical shifts (δ) reported relative to CH_3NO_2.

One-dimensional, solid-state ^{13}C NMR spectroscopy was also performed on the as-prepared polydopamine sample described above. As shown in Figure 5.2, the spectrum showed a pair of resonances spanning from 110 to 150 ppm, characteristic of aromatic species [5]. These signals, which were also present in the solution state spectrum of dopamine HCl (Figure 5.3), indicated that the aromatic ring at the core of the molecule was retained. (Comparisons between solid and solution state NMR spectra have proven to be reliable in many diverse systems, including proteins [6], metal complexes [7], and polymers [8].) Two other features that were not present in the solution-state spectrum of the dopamine monomer provided additional structural information. First, a resonance observed at 173 ppm suggested that the diol structure present in the starting material underwent partial or complete oxidation to its respective 1,2-dione. The oxidative formation of ketones is a hallmark of quinhydrone assembly and a key step in proposed mechanisms for the oligomerization and polymerization of catecholamines [9,10]. Second, resonances observed between 30 and 70 ppm were assigned to aliphatic species. The upfield shift of these ^{13}C resonances, relative to unsaturated olefins, were characteristic of the saturated ethylene linker in dopamine; dehydrogenation was not observed upon cyclization, based on these NMR results. Moreover, as the aforementioned ^{15}N NMR data indicated that the nitrogen atom was part of a heterocycle, the chemical shifts of the aliphatic ^{13}C species (30–70 ppm) further suggested the formation of a saturated indoline product, rather than an unsaturated indole.

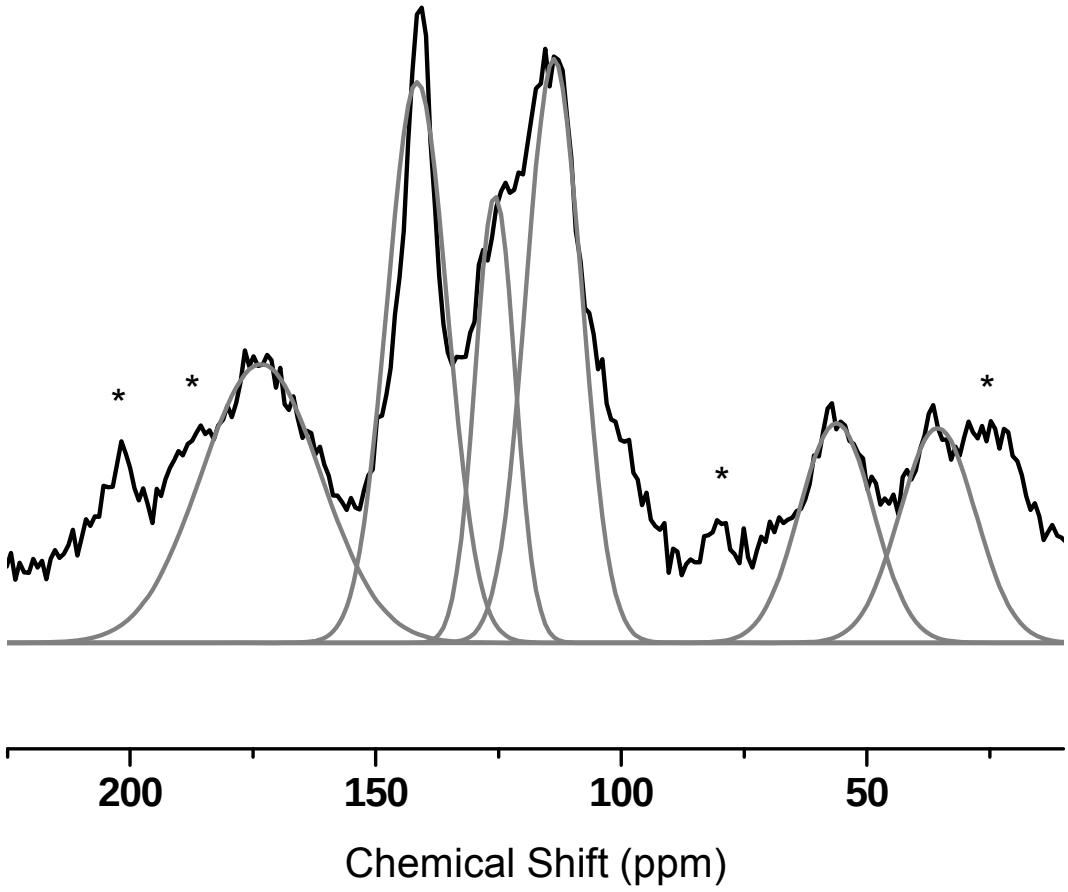

Figure 5.2. Solid state ^{13}C NMR spectrum of unlabeled polydopamine (black) with peak deconvolutions (gray). Relative integrations of the deconvoluted peaks are given in Table 5.1 (asterisks denote spinning side bands).

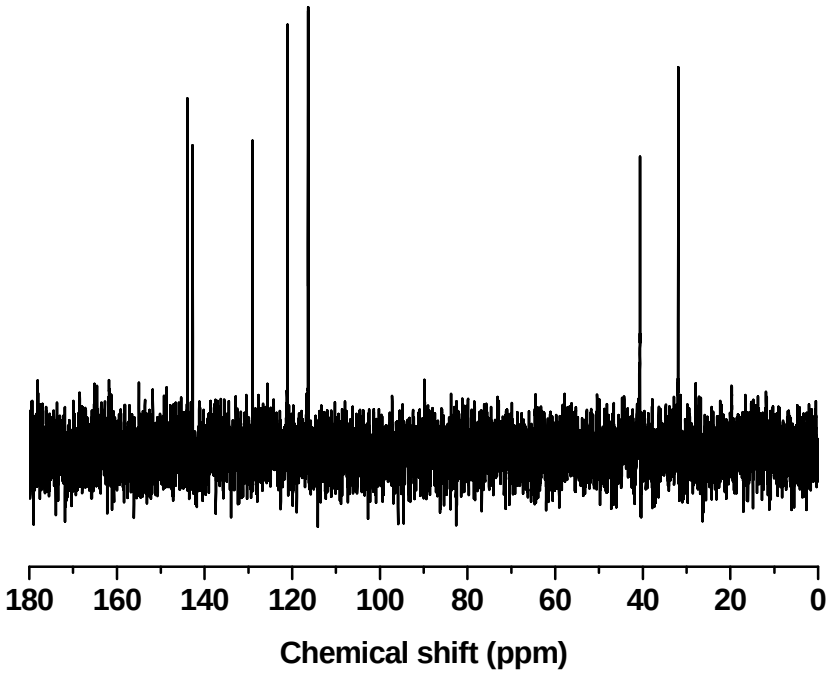

Figure 5.3. ^{13}C solution state NMR spectrum (D_2O) of dopamine HCl.

In an effort to confirm the aforementioned NMR assignments, the peak areas of each of the ^{13}C resonances were quantified. Quantitative ^{13}C ssNMR is often challenged by the long spin-lattice relaxation times of carbon nuclei in the solid state [11–13]. The relaxation times of ^{13}C nuclei in polydopamine, however, were found to be very short. As shown in Figure 5.4, ^{13}C NMR spectra collected on a polydopamine sample at four different spin-lattice relaxation times (t_1 = 5 s, 15 s, and 20 s) showed no changes in peak shape or intensity, despite the presence of secondary, tertiary, and quaternary carbon centers. Such behavior indicated that the ^{13}C nuclear spin-lattice relaxation times were less than 5 s [14], which enabled deconvolution and integration of the ^{13}C ssNMR resonances. The spectrum shown in Figure 5.2 was deconvoluted and the relative integrations of the respective signals are summarized in Table 5.1.

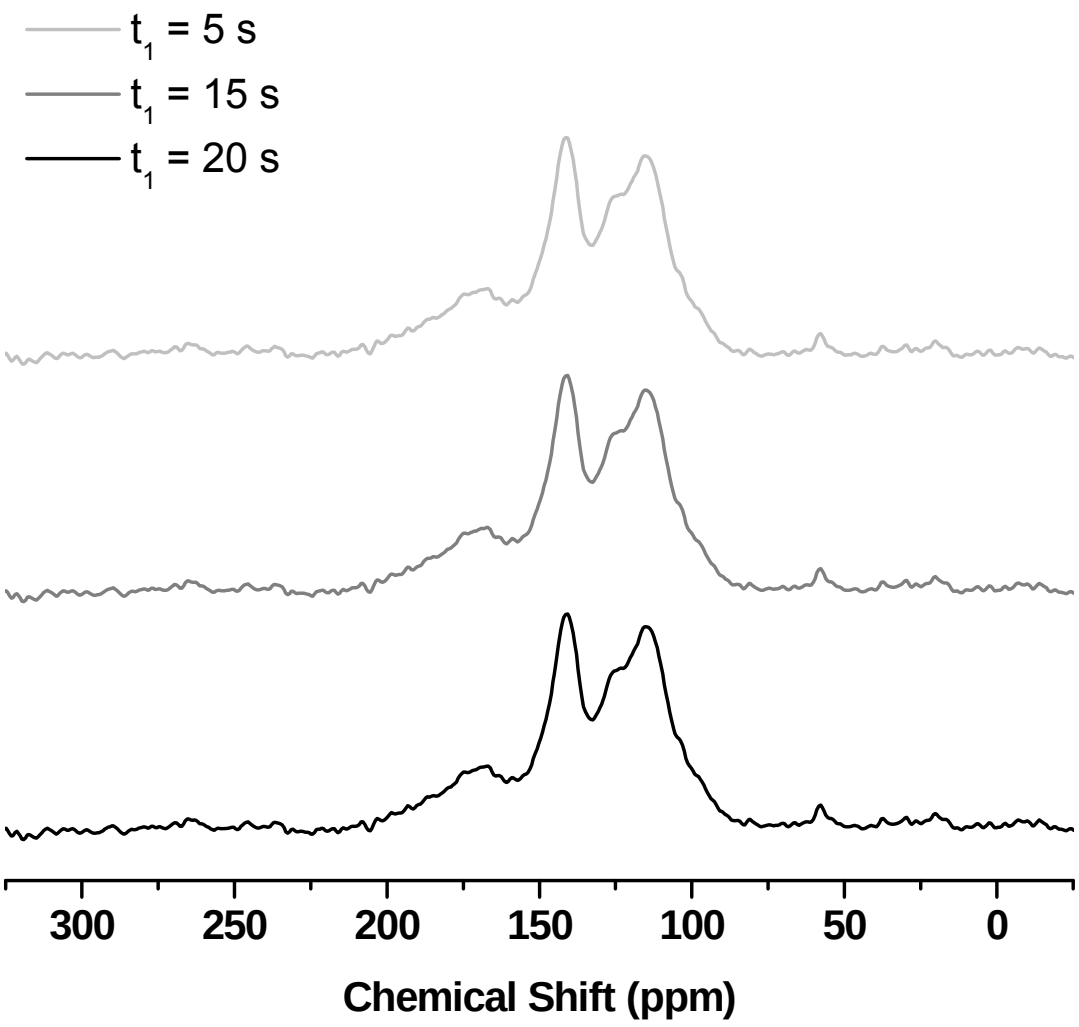

Figure 5.4. Variation of the spin-lattice relaxation time (t1) from 5 s (top) to 15 s (middle) to 20 s (bottom) showed no variation in peak shape or intensity in the solid state ^{13}C spectra of polydopamine, indicating rapid nuclear relaxation.

Proposed Structural Assignment	Relative Integration (arbitrary units)	Peak Maximum (ppm)
Cyclized aliphatic carbon	1.0	36
Cyclized aliphatic carbon	1.0	53
Proteated arene carbons	2.0	114
Quaternary bridgehead	1.1	126
Quaternary bridgehead	1.2	142
Oxygen-bound carbons	2.0	173

Table 5.1. Relative integrations and proposed structural assignments of deconvoluted peaks in the ^{13}C ssNMR spectra shown in Figure 5.2.

Based on the ssNMR data collected, two possible structures of polydopamine were identified (Figure 5.5). These structures, with the carbon centers labeled A–G, were used to assign the peaks observed in the ^{13}C spectrum [15]. The peaks centered at 36 and 53 ppm in the ^{13}C ssNMR spectrum were assigned to carbons G and H, respectively (Figure 5.5), agreeing with their relative integrations of 1.0 each. (The possible structures considered in this study, cyclized indolines 1 and 2, are based on the most commonly proposed structures for eumelanins, and are consistent with the data presented herein [16].) The peak observed at 173 ppm was assigned to the two oxygen-bound carbons (A and B), due to the high downfield shift commonly observed in such deshielded moieties. (Carbons A and B may be partially- or completely-oxidized to a dione; here, they are shown partially oxidized.) As mentioned previously, the signals in the 110 to 150 ppm range corresponded to the four remaining carbon centers in the cyclic core. Based on the proposed structure, the most downfield peak at 142 ppm, which

integrated to 1.2, was attributed to a bridgehead atom adjacent to the electronegative nitrogen (carbon F). Such a carbon center would be expected to produce a resonance further downfield than other carbon atoms in the aromatic region; thus, the resonance at 142 ppm was assigned to carbon F. With the peak at 142 ppm assigned, only the large peak centered at 114 ppm (integration of 2.0) and the smaller shoulder at 126 ppm (integration of 1.1) remained; the sum of these resonances was assigned to carbons C, D, and E. Based on its downfield chemical shift, carbon E, a quaternary center forming the bridge with carbon F, was assigned to the peak at 126 ppm leaving the peak at 114 ppm to be attributed to carbons C and D.

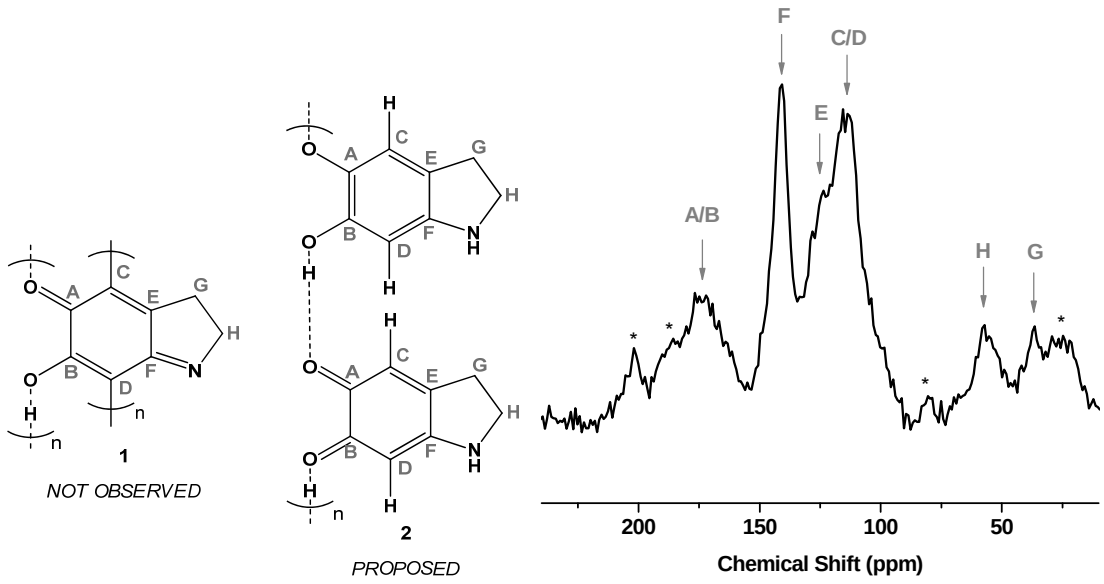

Figure 5.5. Possible structures of polydopamine including and not including aryl-coupled monomers (1 and 2, respectively). ^{13}C NMR spectrum shown at right, including proposed peak assignments based on structure 2 (relative integrations shown in Table 5.1 determined *via* peak deconvolution) (asterisks denote spinning side bands).

Structures 1 and 2 (Figure 5.5) are distinguished by the bonding to carbons C and D. In structure 1, covalent bonds exist between the aryl rings of the monomers; in structure 2, aryl coupling is absent and carbons C and D are bound to hydrogen atoms. The relatively upfield chemical shift of carbons C and D (114 ppm) suggested that these were tertiary, protonated centers rather than quaternary [17], coupled centers, but further confirmation was desired to conclusively define the polymer's structure.

In order to examine the linkages between repeat units in greater detail, a polydopamine sample was prepared using dopamine HCl that was ^{13}C-labeled (99 atom%) at the six atoms comprising the aromatic core (Figure 5.6); the aliphatic carbons were not labeled. Polydopamine powder was prepared from a mixture of 95:5 (w/w) unlabeled : labeled dopamine HCl using the aforementioned polymerization and

purification procedures (see Chapter 4). (^{13}C-labeled dopamine HCl (99 atom%) was diluted with natural abundance dopamine HCl in order to prevent excessive homonuclear dipolar coupling between the NMR-active nuclei [18], which would lead to excessive broadening in the obtained spectrum, as is observed in most solid state ^{1}H NMR spectroscopy [19].) The use of an enriched sample permitted a one-dimensional cross-polarization (CP) study of the isolated aromatic core to examine the structure and bonding in the aryl moiety, with particular attention given to the presence or absence of aryl-aryl linkages between the repeat units [20–22]. An overlay of the spectra obtained with and without an additional 40 μs proton evolution period is shown in Figure 5.7. (Common proton evolution periods are typically less than 600 μs in the solid state [23–25].) Inclusion of this evolution period resulted in a diminished level of magnetization transfer from the protons to the carbons, as partial relaxation of the protons had already occurred prior to CP. As expected for carbons free of adjacent hydrogens, the resonances at 173 (carbons A and B), 142 (carbon F), and 126 ppm (carbon E) showed no significant change in intensity. Conversely, the peak at 114 ppm, corresponding to carbons C and D located in the aromatic core, decreased in intensity upon CP. The change in signal intensity, due to diminished magnetization transfer from protons over the extended evolution time, indicated carbons C and D were bound to hydrogen atoms. Since aryl-aryl linkages are not possible if protons were bound to carbons C and D, the CP study indicated that 1 was not a dominant structural motif in polydopamine.

Aryl-aryl coupling in a fractional amount of the monomer linkages may be ruled out through re-examination of the peak deconvolutions and integrations shown in Figure 5.2 and Table 5.1, respectively. Given the comparatively downfield chemical shifts of the other quaternary carbon centers in the polymer's structure (and comparison to model compounds such as biphenyl [26]; $\delta_{4^\circ\ \mathrm{carbon}}$ = 141 ppm), aryl-aryl coupled quaternary

centers cannot be contained within the resonance at 114 ppm. Moreover, the peaks downfield of 114 ppm did not integrate to higher-than-expected values; likewise, the resonance at 114 ppm did not integrate to a lower-than-expected value, based on structure 2. Thus, the close agreement of these integrations with structure 2 suggested that, within the detection limits of the instrument and the software used to deconvolute and integrate the peaks, there was no spectroscopic evidence for aryl-aryl coupling between the dopamine monomers. (Conservatively assuming a detection limit of 5% using the solid state NMR techniques employed herein [27] and a 5% error in the deconvolution software [28], the extent of aryl-aryl coupling should constitute no more than 7% of the monomer linkages.)

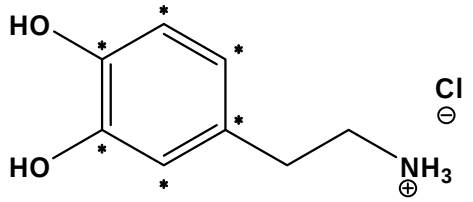

Figure 5.6. ^{13}C-labeled dopamine HCl used to prepared labeled polydopamine (asterisks denotes the ^{13}C-labeled atoms).

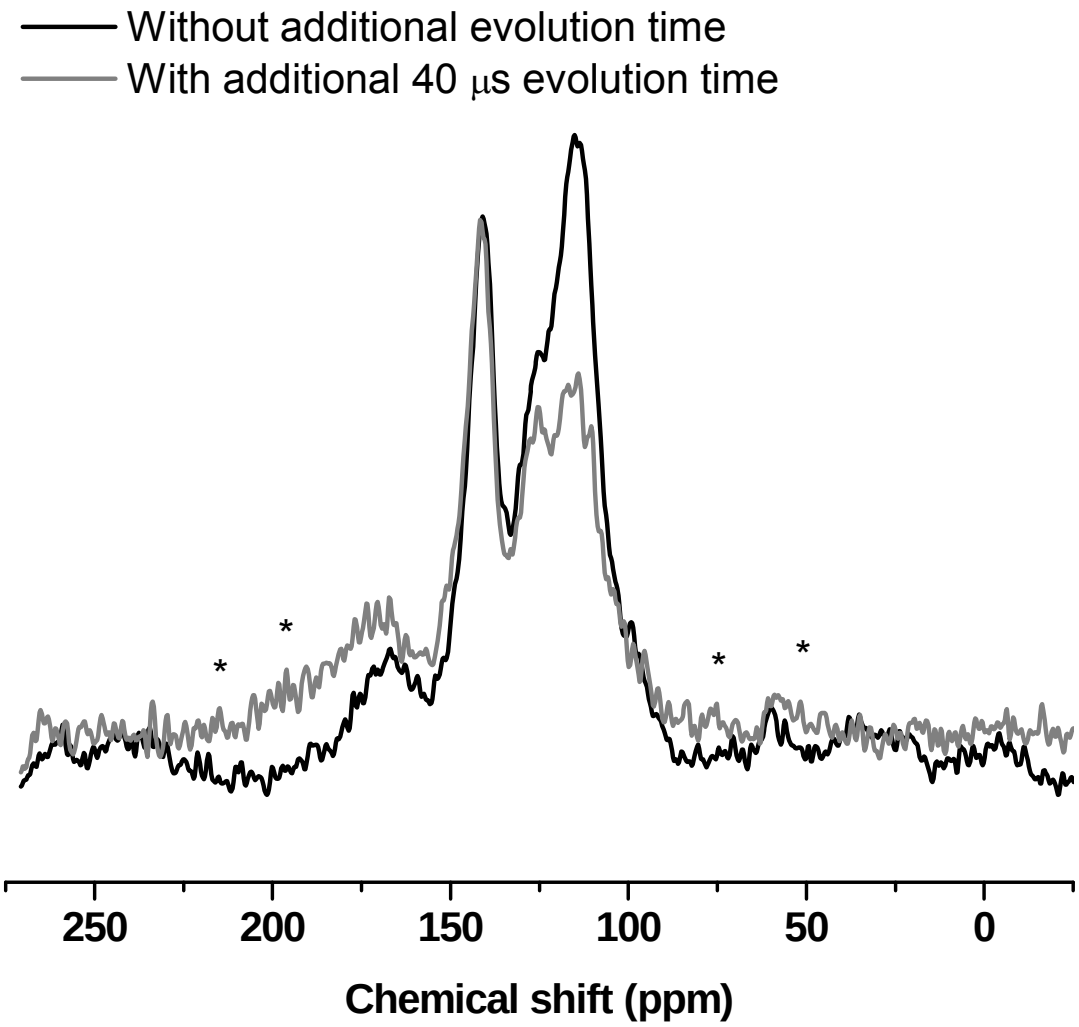

Figure 5.7. Solid state ^{13}C cross cross-polarization NMR spectra of 95:5 (w/w) unlabeled: labeled polydopamine with (gray) and without (black) an additional proton evolution period (40 μs), resulting in perturbation of the resonances of carbons bound to protons (asterisks denote spinning side bands).

Because the NMR studies suggested that covalent bonding between the monomers was not a dominant structural feature, an investigation of the non-covalent forces responsible for polydopamine's structure and bonding was undertaken. FT-IR spectroscopy of polydopamine powder (KBr), shown in Figure 5.8, revealed peaks at 1515 cm^{-1} and 1605 cm^{-1}, consistent with the indole or indoline structures proposed earlier [29]. A large, broad peak spanning 3200 to 3500 cm^{-1} was consistent with the presence of hydroxyl structures as well as water (polydopamine was found to be highly hygroscopic). No carbonyl structures were discernible from this analysis, but these absorbances might be obscured in the broad peak observed between 800 and 1750 cm^{-1}. Nearly identical spectral features were observed in polydopamine-coated KBr samples (Figure 5.9). Matrix-assisted laser desorption/ionization (MADLI) mass spectrometry was also performed using a polydopamine-coated steel target. The mass spectrum of the product (Figure 5.10) revealed the presence of a polymeric product, as indicated by the broad range of peaks spanning m/z ratios from 888 to more than 3500. However, the separation of these peaks, often used to determine the molecular weight of a polymer's repeat unit [15], was much lower than expected: 24, as opposed to the 149 or 151 expected for the proposed repeat units (Figure 5.5). The low m/z ratios were consistent with previously reported mass spectral data for polydopamine coatings (peak separations ranging from 16–26) [1], and suggested fragmentation of the monomers under MALDI conditions.

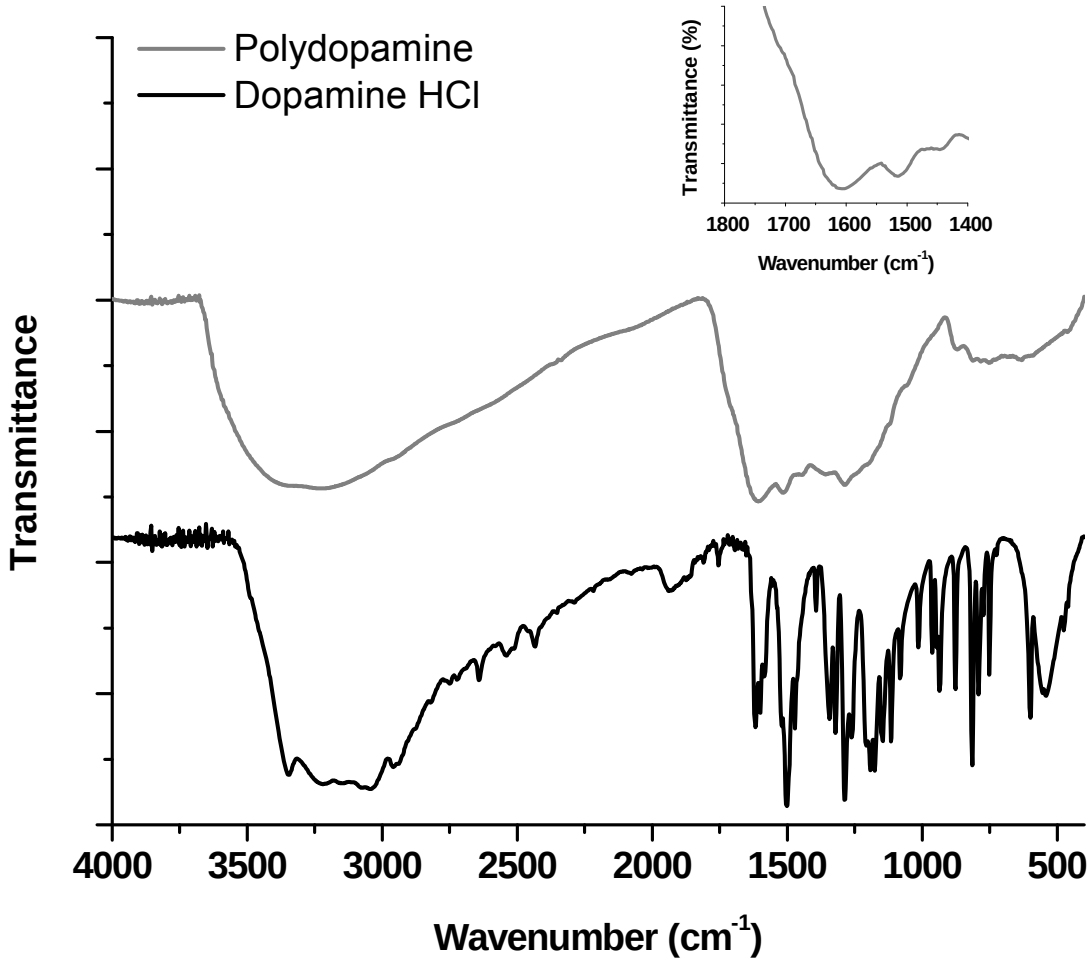

Figure 5.8 FT-IR spectra (KBr) of polydopamine (gray, top) and dopamine HCl (black, bottom). Expansion of polydopamine spectrum (inset) showing peaks at 1515 cm^{-1} and 1605 cm^{-1}, consistent with indole or indoline structures.

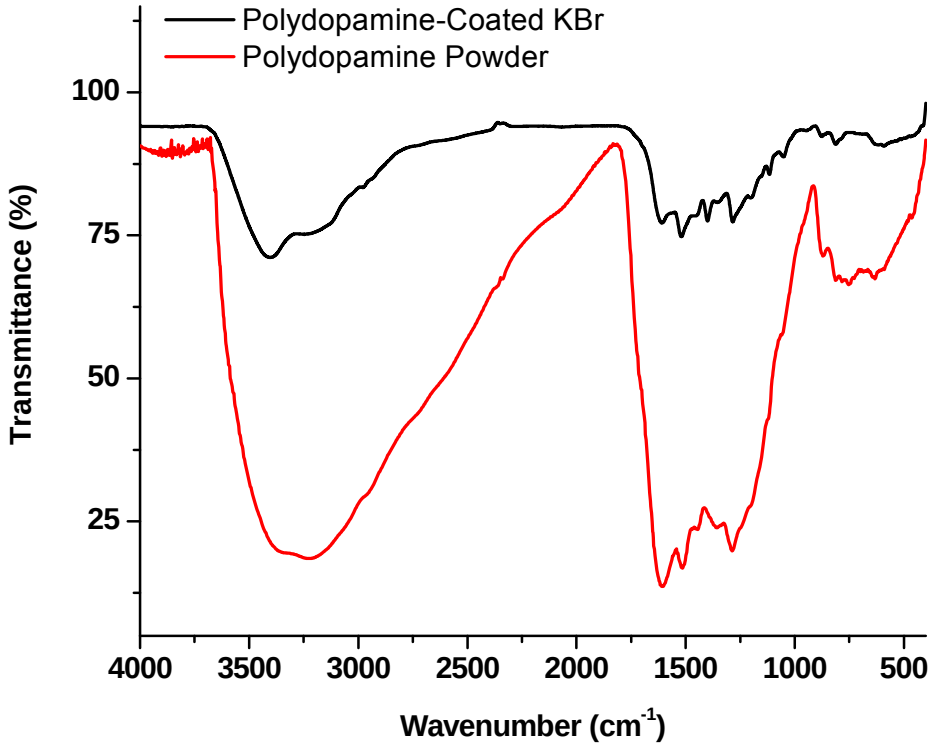

Figure 5.9. FT-IR spectra (KBr) of polydopamine powder (red) and polydopamine coated KBr (black).

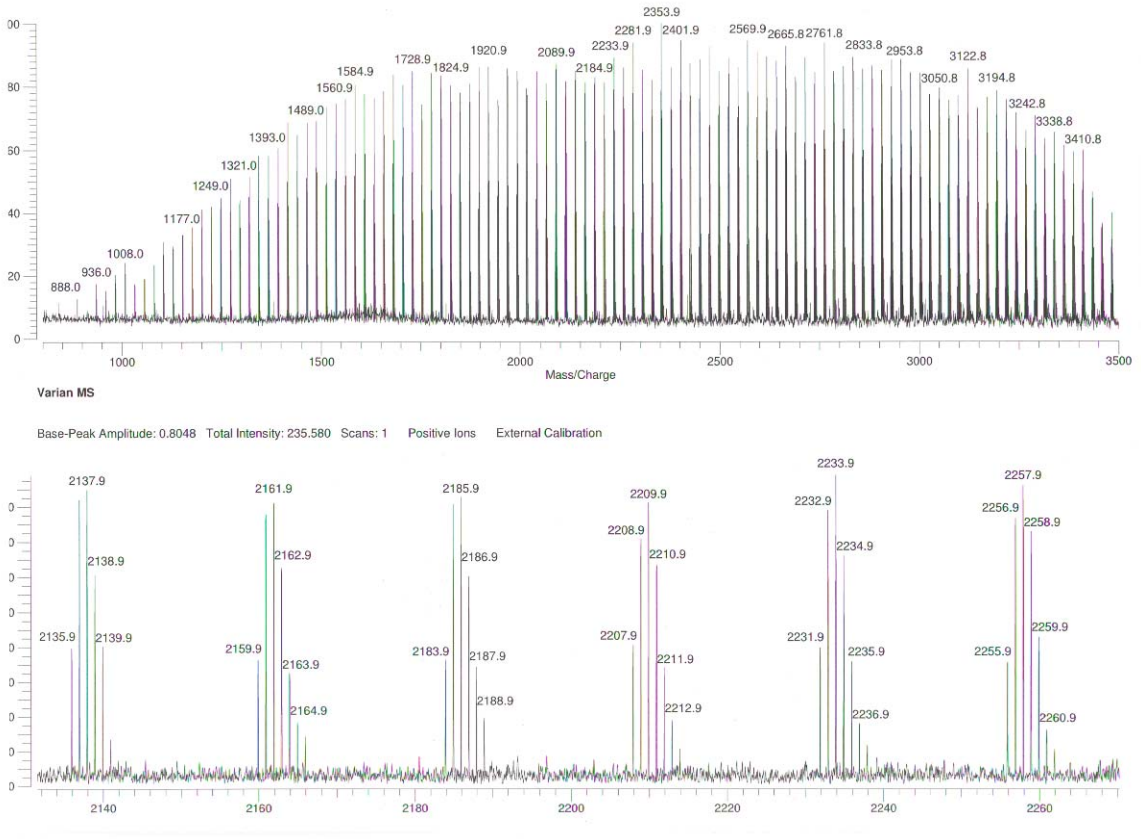

Figure 5.10. MALDI mass spectrum (positive mode) of polydopamine deposited on a steel mass spectroscopy target.

Because melanin and other similar biopolymers are known to incorporate free-radical species into their structures (present as a result of charge transfer between the repeat units) [30–32], such radical moieties may constitute an important component of polydopamine's structure. Analysis of the as-prepared polydopamine sample by electron paramagnetic resonance (EPR) spectroscopy revealed a single peak at a *g* value of 2.0036 (Figure 5.11a), indicating the presence of stable organic radicals in polydopamine's structure. Moreover, using a radical standard (diphenylpicrylhydrazyl, DPPH), it was determined that the spin concentration in the polymer was less than 1 spin per 25 repeat

units. Polydopamine was analyzed in the presence of diphenylpicrylhydrazyl (DPPH) (sealed in a glass capillary packed into the polydopamine sample) to quantify the spin concentration (Figure 5.11b). DPPH is a stable radical-containing, organic molecule and is commonly used to quantify spin concentration in EPR-active samples [33]. Even upon maximizing the polydopamine content in the sample (23.9 mg) and minimizing the DPPH content in the capillary (2.5 mg; the maximum amount that could be reliably weighed on an analytical balance), the DPPH signal (Figure 5.11c) overwhelmed the polydopamine signal. While this precludes quantification of the spin concentration in polydopamine, these results suggest that the spin concentration in polydopamine was very low, and radicals are not dominant structural features in the polymer. Assuming a worst case scenario where the polydopamine spectrum was overlapped exactly by the DPPH spectrum (*i.e.*, the relative integrations of the two samples was 1.0 : 1.0) and a spin concentration of 1.53×10^{21} spins g^{-1} in the DPPH (1 spin per molecule), the maximum spin concentration was 1.60×10^{20} spins g^{-1} in the polydopamine sample. If the repeat unit is taken to be equivalent in molecular weight to the structure shown below (molecular weight: 150.15 g mol^{-1}), the maximum spin concentration in the polymer was no greater than 25 repeat units per spin. The actual spin concentration may be much lower as a result of signal saturation by the DPPH standard. (The appearance of only a single peak in the EPR spectrum, as well as the lack of hyperfine coupling, may indicate a relatively uniform radical structure.) Thus, radicals are evidently present in polydopamine and clearly play a role in the polymer's formation, structure and bonding. The observation of free radical species in the product may also indicate that the previously described oxidation [34] and cyclization [35,36] processes occur *via* radical pathways.

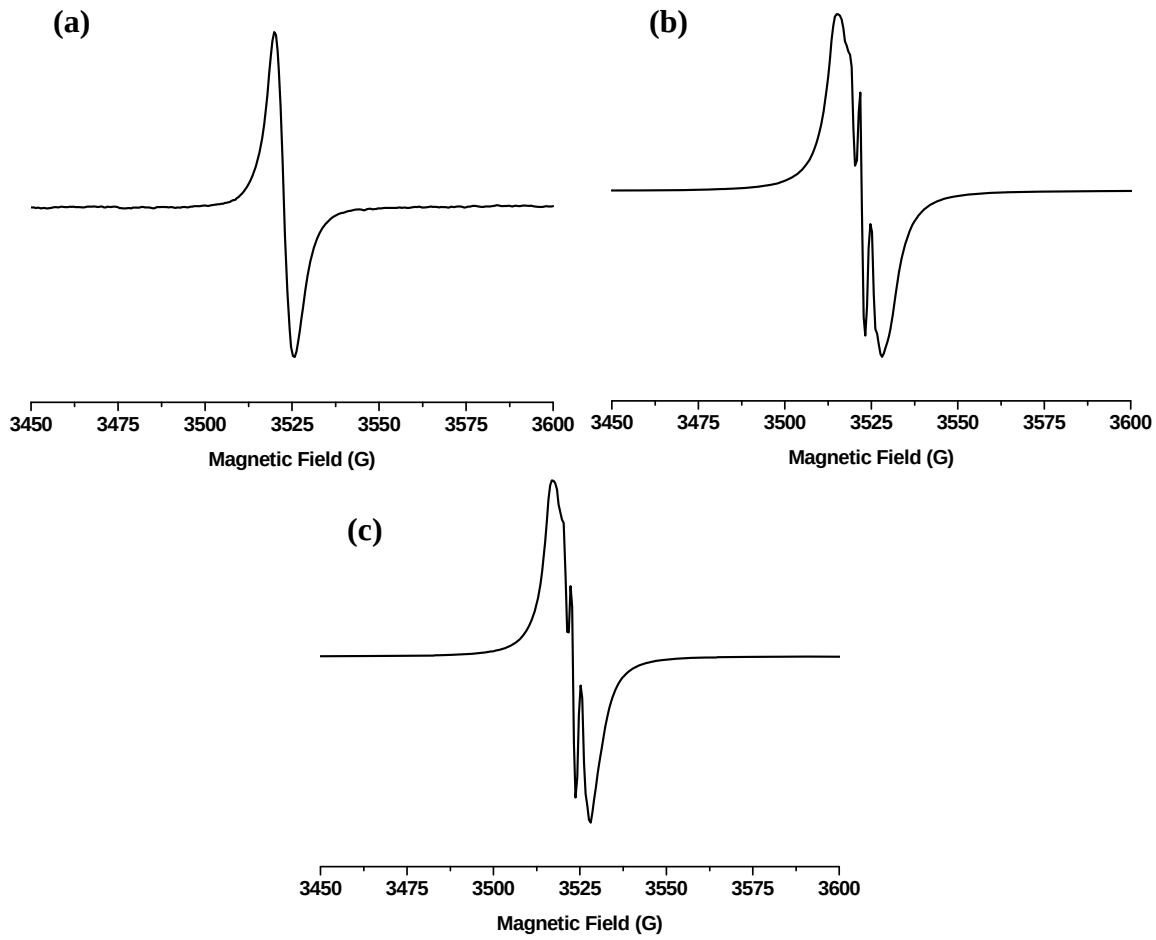

Figure 5.11. (a) Solid state EPR spectrum of as-prepared polydopamine. (b) Solid state EPR spectrum of as-prepared polydopamine (23.9 mg) measured in the presence of DPPH (2.5 mg; sealed in a glass capillary packed into the polydopamine sample). (c) Solid state EPR spectrum of commercial diphenylpicrylhydrazyl (DPPH) sample.

In order to verify that the free radicals observed were present at sufficiently low concentration to avoid perturbation of the chemical shifts or peak intensities in the observed ^{13}C spectrum of polydopamine, the polymer was blended with an internal standard (CBr_4; δ_C = -30 ppm) in the solid state and analyzed *via* solid state ^{13}C NMR spectroscopy. The resonances for the polymer and the internal standard were observed at the expected chemical shifts and intensities based on the mass loadings and structures of

the two components, indicating no detectable paramagnetic shifting or broadening in the observed ^{13}C resonances. Solid state ^{13}C NMR spectroscopy was performed on an unlabeled sample of polydopamine mixed with tetrabromomethane (CBr_4) in a 1.25 : 1 ratio (w/w) (Figure 5.12). The spectrum was recorded with a relaxation delay of 40 s at a pulse angle of 90°. Integration of the range spanning 0–200 ppm (corresponding to the polydopamine) and the peak centered at -30 ppm (corresponding to the CBr_4; consistent with solution state ^{13}C experiments performed on this species [37]) gave a relative integration ratio of 22.95 : 1, (polydopamine : CBr_4). At the weight ratio used in this mixture, and assuming 8 carbon atoms per repeat unit in the polydopamine structure (Figure 5.13), the theoretical integration ratio was 22.04 : 1, (polydopamine : CBr_4. In addition to providing support for the proposed structural model, this result indicated that the NMR spectra observed by solid state ^{13}C NMR were not significantly perturbed by the presence of the stable organic radicals in the polymer's structure, either through paramagnetic shifting or broadening of the peaks.

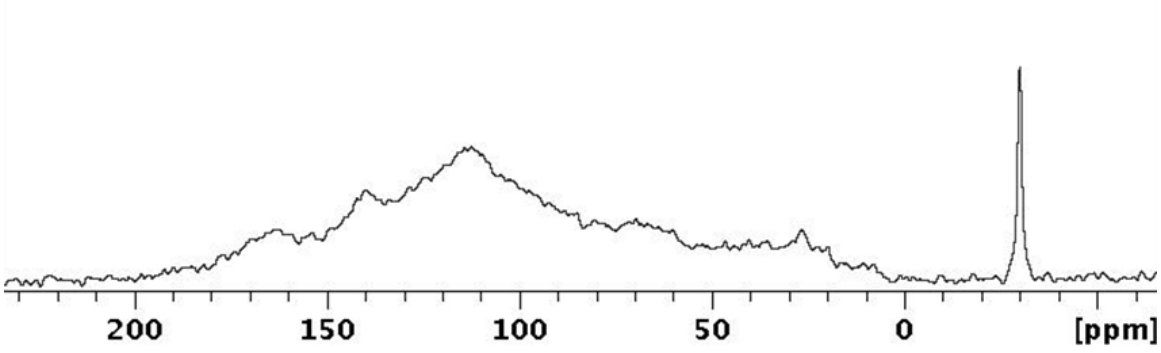

Figure 5.12. Solid state ^{13}C NMR spectrum of polydopamine with CBr_4 (1.15 : 1 ratio, w/w). The two components were present at the expected chemical shifts and relative integrals, indicating that the observed spectra of polydopamine were accurate and not significantly affected by the presence of the stable organic radicals in the polymer's structure.

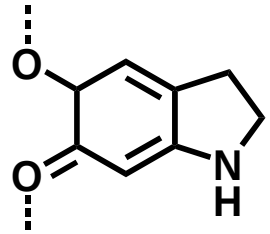

Figure 5.13. Proposed repeat unit in poly(dopamine).

The data described above strongly suggested that the as-prepared polydopamine samples were composed primarily of non-covalent bonding interactions, including hydrogen bonding and charge transfer, as has been observed in other robust, synthetic or biological, supramolecular polymers and materials [38–44]. To further support such a non-covalent model, polydopamine powder was reacted with aqueous sodium hypochlorite (NaOCl, 5-6 %) or potassium periodate (KIO_4, saturated solution), both of which are commonly used for oxidizing alcohols to their corresponding carbonyls [45–47]. It was hypothesized that if polydopamine was comprised of monomers bound by charge transfer, hydrogen bonding, or other supramolecular interactions (Figure 5.16), oxidation of the mixture to the corresponding diones would be expected to degrade the polymer, allowing for analysis of small molecule products. Upon reaction with either of these oxidants, the otherwise insoluble powder dissolved into the aqueous medium and transitioned from dark brown to clear and nearly colorless. The material was then extracted from the aqueous solution using THF (a solvent immiscible with the aqueous, hypochlorite solution of the degraded product), and the solvent was removed under vacuum. Analysis of the crude degradation product by FT-IR spectroscopy (Figure 5.8) revealed the formation of carbonyl structures as evidenced by the absorbances observed at 1715 and 1770 cm^{-1}, consistent with the oxidation of the alcohols or semiquinones present in polydopamine to their corresponding carbonyls (Figure 5.14). Upon reaction

of polydopamine powder with aqueous NaOCl or KIO_4, analysis of the crude product by ^1H NMR and mass spectroscopy revealed a mixture of unidentifiable and inseparable products. Additionally, the oxidized product was found to be hydrolytically and oxidatively unstable over long periods of time, reforming an insoluble solid.

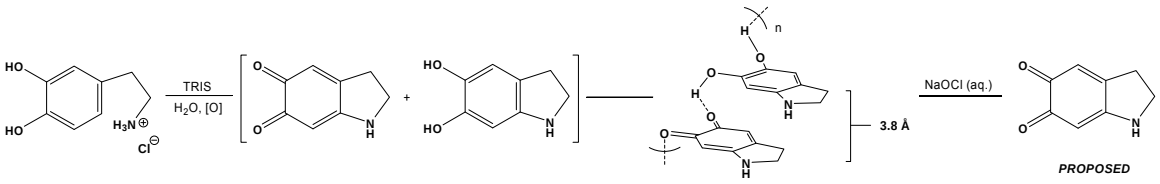

Figure 5.14. Proposed formation and structure of polydopamine, as well as oxidation to the corresponding dione upon exposure to aqueous NaOCl (as supported by solid state NMR, powder X-ray diffraction, and FT-IR spectroscopy).

Previous studies have suggested extended π-π stacking interactions between oligomeric units in eumelanins and quinhydrones [48]. To investigate the possible existence of such long range order in polydopamine, powder X-ray diffraction (PXRD) was performed on the solid state, as-prepared sample. The resultant spectrum (Figure 5.15) showed a broad peak centered at $2\theta = 23.4°$, corresponding to a d-spacing of approximately 3.8 Å. Such spacing was consistent with other π-stacked structures [49] and may facilitate, or be a result of, charge transfer between the faces of the polydopamine monomers.

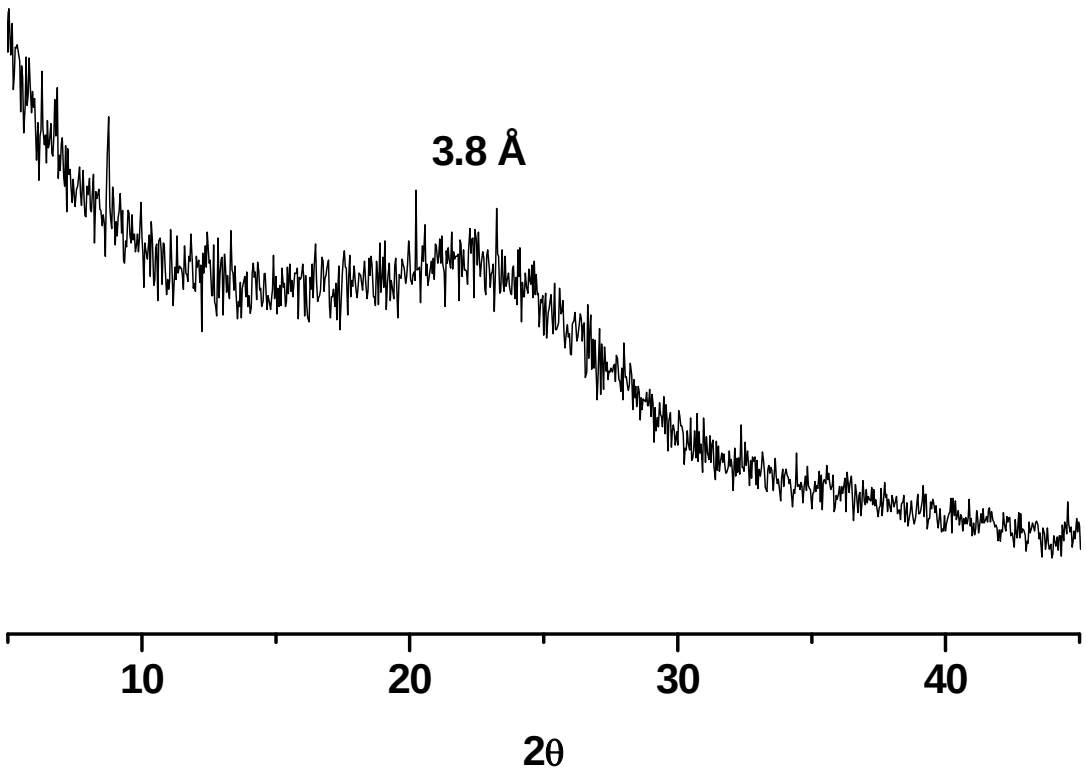

Figure 5.15. Powder X-ray diffraction (PXRD) spectrum of polydopamine.

UV-vis spectroscopy was conducted on quartz slides coated with polydopamine to assess the electronic and photophysical similarities of polydopamine to other eumelanins. Similar to melanin (an archetypal eumelanin) [50], though highly absorbing, polydopamine was found to exhibit a spectrum exhibiting no distinguishable peaks (Figure 5.16). The spectral similarities between synthetic polydopamine and naturally-occurring melanin may suggest that the structure and bonding comprising the two systems are alike.

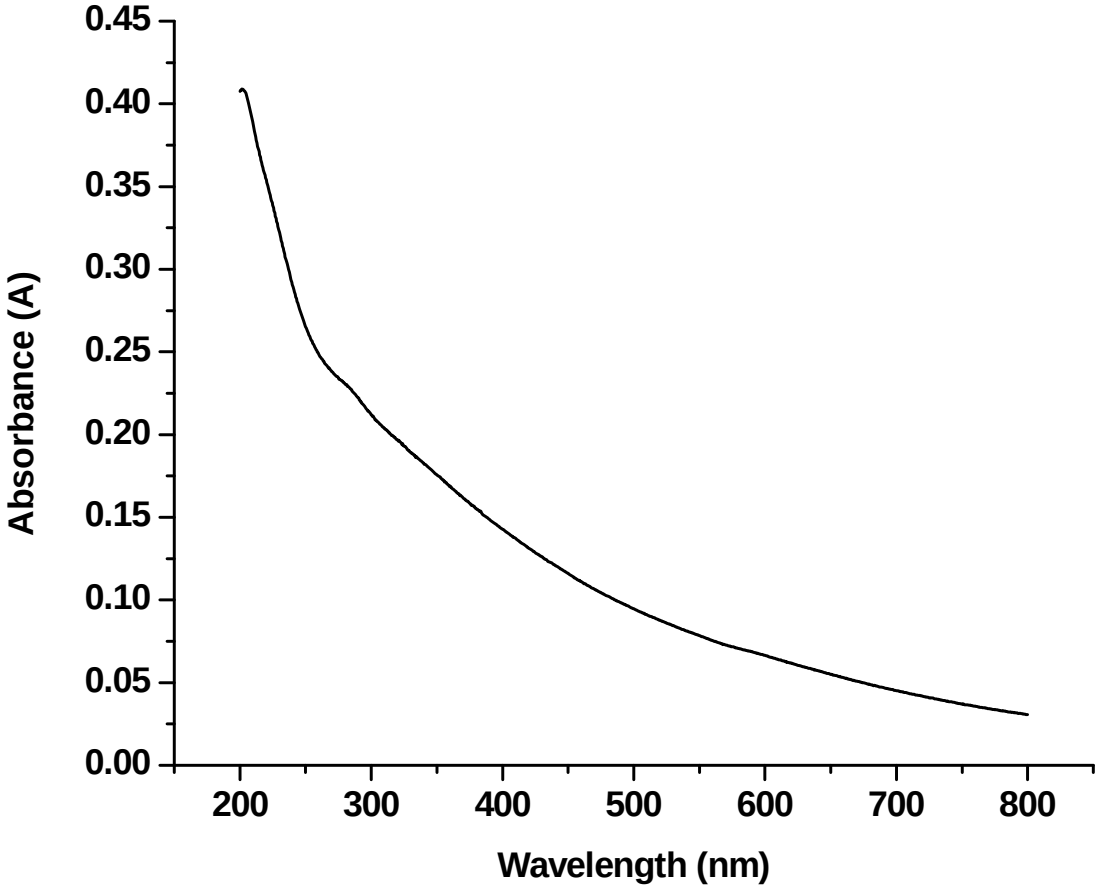

Figure 5.16. UV-vis spectrum of polydopamine deposited on a quartz slide.

Additionally, in conjunction with the non-covalent interactions provided by the hydrogen bonding between oxidized and unoxidized repeat units (including through the N–H bond of the heterocycle), π-stacking provides a route for the formation of polymeric aggregates (Figure 5.17). Similar macroscopic ordering through a combination of hydrogen bonding and π-stacking has been described previously in a wide range of polymeric and crystalline structures [51–54]. Though non-covalent in nature, these bonding arrangements are exceptionally strong, and in the case of polydopamine, leads to its complete insolubility as well as its remarkable stability as a coating [1,55,56].

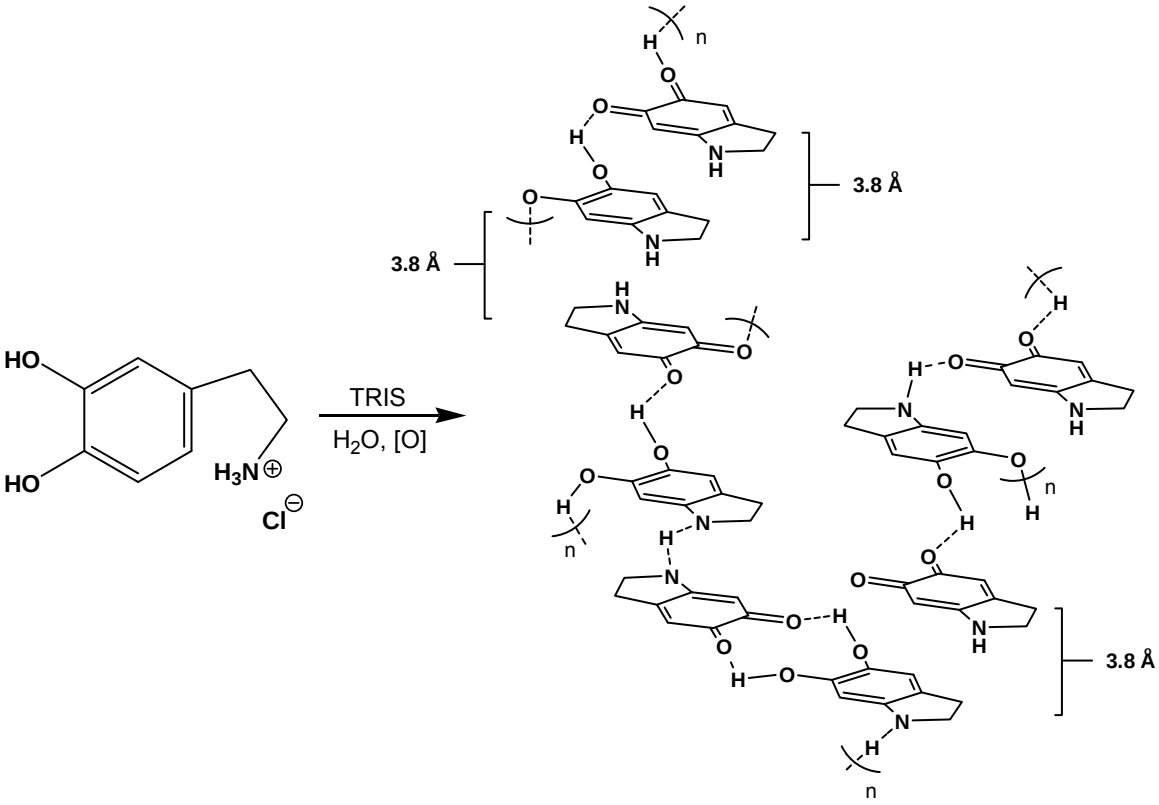

Figure 5.17. Upon reaction of dopamine HCl with TRIS in aerobic aqueous media, polydopamine, and is proposed to be comprised of intra- and inter-chain non-covalent interactions, including hydrogen bonding, π-stacking, charge transfer.

5.3 REFERENCES

[1] H. Lee, S.M. Dellatore, W.M. Miller, P.B. Messersmith, Mussel-Inspired Surface Chemistry for Multifunctional Coatings, Science 318 (5849) (2007) 426–430.

[2] G.C. Levy, R.L. Lichter, Nitrogen-15 Nuclear Magnetic Resonance Spectroscopy, John Wiley & Sons, Inc., New York, 1979.

[3] M. d'Ischia, A. Napolitano, G. Prota, Oxidative Polymerization of 5,6-Dihydroxyindoles. Tracking the Biosynthetic Pathway to Melanin Pigments, Gazzetta Chimica Italiana 126 (12) (1996) 783–789.

[4] D.G. Graham, Oxidative Pathways for Catecholamines in the Genesis of Neuromelanin and Cytotoxic Quinones, Molecular Pharmacology 14 (4) (1978) 633–643.

[5] E. Pretsch, P. Bühlmann, M. Baderstcher, Structure Determination of Organic Compounds, Springer, Berlin, 2009.

[6] V. Chevelkov, Y. Xue, R. Linser, N.R. Skrynnikov, B. Reif, Comparison of Solid-State Dipolar Couplings and Solution Relaxation Data Provides Insight into Protein Backbone Dynamics, Journal of the American Chemical Society 132 (14) (2010) 5015–5017.

[7] I.D. Gay, C.H.. Jones, R.. Sharma, A Multinuclear Solid-State NMR Study of the Dimethyltin Chalcogenides ((CH3)2SnE)3, E = S, Se, Te, Journal of Magnetic Resonance 84 (3) (1989) 501–514.

[8] H.J. Assumption, J.P. Vermeulen, W.L. Jarrett, L.J. Mathias, a. J. van Reenen, High resolution solution and solid state NMR characterization of ethylene/1-butene and ethylene/1-hexene copolymers fractionated by preparative temperature rising elution fractionation, Polymer 47 (1) (2006) 67–74.

[9] A.O. Patil, W.T. Pennington, G.R. Desiraju, D.Y. Curtin, I.C. Paul, Recent Studies on the Formation and Properties of Quinhydrone Complexes, Molecular Crystals and Liquid Crystals 134 (1) (1986) 279–304.

[10] A. V Ragimov, I.I. Ragimov, B.A. Mamedov, S.A. Guseinov, B.I. Liogon'kii, On features of the oligomerization of hydroquinone under auto-oxidation, Polymer Science USSR 24 (10) (1982) 2434–2440.

[11] P.J. Barrie, E.S. Madrali, R. Kandiyoti, Carbon-13 solid-state NMR spin-lattice relaxation time measurements of coals, Energy & Fuels 7 (4) (1993) 479–481.

[12] P. Lauterbur, Anisotropy of the C13 Chemical Shift in Calcite, Physical Review Letters 1 (9) (1958) 343–344.

[13] S.J. Opella, Faster is better: improving the sensitivity of solid-state NMR, Nature Methods 6 (3) (2009) 197–198.

[14] V.I. Bakhmutov, Practical NMR Relaxation for Chemists, John Wiley & Sons, Ltd., West Sussex, England, 2004.

[15] T. Gruendling, S. Weidner, J. Falkenhagen, C. Barner-Kowollik, Mass spectrometry in polymer chemistry: a state-of-the-art up-date, Polymer Chemistry 1 (5) (2010) 599–617.

[16] M.D. Hawley, S. V Tatawawadi, S. Piekarski, R.N. Adams, Electrochemical studies of the oxidation pathways of catecholamines, Journal of the American Chemical Society 89 (2) (1967) 447–50.

[17] D.J. Cookson, B.E. Smith, N. White, Improved Resolution of Low Field Quaternary Carbon Resonances in ^{13}C N.M.R. Spectroscopy, Journal of the Chemical Society, Chemical Communications 2 (1) (1981) 12–13.

[18] W. Kolodziejski, J. Klinowski, Kinetics of Cross-Polarization in Solid-State NMR: A Guide for Chemists, Chemical Reviews 102 (3) (2002) 613–628.

[19] R.S. Stein, B. Elena, L. Emsley, Improving resolution in proton solid-state NMR by removing nitrogen-14 residual dipolar broadening, Chemical Physics Letters 458 (4-6) (2008) 391–395.

[20] M. Fukuchi, A. Ramamoorthy, K. Takegoshi, Efficient cross-polarization using a composite 0 degree pulse for NMR studies on static solids, Journal of Magnetic Resonance 196 (2) (2009) 105–109.

[21] S. Hartmann, E. Hahn, Nuclear Double Resonance in the Rotating Frame, Physical Review 128 (5) (1962) 2042–2053.

[22] A. Pines, M.G. Gibby, J.S. Waugh, Proton-enhanced NMR of dilute spins in solids, The Journal of Chemical Physics 59 (2) (1973) 15–19.

[23] S. Zhang, B. Meier, R. Ernst, Polarization Echoes in NMR, Physical Review Letters 69 (14) (1992) 2149–2151.

[24] S.P. Brown, Probing proton–proton proximities in the solid state, Progress in Nuclear Magnetic Resonance Spectroscopy 50 (4) (2007) 199–251.

[25] H. Takahashi, H. Akutsu, T. Fujiwara, A magic-angle-spinning NMR method for 1H-1H distance measurement using coherent polarization transfer in 13C-labeled organic solids, The Journal of Chemical Physics 129 (15) (2008) 154504.

[26] A.S. Demir, H. Findik, N. Saygili, N. Tuna Subasi, Manganese(III) acetate-mediated synthesis of biaryls under microwave irradiation, Tetrahedron 66 (6) (2010) 1308–1312.

[27] P. Rousselot-Pailley, D. Maux, J.-M. Wieruszeski, J.-L. Aubagnac, J. Martinez, G. Lippens, Impurity Detection in Solid-Phase Organic Chemistry: Scope and Limits of HR MAS NMR, Tetrahedron 56 (29) (2000) 5163–5167.

[28] A.F. Jones, D.L. Misell, The problem of error in deconvolution, Journal of Physics A: General Physics 3 (5) (1970) 462–472.

[29] D.G. O'Sullivan, 657. Vibrational Frequency Correlations in Heterocyclic Molecules. Part VI. Spectral Features of a Range of Compounds Possessing a Benzene Ring Fused to a Five-membered Ring, Journal of the Chemical Society (1960) 3278–3284.

[30] B.-L.L. Seagle, K.A. Rezai, E.M. Gasyna, Y. Kobori, K.A. Rezaei, J.R. Norris, Time-resolved detection of melanin free radicals quenching reactive oxygen species, Journal of the American Chemical Society 127 (32) (2005) 11220–1.

[31] F.W. Cope, R.J. Sever, B.D. Polis, Reversible Free Radical Generation in the Melanin Granules of the Eye by Visible Light, Archives of Biochemistry and Biophysics 100 (2) (1963) 171–177.

[32] T. Sarna, R.C. Sealy, Free Radicals from Eumelanins: Quantum Yields and Wavelength Dependence, Archives of Biochemistry and Biophysics 232 (2) (1984) 574–578.

[33] J. Krzystek, A. Sienkiewicz, L. Pardi, L. Brunel, DPPH as a Standard for High-Field EPR, Journal of Magnetic Resonance 125 (1) (1997) 207–211.

[34] S. Mayer, J. Prandi, Oxygenative radical cyclization with molecular oxygen, Tetrahedron Letters 37 (18) (1996) 3117–3120.

[35] H. Ishibashi, Controlling the Regiochemistry of Radical Cyclizations, Chemical Record 6 (1) (2006) 23–31.

[36] T. V. RajanBabu, Stereochemistry of intramolecular free-radical cyclization reactions, Accounts of Chemical Research 24 (5) (1991) 139–145.

[37] S. Rieth, X. Bao, B.-Y. Wang, C.M. Hadad, J.D. Badjić, Gated molecular recognition and dynamic discrimination of guests, Journal of the American Chemical Society 132 (2) (2010) 773–776.

[38] R.P. Sijbesma, F.H. Beijer, L. Brunsveld, B.J.B. Folmer, J.H.K.K. Hirschberg, R.F.M. Lange, et al., Reversible Polymers Formed from Self-Complementary Monomers Using Quadruple Hydrogen Bonding, Science 278 (5343) (1997) 1601–1604.

[39] H. Kautz, D.J.M. van Beek, R.P. Sijbesma, E.W. Meijer, Cooperative End-to-End and Lateral Hydrogen-Bonding Motifs in Supramolecular Thermoplastic Elastomers, Macromolecules 39 (13) (2006) 4265–4267.

[40] S. Yagai, T. Iwashima, T. Karatsu, A. Kitamura, Synthesis and noncovalent polymerization of self-complementary hydrogen-bonding supramolecular synthons: N,N'-disubstituted 4,6-diamino-pyrimidin-2(1H)-ones, Chemical Communications (9) (2004) 1114–1115.

[41] J. von Byern, I. Grunwald, Biological Adhesive Systems, Springer, Vienna, 2010.

[42] A.R. Hirst, B. Escuder, J.F. Miravet, D.K. Smith, High-tech applications of self-assembling supramolecular nanostructured gel-phase materials: from regenerative medicine to electronic devices, Angewandte Chemie International Edition 47 (42) (2008) 8002–8018.

[43] D.A. Uhlenheuer, K. Petkau, L. Brunsveld, Combining supramolecular chemistry with biology, Chemical Society Reviews 39 (8) (2010) 2817–2826.

[44] H. Cui, M.J. Webber, S.I. Stupp, Self-assembly of peptide amphiphiles: from molecules to nanostructures to biomaterials, Biopolymers 94 (1) (2010) 1–18.

[45] G.A. Mirafzal, A.M. Lozeva, Phase transfer catalyzed oxidation of alcohols with sodium hypochlorite, Tetrahedron Letters 39 (40) (1998) 7263–7266.

[46] R.J.B. Reddaway, The Determination of Vicinal Glycols by Oxidation with Periodate in Non-aqueous Media, Analyst 82 (976) (1957) 506–511.

[47] G. a. Hiremath, P.L. Timmanagoudar, S.T. Nandibewoor, Oxidation of allyl alcohol by alkaline periodate in the presence of micro amounts of palladium(II), Journal of Physical Organic Chemistry 11 (1) (1998) 31–35.

[48] G.W. Zajac, J.M. Gallas, J. Cheng, M. Eisner, S.C. Moss, A.E. Alvarado-Swaisgood, The fundamental unit of synthetic melanin: a verification by tunneling microscopy of X-ray scattering results, Biochimica Et Biophysica Acta 1199 (3) (1994) 271–278.

[49] F. Liao, S. Yin, M.F. Toney, V. Subramanian, Physical discrimination of amine vapor mixtures using polythiophene gas sensor arrays, Sensors and Actuators B: Chemical 150 (1) (2010) 254–263.

[50] N. Kollias, A.H. Baqer, Absorption Mechanisms of Human Melanin in the Visible, 400-720 nm, Journal of Investigative Dermatology 89 (4) (1987) 384–388.

[51] X. Yang, J. Li, X.-H. Zhao, H.-W. Wang, Y.-K. Shan, Hydrogen bonding and pi-pi stacking in the three-dimensional supramolecular complex bis(4,4'-bipyridinium) diaquadioxalatoferrate(II) bis(hydrogen oxalate), Acta Crystallographica. Section C, Crystal Structure Communications 63 (4) (2007) m171–m173.

[52] Z.-L. Chen, Y.-Z. Zhang, F.-P. Liang, A novel nickel(II) coordination polymer incorporating 1,4-phenylenediacetic acid and 1,10-phenanthroline, Acta Crystallographica. Section C, Crystal Structure Communications 62 (2) (2006) m48–m50.

[53] J. Wu, Synthesis, characterization and crystal structure of a 3-D supramolecular Cu/Mn complex with pydc, Crystal Research and Technology 43 (10) (2008) 1097–1100.

[54] G. Yang, X.-L. Yu, X.-M. Chen, L.-N. Ji, Three-Dimensional Structure Constructed via Hydrogen Bonds and π-π Stacking Interaction. Crystal Structure of [Cu(AFO)2(H2O)2](ClO4)2.2(AFO).2H2O (AFO = 4,5-Diazafluoren-9-one), Crystal Research and Technology 35 (8) (2000) 993–1000.

[55] J. Ryu, S.H. Ku, H. Lee, C.B. Park, Mussel-Inspired Polydopamine Coating as a Universal Route to Hydroxyapatite Crystallization, Advanced Functional Materials 20 (13) (2010) 2132–2139.

[56] X.-B. Yin, D.-Y. Liu, Polydopamine-based permanent coating capillary electrochromatography for auxin determination, Journal of Chromatography A 1212 (1-2) (2008) 130–136.

Chapter 6: Validation of Constant Flux Crossflow System Operation by Fundamental Pure Water and Fouling Measurements

6.1 SUMMARY

Membrane fouling is often characterized using a crossflow filtration apparatus. Typically, the transmembrane pressure (TMP) difference is fixed, and the flux is allowed to decline as the membrane fouls and the resistance to mass transfer increases. However, as flux varies, so too does the rate at which foulants are brought to the membrane surface, so the observed fouling behavior is not solely the result of membrane/foulant interactions. Constant flux experiments, where the permeate flux is fixed and the TMP difference varies, minimize such variations in the hydrodynamic conditions at the membrane surface, but constant-TMP difference experiments dominate the fouling literature because they are more straightforward to execute than constant flux experiments. Additionally, most industrial water purification membrane installations operate at constant flux rather than at constant TMP. The construction and operation of a constant flux crossflow fouling apparatus was described in Chapter 4. Here, system accuracy is assessed by some fundamental pure water and fouling measurements. Pure water permeance measurements made in the constant flux crossflow system were compared to values specified by the membrane manufacturer, reported elsewhere, and measured by another technique. Fouling experiments were performed with two membrane/foulant systems: polysulfone ultrafiltration (UF) membranes with a soybean oil emulsion foulant, and PVDF microfiltration (MF) membranes with a polystyrene latex bead suspension foulant. Automatic permeate flux control facilitated flux stepping experiments, which are

---

This chapter adapted from: D.J. Miller, D.R. Paul, B.D. Freeman., A crossflow filtration system for constant permeate flux membrane fouling characterization, Review of Scientific Instruments 84 (3) (2013) 035003.

commonly used to determine the threshold flux or critical flux of a membrane/foulant pair. Comparison of a flux stepping experiment with a literature report yielded good agreement.

6.2 RESULTS AND DISCUSSION

6.2.1 Constant Flux Fouling Tests

Constant flux fouling tests were performed using PS-20 polysulfone UF membranes and 1500 ppm soybean oil emulsion as the foulant solution. The volumetric feed flow rate was 0.8 L/min, corresponding to a crossflow velocity of 0.18 m/s and a Reynolds number of 1000 inside the flow channel of the membrane cell [1], where the channel was approximated as two parallel plates with large aspect ratios, and the channel height was used as the characteristic dimension to calculate the Reynolds number [2]. The feed pressure was 2.1 barg. Fluxes of 40 and 85 $Lm^{-2}h^{-1}$ (LMH) were tested. Before fouling, membranes were operated with pure water for several minutes. The pure water TMP was used to calculate the permeance of the un-fouled membrane. Table 6.1 compares the pure water permeances at 40 and 85 LMH with those specified by the manufacturer and measured independently in stirred dead end cells. Dead end measurements were performed in this study (taken as the average of 25 samples) as reported elsewhere [1]. Differences among values in Table 6.1 could be the result of membrane variability or differences in pretreatment protocol. It is unclear what protocol is used by the manufacturer to wet the porous structure prior to measuring the pure water permeance; more complete wetting of the pores and, therefore, higher permeance, could account for the slightly higher values obtained in the constant flux system and by other dead end filtration measurements [1]. Values measured in the constant flux crossflow system fell between those specified by the manufacturer and those reported elsewhere for

dead end filtration [1], indicating acceptable performance relative to other measurement techniques.

	Manufacturer Specification	Dead End, Reported [1]	Dead End, Measured	Const. Flux Crossflow, 40 LMH	Const. Flux Crossflow, 85 LMH
TMP (bar)	2.1	2.1	2.1	0.043	0.082
Permeance (LMH/bar)	900	1300	900	920	1040

Table 6.1. Pure water permeance comparison of PS-20 UF membranes, including manufacturer specification, dead-end measurements reported elsewhere and performed in this study, and measured in the constant flux crossflow system at two different permeate flux values.

Figure 6.1 compares the fouling response of PS-20 UF membranes at 40 and 85 LMH when exposed to the soybean oil-based emulsion. The data at each flux are from one of the three membrane samples that were tested simultaneously during each experiment; two different experiments where conducted, one at 40 LMH and one at 85 LMH, and fresh membrane samples were used for each test. The data from the other two samples measured simultaneously during each test were comparable to the data presented in this figure, and they are not presented for brevity. The membrane operated at 40 LMH showed little rise in TMP, indicating at most modest fouling. In contrast, the TMP of the membrane operated at 85 LMH rapidly increased, reaching a value equal to the feed pressure (2.1 barg) within a few minutes, indicating rapid fouling. Clearly, the membrane could not be operated at 85 LMH for significant periods of time without catastrophic fouling.

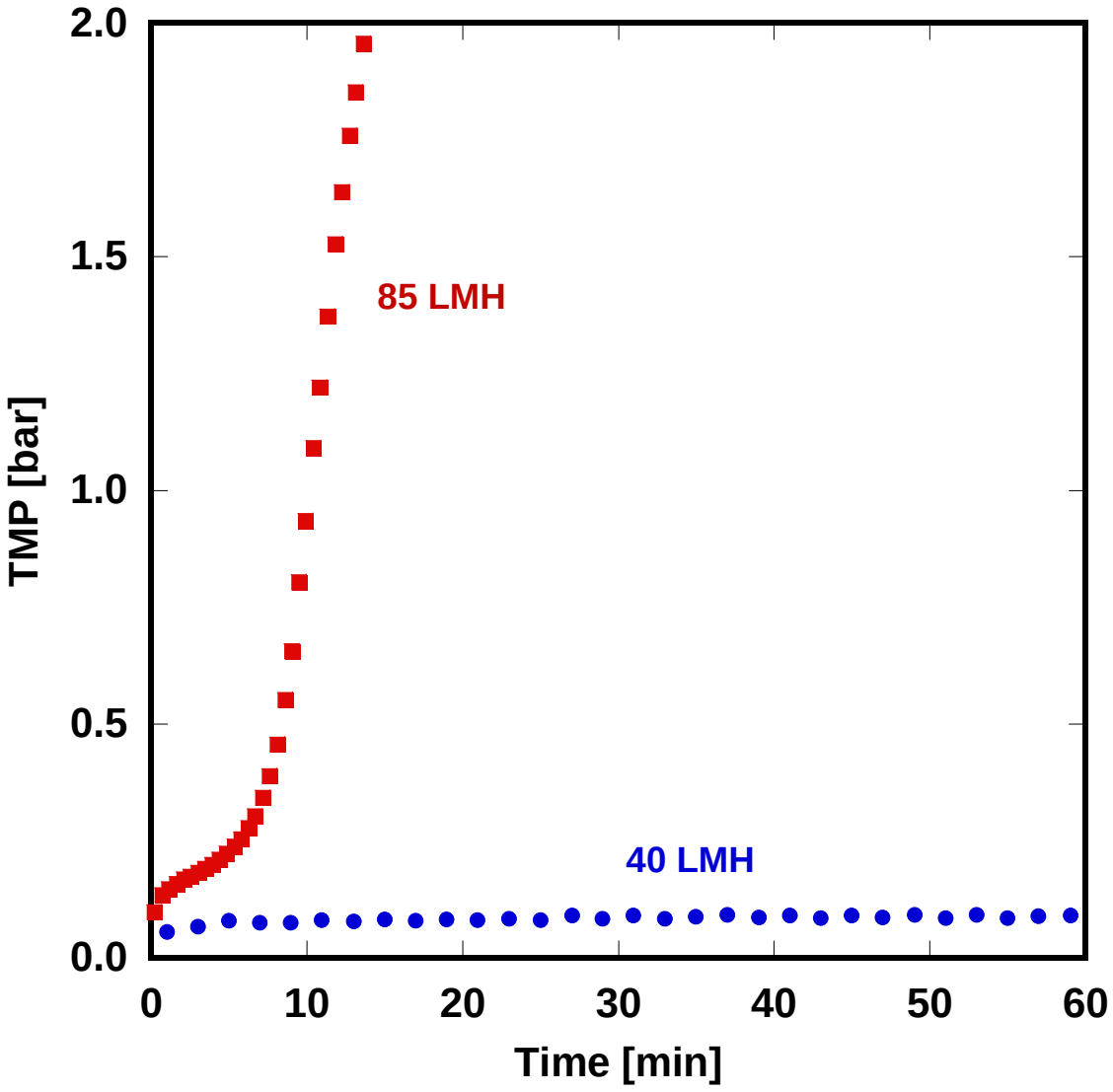

Figure 6.1. Transmembrane pressure evolution during oily water fouling of PS-20 UF membrane operated at 40 and 85 LMH. Foulant: 1500 ppm soybean oil emulsion; feed pressure: 2.1 barg; crossflow velocity: 0.18 m/s.

6.2.2 Critical/Threshold Flux Determination by Flux Stepping

The dramatic difference in TMP evolution at 40 and 85 LMH (as shown in Figure 6.1) indicates that the rate of fouling is much greater at 85 LMH than at 40 LMH, suggesting that the critical or threshold flux lies between these values. To determine the critical/threshold flux of the PS-20 UF membrane with a 1500 ppm soybean oil emulsion foulant, a flux stepping experiment (as described by Choi and Dempsey [3]) was performed. The feed pressure was 2.1 barg and the crossflow velocity was 0.18 m/s (feed flow rate: 0.8 L/min). Fouling was initiated at a flux of 30 LMH and stepped up by 10 LMH every 10 minutes. Figure 6.2a presents the change in TMP at each flux step. At low fluxes, the TMP slowly increased during each 10 minute interval, indicating that the rate of fouling was low at those fluxes. As the flux was increased, the TMP began to increase more rapidly over each flux step. While these changes in the TMP were slow, they suggest that this flux stepping experiment revealed the threshold flux (not the critical flux). If no change in the TMP had been observed at low fluxes, this experiment would have revealed the critical flux.

The threshold flux value was determined as shown in Figure 6.2b. The average TMP was calculated for each 10-minute interval and plotted against the flux. At low fluxes, the average TMP increased linearly with flux. The threshold flux was identified as the flux at which the slope of the average TMP/flux relationship changed due to the increasingly rapid rise in TMP over each successive interval beyond the threshold flux. In this case, the threshold flux was 68 LMH, which is consistent with the disparate fouling behavior observed at 40 LMH and 85 LMH (Figure 6.1). A more detailed discussion of the effects of varying step length, step height, initial flux, and step method may be found in the Appendix and elsewhere [3–5].

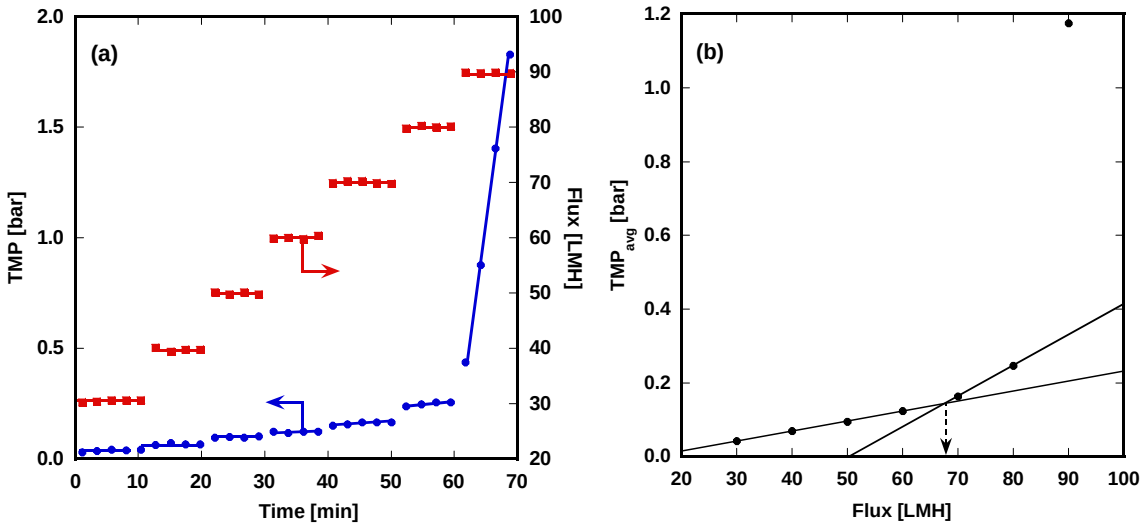

Figure 6.2. Flux stepping experiment with PS-20 UF membrane and 1500 ppm soybean oil emulsion foulant. (a) Transmembrane pressure evolution. Lines through TMP data show trends during each constant flux step and are drawn to guide the eye. The transmembrane pressure over each flux step was never absolutely invariant with time, so this flux stepping experiment revealed the threshold flux. (b) Threshold flux determination. The average TMP of each flux step is plotted against flux; the threshold flux is the flux at which the slope of the average TMP/flux relationship changes (marked with the dashed arrow). Feed pressure: 2.1 barg; crossflow velocity: 0.18 m/s.

6.2.3 The Importance of Permeate Flux Feedback Control

Many literature studies that describe constant flux experimental apparatuses do not mention continuous control (automatic or otherwise) of the permeate flow rate throughout the experiment. Often, in setups that utilize a pump to regulate the permeate flow, authors suggest running the pump at a constant speed to maintain the same flux throughout the experiment [6,7]. Unfortunately, this approach may be insufficient to ensure rigorously constant permeate flux, especially with aggressive foulants or during experiments performed above the critical/threshold flux. In the apparatus described here, high-accuracy Coriolis-style flow meters were used to monitor the permeate flow rates in real time. The LabVIEW program compared the permeate flow to a desired setpoint and adjusted the permeate pump speed through a 0-10 Vdc input. To illustrate the importance of permeate flux feedback control, the voltage applied to the permeate pump (a proxy for pump speed) during automatic control is plotted as a function of time during oily water fouling of a PS-20 UF membrane at 85 LMH (Figure 6.3). The feed pressure was 2.1 barg and the crossflow velocity was 0.18 m/s (feed flow rate: 0.8 L/min). The applied voltage increased from 1.25 V to 1.95 V over the course of the fouling experiment, during which the TMP increased as depicted in Figure 6.1. This voltage rise represents an increase of 56% in pump speed during fouling. If the flux were allowed to decrease during the experiment, the transmembrane pressure would evolve more slowly than it would if the flux were held constant at the target value. At low fluxes, particularly below the critical/threshold flux and in the case of relatively non-aggressive foulants, the fouling rate will be slow and such changes in pump speed may not be required. However, at moderate or high fluxes and with aggressive foulants (as is the case shown here), it was necessary to increase the pump speed to maintain rigorously constant flux operation, which is the intended operational goal of the present apparatus.

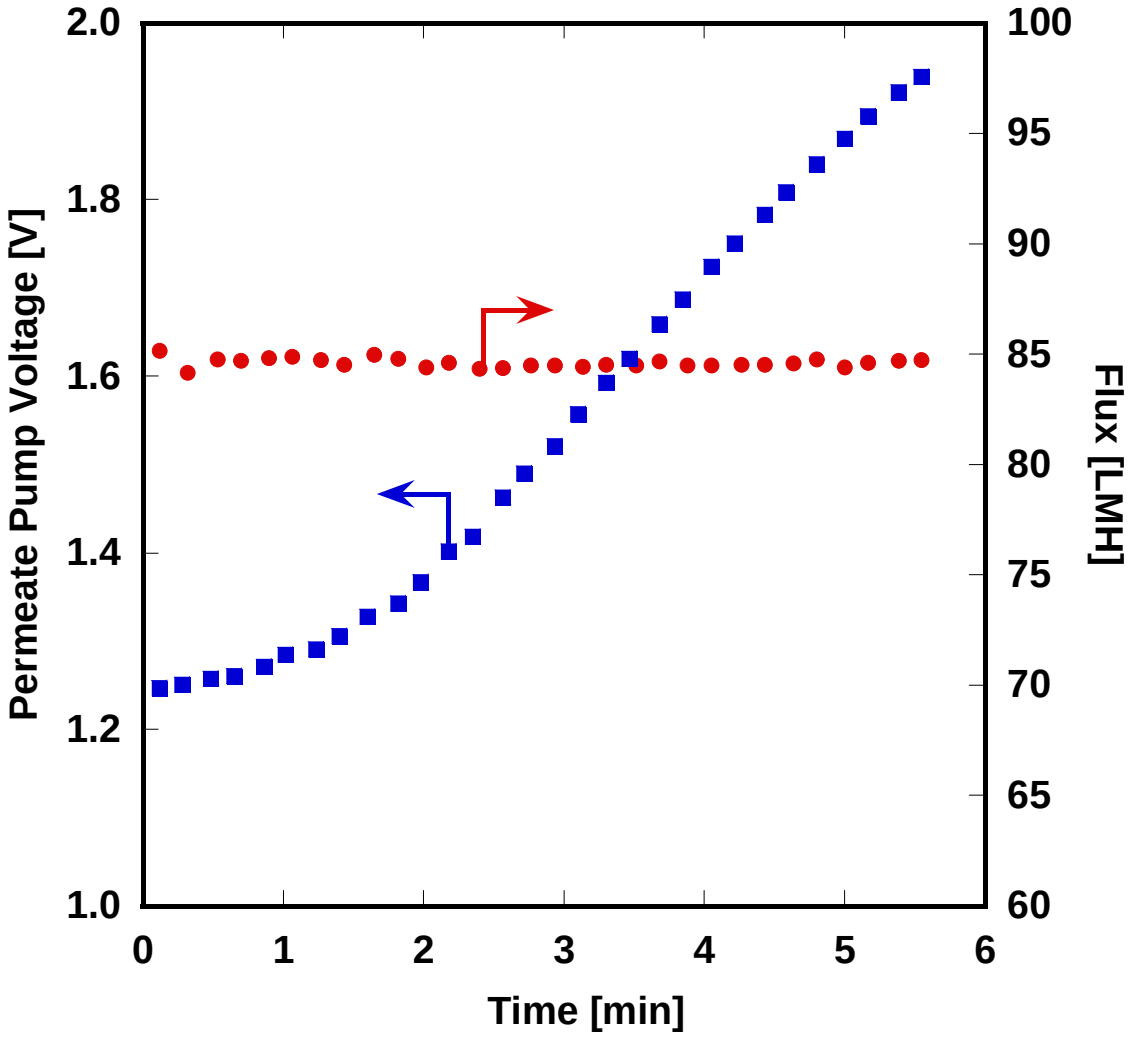

Figure 6.3. Voltage applied to permeate pump to maintain 85 LMH flux during oily water fouling of PS-20 UF membrane. Foulant: 1500 ppm soybean oil emulsion; feed pressure: 2.1 barg; crossflow velocity: 0.18 m/s.

6.2.4 Comparison with Another Study

To validate system operation beyond pure water permeance measurements (Table 6.1), a constant flux fouling experiment reported in the literature was replicated. Kwon *et al.* performed a series of flux stepping experiments using commercial PVDF MF membranes and a polystyrene latex bead suspension as a model foulant [8]. This report

was chosen for comparison due to the detailed reporting of experimental parameters and the commercial availability of membranes and foulant; some other studies use foulants from natural sources *(e.g.*, Dutch canal water) which were not readily available [3,9–11], making a quantitative and rigorous comparison of our results to those in the literature difficult. The polystyrene latex bead suspension was prepared as described in Chapter 4. The filtration apparatus used by Kwon *et al*. regulated membrane flux with a peristaltic pump on the permeate line, and the transmembrane pressure was measured using pressure transducers. Operational parameters were matched as closely as possible to the original study. The feed pressure was 0.20 barg. Constant flux fouling steps were 50 minutes long during which the crossflow velocity was 0.2 m/s; after each fouling step, the crossflow velocity was increased to 0.5 m/s for five minutes during a zero-flux cleaning stage to remove particles that may have accumulated on the membrane surface during the prior fouling stage. Flux steps were 66, 99, 165, 230, and 273 LMH.

Figure 6.4 compares the reported results of Kwon *et al*. with results obtained using the system described in this study. Satisfactory agreement between the studies was obtained. Error bars were estimated as the standard deviation measured over the three replicate cells; transmembrane pressures measured in this study are largely statistically identical to those measured by Kwon *et al*. The minor deviations observed between our results and those of Kwon *et al*. could be the result of differing cell geometries in the two studies. While both cells had rectangular flow paths, the cell used by Kwon *et al.* was much narrower, relative to its length, than the cells used in the present apparatus. Although the crossflow velocity employed here was matched to that of Kwon's study, the differences in cell geometry could affect the hydrodynamic conditions at the membrane surface.

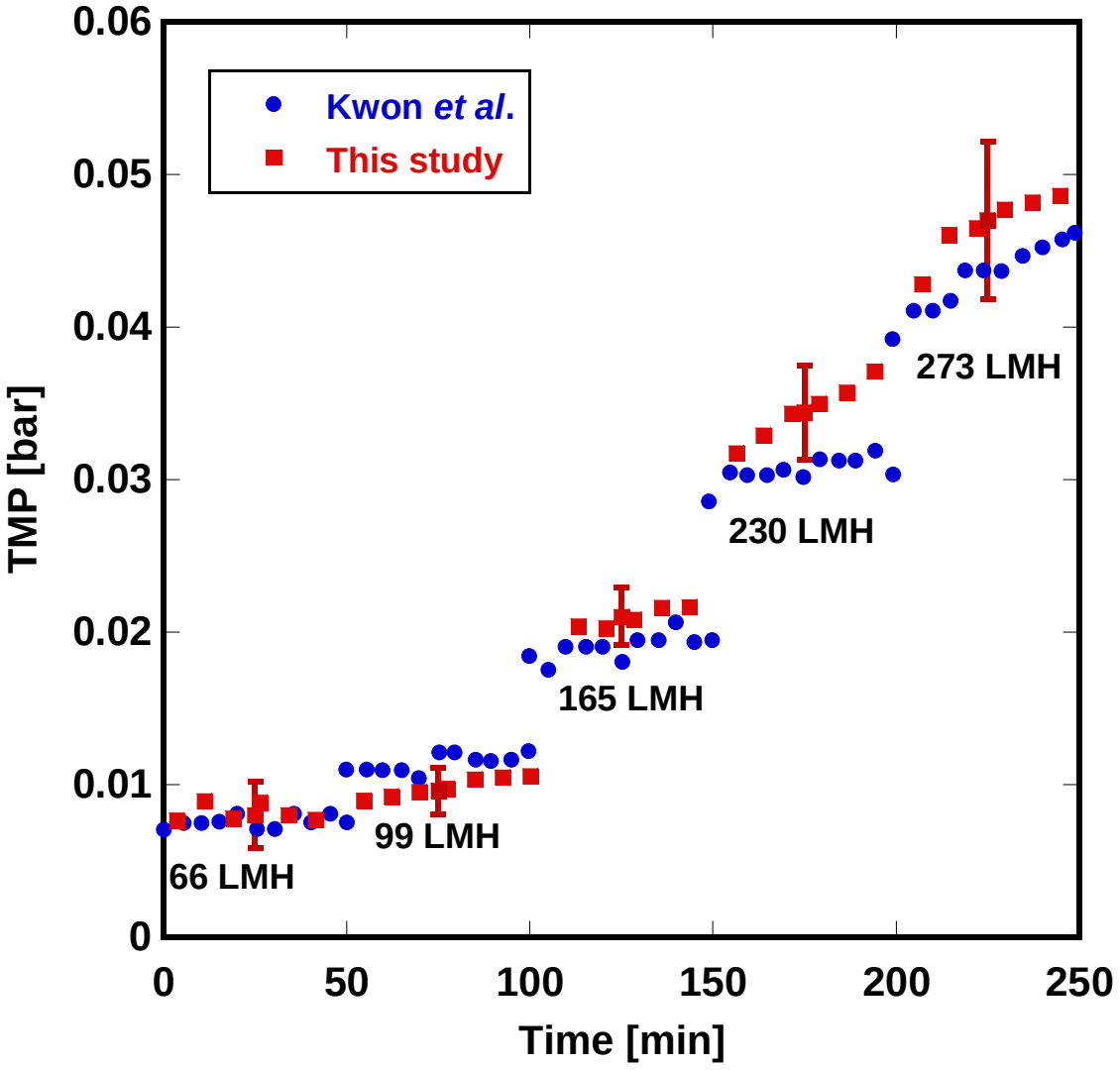

Figure 6.4. Comparison of flux stepping experiment results obtained using the presently described apparatus with results reported by Kwon *et al.*[8] Membrane: Millipore hydrophobic PVDF MF (0.22 µm mean pore size); foulant: 3.0 µm polystyrene bead suspension; feed pressure: 0.20 barg; crossflow velocity: 0.2 m/s during fouling, 0.5 m/s during five minute cleaning stages between fouling steps.

6.3 REFERENCES

[1] B.D. McCloskey, H.B. Park, H. Ju, B.W. Rowe, D.J. Miller, B.D. Freeman, A Bioinspired Fouling-Resistant Surface Modification for Water Purification Membranes, Journal of Membrane Science 413-414 (2012) 82–90.

[2] E.M. Van Wagner, A.C. Sagle, M.M. Sharma, B.D. Freeman, Effect of Crossflow Testing Conditions, including Feed pH and Continuous Feed Filtration, on Commercial Reverse Osmosis Membrane Performance, Journal of Membrane Science 345 (1-2) (2009) 97–109.

[3] K.Y.-J. Choi, B.A. Dempsey, Bench-scale evaluation of critical flux and TMP in low-pressure membrane filtration, Journal of the American Water Works Association 97 (7) (2005) 134–143.

[4] P.S. Beier, G. Jonsson, Critical Flux Determination by Flux-Stepping, AIChE Journal 56 (7) (2010) 1739–1747.

[5] P. van der Marel, A. Zwijnenburg, A. Kemperman, M. Wessling, H. Temmink, W. van der Meer, An improved flux-step method to determine the critical flux and the critical flux for irreversibility in a membrane bioreactor, Journal of Membrane Science 332 (1-2) (2009) 24–29.

[6] M. Turker, J. Hubble, Membrane Fouling in a Constant-Flux Ultrafiltration Cell, Journal of Membrane Science 34 (2-3) (1987) 267–281.

[7] H.K. Vyas, R.J. Bennett, A.D. Marshall, Performance of crossflow microfiltration during constant transmembrane pressure and constant flux operations, International Dairy Journal 12 (5) (2002) 473–479.

[8] D.. Kwon, S. Vigneswaran, A.. Fane, R.B. Aim, Experimental determination of critical flux in cross-flow microfiltration, Separation and Purification Technology 19 (3) (2000) 169–181.

[9] S.F.E. Boerlage, M. Kennedy, Z. Tarawneh, R. De Faber, J.C. Schippers, Development of the MFI-UF in constant flux filtration, Desalination 161 (2) (2004) 103–113.

[10] W. Youravong, M.J. Lewis, A.S. Grandison, Critical Flux in Ultrafiltration of Skimmed Milk, Food and Bioproducts Processing 81 (4) (2003) 303–308.

[11] P. Le Clech, B. Jefferson, I.S. Chang, S.J. Judd, Critical flux determination by the flux-step method in a submerged membrane bioreactor, Journal of Membrane Science 227 (1-2) (2003) 81–93.

Chapter 7: Comparison of Membrane Fouling at Constant Flux and Constant Transmembrane Pressure Conditions

7.1 SUMMARY

Membrane fouling is often characterized in the laboratory by flux decline experiments, where an increase in transport resistance due to accumulation of foulants on and/or in a membrane is manifested as a decrease in permeate flux with filtration time at fixed transmembrane pressure (TMP). However, many industrial microfiltration (MF) and ultrafiltration (UF) applications operate at constant permeate flux, and there are few reports comparing these modes of operation. In this study, emulsified oil fouling of polysulfone UF membranes was studied using both constant permeate flux and constant transmembrane pressure experiments. Mass transfer resistance changes during fouling were compared between constant flux experiments and constant TMP experiments performed at an initial flux equal to the flux imposed during the constant flux experiment. At low fluxes, the transport resistance and its change with permeate volume per unit area agreed within experimental error regardless of operational mode. In contrast, at high fluxes, the change in membrane resistance with permeate volume per unit area was much higher in constant flux than in constant transmembrane pressure experiments. The threshold flux, defined recently as the flux at which the rate of fouling begins to increase rapidly, separates the regimes of good and poor agreement between the two types of experiments. The weak form of the critical flux, below which spontaneous adsorption is the only significant resistance imposed by foulant, was also observed.

7.2 RESULTS AND DISCUSSION

7.2.1 Critical and Threshold Flux Determination

The critical and threshold fluxes of the PS-20 polysulfone UF membrane were evaluated using a well-known flux-stepping protocol [1]. The feed foulant was 1500 ppm soybean oil emulsion. The volumetric feed flow rate was 0.8 L/min, corresponding to a crossflow velocity of 0.18 m/s. The feed pressure was 2.1 barg. The initial flux was 5 $Lm^{-2}h^{-1}$ (LMH), and the flux was increased by 5 LMH every 10 minutes until a flux of 105 LMH was reached, at which the TMP rapidly increased. The result of the flux stepping experiment is shown in Figure 7.1.

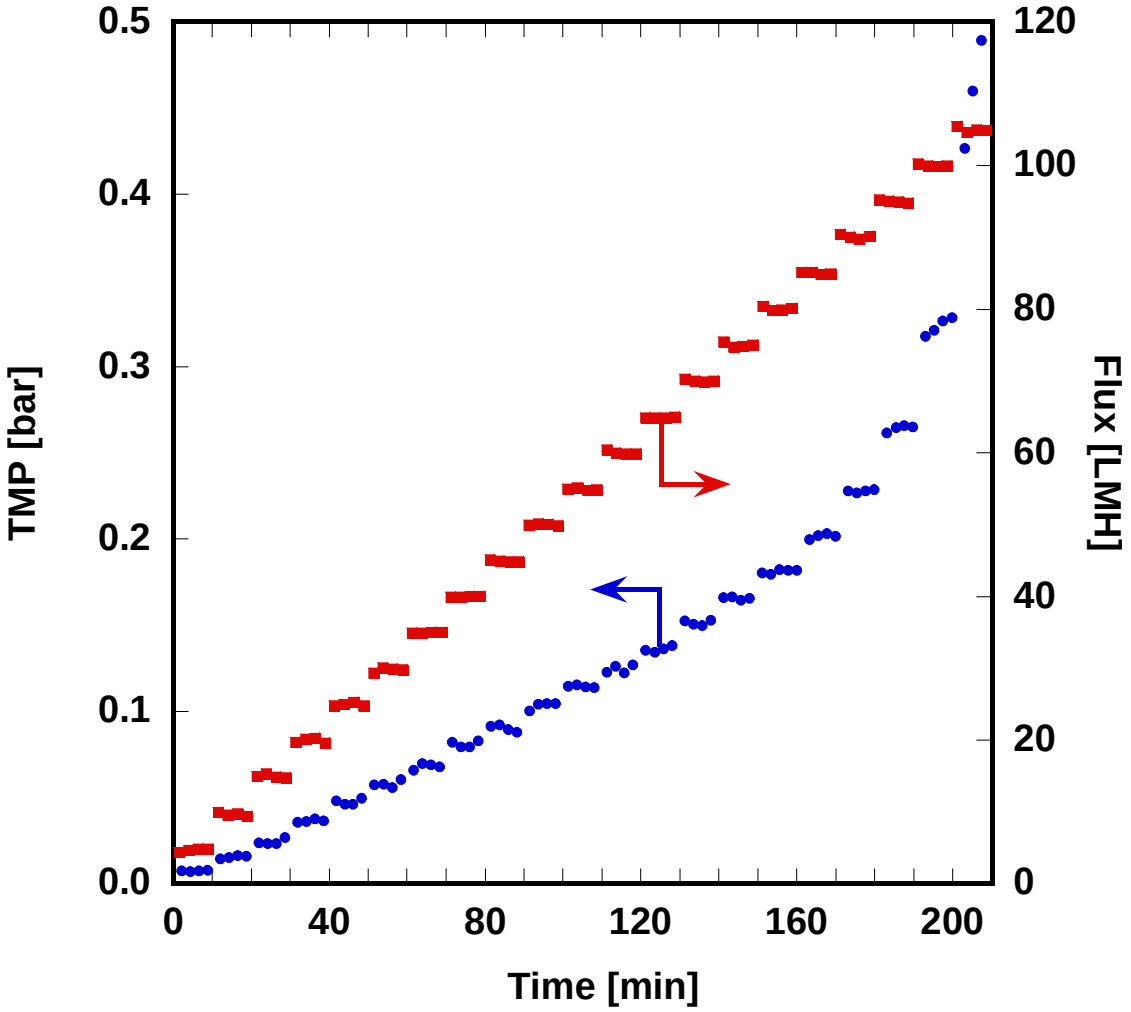

Figure 7.1. Flux stepping experiment with PS-20 UF membrane and 1500 ppm soybean oil emulsion foulant. The flux was gradually increased in 10-minute, constant-flux intervals from 5 to 105 LMH. The TMP was recorded during each flux. Feed pressure: 2.1 barg, crossflow velocity: 0.18 m/s.

Figure 7.2 presents the *average* TMP, calculated as the arithmetic mean of all transmembrane pressures recorded over each constant flux interval shown in Figure 7.1, as a function of imposed permeate flux. TMP_{avg} vs. flux plots are frequently used to determine critical and threshold fluxes from flux stepping experiments [1–3]. Three linear regressions are drawn through the TMP_{avg} values, labeled A, B, and C. Most of the TMP_{avg} values, corresponding to the flux range of 15 LMH to 60 LMH, lie on regression line B. At fluxes higher than 60 LMH, the slope of the TMP_{avg}/flux relationship progressively increases with increasing flux. Regression line C was drawn to find the flux at which this change in slope occurs. The flux increases nonlinearly in region C, so only the first two points beyond region B were used to fit the line identified as C in Figure 7.2. At the lowest fluxes tested, 5 and 10 LMH, TMP_{avg} values deviated from regression line B. Regression line A was drawn through these two points; regression line A also intersects the origin (*i.e.*, zero flux at zero TMP). The intersections of such linear regressions, where the slopes of the regressions change, typically correspond to the critical [1,2] or threshold [3] fluxes. Here, the intersection of regression lines A and B was determined to be the weak form of the critical flux (J_{cw}), and the intersection of regression lines B and C was found to be the threshold flux; the methods used to make these determinations will be described in the following discussion.

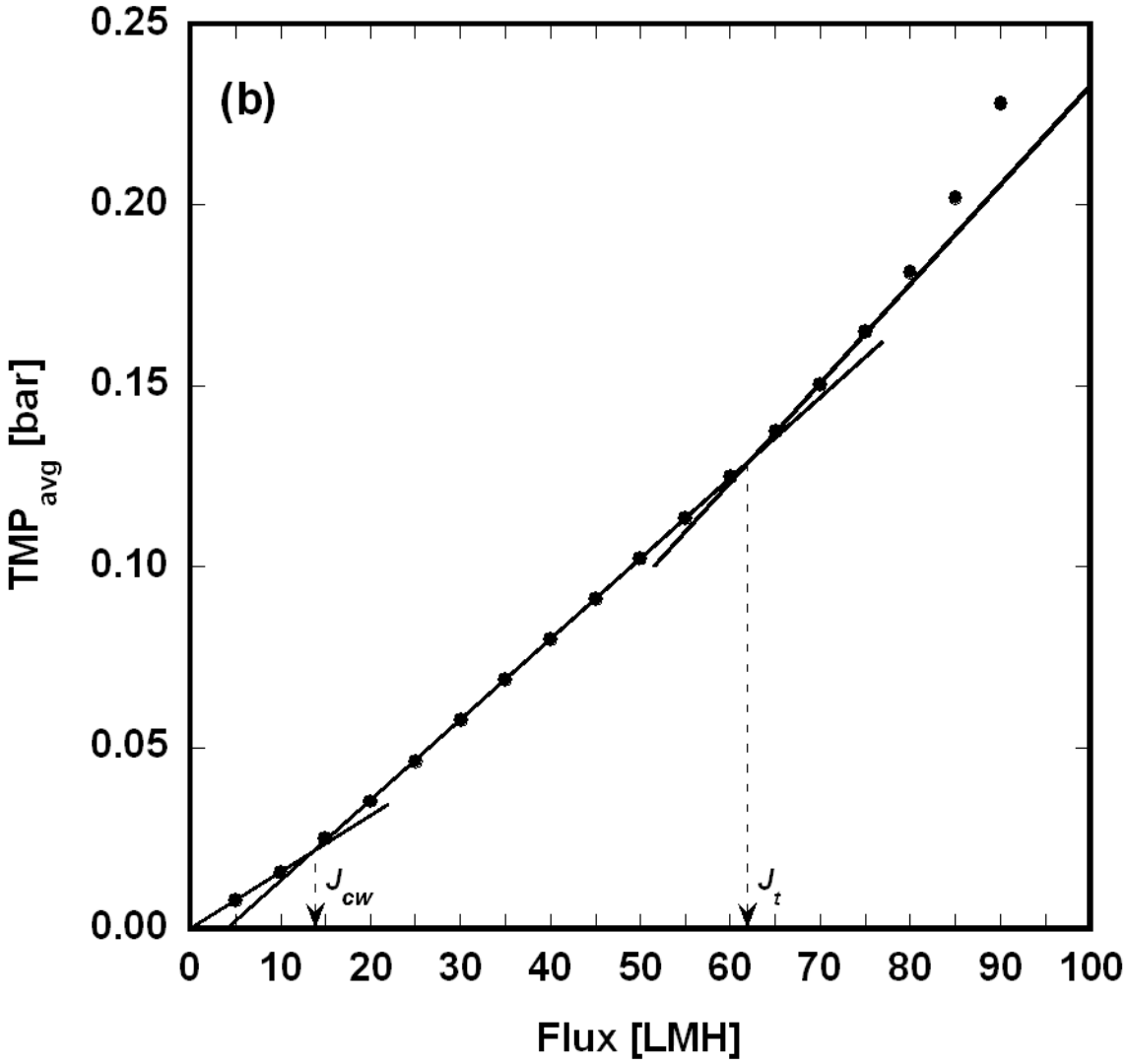

Figure 7.2. Critical and threshold flux determination from flux stepping experiment shown in Figure 7.1. TMP_{avg} was calculated as the arithmetic mean of all transmembrane pressures recorded during each flux step. Based upon the slope of the TMP_{avg}/flux relationship, the data were separated into 3 regions, denoted as A, B, and C. The intersection of regression lines A and B is the weak form of the critical flux (J_{cw}), while the intersection of regression lines B and C is the threshold flux (J_t).

The strict definitions of the strong and weak forms of the critical flux require that no change in resistance occur with time at fluxes below either form of the critical flux [4]. Therefore, below the critical flux, the TMP must remain constant even as the membrane is filtering a potentially fouling feed solution. If the TMP is increasing with time, the resistance is also increasing, and the membrane is operating above the critical flux. At fluxes below the threshold flux, however, the resistance (and, therefore, TMP) may increase at a slow, constant rate with time [4]. TMP profiles were carefully evaluated, especially at the lowest fluxes considered. Figure 7.3 presents the TMP profiles recorded over the first 60 minutes of the flux stepping experiment shown in full in Figure 7.1. At fluxes of 5 and 10 LMH, the TMP profiles are reasonably constant, suggesting that the resistance was not increasing with time. Therefore, the flux where regression lines A and B intersect (cf., Figure 7.2) is a critical flux. Since the definitions of both the strong and weak forms of the critical flux require that the TMP remain constant with time, this flux could not be distinguished as either the strong form or the weak form.

At fluxes greater than 10 LMH, the TMP slowly increased with time over each 10 minute constant flux interval, as shown in Figure 7.3. Furthermore, the rate of TMP increase appeared similar regardless of flux, suggesting that the rate of fouling was similar at all fluxes. As shown by the linear relationship between TMP_{avg} and flux in regression line B (cf., Figure 7.2), the rate of fouling appears to remain constant up to a flux of 62 LMH. At fluxes higher than 62 LMH, the slope of the TMP_{avg}/flux relationship increases, suggesting an increase in the rate of fouling. Since the threshold flux distinguishes a regime of relatively slow, constant fouling from a regime of more rapid fouling [4], 62 LMH is identified as the threshold flux (J_t).

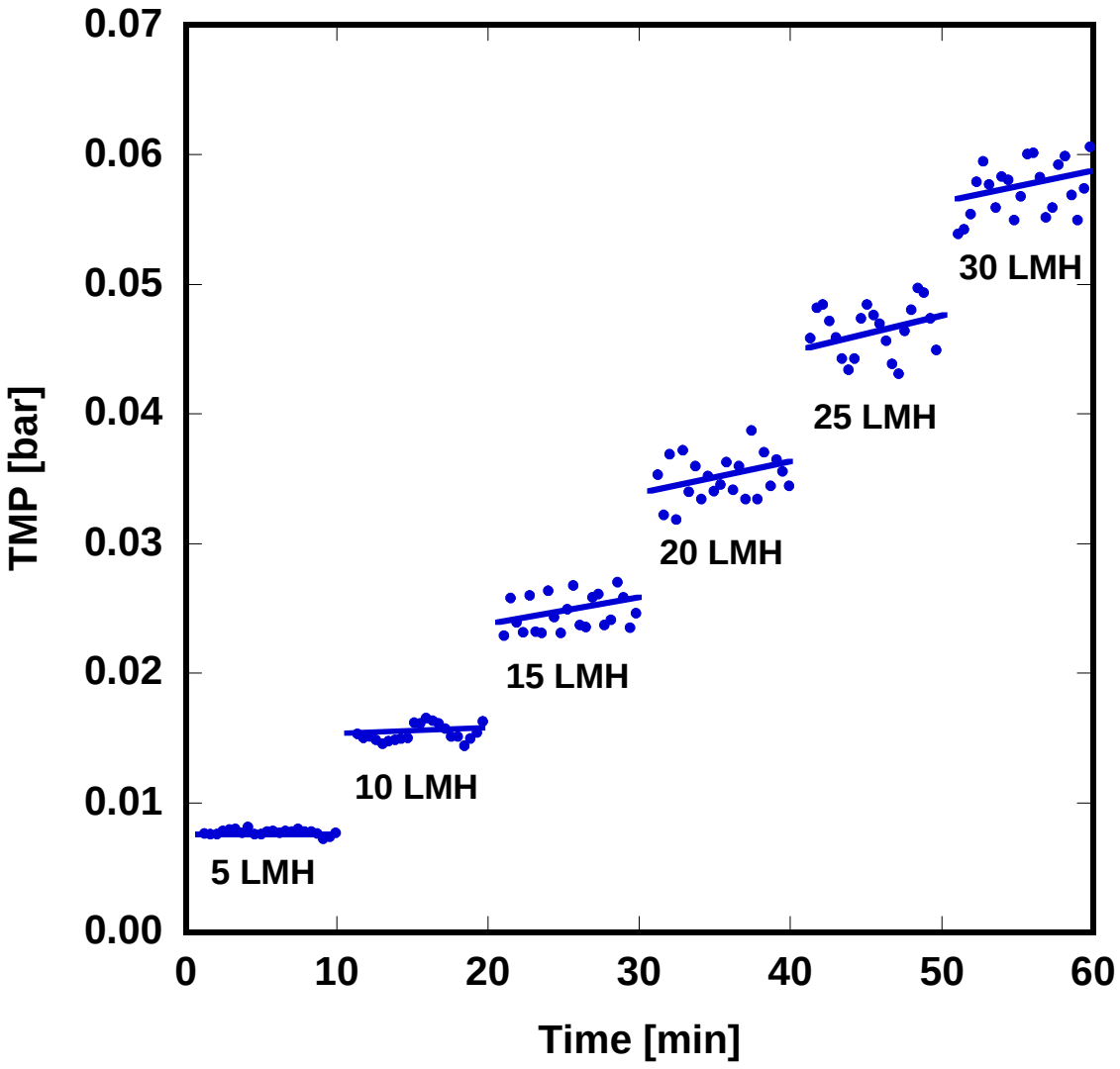

Figure 7.3. Detail of TMP profiles from Figure 7.1 at low fluxes. Although the TMP profiles at fluxes below 62 LMH appear to be invariant with time in Figure 7.1, close inspection reveals that the TMP is gradually increasing over each constant flux interval at fluxes of 15 LMH and greater. As noted by Field and Pearce [4], such a result suggests that 62 LMH is a threshold flux (Figure 7.2), and 14 LMH is the weak form of the critical flux (Figure 7.2). Lines drawn to guide the eye.

Although a relatively recent concept, the threshold flux has been determined by similar use of a TMP_{avg}/flux plot by Le Clech *et al*. [5] as described in the background section. In their study of a membrane bioreactor using a similar flux stepping protocol, a time-invariant TMP was never achieved, but the average TMP over each interval scaled linearly with flux at low fluxes. At higher fluxes, the slope of the average TMP vs. flux relationship increased. Le Clech *et al.* identified a critical flux where this slope change occurred, but they acknowledged that the strict requirement for unchanging TMP with time was not met. In a later discussion of Le Clech's report, Field and Pearce suggested that the term "threshold flux" be used to resolve this ambiguity [4]. Other techniques historically used for critical flux determination, such as pressure cycling [6], have been adapted to determine threshold fluxes [7]. Although similar techniques have been used to determine critical and threshold fluxes, few authors have observed both in the same system. Luo *et al*., for example, observed both the threshold flux and a critical flux for irreversibility in their study of shear-enhanced nanofiltration of dairy effluent [8].

To determine whether the critical flux shown in Figure 7.2 (14 LMH) is the strong form or the weak form of the critical flux, the effect of foulant adsorption to the membrane in the absence of permeate flux was evaluated as described in Section 3.3. Results are shown in Figure 7.4. After exposing the membrane to foulant under conditions of zero permeate flux, the membrane permeance decreased from 900 LMH/bar to 625 LMH/bar. By evaluating fouling under zero flux conditions, the resistance increase due to adsorption, which occurs spontaneously regardless of flux, was separated from that of reversible and irreversible foulant accumulation due to convective flow to the membrane surface [4].

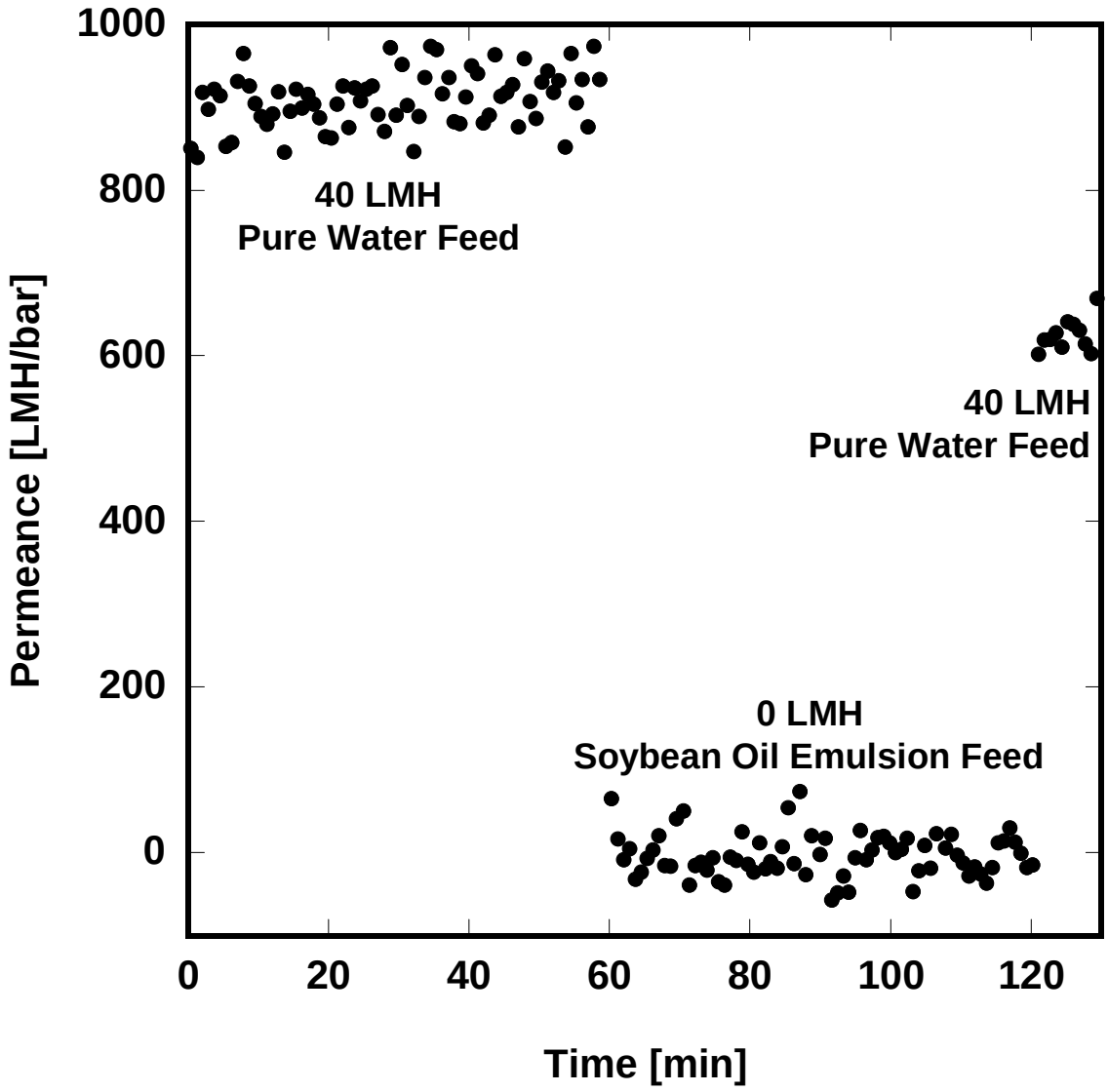

Figure 7.4. Experimental determination of the decrease in permeance due to foulant adsorption. The PS-20 UF membrane was operated with pure water at 40 LMH for 60 min to establish a baseline permeance of 900 LMH/bar. Foulant was adsorbed to the membrane in the absence of convective flow through the pores by reducing the flux to zero and switching the feed to soybean oil emulsion for 60 min. Operation at 40 LMH was resumed with pure water feed for 10 min to measure the permeance after foulant adsorption. Feed pressure: 2.1 barg, crossflow velocity: 0.18 m/s.

Figure 7.5 presents TMP_{avg} values as a function of flux at low fluxes. Experimental data are shown as filled circles, while the linear regressions A and B (also shown in Figure 7.2) are solid lines. These regressions are compared with membrane behavior under two hypothetical fouling scenarios. First, if no foulant adsorption occurs and no foulant accumulates on the membrane due to convective flow towards the surface, the only resistance will be that of the membrane itself. This scenario is represented by the dot-dashed line labeled "Membrane Only." This line was drawn based on the membrane pure water permeance of 900 LMH/bar. Membrane operation along this line when challenged with a fouling feed suggests that the membrane is operating below the strong form of the critical flux at all fluxes considered, because, as described in the background section, the only resistance to permeation below the strong form of the critical flux is due to that of the membrane. In this definition, foulant adsorption or reversible and irreversible accumulation due to convection are not significant contributors to resistance. None of the experimental data lie along this operational line, so the strong form of the critical flux was not observed.

The second hypothetical fouling scenario is represented by the dashed line labeled "Membrane + Adsorption Resistance." This operational line is based on the result of the experiment shown in Figure 7.4, where adsorption of foulant to the membrane surface is a significant contributor to resistance. The dashed line was drawn based on a permeance of 625 LMH/bar, the permeance after adsorption of foulant at zero flux conditions. The experimental data at 5 and 10 LMH nearly lie directly on the dashed line and, therefore, linear regression A (623 LMH/bar) is essentially equal to it. Thus, during filtration of the soybean oil emulsion at 5 and 10 LMH, the membrane and foulant adsorption to the membrane are the major contributors to resistance. Substantial accumulation of foulant due to convective flow towards the membrane likely does not occur at these low fluxes.

As noted in the background section, spontaneous foulant adsorption, but not permeate-driven accumulation, is permitted at fluxes below the weak form of the critical flux. Due to the invariant TMP profiles at 5 and 10 LMH (cf., Figure 7.3), and the close correlation of experimental fouling behavior with the hypothetical scenario representing foulant adsorption only, 14 LMH (*i.e.*, the intersection of lines A and B on Figure 7.4 or 7.5) is likely the weak form of the critical flux.

That the weak form of the critical flux was observed suggests that foulant adsorption is a significant contributor to resistance in this membrane/foulant system. If foulant adsorption had not been significant, it is proposed that the strong form of the critical flux would have been observed, and TMP_{avg} at 10 LMH would have been on linear regression B, and the TMP_{avg} at 5 LMH would have been on the dot-dashed line (cf., Figure 7.5). Regardless of which form of the critical flux was observed, the fact that linear regression B does not pass through the origin suggests that permeate-driven foulant accumulation must not be a dominant fouling mechanism at very low fluxes.

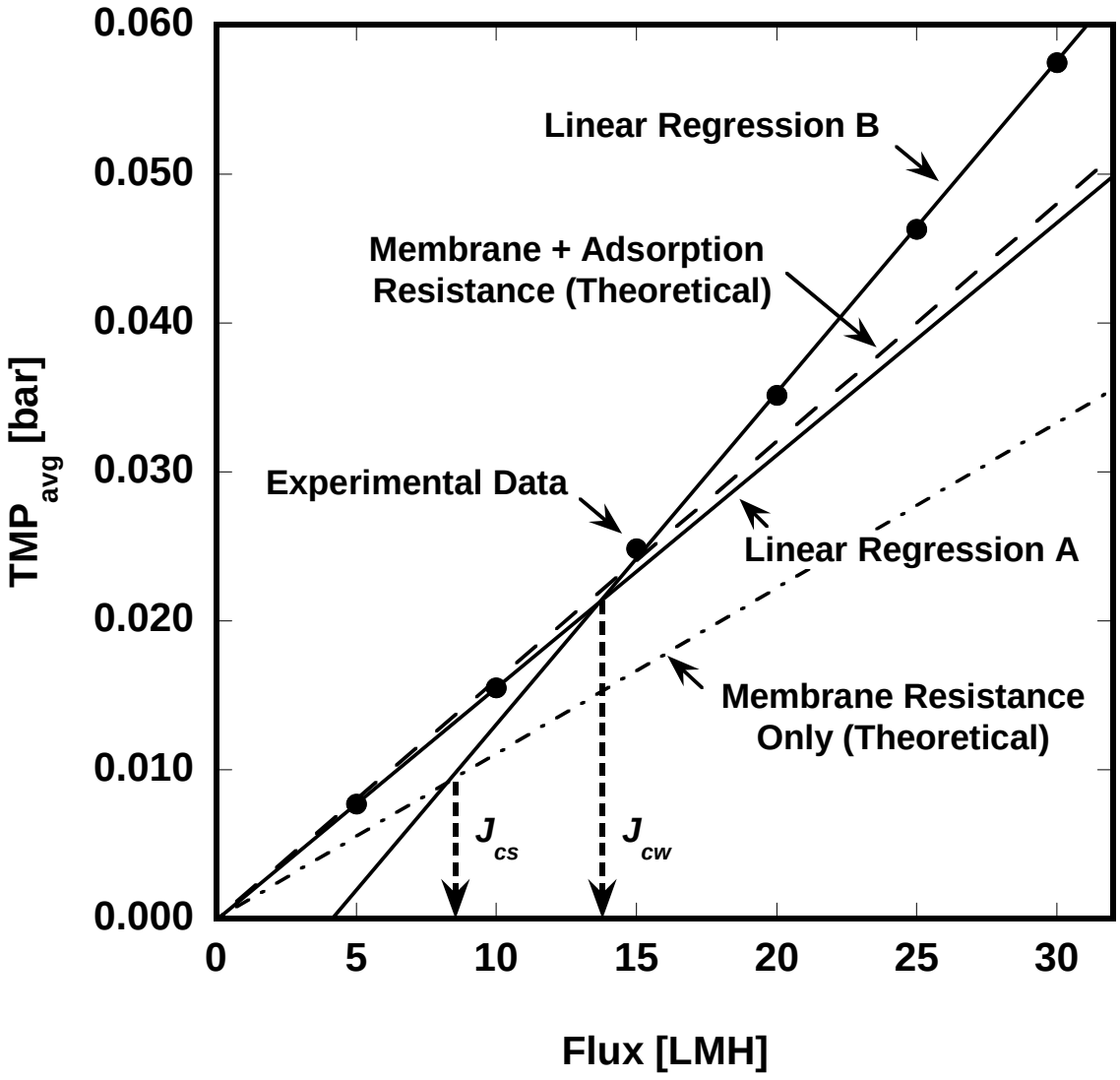

Figure 7.5. Detail of the TMP_{avg}/flux relationship from Figure 7.2 at low fluxes. TMP_{avg} values derived from the flux stepping experiment presented in Figure 7.3 are shown along with the linear regressions A and B (*i.e.*, the solid lines) through those data above and below the weak form of the critical flux (J_{cw}). The TMP/flux relationships are also shown for the hypothetical fouling scenarios where the resistance is identical to that of a clean membrane (the line labeled Membrane Resistance Only) and the resistance accounts for spontaneous foulant adsorption to the membrane (the line labeled Membrane + Adsorption Resistance). It is proposed that the strong and weak forms of the critical flux may be identified as shown.

7.2.2 Constant Flux Fouling

Constant flux fouling experiments were performed on PS-20 UF membranes with 1500 ppm soybean oil emulsion foulant. The feed pressure was 2.1 barg and the volumetric feed flow rate was 0.8 L/min, corresponding to a crossflow velocity of 0.18 m/s. Five fluxes were tested: 25, 40, 55, 85, and 100 LMH, representing two fluxes above and three fluxes below the estimated threshold flux of 62 LMH. The TMP evolution at each flux is presented in Figure 7.6. As the imposed flux increased, the TMP increased. This result is reasonable from the perspective of the both the initial TMP and the TMP during fouling. With increasing flux, the initial TMP (the TMP observed during pure water filtration) increased in proportion to the membrane resistance. During fouling, higher fluxes brought greater amounts of the emulsified oil foulant to the membrane surface, increasing foulant accumulation on the membrane. A significant qualitative difference existed in fouling behavior, however, between the membranes operated above and below the threshold flux. Membranes operated at 25, 40, and 55 LMH (*i.e.*, below the threshold flux) showed a modest increase in TMP in the first few minutes and slowly increasing TMP thereafter. The early TMP rise, where the TMP profile is concave down, was likely due to a combination of concentration polarization and a short period of rapid fouling [9,10], but it does not suggest extensive fouling that would preclude long-term operation.. Marshall, Munro, and Trägårdh found that, even at extremely low fluxes, some fouling of UF membranes could not be prevented during start-up [11].

The membranes operated at fluxes of 85 and 100 LMH, both well above the threshold flux, showed rapid fouling. Above the threshold flux, foulants were brought to the membrane surface more rapidly than they could be removed by crossflow shear forces and diffusion. As foulants accumulated, the imposed flux demanded that the same

volume of permeate be drawn through an increasingly constricted pore structure, exacerbating fouling in any remaining open pores and driving the resistance up quickly.

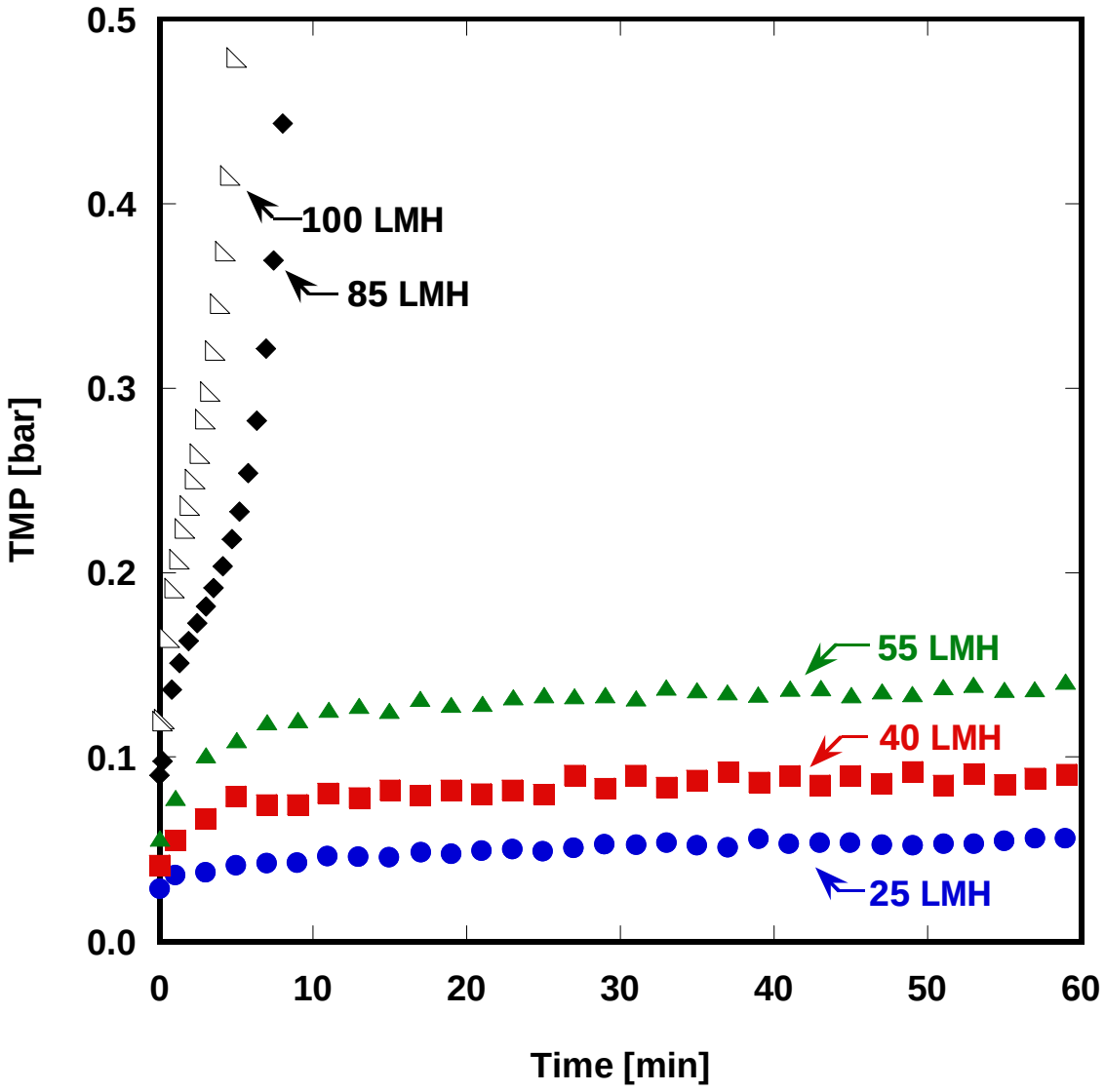

Figure 7.6. TMP evolution of PS-20 UF membranes during constant flux fouling with a 1500 ppm soybean oil emulsion feed. Membranes operated below the threshold flux of 62 LMH exhibited low and slowly increasing TMP's, but those operated above the threshold flux exhibited rapidly increasing TMP's. The curves shown are representative of at least three replicates at each flux. Feed pressure: 2.1 barg, crossflow velocity: 0.18 m/s.

7.2.3 Constant Transmembrane Pressure Fouling

Constant TMP fouling of PS-20 UF membranes was performed with 1500ppm soybean oil emulsion foulant. The volumetric feed flow rate was 0.8 L/min, corresponding to a crossflow velocity of 0.18 m/s. Five transmembrane pressures were tested: 0.027, 0.041, 0.053, 0.077, and 0.096 bar. These TMP values were chosen because they produced initial membrane fluxes identical to those imposed during the constant flux experiments (*e.g.*, a TMP of 0.027 bar produced an initial flux of 25 LMH, etc.). Regardless of whether the initial flux was above or below the threshold flux, the flux decline curves exhibited qualitatively similar behavior, as shown in Figure 7.7. Membranes with initial fluxes below the threshold flux (*i.e.,* TMP = 0.027, 0.041, and 0.053 bar) experienced modest degrees of fouling. The two membranes with initial fluxes above the threshold flux (*i.e.,* TMP = 0.077 and 0.096 bar) fouled quickly to fluxes below the threshold flux. Once at these lower fluxes, the fouling rate decreased, and the flux profiles flattened. Due to the extremely low transmembrane pressures required to produce initial fluxes of 5 and 10 LMH (below the weak form of the critical flux), constant TMP fouling below the weak form of the critical flux was not studied.

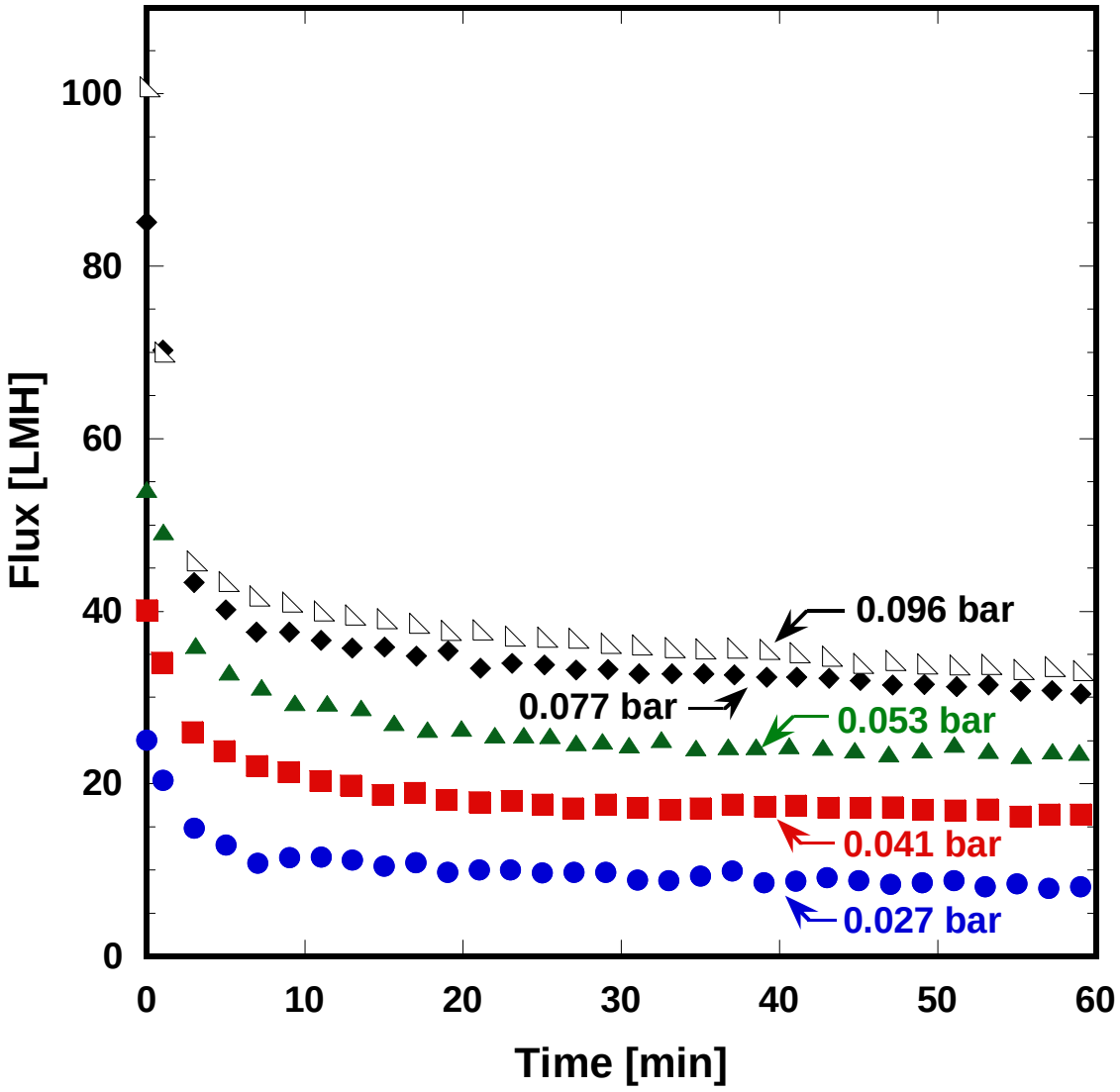

Figure 7.7. Flux decline during constant TMP fouling of PS-20 UF membranes with a 1500 ppm soybean oil emulsion feed. Membranes were operated at five transmembrane pressures sufficient to produce initial fluxes identical to those imposed in the constant flux fouling experiment (cf., Figure 7.6). All curves show qualitatively similar behavior, regardless of whether the initial flux is above or below the threshold flux. The curves shown are representative of at least three replicates at each TMP. The numbers in the figure represent the TMP for each fouling experiment.

7.2.4 Comparison of Constant Flux and Constant Transmembrane Pressure Fouling

From the experimental results in the constant flux and constant TMP experiments, the resistance to mass transfer, R, was calculated according to Equation [2.1]. The resistance values were plotted as a function of the permeate volume normalized by the total filtration area. In the constant TMP experiment, the flux changed with time and, as a result, the rate at which foulant was brought to the membrane surface changed with time. In contrast, the constant flux experiment brought a steady rate of foulant to the membrane surface for the entire experimental duration. By plotting the resistance as a function of permeate volume/area, the resistances may be compared at points where the same amount of permeate has been produced in each experiment (*i.e.*, the membranes have filtered the same amount of feed). Resistances from constant flux experiments were compared to resistances from constant TMP experiments started at the same flux imposed during the constant flux experiment. The typical pure water permeance of the membrane was 900 LMH/bar, so the initial resistance (recorded during pure water filtration just before fouling was initiated) was around 0.0011 bar/LMH.

Figure 7.8 presents resistance comparisons between constant flux and constant TMP fouling at fluxes below the threshold flux (*i.e.,* 62 LMH). Constant flux experiments were performed at 25, 40, and 55 LMH, and constant TMP experiments were performed at 0.027, 0.041, and 0.053 bar, corresponding to initial fluxes of 25, 40, and 55 LMH, respectively. Within experimental error, the resistances during constant flux and constant TMP fouling were indistinguishable. Experimental error was greatest for experiments at the lowest flux due to the low transmembrane pressures required and the uncertainty in the differential pressure transducer readings at the low end of their span. In all three cases, the resistance increased at low permeate volumes and reached a plateau thereafter. Regardless of the applied flux or TMP, all membranes reached a

similar resistance of about 0.0025 bar/LMH. Since all membranes were operating below their threshold flux, foulant accumulation did not contribute strongly to increased membrane resistance as the applied (initial) flux increased. A similar result was observed by Aimar *et al.*, where increasing the flux did not greatly impact the observed resistance during constant flux filtration of whey protein using polysulfone UF membranes [12].

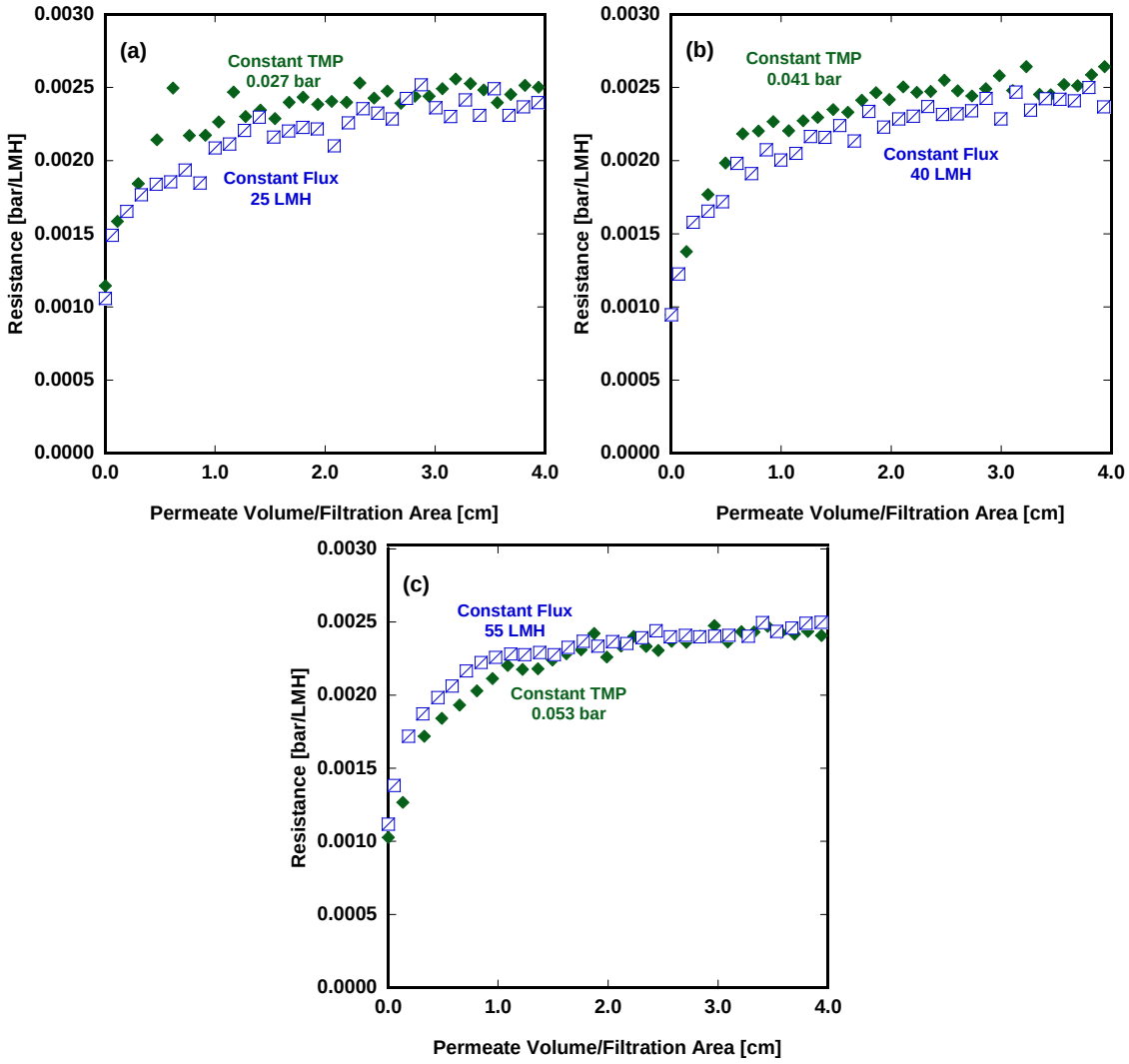

Figure 7.8. Comparisons of mass transfer resistance evolution during constant flux and constant TMP experiments at fluxes below the threshold flux (*i.e.,* 62 LMH), calculated from data shown in Figures 7.6 and 7.7 using Equation [2.1]. (a) Constant flux = 25 LMH, constant TMP = 0.027 bar (initial flux = 25 LMH). (b) Constant flux = 40 LMH, constant TMP = 0.041 bar (initial flux = 40 LMH). (c) Constant flux = 55 LMH, constant TMP = 0.053 bar (initial flux = 55 LMH).

Figure 7.9 presents the resistances developed during constant flux and constant TMP experiments at (initial) fluxes above the threshold flux (*i.e.*, 62 LMH). Constant flux experiments were performed at 85 and 100 LMH. Constant TMP experiments at 0.076 and 0.097 bar produced initial fluxes of 85 and 100 LMH, respectively. Unlike the experiments at (initial) fluxes below the threshold flux, fouling above the threshold flux produced different behavior in constant flux and constant TMP operation. In the constant TMP case, initial fluxes above the threshold flux caused rapid fouling and, consequently, a sharp decline in the flux (cf., Figure 7.7), which manifests itself as an increase in resistance at low permeate volume/area (V/A) (*e.g.*, <1 cm). After the flux fell below the threshold flux, the rate of fouling diminished and little change in membrane resistance was observed thereafter. In constant flux fouling above the threshold flux, a brief period of relatively slow fouling was observed, which closely matched the resistance development in the constant TMP experiment over this same period. However, in the constant flux case, a rapid escalation in resistance was observed near V/A = 1 cm. Because the flux in the constant TMP experiment rapidly fell well below the threshold flux, the hydrodynamic forces responsible for bringing foulant to and from the membrane surface were able to balance, resulting in no further changes in resistance with continuing permeation. In the case of constant flux operation, such a dynamic equilibrium could not be reached, because the high, sustained rate of permeation through the membrane caused the continued accumulation of foulant on the membrane. Similar behavior during constant flux fouling has been reported elsewhere [13–18]. Others have suggested that such an upturn in resistance corresponds to the beginning of cake formation on the membrane surface. For example, Ho and Zydney suggested that pore blockage was the major fouling mechanism during the slow, steady increase in resistance initially observed during constant flux MF of proteins [16]. After the pores were substantially blocked, a

cake layer began to form, rapidly driving up the resistance [16]. Ognier *et al*. proposed a similar hypothesis in their study of constant flux MF of bioreactor effluent [18]. During constant flux filtration, pore closure tends to be a self-propagating phenomenon. As pores gradually become blocked by foulant, the local flux in neighboring pores must increase to maintain the same flux over the entire filtration area. This increase in local flux draws foulant more quickly into the remaining open pores, causing them to foul more quickly. Once many pores are blocked and the local flux is sufficiently high, cake formation begins, dramatically increasing the resistance [18]. Due to this rapid fouling and cake formation under constant flux operation, the membrane TMP values reached the gauge feed pressure after a short time and the experiment was terminated, meaning that constant flux resistance data stopped at permeate volume/area values less than approximately 2 cm.

Most industrial UF and MF systems are operated at constant flux, which permits a consistent rate of permeate production [19,20]. Additionally, depending upon the character of the feed water, the flux may be adjusted to maximize water production while minimizing fouling. Decloux *et al*. showed that, in UF, membranes were more productive with fewer cleanings when operated in constant flux mode than when operated in constant TMP mode [20]. Clearly, however, such benefits may only be realized below the threshold flux, because constant flux operation above the threshold flux appears to be unsustainable. At the very least, constant flux operation at high fluxes would require frequent backwashing or membrane cleaning. Flux optimization protocols, which have been discussed elsewhere, may be used to better understand the most desirable flux (*e.g.*, the "sustainable flux") for long-term industrial operation [4,20]. Sustainable flux determination involves many factors beyond those explored here, including membrane, energy, and cleaning costs [4].

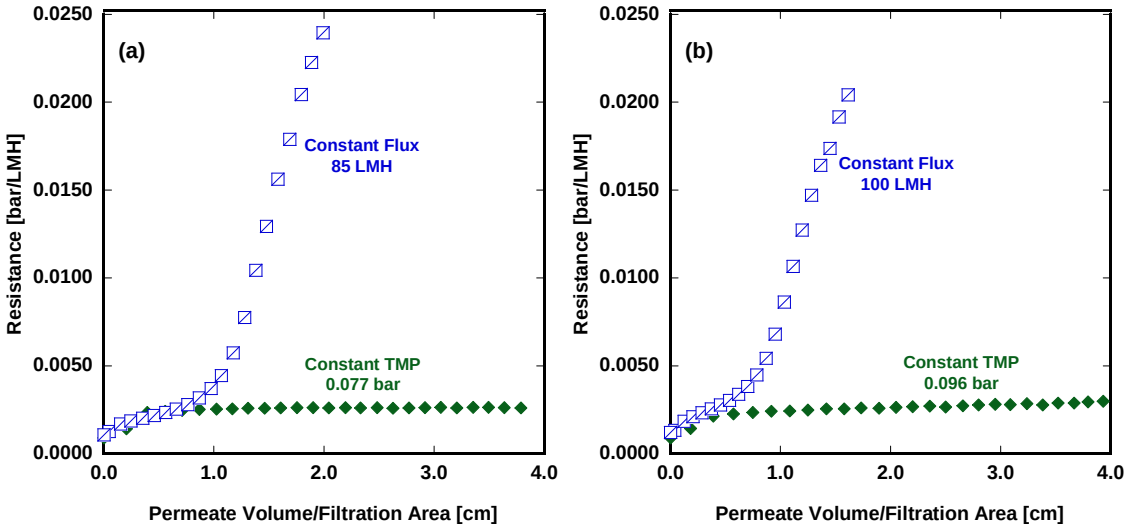

Figure 7.9. Comparisons of resistance evolution during constant flux and constant TMP experiments at fluxes above the threshold flux (62 LMH), calculated from data shown in Figures 7.6 and 7.7 using Equation [2.1]. (a) Constant flux = 85 LMH, constant TMP = 0.077 bar (initial flux = 85 LMH). (b) Constant flux = 100 LMH, constant TMP = 0.096 bar (initial flux =100 LMH).

Organic rejection measurements for all fouling experiments, including both constant flux and constant TMP tests, are shown in Table 7.1. In the constant TMP experiments, the rejection decreased overall from 98.5% to 97.7% as initial flux (and TMP) increased. This decline in rejection is well known in UF. With increasing TMP, the accumulation of foulant on the membrane surface also increased, exacerbating concentration polarization and, therefore, increasing organic permeation through the membrane [21]. For constant flux fouling, the rejection also decreased as flux increased from 25 LMH to 40 LMH; the rejections at 40 LMH and 55 LMH could not be statistically distinguished. However, an increase in rejection was observed as the flux was increased from 55 LMH (below the threshold flux) to 85 LMH (above the threshold flux). A minimum in rejection may exist at 55 LMH, the flux closest to the threshold flux of 62 LMH. A similar result was reported by Chan *et al.*, where a rejection

minimum was observed near the critical flux during protein filtration using regenerated cellulose UF membranes [22]. Below the threshold flux, concentration polarization was enhanced with increasing flux, as in the case of constant TMP fouling, causing a decrease in rejection. At sustained fluxes above the threshold flux, substantial accumulation of foulant on the membrane surface may have hindered organic permeation through the membrane, counteracting the effects of increased concentration polarization at 85 and 100 LMH. Therefore, the rejection increased with increasing flux above the threshold flux [23].

Flux (LMH)	Rejection during Constant Flux Filtration (%)	Rejection during Constant TMP Filtration (%)
25	98.9 ± 0.4	98.5 ± 0.1
40	98.3 ± 0.1	98.4 ± 0.1
55	98.4 ± 0.2	98.3 ± 0.1
85	99.0 ± 0.3	97.7 ± 0.1
100	99.0 ± 0.1	97.7 ± 0.1

Table 7.1. Organic rejection during constant flux and constant TMP fouling experiments. Rejections were calculated based on total organic carbon analysis of permeate and feed. Fluxes shown refer to initial fluxes in the case of constant TMP experiments. Values shown are averages of at least three replicate trials, and errors are standard deviations on those averages.

7.3 REFERENCES

[1] K.Y.-J. Choi, B.A. Dempsey, Bench-scale Evaluation of Critical Flux and TMP in Low-pressure Membrane Filtration, Journal of the American Water Works Association 97 (7) (2005) 134–143.

[2] D.. Kwon, S. Vigneswaran, A.. Fane, R.B. Aim, Experimental determination of critical flux in cross-flow microfiltration, Separation and Purification Technology 19 (3) (2000) 169–181.

[3] D.J. Miller, D.R. Paul, B.D. Freeman, A Crossflow Filtration System for Constant Permeate Flux Membrane Fouling Characterization, Review of Scientific Instruments 84 (3) (2013) 035003.

[4] R.W. Field, G.K. Pearce, Critical, Sustainable and Threshold Fluxes for Membrane Filtration with Water Industry Applications, Advances in Colloid and Interface Science 164 (1-2) (2011) 38–44.

[5] P. Le Clech, B. Jefferson, I.S. Chang, S.J. Judd, Critical Flux Determination by the Flux-step Method in a Submerged Membrane Bioreactor, Journal of Membrane Science 227 (1-2) (2003) 81–93.

[6] B. Espinasse, P. Bacchin, P. Aimar, On an Experimental Method to Measure Critical Flux in Ultrafiltration, Desalination 146 (1-3) (2002) 91–96.

[7] M. Stoller, M. Bravi, A. Chianese, Threshold Flux Measurements of a Nanofiltration Membrane Module by Critical Flux Data Conversion, Desalination 315 (2013) 142–148.

[8] J. Luo, L. Ding, Y. Wan, M.Y. Jaffrin, Threshold flux for shear-enhanced nanofiltration: Experimental observation in dairy wastewater treatment, Journal of Membrane Science 409-410 (2012) 276–284.

[9] R. Ghosh, Study of Membrane Fouling by BSA using Pulsed Injection Technique, Journal of Membrane Science 195 (1) (2002) 115–123.

[10] D.M. Kanani, R. Ghosh, A constant flux based mathematical model for predicting permeate flux decline in constant pressure protein ultrafiltration, Journal of Membrane Science 290 (1-2) (2007) 207–215.

[11] A.D. Marshall, P.A. Munro, G. Trägårdh, Design and Development of a Cross-flow Membrane Rig to Compare Constant Pressure and Constant Flux Operation in Ultrafiltration and Microfiltration, Transactions of the Institution of Chemical Engineers C: Food and Bioproducts Processing 74 (2) (1996) 92–100.

[12] P. Aimar, J.A. Howell, M. Turner, Effects of Concentration Boundary Layer Development on the Flux Limitations in Ultrafiltration, Chemical Engineering Research and Design 67 (3) (1989) 255–261.

[13] Z. Cai, C. Wee, M.M. Benjamin, Fouling Mechanisms in Low-Pressure Membrane Filtration in the Presence of an Adsorbent Cake Layer, Journal of Membrane Science 433 (2013) 32–38.

[14] G. Gésan, G. Daufin, U. Merin, J.-P. Labbé, A. Quémerais, Fouling During Constant Flux Crossflow Microfiltration of Pretreated Whey. Influence of Transmembrane Pressure Gradient, Journal of Membrane Science 80 (1) (1993) 131–145.

[15] G. Gésan, G. Daufin, U. Merin, Performance of Whey Crossflow Microfiltration during Transient and Stationary Operating Conditions, Journal of Membrane Science 104 (3) (1995) 271–281.

[16] C.-C. Ho, A.L. Zydney, Transmembrane Pressure Profiles during Constant Flux Microfiltration of Bovine Serum Albumin, Journal of Membrane Science 209 (2) (2002) 363–377.

[17] P. Kovalsky, G. Bushell, T.D. Waite, Prediction of Transmembrane Pressure Build-up in Constant Flux Microfiltration of Compressible Materials in the Absence and Presence of Shear, Journal of Membrane Science 344 (1-2) (2009) 204–210.

[18] S. Ognier, C. Wisniewski, A. Grasmick, Membrane Bioreactor Fouling in Sub-critical Filtration Conditions: a Local Critical Flux Concept, Journal of Membrane Science 229 (1-2) (2004) 171–177.

[19] B. Alspach, S. Adham, T. Cooke, P. Delphos, J. Garcia-Aleman, J. Jacangelo, et al., Microfiltration and Ultrafiltration Membranes for Drinking Water, Journal of the American Water Works Association 100 (12) (2008) 84–97.

[20] M. Decloux, L. Tatoud, Importance of the Control Mode in Ultrafiltration: Case of Raw Cane Sugar Remelt, Journal of Food Engineering 44 (2) (2000) 119–126.

[21] R.W. Baker, Membrane Technology and Applications, 2nd ed., John Wiley & Sons, West Sussex, England, 2004.

[22] R. Chan, V. Chen, M.P. Bucknall, Ultrafiltration of Protein Mixtures: Measurement of Apparent Critical Flux, Rejection Performance, and Identification of Protein Deposition, Desalination 146 (1-3) (2002) 83–90.

[23] V. Chen, Performance of partially permeable microfiltration membranes under low fouling conditions, Journal of Membrane Science 147 (2) (1998) 265–278.

Chapter 8: Constant Flux Crossflow Filtration Evaluation of Surface-Modified Fouling-Resistant Membranes

8.1 SUMMARY

The surfaces of PS-20 polysulfone ultrafiltration (UF) membranes were modified with polydopamine (PD) and polydopamine-*g*-poly(ethylene glycol) (PD-*g*-PEG) hydrophilic coatings. Unmodified and modified membranes were challenged with a 1500 ppm soybean oil emulsion feed at six different permeate fluxes in constant flux crossflow filtration fouling studies. The threshold flux was determined for each membrane. Above the threshold flux, modified membranes generally exhibited lower transmembrane pressures than unmodified membranes. However, below the threshold flux, modified membranes had higher transmembrane pressures than unmodified membranes, likely due to an increase in mass transfer resistance resulting from the surface modification. In all cases, the additional grafting of PEG brushes resulted in a significant increase in mass transfer resistance. If the membranes are to be operated below the threshold flux to achieve sustainable operation, one might conclude that these surface modifications did not improve the overall performance of the membranes during fouling, since the resistance to mass transfer of the modified membranes was not lower than that of the unmodified analogs. However, the surface modified membranes had a lower initial pure water flux than the unmodified membrane. To account for this difference, PD-*g*-PEG modified membranes were compared to membranes with a thicker PD coating and to an unmodified membrane with a smaller pore size than that used in the surface modification studies; in this way, all three sets of membranes had similar pure water permeances. In this case, the unmodified membrane exhibited a much higher transmembrane pressure (TMP) during fouling than the modified membranes, so when membranes are compared at the same starting permeance, the surface modifications improved fouling resistance.

Therefore, a potential strategy to achieve fouling resistance in a membrane of a desired flux and rejection is to modify the surface of a more permeable (and perhaps lower rejection) membrane, thereby making the resulting modified membrane fouling resistant but leaving it with the desired flux and rejection characteristics.

8.2 RESULTS AND DISCUSSION

8.2.1 Pure Water Permeance

The pure water permeances of unmodified, PD modified, and PD-*g*-PEG modified PS-20 UF membranes were measured by dead end filtration. Results are shown in Table 8.1. The average permeance of unmodified PS-20 membrane was about 900 $Lm^{-2}h^{-1}bar^{-1}$ (LMH/bar), matching the manufacturer specification [1]. The application of PD and PD-*g*-PEG surface modifications reduced the membrane permeance, although the PD surface treatment had a modest impact on permeance, near the limit of uncertainty of the measurement. Similar reductions have been reported elsewhere [2]. While these modifications increased the hydrophilicity of the membrane surface [2,3], they also contributed to the membrane's total mass transfer resistance. The conformal polydopamine coating likely constricts pores to a slight extent, and the grafted PEG chains add additional resistance. The PD modification resulted in a 22% reduction in permeance, and the PD-g-PEG modification resulted in a 36% reduction in permeance relative to that of the unmodified membrane. However, the standard deviations of these measurements were relatively large (±22% for the unmodified membrane and ±14% for the PD modified membrane), reflecting the inherent variability of the small samples cut from the large membrane roll. Although a clear decrease in average permeance was observed with the application of the coatings, the unmodified and PD modified

permeances are the same, within statistical uncertainty, and the unmodified and PD-*g*-PEG modified permeances are near the uncertainty limit.

The unmodified PS-20 membrane has a molecular weight cutoff of 20 kDa (95% PEG rejection) [1]. To provide a very crude, order of magnitude approximation of the average effective pore size of such a membrane, one might use the size of a 20 kDa PEG chain. The Stokes radius of a PEG chain may be calculated from its molecular weight [4]:

$$a = 16.73 \times 10^{-3} M^{0.557} \qquad [8.1]$$

where a is the Stokes radius (in nm), and M is the molecular weight. The Stokes radius of a 20kDa PEG chain is 4.2 nm. Thus, PEG molecules significantly larger than this radius are effectively excluded from the membrane, presumably because they are too large to pass though the pores of the membrane.

The permeance (PM) is the average membrane hydraulic permeability (L_p) divided by the viscosity:

$$PM = \frac{L_p}{\mu} \qquad [8.2]$$

where μ is the fluid viscosity. The viscosity of the permeate will be assumed to be essentially equal to that of water, since the organic rejection of these membranes is very high (>98%), as will be described later. The average membrane hydraulic permeability is given by [5]:

$$L_p = \frac{\varepsilon \mu V}{\mathrm{TMP}} \qquad [8.3]$$

where V is the average permeate fluid velocity and ε is the membrane porosity. Poiseuille's law may be used to relate the fluid velocity through a pore to the pore radius [5]:

$$V = \frac{r^2(\mathrm{TMP})}{8\mu\delta} \qquad [8.4]$$

where r is the average, effective pore radius, and δ is the membrane thickness. The pores are assumed to be straight cylinders through the membrane, and the membrane thickness was 190 μm (averaged from the same samples used for dead end filtration). By combining Equations [8.2] – [8.4], an expression for the permeance of a membrane consisting entirely of pores of radius r may be obtained:

$$PM = \frac{\varepsilon r^2}{8\mu\delta} \qquad [8.5]$$

If the Stokes radius of a 20 kDa PEG chain is used as the pore radius of the unmodified membrane, the radius of either modified membrane may be calculated by taking a ratio of the permeances as expressed in Equation [8.4]:

$$\frac{r_M}{r_{UM}} = \left(\frac{PM_M}{PM_{UM}}\right)^{1/2}\left(\frac{\varepsilon_{UM}}{\varepsilon_M}\right)^{1/2} \qquad [8.6]$$

where r_M and r_{UM} are the average, effective pore radii of the modified (PD or PD-*g*-PEG) and unmodified membranes, PM_M and PM_{UM} are the permeances of the modified and unmodified membranes, and ε_M and ε_{UM} are the porosities of the modified and unmodified membranes, respectively. If one assumes that the porosities of the modified and unmodified membranes are similar, the ratio of radii may be directly related to the ratio of permenaces:

$$\frac{r_M}{r_{UM}} = \left(\frac{PM_M}{PM_{UM}}\right)^{1/2} \qquad [8.7]$$

Table 8.1 shows the average, effective pore radii of the unmodified and modified membranes. The effective pore radius of the unmodified membrane was calculated using

Equation [8.1], and the effective pore radii of the modified membranes were calculated using Equation [8.7].

Membrane	Pure Water Permeance (LMH/bar)	Effective Pore Radius (nm)
Unmodified	900 ± 200	4.2
PD Modified	700 ± 100	3.7
PD-*g*-PEG Modified	570 ± 70	3.3

Table 8.1. Pure water permeance of unmodified, PD modified, and PD-*g*-PEG modified PS-20 UF membranes. Measurements made in dead end filtration with a feed pressure of 2.1 barg. Values shown are averages of at least 25 samples cut from arbitrary locations on the membrane roll. Errors are standard deviations calculated from the averages.

The values given in 8.1 are likely the smallest average pore sizes that would be expected for the modified membranes. The PD and PD-*g*-PEG modifications may occlude some of the smallest pores, which would cause the membrane porosity to decrease. If the modified membranes had porosities less than those of the unmodified membranes, the effective pore radii would be larger than those shown in Table 8.1 (see Equation [8.6]).

Ellipsometry has been used to measure the thickness of polydopamine deposited on the surface of polysulfone films [3]. At the conditions used here (2 mg/mL dopamine, 15 mM TRIS buffer, pH = 8.8, 60 minutes, RT), the reported polydopamine thickness was approximately 12 nm. Increasing the deposition time to 75 minutes resulted in a polydopamine thickness of approximately 17 nm [3]. Based on the estimated effective radii shown in Table 8.1, such polydopamine thicknesses could not develop within the pores of the membrane. Limited diffusion of oxygen into the porous structure may have

resulted in thinner coatings within the porous structure than predicted by deposition on top of a dense polysulfone surface with extensive access to oxygen. Dissolved oxygen has recently been shown to be critical in the oxidative polymerization of dopamine from aqueous solution [6]. Thus, most of the polydopamine was likely deposited on the surface of the membrane. Given that the average size of the oil droplets used in this study is about 1.4 μm, with nearly all droplets in the range of 0.8 to 3.0 μm [7], which is far larger than the average pore size of the membranes considered, having the polydopamine largely on top of the membrane surface puts it in the region where it can most directly interact with the foulant and potentially have the most benefical effect on fouling in this situation.

The graft density of PEG on polydopamine modified PS-20 membrane has also been reported [3]. When PEG was grafted to a polydopamine modified membrane (2 mg/mL dopamine, 15 mM TRIS buffer, pH = 8.8, 60 minutes, RT) under the same conditions used here (1 mg/mL PEG-NH_2, 15 mM TRIS buffer, pH = 8.8, 60 minutes, 60°C), a PEG density of approximately 17 $\mu g/cm^2$ was achieved [3].

Significant sample-to-sample variation in pure water permeance was observed across the width of the membrane roll, contributing to the high standard deviations shown in 8.1 for the unmodified membrane. Interestingly, the modifications appeared to reduce the permeance variability. The standard deviation of the unmodified membrane measurements was 22% of the average; this value decreased to 14% and 12% for the PD and PD-*g*-PEG modifications, respectively. Large pores may have been more readily modified, as their larger diameter may have allowed improved convection of dopamine, oxygen (both of which are required for the formation of polydopamine [6]), or bulky PEG chains to the pore walls. In the following constant flux fouling experiments, these average permeance values were used to guide the selection of membrane samples for

testing; if a sample's pure water permeance was not within 10% of the specified average, it was discarded, and a new sample loaded in its place.

8.2.2 Constant Flux Crossflow Fouling

Constant flux crossflow filtration was performed on unmodified, PD modified, and PD-*g*-PEG modified PS-20 membranes at 25, 40, 55, 70, 85, and 100 $Lm^{-2}h^{-1}$ (LMH). Figure 8.1 presents the transmembrane pressure evolution as a function of the permeate volume divided by the filtration area (V/A) at each flux when the membranes were challenged with a soybean oil emulsion feed. For a constant flux filtration experiment, V/A is proportional to the length (*i.e.*, time) of the fouling experiment. For fluxes of 25, 40, and 55 LMH, data are only shown to a maximum V/A value of 4 cm, because any changes in TMP occurring beyond this point were insubstantial relative to those occurring at smaller V/A values. For fluxes of 70, 85, and 100 LMH, at least one of the three membranes exhibited extreme fouling, causing the transmembrane pressure to reach a value equal to the gauge feed pressure, requiring that the experiment be terminated. In these cases, TMP results are not shown to the same final V/A value for all membranes. The initial transmembrane pressure (*i.e.*, that reported at V/A = 0 in these graphs) is the transmembrane pressure observed during pure water filtration just before fouling was initiated. That is, a V/A value of zero marks the point when the oily water emulsion began to be fed to the membranes. The time for the oily water emulsion to transit from the feed tank to the last membrane in the train of sample cells was approximately 3 seconds, which corresponds to V/A values of 0.002 cm at 25 LMH and 0.008 at 100 LMH, so the fouling experiment started, to good approximation, essentially instantaneously at V/A of zero. Because the unmodified membrane had the highest pure

water permeance (cf.,Table 8.1), it exhibited the lowest initial TMP relative to the modified membranes.

At fluxes of 25, 40, and 55 LMH (Figure 8.1a-c), the TMP of all three membranes increased most at V/A values less than 1 cm, then approached a plateau. Qualitatively similar behavior has been reported elsewhere [8,9]. Ghosh *et al*. suggested that the initial rapid TMP increase is due to a combination of concentration polarization and fouling effects, while a subsequent linear TMP increase that they observed was ascribed to fouling alone [8]. At all three fluxes, the unmodified membrane had the lowest TMP. The PD modified membrane had a TMP higher than that of the unmodified membrane, and the PD-*g*-PEG modified membrane had a TMP substantially higher than that of either the unmodified or PD modified membranes. The higher TMP in the modified membranes is indicative of increased mass transfer resistance resulting from the application of the PD and PD-*g*-PEG modifications to the membrane surface. Similar results have been reported in many other studies, where membranes exhibit a decrease in permeance following surface modification [10–15].

As shown in Figure 8.1d, at 70 LMH, the unmodified membrane exhibited qualitatively different behavior than at lower fluxes (*i.e.*, Figures 8.1a-c). The TMP increases nonlinearly very early in the experiment (*i.e.*, at V/A < 1.0 cm), then increases approximately linearly between V/A values of approximately 1.0 cm and 3.0 cm, similar to the results observed at 25, 40, and 55 LMH. However, unlike the results at lower flux, the TMP of the unmodified membrane at 70 LMH does not approach a plateau but, rather, begins to increase rapidly at V/A > 3.0 cm, indicating a substantial increase in the fouling rate. Several other authors have reported similar results, where a dramatic upturn in TMP occurs after a relatively slow, linear increase [16–21]. Ho and Zydney developed a model based on pore blockage and cake formation laws that was capable of describing

similar behavior in constant flux protein microfiltration (MF) [19]. They suggested that, during the relatively slow, linear increase, pore blockage is the dominant fouling mechanism. Once pores are blocked, a cake layer is able to form [19]. Ognier *et al*. also observed similar behavior during constant flux MF of bioreactor effluent [21]. They proposed that fouling occurs (and the TMP rises) due to sequential pore closure, which occurs in two stages. During the first stage, pores gradually become closed due to the accumulation of foulant on the membrane. To maintain the same flux globally over the entire filtration area, the flux through open pores must increase as other pores gradually become closed. This increase in the local flux accelerates fouling, causing open pores to more quickly become closed. If the local flux becomes sufficiently high, the second stage of fouling begins, during which a cake begins forming on the membrane surface. The formation of this cake dramatically increases the hydraulic resistance, and the TMP rises rapidly to maintain the constant flux condition [21].

After the upturn at V/A = 3.0, the TMP continued rising until it reached a value approximately equal to the gauge feed pressure (2.1 barg), at which point the experiment was terminated. In contrast, the PD modified membrane, although exhibiting a higher initial TMP than the unmodified membrane, experienced a relatively slow and stable rate of fouling after the brief rise in TMP at the beginning of the experiment. This result may suggest that foulant did not form a cake on the PD modified membrane [19]; perhaps the hydrophilic coating mitigated pore blockage sufficiently to prevent cake formation atop blocked pores. The PD-*g*-PEG modified membrane exhibited behavior between that of the unmodified and PD modified membranes at 70 LMH. Like the unmodified membrane, the PD-*g*-PEG modified membrane exhibited a period between V/A = 2.0 cm and V/A = 6.0 cm where the TMP rise was slightly concave up. However, the TMP did not precipitously increase to the maximum TMP possible for the experiment during the

course of these measurements. Rather, the rate of fouling appears to have decreased around V/A = 6.0 cm, and the TMP profile began to plateau near the end of the experiment.

Unlike the cases of 25, 40 and 55 LMH, at 70 LMH, the surface modified membranes, despite their higher initial TMP, ultimately yielded reduced TMP at the highest V/A values considered. The PD modified membrane exhibited much less fouling, based on TMP, than the unmodified membrane, particularly after a V/A of around 4 cm, so the PD modified membrane could be operated stably at these conditions whereas the unmodified membrane could not. The PD-*g*-PEG modified membrane had a higher TMP at all V/A values than the PD-modified membrane, but it also did not exhibit the sharp runaway in TMP exhibited by the unmodified membrane. The long PEG chains, which extend away from the membrane, have high mobility and a large exclusion volume, and they sterically hinder the approach of foulants to the surface [22]. Foulant particles also cannot easily approach the surface by compressing the PEG brushes, as doing so incurs a significant free energy penalty [23]. The increased hydrophilicity of the modified membranes relative to the unmodified membrane, which may have reduced foulant adhesion, likely helped to overcome the higher membrane resistance resulting from the application of the PD and PD-*g*-PEG modifications.

At 85 and 100 LMH (Figure 8.1e, f), the TMP in all three membranes increased to levels requiring the experiment to be terminated. That is, all three experienced an upturn in TMP leading to a rapid rise until the TMP reached the feed pressure. At 85 LMH (Figure 8.1e), the unmodified membrane, while starting at the lowest TMP, reached the maximum TMP first, at a V/A value of approximately 2 cm. In comparison, the unmodified membrane reached the maximum TMP at a V/A of about 7 cm when operated at 70 LMH. Presumably, the higher flux of 85 LMH brought foulants to the

membrane surface more quickly than at 70 LMH, resulting in the more rapid TMP increase. This finding is consistent with other reports in the literature, where TMP increases more rapidly as the imposed flux increases [8,19,20]. The TMP of the unmodified membrane eclipsed that of the PD modified membrane at a V/A value of approximately 1.1 cm and that of the PD-*g*-PEG modified membrane at around 1.3 cm. The PD modified membrane reached the maximum TMP at a V/A value of 3.2 cm. The PD-*g*-PEG modified membrane reached the maximum TMP at a V/A value of 4.2 cm, so it had a lower TMP than the PD modified membrane at V/A values greater than about 2.3 cm. The large excluded volume of the PEG chains, which help to create a substantial buffer to foulant adsorption [22], may have helped retard the rapid formation of a cake layer on the membrane surface observed with the unmodified and PD modified membranes. The PD modification is conformal [24], so the PD modified membrane, while substantially more hydrophilic than the unmodified membrane [3], still may permit the close approach of foulants to the surface, facilitating rapid cake buildup. Although none of the membranes exhibited sustainable performance at this flux, the PD and PD-*g*-PEG modifications clearly mitigated foulant accumulation despite their higher initial TMP than the unmodified membrane.

At 100 LMH (Figure 8.1f), all membranes exhibited rapid fouling. The unmodified membrane reached the maximum TMP (*i.e.*, 2.1 barg) at a V/A value of 1.5 cm, and the PD modified membrane reached this TMP at a V/A value of 2.4 cm. At this high flux, the PD modification was still able to provide some fouling mitigation. The PD-*g*-PEG membrane fouled the most quickly. At this high flux, the reduction in initial membrane permeance caused by the PD-*g*-PEG modification may have contributed to the rapid fouling observed.

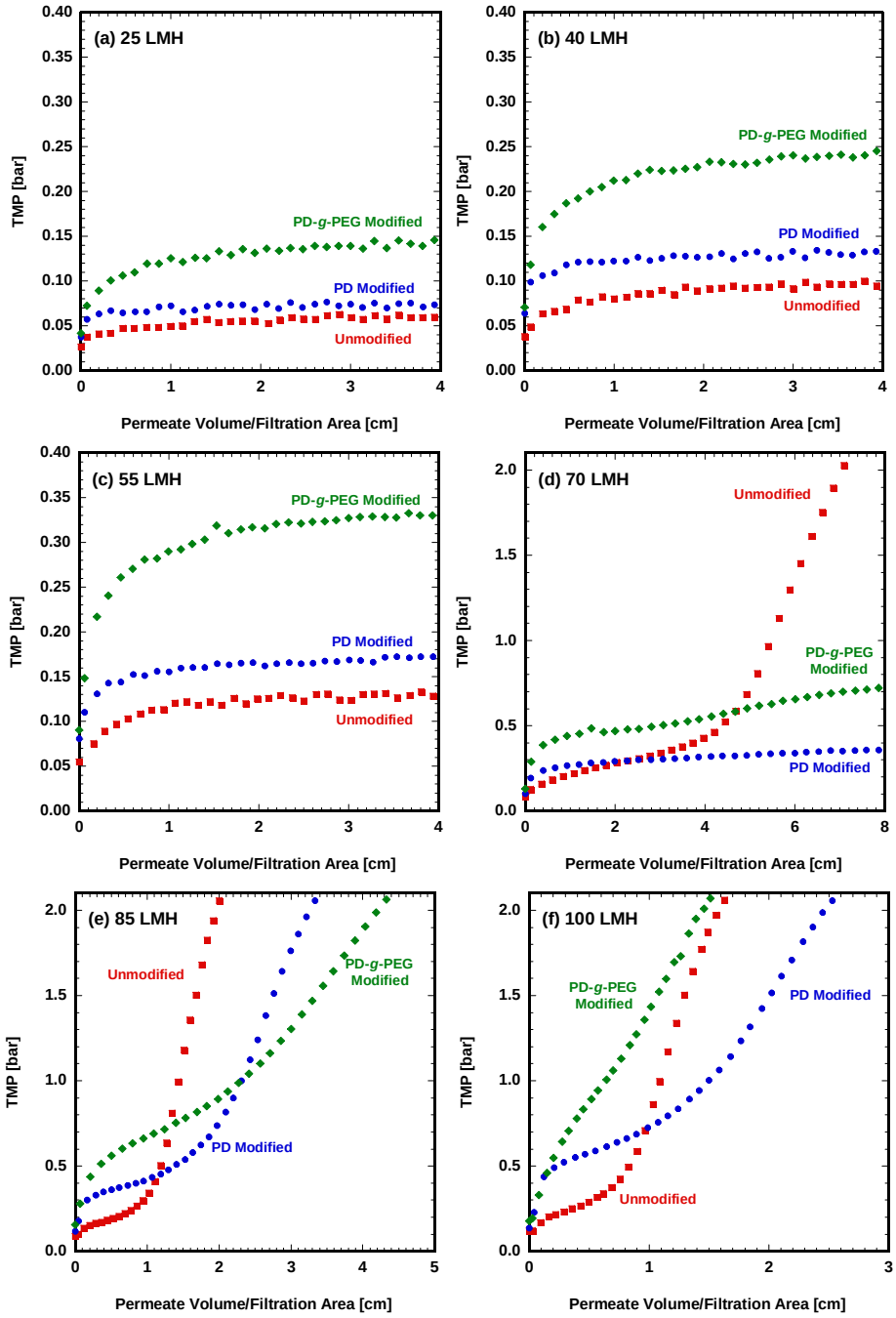

Figure 8.1. TMP evolution during constant flux fouling of unmodified, PD modified, and PD-*g*-PEG modified PS-20 UF membranes with 1500 ppm soybean oil emulsion foulant feed. (a) 25, (b) 40, (c) 55, (d) 70, (e) 85, and (f) 100 LMH. The curves shown are representative of at least three replicates at each flux. Feed pressure: 2.1 barg, crossflow velocity: 0.18 m/s.

The mass transfer resistance, R, of a porous membrane is often defined as the ratio of the transmembrane pressure to the permeate flux, J, as follows [25]:

$$R = \frac{\text{TMP}}{J} \qquad [8.7]$$

The resistance at any V/A value in a constant flux experiment can, therefore, be calculated by dividing the TMP by the flux. The resistance is also reciprocal of the membrane permeance [26]:

$$R = \frac{1}{PM} \qquad [8.8]$$

As shown in Table 8.1, the PD and PD-*g*-PEG modifications decrease membrane permeance (*i.e.*, increase resistance) relative to the unmodified membrane. To gain an improved understanding of the effect of the surface modifications on membrane fouling, the resistances during fouling (calculated using Equation [8.1]) were normalized by the membrane initial resistance (calculated using Equation [8.2]) [17,18,27]:

$$R_N = \frac{R}{R_0} \qquad [8.9]$$

where R_N is the normalized resistance, and R_0 is the initial resistance. The initial resistance was measured during pure water filtration immediately prior to fouling, and it can also be calculated using Equation [8.2] from the pure water permeance measured in dead end filtration (cf., Table 8.1).

Figure 8.2 presents the normalized resistance as a function of V/A for unmodified, PD modified, and PD-*g*-PEG modified membranes at 25, 40, 55, 70, 85, and 100 LMH. At 25 LMH (Figure 8.2a), the unmodified and PD modified membranes have similar normalized resistances. At this low flux, fouling was relatively minor. The unmodified membrane fouled little, reaching a normalized resistance of about 2.25 at V/A = 4.0 cm.

The increased hydrophilicity of the modified membrane likely compensated for the increase in local flux incurred by the pore constriction due to surface modification, and it exhibited a similar normalized resistance. The PD-*g*-PEG modified membrane, however, exhibited a much higher normalized resistance than either the unmodified or PD modified membranes, suggesting that the additional mass transfer resistance imparted by the modification could not be overcome by the increased hydrophilicity. At 40 and 55 LMH (Figure 8.2b, c), the unmodified membrane fouled more significantly than at 25 LMH, reaching a normalized resistance of about 2.75 at V/A = 4 cm in each case. The PD modified membrane, however, maintained approximately the same normalized resistance of 2.25 at V/A = 4 cm when operated at 40 and 55 LMH than it did when operated at 25 LMH. Thus, the PD modification, while increasing the overall resistance, mitigated fouling, because the unmodified membrane exhibited a greater increase in resistance during fouling than the PD modified membrane.

Resistance normalization did not greatly alter the observations at 70 LMH for the unmodified and PD modified membranes (Figure 8.2d). The unmodified membrane reached a normalized resistance of about 24, corresponding to the maximum allowable TMP of 2.1 barg. At 85 and 100 LMH (Figure 8.2e, f), all three membranes reached the maximum TMP of 2.1 barg. The unmodified membrane, for example, exhibited a maximum normalized resistance of approximately 23 at 85 LMH. From Equation [8.1], the resistance at a given TMP decreases with increasing flux. Therefore, because the maximum TMP at any flux was 2.1 bar in our experiments, the maximum resistance (and, consequently, normalized resistance) exhibited by each of the three membranes decreased as the imposed flux increased from 70 LMH to 85 and 100 LMH.

Furthermore, at 85 and 100 LMH, the unmodified membrane always had the greatest maximum normalized resistance, and the PD-*g*-PEG modified membrane always

had the lowest normalized resistance at the end of the experiments. For example, at 85 LMH (Figure 8.2e), the unmodified membrane had a maximum normalized resistance of 23, while the PD modified membrane had a maximum of 18, and the PD-*g*-PEG modified membrane had a maximum of 13. This effect is due to the increased initial resistance of the PD and PD-g-PEG modified membranes relative to the unmodified membrane. The maximum resistance of all three membranes operated at the same flux would be identical (cf., Equation [8.1]); however, because the initial resistances of the PD and PD-*g*-PEG modified membranes were higher than the unmodified membrane, the modified membranes exhibited lower maximum normalized resistances (cf., Equation [8.3]) than the unmodified membrane.

At 85 LMH (Figure 8.2e), both the PD and PD-*g*-PEG modified membranes showed lower normalized resistances than the unmodified membrane at V/A values greater than about 1.1 cm. The PD and PD-*g*-PEG modified membranes showed similar normalized resistances up to V/A = 1.8. Afterwards, the PD-*g*-PEG modified membrane had a lower normalized resistance than the PD modified membrane. At 100 LMH (Figure 8.2f), the unmodified membrane showed the lowest normalized resistance at V/A values less than 0.9 cm. At larger V/A values, the PD modified membrane had the lowest normalized resistance, due to the accelerated increase in resistance in the unmodified membrane at a V/A value of 0.9 and the high value of the PD-*g*-PEG membrane. As shown in Figure 8.1f, the PD-*g*-PEG modified membrane exhibited the highest TMP at all V/A values. In contrast, the PD-*g*-PEG modified membrane had a lower normalized resistance than the unmodified membrane at V/A values greater than about 1.2 cm.

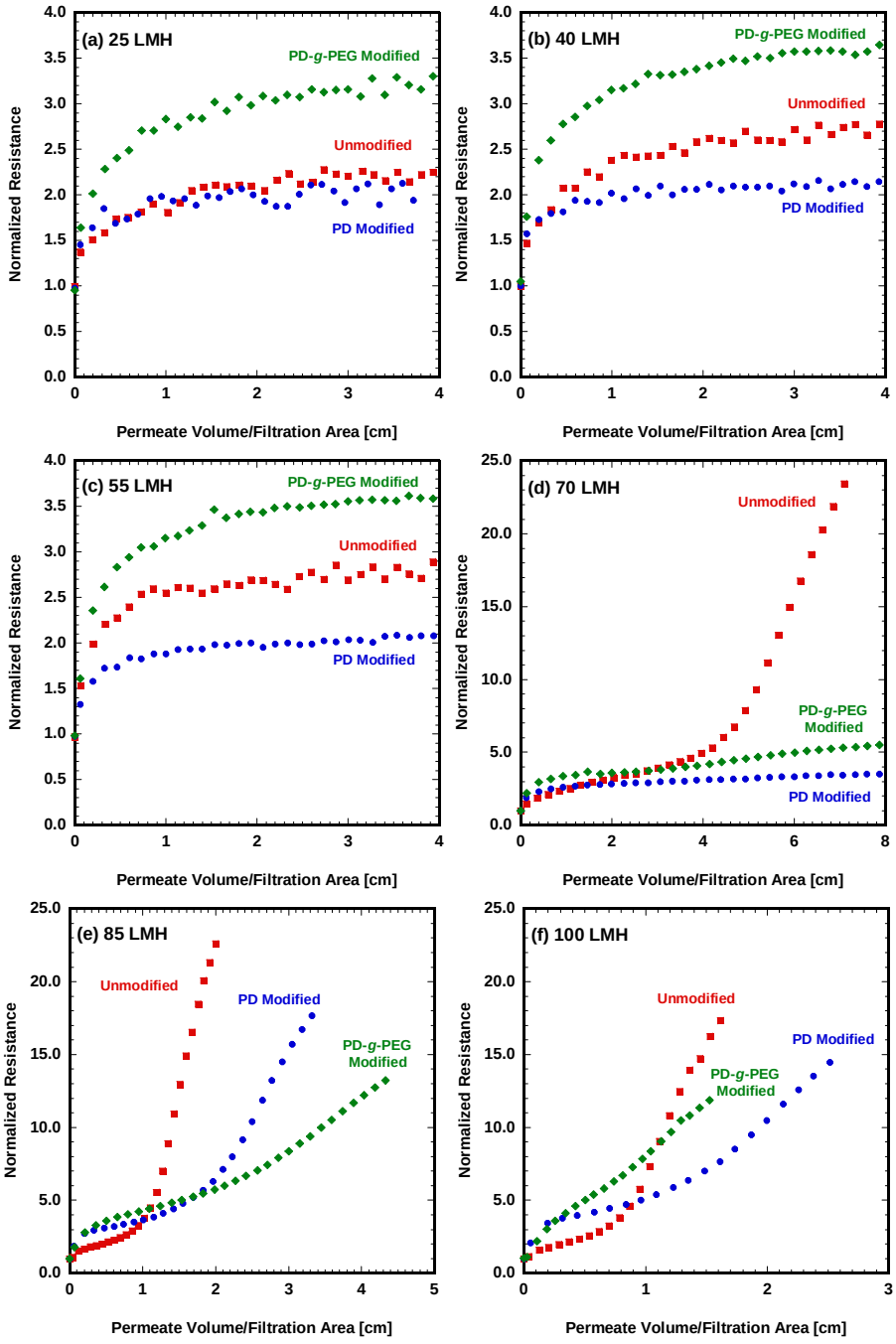

Figure 8.2. Normalized resistance evolution during constant flux fouling of unmodified, PD modified, and PD-*g*-PEG modified PS-20 UF membranes with 1500 ppm soybean oil emulsion feed. Normalized resistances calculated using Equations [8.7] and [8.9] from data shown in Figure 8.1. (a) 25, (b) 40, (c) 55, (d) 70, (e) 85, and (f) 100 LMH.

8.2.3 Threshold Flux Determination

All three membranes showed qualitatively similar behavior during constant flux fouling at 25, 40, and 55 LMH (Figure 8.1a-c). However, as the flux was increased to 70 LMH (Figure 8.1d) or 85 LMH (Figure 8.1e), each membrane exhibited a more dramatic, and qualitatively different, increase in TMP than at lower fluxes. Such a change in the fouling behavior indicated a substantial difference in the rate of fouling at high and low fluxes. Recently, Field *et al.* have described the threshold flux as the flux below which a low, constant rate of fouling occurs. Above the threshold flux, the rate of fouling substantially increases [28].

The threshold flux for each membrane was evaluated by flux stepping. This well-known technique is commonly used to determine critical and threshold fluxes [29–33]. In a flux stepping experiment, the membrane was operated at a constant flux for 20 minutes. After 20 minutes, the flux was increased and maintained at a higher value for another 20 minutes. In this study, the initial flux was 10 LMH, and the flux was increased by 10 LMH upon each step. A discussion of the effects of changing the initial flux, the step length, and the stepping protocol may be found in the Appendix and elsewhere [34]. During each flux step, the increase in TMP was recorded.

Figure 8.3 shows an example of data obtained during flux stepping experiments and three parameters that may be used to gauge the threshold flux. These parameters were described Beier and Jonsson [30] and by Le Clech *et al*. [32]. The flux increase, accomplished by changing the permeate flux set point and allowing LabVIEW to automatically adjust the permeate pump speed to achieve that flux, typically required less than 30 seconds. In response to this flux increase, (from J_n to J_{n+1}), the transmembrane pressure rose quickly. After a few minutes (depending upon how quickly the flux is able

to reach its new setpoint), the TMP entered a period of slow, linear rise as the flux was maintained over the remainder of the 10-minute interval.

Linear regressions were made through the linear portion of the TMP data at each flux. The slope of this regression, d(TMP)/dt, was used as one parameter to determine the threshold flux. In this study, d(TMP)/dt was always greater than zero, even at the lowest flux (*i.e.*, 10 LMH). Therefore, a critical flux could not be determined for any of the membranes, as the critical flux is strictly defined as the flux below which no rise in membrane resistance is observed with time [28,35]. Instead, the flux stepping experiments revealed threshold fluxes.

Another of parameters used to determine the threshold flux was the average transmembrane pressure over the flux step (TMP_{avg}). TMP_{avg} was calculated as the arithmetic mean over all transmembrane pressures recorded during the slow, linear TMP rise after the initial, abrupt increase. The use of TMP_{avg} was proposed by Choi and Dempsey to determine the critical flux when a membrane was challenged with complex, highly-fouling natural waters [29]. Their aim was to develop a critical flux definition that was operationally relevant, since d(TMP)/dt = 0 is rarely observed in practice. In light of the relatively new definition of threshold flux, Choi and Dempsey were likely calculating what is now known as the threshold flux, rather than the critical flux. The third parameter used for threshold flux definition is ΔTMP, which is the TMP difference between the linear regressions of TMP data recorded over two adjacent flux steps at the time of flux increase. Others, such as Le Clech *et al.*, have chosen an arbitrary time after increasing the flux to measure the TMP, from which ΔTMP may be calculated using the last TMP recorded at the previous flux [32]. In this work, the time required for the TMP to reach the linear regime at a new flux varied with flux (*i.e.*, the time became longer as fouling became more severe at higher fluxes), so the present technique was adopted to

standardize measurements at all fluxes. Each of the three threshold flux determination parameters, d(TMP)/dt, TMP_{avg}, and ΔTMP, were plotted as a function of flux.

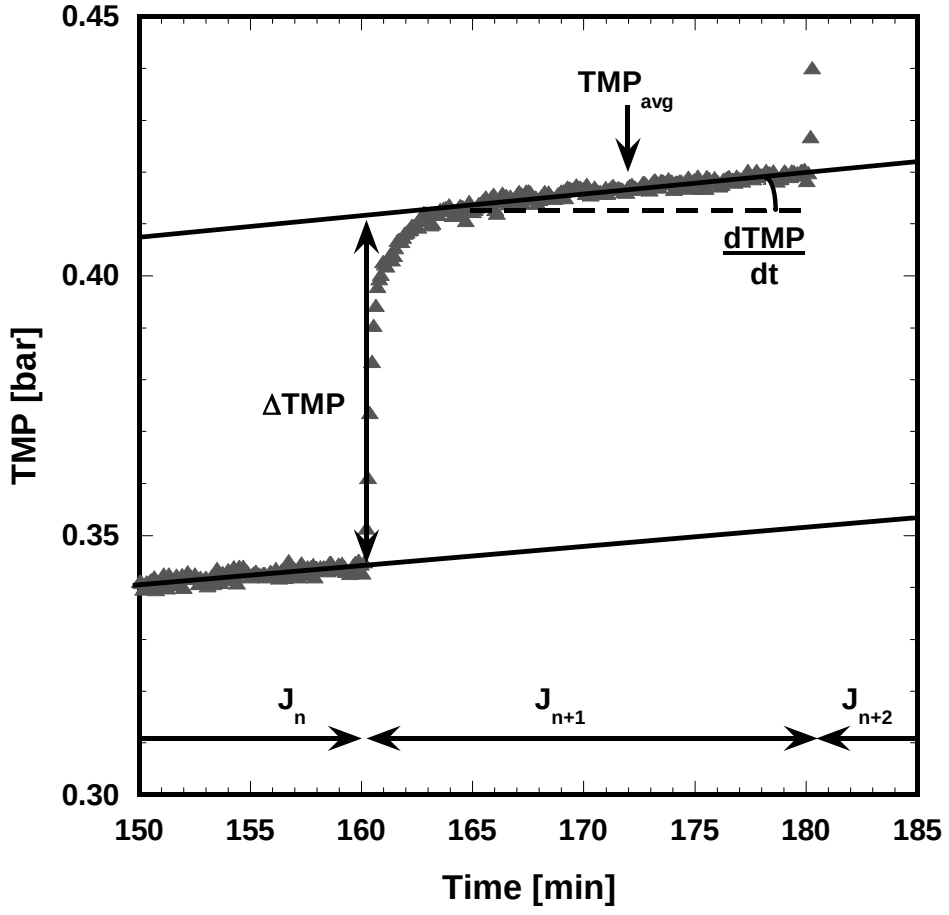

Figure 8.3. An example of determination of the three parameters used to estimate the threshold flux from data obtained by flux stepping experiments. When the flux was increased, the TMP typically increased abruptly, then transitioned to a region where it increased linearly with time. Linear regressions were made through each region of linear TMP increase. ΔTMP at the moment when the flux was increased from one value, J_n, to the next, J_{n+1}, was estimated by extrapolating the linear regions before and after the increase in flux. d(TMP)/dt was the slope of the linear regression. TMP_{avg} was the average of all recorded transmembrane pressures over the linear region. PD modified PS-20 membrane (full data shown in Figure 8.5a).

Figure 8.4 presents the threshold flux determination for the unmodified membrane. Results of the flux stepping experiment are shown in Figure 8.4a. TMP_{avg} values at each flux, calculated from the data in Figure 8.4a, are presented as a function of flux in Figure 8.4b. All TMP_{avg} values for fluxes less than 60 LMH lie on a single linear regression, indicating that the resistance was constant at these fluxes. Above 60 LMH, the slope of the TMP_{avg} vs. flux relationship increases, indicating that the resistance is increasing. The flux at which the slope changes, 65 LMH (indicated by the vertical dotted arrow) is identified as the threshold flux based on this method.

Figure 8.4c presents ΔTMP as a function of flux. The ΔTMP values shown are those observed when the flux was increased to the corresponding value on the horizontal axis (*e.g.*, ΔTMP = 0.020 bar was observed when the flux was increased from 10 LMH to 20 LMH). No ΔTMP value is shown at 10 LMH because 10 LMH was the lowest flux at which the membrane was challenged with the soybean oil emulsion foulant. The threshold flux is the flux above which the relationship between ΔTMP and flux is nonlinear (concave up) [32]. At 40, 50, and 60 LMH, ΔTMP varied linearly with flux. Above 60 LMH, ΔTMP escalated nonlinearly with increasing flux. A horizontal dotted line was drawn to denote the ΔTMP corresponding to the beginning of this nonlinear increase. The threshold flux based on this method, 65 LMH, is identified by the vertical dashed arrow.

Figure 8.4d presents the rate of fouling, d(TMP)/dt, as a function of flux. At flux values below the threshold flux, d(TMP)/dt is low and constant. In this case, d(TMP)/dt is close to, but slightly greater than, zero up to a flux of 60 LMH. Some rise in d(TMP)/dt is seen from 50 LMH to 60 LMH, but the value at 60 LMH is very near the value recorded at 20 LMH (denoted with a horizontal dashed line). Therefore, further increases in d(TMP)/dt beyond the value observed at 60 LMH suggest that the flux has

exceeded the threshold flux. Therefore, the threshold flux (denoted by a vertical dashed arrow) was 65 LMH according to this method.

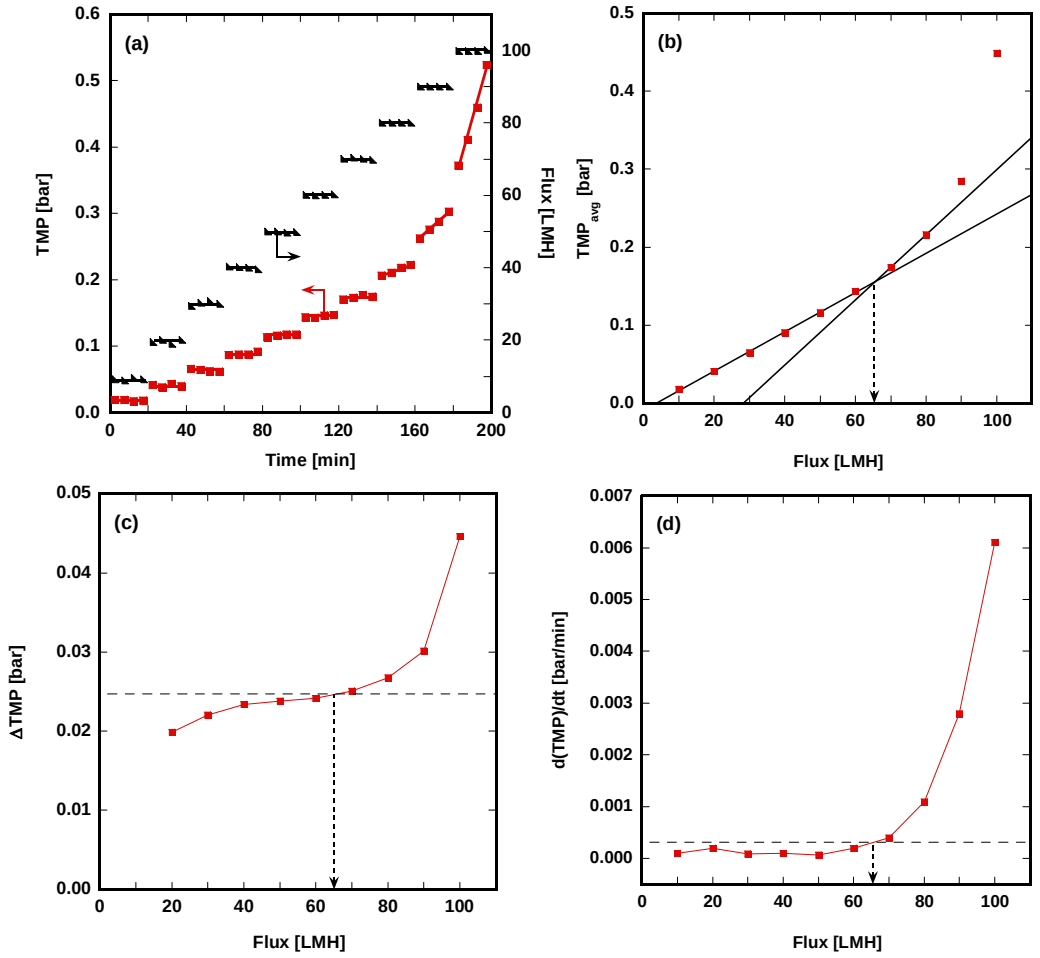

Figure 8.4. Threshold flux determination for an unmodified PS-20 UF membrane challenged with 1500 ppm soybean oil emulsion feed. (a) Flux stepping experiment. Feed pressure: 2.1 barg, crossflow velocity: 0.18 m/s. (b) TMP_{avg} threshold flux method. (c) ΔTMP threshold flux method (d) d(TMP)/dt threshold flux method. Values plotted as a function of flux in (b) – (d) are obtained from the experimental data in (a). For (b) – (d), threshold flux values are denoted by the dashed arrows pointing to the flux axis.

Figure 8.5 presents results of the three different methods to estimate the threshold flux for the PD modified membrane. Results of the flux stepping experiment are shown in Figure 8.5a. TMP_{avg} as a function of flux is presented in Figure 8.5b. Instead of the relatively abrupt change in slope observed for the unmodified membrane (cf., Figure 8.4b), TMP_{avg} values for the PD modified membrane slowly curve upward when plotted as a function of flux. The slope of the TMP_{avg} vs. flux relationship only remains constant at fluxes of 10, 20, and 30 LMH, resulting in an apparent threshold flux value of 33 LMH. Figure 8.5c presents ΔTMP as a function of flux for the PD modified membrane. The ΔTMP values at fluxes of 70 LMH and less vary linearly with flux. A horizontal dashed line separates the region of linear ΔTMP increase from the region where ΔTMP rises rapidly with increasing flux. Using the ΔTMP parameter, a threshold flux value of 72 LMH was estimated. Figure 8.5d shows d(TMP)/dt as a function of flux for the PD modified membrane. No threshold flux could be discerned using this parameter, since only minor changes in d(TMP)/dt were observed with increasing flux up to the maximum flux considered in this study, 100 LMH.

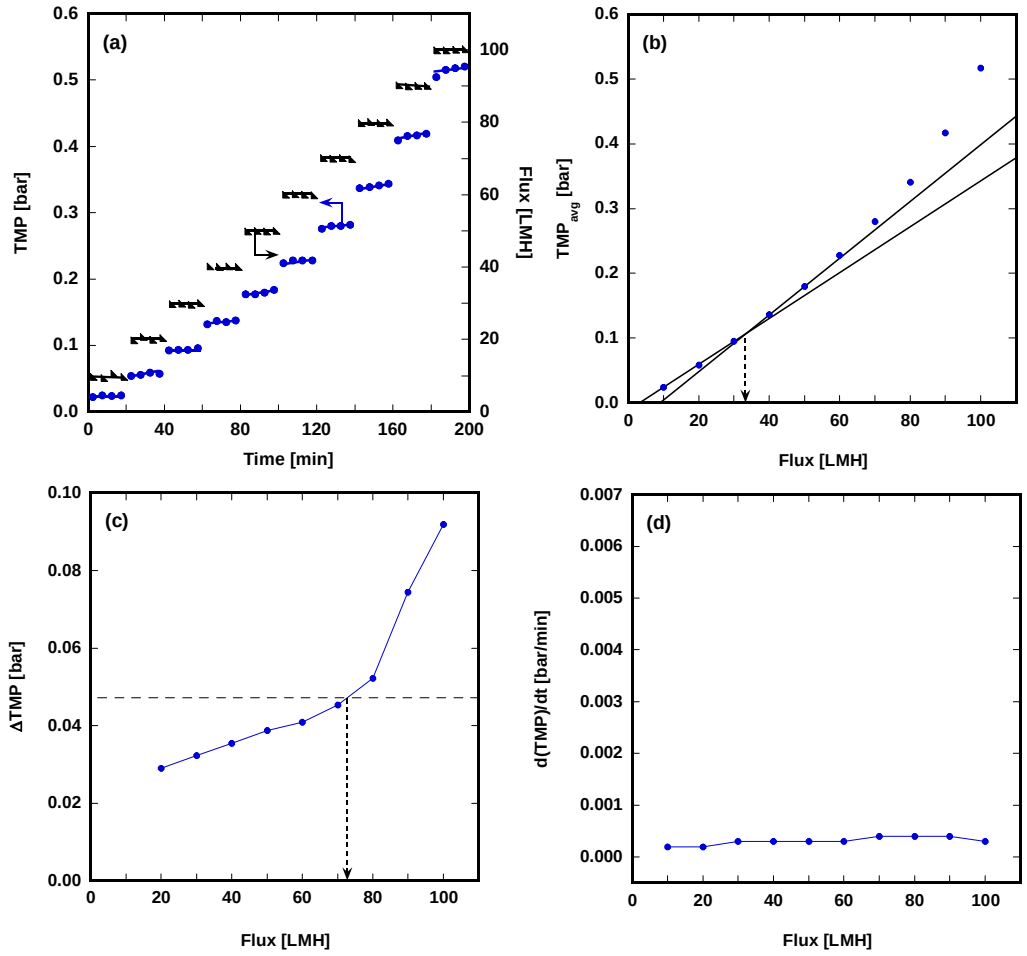

Figure 8.5. Threshold flux determination for a PD modified PS-20 UF membrane challenged with 1500 ppm soybean oil emulsion feed. (a) Flux stepping experiment. Feed pressure: 2.1 barg, crossflow velocity: 0.18 m/s. (b) TMP_{avg} method. (c) ΔTMP method. (d) d(TMP)/dt method. Values plotted as a function of flux in (b) – (d) are obtained from the experiment shown in (a). For (b) and (c), threshold flux values are denoted by the dashed arrow pointing to the flux axis. A threshold flux value could not be determined from (d).

Threshold flux estimation for the PD-*g*-PEG modified membrane is presented in Figure 8.6. Results of the flux stepping experiment are shown in Figure 8.6a. With this membrane, changes in TMP with increasing flux during flux stepping generally occurred more slowly at relatively high fluxes than with the unmodified and PD modified membranes. For example, when the flux was increased from 60 to 70 LMH, the TMP required several minutes to reach the regime of linear increase (as depicted in Figure 8.3). Such behavior may be indicative of some fouling mitigation at high fluxes, with the long PEG chains slowing buildup of foulant relatively far away from the membrane surface.

In Figure 8.6b, TMP_{avg} is plotted as a function of flux. A clear change in slope was evident, suggesting a threshold flux around 58 LMH. Figure 8.6c shows ΔTMP as a function of flux. ΔTMP values at fluxes of 20, 30, 40, and 50 LMH were linear with respect to flux, with an abrupt increase in ΔTMP at fluxes greater than 50 LMH (delineated with a horizontal dashed line), yielding a threshold flux value of 52 LMH. Figure 8.6d presents d(TMP)/dt values as a function of flux. An increase is observed at fluxes higher than 60 LMH (again delineated with a horizontal dashed line), suggesting a threshold flux of 62 LMH.

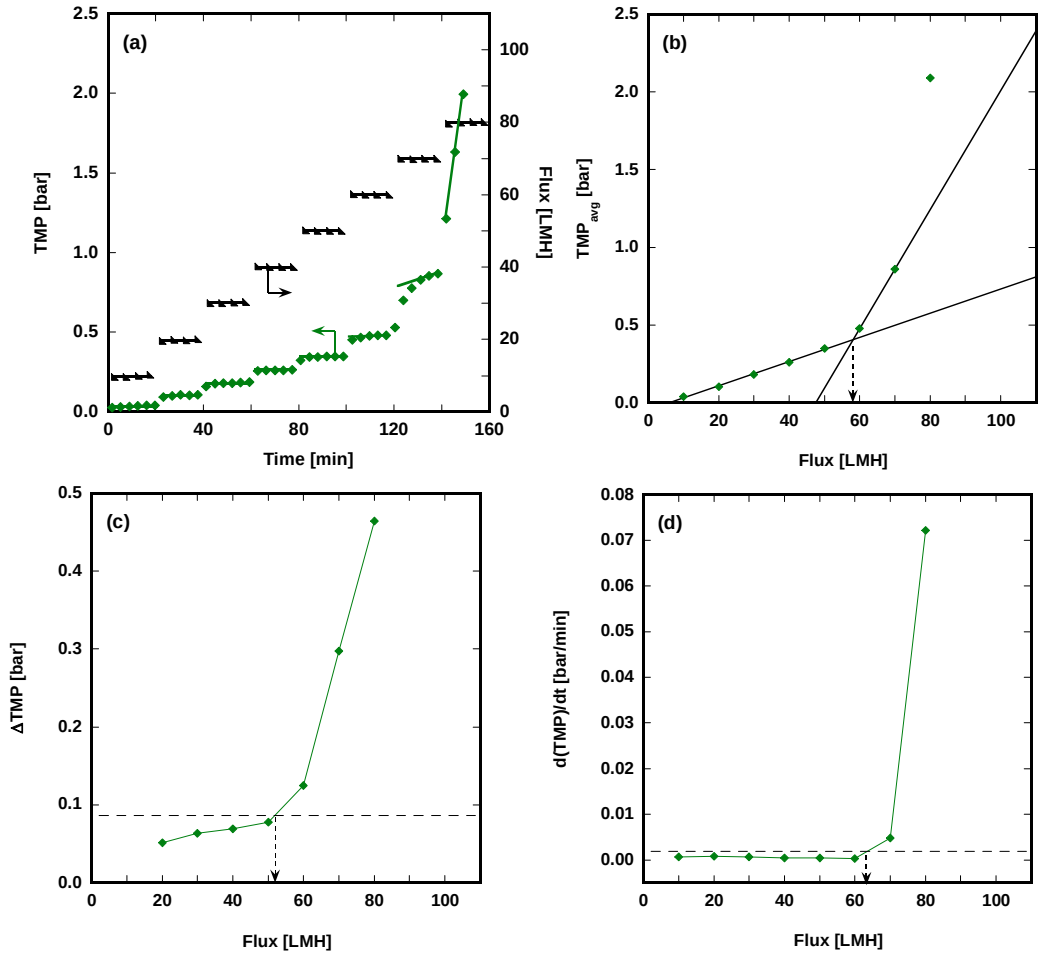

Figure 8.6. Threshold flux determination for a PD-*g*-PEG modified PS-20 UF membrane challenged with 1500 ppm soybean oil emulsion feed. (a) Flux stepping experiment. Feed pressure: 2.1 barg, crossflow velocity: 0.18 m/s. (b) TMP_{avg} method. (c) ΔTMP method. (d) d(TMP)/dt method. Values plotted as a function of flux in (b) – (d) are obtained from the experiment shown in (a). For (b) – (d), threshold flux values are denoted by the dashed arrow pointing to the flux axis.

In Figure 8.4b, Figure 8.5b, and Figure 8.6b, the linear regressions of TMP_{avg} at fluxes below the threshold flux do not pass through the origin. This result may be explained by considering a comparison with the pure water TMP_{avg}/flux relationship, which would pass through the origin and exhibit lower TMP_{avg} values than those exhibited during fouling. Even at the lowest fluxes tested here, fouling rates were non-zero. Therefore, some foulant continuously accumulated on the membrane during each flux step. The non-zero rate of fouling would have caused the TMP_{avg}/flux relationship during fouling to increasingly deviate from the pure water relationship as flux increased. The slope of the TMP_{avg}/flux relationship during fouling would, therefore, have been greater than that in pure water, causing the fouling regression to intersect the flux axis at a value greater than zero. Similar observations have been reported elsewhere [36,37].

A summary of threshold flux values for the three membranes as determined by the three parameters is shown in Table 8.2. As pointed out by Beier and Jonsson, threshold flux determinations should be validated with constant flux fouling studies [30]. For the unmodified membrane, all three threshold flux parameters yielded a value of 65 LMH. This value is in qualitative agreement with the constant flux fouling experiments shown in Figure 8.1 and Figure 8.2. At all fluxes tested below 65 LMH, the transmembrane pressure (and normalized resistance) remained at a relatively low value, so the membrane fouled slowly. At fluxes greater than 65 LMH, the TMP and, consequently, resistance, rose to their maximum values, so the apparent threshold flux of 65 LMH deduced from the three methods described previously is coherent with the fouling data.

The three threshold flux determination parameters yielded different values in the case of the PD modified membrane. For example, the TMP_{avg} parameter gave a threshold flux value of 33 LMH. This value is unreasonably low when compared to the results of the constant flux fouling studies, because fouling studies conducted at 40, 55, and 70

LMH resulted in low TMP and resistance values, indicative of fouling below the threshold flux. A threshold flux of 72 LMH was estimated by plotting ΔTMP as a function of flux. This value is coherent with the results from the fouling studies, since fouling at fluxes higher than 72 LMH (*i.e.*, 85 and 100 LMH) resulted in a rapid rise of the TMP. A threshold flux value could not be determined from d(TMP)/dt, suggesting that the threshold flux was higher than the highest tested flux (*i.e.*, 100 LMH). Since severe fouling was observed at 85 and 100 LMH, the actual threshold flux must be lower than 85 LMH, meaning that d(TMP)/dt was not sensitive to the threshold flux of the PD modified membrane. This scenario, in which different threshold flux determination parameters yield different threshold flux values, reinforces the conclusions drawn by Beier and Jonsson, who stated that critical flux value (or, in this case, threshold flux value) determined by flux stepping experiments must be validated against the results of constant flux experiments [30].

Each of the three threshold flux determination parameters measure different aspects of fouling. The TMP_{avg} parameter, for example, inherently depends upon the step length employed; if the rate of fouling is greater than zero, calculated TMP_{avg} values would increase with increasing step length. Indeed, other authors have reported variations in the determined threshold flux with changing step length [29,30,32]. The d(TMP)/dt parameter, in contrast, is not time-dependent, as long as the rate of fouling does not change over the course of the flux step. The ΔTMP parameter measures the instantaneous TMP response due to a sharp increase in flux. Therefore, this parameter may not be strongly tied to long-term fouling behavior, but instead to the short-term interaction between the membrane and a large influx of foulant. In the case of an unmodified, hydrophobic membrane, the strong hydrophobic foulant readily adsorbs to and accumulates on the membrane. The addition of a hydrophilic coating likely

destabilizes interactions between the membrane and the foulant due to the strongly adsorbed water layer on the surface [38]. The fouling phenomena associated with each of the three parameters may be affected differently, resulting in variations in the determined threshold flux value. Measurement accuracy is likely not the source of variability in threshold flux values, as the accuracy of the differential pressure transducers (used to measure transmembrane pressure) is 0.08% of the reading, and the accuracy of the flow meters (used to measure flux) is 0.2% of the reading.

In the PD-*g*-PEG modified membrane, the three parameters yielded three threshold flux values much closer to each other than those determined for the PD modified membrane. Only the threshold flux value determined by ΔTMP (52 LMH) was not coherent with the fouling data, because constant flux fouling at 55 LMH with the PD-*g*-PEG modified membrane resulted in relatively low TMP and normalized resistance values (Figure 8.1c and Figure 8.2c). As described above, the ΔTMP parameter likely measures the instantaneous response of the membrane to a sharp increase in foulant ingress. The high local flux of the PD-*g*-PEG modified membrane, due to its small effective pore diameter (cf., Table 8.1), may have made this membrane particularly sensitive to this parameter, producing a lower threshold flux value than the other two parameters. At 70 LMH, the TMP and resistance did not reach their maximum values, but an increase in the rate of fouling was observed as a slight, concave up shape in the TMP and resistance profiles between V/A values of 2 and 6 cm (Figures 8.1d and 8.2d). The flux stepping experiment and parameters subsequently used to determine the threshold flux appear sensitive to this behavior, since all three threshold flux determination parameters yielded threshold flux values less than 70 LMH. Because the TMP (and resistance) profiles began to flatten again at V/A values greater than 6 cm, operation of the PD-*g*-PEG modified membrane at 70 LMH may represent an unusual

scenario where sustained operation may be possible at a flux greater than the threshold flux. The PEG chains may facilitate this behavior, since such operation cannot be obtained with either the unmodified or PD modified membranes. The long PEG chains extending from the membrane surface may disrupt the accumulation of a thick, dense layer of foulant on the surface, frustrate adsorption or facilitate removal of the foulant. Therefore, even though an increase in fouling rate was observed between V/A values of 2 and 6 cm (Figures 8.1d and 8.2d), the PD-*g*-PEG modification may have acted to assuage rapid fouling, preventing the increase in TMP (or resistance) to extremely high values at fluxes near the threshold flux. The TMP_{avg} and d(TMP)/dt parameters produced similar threshold flux values which could not be distinguished by the constant flux fouling studies of the PD-*g*-PEG modified membrane. Therefore, the threshold flux of the PD-*g*-PEG modified membrane was taken to be the average of these values, 60 LMH.

Determination Method	Unmodified	PD Modified	PD-*g*-PEG Modified
TMP_{avg}	65	33	58
ΔTMP	65	72	52
d(TMP)/dt	65	>100	62
Estimated Threshold Flux	65	72	60

Table 8.2. Threshold fluxes (LMH) of unmodified, PD modified, and PD-*g*-PEG modified PS-20 UF membranes determined by three different methods, as shown in Figures 8.4 – 8.6.

Several parameters have been used to determine the threshold flux for unmodified and surface modified membranes. In the case of the unmodified membranes, each parameter produced the same threshold flux value. The three parameters produce less-

reproducible threshold flux values for membranes modified with hydrophilic PD and PD-*g*-PEG coatings. As the interactions between the membrane surface and the foulants become less favorable as the surface becomes more hydrophilic (relative to the hydrophobic unmodified membrane), the phenomena measured by each of the three parameters may become less severe, and therefore more difficult to observe. As pointed out by Beier and Jonsson [30], flux stepping techniques should only be used to estimate the critical or threshold flux, and estimated values may be used to plan longer-term constant flux fouling studies to verify regimes of sustainable operation.

8.2.4 Organic Rejection

The organic rejection values of unmodified, PD-modified, and PD-*g*-PEG modified PS-20 membranes at each flux are shown in Table 8.3. For the unmodified membrane, the rejection decreased slightly as flux increased from 25 LMH to 40 LMH. Such a decrease in rejection may be the result of concentration polarization [39,40]. The increase in flux increases accumulation of foulant on the membrane and, consequently, higher oil concentration at the membrane surface. This heightened oil concentration on the feed side of the membrane results in greater oil passage through the membrane pores, thus lowering rejection. Within experimental uncertainty, the rejection was stable as flux was increased from 40 LMH to 70 LMH. However, the rejection increases as flux increases to 85 LMH. A similar result was reported by Chan *et al.*, where an increase in rejection was observed at fluxes above the critical flux of a UF membrane challenged with a protein mixture [39]. This result was attributed to the accumulation of foulant on the membrane sufficient to hinder protein passage through the membrane pores, counteracting the effect of concentration polarization. While 70 LMH is slightly above the estimated threshold flux of 65 LMH, the effect of aggressive fouling may be more

readily observable at the higher fluxes of 85 and 100 LMH. Additionally, permeate samples for rejection analysis were typically taken in the middle of each experiment, before the large rise in TMP at 70 LMH was observed (cf., Figure 8.1d). Permeate samples taken at the end of the 70 LMH test may have revealed higher rejection, as a more substantial foulant layer might have developed. Experiments at 85 and 100 LMH were fairly short due to the rapid TMP increase, so rejection sampling likely captured separation behavior once a significant foulant layer had accumulated.

The PD modified membrane showed rejection behavior that was qualitatively similar to that of the unmodified membrane. At fluxes of 25, 40, and 55 LMH, the PD modified membrane exhibited similar rejections. Values were also close to those obtained for the unmodified membrane. A discernable minimum in rejection was observed at 70 LMH. This flux was just below the threshold flux of 72 LMH. Therefore, at 70 LMH, concentration polarization was most severe, but the effects of significant foulant accumulation above the threshold flux, as suggested by Chan *et al*. [39], were not observed. At 85 and 100 LMH, both values above the threshold flux, an increase in rejection was observed, similar to the case of the unmodified membrane. At all fluxes except for 70 LMH (which is above the threshold flux in the case of the unmodified membrane but below the threshold flux in the case of the PD modified membrane), the unmodified and PD modified membranes exhibited similar rejections.

The PD-*g*-PEG modified membrane showed similar rejections at all fluxes. At fluxes lower than the threshold flux of 60 LMH, the PD-*g*-PEG modified membrane exhibited higher rejection than the PD modified membrane. The additional transport resistance introduced by grafting PEG chains to the membrane surface (and, possibly, within its pores) likely hindered the passage of oil through the membrane. Unlike the unmodified and PD modified membranes, the PD-*g*-PEG modified membrane did not

exhibit an increase in rejection above the threshold flux. Although significant foulant accumulation occurs above the threshold flux, the long PEG chains grafted to the membrane may have disrupted tight packing within the foulant layer. Foulant may have been able to desorb from the foulant layer, passing through the membrane and lowering the observed rejection.

Flux (LMH)	Unmodified	PD Modified	PD-*g*-PEG Modified
25	98.9 ± 0.4	98.4 ± 0.1	98.5 ± 0.1
40	98.3 ± 0.1	98.1 ± 0.5	98.9 ± 0.1
55	98.4 ± 0.2	98.3 ± 0.3	98.9 ± 0.2
70	98.5 ± 0.1	96.5 ± 0.7	98.7 ± 0.1
85	99.0 ± 0.3	99.1 ± 0.3	98.4 ± 0.1
100	99.0 ± 0.1	99.0 ± 0.2	98.7 ± 0.1

Table 8.3. Percent organic rejection for unmodified, PD modified, and PD-*g*-PEG modified PS-20 UF membranes. The total organic concentrations of the feed and permeate were used to calculate rejection. The values shown are averages of at least three trials, and errors are the standard deviations calculated from the averages.

8.2.5 Constant Flux Crossflow Fouling with Membranes of Similar Permeances

Sections 8.2.1 and 8.2.2 clearly demonstrated that membrane surface modification decreased the membrane permeance, resulting in higher TMP's during pure water filtration as well as during fouling at fluxes below the threshold flux of the unmodified membrane (25, 40, and 55 LMH, Figure 8.1a-c). It is of interest, therefore, to assess the fouling performance of unmodified and modified membranes with similar initial (pure water) permeances. PS-10 is a polysulfone UF membrane similar to PS-20, but PS-10 has a lower molecular weight cutoff and, consequently, a lower permeance than PS-20.

The pure water permeance of PS-10, as measured by dead end filtration, was 570 LMH/bar, similar to the permeance of a PS-20 membrane after PD-*g*-PEG modification (cf.,Table 8.1). Furthermore, McCloskey *et al.* have previously demonstrated that increasing the time that a polysulfone UF membrane is in contact with dopamine solution results in a decreased permeance, likely due to thicker polydopamine accumulation on the membrane surface and within its pores [3]. Increasing the polydopamine deposition time from 60 minutes to 75 minutes decreased the permeance of the PD modified PS-20 membrane from 670 LMH/bar (cf.,Table 8.1) to 570 LMH/bar. PD modified membranes subjected to polydopamine deposition for 75 minutes are labeled "PD75 modified."

Constant flux fouling at 25, 40, and 55 LMH was performed on unmodified PS-10, PD75 modified PS-20, and PD-*g*-PEG modified PS-20 membranes. Results are shown in Figure 8.7. Because the PS-10, PD75 modified PS-20, and PD-*g*-PEG modified PS-20 all had similar initial permeances, they all had the same initial TMP at each flux. At all three fluxes, the TMP's of the PD75 and PD-*g*-PEG modified PS-20 were lower than that of the unmodified PS-10 membrane. This result demonstrates the fouling mitigation afforded by the hydrophilic coating. By applying these surface treatments to a membrane with relatively large pores, a hydrophilic membrane may be prepared with a similar permeance to that of a hydrophobic membrane with small pores. This methodology prevents the resistance increase penalty of modifying a membrane and comparing its performance with the unmodified version, as exhibited in Figure 8.1. Surface modified membranes are likely best formulated by starting with a membrane with a nominal pore size larger than that required for a given application and applying the modification to achieve the desired membrane permeance (and rejection). Notably, the two surface modified PS-20 membranes, both of which had a permeance of 570

LMH/bar, showed similar or nearly identical TMP increases during fouling at all three fluxes.

The organic rejections of unmodified PS-10, PD75 modified PS-20, and PD-*g*-PEG modified PS-20 are shown in Table 8.4. The rejection of the unmodified PS-10 membrane was similar at 25 and 40 LMH, but increased at 55 LMH. At 25 and 40 LMH, fouling resulted in a very high organic concentration at the membrane surface, likely causing increased permeation of oil. The higher rejection at 55 LMH may have been the result of significant foulant accumulation on the membrane surface, which restricted the passage of organics through the membrane pores, countering the concentration polarization effect observed at lower fluxes [39]. The PD75 and PD-*g*-PEG modified PS-20 membranes generally showed very similar rejections at all three fluxes. The rejection of the unmodified membranes was higher than that of the unmodified membrane at 25 and 40 LMH, likely due to reduced concentration polarization at these fluxes as the surface modifications helped to mitigate fouling.

Flux (LMH)	Unmodified PS-10	PD75 Modified PS-20	PD-*g*-PEG Modified PS-20
25	97.0 ± 0.2	98.8 ± 0.2	98.5 ± 0.1
40	96.9 ± 0.4	98.8 ± 0.1	98.9 ± 0.1
55	99.0 ± 0.1	99.0 ± 0.1	98.9 ± 0.2

Table 8.4. Percent organic rejection observed for unmodified PS-10, PD75 modified PS-20, and PD-*g*-PEG modified PS-20 membranes. The total organic concentrations of the feed and permeate were used to calculate rejection. Values shown are averages of at least three trials, and errors are the standard deviations calculated from the averages.

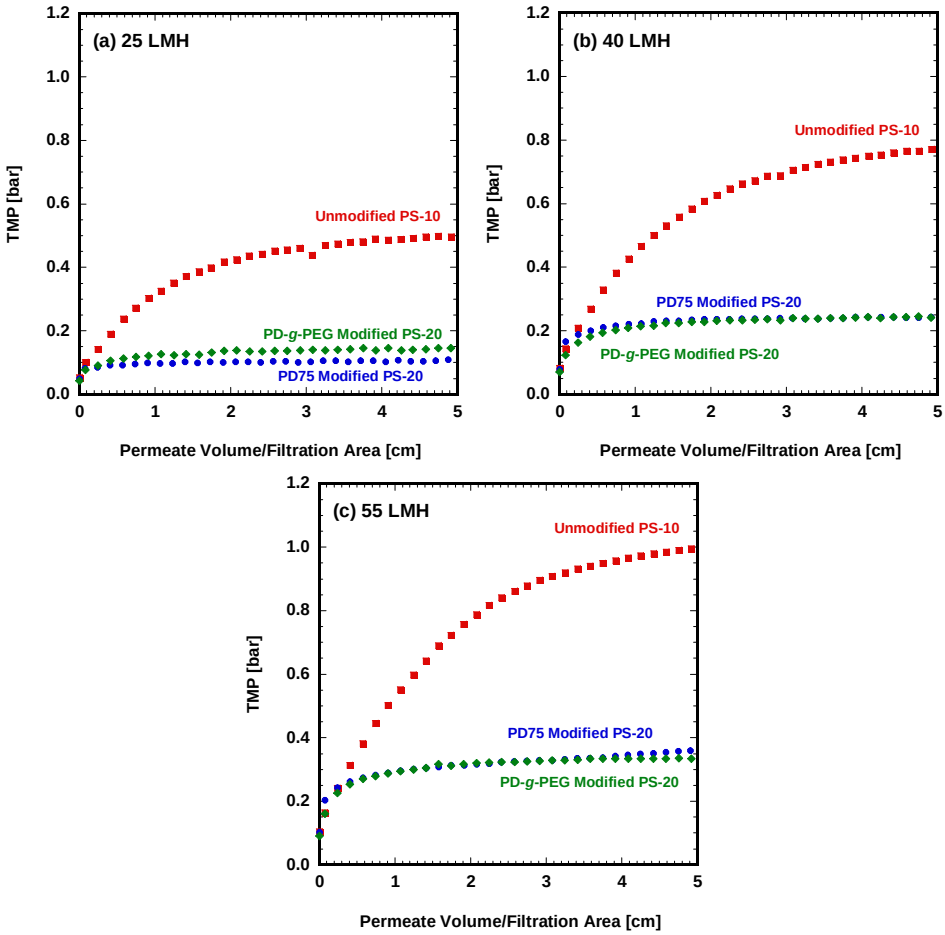

Figure 8.7. Constant flux fouling of (a) unmodified PS-10, (b) PD75 modified PS-20, and (c) PD-*g*-PEG modified PS-20 membranes when challenged with a 1500 ppm soybean oil emulsion feed. All three membranes had a pure water permeance of 570 LMH/bar. Fouling performed at 25, 40 and 55 LMH. The curves shown are representative of at least three replicates at each flux. Feed pressure: 2.1 barg, crossflow velocity: 0.18 m/s.

8.3 REFERENCES

[1] Polysulfone Sheet Membrane Products, Sepro Membranes (2011) PSsheet07.

[2] B.D. McCloskey, H.B. Park, H. Ju, B.W. Rowe, D.J. Miller, B.D. Freeman, A Bioinspired Fouling-Resistant Surface Modification for Water Purification Membranes, Journal of Membrane Science 413-414 (2012) 82–90.

[3] B.D. McCloskey, H.B. Park, H. Ju, B.W. Rowe, D.J. Miller, B.J. Chun, et al., Influence of Polydopamine Deposition Conditions on Pure Water Flux and Foulant Adhesion Resistance of Reverse Osmosis, Ultrafiltration, and Microfiltration Membranes, Polymer 51 (15) (2010) 3472–3485.

[4] S. Singh, K.. Khulbe, T. Matsuura, P. Ramamurthy, Membrane Characterization by Solute Transport and Atomic Force Microscopy, Journal of Membrane Science 142 (1) (1998) 111–127.

[5] S. Mochizuki, A.L. Zydney, Theoretical Analysis of Pore Size Distribution Effects on Membrane Transport, Journal of Membrane Science 82 (3) (1993) 211–227.

[6] H.W. Kim, B.D. McCloskey, T.H. Choi, C. Lee, M.-J. Kim, B.D. Freeman, et al., Oxygen Concentration Control of Dopamine-induced High Uniformity Surface Coating Chemistry, ACS Applied Materials & Interfaces 5 (2) (2013) 233–8.

[7] H. Ju, Water Transport Study in Crosslinked Poly (ethylene oxide) Hydrogels as Fouling-Resistant Membrane Coating Materials, The University of Texas at Austin, 2010.

[8] R. Ghosh, Study of Membrane Fouling by BSA using Pulsed Injection Technique, Journal of Membrane Science 195 (1) (2002) 115–123.

[9] A.D. Marshall, P.A. Munro, G. Trägårdh, Design and Development of a Cross-flow Membrane Rig to Compare Constant Pressure and Constant Flux Operation in Ultrafiltration and Microfiltration, Transactions of the Institution of Chemical Engineers C: Food and Bioproducts Processing 74 (2) (1996) 92–100.

[10] H. Ju, B.D. McCloskey, A.C. Sagle, Y.-H. Wu, V.A. Kusuma, B.D. Freeman, Crosslinked Poly(ethylene oxide) Fouling Resistant Coating Materials for Oil/Water Separation, Journal of Membrane Science 307 (2) (2008) 260–267.

[11] J. Meier-Haack, S. Derenko, J. Seng, Fouling Reduction by Graft-Modification with Hydrophilic Polymers, Separation Science and Technology 42 (13) (2007) 2881–2889.

[12] J. Louie, I. Pinnau, I. Ciobanu, K. Ishida, A. Ng, M. Reinhard, Effects of Polyether–Polyamide Block Copolymer Coating on Performance and Fouling of Reverse Osmosis Membranes, Journal of Membrane Science 280 (1-2) (2006) 762–770.

[13] M. Ulbricht, H. Matuschewski, A. Oechel, H.-G. Hicke, Photo-induced Graft Polymerization Surface Modifications for the Preparation of Hydrophilic and Low-proten-adsorbing Ultrafiltration Membranes, Journal of Membrane Science 115 (1) (1996) 31–47.

[14] A.C. Sagle, E.M. Van Wagner, H. Ju, B.D. McCloskey, B.D. Freeman, M.M. Sharma, PEG-Coated Reverse Osmosis Membranes: Desalination Properties and Fouling Resistance, Journal of Membrane Science 340 (1-2) (2009) 92–108.

[15] E.M. Van Wagner, A.C. Sagle, M.M. Sharma, Y.-H. La, B.D. Freeman, Surface Modification of Commercial Polyamide Desalination Membranes using Poly(ethylene glycol) Diglycidyl Ether to Enhance Membrane Fouling Resistance, Journal of Membrane Science 367 (1-2) (2011) 273–287.

[16] Z. Cai, C. Wee, M.M. Benjamin, Fouling Mechanisms in Low-Pressure Membrane Filtration in the Presence of an Adsorbent Cake Layer, Journal of Membrane Science 433 (2013) 32–38.

[17] G. Gésan, G. Daufin, U. Merin, J.-P. Labbé, A. Quémerais, Fouling During Constant Flux Crossflow Microfiltration of Pretreated Whey. Influence of Transmembrane Pressure Gradient, Journal of Membrane Science 80 (1) (1993) 131–145.

[18] G. Gésan, G. Daufin, U. Merin, Performance of Whey Crossflow Microfiltration during Transient and Stationary Operating Conditions, Journal of Membrane Science 104 (3) (1995) 271–281.

[19] C.-C. Ho, A.L. Zydney, Transmembrane Pressure Profiles during Constant Flux Microfiltration of Bovine Serum Albumin, Journal of Membrane Science 209 (2) (2002) 363–377.

[20] P. Kovalsky, G. Bushell, T.D. Waite, Prediction of Transmembrane Pressure Build-up in Constant Flux Microfiltration of Compressible Materials in the Absence and Presence of Shear, Journal of Membrane Science 344 (1-2) (2009) 204–210.

[21] S. Ognier, C. Wisniewski, A. Grasmick, Membrane Bioreactor Fouling in Sub-critical Filtration Conditions: a Local Critical Flux Concept, Journal of Membrane Science 229 (1-2) (2004) 171–177.

[22] A. Roosjen, H.C. van der Mei, H.J. Busscher, W. Norde, Microbial Adhesion to Poly(ethylene oxide) Brushes: Influence of Polymer Chain Length and Temperature, Langmuir 20 (25) (2004) 10949–55.

[23] A. Halperin, Polymer Brushes that Resist Adsorption of Model Proteins: Design Parameters, Langmuir 15 (7) (1999) 2525–2533.

[24] J. Jiang, L. Zhu, L. Zhu, B. Zhu, Y. Xu, Surface Characteristics of a Self-Polymerized Dopamine Coating Deposited on Hydrophobic Polymer Films, Langmuir 27 (23) (2011) 14180–7.

[25] P. Aimar, J.A. Howell, M. Turner, Effects of Concentration Boundary Layer Development on the Flux Limitations in Ultrafiltration, Chemical Engineering Research and Design 67 (3) (1989) 255–261.

[26] S. Matteucci, Y. Yampolskii, B.D. Freeman, I. Pinnau, Transport of Gases and Vapors in Glassy and Rubbery Polymers, in: Y. Yampolskii, I. Pinnau, B.D. Freeman (Eds.), Materials Science of Membranes for Gas and Vapor Separation, John Wiley & Sons, West Sussex, England, 2006: pp. 1–48.

[27] G. Gésan-Guiziou, E. Boyaval, G. Daufin, Critical Stability Conditions in Crossflow Microfiltration of Skimmed Milk: Transition to Irreversible Deposition, Journal of Membrane Science 158 (1-2) (1999) 211–222.

[28] R.W. Field, G.K. Pearce, Critical, Sustainable and Threshold Fluxes for Membrane Filtration with Water Industry Applications, Advances in Colloid and Interface Science 164 (1-2) (2011) 38–44.

[29] K.Y.-J. Choi, B.A. Dempsey, Bench-scale Evaluation of Critical Flux and TMP in Low-pressure Membrane Filtration, Journal of the American Water Works Association 97 (7) (2005) 134–143.

[30] P.S. Beier, G. Jonsson, Critical Flux Determination by Flux-Stepping, AIChE Journal 56 (7) (2010) 1739–1747.

[31] B. Espinasse, P. Bacchin, P. Aimar, On an Experimental Method to Measure Critical Flux in Ultrafiltration, Desalination 146 (1-3) (2002) 91–96.

[32] P. Le Clech, B. Jefferson, I.S. Chang, S.J. Judd, Critical Flux Determination by the Flux-step Method in a Submerged Membrane Bioreactor, Journal of Membrane Science 227 (1-2) (2003) 81–93.

[33] P. van der Marel, A. Zwijnenburg, A. Kemperman, M. Wessling, H. Temmink, W. van der Meer, An Improved Flux-step Method to Determine the Critical Flux and the Critical Flux for Irreversibility in a Membrane Bioreactor, Journal of Membrane Science 332 (1-2) (2009) 24–29.

[34] D.J. Miller, D.R. Paul, B.D. Freeman, A Crossflow Filtration System for Constant Permeate Flux Membrane Fouling Characterization, Review of Scientific Instruments 84 (3) (2013) 035003.

[35] R.W. Field, D. Wu, J.A. Howell, B.B. Gupta, Critical Flux Concept for Microfiltration Fouling, Journal of Membrane Science 100 (3) (1995) 259–272.

[36] D. Wu, J.A. Howell, R.W. Field, Critical Flux Measurement for Model Colloids, Journal of Membrane Science 152 (1) (1999) 89–98.

[37] M. Stoller, M. Bravi, A. Chianese, Threshold Flux Measurements of a Nanofiltration Membrane Module by Critical Flux Data Conversion, Desalination 315 (2013) 142–148.

[38] M. Elimelech, W.A. Phillip, The Future of Seawater Desalination: Energy, Technology, and the Environment, Science 333 (6043) (2011) 712–7.

[39] R. Chan, V. Chen, M.P. Bucknall, Ultrafiltration of Protein Mixtures: Measurement of Apparent Critical Flux, Rejection Performance, and Identification of Protein Deposition, Desalination 146 (1-3) (2002) 83–90.

[40] R.W. Baker, Membrane Technology and Applications, 2nd ed., John Wiley & Sons, West Sussex, England, 2004.

Chapter 9: Fouling-Resistant Membranes for the Treatment of Flowback Water from Hydraulic Shale Fracturing: a Pilot Study

9.1 SUMMARY

Polyacrylonitrile hollow fiber ultrafiltration (UF) and polyamide spiral wound reverse osmosis (RO) membrane modules were surface-modified by contact with an aqueous solution containing dopamine to deposit polydopamine (PD) on the membrane surfaces and other wetted parts inside the modules. UF modules were further modified by grafting poly(ethylene glycol) (PEG) brushes to the polydopamine coating. PD and PD-*g*-PEG coatings increase the hydrophilicity of the membrane surfaces and have previously been shown to improve fouling resistance towards model oil/water emulsions in laboratory studies. In a pilot-scale test treating hydraulic fracturing flowback water from the Barnett Shale region of Texas, the fouling performance of modified UF and RO membrane modules was compared to that of unmodified analogues. UF modules were used to remove most of the highly fouling organic matter in the feed before desalination by a train of RO elements. PD modified UF modules maintained higher flux, lower transmembrane pressure (TMP) difference, and improved cleaning efficiency relative to unmodified modules. The polydopamine coating did not appear to improve RO fouling behavior, presumably because most of the organic foulants had been removed by UF pretreatment of the feedwater. However, higher and more stable salt rejection was observed in modified RO modules than in unmodified modules.

This chapter adapted from: D. J. Miller, X. Huang, H. Li, S. Kasemset, A. Lee, D. Agnihotri, T. Hayes, D. R. Paul, B. D. Freeman, Fouling-Resistant Membranes for the Treatment of Flowback Water from Hydraulic Shale Fracturing: a Pilot Study, Journal of Membrane Science, 437 (2013) 265-275.

9.2 RESULTS AND DISCUSSION

The performance of UF and RO modules was evaluated when challenged with hydraulic fracturing flowback water from natural gas wells in the Barnett Shale region of north Texas. An unmodified, hollow fiber, polyacrylonitrile UF module was operated simultaneously and in parallel with an identical module that was surface-modified with a PD-*g*-PEG coating. Similarly, results from a train of three spiral wound, unmodified RO modules were compared with those from a train of three polydopamine modified modules. UF modules were cleaned regularly with periodic permeate backwashes and with typical chemically enhanced hot water cleaning and clean-in-place procedures. Autopsy of the modules at the conclusion of the study provided visual confirmation (by the characteristic brown color of polydopamine) that the coating was still in place on the membrane.

9.2.1 Ultrafiltration

In this two-stage pilot, the UF membranes removed suspended particles and highly fouling organic matter from the feed prior to desalination by the RO membranes. The feed turbidity was reported in Nephelometric Turbidity Units (NTU) and is shown in Figure 9.1. Turbidity was highly variable, particularly after ~20 hours of operation, suggesting that the feed became more highly fouling in the latter stages of the study. The turbidity exceeded the UF membrane manufacturer-recommended maximum feed turbidity of 5 NTU for much of the study. Application of a UF module with a more appropriate maximum recommended feed turbidity may have resulted in improved performance.

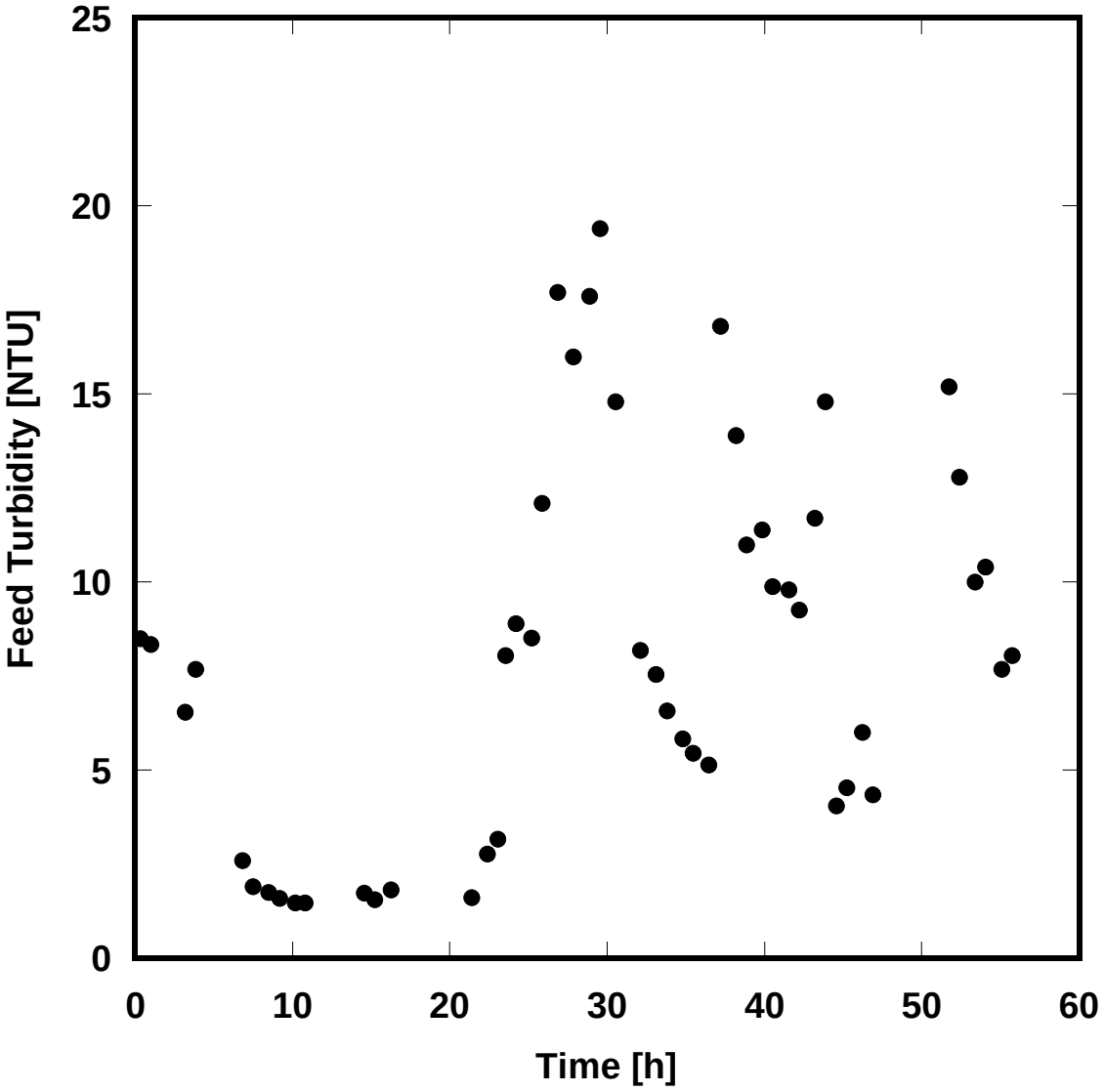

Figure 9.1. UF feed turbidity as a function of operating time. Feed turbidity generally increased and was highly variable in the latter half of the study.

Permeate flux and TMP difference of the UF modules were recorded as a function of time. Figure 9.2 compares the flux of unmodified and PD-*g*-PEG-modified modules over 60 hours. Permeate backwash was performed every 15 minutes; hot water cleaning (HWC) and clean-in-place (CIP) cycles, described in Section 4.3.3, are indicated on the

figure. At the start of the pilot test, the permeate flux of both modules was about 42.5 $Lm^{-2} h^{-1}$ (LMH). Both modules exhibited similar flux deterioration as they fouled during the first 15 hours. After 20 hours of filtration, corresponding to the time that the feed turbidity increased sharply (Figure 9.1), the flux of the modified module became higher than that of the unmodified module. Presumably, the hydrophilic PD-*g*-PEG coating reduced flux deterioration. The modified module had higher flux than the unmodified module for the remainder of the study. By the end of the pilot, the modified module flux was 50% higher than that of the unmodified module.

The PD-*g*-PEG modified module also showed improved recovery relative to the unmodified module upon cleaning, leading to higher ultimate productivity. Especially after the CIP at ~30 hours and the HWC at ~52 hours, the modified module recovered to a significantly higher flux than that of the unmodified module, so the hydrophilic coating appears to facilitate cleaning. Hydrophilic surface modifications have previously been reported to improve the efficacy of cleaning steps, as measured by flux recovery, in RO [1] and UF [2] membranes. According to literature reports, the thin water layer which is strongly bound to a hydrophilic coating reduces strong hydrophobic interactions between hydrophobic foulants and the hydrophobic surface of the native (*i.e.*, uncoated) hydrophobic membrane [3], thereby permitting easier removal of foulants by in situ cleaning protocols such as those used in this study. Improved recovery following cleaning suggests that fouling of the modified membrane is more reversible than that of the unmodified membrane. The rate of flux decline between cleaning procedures was similar in the unmodified and modified modules, suggesting that the rate of fouling of the modules was similar. Therefore, the principle benefit of the PD-*g*-PEG modification appears to be improved flux recovery following cleaning protocols, particularly after

periods where the module was exposed to aggressive fouling conditions, such as the high turbidity of the feed solution that occurred near the mid-point of this study (Figure 9.1).

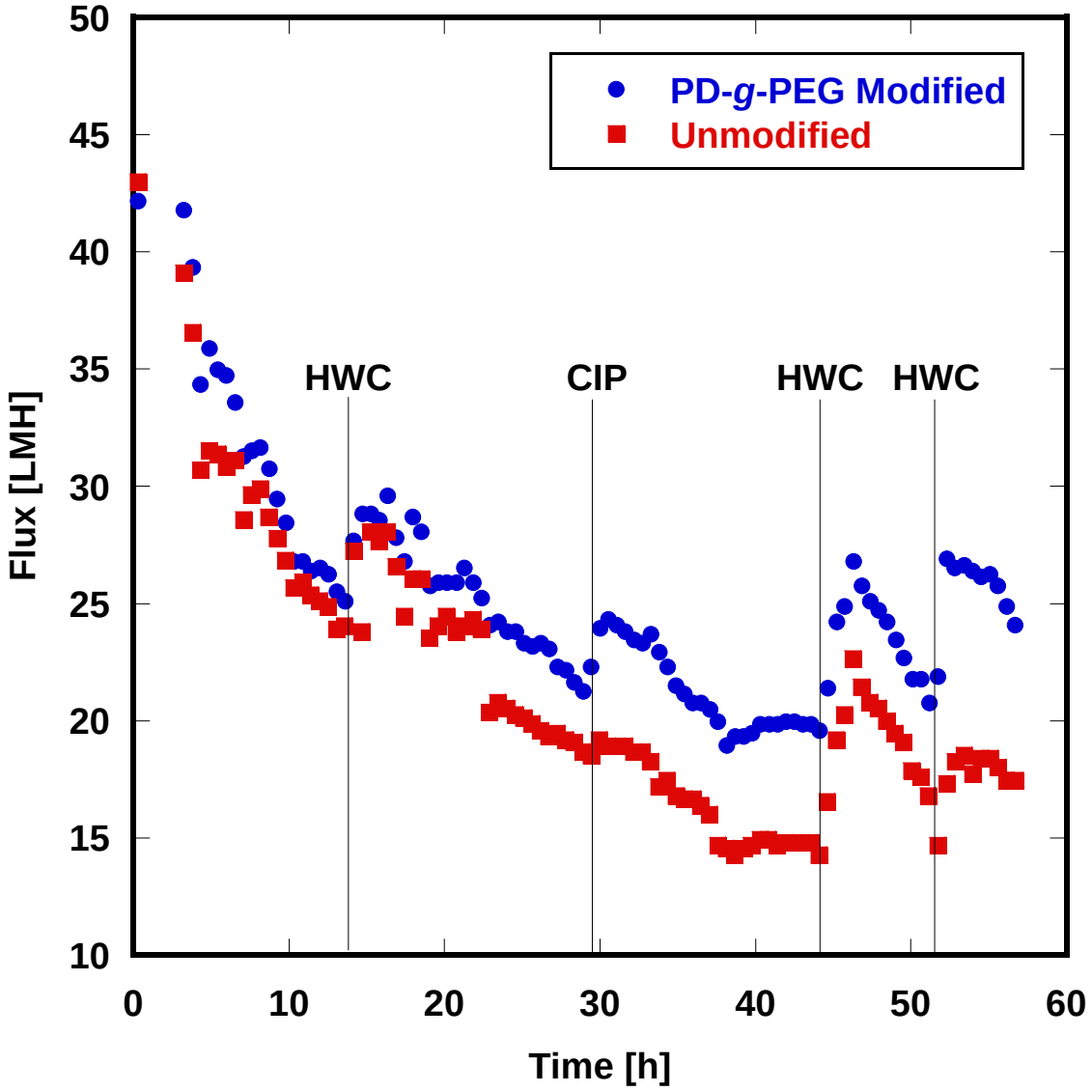

Figure 9.2. Flux of unmodified and PD-*g*-PEG modified UF modules. The modified module showed improved flux relative to the unmodified module after 20 hours of filtration, when the feed turbidity increased. The modified module also recovered flux to a greater degree than the unmodified module after cleaning. HWC is chemically-enhanced hot water cleaning, and CIP is clean-in-place.

The TMP differences of the unmodified and PD-*g*-PEG-modified modules are presented in Figure 9.3. The TMP of the modified module was about 15% lower than that of the unmodified module at the beginning of the study. That is, the TMP was approximately 100 kPa in the unmodified module and 70 kPa in the modified module. Based on this result, the UF membrane with the hydrophilic PD-*g*-PEG surface modification had lower mass transfer resistance relative to the unmodified membrane, since both the modified and unmodified membranes had similar initial fluxes (Figure 9.2), but the modified membrane had a lower TMP. As the study progressed, the difference in TMP between the modified and unmodified modules increased, so that the modified module exhibited a TMP about 20% lower that that of the unmodified module by the conclusion of the study. This difference in TMP over the course of the study supported the hypothesis that the cleaning cycles were more effective on the modified module than on the unmodified module. Apparently irreversible fouling in the unmodified module caused its TMP to gradually increase, while the cleaning cycles were able to effectively maintain or reduce the TMP of the PD-*g*-PEG modified module. In the latter half of the pilot, the TMP of the modified module gradually decreased, suggesting that repeated, periodic cleanings could maintain the TMP near levels observed at the beginning of the study.

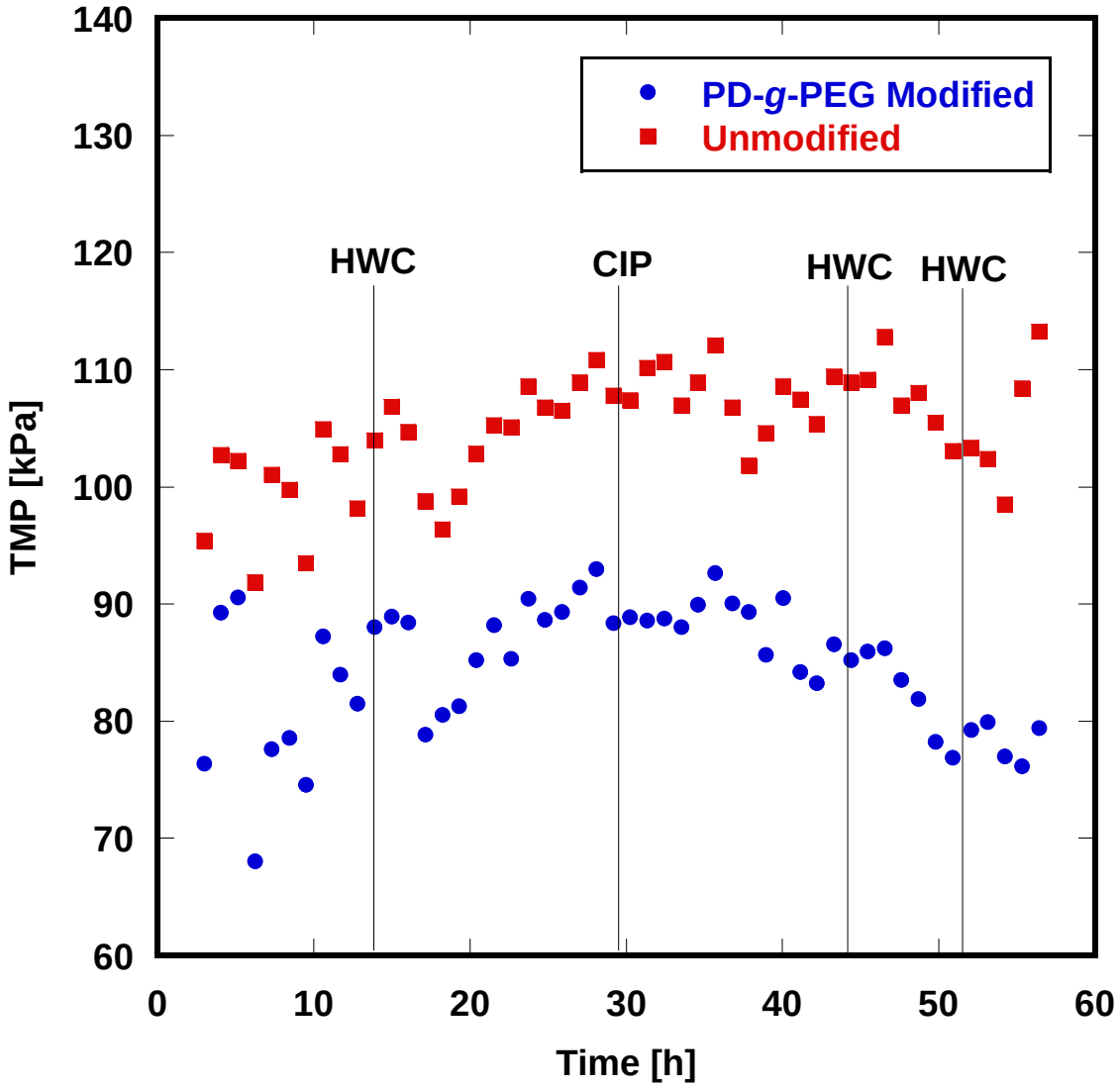

Figure 9.3. TMP evolution in unmodified and PD-*g*-PEG modified UF modules. The modified module maintained a 15-20% lower TMP than the unmodified module during the entire study.

To compare the modified and unmodified UF membrane performance given that both flux and TMP varied during the test, it is useful to consider the membrane permeance (*PM*), which is the flux (*J*) divided by the transmembrane pressure [4]:

$$PM = \frac{J}{\text{TMP}} \qquad [9.1]$$

The reciprocal of permeance is the mass transfer resistance of the membrane. As a membrane fouls, its mass transfer resistance increases, so permeance decreases. A higher permeance or lower rate of decrease in permeance over time would indicate a lower fouling membrane, all other factors being equal. Figure 9.4 compares the permeance values of the modified and unmodified UF membrane modules. The modified module exhibited 25 – 50% higher flux than the unmodified module at 15% - 20% lower TMP, resulting in a significantly higher permeance than that of the unmodified membrane. The ratio of modified module permeance to unmodified module permeance is shown in Figure 9.5. By the conclusion of the pilot test, the modified membrane permeance was approximately two times higher than that of the unmodified membrane, suggesting that the modified module could process up to twice as much water at a given TMP as an unmodified module.

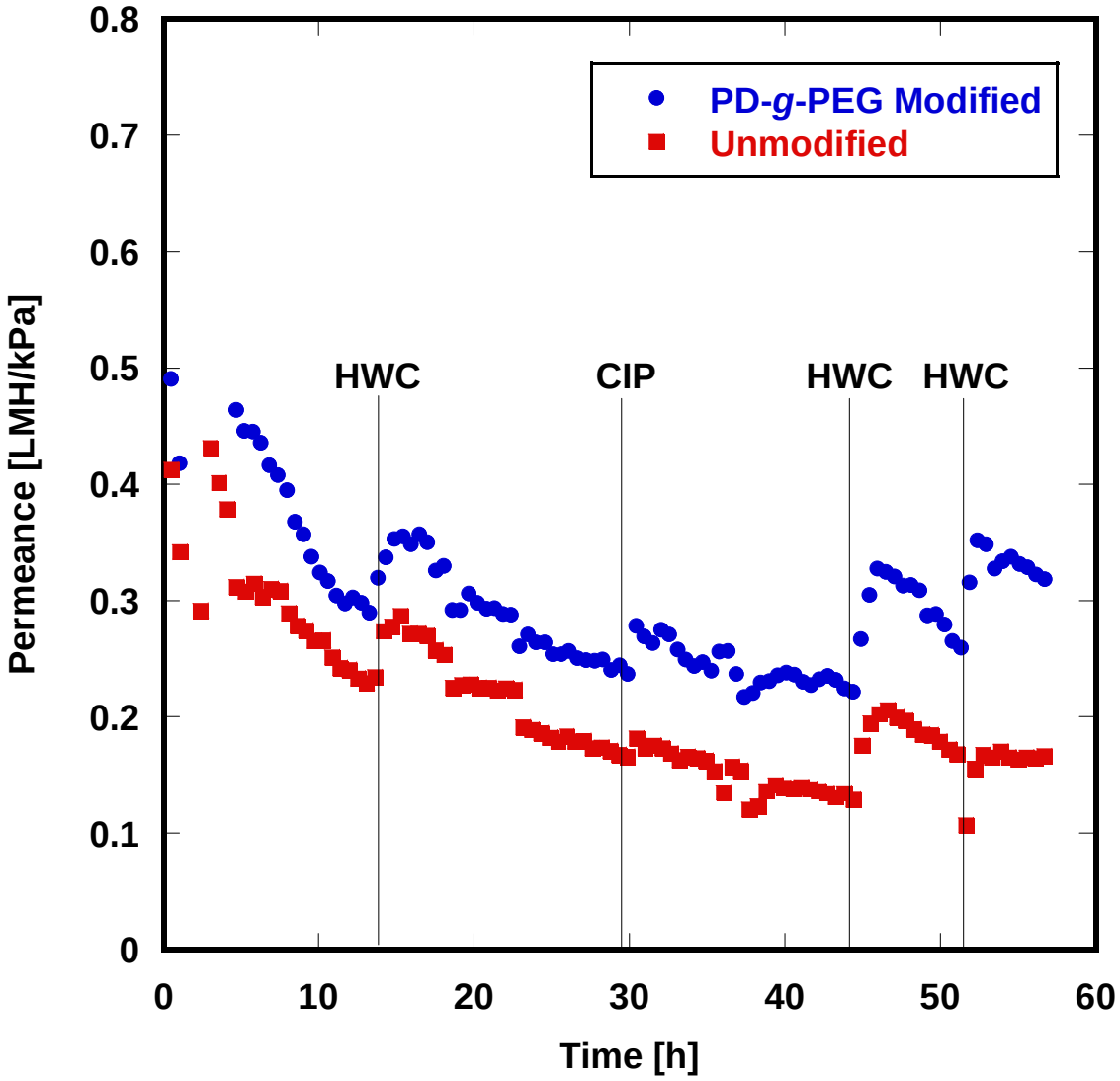

Figure 9.4. Permeance of unmodified and PD-*g*-PEG-modified UF modules. Permeance is a measure of the productivity of the module relative to its energy consumption. The permeance of the modified module was higher than that of the unmodified module due to its higher flux and lower TMP.

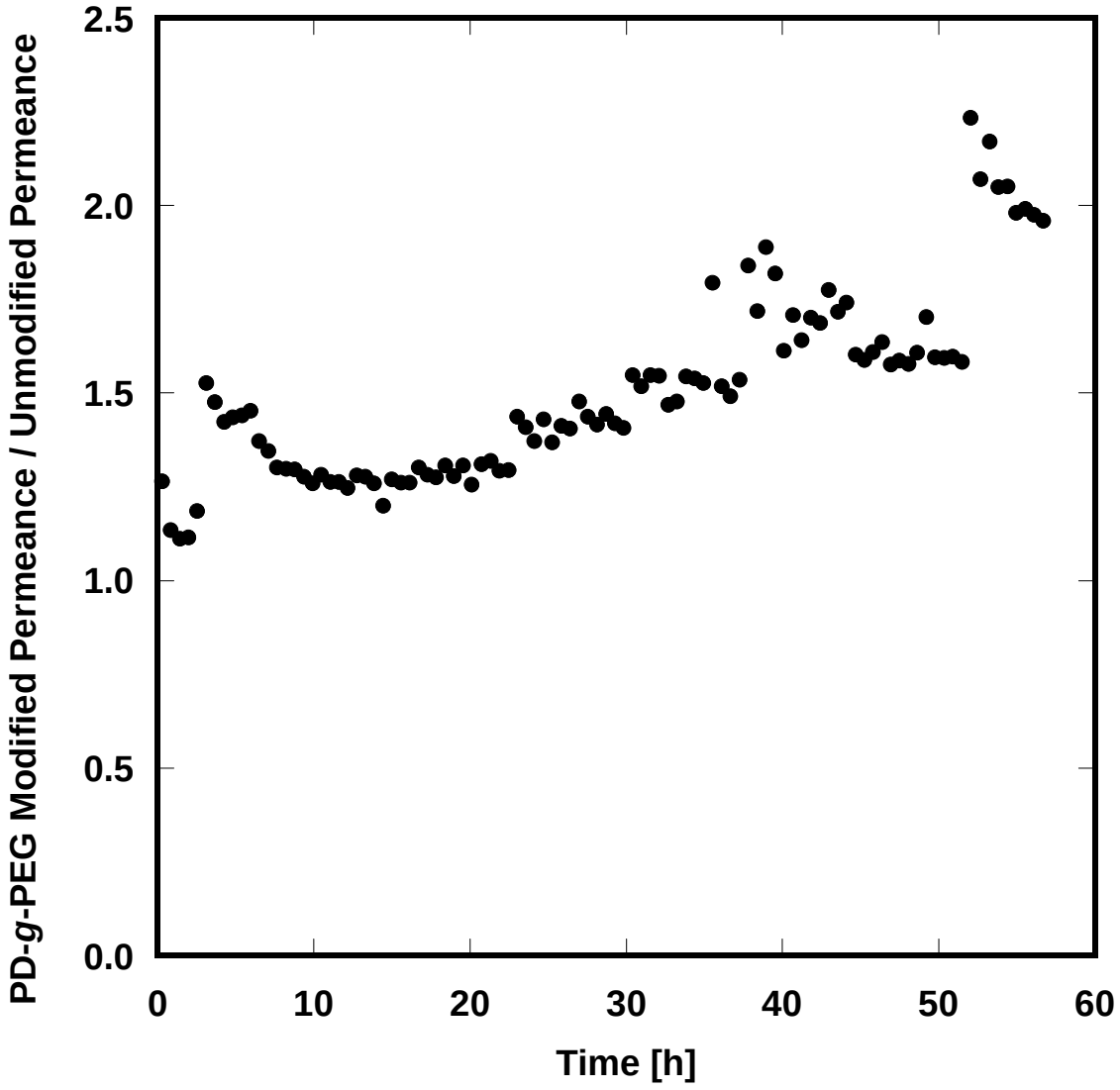

Figure 9.5. Ratio of PD-*g*-PEG modified UF module permeance to unmodified UF module permeance. The modified module was twice as productive as the unmodified module by the conclusion of the pilot study.

9.2.2 Reverse Osmosis

The performance of two RO trains was evaluated by monitoring their permeate fluxes and salt rejections throughout the pilot study. The permeate flux and salt rejection are sensitive to, among other things, feed pressure, feed temperature, and feed salt concentration [5]. Variations in feed temperature and feed salt concentration (measured as total dissolved solids) are shown in Figures 9.6 and 9.7, respectively. The unmodified and PD modified trains were not run concurrently; instead, they were run alternately for 12 hours each. Data were not collected during periods when a train was not operating. Variations in feed temperature reflected the daily cycles in ambient air temperature. Due to changing flowback water characteristics in the field, the feed salt concentration roughly doubled at the midpoint of the study, increasing from approximately 25,000 to more than 50,000 mg/L for some part of the latter half of the study.

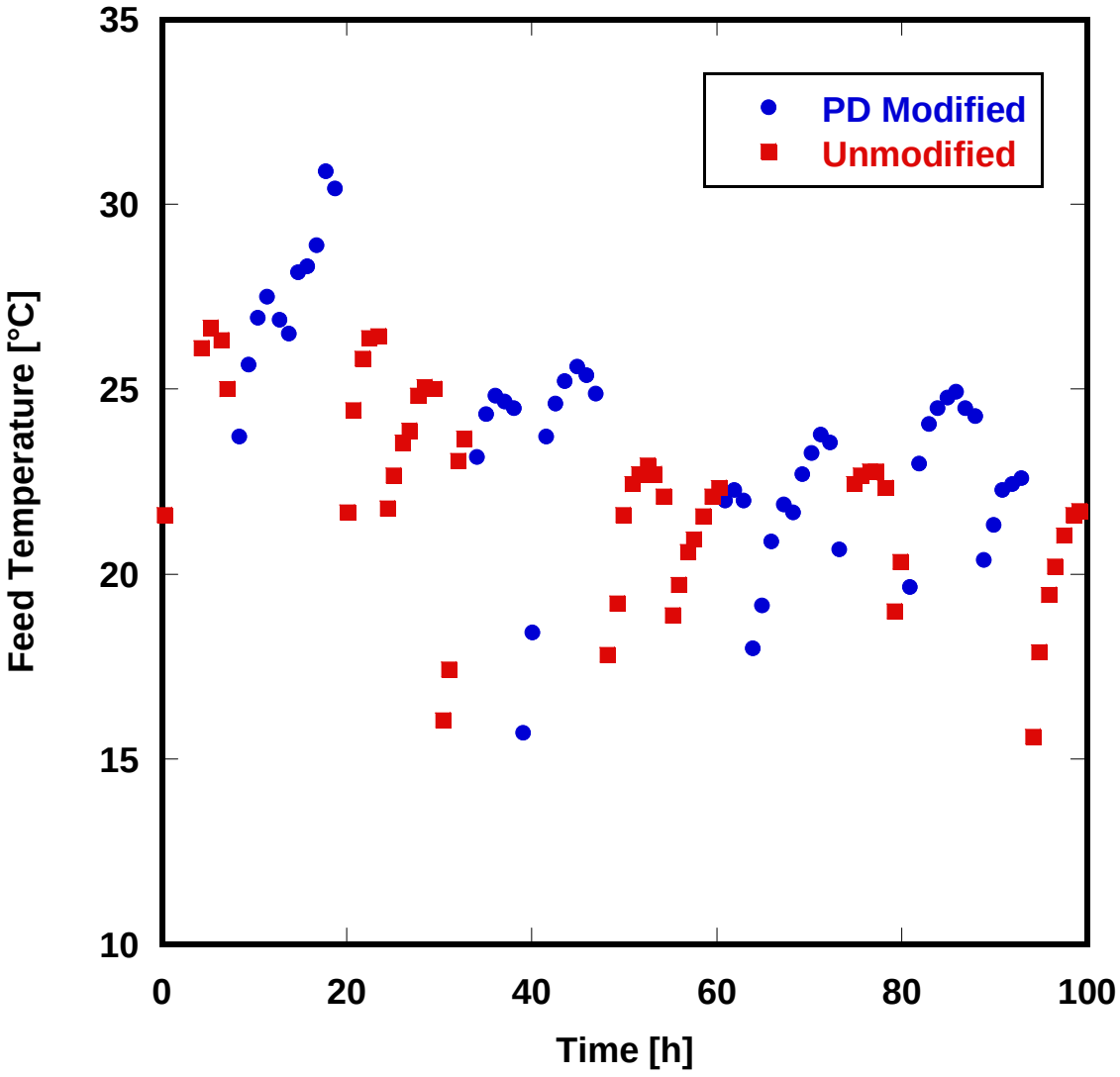

Figure 9.6. Temperature variation in the feeds to PD modified and unmodified RO trains. Variations are the result of daily cycles in ambient temperature.

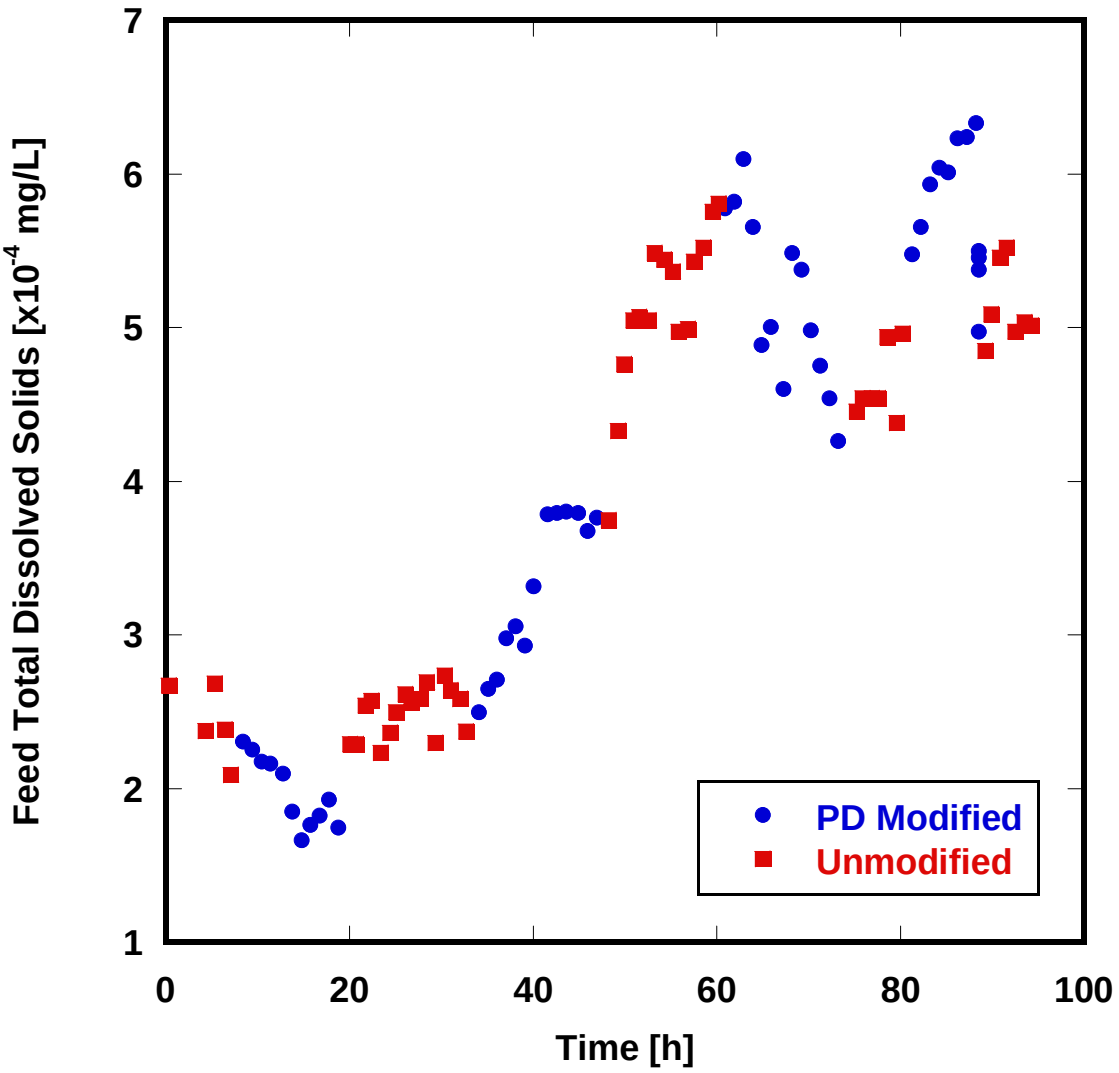

Figure 9.7. Salt concentration (measured as total dissolved solids) of the feed to PD modified and unmodified RO trains. A significant increase in feedwater salt concentration occurred approximately halfway through the study.

The net driving pressure (NDP) is the average driving force available for water permeation through RO membranes [6]. At a fixed feed pressure, the driving force available for water transport through the membrane varies with salt concentration, because the osmotic pressure of the feed is intrinsically linked to its salt content. The NDP is calculated, as described in ASTM Standard D4516 [7], as the transmembrane pressure minus the difference in osmotic pressure ($\Delta\pi$) between the feed and permeate:

$$\text{NDP} = \text{TMP} - \Delta\pi \qquad [9.2]$$

This equation may be expanded as follows:

$$\text{NDP} = \left(P_F - \frac{P_{FB}}{2} - P_P \right) - \left(\pi_{FB} - \pi_P \right) \qquad [9.3]$$

where P_F is the feed pressure, P_{FB} is the pressure drop along the feed-brine side of the module, P_P is the peremeate pressure, π_{FB} is the feed-brine osmotic pressure, and π_P is the permeate osmotic pressure. The osmotic pressure (kPa) of the feed-brine is estimated using [7]:

$$\pi_{FB} = \frac{0.2654 C_{FB} \left(T + 273.15 \right)}{\left(1000 - \frac{C_{FB}}{1000} \right)} \qquad [9.4]$$

where C_{FB} is the feed-brine salt concentration, and T is the feed temperature. The feed-brine salt concentration is based on a log mean average as follows [7]:

$$C_{FB} = C_F \frac{\ln\left(\frac{1}{1-\varphi} \right)}{\varphi} \qquad [9.5]$$

where C_F is the feed salt concentration and φ is the module permeate recovery. The recovery is calculated as the ratio of permeate volumetric flow rate (Q_P) to feed volumetric flow rate (Q_F) [7]:

$$\varphi = \frac{Q_P}{Q_F} \quad [9.6]$$

The salt concentrations C_F and C_P are determined from measurements of the feed and permeate conductivities. Conductivity meters were calibrated with a standard salt solution, as described in the experimental section, to determine the actual concentrations. Finally, the ASTM standard recommends the following approximation for calculation of the permeate osmotic pressure osmotic pressure (kPa) [7]:

$$\pi_P = 0.01\pi_{FB} \quad [9.7]$$

This expression for permeate osmotic pressure is typically used for seawater applications, where the salt concentrations can range from 31,000 to 48,000 mg/L [8]. Hydraulic fracturing flowback water is often at least as highly saline as seawater [9], and the water used in this pilot study was no exception. The feed TDS concentration, initially around 20,000 mg/L for both trains, nearly triples over the course of the pilot to values near 60,000 mg/L. The average feed salt concentration in this study was about 41,000 mg/L, so the expression above for seawater applications was used to calculate the permeate osmotic pressure.

The NDP evolution of the two RO trains is shown in Figure 9.8. The total dissolved solids concentration of the feed water increased significantly around 40 hours into the study (Figure 9.7), so the osmotic pressure of the feed also increased, and the NDP for both trains correspondingly decreased from about 2500 kPa to about 750 kPa. Osmotic pressures were calculated, as shown in Equations [9.2] – [9.7], from conductivity measurements of the feed and permeate. The conductivity meters were calibrated using standard NaCl solutions, so the calculated osmotic pressure is based on the assumption that all salt present is NaCl.

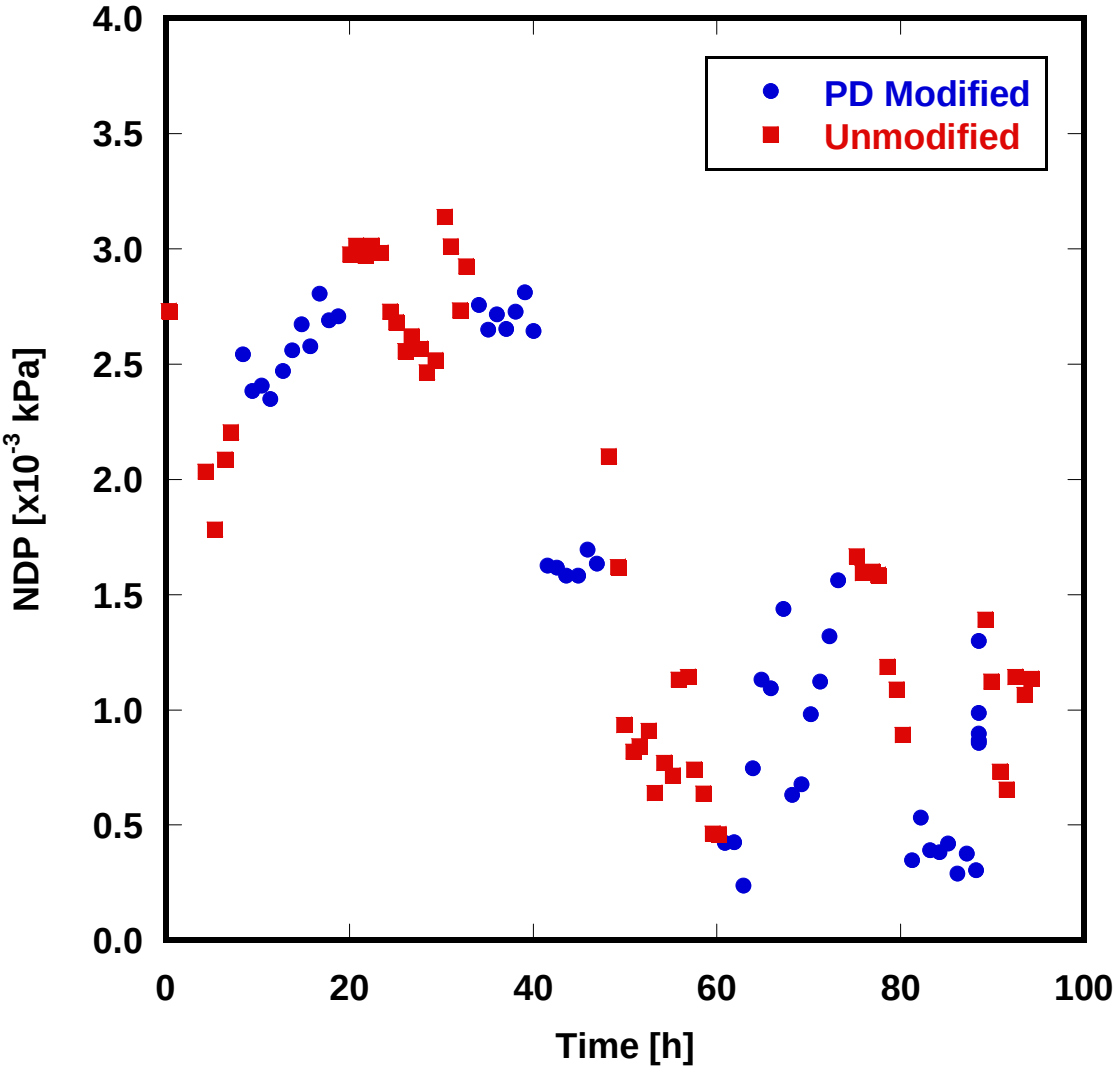

Figure 9.8. NDP of unmodified and PD modified RO trains. The NDP of both trains fell from 20 to 40 hours due to an increase in feed TDS concentration.

Figure 9.9 presents the measured permeate fluxes of unmodified and PD modified RO trains. The fluxes of both the modified and unmodified modules in the first few hours are about 13 LMH. The fluxes of both trains decreased around 40 hours due to the increase in feed salt concentration (and corresponding net driving pressure decrease, cf. Figures 9.7 and 9.8). After 50 hours, the fluxes of both trains fluctuated within a range of

2 – 5 LMH, following the more minor variations observed in feed salt concentration and net driving pressure observed through the end of the study.

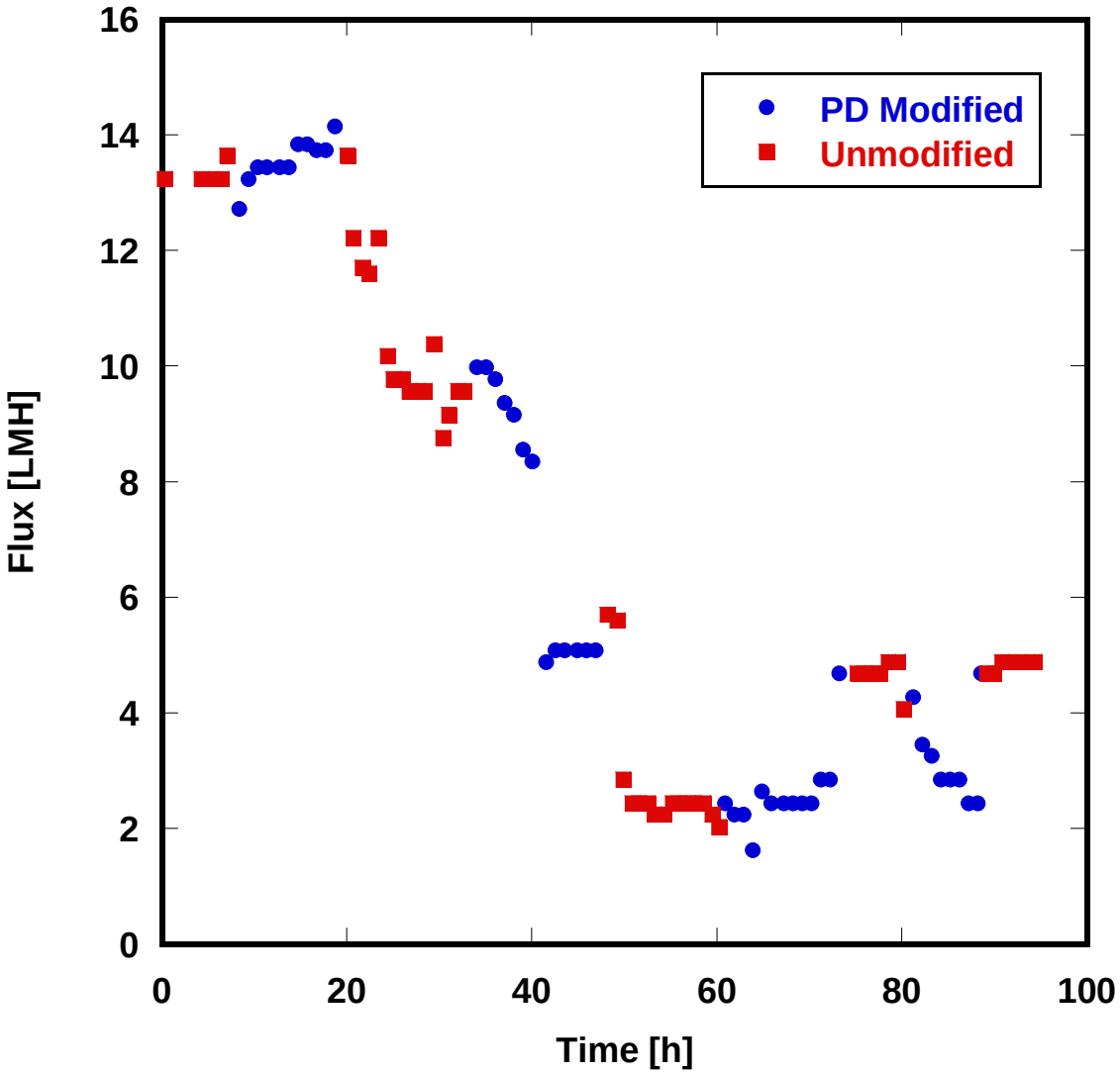

Figure 9.9. Measured permeate flux of unmodified and PD modified RO trains. Fluxes of both trains fell from 20 to 40 hours, corresponding to a substantial increase in feed TDS and, therefore, a decrease in NDP.

Because appreciable variations in feed temperature and salt concentration (and, therefore, net driving pressure) were observed, permeate flux values were normalized to a set of standard condtions. Normalization adjusts the measured flux for variations in temperature, feed pressure, and feed salt concentration, thereby permitting direct comparison of modified and unmodified trains despite changing feed conditions. RO performance data were normalized as described in ASTM Standard D4516 [7] which has been assessed in several literature reports [10–12]. The observed permeate flow was normalized to a set of standard conditions; the conditions for which the manufacturer specifies nominal performance values are convenient for this purpose [10]. For the Hydranautics SWC3+ modules used here, these values are shown in Table 9.1, below.

Standard Condition	Value
Feed Concentration	32,000 mg/L NaCl
Applied Pressure	5515.8 kPa
Operating Temperature	25°C
Permeate Recovery	0.1
Element Permeate Volumetric Flow	1104 L/hr
Element Pressure Drop	68.9 kPa

Table 9.1. Standard operating conditions for which nominal performance values are specified.

Normalization of the permeate flow is based on the solution-diffusion model for water transport through a dense polymer film [11]. The permeate flow is normalized to a standard net driving pressure and a standard feed temperature as follows [7]:

$$Q_{Ps} = \frac{(\mathrm{NDP}_s)(TCF_s)}{(\mathrm{NDP}_a)(TCF_s)} Q_{Pa} \quad [9.8]$$

where *TCF* is the temperature correction factor. The subscript *s* denotes the standard conditions to which data are normalized, and *a* denotes the actual experimental conditions. NDP_s is calculated as shown in Equation [9.3], with the applied pressure (the difference between the feed pressure, P_F, and the permeate pressure, P_P) and the element pressure drop (P_{FB}) taken from Table 9.1. The temperature correction factor is derived from the Arrhenius response of water flux to temperature variations [13]:

$$TCF = \exp\left[K_e \left(\frac{1}{T + 273.15} \right) - \left(\frac{1}{298.15} \right) \right] \quad [9.9]$$

where the constant K_e is provided by the manufacturer (here, K_e = 2700). Because the standard temperature is 25°C (Table 9.1), TCF_s is equal to unity. Finally, the normalized flux is calculated by dividing the normalized permeate flow rate by the total membrane area (*A*):

$$J_s = \frac{Q_{Ps}}{A} \quad [9.10]$$

Normalized fluxes of the unmodified and PD-modified RO trains are shown in Figure 9.10. The normalized fluxes of both trains ranged between 5 LMH and 25 LMH and were generally higher than the actual permeate fluxes (Figure 9.9) at any time. Normalization according to ASTM standard protocols [7] did not eliminate variability in flux data due to changes in feed temperature, feed concentration, and net driving pressure. Instead, the normalization exacerbated fluctuations, especially in data collected towards the end of the study (50 – 100 hours). The introduction of such variability may be due to the large magnitude of the correction factors used to account for changes in temperature and net driving pressure. Additionally, the normalization procedure does not

account for other influences on permeate flux, such as concentration polarization. Concentration polarization is well-known to affect the passage of water and salt across the membrane [14] and itself varies with permeate flux [15]. A similar result has been reported by Safar *et al.* [10], where normalization by the ASTM method results in higher variability than that observed in the measured data. Another possible reason for the variability of normalized data may be the ASTM assumption that all salt present is NaCl. Variations in the conductivity may not be properly reflected in the salt concentration (and, consequently, osmotic pressure) calculations if the feed and permeate streams are comprised of complex mixtures of monovalent and multivalent salts.

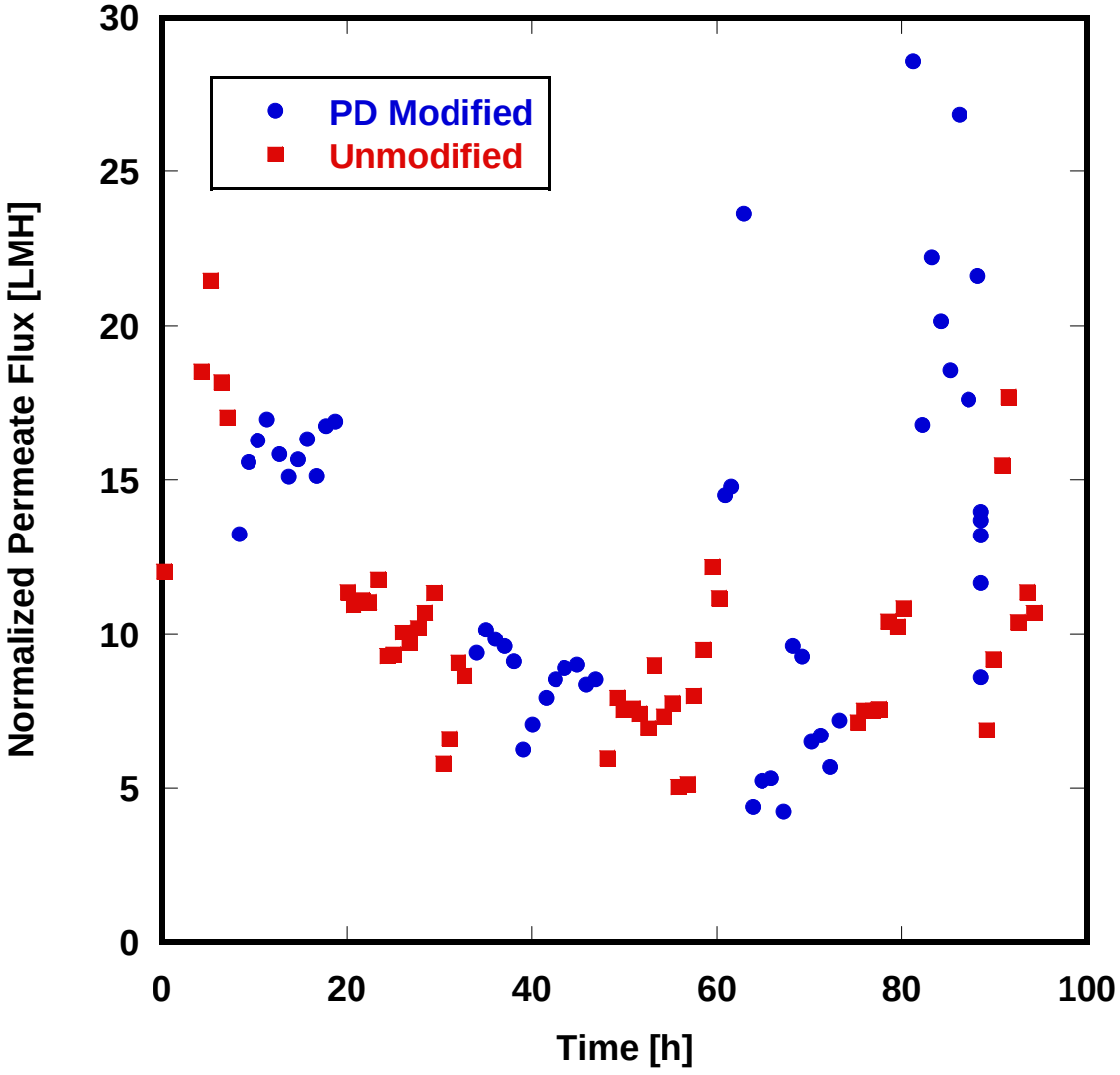

Figure 9.10. Normalized permeate flux of unmodified and PD modified RO trains. Data scatter was observed in the latter half of the study when the feed TDS concentration increased. No appreciable benefit of the PD coating was observed in permeate flux measurements.

Unlike the UF results, the polydopamine-modified RO train did not exhibit systematically improved permeate flux relative to the unmodified train in either the measured data (Figure 9.9) or after normalization. While PD-coated RO membranes exhibited improved resistance to fouling by a simple oil/water emulsion in laboratory tests [16], the RO membrane feed water in this pilot study had already been treated by the UF modules, so it was largely free of organic foulants. For this reason, the RO feed water was likely not highly fouling, and little benefit of a fouling resistant coating was realized with regard to permeate production.

A comparison of apparent salt rejection values between the modified and unmodified RO trains is made in Figures 9.11 and 9.12. Figure 9.11 presents the measured apparent salt rejections. No corrections were made for concentration polarization.

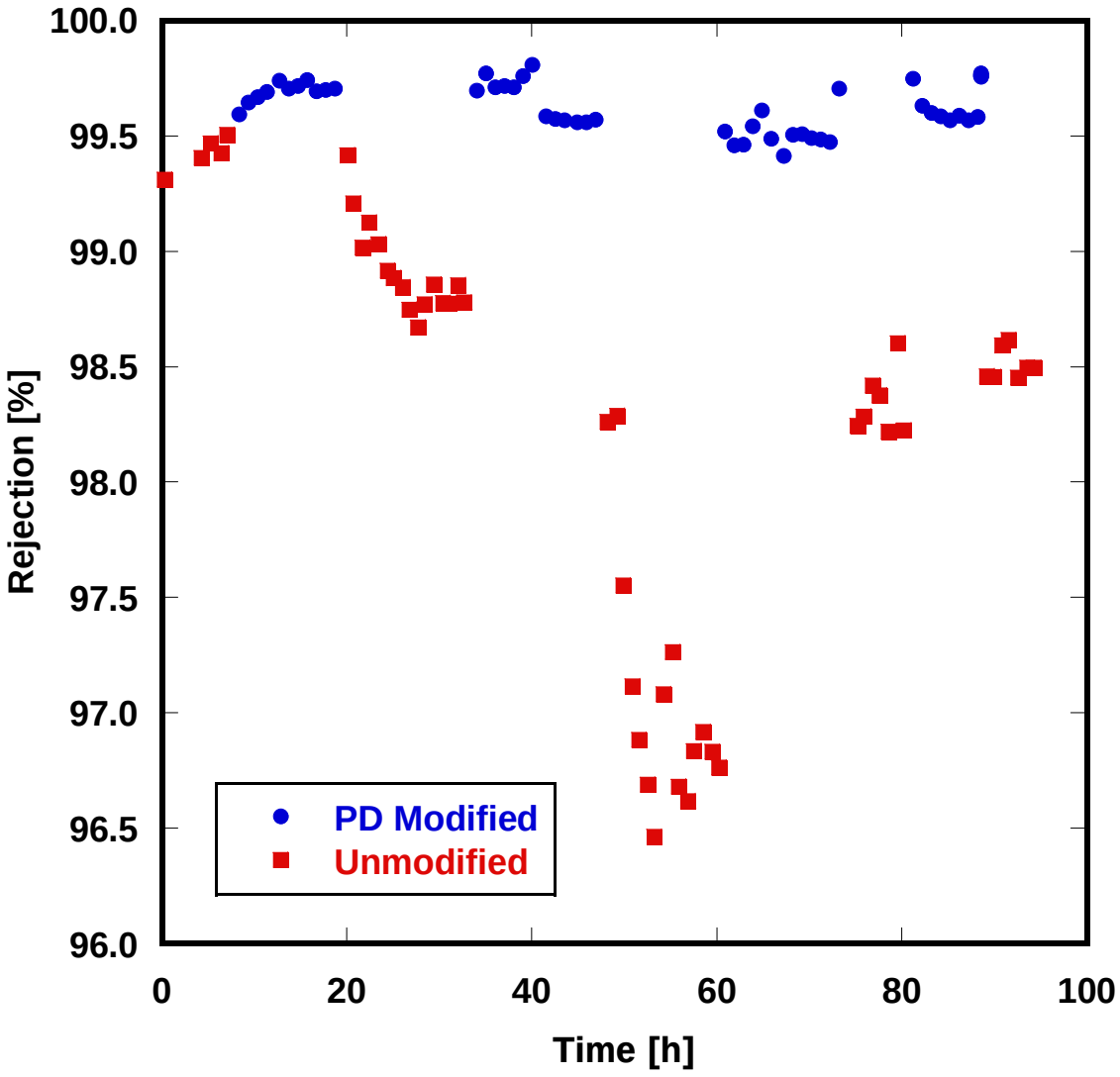

Figure 9.11. Measured salt rejections of PD modified and unmodified RO trains. The modified train showed a higher and more stable rejection than the unmodified train.

Like permeate flux, the salt passage of an RO membrane is also sensitive to operating conditions such as the feed salt concentration, permete flow rate, and temperature [7].. Salt rejection data were normalized using ASTM standard D4516 to the conditions shown in Table 9.1. Unlike the calculation for normalization of the permeate

flow, the normalization of salt passage presented in ASTM standard D4516 is not based on the solution-diffusion model and was likely developed empirically [11]. The salt passage (*SP*) at standard conditions is calculated by [7]:

$$SP_s = \frac{(EPF_a)(STCF_a)C_{FBs}C_{Fa}}{(EPF_s)(STCF_s)C_{FBa}C_{Fs}} SP_a \qquad [9.11]$$

where *EPF* is the element permeate volumetric flow rate and STCF is the salt passage temperature correction factor. EPF_s is not necessarily identical to Q_{ps} calculated above [7] and is, instead, the manufacturer-specified permeate flow shown in Table 9.1. C_{Fs} is also taken from Table 9.1. Equation [9.5] is used to calculate C_{FBa} and C_{FBs}; in the case of C_{FBs}, the permeate recovery φ is the manufacturer-specified permeate recovery under standard operating conditions (Table 9.1). Element manufacturers sometimes provide an expression for the salt transport temperature correction coefficient. Otherwise, the temperature correction factor (*TCF*, Equation [9.9]) may be used, as was the case here. $STCF_s$ was, therefore, equal to unity. The actual salt passage, expressed as a decimal, is given by:

$$SP_a = \frac{C_{Pa}}{C_{FBa}} \qquad [9.12]$$

Finally, the salt rejection ($\Re$) normalized to standard conditions may be calculated:

$$\Re_s = (1 - SP_s) \times 100\% \qquad [13]$$

where *SP* is the salt passage.

Figure 9.12 presents the normalized salt rejection. Rejection normalization accounts for The measured rejection of the unmodified train ranges from over 99.5% to below 96.5% (Figure 9.11), below the manufacturer-specified minimum salt rejection of

97%. Once normalized to the manufacturer-specified operating conditions, however, the unmodified train measured rejection varied between 99.85% and 99.95% (Figure 9.12), consistent with the manufacturer-specified minimum salt rejection. In both the measured and normalized salt rejections, the PD modified train exhibited higher and more stable rejection than the unmodified train. Previous studies have reported improved salt rejection of commercial membranes modified with hydrophilic surface coatings [17]. One possible hypothesis for such improvements is that the coating seals minor defects inherently present in the thin, selective polyamide layer. Other studies have noted the presence of defects in ultathin polymeric separation layers, including Lonsdale, Merten, and Riley's seminal publication describing the preparation of cellulose acetate RO membranes where lower-than-expected salt rejection was measured [18]. Sagle *et al*. observed improved salt rejection values upon coating polyamide RO membranes with PEG-based hydrogels and suggested that the highly-permeable PEG layer could caulk defects in the separation layer [19]. The findings of this study, where the application of a PD coating to thin, interfacially polymerized polyamide RO membranes resulted in an improvement in salt rejection, are consistent with these other reports.

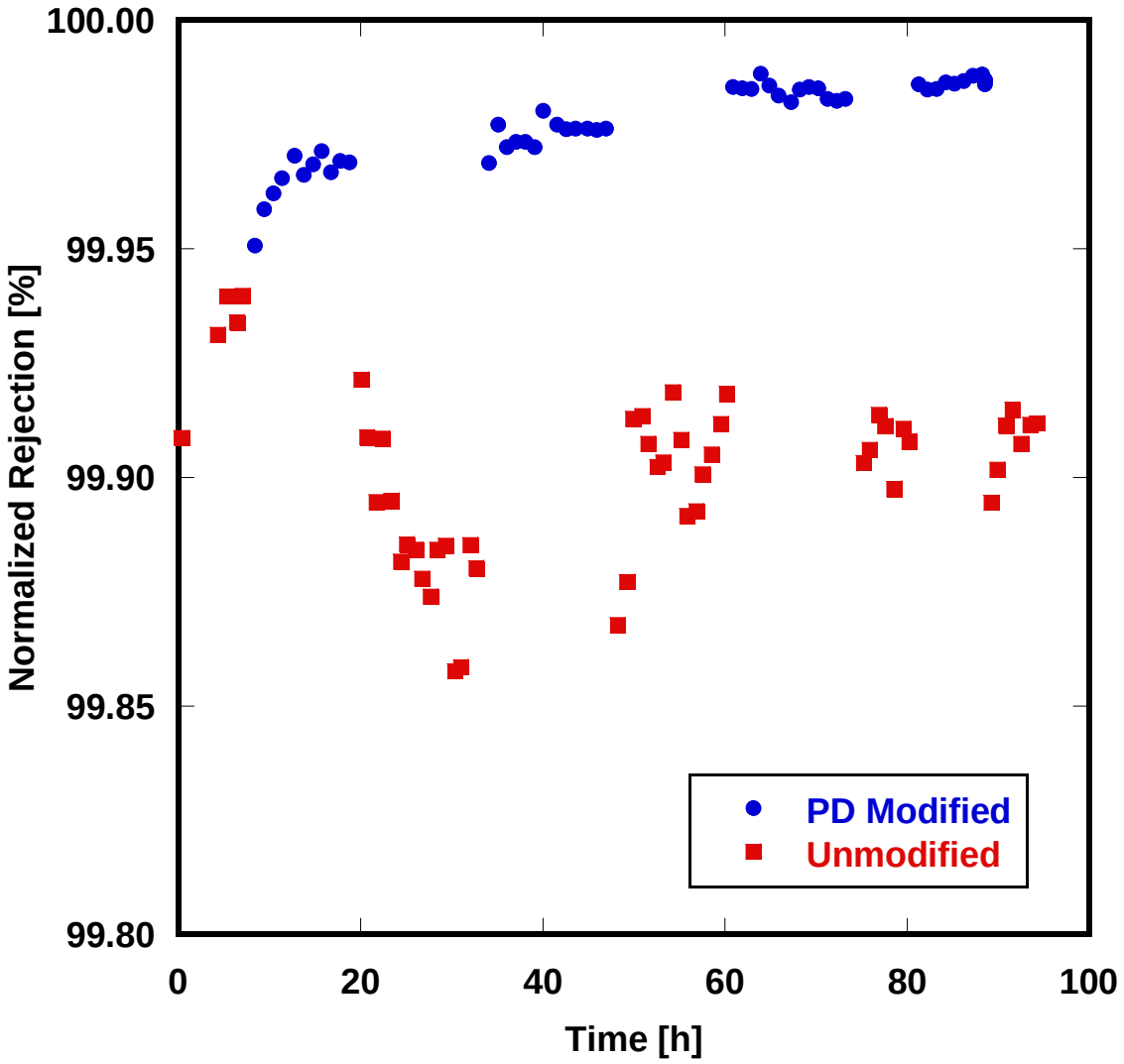

Figure 9.12. Normalized salt rejection of unmodified and PD modified RO trains. The modified train showed a higher and more stable rejection than the unmodified train.

Table 9.2 records the average measured (*i.e.*, not normalized to standard conditions) rejection of individual ions, including chloride, calcium, magnesium, and total hardness over the duration of the pilot test. Calcium, magnesium, and total hardness were measured by titration as $CaCO_3$. Calcium and magnesium concentrations were subsequently calculated using their respective atomic masses. The coated modules

showed improved rejection of all ions, corrobroating the rejection results obtained with conductivity measurements (Figures 9.11 and 9.12). Generally, RO membranes reject multivalent ions more effectively than monovalent ions, as was the case here [5].

	Unmodified SWC3+			PD Modified SWC3+		
	Feed (mg/L)	Permeate (mg/L)	Rejection (%)	Feed (mg/L)	Permeate (mg/L)	Rejection (%)
Cl^-	33500	597	98.2	36800	129	99.6
Ca^{2+}	3790	59	98.5	3790	2	99.9
Mg^{2+}	1880	31	98.4	304	1	99.7
Total Hardness	1650	19	98.9	10700	9	99.9

Table 9.2. Measured rejection of chloride, calcium, magnesium, and total hardness (measured as $CaCO_3$), averaged over the entire pilot duration.

9.3 REFERENCES

[1] L. Zou, I. Vidalis, D. Steele, A. Michelmore, S.P. Low, J.Q.J.C. Verberk, Surface Hydrophilic Modification of RO Membranes by Plasma Polymerization for Low Organic Fouling, Journal of Membrane Science 369 (1-2) (2011) 420–428.

[2] A. Maartens, E.P. Jacobs, P. Swart, UF of Pulp and Paper Effluent: Membrane Fouling-Prevention and Cleaning, Journal of Membrane Science 209 (1) (2002) 81–92.

[3] M. Elimelech, W.A. Phillip, The Future of Seawater Desalination: Energy, Technology, and the Environment, Science 333 (6043) (2011) 712–7.

[4] S. Matteucci, Y. Yampolskii, B.D. Freeman, I. Pinnau, Transport of Gases and Vapors in Glassy and Rubbery Polymers, in: Y. Yampolskii, I. Pinnau, B.D. Freeman (Eds.), Materials Science of Membranes for Gas and Vapor Separation, John Wiley & Sons, West Sussex, England, 2006: pp. 1–48.

[5] R.W. Baker, Membrane Technology and Applications, 2nd ed., John Wiley & Sons, West Sussex, England, 2004.

[6] S. Liang, C. Liu, L. Song, Two-Step Optimization of Pressure and Recovery of Reverse Osmosis Desalination Process, Environmental Science & Technology 43 (9) (2009) 3272–3277.

[7] Standard Practice for Standardizing Reverse Osmosis Performance Data, ASTM Standard D4516-00 (2010).

[8] L.F. Greenlee, D.F. Lawler, B.D. Freeman, B. Marrot, P. Moulin, Reverse Osmosis Desalination: Water Sources, Technology, and Today's Challenges, Water Research 43 (9) (2009) 2317–48.

[9] M. Blauch, R. Myers, T. Moore, B. Lipinski, N. Houston, Marcellus Shale Post-Frac Flowback Waters - Where is All the Salt Coming from and What are the Implications?, in: Proceedings of SPE Eastern Regional Meeting, Society of Petroleum Engineers, 2009: pp. 1–20.

[10] M. Safar, M. Jafar, M. Abdel-Jawad, S. Bou-Hamad, Standardization of RO membrane performance, Desalination 118 (1-3) (1998) 13–21.

[11] Y. Zhao, J.S. Taylor, Assessment of ASTM D 4516 for Evaluation of Reverse Osmosis Membrane Performance, Desalination 180 (1-3) (2005) 231–244.

[12] H.I. Al-Qahtany, N.M.S. Al-Bastaki, Effect of Aging on the Performance of RO Hollow Fiber Membranes in a Section of an RO Plant, Desalination 101 (2) (1995) 177–183.

[13] H. Mehdizadeh, J.M. Dickson, P.K. Eriksson, Temperature Effects on the Performance of Thin-Film Composite, Aromatic Polyamide Membranes, Industrial & Engineering Chemistry Research 28 (6) (1989) 814–824.

[14] D.C. Brandt, G.F. Leitner, W.E. Leitner, Reverse Osmosis Membranes State of the Art, in: Z. Amjad (Ed.), Reverse Osmosis: Membrane Technology, Water Chemistry, and Industrial Applications, Van Nostrand Reinhold, New York, NY, 1993: pp. 1–36.

[15] E.M. Van Wagner, A.C. Sagle, M.M. Sharma, B.D. Freeman, Effect of Crossflow Testing Conditions, including Feed pH and Continuous Feed Filtration, on Commercial Reverse Osmosis Membrane Performance, Journal of Membrane Science 345 (1-2) (2009) 97–109.

[16] B.D. McCloskey, H.B. Park, H. Ju, B.W. Rowe, D.J. Miller, B.D. Freeman, A Bioinspired Fouling-Resistant Surface Modification for Water Purification Membranes, Journal of Membrane Science 413-414 (2012) 82–90.

[17] W.E. Mickols, Composite Membrane with Polyalkylene Oxide Modified Polyamide Surface, U.S. Patent 6,280,853 B1, 2001.

[18] H.K. Lonsdale, U. Merten, R.L. Riley, Transport Properties of Cellulose Acetate Osmotic Membranes, Journal of Applied Polymer Science 9 (4) (1965) 1341–1362.

[19] A.C. Sagle, E.M. Van Wagner, H. Ju, B.D. McCloskey, B.D. Freeman, M.M. Sharma, PEG-Coated Reverse Osmosis Membranes: Desalination Properties and Fouling Resistance, Journal of Membrane Science 340 (1-2) (2009) 92–108.

Chapter 10: Short-term adhesion and long-term biofouling testing of polydopamine and poly(ethylene glycol) surface modifications for biofouling control on membranes and feed spacers

10.1 SUMMARY

Ultrafiltration (UF) membranes were hydrophilized with polydopamine (PD) and polydopamine-*g*-poly(ethylene glycol) (PD-*g*-PEG) surface coatings. The fouling propensity of modified and unmodified membranes was evaluated by short-term batch protein and bacterial adhesion tests and by continuous biofouling experiments in a membrane fouling simulator. The goals of the study were: 1) to determine the effectiveness of PD and polydopamine-*g*-poly(ethylene glycol) membrane coatings for biofouling control and 2) to compare techniques commonly used in assessment of membrane biofouling propensity with realistic biofouling experiments. Short-term adhesion tests were carried out under static, no-flow conditions for one hour using bovine serum albumin, a common model globular protein, and *Pseudomonas aeruginosa,* a common model Gram negative bacterium. Biofouling tests were performed in a membrane fouling simulator for several days under flow conditions similar to those encountered in industrial modules with the autochthonous drinking water population and with organic substrate dosage. PD and PD-*g*-PEG modified membranes showed significantly reduced adhesion of bovine serum albumin and *P. aeruginosa* in the short-term adhesion tests, but no reduction of biofouling was observed during longer biofouling experiments. These results demonstrate that short-term batch adhesion experiments using model proteins or bacteria under static conditions are not indicative of ultimate biofouling

This chapter adapted from: D. J. Miller, P. A. Araújo, P.Correia, M. M. Ramsey, J. C. Kruithof, M. C. M. van Loosdrecht, B. D. Freeman, D. R. Paul, M. Whiteley, J. S. Vrouwenvelder, Short-term adhesion and long-term biofouling testing of polydopamine and poly(ethylene glycol) surface modifications of membranes and feed spacers for biofouling control, Water Research 46 (12) (2012) 3737-3753.

potential, while continuous biofouling experiments showed that membrane surface modification by PD and PD-*g*-PEG is not effective for biofouling control.

10.2 PRACTICAL IMPLICATIONS OF EARLY MICROBIAL ATTACHMENT FOR BIOFOULING

Biofilm formation is a multi-stage process [1]. A conditioning film comprised of proteins or other natural organic material forms within seconds of first water contact [2]; this film promotes, and may be requisite for, bacterial adhesion [3]. Fast-adhering strains attach to a surface within minutes and can reach a surface density equivalent to the bulk suspension density within an hour [2]. After early attachment of cells to the conditioning film, bacteria colonize the surface and replicate to form a biofilm [4]. Understandably, many authors have emphasized the role of initial microbial attachment in the study of biofilm formation, but it is not clear whether the degree of initial protein and cell attachment is a good indicator of ultimate biofilm accumulation.

Literature is divided concerning the effect of early attachment on long-term biofilm growth. Several other studies have reported little or no correlation between short-term microbial adhesion and biofouling, but few, if any, are found in the membrane literature. Simões et al. studied the adhesion of organisms from drinking water to styrene particles [5]. They found a relationship between initial adhesion and biofilm formation only at short times (<24 hours); at longer biofilm formation times, the correlation deteriorates. Even microbes like *Methylobacterium* sp. and *M. mucogenicum*, which are only weakly adherent, and *B. cepacia*, *Sph. capsulata*, and *Staphylococcus* sp., largely considered non-adherent, were all able to form biofilms after 24-48 hours. Gjaltema and co-workers studied 2-hour adhesion of *P. putida* and 16-day biofilm growth on glass beads with several different surface modifications. Chemical surface modifications were found to have little influence on biofilm development. Roughened surfaces showed

reduced 2-hour adhesion, but 16-day biofilm growth was exacerbated on rough beads [6]. Nejadnik et al. evaluated poly(ethylene oxide)/poly(propylene oxide) copolymer brushes for their efficacy in reducing adhesion and growth of several organisms, including *Staphylococcus aureus*, *Staphylococcus epidermidis,* and *P. aeruginosa*, on silicone rubber. The brush coatings reduced *Staphylococcus* adhesion over 30 minutes but did not prevent biofilm growth over 20 hours. *P. aeruginosa* was able to adhere to and grow biofilm on both treated and untreated samples. Biofilms of all three organisms growing on the hydrophilic brush coatings showed higher viability than those on the bare silicone rubber [7]. Surface modifications, even when effective in reducing or preventing initial adhesion of microorganisms, are largely ineffective in preventing biofilm formation over longer durations.

Despite such evidence suggesting that initial attachment is not predictive of biofilm growth, many authors maintain that prevention of microbial adhesion is a viable strategy for development of anti-fouling materials. To this end, membrane biofouling susceptibility is often judged by short-term experiments in which only initial bacterial adhesion is observed rather than by longer biofouling experiments representative of industrial installations. In early work framed by the impact of biofouling at Water Factory 21, Ridgway *et al*. investigated attachment and detachment of *Mycobacterium* sp. to cellulose diacetate RO membranes; they found that most bacterial adhesion occurred within two hours [8,9]. A hypothesis that, "because mycobacteria appear to be involved in the earliest stages of membrane fouling, it may be possible to control or reduce the rate of biofouling by interfering with the ability of these bacteria to adhere to and colonize the membrane surface" [10] was hence put forth and is pervasive in the biofouling literature.

Recent reports demonstrate the continued use of short bacterial adhesion tests as a measure of membrane biofouling susceptibility. In a report on *Stenotrophomonas*

maltophilia adhesion to polystyrene, Pompilio stated that "preventing primary adhesion would prevent biofilm formation" [11]. Chen and co-workers found decreased *H. pacifica* adhesion to zeolite-covered stainless steel relative to the bare metal during 24-hour incubation; they claimed that this result indicates that the zeolite coating is a good "anti-fouling" material [12]. Poly(acrylonitrile)-*g*-poly(ethylene oxide) UF membranes were studied by Adout in one-hour studies with *Escherichia coli* [13]. Bernstein and co-workers recently examined *P. fluorescens* deposition on surface-modified polyamide RO membranes over 30 minutes to "open a route to rational design and preparation of modified membranes…for biofouling mitigation" [14]. Yang, *et al*. evaluated surface-grafted polycations as an anti-biofouling modification of microporous polypropylene membranes. Modified membranes showed decreased adhesion of *E. coli* and *E. aureus* over 60 minutes and the authors claimed that "these membranes have capability of combating with biofouling" [15]. Silver was incorporated into poly(ether sulfone) membranes using 2,4,6-triaminopyrimidine compatibilizer by Basri *et al*. to create hybrid membranes with increased hydrophilicity, tensile strength, and smoothness. Membranes with these improved surface properties, which "are prominent factors in preventing or minimizing biofouling problems in membrane application[s]," were incubated with *E. coli* for only four hours [16]. Studies such as these, which employ short timescales where only early adhesion is evaluated, likely yield little evidence of the long-term biofouling propensity of membranes and membrane modules.

Direct comparisons of surface-hydrophilized membranes to unmodified membranes at the pilot or full scales are extremely rare in the academic biofouling literature. This dearth of studies may speak to the difficulty of translating many laboratory membrane surface modifications to assembled membrane modules. The deposition of polydopamine provides a route to facile, post-manufacture modification by

simply pumping alkaline dopamine solution through the membrane module, forming a hydrophilic coating on all wetted parts. PEG-NH_2 could be subsequently grafted to the polydopamine coating in a similar fashion. This study evaluates PD and PD-*g*-PEG membrane surface modifications using membrane fouling simulators recently developed by Vrouwenvelder [17,18]. These tools, which incorporate flat-sheet membranes and feed spacers, effectively simulate the hydrodynamic conditions of spiral-wound membrane modules and have been shown to reflect biofouling patterns encountered in full-scale installations [19]. Importantly, the simulators may be operated for any desired duration, permitting long-term biofouling testing. Therefore, we are able to directly compare hydrophilized membranes and feed spacers to their unmodified counterparts under conditions that closely approximate industrial membrane installations.

10.3 RESULTS

10.3.1 Membrane modification

Examples of PS-20 polysulfone UF membranes and polypropylene feed spacers which were coated with PD *in situ* and subsequently removed from the membrane fouling simulator for photography are shown in Figure 10.1. The characteristic brown color of PD surface deposition is apparent on both the polysulfone UF membrane and the polypropylene feed spacer when compared to the unmodified samples. The cross-hatch pattern of the feed spacer is visible on the membrane surface, a result of incomplete PD coverage where the spacer was in contact with the membrane during *in situ* modification. This observation led to application of *ex situ* coating techniques (see Chapter 4). Membranes and feed spacers coated ex situ are shown in Figure 10.2. The polydopamine-coated membrane sample does not exhibit the cross-hatched pattern of the

membrane in Figure 10.1 because it was not in contact with the polypropylene feed spacer during the coating process, permitting more complete coverage of the coating.

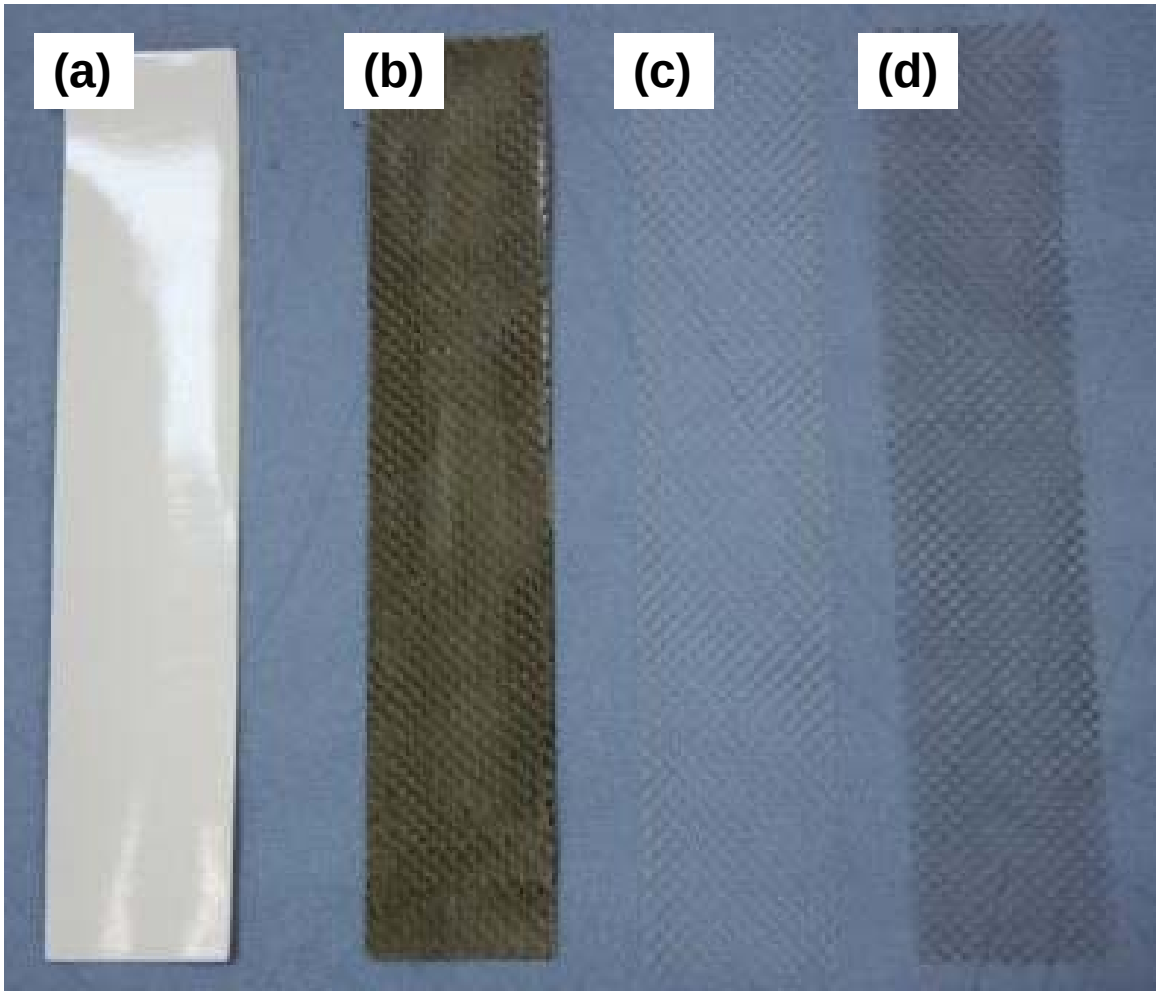

Figure 10.1. (a) Unmodified membrane, (b) PD modified membrane, (c) unmodified feed spacer, and (d) PD modified feed spacer. Membranes and feed spacers were modified *in situ* in a membrane fouling simulator and subsequently removed for inspection. The brown color is indicative of the PD coating; the pattern on the PD modified membrane (b) is a result of contact with the feed spacer (d) during coating.

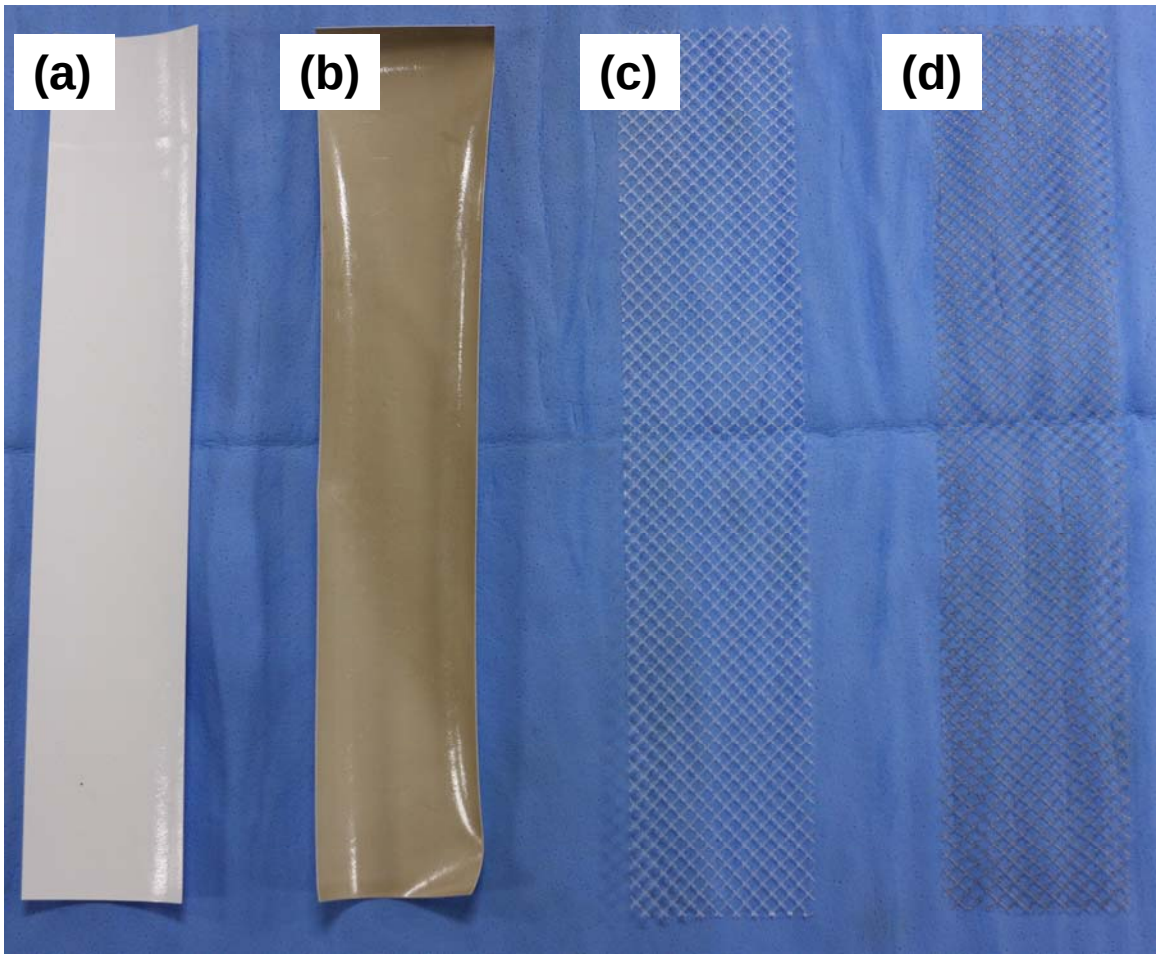

Figure 10.2. (a) Unmodified membrane, (b) PD modified membrane, (c) unmodified feed spacer, and (d) PD modified feed spacer. Membranes and feed spacers were modified *ex situ*. The brown color is indicative of the PD coating. Because the membrane (b) was not in contact with the feed spacer (d) during coating, it does not show the patterned appearance of the PD modified membrane in Figure 10.3.

10.3.2 Short-term batch protein and bacteria adhesion tests

The effect of PD and PD-*g*-PEG coatings on short-term BSA and *P. aeruginosa* adhesion was examined. Unmodified, PD modified, and PD-*g*-PEG modified PS-20 UF membranes were exposed to fluorescent BSA and luminescent *P. aeruginosa* suspensions for one hour. Fluorescence and luminescence intensities were measured; intensities were normalized to a value of 100 for the unmodified sample in both cases. Relative adsorption of proteins or bacteria may be deduced by comparing fluorescence or luminescence intensity of unmodified samples to that of PD or PD-*g*-PEG modified samples. Results of the BSA adhesion studies are shown in Figure 10.3. The polydopamine-modified membrane showed two orders of magnitude lower fluorescence than the unmodified sample and the PD-*g*-PEG modified membrane showed further reduction in fluorescence intensity. Figure 10.4 shows that polydopamine and PD-*g*-PEG modifications resulted in a 75% reduction in *P. aeruginosa* luminescence relative to an unmodified membrane. In the case of the bacteria adhesion, no statistical difference was observed between PD and PD-*g*-PEG modified membranes. The PD and PD-*g*-PEG coatings, therefore, significantly reduced both protein and bacterial binding to the membranes during the short-term, static adhesion tests.

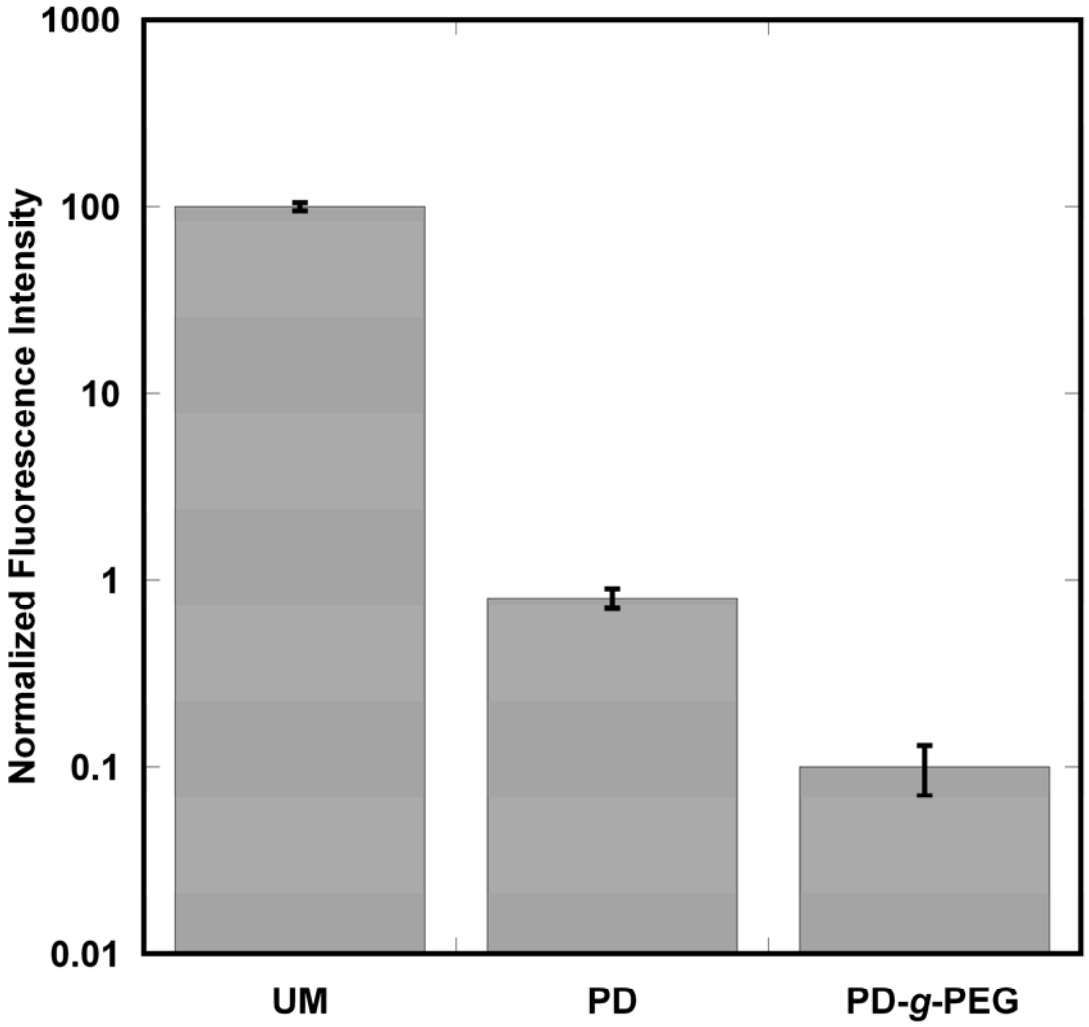

Figure 10.3. Normalized fluorescence intensity of PS-20 UF membranes after 1 h static contact with a 0.1 mg/mL solution of rhodamine-tagged bovine serum albumin. Values normalized to fluorescence of the unmodified sample, which was assigned an intensity of 100. Error bars are standard deviation over nine replicates. UM = unmodified, PD = polydopamine modified, PD-*g*-PEG = polydopamine-*g*-PEG modified.

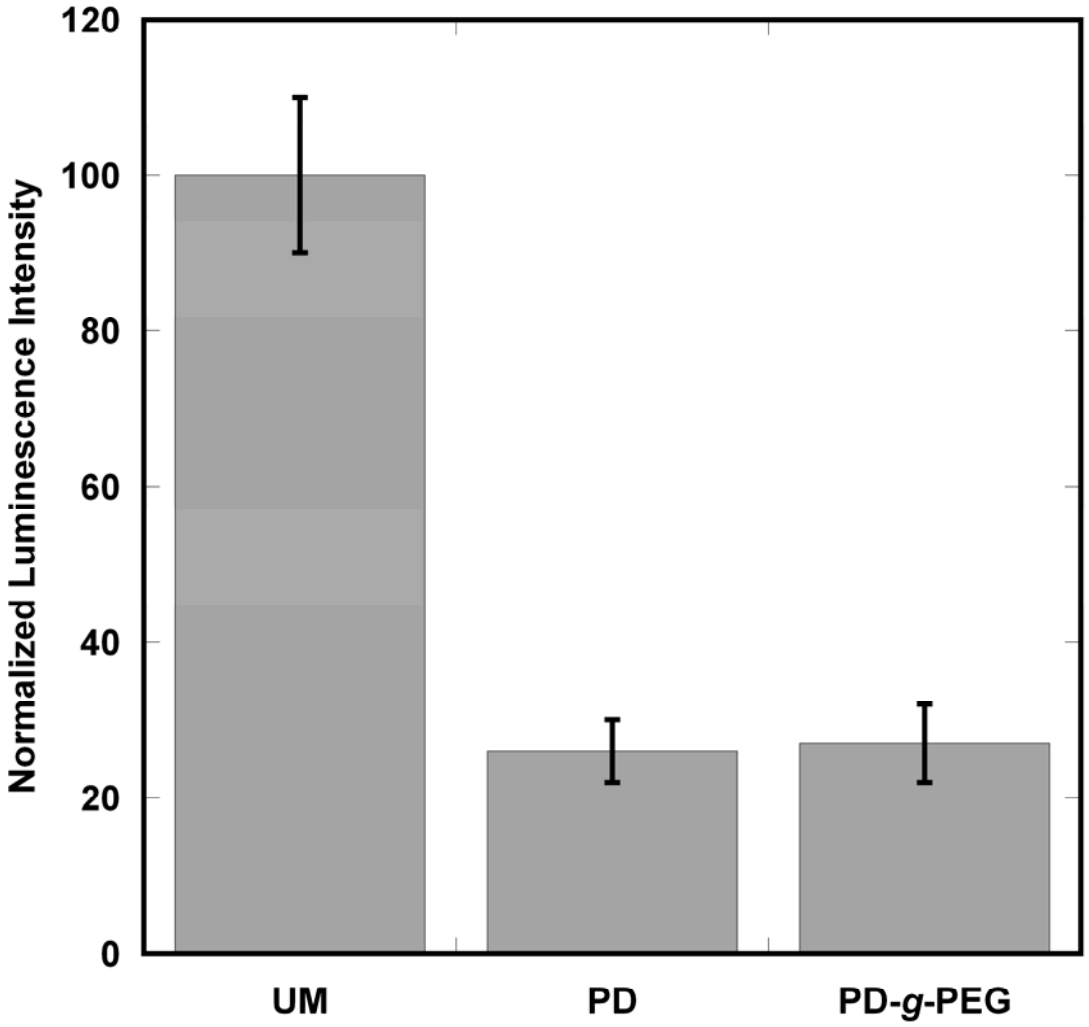

Figure 10.4. Normalized luminescence intensity of PS-20 UF membranes after 1 h static contact with a suspension of luminescent *P. aeruginosa* culture (OD_{600} = 0.1). Values normalized to luminescence of the unmodified sample, which was assigned an intensity of 100. Error bars are standard error over eight replicates. UM = unmodified, PD = polydopamine modified, PD-*g*-PEG = polydopamine-*g*-PEG modified.

10.3.3 Long-term continuous biofouling tests

Three experiments were conducted to assess the efficacy of PD and PD-*g*-PEG coatings in preventing biofouling on polysulfone UF membranes and polypropylene feed spacers over several days in membrane fouling simulators. In the first experiment, membranes and feed spacers were modified *in situ* and the temperature of the feed water was not controlled. Feed channel pressure drop evolution for the first experiment is shown in Figure 10.5a. The membrane fouling simulator which received no substrate dosing did not show any development of feed channel pressure drop. Membrane fouling simulators containing both unmodified and modified samples receiving substrate showed similar increases in feed channel pressure drop over the 10-day study. The membrane fouling simulator containing PD-*g*-PEG modified membranes and feed spacers showed a higher initial feed channel pressure drop at the experiment outset; evaluation of the pressure drop development as a percentage of initial feed channel pressure drop (Figure 10.5b) shows similar trends for all membrane fouling simulators, regardless of whether the contained samples were modified or unmodified. ATP and TOC concentrations in biomass after ten days of monitor operation are shown in Figures 10.5c and 10.5d, respectively. With substrate dosage, unmodified, polydopamine-modified and PD-*g*-PEG modified samples showed similar ATP and TOC concentrations, but all samples receiving substrate showed ATP and TOC concentrations orders of magnitude higher than the samples which received no substrate and, therefore, did not grow biofilm. PD and PD-*g*-PEG modifications to the membranes and feed spacers did not inhibit biofouling.

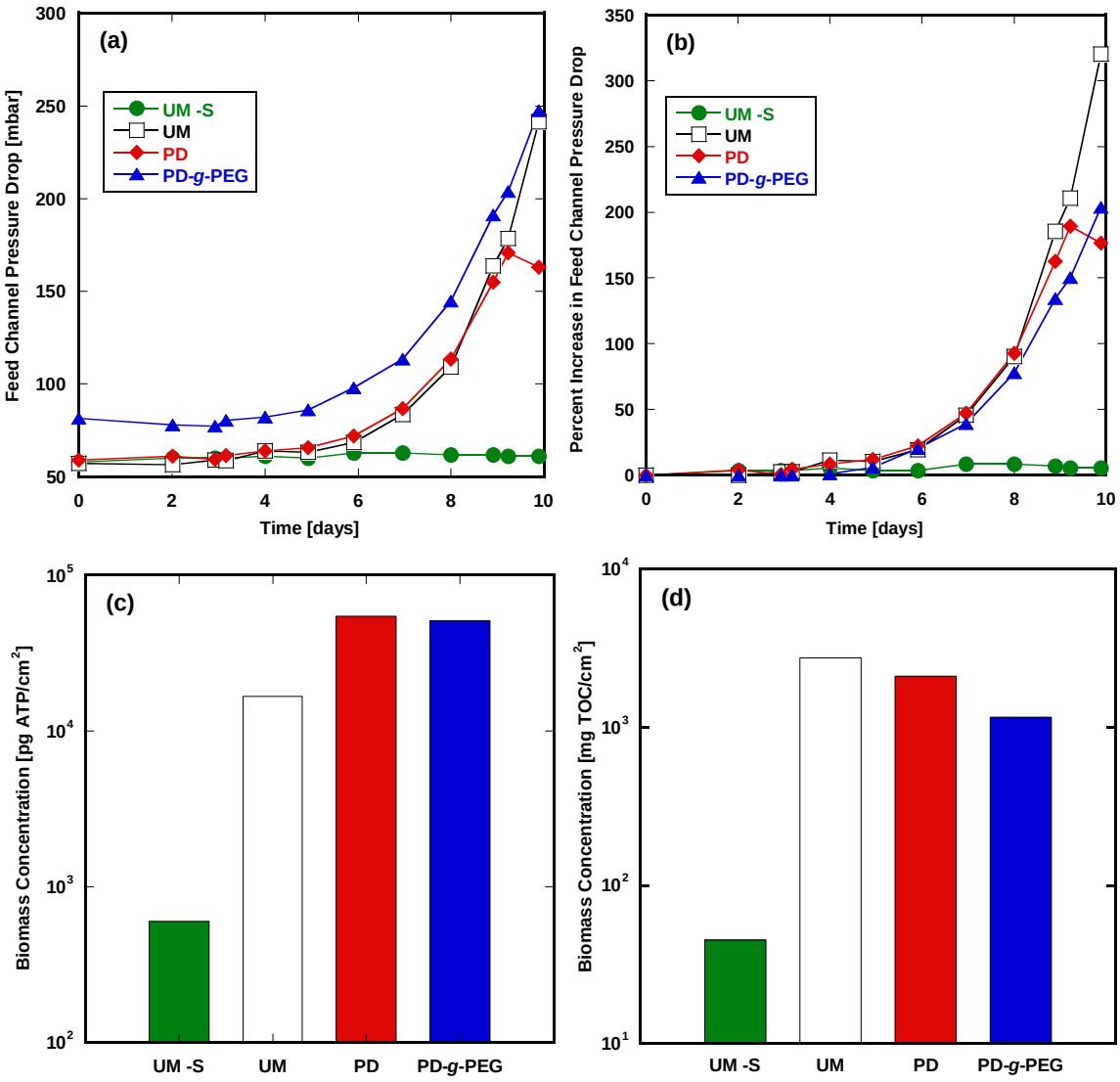

Figure 10.5. (a) Feed channel pressure drop increase, (b) percent increase in feed channel pressure drop, (c) ATP concentration, and (d) TOC concentration of the MFS study performed at 12°C with *in-situ* coated membranes and feed spacers. UM –S = unmodified membrane and feed spacer, no substrate dosage; UM = unmodified membrane and feed spacer, with substrate dosage; PD = polydopamine modified membrane and feed spacer; PD-*g*-PEG = polydopamine-*g*-PEG modified membrane and feed spacer.

To accelerate biofilm growth, feed water temperature was elevated to 20°C in the second biofouling experiment. Membranes and feed spacers were again modified *in situ*. Feed channel pressure drops, which reached 500 mbar after about four days, are plotted in Figure 10.6a and are shown as a percentage of their initial value in Figure 10.6b. As in the first experiment, PD and PD-*g*-PEG coatings had little impact on feed channel pressure drop increase. ATP and TOC concentrations are given in Figures 10.6c and 10.6d, respectively. Unmodified and modified membrane samples receiving substrate dosing all showed similar ATP and TOC levels; the membrane fouling simulator which did not receive substrate dosing yielded markedly lower ATP and TOC concentrations. At the higher temperature of the second experiment, biofouling was not inhibited by PD or by PD-*g*-PEG modifications.

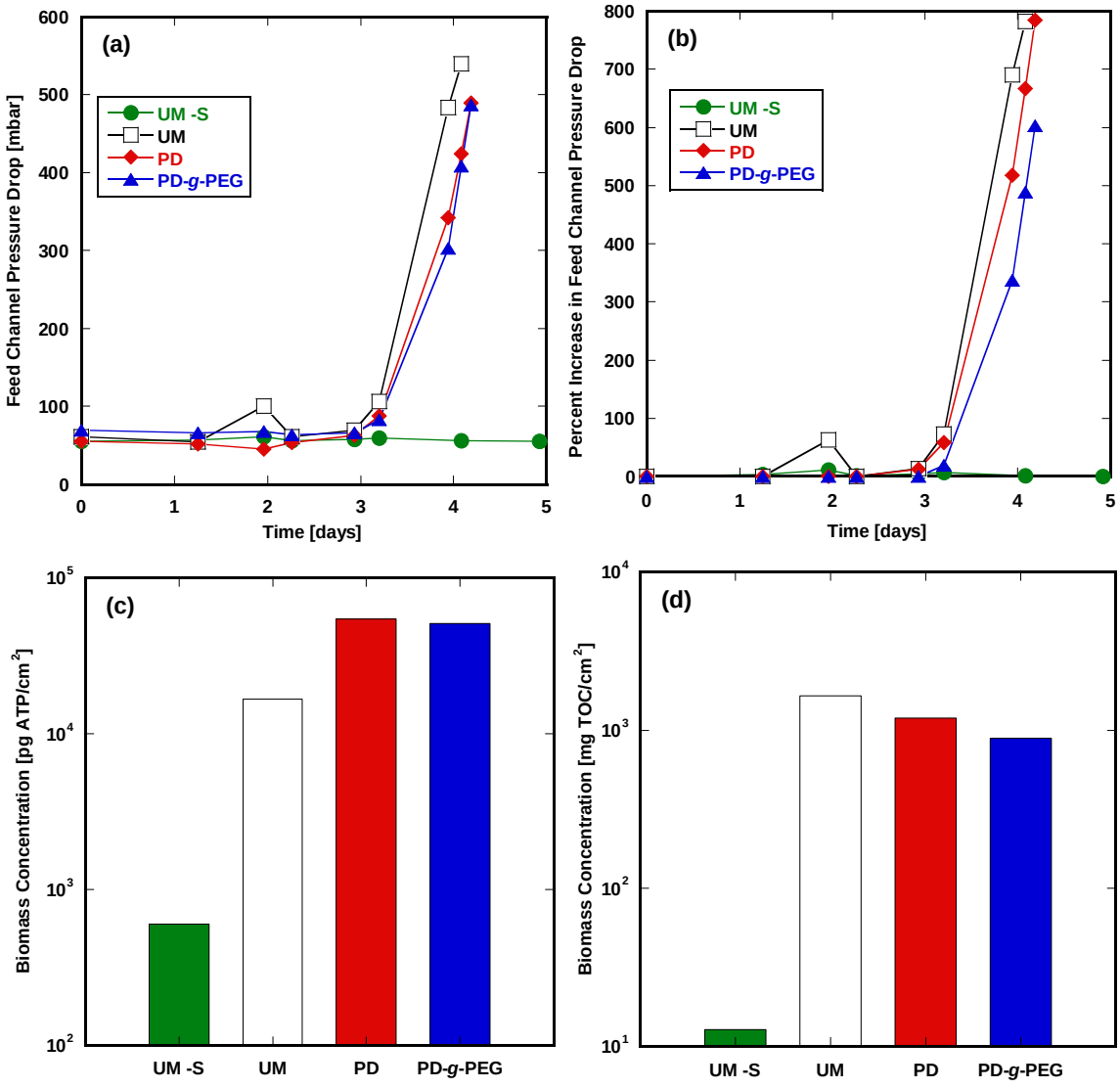

Figure 10.6. (a) Feed channel pressure drop increase, (b) percent increase in feed channel pressure drop, (c) ATP concentration, and (d) TOC concentration of the MFS study performed at 20°C with *in-situ* coated membranes and feed spacers. UM –S = unmodified membrane and feed spacer, no substrate dosage; UM = unmodified membrane and feed spacer, with substrate dosage; PD = polydopamine modified membrane and feed spacer; PD-*g*-PEG = polydopamine-*g*-PEG modified membrane and feed spacer.

For the third set of experiments, membrane and feed spacer samples were modified *ex situ* and the feed water temperature was controlled at 20°C. Modifying the membranes and feed spacers separately before membrane fouling simulator assembly ensures that the surface of each is fully coated, eliminating the possibility that insufficient coating coverage where the spacer and the membrane make contact permitted microbial attachment and growth. Previous studies revealed the onset of biofilm growth occurs in the crevices of feed spacers near the membrane surface where feed water stagnates, promoting microbial attachment [18]. Feed channel pressure drops are plotted in Figure 10.7a and are shown as a percentage of their initial value in Figure 10.7b. As in the first and second biofouling experiments, PD and PD-*g*-PEG coatings had no observable impact on feed channel pressure drop increase. ATP and TOC concentrations, shown in Figures 10.7c and 10.7d, respectively, were again in the same order of magnitude for unmodified and modified membranes receiving substrate dosing, but were much higher than the values of the negative control which did not receive substrate dosing. The PD and PD-*g*-PEG modifications applied to membranes and feed spacers *ex situ* did not inhibit biofouling.

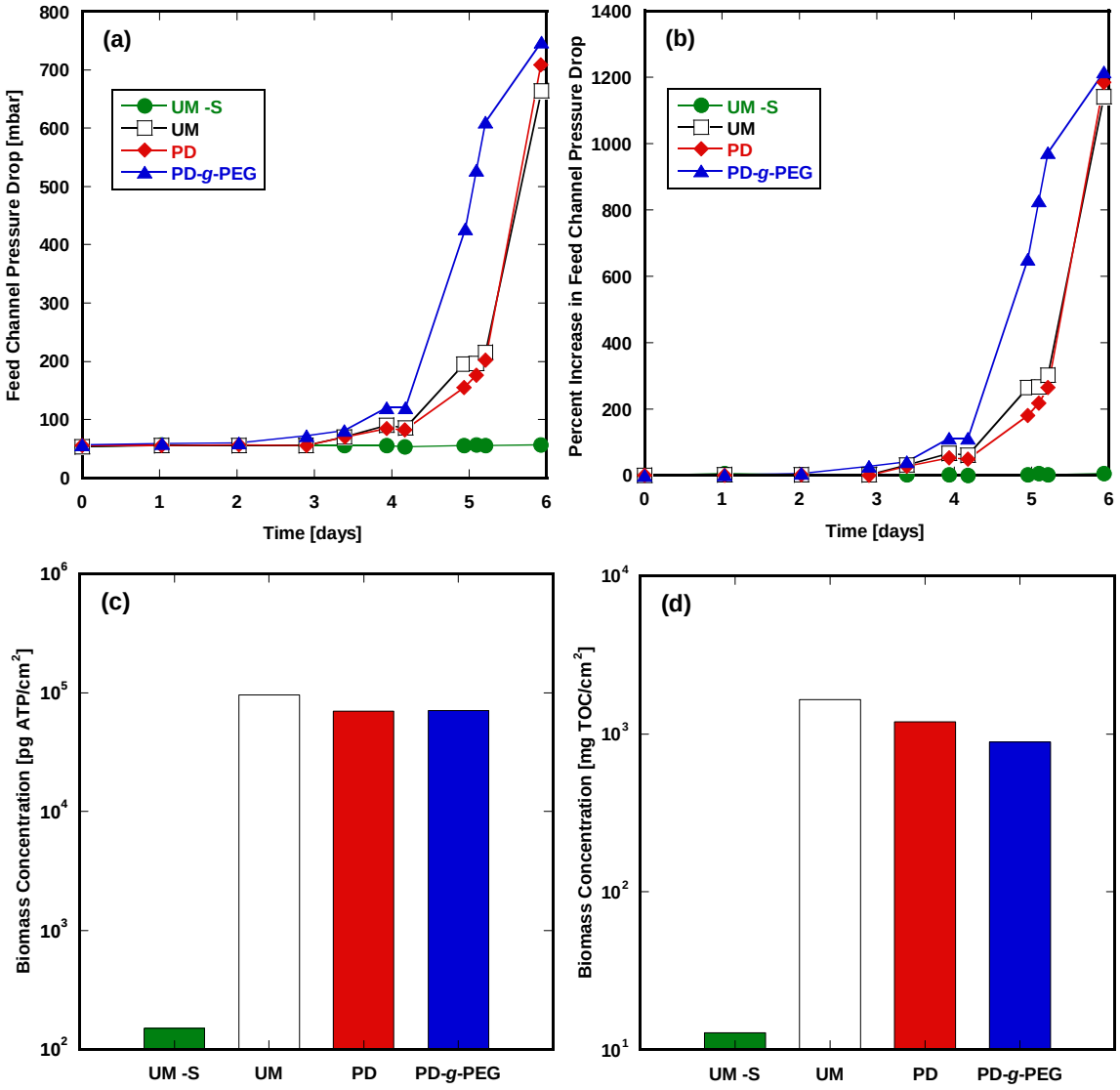

Figure 10.7. (a) Feed channel pressure drop increase, (b) percent increase in feed channel pressure drop, (c) ATP concentration, and (d) TOC concentration of the MFS study performed at 20°C with *ex-situ* coated membranes and feed spacers. UM –S = unmodified membrane and feed spacer, no substrate dosage; UM = unmodified membrane and feed spacer, with substrate dosage; PD = PD modified membrane and feed spacer; PD-*g*-PEG = polydopamine-*g*-PEG modified membrane and feed spacer.

10.4 DISCUSSION

10.4.1 Hydrophilic coatings do not limit biofouling

Surface hydrophilicity is considered a major determinant of membrane fouling propensity [20]. Hydrophilic surfaces attract a strongly-bound water layer which acts as a buffer, minimizing direct foulant-surface interaction and discouraging hydrophobic-hydrophobic interactions [21]. A thin coating of PD is able to impart a dramatic increase in hydrophilicity on a variety of surfaces. Additionally, PEG may be grafted to PD modified surfaces to further increase hydrophilicity. Many membranes have shown improved oily water fouling resistance when modified with PD and PD-*g*-PEG [22]. Hydrophilic materials, especially PEG, are often resistant to protein adhesion [23]. Materials resistant to protein adhesion are likely also resistant to bacteria adhesion [3].

In this study, the hydrophilic PD and PD-*g*-PEG coatings did not limit biofouling. Regardless of feed water temperature (12°C or 20°C) or modification technique (*in situ* or *ex situ*), membrane fouling simulators containing surface-modified membranes and feed spacers showed behavior similar to those containing unmodified samples. All samples which received substrate accumulated biofouling to a much greater extent than the negative controls which received no substrate dosing. The hydrophilic coatings were not able to suppress proliferation of the biofilm and the membrane fouling simulator with modified membranes and feed spacers foul as severely as those containing unmodified samples. Comparisons of hydrophilized, surface-modified membranes to their hydrophobic, native counterparts are scarce in the literature. Xu *et al.*, however, provide a report of biofouling in pilot-scale nanofiltration and reverse osmosis membranes of varying hydrophilicities. They concluded that membrane surface characteristics influence membrane fouling behavior during early stages of operation, but all membranes, regardless of surface hydrophilicity, experienced biofouling over the total

duration of the study [24]. This report reinforces our finding that short-term indicators of membrane fouling are not indicative of long-term performance.

10.4.2 Short-term protein and bacteria adhesion are not indicative of biofouling propensity

As discussed in section 10.2, a number of authors use short-term experiments to asses the biofouling propensity of membranes. To evaluate short-term experiments as a metric of long-term membrane biofouling, two experimental approaches were explored during this study: static protein and bacterial adhesion to the membrane surface over one hour and biofilm growth in a crossflow channel containing a feed spacer over several days. The two methodologies yielded dissimilar results. During short-term static adhesion tests, the PD and PD-*g*-PEG coatings showed remarkable efficacy in reducing attachment of BSA and of *P. aeruginosa*. However, during longer biofouling studies, under flow conditions representative of membrane modules and with substrate dosing, the coatings failed to inhibit biofouling.

Short-term tests of protein and/or cell adhesion to membranes do not predict ultimate membrane biofouling behavior. The membrane fouling simulator has, in previous studies, been shown to successfully mimic biofouling in full-size modules [17]. The adhesion tests, however, fail to reproduce several conditions relevant to biofilm growth in modules. First, the short duration of the adhesion tests means that the microbes are not able to proliferate to any appreciable extent. Low adhesion at short times may have little bearing on ultimate biofilm growth—even a few adhered organisms may generate a biofilm. Gjaletema *et al*. modified glass beads to reduce early adhesion by an order of magnitude, but biofilms grew from even these small adherent populations [6]. Second, the feed to the membrane fouling simulators and to industrial modules is typically not comprised of a single organism or protein; instead, these feeds often contain

complex flora [25]. Although both BSA and *P. aeruginosa* represent widely-accepted laboratory models of globular proteins and bacteria, respectively, other organic molecules, organisms, or mixtures of organisms may enhance biofilm growth through synergistic relationships. Tang and co-workers showed that microbes isolated from biofilms growing on UF and nanofiltration membranes in a dairy processing plant failed to grow a biofilm when tested from pure culture [26]. Finally, the membrane fouling simulator provides a turbulent hydrodynamic environment near the membrane surface by inclusion of feed spacer in continuous crossflow. While the spacer creates regions of high shear near the membrane, which reduces bacterial adhesion [27,28], it also creates stagnation points where fluid velocities are low and bacteria may more easily adhere. Indeed, biofilm growth has been observed to originate from the junctions of fibers comprising the feed spacers [17]. Once the biofilm is established, the turbulence created by the spacer is of little consequence; in fact, the high shear forces tend to select for organisms which can withstand them and mechanically robust biofilms proliferate as described by Flemming [2]. Combined with the constant stream of nutrients provided by the feed water, considered to be one of the most important promoters of biofilm development [2], the continuous-flow environment of the membrane module is likely more hospitable to long-term biofilm growth and biofouling than the quiescent water of the static adhesion test.

10.5 REFERENCES

[1] H.-C. Flemming, G. Schaule, Biofouling on Membranes - A Microbiological Approach, Desalination 70 (1-3) (1988) 95–119.

[2] H.-C. Flemming, Biofouling in water systems--cases, causes and countermeasures, Applied Microbiology and Biotechnology 59 (6) (2002) 629–40.

[3] R.G. Chapman, E. Ostuni, M.N. Liang, G. Meluleni, E. Kim, L. Yan, et al., Polymeric Thin Films That Resist the Adsorption of Proteins and the Adhesion of Bacteria, Langmuir 17 (4) (2001) 1225–1233.

[4] M.C.M. van Loosdrecht, J. Lyklema, W. Norde, A.J.B. Zehnder, Influence of Interfaces on Microbial Activity, Microbiological Reviews 54 (1) (1990) 75–87.

[5] L.C. Simões, M. Simões, M.J. Vieira, Adhesion and biofilm formation on polystyrene by drinking water-isolated bacteria, Antonie Van Leeuwenhoek 98 (3) (2010) 317–29.

[6] A. Gjaltema, N. van der Marel, M.C.M. van Loosdrecht, J.J. Heijnen, Adhesion and Biofilm Development on Suspended Carriers in Airlift Reactors: Hydrodynamic Conditions versus Surface Characteristics, Biotechnology and Bioengineering 55 (6) (1997) 880–9.

[7] M.R. Nejadnik, H.C. van der Mei, W. Norde, H.J. Busscher, Bacterial adhesion and growth on a polymer brush-coating, Biomaterials 29 (30) (2008) 4117–21.

[8] H.F. Ridgway, M.G. Rigby, D.G. Argo, Adhesion of a Mycobacterium sp. to Cellulose Diacetate Membranes Used in Reverse Osmosis, Applied and Environmental Microbiology 47 (1) (1984) 61–7.

[9] H.F. Ridgway, Microbial Adhesion and Biofouling of Reverse Osmosis Membranes, Chemical Industries 35 (1988) 429–481.

[10] H.F. Ridgway, M.G. Rigby, D.G. Argo, Bacterial Adhesion and Fouling of Reverse Osmosis Membranes, Journal of the American Water Works Association 77 (7) (1985) 97–106.

[11] A. Pompilio, R. Piccolomini, C. Picciani, D. D'Antonio, V. Savini, G. Di Bonaventura, Factors associated with adherence to and biofilm formation on polystyrene by Stenotrophomonas maltophilia: the role of cell surface hydrophobicity and motility, FEMS Microbiology Letters 287 (1) (2008) 41–7.

[12] G. Chen, D.E. Beving, R.S. Bedi, Y.S. Yan, S.L. Walker, Initial Bacterial Deposition on Bare and Zeolite-Coated Aluminum Alloy and Stainless Steel, Langmuir 25 (3) (2009) 1620–6.

[13] A. Adout, S. Kang, A. Asatekin, A.M. Mayes, M. Elimelech, Ultrafiltration Membranes Incorporating Amphiphilic Comb Copolymer Additives Prevent Irreversible Adhesion of Bacteria, Environmental Science & Technology 44 (7) (2010) 2406–11.

[14] R. Bernstein, S. Belfer, V. Freger, Bacterial Attachment to RO Membranes Surface-Modified by Concentration-Polarization-Enhanced Graft Polymerization, Environmental Science & Technology 45 (14) (2011) 5973–80.

[15] Y.-F. Yang, H.-Q. Hu, Y. Li, L.-S. Wan, Z.-K. Xu, Membrane surface with antibacterial property by grafting polycation, Journal of Membrane Science 376 (1-2) (2011) 132–141.

[16] H. Basri, A.F. Ismail, M. Aziz, Microstructure and anti-adhesion properties of PES/TAP/Ag hybrid ultrafiltration membrane, Desalination 287 (2012) 71–77.

[17] J.S. Vrouwenvelder, J.A.M. van Paassen, L.P. Wessels, A.F. van Dam, S.M. Bakker, The Membrane Fouling Simulator: A practical tool for fouling prediction and control, Journal of Membrane Science 281 (1-2) (2006) 316–324.

[18] J.S. Vrouwenvelder, S.M. Bakker, L.P. Wessels, J.A.M. van Paassen, The Membrane Fouling Simulator as a new tool for biofouling control of spiral-wound membranes, Desalination 204 (1-3) (2007) 170–174.

[19] J.S. Vrouwenvelder, D.A. Graf von der Schulenburg, J.C. Kruithof, M.L. Johns, M.C.M. van Loosdrecht, Biofouling of spiral-wound nanofiltration and reverse osmosis membranes: A feed spacer problem, Water Research 43 (3) (2009) 583–94.

[20] G.M. Geise, H.-S. Lee, D.J. Miller, B.D. Freeman, J.E. McGrath, D.R. Paul, Water Purification by Membranes: The Role of Polymer Science, Journal of Polymer Science Part B: Polymer Physics 48 (15) (2010) 1685–1718.

[21] E.M. Vrijenhoek, S. Hong, M. Elimelech, Influence of membrane surface properties on initial rate of colloidal fouling of reverse osmosis and nanofiltration membranes, Journal of Membrane Science 188 (1) (2001) 115–128.

[22] B.D. McCloskey, H.B. Park, H. Ju, B.W. Rowe, D.J. Miller, B.D. Freeman, A Bioinspired Fouling-Resistant Surface Modification for Water Purification Membranes, Journal of Membrane Science 413-414 (2012) 82–90.

[23] M. Zhou, H. Liu, J.E. Kilduff, R. Langer, D.G. Anderson, G. Belfort, High Throughput Synthesis and Screening of New Protein Resistant Surfaces for Membrane Filtration, AIChE Journal 56 (7) (2009) 1932–1945.

[24] P. Xu, C. Bellona, J.E. Drewes, Fouling of nanofiltration and reverse osmosis membranes during municipal wastewater reclamation: Membrane autopsy results from pilot-scale investigations, Journal of Membrane Science 353 (1-2) (2010) 111–121.

[25] H.F. Ridgway, C.A. Justice, C. Whittaker, D.G. Argo, B.H. Olson, Biofilm fouling of RO membranes - its nature and effect on treatment of water for reuse, Journal of the American Water Works Association 76 (6) (1984) 94–102.

[26] X. Tang, S.H. Flint, J.D. Brooks, R.J. Bennett, Factors affecting the attachment of micro-organisms isolated from ultrafiltration and reverse osmosis membranes in dairy processing plants, Journal of Applied Microbiology 107 (2) (2009) 443–51.

[27] J.E. Duddridge, C.A. Kent, J.F. Laws, Effect of Surface Shear Stress on the Attachment of Pseudomonas fluorescens to Stainless Steel under Defined Flow Conditions, Biotechnology and Bioengineering 24 (8) (1982) 1930.

[28] Y.L. Lau, D. Liu, Effect of Flow Rate on Biofilm Accumulation in Open Channels, Water Research 27 (3) (1993) 355–360.

Chapter 11: Conclusions and Recommendations

11.1 Conclusions

11.1.1 Polydopamine Structure Determination

Using a broad range of solid-state spectroscopic techniques, the repeat units present in polydopamine, prepared in powder form under aerobic, alkaline conditions, were found to consist primarily of non-covalent interactions. Such a model is in agreement with many previously reported studies on quinhydrones and other similar macromolecules [1–4], but contrasts with some reports proposing covalent bonds between the repeat units in polydopamine [5–8]. Solid-state ^{15}N NMR spectroscopy confirmed the formation of a heterocyclic species, and solid-state CP ^{13}C NMR experiments indicated the presence of protons bound to the aryl core of the polymer. Additionally, powder x-ray diffraction indicated that the monomers formed stacked structures with a d-spacing (3.8 Å) consistent with that observed in other π-stacked materials [9]. Based upon these composite results, polydopamine is not a covalently bound polymer, but it is instead an aggregate of monomers held together by strong, non-covalent forces including charge transfer, π-stacking, and hydrogen bonding. The combination of these non-covalent interactions (all of which have been observed in quinhydrones [1,10,11], which can form similarly robust and insoluble materials) results in high stability and insolubility of polydopamine coatings.

The similarities between dopamine polymerization and that of eumelanins and quinhydrones are of particular interest, and the insights from this study may be of broad applicability and provide a deeper fundamental understanding of the formation mechanism of such materials. Three characteristic steps which govern the formation of eumelanins (synthetic or natural) and quinhydrones are proposed: (1) aerobic oxidation of

phenolic hydroxyls to carbonyls, (2) cyclization of a pendant amine, if one is present, to form a 5-membered α-hydroxyketone (which may then intermolecularly disproportionate to diol and dione intermediates), and (3) polymerization *via* charge transfer, hydrogen bonding, and/or π-π stacking.

11.1.2 Membrane Fouling

A constant flux crossflow fouling apparatus was designed, constructed and successfully used to characterize membrane fouling behavior. The permeate flux was monitored in real time by Coriolis type flow meters and regulated by peristaltic pumps. Feedback control was implemented so that permeate pump speed was continuously adjusted, ensuring rigorously constant flux operation. Such control was critical in fouling studies with aggressive foulants, such as oily water. System accuracy was validated by comparing the pure water permeance of a control membrane to values reported: (1) by the membrane manufacturer, (2) by other researchers in the literature, and (3) measured in dead end filtration in our laboratories. Fouling experiments were performed on polysulfone ultrafiltration (UF) membranes with a soybean oil emulsion foulant and on poly(vinylidene fluoride) microfiltration (MF) membranes with a polystyrene latex bead suspension foulant. Threshold flux determination using a well-known flux stepping technique was facilitated by automatic control of the flux rate. For the polystyrene latex bead suspension, results from a flux stepping experiment were in good agreement with results presented in the literature.

Fouling of PS-20 polysulfone UF membranes by a soybean oil emulsion feed was assessed under constant permeate flux and constant transmembrane pressure (TMP) conditions. The weak form of the critical flux and the threshold flux were determined by flux stepping. Constant flux fouling was performed at fluxes above and below the

threshold flux. Below the threshold flux, modest increases in TMP were observed. Above the threshold flux, fouling was severe, and the TMP rapidly increased. Constant TMP experiments were performed at pressures that produced initial fluxes equal to the fluxes imposed in the constant flux experiments. Regardless of whether the initial flux was above or below the threshold flux, all constant TMP experiments showed qualitatively similar behavior. Constant flux and constant TMP experiments were compared by plotting total resistance as a function of permeate volume per unit membrane area, V/A. At (initial) fluxes below the threshold flux, the resistances as a function of V/A in both modes of operation were indistinguishable within experimental error. Above the threshold flux, the constant TMP resistance rose initially but reached a plateau with V/A because the flux fell rapidly to a value below the threshold flux and fouling lessened in severity. The resistance during constant flux fouling rose to the same value at which the constant TMP resistance reached a plateau, but thereafter rapidly increased. Organic rejection decreased with increasing initial flux (increasing TMP) in constant TMP experiments, probably due to enhanced concentration polarization at high transmembrane pressures. Similarly, the organic rejection decreased with increasing flux during constant flux filtration at fluxes below the threshold flux. Above the threshold flux, organic rejection increased, likely due to restricted permeation through substantial foulant accumulated on the membrane surface.

PS-20 UF membranes were modified with polydopamine (PD) and polydopamine-*g*-poly(ethylene glycol) (PD-*g*-PEG) hydrophilic coatings. The fouling behavior of the modified membranes was compared to that of an unmodified membrane when challenged with a soybean oil emulsion under constant flux filtration at six different fluxes. The threshold flux was determined for the unmodified and modified membranes by flux stepping. The results of constant flux studies were used to verify the

threshold fluxes obtained from flux stepping experiments. For all three membranes, at fluxes below the threshold flux, membranes showed a brief increase in TMP at the start of fouling, but thereafter, a very slow TMP increase at large permeated volumes. Above the threshold flux, membranes generally showed a characteristic concave up increase in TMP, indicating a rapid rate of fouling. At fluxes below the threshold flux, unmodified membranes showed the lowest TMP during fouling. PD and PD-*g*-PEG modified membranes exhibited TMP's higher than that of the unmodified membrane, likely due to the decreased permeance resulting from the application of the surface modifications on the membrane surface and within its porous structure. At fluxes higher than the threshold flux, the modified membranes initially exhibited TMP's greater than that of the unmodified membrane, but rapid fouling of the unmodified membrane typically resulted in the modified membranes having lower TMP's than the unmodified membrane as fouling progressed.

Modified membranes were also compared to unmodified membranes with similar initial permeance. PS-10, a polysulfone UF membrane with a smaller pore size than PS-20, was used. The polydopamine modification time of the PS-20 membrane was increased so that the permeance of the PD and PD-*g*-PEG modified PS-20 membranes were similar. In this scenario, where all three membranes had similar pure water permeances, the TMP of the unmodified PS-10 membrane was significantly higher than that of the PD and PD-*g*-PEG modified PS-20 membranes, which exhibited very similar behavior. When the membranes had the same initial permeance and, therefore, the same local flux through the pores at the start of fouling, the hydrophilic surface modification effectively mitigated fouling. The particular nature of the surface modification, either a conformal coating or grafted brushes, did not measurably impact the observed fouling behavior.

Polydopamine was used to modify commercial UF and reverse osmosis (RO) membrane modules. UF modules were further modified by grafting PEG to the polydopamine coating. Modified and unmodified modules were employed in a pilot study where they were challenged with flowback water from hydraulic fracturing operations in the Barnett shale gas basin. Modified UF membranes showed improved flux and decreased TMP and, therefore, higher permeances than their unmodified counterparts. Furthermore, both modified and unmodified UF modules were cleaned regularly with mild chemical cleaning regimens (either mildly basic hot water or caustic hot water followed by citric acid). Both the modified and unmodified modules showed enhanced flux recovery after cleaning, but the modified membranes maintained a performance advantage throughout the pilot test. The PD modified RO modules did not show enhanced flux or depressed TMP relative to the unmodified modules, likely due to the cleanliness of the RO feed after UF pretreatment and the relatively short duration (~100 hours) of the pilot test. Salt rejection, however, was both higher and more stable in the modified modules than in the unmodified modules, perhaps due in part to caulking of minor defects in the thin polyamide separation layer by polydopamine. Previous studies on polydopamine membrane coatings focused on laboratory-scale experiments, but the pilot study demonstrated that polydopamine and PEG can be employed in the modification of industrial membrane modules; the modifications improved the fouling behavior of those modules when challenged with complex, highly-fouling feedwater. PD and PD-*g*-PEG modifications can improve the quantity and quality of permeate from membrane-based industrial water purification.

Finally, the effect of PD and PD-*g*-PEG modifications on biofouling was assessed in short-term, static adhesion tests and in long-term biofilm growth tests under hydrodynamic conditions similar to those encountered in membrane modules. PD and

PD-*g*-PEG modified PS-20 polysulfone UF membranes showed significantly decreased adhesion of bovine serum albumin and *P. aeruginosa* during one-hour static adhesion tests. However, during biofouling studies where feed spacers and membranes were exposed to substrate-doped feedwater in membrane fouling simulators, PD and PD-*g*-PEG surface modifications did not noticeably inhibit biofouling. Short-term membrane surface adhesion tests were not suitable predictors of membrane module biofouling potential. While PD and PD-*g*-PEG coatings have improved the membrane performance when challenged with other foulants [12], such as emulsified soybean oil, the biofouling study demonstrated that PD and PD-*g*-PEG coatings considered were not able to effectively control biofouling. Unlike foulants accumulating on membrane surfaces due to exposure to emulsified oil, biofilms are comprised of diverse communities of living microorganisms. Although the initial adhesion of microbes may be reduced by hydrophilic surface modifications, the ability of microbes to rapidly reproduce and form synergistic communities makes biofouling prevention difficult.

11.2 RECOMMENDATIONS

Constant flux fouling studies comparing PD and PD-*g*-PEG modified membranes to unmodified membranes demonstrated that, at fluxes below the threshold flux, the modified membrane may show a higher TMP than the unmodified membrane due to the additional mass transfer resistance imposed by the modification. Previous work has demonstrated the possibility of varying the polydopamine thickness, and therefore the membrane permeance, by adjusting the deposition conditions, such as the deposition time or dopamine solution concentration [13,14]. The PEG molecular weight or PEG grafting density may also be varied to adjust the permeance [13]. All of the modifications performed on samples used in constant flux fouling studies were prepared using the same

polydopamine and PEG modification conditions, so a reasonable next course of study would be to evaluate the effect of systematically changing these conditions. Because the polydopamine coating can be made extraordinarily thin and still maintain its hydrophilic character [13], a thin coating may confer the desired hydrophilicity while only negligibly increasing the overall membrane mass transfer resistance.

Previous studies on PD and PD-*g*-PEG modified membranes have been performed using constant TMP crossflow fouling [12]; these studies clearly demonstrated the improved flux of modified membranes relative to unmodified membranes. With the increased resistance of the modified membranes, however, the initial flux of the modified membrane is lower than that of an unmodified membrane if both are operated at the same TMP. Constant TMP experiments operated in this way, therefore, favor the modified membrane, perhaps because the rate of fouling at the start of the experiment (when the fouling is most severe) will be lower for the modified membrane than for the unmodified membrane. Likewise, constant flux experiments tend to favor the unmodified membrane if both are operated at the same overall flux, since the increased resistance of the modified membrane also increases the local flux through its pores relative to the unmodified membrane, resulting in their more rapid blockage. Two intermediate fouling experiments should be performed: (1) constant TMP where modified and unmodified membranes are operated different TMP's such that they have the same *initial flux*, and (2) constant flux where modified and unmodified membranes are operated at different fluxes such that they have the same *initial TMP*. It is hypothesized that, in the proposed constant TMP experiment (1), the modified membrane may not show the dramatic improvement over the unmodified membrane previously reported [12], and in the proposed constant flux experiment (2), the modified membrane may not show the dramatic disadvantage relative to the unmodified membrane reported in Chapter 8.

Furthermore, the results of the constant flux fouling studies described in Chapter 8 suggest that it is imperative to marry membrane design with the development of surface modifications for fouling resistance. When fouling results from a modified PS-20 UF membrane were compared with those from an unmodified PS-20 UF membrane, the modified membrane exhibited higher TMP values than the unmodified membrane at fluxes below the threshold flux. Although many factors are used to determine the most desirable flux for prolonged industrial operation (the "sustainable flux" [15]), operation below the threshold flux typically leads to operation that can be maintained with periodic cleaning [15]. Therefore, operation at fluxes below the threshold flux is likely to be of greatest practical interest. When the modified PS-20 UF membrane was compared to an unmodified PS-10 membrane with a similar initial resistance, however, the benefit of the hydrophilic surface modification was clear, even at fluxes well below the threshold flux. Therefore, a reasonable way to develop fouling-resistant membranes is to begin with a membrane with larger pores than required for the particular application and modify its surface to produce the desired permeance.

Laboratory fouling studies were carried out under a variety of conditions, including constant flux at several different fluxes and constant TMP at several different transmembrane pressures. Similar resistance development was observed in the constant flux and constant TMP experiments under some conditions. In this study, some insight was gained into fouling mechanisms by the shape of the TMP profiles obtained during constant flux fouling (Chapters 7 and 8). The observed behavior was not, however, mathematically modeled. Well-known models for the flux decline in dead-end [16] and crossflow [17] constant pressure filtration have been developed and successfully used to model fouling phenomena. In light of the similarity of resistance development at fluxes less than the threshold flux in constant TMP and constant flux crossflow experiments, it

would be of significant interest to determine the applicability of existent models to constant flux fouling. Ultimately, such models may enable the prediction of fouling behavior or provide insight into optimal conditions under which membranes may be sustainably operated. Models may also reveal fouling mechanisms (cake filtration, complete blocking, intermediate blocking).

Laboratory fouling studies were carried out with exclusively with a soybean oil emulsion because emulsified oils are a common component of industrial wastewater [18]. The pilot study was performed to assess the performance of polydopamine-modified membranes when challenged with realistic industrial feedwaters. However, the extension of laboratory studies to other foulants may provide fundamental insight into membrane fouling behavior when challenged with other foulants that may be of interest in other applications. Suggested foulants include other oils, mixtures of oils, latex beads, silica particles, and proteins.

While the PD and PD-*g*-PEG coatings were capable of improving the fouling performance of membranes filtering emulsified oil and hydraulic fracturing flowback water, the coatings did not appear to mitigate biofouling in the tested conducted within the scope of this thesis. If biofouling cannot realistically be prevented in membrane modules, removal *via* cleaning protocols is the only means of reducing biofilm impact on membrane performance. Although the hydrophilic coatings employed here did not appreciably reduce biofouling, they may facilitate cleaning, enabling greater recovery of membrane performance. A study of feed channel pressure drop recovery (in membrane fouling simulators) after cleaning should be pursued on modified and unmodified membranes and feed spacers. Additionally, although the presence or absence of permeate production does not affect the observed feed channel pressure drop, the hydrophilic coatings may impact changes in flux and rejection with biofouling development.

Biofilms may adopt different architectures on modified and unmodified membranes and feed spacers; impact of the surface modification on flux decline and rejection properties in the presence of biofouling should be investigated.

The pilot study demonstrated that the PD-*g*-PEG modification improves the permeance of UF membranes during fouling when challenged with a complex, highly fouling hydraulic fracturing wastewater feed. The greatest benefit was realized after cleaning, so the surface modification probably facilitates the removal of reversibly adhered foulant. Based on post-operation autopsy, the PD-*g*-PEG coating did not appear to deteriorate during this short pilot study. However, more extensive evaluation of the coating tolerance toward various cleaning regimens for prolonged operational times is warranted. Investigation of coating stability is also important in light of the study proposed above to investigate the effect of cleaning protocols on biofouling. Studies on coating durability could be started at the laboratory level by, for example, measurement of modified membrane permeance in dead end filtration or coating thickness *via* ellipsometry after exposure to various cleaning protocols. Later, tests of pilot-scale modules could be undertaken.

Furthermore, as the coatings constitute addition of organic material to the membrane system, biofilms themselves could cause coating degradation as their constituent microorganisms metabolize the polydopamine and poly(ethylene glycol), potentially exacerbating biofouling. Modified and unmodified membranes/feed spacers could be evaluated without addition of substrate to the feedwater; development of biofilm on the modified membranes/feed spacers without feed water substrate dosage would indicate that microbes are able to use the coatings as nutrient sources.

Finally, the investigation of the polydopamine chemical structure may shed some light on the aggregation and polymerization of families of catecholamines, including the

precursors of such biologically important molecules as melanin. In addition to exploring the fundamental structure and reactivity of this ubiquitous class of biopolymers, the spectroscopic results described herein may lead to new and previously unidentified routes toward optimizing the polymers' properties (*e.g.*, biocidal activity, stability to chemical reagents such as halogens, etc.). For example, dopamine derivatives or other catecholamines functionalized at the 3,6-positions may improve polydopamine's fouling resistant behavior, while retaining the ability of these monomers to be polymerized. Additionally, derivatives of dopamine that have increased numbers of hydrogen bond donors or acceptors, such as DOPA, which bears a pendant carboxylic acid moiety, may improve surface adhesion or resistance to chemical degradation. Importantly, other similar catecholamines or catechol-containing compounds should be investigated to determine if they exhibit similar universal deposition behavior to that of polydopamine and whether they impart similar hydrophilicity and fouling resistant character to substrates onto which they are deposited.

11.3 REFERENCES

[1] A.O. Patil, W.T. Pennington, G.R. Desiraju, D.Y. Curtin, I.C. Paul, Recent Studies on the Formation and Properties of Quinhydrone Complexes, Molecular Crystals and Liquid Crystals 134 (1) (1986) 279–304.

[2] A. V Ragimov, I.I. Ragimov, B.A. Mamedov, S.A. Guseinov, B.I. Liogon'kii, On features of the oligomerization of hydroquinone under auto-oxidation, Polymer Science USSR 24 (10) (1982) 2434–2440.

[3] A. Furlani, M. V Russo, F. Cataldo, Oxidative polymerization of p-benzoquinone and hydroquinone. Conductivity of doped and undoped polymerization products, Synthetic Metals 29 (1) (1989) 507–510.

[4] A. V Ragimov, B.A. Mamedov, B.I. Liogon'kii, The alkali initiated polymerization of p-benzoquinone, Polymer Science USSR 19 (11) (1977) 2922–2928.

[5] H. Lee, S.M. Dellatore, W.M. Miller, P.B. Messersmith, Mussel-Inspired Surface Chemistry for Multifunctional Coatings, Science 318 (5849) (2007) 426–430.

[6] F. Yu, S. Chen, Y. Chen, H. Li, L. Yang, Y. Chen, et al., Experimental and theoretical analysis of polymerization reaction process on the polydopamine membranes and its corrosion protection properties for 304 Stainless Steel, Journal of Molecular Structure 982 (1-3) (2010) 152–161.

[7] X.-B. Yin, D.-Y. Liu, Polydopamine-based permanent coating capillary electrochromatography for auxin determination, Journal of Chromatography A 1212 (1-2) (2008) 130–136.

[8] L. Zhang, J. Shi, Z. Jiang, Y. Jiang, S. Qiao, J. Li, et al., Bioinspired preparation of polydopamine microcapsule for multienzyme system construction, Green Chemistry 13 (2) (2011) 300.

[9] F. Liao, S. Yin, M.F. Toney, V. Subramanian, Physical discrimination of amine vapor mixtures using polythiophene gas sensor arrays, Sensors and Actuators B: Chemical 150 (1) (2010) 254–263.

[10] D. Bijl, H. Kainer, A.C. Rose-Innes, Stabilization of Free Radicals by Adsoption: Detection by Paramagnetic Resonance, Nature 174 (4435) (1954) 830–831.

[11] H.R. Devlin, I.J. Harris, Mechanism of the oxidation of aqueous phenol with dissolved oxygen, Industrial & Engineering Chemistry Fundamentals 23 (4) (1984) 387–392.

[12] B.D. McCloskey, H.B. Park, H. Ju, B.W. Rowe, D.J. Miller, B.D. Freeman, A Bioinspired Fouling-Resistant Surface Modification for Water Purification Membranes, Journal of Membrane Science 413-414 (2012) 82–90.

[13] B.D. McCloskey, H.B. Park, H. Ju, B.W. Rowe, D.J. Miller, B.J. Chun, et al., Influence of Polydopamine Deposition Conditions on Pure Water Flux and Foulant Adhesion Resistance of Reverse Osmosis, Ultrafiltration, and Microfiltration Membranes, Polymer 51 (15) (2010) 3472–3485.

[14] S. Kasemset, A. Lee, D.J. Miller, B.D. Freeman, M.M. Sharma, Effect of Polydopamine Deposition Conditions on Fouling Resistance, Physical Properties, and Permeation Properties of Reverse Osmosis Membranes in Oil/Water Separation, Journal of Membrane Science 425-426 (2013) 208–216.

[15] R.W. Field, G.K. Pearce, Critical, Sustainable and Threshold Fluxes for Membrane Filtration with Water Industry Applications, Advances in Colloid and Interface Science 164 (1-2) (2011) 38–44.

[16] J. Hermia, Constant Pressure Blocking Filtration Laws - Application to Power-law Non-Newtonian Fluids, Transactions of the Institution of Chemical Engineers 60 (3) (1982) 183–187.

[17] R.W. Field, D. Wu, J.A. Howell, B.B. Gupta, Critical Flux Concept for Microfiltration Fouling, Journal of Membrane Science 100 (3) (1995) 259–272.

[18] J. Mueller, Y. Cen, R.H. Davis, Crossflow Microfiltration of Oily Water, Journal of Membrane Science 129 (2) (1997) 221–235.

Appendix: Flux Stepping Experiments for Critical and Threshold Flux Determination

A notable benefit of performing fouling experiments in the constant flux mode is the ability to perform flux stepping experiments, where the flux is gradually increased over several constant flux intervals [1,2]. The transmembrane pressure (TMP) profile is observed over each constant flux step, and several different parameters (calculated from the TMP data) may be used to determine the threshold or critical fluxes [1,3], as described in greater detail in Chapter 7.

Several authors have discussed the effects of changing the step length, step height, and initial flux on the observed critical or threshold flux value [1]. The effect of changing step length is probably the most widely studied. Choi and Dempsey, for example, observed a decrease in critical flux values as the step length was increased from 10 minutes to 20 minutes to 30 minutes in the ultrafiltration (UF) of humic acid [2]. In contrast, Beier and Jonsson observed an increase in the critical flux with increasing step length during the microfiltration of yeast [1]. Le Clech observed a decrease in critical flux value as the step length was increased from 30 minutes to 120 minutes in a membrane bioreactor, but no change in the critical flux at flux step lengths of 10 minutes, 20 minutes, and 30minutes. Similarly, Kwon and Vigneswaran [4] and Guo *et al.* [5] reported no change in the critical flux with variations in the step length. Le Clech found that changing step height had the greatest impact on the determined critical flux [3]. Beier and Jonsson also suggested that larger step heights and greater initial fluxes may contribute to decreased critical flux values [1].

Results of flux stepping experiments for threshold and critical flux determination are shown in Chapters 6, 7, and 8. Here, the effects of step length and initial flux on the

determined threshold flux value are explored. As discussed in Chapter 7, the weak form of the critical flux may be observed at very low fluxes. However, the threshold flux was found to separate the regimes of good and poor agreement between resistance development in constant flux and constant TMP experiments. Furthermore, Field *et al*. suggest that the threshold flux is particularly relevant for industrial operation, as it is the flux at which the rate of fouling increases from relatively slow (where fouling may be controlled with cleaning) to relatively rapid (where fouling impedes sustainable operation) [6]. For these reasons, only the effects on threshold flux will be considered here.

All membranes were Sepro PS-20 polysulfone UF membranes, and the foulant was 1500 ppm soybean oil emulsion (both as described in Chapter 4). Flux stepping experiments were carried out at a feed pressure of 30 psig and a feed flow rate of 0.8 L/min, corresponding to a crossflow velocity of 0.18 m/s. As shown in Chapter 8, all three threshold flux determination parameters (TMP_{avg}, ΔTMP, and d(TMP)/dt) produced identical threshold flux values for the unmodified PS-20 membrane. For brevity, only the TMP_{avg} parameter will be used in this Appendix.

Figure A.1 shows a flux stepping experiment (a) with a step length of 10 minutes, initial flux of 10 $Lm^{-2}h^{-1}$ (LMH), and a step height of 10 LMH. The threshold flux was 65 LMH, as denoted by the vertical dashed arrow in (b).

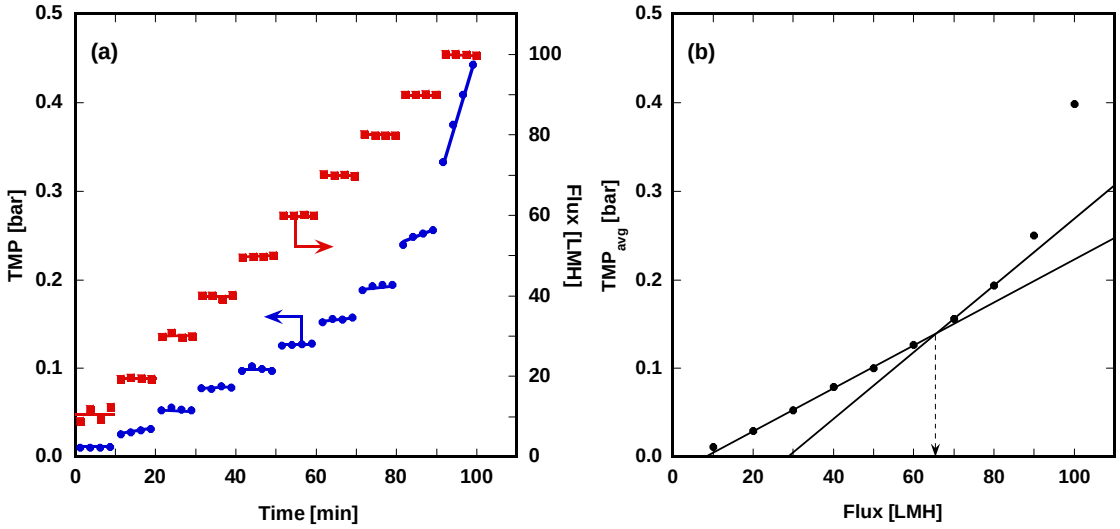

Figure A.1. (a) Flux stepping experiment. Flux step length: 10 min., initial flux: 10 LMH, step height: 10 LMH. (b) Threshold flux determination by TMP_{avg} parameter. Threshold flux = 65 LMH, denoted by vertical dashed arrow.

Figure A.2 presents a flux stepping experiment (a) where the initial flux was increased to 30 LMH, but the step length and step height were maintained at 10 minutes and 10 LMH, respectively. The threshold flux was 68 LMH, as denoted by the vertical dashed arrow in (b).

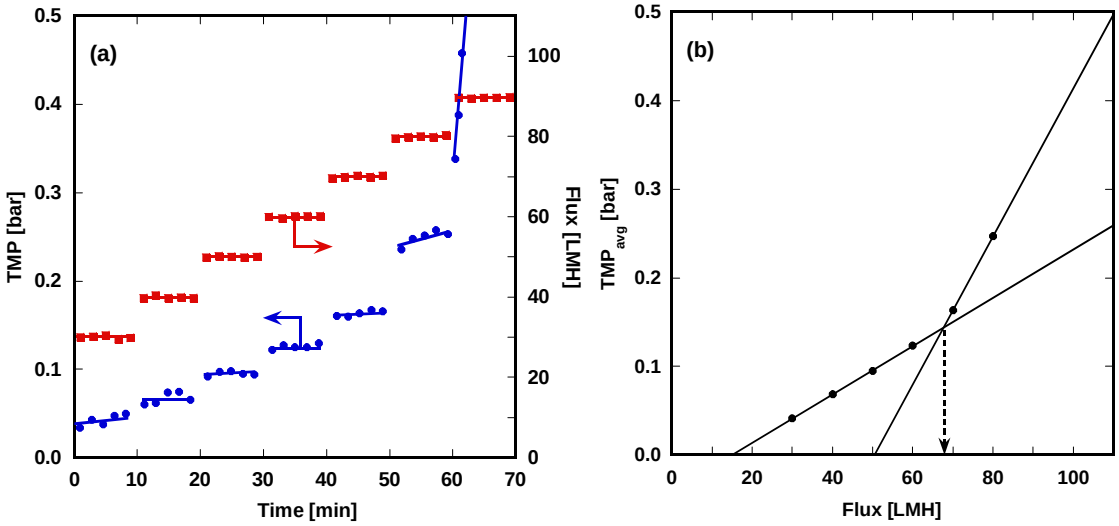

Figure A.2. (a) Flux stepping experiment. Flux step length: 10 min., initial flux: 30 LMH, step height: 10 LMH. (b) Threshold flux determination by TMP_{avg} parameter. Threshold flux = 68 LMH, denoted by vertical dashed arrow. Data also shown in Figure 6.2.

Figure A.3 shows a flux stepping experiment (a) with a step length of 20 minutes, an initial flux of 10 LMH, and a step height of 10 LMH. The threshold flux was 65 LMH, as denoted by the vertical dashed arrow in (b).

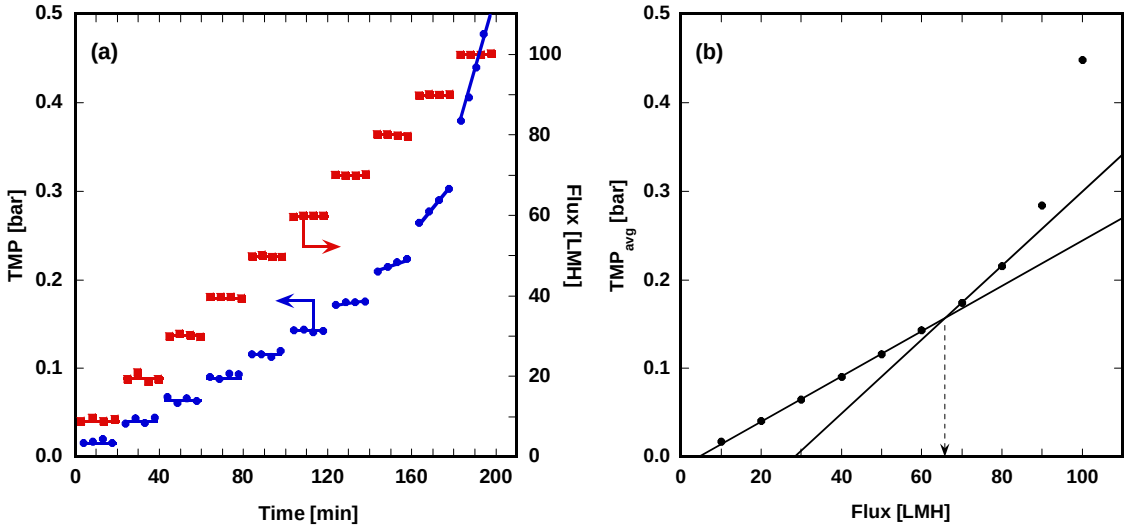

Figure A.3. (a) Flux stepping experiment. Flux step length: 20 min., initial flux: 10 LMH, step height: 10 LMH. (b) Threshold flux determination by TMP_{avg} parameter. Threshold flux = 65 LMH, denoted by vertical dashed arrow. Data also shown in Figure 8.4.

Figure A.4 presents a flux stepping experiment (a) were the step length was 20 minutes, the initial flux was 30 LMH, and the step height was 10 LMH. The threshold flux was 68 LMH, as denoted by the vertical dashed arrow in (b).

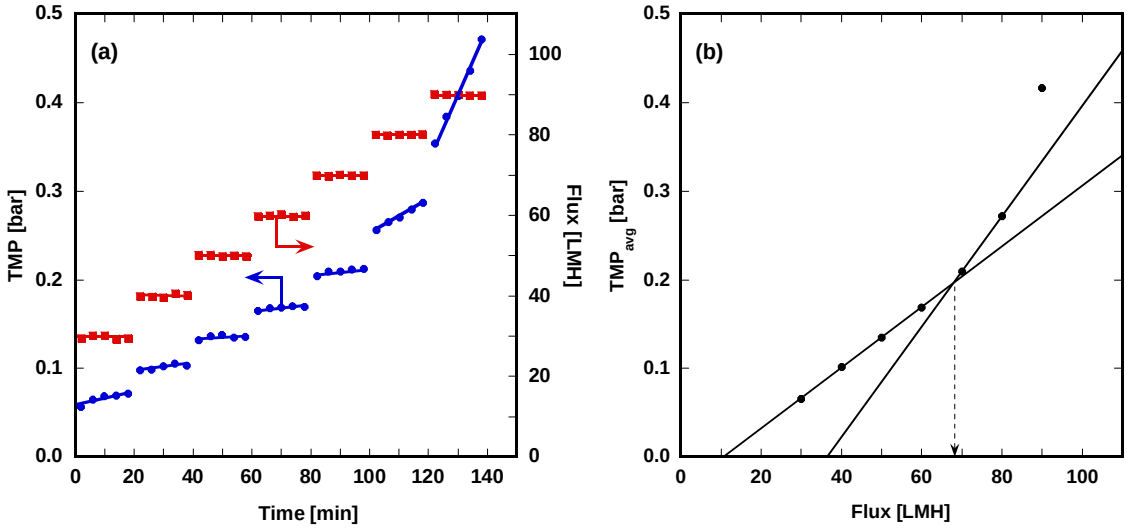

Figure A.4. (a) Flux stepping experiment. Flux step length: 20 min., initial flux: 30 LMH, step height: 10 LMH. (b) Threshold flux determination by TMP_{avg} parameter. Threshold flux = 69 LMH, denoted by vertical dashed arrow.

A summary of the experiments shown in Figures A.1 – A.4 is presented in Table A.1. Increasing the step length from 10 minutes to 20 minutes appears to have no effect on the threshold flux value. The threshold fluxes determined using an initial flux of 30 LMH are slightly higher than those determined using an initial flux of 10 LMH, but the increase of 3-4 LMH is so small as to be of little practical significance.

	Initial Flux	
Step Length	10 LMH	30 LMH
10 min	65 LMH	68 LMH
20 min	65 LMH	69 LMH

Table A.1. Summary of threshold flux values determined by flux stepping protocols with various initial fluxes and step lengths.

To observe the weak form of the critical flux, as described in Chapter 7, a flux stepping experiment was required with at least one step at a flux less than 10 LMH. For this reason, a flux stepping experiment was performed with an initial flux of 5 LMH, a step height of 5 LMH, and a step length of 10 minutes. The results are presented in Figure A.5. As shown in (b), and as described in Section 7.2.1, the weak form of the critical flux (J_{cw}) and the threshold flux (J_t) were apparent by the TMP_{avg}/flux relationship. The threshold flux value decreased slightly to 62 LMH relative to the experiments shown in Table A.1.

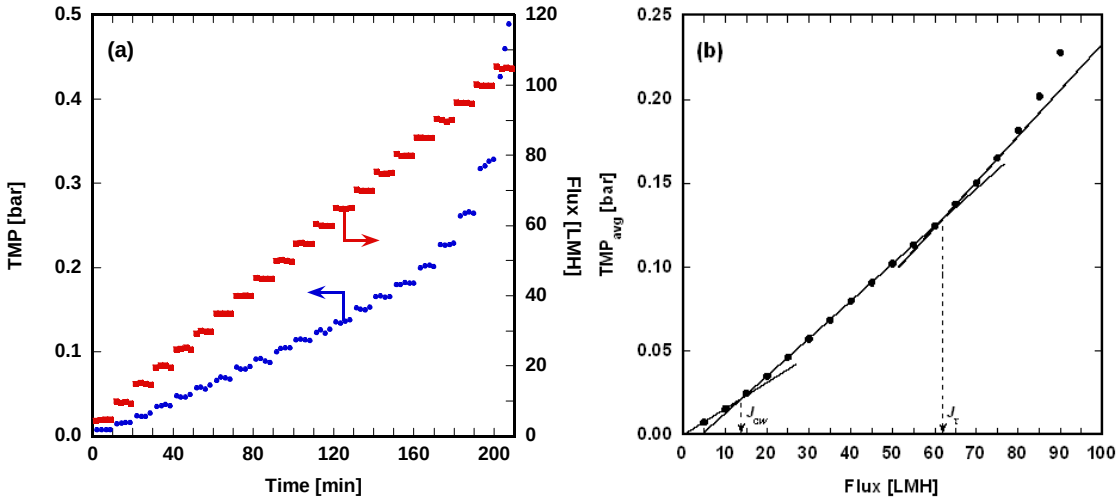

Figure A.5. (a) Flux stepping experiment. Flux step length: 10 min., initial flux: 5 LMH, step height: 5 LMH. (b) The weak form of the critical flux and the threshold flux are both evident by the TMP_{avg} parameter. Weak form of the critical flux = 14 LMH, threshold flux = 62 LMH, denoted by vertical dashed arrows. Data also shown in Figure 7.1.

Several authors have investigated the critical flux for irreversibility by flux stepping experiments wherein the flux is cycled up and down, and hysteresis in TMP is observed [1,7–10]. Here, the cycling method of Espinasse was followed [7]. Results are shown in Figure A.6. The flux cycling experiment is shown in (a). The initial flux was 10 LMH and the step length was 10 minutes. Except for the first step, the flux was periodically stepped up by 20 LMH, then stepped down by 10 LMH to a previous value. The TMP_{avg}/flux relationship is shown in (b). At fluxes where irreversible fouling is not significant, the TMP would return very near its prior value when the flux was stepped down to a previous flux. As the fluxes were gradually increased, hysteresis was observed, as shown in (c). A horizontal dashed line is shown, denoting the relatively stable and near-zero hysteresis levels up to a flux of 70 LMH. At 80 LMH, the hysteresis eclipses that observed at any previous flux. The critical flux for irreversibility was

denoted as 72 LMH. Therefore, the critical flux for irreversibility is slightly higher than the threshold flux for this membrane/foulant pair (62-69 LMH, Figures A.1 – A.5) and significantly higher than the weak form of the critical flux (14 LMH, Figure 7.2). This result suggests that the fouling occurring at fluxes up to a flux of 72 LMH (which includes a significant regime of non-zero fouling above the weak form of the critical flux, 14 – 72 LMH), the fouling is reversible. Bacchin *et al*. suggests that the critical flux for irreversibility may, under some circumstances, be identical to the strong form or weak form of the critical flux [11]. Clearly, such is not the case here, but the critical flux for irreversibility is very near the threshold flux value(s) determined previously. Therefore, the fouling that occurs below the threshold flux (which is slow) may be largely reversible, and irreversible fouling only occurs to a substantial extent above the threshold flux, when the rate of fouling increases significantly [6].

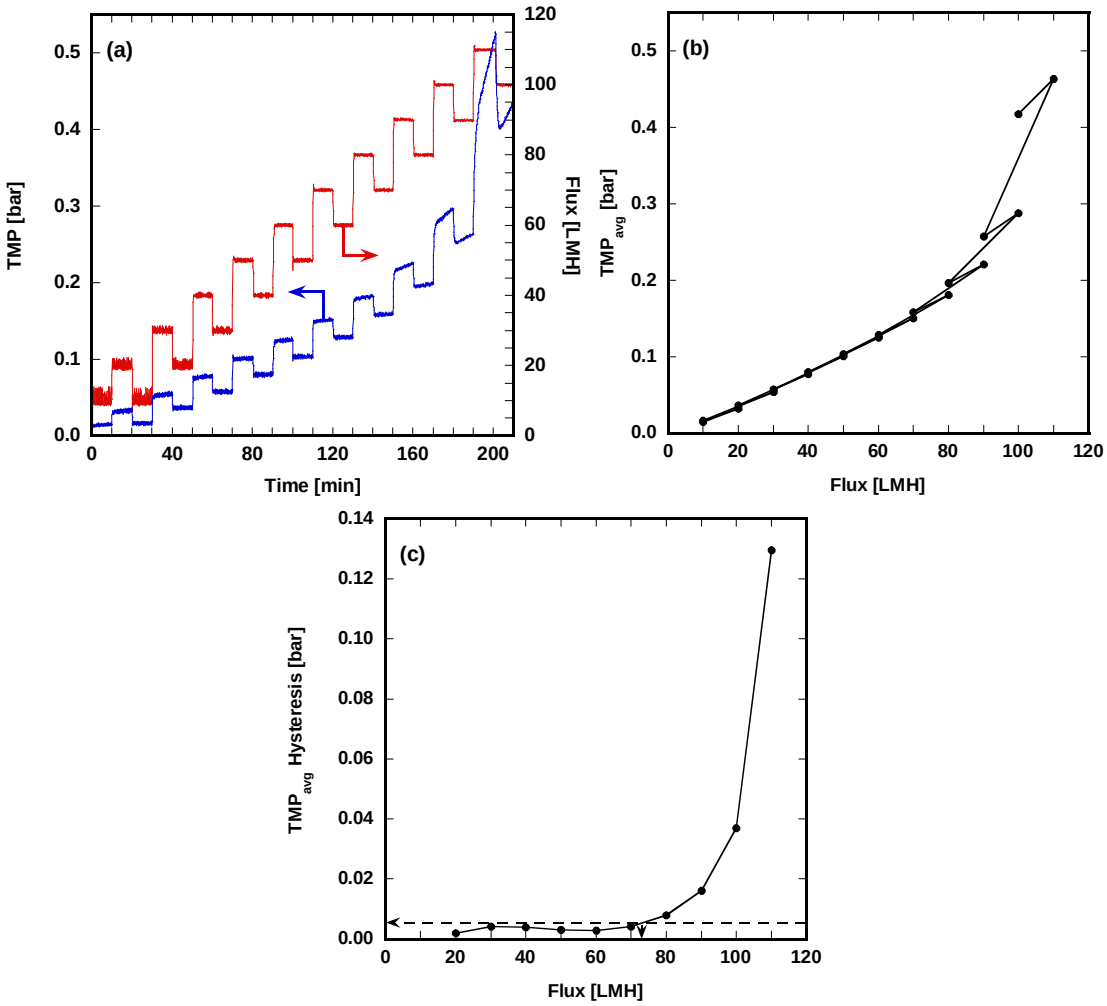

Figure A.6 (a) Flux step up/step down experiment. Flux step length: 10 min., initial flux: 10 LMH, step up height (except first step): 20 LMH, step down height: 10 LMH. Full data shown for clarity. (b) TMP_{avg} as a function of flux. Fluxes Lines connecting data points are shown to indicate flux step pathway. (c) Hysteresis in TMP_{avg} values. Hysteresis values plotted on the vertical axis are the difference in TMP_{avg} values at a flux before and after stepping up to the fluxes shown on the horizontal axis (*e.g.*, the value corresponding to a flux of 20 LMH is the hysteresis observed in TMP_{avg} values at 10 LMH before and after stepping up to a flux of 20 LMH.) The critical flux for irreversibility is denoted by the vertical arrow. Critical flux for irreversibility = 72 LMH.

A.1 REFERENCES

[1] P.S. Beier, G. Jonsson, Critical Flux Determination by Flux-Stepping, AIChE Journal 56 (7) (2010) 1739–1747.

[2] K.Y.-J. Choi, B.A. Dempsey, Bench-scale Evaluation of Critical Flux and TMP in Low-pressure Membrane Filtration, Journal of the American Water Works Association 97 (7) (2005) 134–143.

[3] P. Le Clech, B. Jefferson, I.S. Chang, S.J. Judd, Critical Flux Determination by the Flux-step Method in a Submerged Membrane Bioreactor, Journal of Membrane Science 227 (1-2) (2003) 81–93.

[4] D.Y. Kwon, S. Vigneswaran, Influence of particle size and surface charge on critical flux of crossflow microfiltration, Water Science and Technology 38 (4-5) (1998) 481–488.

[5] W.S. Guo, S. Vigneswaran, H.H. Ngo, Effect of flocculation and/or adsorption as pretreatment on the critical flux of crossflow microfiltration, Desalination 172 (1) (2005) 53–62.

[6] R.W. Field, G.K. Pearce, Critical, Sustainable and Threshold Fluxes for Membrane Filtration with Water Industry Applications, Advances in Colloid and Interface Science 164 (1-2) (2011) 38–44.

[7] B. Espinasse, P. Bacchin, P. Aimar, On an Experimental Method to Measure Critical Flux in Ultrafiltration, Desalination 146 (1-3) (2002) 91–96.

[8] P. van der Marel, A. Zwijnenburg, A. Kemperman, M. Wessling, H. Temmink, W. van der Meer, An Improved Flux-step Method to Determine the Critical Flux and the Critical Flux for Irreversibility in a Membrane Bioreactor, Journal of Membrane Science 332 (1-2) (2009) 24–29.

[9] L. Defrance, M.Y. Jaffrin, Reversibility of fouling formed in activated sludge filtration, Journal of Membrane Science 157 (1) (1999) 73–84.

[10] V. Chen, A.G. Fane, S. Madaeni, I.G. Wenten, Particle deposition during membrane filtration of colloids: transition between concentration polarization and cake formation, Journal of Membrane Science 125 (1) (1997) 109–122.

[11] P. Bacchin, P. Aimar, R.W. Field, Critical and sustainable fluxes: Theory, experiments and applications, Journal of Membrane Science 281 (1-2) (2006) 42–69.

Bibliography

Adout, A., Kang, S., Asatekin, A., Mayes, A. M. and Elimelech, M. Ultrafiltration Membranes Incorporating Amphiphilic Comb Copolymer Additives Prevent Irreversible Adhesion of Bacteria. *Environmental Science & Technology*, 44(7) 2406–2411 (2010). doi:10.1021/es902908g

Aimar, P., Howell, J. A. and Turner, M. Effects of Concentration Boundary Layer Development on the Flux Limitations in Ultrafiltration. *Chemical Engineering Research and Design*, 67(3) 255–261 (1989).

Akter, T. and Kim, W. S. Reversibly stretchable transparent conductive coatings of spray-deposited silver nanowires. *ACS Applied Materials & Interfaces*, 4(4) 1855–1859 (2012). doi:10.1021/am300058j

Al-Qahtany, H. I. and Al-Bastaki, N. M. S. Effect of Aging on the Performance of RO Hollow Fiber Membranes in a Section of an RO Plant. *Desalination*, 101(2) 177–183 (1995). doi:10.1016/0011-9164(95)00020-3

Alspach, B., Adham, S., Cooke, T., Delphos, P., Garcia-Aleman, J., Jacangelo, J., Karimi, A., Pressman, J., Schaefer, J. and Sethi, S. Microfiltration and Ultrafiltration Membranes for Drinking Water. *Journal of the American Water Works Association*, 100(12) 84–97 (2008).

Anderson, T. H., Yu, J., Estrada, A., Hammer, M. U., Waite, J. H. and Israelachvili, J. N. The Contribution of DOPA to Substrate-Peptide Adhesion and Internal Cohesion of Mussel-Inspired Synthetic Peptide Films. *Advanced Functional Materials*, 20(23) 4196–4205 (2010). doi:10.1002/adfm.201000932

Araújo, P. A., Miller, D. J., Correia, P. B., Van Loosdrecht, M. C. M., Kruithof, J. C., Freeman, B. D., Paul, D. R. and Vrouwenvelder, J. S. Impact of feed spacer and membrane modification by hydrophilic, bactericidal and biocidal coating on biofouling control. *Desalination*, 295 1–10 (2012). doi:10.1016/j.desal.2012.02.026

Arena, J. T., McCloskey, B., Freeman, B. D. and McCutcheon, J. R. Surface Modification of Thin Film Composite Membrane Support Layers with Polydopamine: Enabling Use of Reverse Osmosis Membranes in Pressure Retarded Osmosis. *Journal of Membrane Science*, 375(1-2) 55–62 (2011). doi:10.1016/j.memsci.2011.01.060

Arnot, T. C., Field, R. W. and Koltuniewicz, A. B. Cross-flow and dead-end microfiltration of oily-water emulsions Part II. Mechanisms and modelling of flux

decline. *Journal of Membrane Science*, 169(1) 1–15 (2000). doi:10.1016/S0376-7388(99)00321-X

Asatekin, A. and Mayes, A. M. Oil industry wastewater treatment with fouling resistant membranes containing amphiphilic comb copolymers. *Environmental Science & Technology*, 43(12) 4487–4492 (2009). Retrieved from http://www.ncbi.nlm.nih.gov/pubmed/19603666

Assumption, H. J., Vermeulen, J. P., Jarrett, W. L., Mathias, L. J. and Van Reenen, a. J. High resolution solution and solid state NMR characterization of ethylene/1-butene and ethylene/1-hexene copolymers fractionated by preparative temperature rising elution fractionation. *Polymer*, 47(1) 67–74 (2006). doi:10.1016/j.polymer.2005.11.020

Atkinson, P. M. and Lloyd, D. R. Anisotropic flat sheet membrane formation via TIPS: atmospheric convection and polymer molecular weight effects. *Journal of Membrane Science*, 175(2) 225–238 (2000). doi:10.1016/S0376-7388(00)00422-1

Azari, S. and Zou, L. Using zwitterionic amino acid l-DOPA to modify the surface of thin film composite polyamide reverse osmosis membranes to increase their fouling resistance. *Journal of Membrane Science*, 401-402 68–75 (2012). doi:10.1016/j.memsci.2012.01.041

Bacchin, P., Aimar, P. and Field, R. W. Critical and sustainable fluxes: Theory, experiments and applications. *Journal of Membrane Science*, 281(1-2) 42–69 (2006). doi:10.1016/j.memsci.2006.04.014

Bagheri Gh, A. Thermodynamic studies on complexation of dopamine with gadolinium(III) in water–ethanol system. *Journal of Molecular Liquids*, 156(2-3) 141–145 (2010). doi:10.1016/j.molliq.2010.07.002

Baker, R. W. *Membrane Technology and Applications* (2nd ed.). West Sussex, England: John Wiley & Sons (2004).

Bakhmutov, V. I. *Practical NMR Relaxation for Chemists* (pp. 19–29). West Sussex, England: John Wiley & Sons (2004).

Barrie, P. J., Madrali, E. S. and Kandiyoti, R. Carbon-13 solid-state NMR spin-lattice relaxation time measurements of coals. *Energy & Fuels*, 7(4) 479–481 (1993). doi:10.1021/ef00040a007

Basri, H., Ismail, A. F. and Aziz, M. Microstructure and anti-adhesion properties of PES/TAP/Ag hybrid ultrafiltration membrane. *Desalination*, 287 71–77 (2012). doi:10.1016/j.desal.2011.09.031

Beckwith, R. Hydraulic Fracturing: the Fuss, the facts, the Future. *Journal of Petroleum Technology*, 62(12) 34–41 (2010).

Beier, P. S. and Jonsson, G. Critical Flux Determination by Flux-Stepping. *AIChE Journal*, 56(7) 1739–1747 (2010). doi:10.1002/aic

Belfort, G., Davis, R. H. and Zydney, A. L. The behavior of suspensions and macromolecular solutions in crossflow microfiltration. *Journal of Membrane Science*, 96(1-2) 1–58 (1994). doi:10.1016/0376-7388(94)00119-7

Bernsmann, F., Ball, V., Addiego, F., Ponche, A., Michel, M., Gracio, J. J. de A., Toniazzo, V. and Ruch, D. Dopamine-Melanin Film Deposition Depends on the Used Oxidant and Buffer Solution. *Langmuir*, 27(6) 2819–2825 (2011). doi:10.1021/la104981s

Bernsmann, F., Ponche, A., Ringwald, C., Hemmerlé, J., Raya, J., Bechinger, B., Voegel, J.-C., Schaaf, P. and Ball, V. Characterization of Dopamine−Melanin Growth on Silicon Oxide. *Journal of Physical Chemistry C*, 113(19) 8234–8242 (2009). doi:10.1021/jp901188h

Bernstein, R., Belfer, S. and Freger, V. Bacterial Attachment to RO Membranes Surface-Modified by Concentration-Polarization-Enhanced Graft Polymerization. *Environmental Science & Technology*, 45(14) 5973–5980 (2011). doi:10.1021/es1043694

Bertrand, G. Sur une nouvelle oxydase, ou ferment solubleoxydant, d'origine vegetale. *Comptes Rendus de l'Académie des Sciences*, 122 1215–1217 (1896).

Berzelius, J. J. Lehrbuch der Chemie. *Lehrbuch der Chemie*, 9 22–24 (1840).

Beuvier, E., Berthaud, K., Cegarra, S., Dasen, A., Pochet, S., Buchin, S. and Duboz, G. Ripening and quality of Swiss-type cheese made from raw, pasteurized or microfiltered milk. *International Dairy Journal*, 7(5) 311–323 (1997). doi:10.1016/S0958-6946(97)00015-0

Bhattacharya, A. and Misra, B. N. Grafting: a versatile means to modify polymersTechniques, factors and applications. *Progress in Polymer Science*, 29(8) 767–814 (2004). doi:10.1016/j.progpolymsci.2004.05.002

Bierenbaum, H. S., Plainfield, R. B., Isaacson, R. and Lantos, P. R. Breathable Medical Dressing. U.S. Patent No. 3426754 (1969).

Bijl, D., Kainer, H. and Rose-Innes, A. C. Stabilization of Free Radicals by Adsoption: Detection by Paramagnetic Resonance. *Nature*, 174(4435) 830–831 (1954). doi:10.1038/174830a0

Blauch, M., Myers, R., Moore, T., Lipinski, B. and Houston, N. Marcellus Shale Post-Frac Flowback Waters - Where is All the Salt Coming from and What are the Implications? In *Proceedings of SPE Eastern Regional Meeting* (pp. 1–20). Society of Petroleum Engineers (2009). doi:10.2118/125740-MS

Bloch, B. Chemische Untersuchungen über das spezifische pigmentbildende Ferment der Haut, die Dopaoxydase. *Zeitschrift für physiologische Chemie*, 98 226–254 (n.d.).

Boerlage, S. F. E., Kennedy, M., Tarawneh, Z., De Faber, R. and Schippers, J. C. Development of the MFI-UF in constant flux filtration. *Desalination*, 161(2) 103–113 (2004). doi:10.1016/S0011-9164(04)90046-X

Bokhorst, H., Altena, F. W. and Smolders, C. A. Formation of asymmetric cellulose acetate membranes. *Desalination*, 38 349–360 (1981). doi:10.1016/S0011-9164(00)86079-8

Bonapace, J., Giglio, M., Moggia, J. and Krenz, M. Water Conservation: Reducing Freshwater Consumption by Using Produced Water for Base Fluid in Hydraulic Fracturing-Case Histories in Argentina. In *Proceedings of SPE Latin America and Caribbean Petroleum Engineering Conference*. Society of Petroleum Engineers (2012). doi:10.2118/151819-MS

Borovanský, J. History of Melanosome Research. In Patrick A Riley and J. Borovanský (Eds.), *Melanins and Melanosomes: Biosynthesis, Biogenesis, Physiological, and Pathological Functions* (pp. 1–19). Weinheim, Germany: Wiley-Blackwell (2011).

Bourquelot, E. E. and Bertrand, A. Le bleuissement et le noircissement des champignons. *Comptes Rendus de l'Académie des Sciences*, 2 582–584 (1895).

Bourquelot, E. E. and Bertrand, G. Sur la coloration des tissus et du suc de certains champignons au contact de l'air. *Journal de Pharmacie et de Chimie*, 3(6) 177–182 (1896).

Brandt, D. C., Leitner, G. F. and Leitner, W. E. Reverse Osmosis Membranes State of the Art. In Z. Amjad (Ed.), *Reverse Osmosis: Membrane Technology, Water Chemistry,*

and Industrial Applications (pp. 1–36). New York, NY: Van Nostrand Reinhold (1993).

Bridelli, M. G. and Crippa, P. R. Infrared and water sorption studies of the hydration structure and mechanism in natural and synthetic melanin. *The Journal of Physical Chemistry B*, 114(29) 9381–9390 (2010). doi:10.1021/jp101833k

Broens, L., Koenhen, D. M. and Smolders, C. A. On the mechanism of formation of asymmetric ultra- and hyper-filtration membranes. *Desalination*, 22(1-3) 205–219 (1977). doi:10.1016/S0011-9164(00)88376-9

Brown, S. P. Probing proton–proton proximities in the solid state. *Progress in Nuclear Magnetic Resonance Spectroscopy*, 50(4) 199–251 (2007). doi:10.1016/j.pnmrs.2006.10.002

Burghardt, W. R., Yilmaz, L. and McHugh, A. J. Glass transition, crystallization and thermoreversible gelation in ternary PPO solutions; relationship to asymmetric membrane formation. *Polymer*, 28(12) 2085–2092 (1987). doi:10.1016/0032-3861(87)90046-2

Burzio, L. A. and Waite, J. H. Cross-Linking in Adhesive Quinoproteins: Studies with Model Decapeptides. *Biochemistry*, 39(36) 11147–11153 (2000). doi:10.1021/bi0002434

Cai, Z., Wee, C. and Benjamin, M. M. Fouling Mechanisms in Low-Pressure Membrane Filtration in the Presence of an Adsorbent Cake Layer. *Journal of Membrane Science*, 433 32–38 (2013). doi:10.1016/j.memsci.2013.01.007

Caneba, G. T. and Soong, D. S. Polymer membrane formation through the thermal-inversion process. 1. Experimental study of membrane structure formation. *Macromolecules*, 18(12) 2538–2545 (1985). doi:10.1021/ma00154a031

Cataldo, F. On the Structure of Macromolecules Obtained by Oxidative Polymerization of Polyhydroxyphenols and Quinones. *Polymer International*, 46(4) 263–268 (1998). doi:10.1002/(SICI)1097-0126(199808)46:4<263::AID-PI983>3.0.CO;2-0

Çelen, B., Ekiz, D., Pişkin, E. and Demirel, G. Green catalysts based on bio-inspired polymer coatings and electroless plating of silver nanoparticles. *Journal of Molecular Catalysis A: Chemical*, 350(1-2) 97–102 (2011). doi:10.1016/j.molcata.2011.09.017

Chan, R and Chen, V. The Effects of Electrolyte Concentration and pH on Protein Aggregation and Deposition: Critical Flux and Constant Flux Membrane Filtration.

Journal of Membrane Science, 185(2) 177–192 (2001). doi:10.1016/S0376-7388(00)00645-1

Chan, Robert, Chen, V. and Bucknall, M. P. Ultrafiltration of Protein Mixtures: Measurement of Apparent Critical Flux, Rejection Performance, and Identification of Protein Deposition. *Desalination*, 146(1-3) 83–90 (2002). doi:10.1016/S0011-9164(02)00493-9

Chapman, R. G., Ostuni, E., Liang, M. N., Meluleni, G., Kim, E., Yan, L., Pier, G., Warren, H. S. and Whitesides, G. M. Polymeric Thin Films That Resist the Adsorption of Proteins and the Adhesion of Bacteria. *Langmuir*, 17(4) 1225–1233 (2001). doi:10.1021/la001222d

Chddress, A. E. and Deshmukh, S. S. Effect ofhumic substances and anionic surfactants on the surface charge and performance of reverse osmosis membranes. *Desalination*, 118(1-3) 167–174 (1998).

Chen, C., Wang, L., Tan, Y., Qin, C., Xie, F., Fu, Y., Xie, Q., Chen, J. and Yao, S. High-performance amperometric biosensors and biofuel cell based on chitosan-strengthened cast thin films of chemically synthesized catecholamine polymers with glucose oxidase effectively entrapped. *Biosensors & Bioelectronics*, 26(5) 2311–2316 (2011). doi:10.1016/j.bios.2010.09.058

Chen, G., Beving, D. E., Bedi, R. S., Yan, Y. S. and Walker, S. L. Initial Bacterial Deposition on Bare and Zeolite-Coated Aluminum Alloy and Stainless Steel. *Langmuir*, 25(3) 1620–1626 (2009). doi:10.1021/la803285j

Chen, J., Chen, X., Yin, X., Ma, J. and Jiang, Z. Bioinspired fabrication of composite pervaporation membranes with high permeation flux and structural stability. *Journal of Membrane Science*, 344(1-2) 136–143 (2009). doi:10.1016/j.memsci.2009.07.044

Chen, S., Chen, Y., Lei, Y. and Yin, Y. Novel strategy in enhancing stability and corrosion resistance for hydrophobic functional films on copper surfaces. *Electrochemistry Communications*, 11(8) 1675–1679 (2009). doi:10.1016/j.elecom.2009.06.021

Chen, V. Performance of partially permeable microfiltration membranes under low fouling conditions. *Journal of Membrane Science*, 147(2) 265–278 (1998). doi:10.1016/S0376-7388(98)00141-0

Chen, V., Fane, A. G., Madaeni, S. and Wenten, I. G. Particle deposition during membrane filtration of colloids: transition between concentration polarization and

cake formation. *Journal of Membrane Science*, 125(1) 109–122 (1997). doi:10.1016/S0376-7388(96)00187-1

Chen, W., Su, Y., Peng, J., Zhao, X., Jiang, Z., Dong, Y., Zhang, Y., Liang, Y. and Liu, J. Efficient wastewater treatment by membranes through constructing tunable antifouling membrane surfaces. *Environmental Science & Technology*, 45(15) 6545–6552 (2011). doi:10.1021/es200994n

Chen, Z.-L., Zhang, Y.-Z. and Liang, F.-P. A novel nickel(II) coordination polymer incorporating 1,4-phenylenediacetic acid and 1,10-phenanthroline. *Acta Crystallographica. Section C, Crystal Structure Communications*, 62(2) m48–m50 (2006). doi:10.1107/S0108270105042575

Cheryan, M. and Rajagopalan, N. Membrane Processing of Oily Streams. Wastewater Treatment and Waste Reduction. *Journal of Membrane Science*, 151(1) 13–28 (1998). doi:10.1016/S0376-7388(98)00190-2

Chevelkov, V., Xue, Y., Linser, R., Skrynnikov, N. R. and Reif, B. Comparison of Solid-State Dipolar Couplings and Solution Relaxation Data Provides Insight into Protein Backbone Dynamics. *Journal of the American Chemical Society*, 132(14) 5015–5017 (2010). doi:10.1021/ja100645k

Chien, H.-W., Kuo, W.-H., Wang, M.-J., Tsai, S.-W. and Tsai, W.-B. Tunable Micropatterned Substrates Based on Poly(dopamine) Deposition via Microcontact Printing. *Langmuir*, 28(13) 5775–5782 (2012). doi:10.1021/la300147p

Choi, K. Y.-J. and Dempsey, B. A. Bench-scale Evaluation of Critical Flux and TMP in Low-pressure Membrane Filtration. *Journal of the American Water Works Association*, 97(7) 134–143 (2005).

Clancy, C. M. R. and Simon, J. D. Ultrastructural Organization of Eumelanin from Sepia officinalis Measured by Atomic Force Microscopy. *Biochemistry*, 40(44) 13353–13360 (2001). doi:10.1021/bi010786t

Clark, M. B., Gardella, J. A., Schultz, T. M., Patil, D. G. and Salvati, L. Solid-state analysis of eumelanin biopolymers by electron spectroscopy for chemical analysis. *Analytical Chemistry*, 62(9) 949–956 (1990). doi:10.1021/ac00208a011

Cohen, C., Tanny, G. B. and Prager, S. Diffusion-controlled formation of porous structures in ternary polymer systems. *Journal of Polymer Science: Polymer Physics Edition*, 17(3) 477–489 (1979). doi:10.1002/pol.1979.180170312

Combe, C., Molis, E., Lucas, P., Riley, R. and Clark, M. . The effect of CA membrane properties on adsorptive fouling by humic acid. *Journal of Membrane Science*, 154(1) 73–87 (1999). doi:10.1016/S0376-7388(98)00268-3

Cooksey, C. J., Land, E. J., Rushton, F. A. P., Ramsden, C. A. and Riley, P. A. Tyrosinase-Mediated Cytotoxicity of 4-Substituted Phenols: Use of QSAR to Forecast Reactivities of Thiols towards the Derived ortho -Quinones. *Quantitative Structure-Activity Relationships*, 15(6) 498–503 (1996). doi:10.1002/qsar.19960150606

Cookson, D. J., Smith, B. E. and White, N. Improved Resolution of Low Field Quaternary Carbon Resonances in 13C N.M.R. Spectroscopy. *Journal of the Chemical Society, Chemical Communications*, 2(1) 12–13 (1981). doi:10.1039/c39810000012

Cope, F. W., Sever, R. J. and Polis, B. D. Reversible Free Radical Generation in the Melanin Granules of the Eye by Visible Light. *Archives of Biochemistry and Biophysics*, 100(2) 171–177 (1963). doi:10.1016/0003-9861(63)90058-4

Corradoini, M. G., Napolitano, A. and Prota, G. A biosynthetic approach to the structure of eumelanins. The isolation of oligomers from 5,6-dihydroxy-1-methylindole. *Tetrahedron*, 42(7) 2083–2088 (1986). doi:10.1016/S0040-4020(01)87625-0

Coufort, C., Derlon, N., Ochoa-Chaves, J., Liné, A. and Paul, E. Cohesion and detachment in biofilm systems for different electron acceptor and donors. *Water Science & Technology*, 55(8-9) 421–428 (2007). doi:10.2166/wst.2007.286

Craig, J. P., Knudsen, J. P. and Holland, V. F. Characterization of Acrylic Fiber Structure. *Textile Research Journal*, 32(6) 435–448 (1962). doi:10.1177/004051756203200601

Crippa, P. R., Cristofoletti, V. and Romeo, N. A band model for melanin deduced from optical absorption and photoconductivity experiments. *Biochimica et Biophysica Acta - General Subjects*, 538(1) 164–170 (1978). doi:10.1016/0304-4165(78)90260-X

Cui, H., Webber, M. J. and Stupp, S. I. Self-assembly of peptide amphiphiles: from molecules to nanostructures to biomaterials. *Biopolymers*, 94(1) 1–18 (2010). doi:10.1002/bip.21328

Cui, J., Wang, Y., Postma, A., Hao, J., Hosta-Rigau, L. and Caruso, F. Monodisperse Polymer Capsules: Tailoring Size, Shell Thickness, and Hydrophobic Cargo

Loading via Emulsion Templating. *Advanced Functional Materials*, 20(10) 1625–1631 (2010). doi:10.1002/adfm.201000209

Czekaj, P., López, F. and Güell, C. Membrane fouling during microfiltration of fermented beverages. *Journal of Membrane Science*, 166(2) 199–212 (2000). doi:10.1016/S0376-7388(99)00261-6

d'Ischia, M., Napolitano, A. and Pezzella, A. 5,6-Dihydroxyindole Chemistry: Unexplored Opportunities Beyond Eumelanin. *European Journal of Organic Chemistry*, 2011(28) 5501–5516 (2011). doi:10.1002/ejoc.201100796

d'Ischia, M., Napolitano, A., Pezzella, A., Meredith, P. and Sarna, T. Chemical and structural diversity in eumelanins: unexplored bio-optoelectronic materials. *Angewandte Chemie International Edition*, 48(22) 3914–3921 (2009). doi:10.1002/anie.200803786

d'Ischia, M., Napolitano, A. and Prota, G. Oxidative Polymerization of 5,6-Dihydroxyindoles. Tracking the Biosynthetic Pathway to Melanin Pigments. *Gazzetta Chimica Italiana*, 126(12) 783–789 (1996).

d'Ischia, M., Napolitano, A., Tsiakas, K. and Prota, G. New intermediates in the oxidative polymerisation of 5,6-dihydroxyindole to melanin promoted by the peroxidase/H2O2 system. *Tetrahedron*, 46(16) 5789–5796 (1990). doi:10.1016/S0040-4020(01)87775-9

Dai, W. . and Barbari, T. . Hydrogel membranes with mesh size asymmetry based on the gradient crosslinking of poly(vinyl alcohol). *Journal of Membrane Science*, 156(1) 67–79 (1999). doi:10.1016/S0376-7388(98)00330-5

Dalsin, J. L., Hu, B.-H., Lee, B. P. and Messersmith, P. B. Mussel adhesive protein mimetic polymers for the preparation of nonfouling surfaces. *Journal of the American Chemical Society*, 125(14) 4253–4258 (2003). doi:10.1021/ja0284963

Dalsin, J. L. and Messersmith, P. B. Bioinspired antifouling polymers. *Materials Today*, 8(9) 38–46 (2005). doi:10.1016/S1369-7021(05)71079-8

Decloux, M. and Tatoud, L. Importance of the Control Mode in Ultrafiltration: Case of Raw Cane Sugar Remelt. *Journal of Food Engineering*, 44(2) 119–126 (2000). doi:10.1016/S0260-8774(99)00175-2

Defrance, L. and Jaffrin, M. Y. Reversibility of fouling formed in activated sludge filtration. *Journal of Membrane Science*, 157(1) 73–84 (1999). doi:10.1016/S0376-7388(98)00356-1

Demir, A. S., Findik, H., Saygili, N. and Tuna Subasi, N. Manganese(III) acetate-mediated synthesis of biaryls under microwave irradiation. *Tetrahedron*, 66(6) 1308–1312 (2010). doi:10.1016/j.tet.2009.12.018

Devlin, H. R. and Harris, I. J. Mechanism of the oxidation of aqueous phenol with dissolved oxygen. *Industrial & Engineering Chemistry Fundamentals*, 23(4) 387–392 (1984). doi:10.1021/i100016a002

Dreyer, D. R., Miller, D. J., Freeman, B. D., Paul, D. R. and Bielawski, C. W. Elucidating the Structure of Poly(dopamine). *Langmuir*, 28(15) 6428–6435 (2012). doi:10.1021/la204831b

Duddridge, J. E., Kent, C. A. and Laws, J. F. Effect of surface shear stress on the attachment of pseudomonas fluorescens to stainless steel under defined flow conditions. *Biotechnology and Bioengineering*, 24(8) 153–164 (1982). doi:10.1002/bit.260240825

Economides, M. J. and Nikolaou, M. Technologies for Oil and Gas Production: Present and Future. *AIChE Journal*, 57(8) 1974–1982 (2011). doi:10.1002/aic.12714

Elimelech, M. and Phillip, W. A. The Future of Seawater Desalination: Energy, Technology, and the Environment. *Science*, 333(6043) 712–717 (2011). doi:10.1126/science.1200488

Elliot, J. R. and Lira, C. T. *Introductory Chemical Engineering Thermodynamics*. Upper Saddle River, NJ: Prentice Hall PTR (1999).

Espinasse, B., Bacchin, P. and Aimar, P. On an Experimental Method to Measure Critical Flux in Ultrafiltration. *Desalination*, 146(1-3) 91–96 (2002).

Fei, B., Qian, B., Yang, Z., Wang, R., Liu, W., Mak, C. and Xin, J. Coating carbon nanotubes by spontaneous oxidative polymerization of dopamine. *Carbon*, 46(13) 1795–1797 (2008). doi:10.1016/j.carbon.2008.06.049

Feng, J., Sun, M., Li, J., Xu, L., Liu, X. and Jiang, S. Polydopamine supported preparation method for solid-phase microextraction coatings on stainless steel wire. *Journal of Chromatography A*, 1218(23) 3601–3607 (2011). doi:10.1016/j.chroma.2011.04.018

Feng, J., Sun, M., Xu, L., Li, J., Liu, X. and Jiang, S. Preparation of metal wire supported solid-phase microextraction fiber coated with multi-walled carbon nanotubes. *Journal of Separation Science*, 34(18) 2482–2488 (2011). doi:10.1002/jssc.201100375

Feng, J.-J., Zhang, P.-P., Wang, A.-J., Liao, Q.-C., Xi, J.-L. and Chen, J.-R. One-step synthesis of monodisperse polydopamine-coated silver core–shell nanostructures for enhanced photocatalysis. *New Journal of Chemistry*, 36(1) 148–154 (2012). doi:10.1039/c1nj20850k

Field, R W, Wu, D., Howell, J. A. and Gupta, B. B. Critical Flux Concept for Microfiltration Fouling. *Journal of Membrane Science*, 100(3) 259–272 (1995). doi:10.1016/0376-7388(94)00265-Z

Field, R. Fundamentals of Fouling. In K.-V. Pinemann and S. P. Nunes (Eds.), *Membrane Technology: Membranes for Water Treatment* (Vol. 4, pp. 1–24). Weinheim, Germany: Wiley-VCH (2010). doi:10.1002/9783527631407.ch1

Field, Robert W and Pearce, G. K. Critical, Sustainable and Threshold Fluxes for Membrane Filtration with Water Industry Applications. *Advances in Colloid and Interface Science*, 164(1-2) 38–44 (2011). doi:10.1016/j.cis.2010.12.008

Filatovs, J., McGinness, J. and Corry, P. Thermal and electronic contributions to switching in melanins. *Biopolymers*, 15(11) 2309–2312 (1976). doi:10.1002/bip.1976.360151120

Flemming, H.-C. Biofouling in Water Systems--Cases, Causes and Countermeasures. *Applied Microbiology and Biotechnology*, 59(6) 629–640 (2002). doi:10.1007/s00253-002-1066-9

Flemming, H.-C. and Schaule, G. Biofouling on Membranes - A Microbiological Approach. *Desalination*, 70(1-3) 95–119 (1988). doi:10.1016/0011-9164(88)85047-1

Flemming, Hans-Curt, Neu, T. R. and Wozniak, D. J. The EPS Matrix: The "House of Biofilm Cells". *Journal of Bacteriology*, 189(22) 7945–7947 (2007). doi:10.1128/JB.00858-07

Francis, P. S. *NTIS Report No. PB-177083*. United States Department of Commerce (1966).

Freeman, B. D. and Pinnau, I. Gas and Liquid Separations Using Membranes: An Overview. In I. Pinnau and B. D. Freeman (Eds.), *Advanced Materials for Membrane Separations* (pp. 1–23) (2004). doi:10.1021/bk-2004-0876.ch001

Fu, Y., Li, P., Bu, L., Wang, T., Xie, Q., Xu, X., Lei, L., Zou, C. and Yao, S. Chemical/Biochemical Preparation of New Polymeric Bionanocomposites with Enzyme Labels Immobilized at High Load and Activity for High-Performance

Electrochemical Immunoassay. *The Journal of Physical Chemistry C*, 114(3) 1472–1480 (2010). doi:10.1021/jp9092767

Fu, Y., Li, P., Wang, T., Bu, L., Xie, Q., Xu, X., Lei, L., Zou, C., Chen, J. and Yao, S. Novel polymeric bionanocomposites with catalytic Pt nanoparticles label immobilized for high performance amperometric immunoassay. *Biosensors & Bioelectronics*, 25(7) 1699–1704 (2010). doi:10.1016/j.bios.2009.12.010

Fukuchi, M., Ramamoorthy, A. and Takegoshi, K. Efficient cross-polarization using a composite 0 degree pulse for NMR studies on static solids. *Journal of Magnetic Resonance*, 196(2) 105–109 (2009). doi:10.1016/j.jmr.2008.10.013

Furlani, A., Russo, M. V and Cataldo, F. Oxidative polymerization of p-benzoquinone and hydroquinone. Conductivity of doped and undoped polymerization products. *Synthetic Metals*, 29(1) 507–510 (1989). doi:10.1016/0379-6779(89)90341-X

Gaides, G. E. and McHugh, A. J. Gelation in an amorphous polymer: a discussion of its relation to membrane formation. *Polymer*, 30(11) 2118–2123 (1989). doi:10.1016/0032-3861(89)90303-0

Gan, Q., Field, R. W., Bird, M. R., England, R., Howell, J. A., McKechnie, M. T. and O'Shaughnessy, C. L. Beer Clarification by Cross-Flow Microfiltration: Fouling Mechanisms and Flux Enhancement. *Chemical Engineering Research and Design*, 75(1) 3–8 (1997). doi:10.1205/026387697523327

Gao, Z., Walton, N. I., Malugin, A., Ghandehari, H. and Zharov, I. Preparation of dopamine-modified boron nanoparticles. *Journal of Materials Chemistry*, 22(3) 877–882 (2012). doi:10.1039/c1jm12655e

Gaudlip, A. W., Paugh, L. O. and Hayes, T. D. Marcellus Shale Water Management Challenges in Pennsylvania. In *Proceedings of SPE Shale Gas Production Conference*. Society of Petroleum Engineers (2008). doi:10.2118/119898-MS

Gay, I. D., Jones, C. H. . and Sharma, R. . A Multinuclear Solid-State NMR Study of the Dimethyltin Chalcogenides ((CH3)2SnE)3, E = S, Se, Te. *Journal of Magnetic Resonance*, 84(3) 501–514 (1989). doi:10.1016/0022-2364(89)90116-9

Geise, G. M., Lee, H.-S., Miller, D. J., Freeman, B. D., McGrath, J. E. and Paul, D. R. Water Purification by Membranes: The Role of Polymer Science. *Journal of Polymer Science Part B: Polymer Physics*, 48(15) 1685–1718 (2010). doi:10.1002/polb.22037

Gésan, G., Daufin, G. and Merin, U. Performance of Whey Crossflow Microfiltration during Transient and Stationary Operating Conditions. *Journal of Membrane Science*, 104(3) 271–281 (1995). doi:10.1016/0376-7388(95)00037-D

Gésan, G., Daufin, G., Merin, U., Labbé, J.-P. and Quémerais, A. Fouling During Constant Flux Crossflow Microfiltration of Pretreated Whey. Influence of Transmembrane Pressure Gradient. *Journal of Membrane Science*, 80(1) 131–145 (1993). doi:10.1016/0376-7388(93)85138-M

Gésan-Guiziou, G., Boyaval, E. and Daufin, G. Critical Stability Conditions in Crossflow Microfiltration of Skimmed Milk: Transition to Irreversible Deposition. *Journal of Membrane Science*, 158(1-2) 211–222 (1999). doi:10.1016/S0376-7388(99)00017-4

Ghosh, R. Study of Membrane Fouling by BSA using Pulsed Injection Technique. *Journal of Membrane Science*, 195(1) 115–123 (2002). doi:10.1016/S0376-7388(01)00550-6

Gjaltema, A., Van der Marel, N., Van Loosdrecht, M. C. M. and Heijnen, J. J. Adhesion and Biofilm Development on Suspended Carriers in Airlift Reactors: Hydrodynamic Conditions versus Surface Characteristics. *Biotechnology and Bioengineering*, 55(6) 880–889 (1997). doi:10.1002/(SICI)1097-0290(19970920)55:6<880::AID-BIT6>3.0.CO;2-C

Gombotz, W. R., Guanghui, W. and Hoffman, a. S. Immobilization of poly(ethylene oxide) on poly(ethylene terephthalate) using a plasma polymerization process. *Journal of Applied Polymer Science*, 37(1) 91–107 (1989). doi:10.1002/app.1989.070370108

Gore, R. W. Process for Producing Porous Products. U. S. Patent No. 3953566 (1976).

Graham, D. G. Oxidative Pathways for Catecholamines in the Genesis of Neuromelanin and Cytotoxic Quinones. *Molecular Pharmacology*, 14(4) 633–643 (1978).

Greenlee, L. F., Lawler, D. F., Freeman, B. D., Marrot, B. and Moulin, P. Reverse Osmosis Desalination: Water Sources, Technology, and Today's Challenges. *Water Research*, 43(9) 2317–2348 (2009). doi:10.1016/j.watres.2009.03.010

Griebe, T. and Flemming, H.-C. Biocide-free antifouling strategy to protect RO membranes from biofouling. *Desalination*, 118(1-3) 153–156 (1998). doi:10.1016/S0011-9164(98)00113-1

Gruendling, T., Weidner, S., Falkenhagen, J. and Barner-Kowollik, C. Mass spectrometry in polymer chemistry: a state-of-the-art up-date. *Polymer Chemistry*, 1(5) 599–617 (2010). doi:10.1039/b9py00347a

Güell, C. and Davis, R. H. Membrane fouling during microfiltration of protein mixtures. *Journal of Membrane Science*, 119(2) 269–284 (1996). doi:10.1016/0376-7388(96)80001-J

Guidelines for Drinking-water Quality (4th ed., Vol. 38). Geneva, Switzerland: World Health Organization (2011). Retrieved from http://www.ncbi.nlm.nih.gov/pubmed/15806952

Guo, W. S., Vigneswaran, S. and Ngo, H. H. Effect of flocculation and/or adsorption as pretreatment on the critical flux of crossflow microfiltration. *Desalination*, 172(1) 53–62 (2005). doi:10.1016/j.desal.2004.06.196

Gupta, D. and Hlidek, B. Frac-Fluid Recycling and Water Conservation: A Case History. *SPE Production & Operations*, 25(1) 65–69 (2010). doi:10.2118/119478-PA

Halperin, A. Polymer Brushes that Resist Adsorption of Model Proteins: Design Parameters. *Langmuir*, 15(7) 2525–2533 (1999). doi:10.1021/la981356f

Hanemaaijer, J. H., Robbertsen, T., Van den Boomgaard, T. and Gunnink, J. W. Fouling of ultrafiltration membranes. The role of protein adsorption and salt precipitation. *Journal of Membrane Science*, 40(2) 199–217 (1989). doi:10.1016/0376-7388(89)89005-2

Harrison, W. H., Whisler, W. W. and Hill, B. J. Catecholamine oxidation and ionization properties indicated from the H+ release, tritium exchange, and spectral changes which occur during ferricyanide oxidation. *Biochemistry*, 7(9) 3089–3094 (1968).

Hartmann, S. and Hahn, E. Nuclear Double Resonance in the Rotating Frame. *Physical Review*, 128(5) 2042–2053 (1962). doi:10.1103/PhysRev.128.2042

Hawley, M D, Tatawawadi, S. V, Piekarski, S. and Adams, R. N. Electrochemical studies of the oxidation pathways of catecholamines. *Journal of the American Chemical Society*, 89(2) 447–450 (1967).

Hawley, M. D., Tatawawadi, S. V., Piekarski, S. and Adams, R. N. Additions and Corrections - Electrochemical Studies of the Oxidation Pathways of Catecholamines. *Journal of the American Chemical Society*, 90(4) 1093 (1968). doi:10.1021/ja01006a604

Hayes, T. D. and Severin, B. F. *Characterization of Flowback Waters from the Marcellus and the Barnett Shale Regions*. RPSEA Report 08122-05.09 (2012).

Headen, T. F., Howard, C. A., Skipper, N. T., Wilkinson, M. A., Bowron, D. T. and Soper, A. K. Structure of π-π Interactions in Aaromatic Liquids. *Journal of the American Chemical Society*, 132(16) 5735–5742 (2010). doi:10.1021/ja909084e

Hermia, J. Constant Pressure Blocking Filtration Laws - Application to Power-law Non-Newtonian Fluids. *Transactions of the Institution of Chemical Engineers*, 60(3) 183–187 (1982).

Hiremath, G. a., Timmanagoudar, P. L. and Nandibewoor, S. T. Oxidation of allyl alcohol by alkaline periodate in the presence of micro amounts of palladium(II). *Journal of Physical Organic Chemistry*, 11(1) 31–35 (1998). doi:10.1002/(SICI)1099-1395(199801)11:1<31::AID-POC968>3.0.CO;2-7

Hirst, A. R., Escuder, B., Miravet, J. F. and Smith, D. K. High-tech Applications of Self-Assembling Supramolecular Nanostructured Gel-Phase Materials: From Regenerative Medicine to Electronic Devices. *Angewandte Chemie International Edition*, 47(42) 8002–8018 (2008). doi:10.1002/anie.200800022

Ho, C.-C. and Zydney, A. L. Transmembrane Pressure Profiles during Constant Flux Microfiltration of Bovine Serum Albumin. *Journal of Membrane Science*, 209(2) 363–377 (2002). doi:10.1016/S0376-7388(02)00282-X

Ho, W. S. and Sirkar, K. K. *Membrane Handbook*. New York: Van Nostrand Reinhold (1992).

Holm-Hansen, O. and Booth, C. R. The Measurement of Adenosine Triphosphate in the Ocean and its Ecological Significance. *Limnology and Oceanography*, 11(4) 510–519 (1966).

Hong, S., Lee, J. S., Ryu, J., Lee, S. H., Lee, D. Y., Kim, D.-P., Park, C. B. and Lee, H. Bio-inspired strategy for on-surface synthesis of silver nanoparticles for metal/organic hybrid nanomaterials and LDI-MS substrates. *Nanotechnology*, 22(49) 494020 (2011). doi:10.1088/0957-4484/22/49/494020

Horak, V. and Gillette, J. R. A Study of the Oxidation-Reduction State of Synthetic 3,4-Dihydroxy-DL-phenylalanine Melanin. *Molecular Pharmacology*, 7(4) 429–433 (1971).

Howe, K. J. and Clark, M. M. Fouling of microfiltration and ultrafiltration membranes by natural waters. *Environmental Science & Technology*, 36(16) 3571–3576 (2002).

Howell, J A, Wu, D. and Field, R. W. Transmission of bovine albumin under controlled flux ultrafiltration. *Journal of Membrane Science*, 152(1) 117–127 (1999). doi:10.1016/S0376-7388(98)00202-6

Howell, John A. Sub-critical flux operation of microfiltration. *Journal of Membrane Science*, 107(1-2) 165–171 (1995). doi:10.1016/0376-7388(95)00114-R

Hu, H., Yu, B., Ye, Q., Gu, Y. and Zhou, F. Modification of carbon nanotubes with a nanothin polydopamine layer and polydimethylamino-ethyl methacrylate brushes. *Carbon*, 48(8) 2347–2353 (2010). doi:10.1016/j.carbon.2010.03.014

Hughes, D. and Field, R. W. Crossflow filtration of washed and unwashed yeast suspensions at constant shear under nominally sub-critical conditions. *Journal of Membrane Science*, 280(1-2) 89–98 (2006). doi:10.1016/j.memsci.2006.01.022

Hurrell, R. F. and Finot, P.-A. Nutritional consequences of the reactions between proteins and oxidized polyphenolic acids. *Advances in Experimental Medicine and Biology*, 177 423–435 (1984).

Hvid, K. B., Nielsen, P. S. and Stengaard, F. F. Preparation and characterization of a new ultrafiltration membrane. *Journal of Membrane Science*, 53(3) 189–202 (1990). doi:10.1016/0376-7388(90)80014-D

Inada, A., Nakamura, Y. and Morita, Y. An effective dehydrogenation of indolines to indoles with cobalt(II) Schiff's base complexes. *Chemistry Letters*, 9(10) 1287–1290 (1980). doi:10.1246/cl.1980.1287

Iqbal, Z., Alsudir, S., Miah, M. and Lai, E. P. C. Rapid CE-UV binding tests of environmentally hazardous compounds with polymer-modified magnetic nanoparticles. *Electrophoresis*, 2181–2187 (2011). doi:10.1002/elps.201100106

Ishibashi, H. Controlling the Regiochemistry of Radical Cyclizations. *Chemical Record*, 6(1) 23–31 (2006). doi:10.1002/tcr.20069

Ito, S. A chemist's view of melanogenesis. *Pigment Cell Research*, 16(3) 230–6 (2003).

Ito, Y., Kotera, S., Inaba, M., Kono, K. and Imanishi, Y. Control of pore size of polycarbonate membrane with straight pores by poly(acrylic acid) grafts. *Polymer*, 31(11) 2157–2161 (1990). doi:10.1016/0032-3861(90)90090-L

IUPAC. *Compendium of Chemical Terminology*. (A. D. M. and A. Wilkinson, Ed.) (2nd ed.). Oxford: Blackwell Scientific Publications (1997).

Iversen, L. L. The Catecholamines. *Nature*, 214(5083) 8–14 (1967). doi:10.1038/214008a0

Iwata, H., Ivanchenko, M. I. and Miyaki, Y. Preparation of anti-oil stained membrane by grafting polyethylene glycol macromer onto polysulfone membrane. *Journal of Applied Polymer Science*, 54(1) 125–128 (1994). doi:10.1002/app.1994.070540113

Iwata, H. and Matsuda, T. Preparation and properties of novel environment-sensitive membranes prepared by graft polymerization onto a porous membrane. *Journal of Membrane Science*, 38(2) 185–199 (1988). doi:10.1016/S0376-7388(00)80879-0

Jacobson, F. W. and Millott, N. Phenolases and Melanogenesis in the Coelomic Fluid of the Echinoid Diadema antillarum Phillippi. *Proceedings of the Royal Society of London B*, 141(903) 231–247 (1953).

Jameson, R. F., Hunter, G. and Kiss, T. A 1H nuclear magnetic resonance study of the deprotonation of L-dopa and adrenaline. *Journal of the Chemical Society, Perkin Transactions 2*, (7) 1105–1110 (1980). doi:10.1039/p29800001105

Jastrzebska, M M, Stepień, K., Wilczok, J., Porebska-Budny, M. and Wilczok, T. Semiconductor properties of melanins prepared from catecholamines. *General Physiology and Biophysics*, 9(4) 373–383 (1990).

Jastrzebska, Maria M, Isotalo, H., Paloheimo, J. and Stubb, H. Electrical conductivity of synthetic DOPA-melanin polymer for different hydration states and temperatures. *Journal of Biomaterials Science, Polymer Edition*, 7(7) 577–586 (1996). doi:10.1163/156856295X00490

Jeong, K. J., Wang, L., Stefanescu, C. F., Lawlor, M. W., Polat, J., Dohlman, C. H., Langer, R. S. and Kohane, D. S. Polydopamine coatings enhance biointegration of a model polymeric implant. *Soft Matter*, 7(18) 8305–8312 (2011). doi:10.1039/c1sm05918a

Jia, M., Qin, L., He, X.-W. and Li, W.-Y. Preparation and application of lysozyme imprinted monolithic column with dopamine as the functional monomer. *Journal of Materials Chemistry*, 22(2) 707–713 (2012). doi:10.1039/c1jm13134f

Jiang, H., Yang, L., Li, C., Yan, C., Lee, P. S. and Ma, J. High–rate electrochemical capacitors from highly graphitic carbon–tipped manganese oxide/mesoporous carbon/manganese oxide hybrid nanowires. *Energy & Environmental Science*, 4(5) 1813–1819 (2011). doi:10.1039/c1ee01032h

Jiang, J., Zhu, L., Zhu, L., Zhu, B. and Xu, Y. Surface Characteristics of a Self-Polymerized Dopamine Coating Deposited on Hydrophobic Polymer Films. *Langmuir*, 27(23) 14180–14187 (2011). doi:10.1021/la202877k

Jimbo, T., Higa, M., Minoura, N. and Tanioka, A. Surface Characterization of Poly(acrylonitrile) Membranes Graft-Polymerized with Ionic Monomers As Revealed by ζ Potential Measurement. *Macromolecules*, 31(4) 1277–1284 (1998). doi:10.1021/ma970692k

Jimbow, K., Quevedo Jr., W. C., Fitzpatrick, T. B. and Szabo, G. Some Aspects of Melanin Biology: 1950-1975. *Journal of Investigative Dermatology*, 67(1) 72–89 (1976). doi:10.1111/1523-1747.ep12512500

Jones, A. F. and Misell, D. L. The problem of error in deconvolution. *Journal of Physics A: General Physics*, 3(5) 462–472 (1970). doi:10.1088/0305-4470/3/5/002

Joule, J. A. and Mills, K. *Heterocyclic Chemistry*. Chichester, U.K.: Wiley (2010).

Ju, H. *Water Transport Study in Crosslinked Poly (ethylene oxide) Hydrogels as Fouling-Resistant Membrane Coating Materials*. The University of Texas at Austin (2010).

Ju, H., McCloskey, B. D., Sagle, A. C., Kusuma, V. A. and Freeman, B. D. Preparation and Characterization of Crosslinked Poly(ethylene glycol) Diacrylate Hydrogels as Fouling-resistant Membrane Coating Materials. *Journal of Membrane Science*, 330(1-2) 180–188 (2009). doi:10.1016/j.memsci.2008.12.054

Ju, H., McCloskey, B. D., Sagle, A. C., Wu, Y.-H., Kusuma, V. A. and Freeman, B. D. Crosslinked Poly(ethylene oxide) Fouling Resistant Coating Materials for Oil/Water Separation. *Journal of Membrane Science*, 307(2) 260–267 (2008). doi:10.1016/j.memsci.2007.09.028

Kanani, D. M. and Ghosh, R. A constant flux based mathematical model for predicting permeate flux decline in constant pressure protein ultrafiltration. *Journal of Membrane Science*, 290(1-2) 207–215 (2007). doi:10.1016/j.memsci.2006.12.030

Kang, K., Choi, I. S. and Nam, Y. A biofunctionalization scheme for neural interfaces using polydopamine polymer. *Biomaterials*, 32(27) 6374–80 (2011). doi:10.1016/j.biomaterials.2011.05.028

Kang, S. and Elimelech, M. Bioinspired single bacterial cell force spectroscopy. *Langmuir*, 25(17) 9656–9659 (2009). doi:10.1021/la902247w

Kasemset, S., Lee, A., Miller, D. J., Freeman, B. D. and Sharma, M. M. Effect of Polydopamine Deposition Conditions on Fouling Resistance, Physical Properties, and Permeation Properties of Reverse Osmosis Membranes in Oil/Water Separation. *Journal of Membrane Science*, 425-426 208–216 (2013). doi:10.1016/j.memsci.2012.08.049

Kautz, H., Van Beek, D. J. M., Sijbesma, R. P. and Meijer, E. W. Cooperative End-to-End and Lateral Hydrogen-Bonding Motifs in Supramolecular Thermoplastic Elastomers. *Macromolecules*, 39(13) 4265–4267 (2006a). doi:10.1021/ma060706z

Kautz, H., Van Beek, D. J. M., Sijbesma, R. P. and Meijer, E. W. Cooperative End-to-End and Lateral Hydrogen-Bonding Motifs in Supramolecular Thermoplastic Elastomers. *Macromolecules*, 39(13) 4265–4267 (2006b). doi:10.1021/ma060706z

Kawase, M., Miyake, Y. and Kikugawa, Y. Dehydrogenation of indolines to indoles via azasulphonium salts or N-chloramines. *Journal of the Chemical Society, Perkin Transactions 1*, 1401–1404 (1984). doi:10.1039/p19840001401

Kaxiras, E., Tsolakidis, A., Zonios, G. and Meng, S. Structural Model of Eumelanin. *Physical Review Letters*, 97(21) 218102/1–218102/4 (2006). doi:10.1103/PhysRevLett.97.218102

Kerr, R. A. Not Under My Backyard, Thank You. *Science*, 328(5986) 1625 (2010). doi:10.1126/science.328.5986.1625

Kesting, R. E. *Synthetic Polymeric Membranes*. New York: McGraw-Hill (1971).

Ketcha, D. M. The manganese(III) acetate oxidation of N-protected indolines. *Tetrahedron Letters*, 29(18) 2151–2154 (1988). doi:10.1016/S0040-4039(00)86696-4

Kim, B. H., Lee, D. H., Kim, J. Y., Shin, D. O., Jeong, H. Y., Hong, S., Yun, J. M., Koo, C. M., Lee, H. and Kim, S. O. Mussel-inspired block copolymer lithography for low surface energy materials of teflon, graphene, and gold. *Advanced Materials*, 23(47) 5618–5622 (2011). doi:10.1002/adma.201103650

Kim, H. W., McCloskey, B. D., Choi, T. H., Lee, C., Kim, M.-J., Freeman, B. D. and Park, H. B. Oxygen Concentration Control of Dopamine-induced High Uniformity Surface Coating Chemistry. *ACS Applied Materials & Interfaces*, 5(2) 233–238 (2013). doi:10.1021/am302439g

Kim, S., Lee, S., Hong, S., Oh, Y., Seoul, M., Kweon, J. and Kim, T. Biofouling of reverse osmosis membranes: Microbial quorum sensing and fouling propensity. *Desalination*, 247(1-3) 303–315 (2009). doi:10.1016/j.desal.2008.12.033

King, G. E. Hydraulic Fracturing 101: What Every Representative, Environmentalist, Regulator, Reporter, Investor, University Researcher, Neighbor and Engineer Should Know About Estimating Frac Risk and Improving Frac Performance in Unconventional Gas and Oil Wells. In *Proceedings of SPE Hydraulic Fracturing Technology Conference* (pp. 1–80). Society of Petroleum Engineers (2012). doi:10.2118/152596-MS

Knoell, T. Chlorine's Impact on the Performance and Properties of Polyamide Membranes. *Ultrapure Water*, UP230324 24–30 (2006).

Knudsen, J. P. The Influence of Coagulation Variables on the Structure and Physical Properties of an Acrylic Fiber. *Textile Research Journal*, 33(1) 13–20 (1963). doi:10.1177/004051756303300103

Koenhen, D. M., Mulder, M. H. V. and Smolders, C. a. Phase separation phenomena during the formation of asymmetric membranes. *Journal of Applied Polymer Science*, 21(1) 199–215 (1977). doi:10.1002/app.1977.070210118

Kollias, N. and Baqer, A. H. Absorption Mechanisms of Human Melanin in the Visible, 400-720 nm. *Journal of Investigative Dermatology*, 89(4) 384–388 (1987). doi:10.1111/1523-1747.ep12471764

Kolodziejski, W. and Klinowski, J. Kinetics of Cross-Polarization in Solid-State NMR: A Guide for Chemists. *Chemical Reviews*, 102(3) 613–628 (2002).

Koltuniewicz, A. B., Field, R. W. and Arnot, T. C. Cross-flow and dead-end microfiltration of oily-water emulsion. Part I: Experimental study and analysis of flux decline. *Journal of Membrane Science*, 102(1-3) 193–207 (1995). doi:10.1016/0376-7388(94)00320-X

Korytowski, W. and Sarna, T. Bleaching of Melanin Pigments. *The Journal of Biological Chemistry*, 265(21) 12410–12416 (1990).

Kovalsky, P., Bushell, G. and Waite, T. D. Prediction of Transmembrane Pressure Build-up in Constant Flux Microfiltration of Compressible Materials in the Absence and Presence of Shear. *Journal of Membrane Science*, 344(1-2) 204–210 (2009). doi:10.1016/j.memsci.2009.08.005

Krzystek, J., Sienkiewicz, A., Pardi, L. and Brunel, L. DPPH as a Standard for High-Field EPR. *Journal of Magnetic Resonance*, 125(1) 207–211 (1997). doi:10.1006/jmre.1996.1098

Ku, S. H., Lee, J. S. and Park, C. B. Spatial Control of Cell Adhesion and Patterning through Mussel-Inspired Surface Modification by Polydopamine. *Langmuir*, 26(6) 15104–15108 (2010). doi:10.1021/la102825p

Ku, S. H. and Park, C. B. Human endothelial cell growth on mussel-inspired nanofiber scaffold for vascular tissue engineering. *Biomaterials*, 31(36) 9431–9437 (2010). doi:10.1016/j.biomaterials.2010.08.071

Ku, S. H., Ryu, J., Hong, S. K., Lee, H. and Park, C. B. General functionalization route for cell adhesion on non-wetting surfaces. *Biomaterials*, 31(9) 2535–2541 (2010). doi:10.1016/j.biomaterials.2009.12.020

Kuang, J. and Messersmith, P. B. Universal surface-initiated polymerization of antifouling zwitterionic brushes using a mussel-mimetic Peptide initiator. *Langmuir*, 28(18) 7258–7266 (2012). doi:10.1021/la300738e

Kuehne, M. E. and Hall, T. C. Oxidation of primary amines and indoline with palladium dichloride and gold trichloride. *Journal of Organic Chemistry*, 41(16) 2742–2746 (1976). doi:10.1021/jo00878a021

Kulma, A. and Szopa, J. Catecholamines are active compounds in plants. *Plant Science*, 172(3) 433–440 (2007). doi:10.1016/j.plantsci.2006.10.013

Kwon, D. Y. and Vigneswaran, S. Influence of particle size and surface charge on critical flux of crossflow microfiltration. *Water Science and Technology*, 38(4-5) 481–488 (1998). doi:10.1016/S0273-1223(98)00548-4

Kwon, D.Y, Vigneswaran, S., Fane, A. . and Aim, R. B. Experimental determination of critical flux in cross-flow microfiltration. *Separation and Purification Technology*, 19(3) 169–181 (2000). doi:10.1016/S1383-5866(99)00088-X

Lai, M., Cai, K., Zhao, L., Chen, X., Hou, Y. and Yang, Z. Surface functionalization of TiO2 nanotubes with bone morphogenetic protein 2 and its synergistic effect on the differentiation of mesenchymal stem cells. *Biomacromolecules*, 12(4) 1097–1105 (2011). doi:10.1021/bm1014365

Landholt. Ueber das Melanin der Augenhäute. *Hoppe-Seyler's Zeitschrift für Physiologische Chemie*, 28 192–211 (1899).

Lau, Y. L. and Liu, D. Effect of Flow Rate on Biofilm Accumulation in Open Channels. *Water Research*, 27(3) 355–360 (1993). doi:10.1016/0043-1354(93)90034-F

Lauterbur, P. Anisotropy of the C13 Chemical Shift in Calcite. *Physical Review Letters*, 1(9) 343–344 (1958). doi:10.1103/PhysRevLett.1.343

LaVoie, M. J., Ostaszewski, B. L., Weihofen, A., Schlossmacher, M. G. and Selkoe, D. J. Dopamine covalently modifies and functionally inactivates parkin. *Nature Medicine*, 11(11) 1214–1221 (2005). doi:10.1038/nm1314

Le Clech, P., Jefferson, B., Chang, I. S. and Judd, S. J. Critical Flux Determination by the Flux-step Method in a Submerged Membrane Bioreactor. *Journal of Membrane Science*, 227(1-2) 81–93 (2003). doi:10.1016/j.memsci.2003.07.021

Lee, B. P., Messersmith, P. B., Israelachvili, J. N. and Waite, J. H. Mussel-Inspired Adhesives and Coatings. *Annual Review of Materials Research*, 41 99–132 (2011). doi:10.1146/annurev-matsci-062910-100429

Lee, H., Dellatore, S. M., Miller, W. M. and Messersmith, P. B. Mussel-Inspired Surface Chemistry for Multifunctional Coatings. *Science*, 318(5849) 426–430 (2007). doi:10.1126/science.1147241

Lee, H., Lee, Y., Statz, A. R., Rho, J., Park, T. G. and Messersmith, P. B. Substrate-Independent Layer-by-Layer Assembly by Using Mussel-Adhesive-Inspired Polymers. *Advanced Materials*, 20(9) 1619–1623 (2008). doi:10.1002/adma.200702378

Lee, H., Rho, J. and Messersmith, P. B. Facile Conjugation of Biomolecules onto Surfaces via Mussel Adhesive Protein Inspired Coatings. *Advanced Materials*, 21(4) 431–434 (2009). doi:10.1002/adma.200801222

Lee, H., Scherer, N. F. and Messersmith, P. B. Single-molecule mechanics of mussel adhesion. *Proceedings of the National Academy of Sciences of the United States of America*, 103(35) 12999–13003 (2006). doi:10.1073/pnas.0605552103

Lee, M., Ku, S. H., Ryu, J. and Park, C. B. Mussel-inspired functionalization of carbon nanotubes for hydroxyapatite mineralization. *Journal of Materials Chemistry*, 20(40) 8848–8853 (2010). doi:10.1039/c0jm01339k

Levy, G. C. and Lichter, R. L. *Nitrogen-15 Nuclear Magnetic Resonance Spectroscopy*. New York: John Wiley & Sons (1979).

Li, B., Liu, W., Jiang, Z., Dong, X., Wang, B. and Zhong, Y. Ultrathin and Stable Active Layer of Dense Composite Membrane Enabled by Poly(dopamine). *Langmuir*, 25(13) 7368–7374 (2009). doi:10.1021/la900262p

Li, C. Y., Wang, W. C., Xu, F. J., Zhang, L. Q. and Yang, W. T. Preparation of pH-sensitive membranes via dopamine-initiated atom transfer radical polymerization. *Journal of Membrane Science*, 367(1-2) 7–13 (2011). doi:10.1016/j.memsci.2010.09.057

Li, F., Feng, Y., Yang, L., Li, L., Tang, C. and Tang, B. A selective novel non-enzyme glucose amperometric biosensor based on lectin-sugar binding on thionine modified electrode. *Biosensors & Bioelectronics*, 26(5) 2489–2494 (2011). doi:10.1016/j.bios.2010.10.040

Li, F., Yang, L., Zhao, C. and Du, Z. Electroactive gold nanoparticles/polyaniline/polydopamine hybrid composite in neutral solution as high-performance sensing platform. *Analytical Methods*, 3(7) 1601–1606 (2011). doi:10.1039/c1ay05126a

Li, J., Wang, Z., Li, P., Zong, N. and Li, F. A sensitive non-enzyme sensing platform for glucose based on boronic acid–diol binding. *Sensors and Actuators B: Chemical*, 161(1) 832–837 (2012). doi:10.1016/j.snb.2011.11.042

Li, R. H. and Barbari, T. A. Performance of poly(vinyl alcohol) thin-gel composite ultrafiltration membranes. *Journal of Membrane Science*, 105(1-2) 71–78 (1995). doi:10.1016/0376-7388(95)00048-H

Liang, R.-P., Meng, X.-Y., Liu, C.-M. and Qiu, J.-D. PDMS microchip coated with polydopamine/gold nanoparticles hybrid for efficient electrophoresis separation of amino acids. *Electrophoresis*, 32(23) 3331–40 (2011). doi:10.1002/elps.201100403

Liang, S., Liu, C. and Song, L. Two-Step Optimization of Pressure and Recovery of Reverse Osmosis Desalination Process. *Environmental Science & Technology*, 43(9) 3272–3277 (2009). doi:10.1021/es803692h

Liao, F., Yin, S., Toney, M. F. and Subramanian, V. Physical discrimination of amine vapor mixtures using polythiophene gas sensor arrays. *Sensors and Actuators B: Chemical*, 150(1) 254–263 (2010). doi:10.1016/j.snb.2010.07.006

Liao, Y., Cao, B., Wang, W.-C., Zhang, L., Wu, D. and Jin, R. A facile method for preparing highly conductive and reflective surface-silvered polyimide films. *Applied Surface Science*, 255(19) 8207–8212 (2009). doi:10.1016/j.apsusc.2009.05.038

Lin, Haiqin, Van Wagner, E., Swinnea, J. S., Freeman, B. D., Pas, S. J., Hill, A. J., Kalakkunnath, S. and Kalika, D. S. Transport and structural characteristics of crosslinked poly(ethylene oxide) rubbers. *Journal of Membrane Science*, 276(1-2) 145–161 (2006). doi:10.1016/j.memsci.2005.09.040

Lin, Haiqing, Kai, T., Freeman, B. D., Kalakkunnath, S. and Kalika, D. S. The Effect of Cross-Linking on Gas Permeability in Cross-Linked Poly(Ethylene Glycol Diacrylate). *Macromolecules*, 38(20) 8381–8393 (2005). doi:10.1021/ma0510136

Liu, A., Zhao, L., Bai, H., Zhao, H., Xing, X. and Shi, G. Polypyrrole actuator with a bioadhesive surface for accumulating bacteria from physiological media. *ACS Applied Materials & Interfaces*, 1(4) 951–955 (2009). doi:10.1021/am9000387

Liu, C. and Martin, C. R. Composite membranes from photochemical synthesis of ultrathin polymer films. *Nature*, 352(6330) 50–52 (1991). doi:10.1038/352050a0

Liu, H., Xi, P., Xie, G., Shi, Y., Hou, F., Huang, L., Chen, F., Zeng, Z., Shao, C. and Wang, J. Simultaneous Reduction and Surface Functionalization of Graphene Oxide for Hydroxyapatite Mineralization. *The Journal of Physical Chemistry C*, 116(5) 3334–3341 (2012). doi:10.1021/jp2102226

Liu, K., Wei, W.-Z., Zeng, J.-X., Liu, X.-Y. and Gao, Y.-P. Application of a novel electrosynthesized polydopamine-imprinted film to the capacitive sensing of nicotine. *Analytical and Bioanalytical Chemistry*, 385(4) 724–729 (2006). doi:10.1007/s00216-006-0489-z

Liu, L., Wakamatsu, K., Ito, S. and Williamson, P. R. Catecholamine Oxidative Products, but Not Melanin, Are Produced by Cryptococcus neoformans during Neuropathogenesis in Mice. *Infection and Immunity*, 67(1) 108–112 (1999).

Liu, Q., Yu, B., Ye, W. and Zhou, F. Highly selective uptake and release of charged molecules by pH-responsive polydopamine microcapsules. *Macromolecular Bioscience*, 11(9) 1227–1234 (2011). doi:10.1002/mabi.201100061

Liu, W., Li, B., Cao, R., Jiang, Z., Yu, S., Liu, G. and Wu, H. Enhanced pervaporation performance of poly (dimethyl siloxane) membrane by incorporating titania microspheres with high silver ion loading. *Journal of Membrane Science*, 378(1-2) 382–392 (2011). doi:10.1016/j.memsci.2011.05.027

Loeb, S. and Sourirajan, S. Sea Water Demineralization by Means of an Osmotic Membrane. *Advances in Chemistry Series*, 38 117–132 (1963).

Long, Y., Wu, J., Wang, H., Zhang, X., Zhao, N. and Xu, J. Rapid sintering of silver nanoparticles in an electrolyte solution at room temperature and its application to fabricate conductive silver films using polydopamine as adhesive layers. *Journal of Materials Chemistry*, 21(13) 4875–4881 (2011). doi:10.1039/c0jm03838e

Longuet-Higgins, H. C. On the origin of the free radical property of melanins. *Archives of Biochemistry and Biophysics*, 86(2) 231–232 (1960). doi:10.1016/0003-9861(60)90410-0

Lonsdale, H. K. The Growth of Membrane Technology. *Journal of Membrane Science*, 10(2-3) 81–181 (1982). doi:10.1016/S0376-7388(00)81408-8

Lonsdale, H. K., Merten, U. and Riley, R. L. Transport Properties of Cellulose Acetate Osmotic Membranes. *Journal of Applied Polymer Science*, 9(4) 1341–1362 (1965). doi:10.1002/app.1965.070090413

Louie, J., Pinnau, I., Ciobanu, I., Ishida, K., Ng, A. and Reinhard, M. Effects of Polyether–Polyamide Block Copolymer Coating on Performance and Fouling of Reverse Osmosis Membranes. *Journal of Membrane Science*, 280(1-2) 762–770 (2006). doi:10.1016/j.memsci.2006.02.041

Lu, C.-C., Zhang, M., Li, A.-J., He, X.-W. and Yin, X.-B. 3,4-Dihydroxy-L-phenylalanine for Preparation of Gold Nanoparticles and as Electron Transfer Promoter in H2O2 Biosensor. *Electroanalysis*, 23(10) 2421–2428 (2011). doi:10.1002/elan.201100291

Luczak, T. Preparation and characterization of the dopamine film electrochemically deposited on a gold template and its applications for dopamine sensing in aqueous solution. *Electrochimica Acta*, 53(19) 5725–5731 (2008). doi:10.1016/j.electacta.2008.03.052

Luo, J., Ding, L., Wan, Y. and Jaffrin, M. Y. Threshold flux for shear-enhanced nanofiltration: Experimental observation in dairy wastewater treatment. *Journal of Membrane Science*, 409-410 276–284 (2012). doi:10.1016/j.memsci.2012.03.065

Lynge, M. E., Van der Westen, R., Postma, A. and Städler, B. Polydopamine--a nature-inspired polymer coating for biomedical science. *Nanoscale*, 3(12) 4916–4928 (2011). doi:10.1039/c1nr10969c

Maartens, A., Jacobs, E. P. and Swart, P. UF of Pulp and Paper Effluent: Membrane Fouling-Prevention and Cleaning. *Journal of Membrane Science*, 209(1) 81–92 (2002). doi:10.1016/S0376-7388(02)00266-1

Manini, P., D'Ischia, M., Milosa, M. and Prota, G. Acid-Promoted Competing Pathways in the Oxidative Polymerization of 5,6-Dihydroxyindoles and Related Compounds: Straightforward Cyclotrimerization Routes to Diindolocarbazole Derivatives. *Journal of Organic Chemistry*, 63(20) 7002–7008 (1998). doi:10.1021/jo980875k

Marshall, A. D., Munro, P. A. and Trägårdh, G. The effect of protein fouling in microfiltration and ultrafiltration on permeate flux, protein retention and selectivity: A literature review. *Desalination*, 91(1) 65–108 (1993). doi:10.1016/0011-9164(93)80047-Q

Marshall, A. D., Munro, P. A. and Trägårdh, G. Design and Development of a Cross-flow Membrane Rig to Compare Constant Pressure and Constant Flux Operation in Ultrafiltration and Microfiltration. *Transactions of the Institution of Chemical Engineers C: Food and Bioproducts Processing*, 74(2) 92–100 (1996).

Martma, K., Habicht, K.-L., Ramirez, X. M., Tepp, K., Käämbre, T., Volobujeva, O. and Shimmo, R. Polydopamine as an adhesive coating for open tubular capillary electrochromatography. *Electrophoresis*, 32(9) 1054–1060 (2011). doi:10.1002/elps.201000569

Mason, H. S. The Chemistry of Melanin. III. Mechanism of Oxidation of 3,4-Dihydroxyphenylalanine by Tyrosinase. *Journal of Biological Chemistry*, 172 83–99 (1948).

Matsuyama, H., Berghmans, S. and Lloyd, D. R. Formation of hydrophilic microporous membranes via thermally induced phase separation. *Journal of Membrane Science*, 142(2) 213–224 (1998). doi:10.1016/S0376-7388(97)00330-X

Matsuyama, H., Berghmans, S. and Lloyd, D. R. Formation of anisotropic membranes via thermally induced phase separation. *Polymer*, 40(9) 2289–2301 (1999). doi:10.1016/S0032-3861(98)00040-8

Matteucci, S., Yampolskii, Y., Freeman, B. D. and Pinnau, I. Transport of Gases and Vapors in Glassy and Rubbery Polymers. In Y. Yampolskii, I. Pinnau and B. D. Freeman (Eds.), *Materials Science of Membranes for Gas and Vapor Separation* (pp. 1–48). West Sussex, England: John Wiley & Sons (2006).

Mayer, S. and Prandi, J. Oxygenative radical cyclization with molecular oxygen. *Tetrahedron Letters*, 37(18) 3117–3120 (1996). doi:10.1016/0040-4039(96)00505-9

McCloskey, Bryan D., Ju, H. and Freeman, B. D. Composite Membranes Based on a Selective Chitosan−Poly(ethylene glycol) Hybrid Layer: Synthesis,

Characterization, and Performance in Oil−Water Purification. *Industrial & Engineering Chemistry Research*, 49(1) 366–373 (2010). doi:10.1021/ie901197u

McCloskey, Bryan D., Park, H. B., Ju, H., Rowe, B. W., Miller, D. J., Chun, B. J., Kin, K. and Freeman, B. D. Influence of Polydopamine Deposition Conditions on Pure Water Flux and Foulant Adhesion Resistance of Reverse Osmosis, Ultrafiltration, and Microfiltration Membranes. *Polymer*, 51(15) 3472–3485 (2010). doi:10.1016/j.polymer.2010.05.008

McCloskey, Bryan D., Park, H. B., Ju, H., Rowe, B. W., Miller, D. J. and Freeman, B. D. A Bioinspired Fouling-Resistant Surface Modification for Water Purification Membranes. *Journal of Membrane Science*, 413-414 82–90 (2012). doi:10.1016/j.memsci.2012.04.021

McCloskey, Bryan David. *Novel Surface Modifications and Materials for Fouling Resistant Water Purification Membranes*. The University of Texas at Austin (2009).

McDowell, L. M., Burzio, L. A., Waite, J. H. and Schaefer, J. Rotational Echo Double Resonance Detection of Cross-links Formed in Mussel Byssus under High-Flow Stress. *Journal of Biological Chemistry*, 274(29) 20293–20295 (1999). doi:10.1074/jbc.274.29.20293

McGinness, J., Corry, P. and Proctor, P. Amorphous Semiconductor Switching in Melanins. *Science*, 183(4127) 853–855 (1974). doi:10.1126/science.183.4127.853

Mehdizadeh, H., Dickson, J. M. and Eriksson, P. K. Temperature Effects on the Performance of Thin-Film Composite, Aromatic Polyamide Membranes. *Industrial & Engineering Chemistry Research*, 28(6) 814–824 (1989). doi:10.1021/ie00090a025

Meier-Haack, J., Derenko, S. and Seng, J. Fouling Reduction by Graft-Modification with Hydrophilic Polymers. *Separation Science and Technology*, 42(13) 2881–2889 (2007). doi:10.1080/01496390701558326

Meltzer, T. H. *Filtration in the Pharmaceutical Industry*. New York: Marcel Dekker (1987).

Meredith, P. and Riesz, J. Radiative Relaxation Quantum Yields for Synthetic Eumelanin. *Photochemistry and Photobiology*, 79(2) 211–216 (2004). doi:10.1562/0031-8655(2004)079<0211:RCRQYF>2.0.CO;2

Meredith, P. and Sarna, T. The physical and chemical properties of eumelanin. *Pigment Cell Research*, 19(6) 572–594 (2006). doi:10.1111/j.1600-0749.2006.00345.x

Metsämuuronen, S., Howell, J. and Nyström, M. Critical flux in ultrafiltration of myoglobin and baker's yeast. *Journal of Membrane Science*, 196(1) 13–25 (2002). doi:10.1016/S0376-7388(01)00572-5

Metsämuuronen, S. and Nyström, M. Critical flux in cross-flow ultrafiltration of protein solutions. *Desalination*, 175(1) 37–47 (2005). doi:10.1016/j.desal.2004.11.003

Mi, Y., Wang, Z., Liu, X., Yang, S., Wang, H., Ou, J., Li, Z. and Wang, J. A simple and feasible in-situ reduction route for preparation of graphene lubricant films applied to a variety of substrates. *Journal of Materials Chemistry*, 22(16) 8036–8042 (2012). doi:10.1039/c2jm16656a

Mickols, W. E. Composite Membrane with Polyalkylene Oxide Modified Polyamide Surface. U.S. Patent No. 6280853 (2001).

Miller, A. J. and Mihm, M. C. Mechanisms of Disease: Melanoma. *The New England Journal of Medicine*, 355(1) 51–65 (2006). doi:10.1056/NEJMra052166

Miller, D. J., Araújo, P. A., Correia, P., Ramsey, M. M., Kruithof, J. C., Van Loosdrecht, M. C. M., Freeman, B. D., Paul, D. R., Whiteley, M. and Vrouwenvelder, J. S. Short-term adhesion and long-term biofouling testing of polydopamine and poly(ethylene glycol) surface modifications of membranes and feed spacers for biofouling control. *Water Research*, 46(12) 3737–3753 (2012). doi:10.1016/j.watres.2012.03.058

Miller, D. J., Paul, D. R. and Freeman, B. D. A Crossflow Filtration System for Constant Permeate Flux Membrane Fouling Characterization. *Review of Scientific Instruments*, 84(3) 035003 (2013). doi:10.1063/1.4794909

Mirafzal, G. A. and Lozeva, A. M. Phase transfer catalyzed oxidation of alcohols with sodium hypochlorite. *Tetrahedron Letters*, 39(40) 7263–7266 (1998). doi:10.1016/S0040-4039(98)01584-6

Mochizuki, S. and Zydney, A. L. Theoretical Analysis of Pore Size Distribution Effects on Membrane Transport. *Journal of Membrane Science*, 82(3) 211–227 (1993). doi:10.1016/0376-7388(93)85186-Z

Mohammadi, T., Kazemimoghadam, M. and Saadabadi, M. Modeling of membrane fouling and flux decline in reverse osmosis during separation of oil in water emulsions. *Desalination*, 157(1-3) 369–375 (2003). doi:10.1016/S0011-9164(03)00419-3

Mondal, S. and Wickramasinghe, S. Produced water treatment by nanofiltration and reverse osmosis membranes. *Journal of Membrane Science*, 322(1) 162–170 (2008). doi:10.1016/j.memsci.2008.05.039

Montgomery, C. T. and Smith, M. B. Hydraulic Fracturing: History of an Enduring Technology. *Journal of Petroleum Technology*, 62(12) 26–32 (2010).

Mörner, K. A. H. Zur Kenntnis von der Farbstoffen der melanotischen Geschwülste. *Zeitschrift für physiologische Chemie*, 11 66–141 (1887).

Morresi, L., Ficcadenti, M., Pinto, N., Murri, R., Cuccioloni, M., Angeletti, M. and Tombesi, P. Optical and electrical behavior of synthetic melanin thin films spray-coated. *Energy Procedia*, 2(1) 177–182 (2010). doi:10.1016/j.egypro.2010.07.025

Morris, T. A., Peterson, A. W. and Tarlov, M. J. Selective Binding of RNase B Glycoforms by Polydopamine-Immobilized Concanavalin A. *Analytical Chemistry*, 81(13) 5413–5420 (2009). doi:10.1021/ac900715d

Mueller, J., Cen, Y. and Davis, R. H. Crossflow microfiltration of oily water. *Journal of Membrane Science*, 129(2) 221–235 (1997). doi:10.1016/S0376-7388(96)00344-4

Mulder, M. H. V., Hendrikman, J. O., Wijmans, J. G. and Smolders, C. a. A rationale for the preparation of asymmetric pervaporation membranes. *Journal of Applied Polymer Science*, 30(7) 2805–2820 (1985). doi:10.1002/app.1985.070300708

Napolitano, A., Pezzella, A., Prota, G., Seraglia, R. and Traldi, P. Structural Analysis of Synthetic Melanins from 5,6-Dihydroxyindole by Matrix-assisted Laser Desorption/Ionization Mass Spectrometry. *Rapid Communications in Mass Spectrometry*, 10(4) 468–472 (1996). doi:10.1002/(SICI)1097-0231(19960315)10:4<468::AID-RCM506>3.0.CO;2-6

Nejadnik, M. R., Van der Mei, H. C., Norde, W. and Busscher, H. J. Bacterial adhesion and growth on a polymer brush-coating. *Biomaterials*, 29(30) 4117–4121 (2008). doi:10.1016/j.biomaterials.2008.07.014

Nicot, J.-P. and Scanlon, B. R. Water Use for Shale-Gas Production in Texas, U.S. *Environmental Science & Technology*, 46(6) 3580–3586 (2012). doi:10.1021/es204602t

Nogales, A., Hsiao, B. S., Somani, R. H., Srinivas, S., Tsou, A. H., Balta-Calleja, F. J. and Ezquerra, T. A. Shear-induced crystallization of isotactic polypropylene with different molecular weight distributions: in situ small- and wide-angle X-ray

scattering studies. *Polymer*, 42(12) 5247–5256 (2001). doi:10.1016/S0032-3861(00)00919-8

Nunes, S. P., Sforça, M. L. and Peinemann, K.-V. Dense hydrophilic composite membranes for ultrafiltration. *Journal of Membrane Science*, 106(1-2) 49–56 (1995). doi:10.1016/0376-7388(95)00076-O

O'Sullivan, D. G. 657. Vibrational Frequency Correlations in Heterocyclic Molecules. Part VI. Spectral Features of a Range of Compounds Possessing a Benzene Ring Fused to a Five-membered Ring. *Journal of the Chemical Society*, 3278–3284 (1960). doi:10.1039/jr9600003278

Ognier, S., Wisniewski, C. and Grasmick, A. Membrane Bioreactor Fouling in Sub-critical Filtration Conditions: a Local Critical Flux Concept. *Journal of Membrane Science*, 229(1-2) 171–177 (2004). doi:10.1016/j.memsci.2003.10.026

Okuda, H., Wakamatsu, K., Ito, S. and Sota, T. Possible Oxidative Polymerization Mechanism of 5,6-Dihydroxyindole from ab Initio Calculations. *Journal of Physical Chemistry A*, 112(44) 11213–11222 (2008). doi:10.1021/jp711025m

Opella, S. J. Faster is better: improving the sensitivity of solid-state NMR. *Nature Methods*, 6(3) 197–198 (2009). doi:10.1038/nmeth0309-197

Orchard, G. E. and Calonje, E. The Effect of Melanin Bleaching on Immunohistochemical Staining in Heavily Pigmented Melanocytic Neoplasms. *The American Journal of Dermatopathology*, 20(4) 357–361 (1998). doi:10.1097/00000372-199808000-00006

Ou, J., Wang, J., Liu, S., Zhou, J., Ren, S. and Yang, S. Microtribological and electrochemical corrosion behaviors of polydopamine coating on APTS-SAM modified Si substrate. *Applied Surface Science*, 256(3) 894–899 (2009). doi:10.1016/j.apsusc.2009.08.081

Ou, J., Wang, J., Liu, S., Zhou, J. and Yang, S. Self-Assembly and Tribological Property of a Novel 3-Layer Organic Film on Silicon Wafer with Polydopamine Coating as the Interlayer. *Journal of Physical Chemistry C*, 113(47) 20429–20434 (2009). doi:10.1021/jp9073416

Ou, J., Wang, J., Qiu, Y., Liu, L. and Yang, S. Mechanical property and corrosion resistance of zirconia/polydopamine nanocomposite multilayer films fabricated via a novel non-electrostatic layer-by-layer assembly technique. *Surface and Interface Analysis*, 43(4) 803–808 (2011). doi:10.1002/sia.3631

Ou, J., Wang, J., Zhang, D., Zhang, P., Liu, S., Yan, P., Liu, B. and Yang, S. Fabrication and biocompatibility investigation of TiO2 films on the polymer substrates obtained via a novel and versatile route. *Colloids and Surfaces B: Biointerfaces*, 76(1) 123–127 (2010). doi:10.1016/j.colsurfb.2009.10.024

Ouyang, R., Lei, J. and Ju, H. Surface molecularly imprinted nanowire for protein specific recognition. *Chemical Communications*, (44) 5761–5763 (2008). doi:10.1039/b810248a

Ouyang, R., Lei, J. and Ju, H. Artificial receptor-functionalized nanoshell: facile preparation, fast separation and specific protein recognition. *Nanotechnology*, 21(18) 185502 (2010). doi:10.1088/0957-4484/21/18/185502

Palumbo, P., d'Ischia, M. and Prota, G. Tyrosinase-promoted oxidation of 5, 6-dihydroxyindole-2-carboxylic acid to melanin. Isolation and characterization of oligomer intermediates. *Tetrahedron*, 43(18) 4203–4206 (1987). doi:10.1016/S0040-4020(01)83461-X

Pan, F., Jia, H., Qiao, S., Jiang, Z., Wang, J., Wang, B. and Zhong, Y. Bioinspired fabrication of high performance composite membranes with ultrathin defect-free skin layer. *Journal of Membrane Science*, 341(1-2) 279–285 (2009). doi:10.1016/j.memsci.2009.06.020

Panzella, L., Pezzella, A., Napolitano, A. and D'Ischia, M. The First 5,6-Dihydroxyindole Tetramer by Oxidation of 5,5',6,6'-Tetrahydroxy- 2,4'-biindolyl and an Unexpected Issue of Positional Reactivity en Route to Eumelanin-Related Polymers. *Organic Letters*, 9(7) 1411–1414 (2007). doi:10.1021/ol070268w

Parthasarathy, A., Brumlik, C. J., Martin, C. R. and Collins, G. E. Interfacial polymerization of thin polymer films onto the surface of a microporous hollow-fiber membrane. *Journal of Membrane Science*, 94(1) 249–254 (1994). doi:10.1016/0376-7388(93)E0206-Y

Pasenkiewicz-Gierula, M. and Sealy, R. C. Analysis of the ESR spectrum of synthetic dopa melanin. *Biochimica et Biophysica Acta - General Subjects*, 884(3) 510–516 (1986). doi:10.1016/0304-4165(86)90202-3

Pasmore, M., Todd, P., Smith, S., Baker, D., Silverstein, J., Coons, D. and Bowman, C. N. Effects of ultrafiltration membrane surface properties on Pseudomonas aeruginosa biofilm initiation for the purpose of reducing biofouling. *Journal of Membrane Science*, 194(1) 15–32 (2001). doi:10.1016/S0376-7388(01)00468-9

Patil, A. O., Pennington, W. T., Desiraju, G. R., Curtin, D. Y. and Paul, I. C. Recent Studies on the Formation and Properties of Quinhydrone Complexes. *Molecular Crystals and Liquid Crystals*, 134(1) 279–304 (1986). doi:10.1080/00268948608079591

Paul, D. R. Diffusion During the Coagulation Step of Wet-Spinning. *Journal of Applied Polymer Science*, 12(3) 383–402 (1968). doi:10.1002/app.1968.070120301

Paulo, C. S. O., Vidal, M. and Ferreira, L. S. Antifungal Nanoparticles and Surfaces. *Biomacromolecules*, 11(10) 2810–2817 (2010). doi:10.1021/bm100893r

Peng, J., Feng, L.-N., Zhang, K., Li, J.-J., Jiang, L.-P. and Zhu, J.-J. Multifunctional Manganese Carbonate Microspheres with Superparamagnetic and Fluorescent Properties: Synthesis and Biological Application. *Chemistry*, 17(39) 10916–10923 (2011). doi:10.1002/chem.201100899

Percival, S. L., Walker, J. T. and Hunter, P. R. *Microbiological Aspects of Biofilms and Drinking Water*. Boca Raton, FL: CRC Press (2000).

Petersen, R. J. Composite reverse osmosis and nanofiltration membranes. *Journal of Membrane Science*, 83(1) 81–150 (1993). doi:10.1016/0376-7388(93)80014-O

Pezzella, A., Napolitano, A., D'Ischia, M. and Prota, G. Oxidative Polymerisation of 5,6-Dihydroxyindole-2-carboxylic Acid to Melanin: A New Insight. *Tetrahedron*, 52(23) 7913–7920 (1996). doi:10.1016/0040-4020(96)00362-6

Pezzella, A., Vogna, D. and Prota, G. Atropoisomeric melanin intermediates by oxidation of the melanogenic precursor 5,6-dihydroxyindole-2-carboxylic acid under biomimetic conditions. *Tetrahedron*, 58(19) 3681–3687 (2002). doi:10.1016/S0040-4020(02)00335-6

Piattelli, M., Fattorusso, E., Magno, S. and Nicolaus, R. A. The Structure of Melanins and Melanogenesis—III. *Tetrahedron*, 19(12) 2061–2072 (1963). doi:10.1016/0040-4020(63)85021-8

Pines, A., Gibby, M. G. and Waugh, J. S. Proton-enhanced NMR of dilute spins in solids. *The Journal of Chemical Physics*, 59(2) 15–19 (1973). doi:10.1063/1.1680061

Pinnau, I. Recent advances in the formation of ultrathin polymeric membranes for gas separations. *Polymers for Advanced Technologies*, 5(11) 733–744 (1994). doi:10.1002/pat.1994.220051106

Pinnau, I. and Koros, W. J. Structures and gas separation properties of asymmetric polysulfone membranes made by dry, wet, and dry/wet phase inversion. *Journal of Applied Polymer Science*, 43(8) 1491–1502 (1991). doi:10.1002/app.1991.070430811

Poh, C. K., Shi, Z., Lim, T. Y., Neoh, K. G. and Wang, W. The effect of VEGF functionalization of titanium on endothelial cells in vitro. *Biomaterials*, 31(7) 1578–1585 (2010). doi:10.1016/j.biomaterials.2009.11.042

Polysulfone Sheet Membrane Products. *Sepro Membranes*, PSsheet07 (2011). Retrieved from http://www.sepromembranes.com/pdf/PSsheet07.pdf

Pompilio, A., Piccolomini, R., Picciani, C., D'Antonio, D., Savini, V. and Di Bonaventura, G. Factors associated with adherence to and biofilm formation on polystyrene by Stenotrophomonas maltophilia: the role of cell surface hydrophobicity and motility. *FEMS Microbiology Letters*, 287(1) 41–47 (2008). doi:10.1111/j.1574-6968.2008.01292.x

Pop-Georgievski, O., Popelka, Š., Houska, M., Chvostová, D., Proks, V. and Rypáček, F. Poly(ethylene oxide) layers grafted to dopamine-melanin anchoring layer: stability and resistance to protein adsorption. *Biomacromolecules*, 12(9) 3232–3242 (2011). doi:10.1021/bm2007086

Postma, A., Yan, Y., Wang, Y., Zelikin, A. N., Tjipto, E. and Caruso, F. Self-Polymerization of Dopamine as a Versatile and Robust Technique to Prepare Polymer Capsules. *Chemistry of Materials*, 21(14) 3042–3044 (2009). doi:10.1021/cm901293e

Pretsch, E., Bühlmann, P. and Baderstcher, M. *Structure Determination of Organic Compounds*. Berlin: Springer (2009).

Producing Food. Food and Agricultrure Organization of the United Nations (2009).

Prota, G. *Melanins and Melanogenesis*. San Diego: Academic Press (1992).

Pullman, A. and Pullman, B. The band structure of melanins. *Biochimica et Biophysica Acta*, 54(2) 384–385 (1961). doi:10.1016/0006-3002(61)90389-4

Purkyně, J. E. *Bericht uber die Versammlung deutscher Naturforscher und Aerzte in Prag im September 1837*. (K. M. von Sternberg and J. V. Krombholz, Eds.) (pp. 174 – 180). Prague: Druck von G. Haase Söhne (1838).

Raasch, C. Falling Natural Gas Prices Hit States' Pocketbooks. *USA Today*, p. 3B (2012, May 2).

Ragimov, A. V, Mamedov, B. A. and Liogon'kii, B. I. The alkali initiated polymerization of p-benzoquinone. *Polymer Science USSR*, 19(11) 2922–2928 (1977). doi:10.1016/0032-3950(77)90312-4

Ragimov, A. V, Ragimov, I. I., Mamedov, B. A., Guseinov, S. A. and Liogon'kii, B. I. On features of the oligomerization of hydroquinone under auto-oxidation. *Polymer Science USSR*, 24(10) 2434–2440 (1982). doi:10.1016/0032-3950(82)90116-2

RajanBabu, T. V. Stereochemistry of intramolecular free-radical cyclization reactions. *Accounts of Chemical Research*, 24(5) 139–145 (1991). doi:10.1021/ar00005a003

Rana, D. and Matsuura, T. Surface Modifications for Antifouling Membranes. *Chemical Reviews*, 110(4) 2448–2471 (2010). doi:10.1021/cr800208y

Raper, H. S. The Aerobic Oxidases. *Physiological Reviews*, 8(2) 245–282 (1928).

Rassenfoss, S. From Flowback to Fracturing: Water Recycling Grows in the Marcellus Shale. *Journal of Petroleum Technology*, 63(7) 48–51 (2011).

Reddaway, R. J. B. The Determination of Vicinal Glycols by Oxidation with Periodate in Non-aqueous Media. *Analyst*, 82(976) 506–511 (1957). doi:10.1039/an9578200506

Ren, Y., Rivera, J. G., He, L., Kulkarni, H., Lee, D.-K. and Messersmith, P. B. Facile, high efficiency immobilization of lipase enzyme on magnetic iron oxide nanoparticles via a biomimetic coating. *BMC Biotechnology*, 11 63 (2011). doi:10.1186/1472-6750-11-63

Ridgway, H F, Rigby, M. G. and Argo, D. G. Adhesion of a Mycobacterium sp. to Cellulose Diacetate Membranes Used in Reverse Osmosis. *Applied and Environmental Microbiology*, 47(1) 61–67 (1984).

Ridgway, Harry F. Microbial Adhesion and Biofouling of Reverse Osmosis Membranes. *Chemical Industries*, 35 429–481 (1988).

Ridgway, Harry F, Justice, C. A., Whittaker, C., Argo, D. G. and Olson, B. H. Biofilm fouling of RO membranes - its nature and effect on treatment of water for reuse. *Journal of the American Water Works Association*, 76(6) 94–102 (1984).

Ridgway, Harry F, Rigby, M. G. and Argo, D. G. Bacterial Adhesion and Fouling of Reverse Osmosis Membranes. *Journal of the American Water Works Association*, 77(7) 97–106 (1985).

Riesz, J., Gilmore, J. and Meredith, P. Quantitative Scattering of Melanin Solutions. *Biophysical Journal*, 90(11) 4137–4144 (2006). doi:10.1529/biophysj.105.075713

Rieth, S., Bao, X., Wang, B.-Y., Hadad, C. M. and Badjić, J. D. Gated molecular recognition and dynamic discrimination of guests. *Journal of the American Chemical Society*, 132(2) 773–776 (2010). doi:10.1021/ja908436c

Riley, P A. Melanin. *International Journal of Biochemistry and Cell Biology*, 29(11) 1235–1239 (1997). doi:10.1016/S1357-2725(97)00013-7

Rim, N. G., Kim, S. J., Shin, Y. M., Jun, I., Lim, D. W., Park, J. H. and Shin, H. Mussel-inspired surface modification of poly(L-lactide) electrospun fibers for modulation of osteogenic differentiation of human mesenchymal stem cells. *Colloids and Surfaces B: Biointerfaces*, 91 189–97 (2012). doi:10.1016/j.colsurfb.2011.10.057

Roosjen, A., Kaper, H. J., Van der Mei, H. C., Norde, W. and Busscher, H. J. Inhibition of Adhesion of Yeasts and Bacteria by Poly(ethylene oxide)-brushes on Glass in a Parallel Plate Flow Chamber. *Microbiology*, 149(11) 3239–3246 (2003). doi:10.1099/mic.0.26519-0

Roosjen, A., Van der Mei, H. C., Busscher, H. J. and Norde, W. Microbial Adhesion to Poly(ethylene oxide) Brushes: Influence of Polymer Chain Length and Temperature. *Langmuir*, 20(25) 10949–10955 (2004). doi:10.1021/la048469l

Rousselot-Pailley, P., Maux, D., Wieruszeski, J.-M., Aubagnac, J.-L., Martinez, J. and Lippens, G. Impurity Detection in Solid-Phase Organic Chemistry: Scope and Limits of HR MAS NMR. *Tetrahedron*, 56(29) 5163–5167 (2000). doi:10.1016/S0040-4020(00)00430-0

Rubianes, M. D. and Strumia, M. C. Polyethylenimine Functionalized with Dopamine: Characterization and Electrocatalytic Properties. *Electroanalysis*, 22(11) 1200–1206 (2010). doi:10.1002/elan.200900552

Ryu, J., Ku, S. H., Lee, H. and Park, C. B. Mussel-Inspired Polydopamine Coating as a Universal Route to Hydroxyapatite Crystallization. *Advanced Functional Materials*, 20(13) 2132–2139 (2010). doi:10.1002/adfm.200902347

Ryu, J., Ku, S. H., Lee, M. and Park, C. B. Bone-like peptide/hydroxyapatite nanocomposites assembled with multi-level hierarchical structures. *Soft Matter*, 7(16) 7201–7206 (2011). doi:10.1039/c1sm05307h

Sadeghi, F, Tabatabaei, S. H., Ajji, A. and Carreau, P. J. Effect of PVDF characteristics on extruded film morphology and porous membranes feasibility by stretching. *Journal of Polymer Science Part B: Polymer Physics*, 47(12) 1219–1229 (2009). doi:10.1002/polb.21725

Sadeghi, Farhad, Ajji, A. and Carreau, P. J. Analysis of row nucleated lamellar morphology of polypropylene obtained from the cast film process: Effect of melt rheology and process conditions. *Polymer Engineering & Science*, 47(7) 1170–1178 (2007). doi:10.1002/pen.20837

Safar, M., Jafar, M., Abdel-Jawad, M. and Bou-Hamad, S. Standardization of RO membrane performance. *Desalination*, 118(1-3) 13–21 (1998). doi:10.1016/S0011-9164(98)00070-8

Sagle, A. C., Ju, H., Freeman, B. D. and Sharma, M. M. PEG-Based Hydrogel Membrane Coatings. *Polymer*, 50(3) 756–766 (2009). doi:10.1016/j.polymer.2008.12.019

Sagle, A. C., Van Wagner, E. M., Ju, H., McCloskey, B. D., Freeman, B. D. and Sharma, M. M. PEG-Coated Reverse Osmosis Membranes: Desalination Properties and Fouling Resistance. *Journal of Membrane Science*, 340(1-2) 92–108 (2009). doi:10.1016/j.memsci.2009.05.013

Sánchez-Cortés, S., Francioso, O., García-Ramos, J. ., Ciavatta, C. and Gessa, C. Catechol polymerization in the presence of silver surface. *Colloids and Surfaces A*, 176(2-3) 177–184 (2001). doi:10.1016/S0927-7757(00)00630-0

Sarna, T. and Sealy, R. C. Free Radicals from Eumelanins: Quantum Yields and Wavelength Dependence. *Archives of Biochemistry and Biophysics*, 232(2) 574–578 (1984). doi:10.1016/0003-9861(84)90575-7

Scheffer, J., Wong, Y. F., Patil, A. O., Curtin, D. Y. and Paul, I. C. CPMAS (cross-polarization magic angle spinning) carbon-13 NMR spectra of quinones, hydroquinones, and their complexes. Use of CMR to follow a reaction in the solid state. *Journal of the American Chemical Society*, 107(17) 4898–4904 (1985). doi:10.1021/ja00303a014

Schüsler-Van Hees, M. T. I. W., Beijersbergen Van Henegouwen, G. M. J. and Stoutenberg, P. Autoxidation of catechol(amine)s. *Pharmaceutisch Weekblad Scientific Edition*, 7(6) 245–251 (1985). doi:10.1007/BF01959197

Seagle, B.-L. L., Rezai, K. A., Gasyna, E. M., Kobori, Y., Rezaei, K. A. and Norris, J. R. Time-Resolved Detection of Melanin Free Radicals Quenching Reactive Oxygen Species. *Journal of the American Chemical Society*, 127(32) 11220–11221 (2005). doi:10.1021/ja052773z

Seah, H., Tan, T. P., Chong, M. L. and Leong, J. NEWater—multi safety barrier approach for indirect potable use. *Water Science & Technology: Water Supply*, 8(5) 573–588 (2008). doi:10.2166/ws.2008.130

Senoh, S., Creveling, C. R., Udenfriend, S. and Witkop, B. Chemical, Enzymatic and Metabolic Studies on the Mechanism of Oxidation of Dopamine. *Journal of the American Chemical Society*, 81(23) 6236–6240 (1959). doi:10.1021/ja01532a030

Senoh, S. and Witkop, B. Formation and Rearrangements of Aminochromes from a New Metabolite of Dopamine and Some of its Derivatives. *Journal of the American Chemical Society*, 81(23) 6231–6235 (1959). doi:10.1021/ja01532a029

Sever, M. J. and Wilker, J. J. Absorption spectroscopy and binding constants for first-row transition metal complexes of a DOPA-containing peptide. *Dalton Transactions*, 6 813–822 (2006). doi:10.1039/b509586g

Shalev, T., Gopin, A., Bauer, M., Stark, R. W. and Rahimipour, S. Non-leaching antimicrobial surfaces through polydopamine bio-inspired coating of quaternary ammonium salts or an ultrashort antimicrobial lipopeptide. *Journal of Materials Chemistry*, 22(5) 2026–2032 (2012). doi:10.1039/c1jm13994k

Shannon, M. A., Bohn, P. W., Elimelech, M., Georgiadis, J. G., Mariñas, B. J. and Mayes, A. M. Science and technology for water purification in the coming decades. *Nature*, 452(7185) 301–310 (2008). doi:10.1038/nature06599

Shen, W., Cai, K., Yang, Z., Yan, Y., Yang, W. and Liu, P. Improved endothelialization of NiTi alloy by VEGF functionalized nanocoating. *Colloids and Surfaces B: Biointerfaces*, 94 347–353 (2012). doi:10.1016/j.colsurfb.2012.02.009

Shim, Y., Lee, H.-J., Lee, S., Moon, S.-H. and Cho, J. Effects of Natural Organic Matter and Ionic Species on Membrane Surface Charge. *Environmental Science & Technology*, 36(17) 3864–3871 (2002).

Shin, Y. M., Lee, Y. Bin and Shin, H. Time-dependent mussel-inspired functionalization of poly(L-lactide-co-ε-caprolactone) substrates for tunable cell behaviors. *Colloids and Surfaces B: Biointerfaces*, 87(1) 79–87 (2011). doi:10.1016/j.colsurfb.2011.05.004

Si, J. and Yang, H. Preparation and characterization of bio-compatible Fe3O4@Polydopamine spheres with core/shell nanostructure. *Materials Chemistry and Physics*, 128(3) 519–524 (2011). doi:10.1016/j.matchemphys.2011.03.039

Sijbesma, R. P., Beijer, F. H., Brunsveld, L., Folmer, B. J. B., Hirschberg, J. H. K. K., Lange, R. F. M., Lowe, J. K. L. and Meijer, E. W. Reversible Polymers Formed from Self-Complementary Monomers Using Quadruple Hydrogen Bonding. *Science*, 278(5343) 1601–1604 (1997). doi:10.1126/science.278.5343.1601

Sileika, T. S., Kim, H.-D., Maniak, P. and Messersmith, P. B. Antibacterial performance of polydopamine-modified polymer surfaces containing passive and active components. *ACS Applied Materials & Interfaces*, 3(12) 4602–10 (2011). doi:10.1021/am200978h

Sim, L.-N., Ye, Y., Chen, V. and Fane, A. G. Comparison of MFI-UF constant pressure, MFI-UF constant flux and Crossflow Sampler – Modified Fouling Index Ultrafiltration (CFS-MFIUF). *Water Research*, 45(4) 1639–1650 (2010). doi:10.1016/j.watres.2010.12.001

Simões, L. C., Simões, M. and Vieira, M. J. Adhesion and biofilm formation on polystyrene by drinking water-isolated bacteria. *Antonie van Leeuwenhoek*, 98(3) 317–329 (2010). doi:10.1007/s10482-010-9444-2

Simon, G. Zür Entwickelungsgeschichte der Haare. *Joh. Müllers Archiv für Anatomie*, 367 (1841).

Singh, S., Khulbe, K. ., Matsuura, T. and Ramamurthy, P. Membrane Characterization by Solute Transport and Atomic Force Microscopy. *Journal of Membrane Science*, 142(1) 111–127 (1998). doi:10.1016/S0376-7388(97)00329-3

Sinnokrot, M. O. and Sherrill, C. D. High-accuracy quantum mechanical studies of pi-pi interactions in benzene dimers. *The Journal of Physical Chemistry A*, 110(37) 10656–68 (2006). doi:10.1021/jp0610416

Sioutopoulos, D. C. and Karabelas, A. J. Correlation of organic fouling resistances in RO and UF membrane filtration under constant flux and constant pressure. *Journal of Membrane Science*, 407-408 34–46 (2012). doi:10.1016/j.memsci.2012.03.036

Sivik, B., Wahlgren, M. and Miezis, Y. A rheological screening method for membrane modifying polymers. *Desalination*, 77 181–193 (1990). doi:10.1016/0011-9164(90)85025-6

Standard Practice for Standardizing Reverse Osmosis Performance Data. *ASTM Standard D4516-00* (2010). doi:10.1520/D4516-00R10

Standard Test Methods for Operating Characteristics of Reverse Osmosis and Nanofiltration Devices. *ASTM Standard D4194-03* (2008).

Stark, K. B., Gallas, J. M., Zajac, G. W., Golab, J. T., Gidanian, S., McIntire, T. and Farmer, P. J. Effect of Stacking and Redox State on Optical Absorption Spectra of Melanins -- Comparison of Theoretical and Experimental Results. *Journal of Physical Chemistry B*, 109(5) 1970–1977 (2005). doi:10.1021/jp046710z

Stein, R. S., Elena, B. and Emsley, L. Improving resolution in proton solid-state NMR by removing nitrogen-14 residual dipolar broadening. *Chemical Physics Letters*, 458(4-6) 391–395 (2008). doi:10.1016/j.cplett.2008.05.008

Stoller, M., Bravi, M. and Chianese, A. Threshold Flux Measurements of a Nanofiltration Membrane Module by Critical Flux Data Conversion. *Desalination*, 315 142–148 (2013). doi:10.1016/j.desal.2012.11.013

Sulaimon, S. S. and Kitchell, B. E. The biology of melanocytes. *Veterinary Dermatology*, 14(2) 57–65 (2003). doi:10.1046/j.1365-3164.2003.00327.x

Sun, K., Xie, Y., Ye, D., Zhao, Y., Cui, Y., Long, F., Zhang, W. and Jiang, X. Mussel-inspired anchoring for patterning cells using polydopamine. *Langmuir*, 28(4) 2131–2136 (2012). doi:10.1021/la2041967

Sureshkumar, M. and Lee, C.-K. Polydopamine coated magnetic-chitin (MCT) particles as a new matrix for enzyme immobilization. *Carbohydrate Polymers*, 84(2) 775–780 (2011). doi:10.1016/j.carbpol.2010.03.036

Sureshkumar, M., Lee, P.-N. and Lee, C.-K. Stepwise assembly of multimetallic nanoparticles via self-polymerized polydopamine. *Journal of Materials Chemistry*, 21(33) 12316–12320 (2011). doi:10.1039/c1jm11914a

Sureshkumar, M., Siswanto, D. Y. and Lee, C.-K. Magnetic antimicrobial nanocomposite based on bacterial cellulose and silver nanoparticles. *Journal of Materials Chemistry*, 20(33) 6948–6955 (2010). doi:10.1039/c0jm00565g

Surjaatmadja, J., McDaniel, B., Case, L., East, L. and Pyecroft, J. Consideration for Future Stimulation Options Is Vital in Deciding Horizontal Well Drilling and Completion Schemes for Production Optimization. *SPE Production & Operations*, 23(2) 27–31 (2008). doi:10.2118/103774-PA

Suzuki, M., Kishida, a., Iwata, H. and Ikada, Y. Graft copolymerization of acrylamide onto a polyethylene surface pretreated with glow discharge. *Macromolecules*, 19(7) 1804–1808 (1986). doi:10.1021/ma00161a005

Swan, G. A. Structure, chemistry, and biosynthesis of the melanins. *Progress in the Chemistry of Organic Natural Products*, 31 521–582 (1974). doi:10.1007/978-3-7091-7094-6_9

Swift, J. A. Speculations on the molecular structure of eumelanin. *International Journal of Cosmetic Science*, 31(2) 143–150 (2009). doi:10.1111/j.1468-2494.2008.00488.x

Tabatabaei, S., Carreau, P. and Ajji, a. Microporous membranes obtained from polypropylene blend films by stretching. *Journal of Membrane Science*, 325(2) 772–782 (2008). doi:10.1016/j.memsci.2008.09.001

Takahashi, H., Akutsu, H. and Fujiwara, T. A magic-angle-spinning NMR method for 1H-1H distance measurement using coherent polarization transfer in 13C-labeled organic solids. *The Journal of Chemical Physics*, 129(15) 154504 (2008). doi:10.1063/1.2993170

Tan, Y., Deng, W., Li, Y., Huang, Z., Meng, Y., Xie, Q., Ma, M. and Yao, S. Polymeric bionanocomposite cast thin films with in situ laccase-catalyzed polymerization of dopamine for biosensing and biofuel cell applications. *The Journal of Physical Chemistry B*, 114(15) 5016–5024 (2010). doi:10.1021/jp100922t

Tang, X., Flint, S. H., Brooks, J. D. and Bennett, R. J. Factors affecting the attachment of micro-organisms isolated from ultrafiltration and reverse osmosis membranes in dairy processing plants. *Journal of Applied Microbiology*, 107(2) 443–451 (2009). doi:10.1111/j.1365-2672.2009.04214.x

Taniguchi, M. and Belfort, G. Low protein fouling synthetic membranes by UV-assisted surface grafting modification: varying monomer type. *Journal of Membrane Science*, 231(1-2) 147–157 (2004). doi:10.1016/j.memsci.2003.11.013

Taniguchi, M., Kilduff, J. E. and Belfort, G. Low fouling synthetic membranes by UV-assisted graft polymerization: monomer selection to mitigate fouling by natural organic matter. *Journal of Membrane Science*, 222(1-2) 59–70 (2003a). doi:10.1016/S0376-7388(03)00192-3

Taniguchi, M., Kilduff, J. E. and Belfort, G. Modes of Natural Organic Matter Fouling during Ultrafiltration. *Environmental Science & Technology*, 37(8) 1676–1683 (2003b). doi:10.1021/es020555p

Tao, C., Yang, S., Zhang, J. and Wang, J. Surface modification of diamond-like carbon films with protein via polydopamine inspired coatings. *Applied Surface Science*, 256(1) 294–297 (2009). doi:10.1016/j.apsusc.2009.08.024

Taskier, H. T. Hydrophilic Microporous Film. U.S. Patent No. 3853601 (1974).

Taylor, M., Urquhart, A. J., Anderson, D. G., Williams, P. M., Langer, R., Alexander, M. R. and Davies, M. C. A Methodology for Investigating Protein Adhesion and Adsorption to Microarrayed Combinatorial Polymers. *Macromolecular Rapid Communications*, 29(15) 1298–1302 (2008). doi:10.1002/marc.200800171

The United Nations World Water Development Report 3. Paris, France: The United Nations Educational, Scientific, and Cultural Organization (2009).

The United Nations World Water Development Report 3: Facts and Figures. Paris, France: The United Nations Educational, Scientific, and Cultural Organization (2009).

Tsai, W.-B., Chen, W.-T., Chien, H.-W., Kuo, W.-H. and Wang, M.-J. Poly(dopamine) coating of scaffolds for articular cartilage tissue engineering. *Acta Biomaterialia*, 7(12) 4187–4194 (2011). doi:10.1016/j.actbio.2011.07.024

Tse, D. C. S., McCreery, R. L. and Adams, R. N. Potential oxidative pathways of brain catecholamines. *Journal of Medicinal Chemistry*, 19(1) 37–40 (1976). doi:10.1021/jm00223a008

Tseng, Y. C. and Park, K. Synthesis of photoreactive poly(ethylene glycol) and its application to the prevention of surface-induced platelet activation. *Journal of Biomedical Materials Research*, 26(3) 373–391 (1992). doi:10.1002/jbm.820260308

Turker, M. and Hubble, J. Membrane Fouling in a Constant-Flux Ultrafiltration Cell. *Journal of Membrane Science*, 34(2-3) 267–281 (1987). doi:10.1016/S0376-7388(00)83168-3

Turton, R., Bailie, R. C., Whiting, W. B. and Shaeiwitz, J. A. *Analysis, Synthesis, and Design of Chemical Processes* (2nd ed.). Upper Saddle River, NJ: Prentice Hall PTR (2003).

Uchida, E., Uyama, Y. and Ikada, Y. Grafting of Water-Soluble Chains onto a Polymer Surface. *Langmuir*, 10(2) 481–485 (1994). doi:10.1021/la00014a023

Uhlenheuer, D. A., Petkau, K. and Brunsveld, L. Combining supramolecular chemistry with biology. *Chemical Society Reviews*, 39(8) 2817–2826 (2010). doi:10.1039/b820283b

Ulbricht, M. Advanced functional polymer membranes. *Polymer*, 47(7) 2217–2262 (2006). doi:10.1016/j.polymer.2006.01.084

Ulbricht, M. and Belfort, G. Surface modification of ultrafiltration membranes by low temperature plasma. I. Treatment of polyacrylonitrile. *Journal of Applied Polymer Science*, 56(3) 325–343 (1995). doi:10.1002/app.1995.070560304

Ulbricht, M. and Belfort, G. Surface modification of ultrafiltration membranes by low temperature plasma II. Graft polymerization onto polyacrylonitrile and polysulfone. *Journal of Membrane Science*, 111(2) 193–215 (1996). doi:10.1016/0376-7388(95)00207-3

Ulbricht, M., Matuschewski, H., Oechel, A. and Hicke, H.-G. Photo-induced Graft Polymerization Surface Modifications for the Preparation of Hydrophilic and Low-proten-adsorbing Ultrafiltration Membranes. *Journal of Membrane Science*, 115(1) 31–47 (1996). doi:10.1016/0376-7388(95)00264-2

Ulbricht, M., Oechel, A., Lehmann, C., Tomaschewski, G. and Hicke, H.-G. Gas-phase photoinduced graft polymerization of acrylic acid onto polyacrylonitrile ultrafiltration membranes. *Journal of Applied Polymer Science*, 55(13) 1707–1723 (1995). doi:10.1002/app.1995.070551301

Van der Marel, P., Zwijnenburg, A., Kemperman, A., Wessling, M., Temmink, H. and Van der Meer, W. An Improved Flux-step Method to Determine the Critical Flux and the Critical Flux for Irreversibility in a Membrane Bioreactor. *Journal of Membrane Science*, 332(1-2) 24–29 (2009). doi:10.1016/j.memsci.2009.01.046

Van Loosdrecht, M. C. M., Lyklema, J., Norde, W. and Zehnder, A. J. B. Influence of Interfaces on Microbial Activity. *Microbiological Reviews*, 54(1) 75–87 (1990).

Van Wagner, E. M., Sagle, A. C., Sharma, M. M. and Freeman, B. D. Effect of Crossflow Testing Conditions, including Feed pH and Continuous Feed Filtration, on Commercial Reverse Osmosis Membrane Performance. *Journal of Membrane Science*, 345(1-2) 97–109 (2009). doi:10.1016/j.memsci.2009.08.033

Van Wagner, E. M., Sagle, A. C., Sharma, M. M., La, Y.-H. and Freeman, B. D. Surface Modification of Commercial Polyamide Desalination Membranes using Poly(ethylene glycol) Diglycidyl Ether to Enhance Membrane Fouling Resistance.

Journal of Membrane Science, 367(1-2) 273–287 (2011). doi:10.1016/j.memsci.2010.11.001

Veil, J. A., Puder, M. G., Elcock, D. and Redweik, R. J. *A White Paper Describing Produced Water from Production of Crude Oil, Natural Gas, and Coal Bed Methane* (2004).

Vigo, F., Uliana, C. and Traverso, M. Poly(vinyl chloride) ultrafiltration membranes modified by glow discharge grafting of poly(acrylic acid). *European Polymer Journal*, 27(8) 779–783 (1991). doi:10.1016/0014-3057(91)90008-C

Vital Water Graphics: An Overview of the State of the World's Fresh and Marine Waters. Nairobi, Kenya: United Nations Environment Programme (2008). Retrieved from http://www.unep.org/dewa/vitalwater/rubrique2.html

Vitkin, I. A., Woolsey, J., Wilson, B. C. and Anderson, R. R. Optical and Thermal Characterization of Natural (Sepia officinalis) Melanin. *Photochemistry and Photobiology*, 59(4) 455–462 (1994). doi:10.1111/j.1751-1097.1994.tb05064.x

Von Byern, J and Grunwald, I. *Biological Adhesive Systems*. Vienna: Springer (2010).

Von Byern, Janek and Grunwald, I. *Biological Adhesive Systems: From Nature to Technical and Medical Application*. Vienna: Springer (2010).

Vrijenhoek, E. M., Hong, S. and Elimelech, M. Influence of membrane surface properties on initial rate of colloidal fouling of reverse osmosis and nanofiltration membranes. *Journal of Membrane Science*, 188(1) 115–128 (2001). doi:10.1016/S0376-7388(01)00376-3

Vrouwenvelder, J. S., Bakker, S. M., Wessels, L. P. and Van Paassen, J. A. M. The Membrane Fouling Simulator as a New Tool for Biofouling Control of Spiral-wound Membranes. *Desalination*, 204(1-3) 170–174 (2007). doi:10.1016/j.desal.2006.04.028

Vrouwenvelder, J. S., Beyer, F., Dahmani, K., Hasan, N., Galjaard, G., Kruithof, J. C. and Van Loosdrecht, M. C. M. Phosphate Limitation to Control Biofouling. *Water Research*, 44(11) 3454–3466 (2010). doi:10.1016/j.watres.2010.03.026

Vrouwenvelder, J. S., Graf von der Schulenburg, D. A., Kruithof, J. C., Johns, M. L. and Van Loosdrecht, M. C. M. Biofouling of spiral-wound nanofiltration and reverse osmosis membranes: A feed spacer problem. *Water Research*, 43(3) 583–594 (2009). doi:10.1016/j.watres.2008.11.019

Vrouwenvelder, J. S., Kruithof, J. C. and Van Loosdrecht, M. C. M. Integrated Approach for Biofouling Control. *Water Science & Technology*, 62(11) 2477–2490 (2010). doi:10.2166/wst.2010.747

Vrouwenvelder, J. S., Manolarakis, S. A., Van der Hoek, J. P., Van Paassen, J. A. M., Van der Meer, W. G. J., Van Agtmaal, J. M. C., Prummel, H. D. M., Kruithof, J. C. and Van Loosdrecht, M. C. M. Quantitative biofouling diagnosis in full scale nanofiltration and reverse osmosis installations. *Water Research*, 42(19) 4856–4868 (2008). doi:10.1016/j.watres.2008.09.002

Vrouwenvelder, J. S., Van Paassen, J. A. M., Kruithof, J. C. and Van Loosdrecht, M. C. M. Sensitive pressure drop measurements of individual lead membrane elements for accurate early biofouling detection. *Journal of Membrane Science*, 338(1-2) 92–99 (2009). doi:10.1016/j.memsci.2009.04.016

Vrouwenvelder, J. S., Van Paassen, J. A. M., Wessels, L. P., Van Dam, A. F. and Bakker, S. M. The Membrane Fouling Simulator: A practical tool for fouling prediction and control. *Journal of Membrane Science*, 281(1-2) 316–324 (2006). doi:10.1016/j.memsci.2006.03.046

Vyas, H. K., Bennett, R. J. and Marshall, A. D. Performance of crossflow microfiltration during constant transmembrane pressure and constant flux operations. *International Dairy Journal*, 12(5) 473–479 (2002). doi:10.1016/S0958-6946(02)00020-1

Wan, Y., Zhang, D., Wang, Y., Qi, P. and Hou, B. Direct immobilisation of antibodies on a bioinspired architecture as a sensing platform. *Biosensors & Bioelectronics*, 26(5) 2595–2600 (2011). doi:10.1016/j.bios.2010.11.013

Wang, A.-J., Liao, Q.-C., Feng, J.-J., Yan, Z.-Z. and Chen, J.-R. In situ synthesis of polydopamine–Ag hollow microspheres for hydrogen peroxide sensing. *Electrochimica Acta*, 61 31–35 (2012). doi:10.1016/j.electacta.2011.11.063

Wang, G., Huang, H., Zhang, G., Zhang, X., Fang, B. and Wang, L. Dual amplification strategy for the fabrication of highly sensitive interleukin-6 amperometric immunosensor based on poly-dopamine. *Langmuir*, 27(3) 1224–1231 (2011). doi:10.1021/la1033433

Wang, G., Huang, H., Zhang, G., Zhang, X. and Wang, L. Dual functional electrochemical sensor based on Au–polydopamine–Fe3O4 nanocomposites. *Analytical Methods*, 3(11) 2475–2477 (2011). doi:10.1039/c1ay05404j

Wang, L., Jeong, K. J., Chiang, H. H., Zurakowski, D., Behlau, I., Chodosh, J., Dohlman, C. H., Langer, R. and Kohane, D. S. Hydroxyapatite for keratoprosthesis

biointegration. *Investigative Ophthalmology & Visual Science*, 52(10) 7392–7399 (2011). doi:10.1167/iovs.11-7601

Wang, P., Tan, K. L., Kang, E. T. and Neoh, K. G. Plasma-induced immobilization of poly(ethylene glycol) onto poly(vinylidene fluoride) microporous membrane. *Journal of Membrane Science*, 195(1) 103–114 (2002). doi:10.1016/S0376-7388(01)00548-8

Wang, R., Neoh, K. G., Shi, Z., Kang, E.-T., Tambyah, P. A. and Chiong, E. Inhibition of Escherichia coli and Proteus mirabilis adhesion and biofilm formation on medical grade silicone surface. *Biotechnology and Bioengineering*, 109(2) 336–345 (2012). doi:10.1002/bit.23342

Wang, W., Jiang, Y., Liao, Y., Tian, M., Zou, H. and Zhang, L. Fabrication of silver-coated silica microspheres through mussel-inspired surface functionalization. *Journal of Colloid and Interface Science*, 358(2) 567–574 (2011). doi:10.1016/j.jcis.2011.03.023

Wang, W., Jiang, Y., Wen, S., Liu, L. and Zhang, L. Preparation and characterization of polystyrene/Ag core-shell microspheres--a bio-inspired poly(dopamine) approach. *Journal of Colloid and Interface Science*, 368(1) 241–249 (2012). doi:10.1016/j.jcis.2011.10.047

Wang, W., Zhang, A., Liu, L., Tian, M. and Zhang, L. Dopamine-Induced Surface Functionalization for the Preparation of Al–Ag Bimetallic Microspheres. *Journal of The Electrochemical Society*, 158(4) D228–D233 (2011). doi:10.1149/1.3551496

Wang, Y., Liu, L., Li, M., Xu, S. and Gao, F. Multifunctional carbon nanotubes for direct electrochemistry of glucose oxidase and glucose bioassay. *Biosensors and Bioelectronics*, 30(1) 107–111 (2011). doi:10.1016/j.bios.2011.08.038

Water, Sanitation, and Hygiene Links to Health: Facts and Figures. *World Health Organization* (2004). Retrieved from http://www.who.int/water_sanitation_health/publications/facts2004/en/index.html

Watt, A. A. R., Bothma, J. P. and Meredith, P. The supramolecular structure of melanin. *Soft Matter*, 5(19) 3754–3760 (2009). doi:10.1039/b902507c

Webber, M. E. Catch-22: Water vs. Energy. *Scientific American*, 18(4) 34–41 (2008). doi:10.1038/scientificamericanearth0908-34

Wei, Q., Zhang, F., Li, J., Li, B. and Zhao, C. Oxidant-induced dopamine polymerization for multifunctional coatings. *Polymer Chemistry*, 1(9) 1430–1433 (2010). doi:10.1039/c0py00215a

Wesslén, B., Kober, M., Freij-Larsson, C., Ljungh, A. and Paulsson, M. Protein adsorption of poly(ether urethane) surfaces modified by amphiphilic and hydrophilic polymers. *Biomaterials*, 15(4) 278–284 (1994). Retrieved from http://www.ncbi.nlm.nih.gov/pubmed/8031988

Wienk, I. M., Boom, R. M., Beerlage, M. a. M., Bulte, a. M. W., Smolders, C. a. and Strathmann, H. Recent advances in the formation of phase inversion membranes made from amorphous or semi-crystalline polymers. *Journal of Membrane Science*, 113(2) 361–371 (1996). doi:10.1016/0376-7388(95)00256-1

Wijmans, J. ., Kant, J., Mulder, M. H. . and Smolders, C. . Phase separation phenomena in solutions of polysulfone in mixtures of a solvent and a nonsolvent: relationship with membrane formation. *Polymer*, 26(10) 1539–1545 (1985). doi:10.1016/0032-3861(85)90090-4

Wolbarsht, M. L., Walsh, A. W. and George, G. Melanin, a unique biological absorber. *Applied Optics*, 20(13) 2184–2186 (1981). doi:10.1364/AO.20.002184

Wu, C., Fan, W., Chang, J. and Xiao, Y. Mussel-inspired porous SiO2 scaffolds with improved mineralization and cytocompatibility for drug delivery and bone tissue engineering. *Journal of Materials Chemistry*, 21(45) 18300–18307 (2011). doi:10.1039/c1jm12770e

Wu, D., Howell, J. A. and Field, R. W. Critical Flux Measurement for Model Colloids. *Journal of Membrane Science*, 152(1) 89–98 (1999). doi:10.1016/S0376-7388(98)00200-2

Wu, J. Synthesis, characterization and crystal structure of a 3-D supramolecular Cu/Mn complex with pydc. *Crystal Research and Technology*, 43(10) 1097–1100 (2008). doi:10.1002/crat.200800020

Xi, Z.-Y., Xu, Y.-Y., Zhu, L.-P., Wang, Y. and Zhu, B.-K. A facile method of surface modification for hydrophobic polymer membranes based on the adhesive behavior of poly(DOPA) and poly(dopamine). *Journal of Membrane Science*, 327(1-2) 244–253 (2009). doi:10.1016/j.memsci.2008.11.037

Xie, J., Michael, P. L., Zhong, S., Ma, B., MacEwan, M. R. and Lim, C. T. Mussel inspired protein-mediated surface modification to electrospun fibers and their

potential biomedical applications. *Journal of Biomedical Materials Research A*, 100(4) 929–938 (2012). doi:10.1002/jbm.a.34030

Xie, W., Geise, G. M., Freeman, B. D., Lee, H.-S., Byun, G. and McGrath, J. E. Polyamide Interfacial Composite Membranes Prepared from m-Phenylene Diamine, Trimesoyl Chloride and a New Disulfonated Diamine. *Journal of Membrane Science*, 403-404 31–33 (2012). doi:10.1016/j.memsci.2012.02.038

Xu, Haolan, Liu, X. and Wang, D. Interfacial Basicity-Guided Formation of Polydopamine Hollow Capsules in Pristine O/W Emulsions – Toward Understanding of Emulsion Template Roles. *Chemistry of Materials*, 23(23) 5105–5110 (2011). doi:10.1021/cm2028417

Xu, Hong, Shi, X., Ma, H., Lv, Y., Zhang, L. and Mao, Z. The preparation and antibacterial effects of dopa-cotton/AgNPs. *Applied Surface Science*, 257(15) 6799–6803 (2011). doi:10.1016/j.apsusc.2011.02.129

Xu, L. Q., Jiang, H., Neoh, K.-G., Kang, E.-T. and Fu, G. D. Poly(dopamine acrylamide)-co-poly(propargyl acrylamide)-modified titanium surfaces for "click" functionalization. *Polymer Chemistry*, 3(4) 920–927 (2012). doi:10.1039/c2py00552b

Xu, L. Q., Yang, W. J., Neoh, K.-G., Kang, E.-T. and Fu, G. D. Dopamine-Induced Reduction and Functionalization of Graphene Oxide Nanosheets. *Macromolecules*, 43(20) 8336–8339 (2010). doi:10.1021/ma101526k

Xu, P., Bellona, C. and Drewes, J. E. Fouling of nanofiltration and reverse osmosis membranes during municipal wastewater reclamation: Membrane autopsy results from pilot-scale investigations. *Journal of Membrane Science*, 353(1-2) 111–121 (2010). doi:10.1016/j.memsci.2010.02.037

Yagai, S., Iwashima, T., Karatsu, T. and Kitamura, A. Synthesis and noncovalent polymerization of self-complementary hydrogen-bonding supramolecular synthons: N,N'-disubstituted 4,6-diamino-pyrimidin-2(1H)-ones. *Chemical Communications*, (9) 1114–1115 (2004). doi:10.1039/b401132e

Yan, P., Wang, J., Wang, L., Liu, B., Lei, Z. and Yang, S. The in vitro biomineralization and cytocompatibility of polydopamine coated carbon nanotubes. *Applied Surface Science*, 257(11) 4849–4855 (2011). doi:10.1016/j.apsusc.2010.12.111

Yang, G., Yu, X.-L., Chen, X.-M. and Ji, L.-N. Three-Dimensional Structure Constructed via Hydrogen Bonds and π-π Stacking Interaction. Crystal Structure of [Cu(AFO)2(H2O)2](ClO4)2.2(AFO).2H2O (AFO = 4,5-Diazafluoren-9-one).

Crystal Research and Technology, 35(8) 993–1000 (2000). doi:10.1002/1521-4079(200008)35:8<993::AID-CRAT993>3.0.CO;2-V

Yang, J., Lee, S., Lee, E., Lee, J. and Hong, S. Effect of solution chemistry on the surface property of reverse osmosis membranes under seawater conditions. *Desalination*, 247(1-3) 148–161 (2009). doi:10.1016/j.desal.2008.12.020

Yang, L., Phua, S. L., Teo, J. K. H., Toh, C. L., Lau, S. K., Ma, J. and Lu, X. A biomimetic approach to enhancing interfacial interactions: polydopamine-coated clay as reinforcement for epoxy resin. *ACS Applied Materials & Interfaces*, 3(8) 3026–3032 (2011). doi:10.1021/am200532j

Yang, S. H., Kang, S. M., Lee, K.-B., Chung, T. D., Lee, H. and Choi, I. S. Mussel-inspired encapsulation and functionalization of individual yeast cells. *Journal of the American Chemical Society*, 133(9) 2795–2797 (2011). doi:10.1021/ja1100189

Yang, X., Li, J., Zhao, X.-H., Wang, H.-W. and Shan, Y.-K. Hydrogen bonding and pi-pi stacking in the three-dimensional supramolecular complex bis(4,4'-bipyridinium) diaquadioxalatoferrate(II) bis(hydrogen oxalate). *Acta Crystallographica. Section C, Crystal Structure Communications*, 63(4) m171–m173 (2007). doi:10.1107/S0108270107006440

Yang, Y.-F., Hu, H.-Q., Li, Y., Wan, L.-S. and Xu, Z.-K. Membrane surface with antibacterial property by grafting polycation. *Journal of Membrane Science*, 376(1-2) 132–141 (2011). doi:10.1016/j.memsci.2011.04.012

Ye, W., Hu, H., Zhang, H., Zhou, F. and Liu, W. Multi-walled carbon nanotube supported Pd and Pt nanoparticles with high solution affinity for effective electrocatalysis. *Applied Surface Science*, 256(22) 6723–6728 (2010). doi:10.1016/j.apsusc.2010.04.080

Ye, W., Wang, D., Zhang, H., Zhou, F. and Liu, W. Electrochemical growth of flowerlike gold nanoparticles on polydopamine modified ITO glass for SERS application. *Electrochimica Acta*, 55(6) 2004–2009 (2010). doi:10.1016/j.electacta.2009.11.022

Yin, X.-B. and Liu, D.-Y. Polydopamine-based permanent coating capillary electrochromatography for auxin determination. *Journal of Chromatography A*, 1212(1-2) 130–136 (2008). doi:10.1016/j.chroma.2008.10.001

Youravong, W., Lewis, M. J. and Grandison, A. S. Critical Flux in Ultrafiltration of Skimmed Milk. *Food and Bioproducts Processing*, 81(4) 303–308 (2003). doi:10.1205/096030803322756385

Yu, B., Liu, J., Liu, S. and Zhou, F. Pdop layer exhibiting zwitterionicity: a simple electrochemical interface for governing ion permeability. *Chemical Communications*, 46(32) 5900–5902 (2010). doi:10.1039/c0cc00596g

Yu, B., Wang, D. A., Ye, Q., Zhou, F. and Liu, W. Robust polydopamine nano/microcapsules and their loading and release behavior. *Chemical Communications*, (44) 6789–6791 (2009). doi:10.1039/b910679k

Yu, F., Chen, S., Chen, Y., Li, H., Yang, L., Chen, Y. and Yin, Y. Experimental and theoretical analysis of polymerization reaction process on the polydopamine membranes and its corrosion protection properties for 304 Stainless Steel. *Journal of Molecular Structure*, 982(1-3) 152–161 (2010). doi:10.1016/j.molstruc.2010.08.021

Yu, F., Chen, S., Li, H., Yang, L. and Yin, Y. Application of Self Assembled 6-aminohexanol layers for corrosion protection of 304 stainless steel surface. *Thin Solid Films*, 520(15) 4990–4995 (2012). doi:10.1016/j.tsf.2012.03.006

Yu, H., Hu, M., Xu, Z., Wang, J. and Wang, S. Surface modification of polypropylene microporous membranes to improve their antifouling property in MBR: NH plasma treatment. *Separation and Purification Technology*, 45(1) 8–15 (2005). doi:10.1016/j.seppur.2005.01.012

Yu, H., Xie, Y., Hu, M., Wang, J., Wang, S. and Xu, Z. Surface modification of polypropylene microporous membrane to improve its antifouling property in MBR: CO plasma treatment. *Journal of Membrane Science*, 254(1-2) 219–227 (2005). doi:10.1016/j.memsci.2005.01.010

Zajac, G. W., Gallas, J. M., Cheng, J., Eisner, M., Moss, S. C. and Alvarado-Swaisgood, A. E. The fundamental unit of synthetic melanin: a verification by tunneling microscopy of X-ray scattering results. *Biochimica et Biophysica Acta*, 1199(3) 271–278 (1994). doi:10.1016/0304-4165(94)90006-X

Zeng, R., Luo, Z., Zhou, D., Cao, F. and Wang, Y. A novel PEG coating immobilized onto capillary through polydopamine coating for separation of proteins in CE. *Electrophoresis*, 31(19) 3334–3341 (2010). doi:10.1002/elps.201000228

Zeni, M., Bellobono, I. R., Muffato, F., Polissi, A., Selli, E. and Rastelli, E. Photosynthetic membranes. VI. Characterization of ultrafiltration membranes prepared by photografting zeolite-epoxy-diacrylate resin composites onto cellulose. *Journal of Membrane Science*, 36 277–295 (1988). doi:10.1016/0376-7388(88)80023-1

Zhang, A., He, J., Guan, Y., Li, Z., Zhang, Y. and Zhu, J. X. Oxidative polymerization of hydroquinone using deoxycholic acid supramolecular template. *Science China Chemistry*, 55(5) 830–835 (2012). doi:10.1007/s11426-012-4504-2

Zhang, H., Hu, H., Ye, W. and Zhou, F. Conferring polytetrafluoroethylene micropowders with hydrophilicity using dopamine chemistry and the application as water-based lubricant additive. *Journal of Applied Polymer Science*, 122(5) 3145–3151 (2011). doi:10.1002/app.34330

Zhang, L., Shi, J., Jiang, Z., Jiang, Y., Meng, R., Zhu, Y., Liang, Y. and Zheng, Y. Facile preparation of robust microcapsules by manipulating metal-coordination interaction between biomineral layer and bioadhesive layer. *ACS Applied Materials & Interfaces*, 3(2) 597–605 (2011). doi:10.1021/am101184h

Zhang, L., Shi, J., Jiang, Z., Jiang, Y., Qiao, S., Li, J., Wang, R., Meng, R., Zhu, Y. and Zheng, Y. Bioinspired preparation of polydopamine microcapsule for multienzyme system construction. *Green Chemistry*, 13(2) 300–306 (2011). doi:10.1039/c0gc00432d

Zhang, M., He, X., Chen, L. and Zhang, Y. Preparation of IDA-Cu functionalized core–satellite Fe3O4/polydopamine/Au magnetic nanocomposites and their application for depletion of abundant protein in bovine blood. *Journal of Materials Chemistry*, 20(47) 10696–10704 (2010). doi:10.1039/c0jm01336f

Zhang, S., Meier, B. and Ernst, R. Polarization Echoes in NMR. *Physical Review Letters*, 69(14) 2149–2151 (1992). Retrieved from http://www.ncbi.nlm.nih.gov/pubmed/10046411

Zhang, Y., Wang, H., Nie, J., Zhou, H., Shen, G. and Yu, R. Mussel-inspired fabrication of encoded polymer films for electrochemical identification. *Electrochemistry Communications*, 11(10) 1936–1939 (2009). doi:10.1016/j.elecom.2009.08.024

Zhao, Y. and Taylor, J. S. Assessment of ASTM D 4516 for Evaluation of Reverse Osmosis Membrane Performance. *Desalination*, 180(1-3) 231–244 (2005). doi:10.1016/j.desal.2004.11.089

Zheng, L., Xiong, L., Zheng, D., Li, Y., Liu, Q., Han, K., Liu, W., Tao, K., Yang, S. and Xia, J. Bilayer lipid membrane biosensor with enhanced stability for amperometric determination of hydrogen peroxide. *Talanta*, 85(1) 43–48 (2011). doi:10.1016/j.talanta.2011.02.048

Zheng, Y., Zhang, L., Shi, J., Liang, Y., Wang, X. and Jiang, Z. Mussel-inspired surface capping and pore filling to confer mesoporous silica with high loading and enhanced

stability of enzyme. *Microporous and Mesoporous Materials*, 152 122–127 (2012). doi:10.1016/j.micromeso.2011.11.049

Zhou, M., Liu, H., Kilduff, J. E., Langer, R., Anderson, D. G. and Belfort, G. High Throughput Synthesis and Screening of New Protein Resistant Surfaces for Membrane Filtration. *AIChE Journal*, 56(7) 1932–1945 (2009). doi:10.1002/aic.12104

Zhou, W.-H., Lu, C.-H., Guo, X.-C., Chen, F.-R., Yang, H.-H. and Wang, X.-R. Mussel-inspired molecularly imprinted polymer coating superparamagnetic nanoparticles for protein recognition. *Journal of Materials Chemistry*, 20(5) 880–883 (2010). doi:10.1039/b916619j

Zhu, B. and Edmondson, S. Polydopamine-Melanin Initiators for Surface-Initiated ATRP. *Polymer*, 52(10) 2141–2149 (2011). doi:10.1016/j.polymer.2011.03.027

Zhu, L.-P., Jiang, J.-H., Zhu, B.-K. and Xu, Y.-Y. Immobilization of bovine serum albumin onto porous polyethylene membranes using strongly attached polydopamine as a spacer. *Colloids and Surfaces B: Biointerfaces*, 86(1) 111–118 (2011). doi:10.1016/j.colsurfb.2011.03.027

Zou, L., Vidalis, I., Steele, D., Michelmore, A., Low, S. P. and Verberk, J. Q. J. C. Surface Hydrophilic Modification of RO Membranes by Plasma Polymerization for Low Organic Fouling. *Journal of Membrane Science*, 369(1-2) 420–428 (2011). doi:10.1016/j.memsci.2010.12.023

Zydney, A. L. Protein Separations Using Membrane Filtration: New Opportunities for Whey Fractionation. *International Dairy Journal*, 8(3) 243–250 (1998). doi:10.1016/S0958-6946(98)00045-4

Vita

Daniel Joseph Lang Miller was born in Baltimore, MD. He graduated from the John Carroll School in Churchville, MD in 2002. Dan then attended Bucknell University in Lewisburg, PA, from which he graduated *magna cum laude* with a Bachelor of Science in Chemical Engineering. While at Bucknell, Dan participated in undergraduate research in the laboratory of Dr. Eric Tillman. Dan also held a Summer Undergraduate Research Fellowship at the National Institute of Standards and Technology in Gaithersburg, MD, where he studied under Dr. Steve Kline. Dan began his doctoral studies at the University of Texas at Austin in 2006 under the tutelage of Drs. Don Paul and Benny Freeman. In 2008, Dan was selected for a National Science Foundation Graduate Research Fellowship. Outside of the laboratory, Dan competed on the American Country Dance Association circuit, where he won a Division IV Couples national title before advancing to Division III. Dan graduated from the University of Texas at Austin with a Doctor of Philosophy in Chemical Engineering in May 2013.

Permanent email: danieljmiller@utexas.edu

This dissertation was typed by the author.